Radiation Characteristics of the Atmosphere and the Earth's Surface

N74-22042

Unclas
37448

K Ya Kondrat'ev (Ed.)

(NASA-TT-F-678) RADIATION CHARACTERISTICS OF THE ATMOSPHERE AND THE EARTH'S SURFACE (Amerind Publishing Co. Pvt. Ltd., New Delhi) 597 p HC $11.00

CSCL 04A H1/13

Published for the National Aeronautics and Space Administration and the National Science Foundation, Washington, D.C. by Amerind Publishing Co. Pvt. Ltd., New Delhi

This book contains a great body of information on the most important features of atmospheric radiation such as the quantitative characteristics of molecular absorption and scattering, information regarding spectral and angular distributions, as well as about the three-dimensional structure of shortwave and longwave radiation fields, data on the net radiation flux of the earth's surface, the atmosphere and the so-called earth's surface-atmosphere system, information about the earth's radiation field, etc.

The book describes briefly the model of the structure and composition of the atmosphere. The authors have examined the fundamental optical characteristics of absorption and scattering of radiation by the atmosphere due primarily to the elementary processes of molecular absorption and

(continued on back flap)

TT 71-58003
NASA TT F-678
CATEGORY - 13

RADIATION CHARACTERISTICS OF THE ATMOSPHERE AND THE EARTH'S SURFACE

(RADIATSIÓNNYE KHARAKTERISTIKI ATMOSFERY I ZEMNOI POVERKHNOSTI)

Edited by
K. Ya. Kondrat'ev

Gidrometeorologicheskoe Press
Leningrad, 1969

Translated from Russian

Published for the National Aeronautics and Space Administration
and the National Science Foundation, Washington, D. C.
by Amerind Publishing Co. Pvt. Ltd., New Delhi

1973

© 1973 Amerind Publishing Co. Pvt. Ltd., New Delhi

Translated and Published for the National Aeronautics and Space Administration pursuant to an agreement with the National Science Foundation, Washington, D. C. by Amerind Publishing Co. Pvt. Ltd., 66 Janpath, New Delhi 110001

Translator : Miss Vijay Pandit
General Editor : Dr. V. S. Kothekar

Available from the U. S. Department of Commerce
National Technical Information Service
Springfield, Virginia 22151

Printed at Prem Printing Press, Lucknow, India

UDC 551.521

A great deal of experimental and theoretical material on the atmospheric radiation is available at present. However, so far no adequate reference books have appeared on this subject so that specialists in different branches of science and engineering had to use manuals which are out of date.

This publication contains a great body of data on the most important features of atmospheric radiation such as the quantitative characteristics of molecular absorption and scattering, information regarding spectral and angular distributions, as well as about the three-dimensional structure of shortwave and longwave radiation fields, data on the net radiation flux of the earth's surface, the atmosphere and the so-called earth's surface-atmosphere system, information about the earth's radiation field, etc.

The present monograph will prove to be of value to specialists in meteorology and the physics of the atmosphere, to those engaged in related fields, as well as to students.

TRANSLATOR'S NOTE

In the translation of a highly specialized monograph, such as the present volume, one is bound to come across many obstacles both of a technical nature and otherwise. For instance, the translator found it particularly difficult to use an appropriate equivalent for the Russian word *indicatrix*, a word that has been used very often in the book to denote *coefficient* at some places and *phase function* at others.

The translator put up this and other translation problems to Prof. Kondrat'ev himself. In his reply, the author made several comments of which the following are reproduced :

> "You cannot use 'scattering function' instead of 'scattering coefficient'. You can translate the whole passage [Ch. 2, para 1, p. 26] as follows : 'To describe the process of interaction, the absorption coefficient, the scattering coefficient and the scattering function are used'. "*

For the benefit of the reader Prof. Kondrat'ev recommends two of his recent monographs published in English translation as reference books. These are : *Radiation in the Atmosphere,* Academic Press, New York, 1969; and *Radiation Processes in the Atmosphere,* WMO Monograph, Geneva, 1972.

The translator offers her sincere thanks to Dr. A. P. Mitra, Deputy Director, National Physical Laboratory of India and to Dr. (Miss) A. Mani, Indian Meteorological Department for many useful technical suggestions.

*From a letter to the translator written by Mrs. Helen Valikhan, Secretary to Prof. K. Ya. Kondrat'ev, Corr. Member of the USSR Academy of Sciences, Head of the Department of Atmospheric Physics, Leningrad University, Institute of Physics, USSR, dated August 24, 1972.

Thus, Chapter 1 contains a brief description of the model of the structure and composition of the atmosphere (the significance of these data also lies in their contribution to the transfer of radiation in the atmosphere). However, it is too early as yet to speak of the possibility of the construction of a radiation model of the atmosphere; the only practical course at the moment is to analyze the situation from the point of view of the existence of original data in order to construct such a model. The present monograph can become the foundation for such an analysis.

In Chapter 2 the authors have examined the fundamental optical characteristics of absorption and scattering of radiation by the atmosphere, referring primarily to the elementary processes of molecular absorption and scattering on individual particles. At the end of the chapter there is a brief summary of the data characteristic of the scattering functions in a real atmosphere.

A survey of data on the spectral and integrated transparency of total atmospheric thickness is presented in Chapter 3. A detailed study of the principles of spectral and space-time variability of the albedo of natural underlying surfaces, clouds and the earth's surface-atmosphere system has been given in outline in Chapter 4.

Chapters 5-7 are devoted to the study of the principles of variability of direct solar, scattered, reflected and total radiations. These chapters present an analysis of data on spectral and angular distributions of radiation and provide information on the space-time variability of fluxes and totals of shortwave radiation. Considerable attention has been given to data on the incidence of radiation on an inclined surface. The radiative influx of heat on account of shortwave radiation has been briefly discussed.

Information on different characteristics of thermal emission of the atmosphere has been presented in Chapter 8. This chapter also contains data on spectral and angular distributions of thermal emission, vertical profiles and geographic distributions not only of the fluxes of thermal emission but also of the longwave radiative balance. As in the chapters on shortwave radiation, the problem of the variability principles of the fluxes of thermal emission on an inclined surface has also been examined. The last section of this chapter describes the characteristic of the mesostructure of the thermal emission field of the earth as a planet.

Chapter 9 contains data on net radiation of the underlying surface, the atmosphere and the earth's surface-atmosphere system and characterizes the three-dimensional spatial structure of the field of net radiation as well as its variation with respect to time. The chapter also presents information on the total radiative influx of heat.

The authors appreciate the fact that this first attempt at composing a

FOREWORD

The problem of radiative transfer in the atmosphere has become a focus of interest for specialists not only in the field of atmospheric physics but also in other scientific disciplines. The interest in this problem as related to atmospheric physics has increased considerably with the appearance and development of weather satellites, especially in relation to the solution of reverse problems of meteorology-problems of reconstruction of vertical profiles of the meteorological elements (temperature, density of air, moisture and others) from the data on the measurement of the quantitative characteristics of the field of outgoing radiation. A great deal of attention is now being given to the study of nonadiabatic (or radiative) factors of weather and climate in the development of the theory of climate and to a numerical model of the general atmospheric circulation. There has been a timely accumulation of information in the field of atmospheric radiation for sciences such as agrobiology, radio-physiology, therapy, etc. The characteristics of the earth's radiation field turn out to be extremely important for the solution of complex technical problems connected with the orbiting of cosmic vehicles and for many other technical applications.

K. Ya. Kondrat'ev published a book called *Actinometry* in 1965 in which he presented a fairly complete survey of the problem of transfer of radiation in the atmosphere. However, this book sold out very fast. The present monograph is in the way of a reference book and is based substantially on the material contained in *Actinometry*; and, besides, it includes a large collection of new data on radiation characteristics of the atmosphere. All the sections of this book have been prepared by specialists in their respective limited fields. The majority of the authors are faculty members in the Department of the Physics of the Atmosphere, Leningrad State University named after A. A. Zhdanov. The inclusion of a large number of authors made it difficult to ensure a stylistic uniformity in the presentation of this monograph. However, it resolved the more important problem of a concise presentation of the material, which is also fairly complete and up-to-date (in many cases original data have been reported). The basic information in the monograph comprises results of measurements and computations of the radiation characteristics of the atmosphere. The text only briefly explains the ideas and indicates the sources of the data examined.

Practical interests demand the development of a radiation model similar to the known models of the structure and composition of the atmosphere.

reference monograph on the radiation characteristics of the atmosphere and the underlying surface is, inevitably, far from complete, and would, therefore, welcome any suggestions and comments, which could be sent at the following address : Gidrometeoizdat, 23 Second Lane, Leningrad, V-53.

Member-Correspondent K. Ya. Kondrat'ev

PRECEDING PAGE BLANK NOT FILMED

CONTENTS

Foreword vii
Notation xvii

Chapter 1. Structure and Composition of the Atmosphere .. 1
1. General Terminology (*V. N. Konashenok*) 1
2. Structure of the Atmosphere (*V. N. Konashenok*) 2
3. Gaseous Constituents of the Atmosphere (*V. N. Konashenok*) .. 3
3.1. Units of measurements of gaseous content .. 3
3.2. General information about the constituents of air near the earth's surface 12
3.3. Water vapor (*S. D. Andreev*) 12
3.4. Ozone 19
3.5. Carbon dioxide 25
3.6. Methane 26
3.7. Oxides of nitrogen 27
4. Atmospheric Aerosol (*L. S. Ivlev*) 28
4.1. Experimental investigation of vertical distribution of atmospheric aerosol 28
4.2. Size distribution of atmospheric aerosol particles .. 38
4.3. Sources of aerosol and mechanism of distribution in the atmosphere 39
4.4. *Aerosol models* .. 40

Chapter 2. Optical Characteristics of the Atmosphere .. 45
1. Coefficient of Absorption of Atmospheric Gases in the Visible and Ultraviolet Regions of Spectrum (*A. P. Gal'tsev*) .. 46
1.1. Oxygen O_2 47
1.2. Molecular nitrogen N_2 50
1.3. Nitric oxide NO 54
1.4. Ozone O_3 54
1.5. Water vapor H_2O 55
1.6. Remaining gases 60
2. Optical Characteristics of Atmospheric Gases in the Ultraviolet Region of the Spectrum (*A. P. Gal'tsev*) 62
2.1. Water vapor 64
2.2. Carbon dioxide CO_2 69

2.3. Ozone O_3 73
2.4. Minor components of the atmosphere : CH_4, N_2O and CO 74

3. Characteristics of Scattering of Visible and Infrared Radiation by Aerosol Particles and Air Molecules (*L. S. Ivlev*) .. 79
3.1. Small particles and molecules of air 81
3.2. Large particles 82
3.3. Transparent particles of different sizes 85
3.4. Particles with complex index of refraction .. 87
3.5. Polydispersional aerosol 96

4. Localized Scattering Function in Real Atmosphere (*G. M. Petalin*) 106

Chapter 3. Spectral Transparency of Real Atmosphere .. 119

1. Attenuation of Monochromatic Radiation at Various Inclinations in the Atmosphere. Optical Mass (*I. Ya. Badinov*) .. 122

2. Selective Absorption in Case of Inhomogeneous Atmosphere (*I. Ya. Badinov*) 133
2.1. Method of reduced absorbent masses 133
2.2. Approximation with two parameters 133

3. Atmospheric Transparency Caused by Molecular Scattering (*I. Ya. Badinov*) 134

4. Aerosol Attenuation in Real Atmosphere (*I. Ya. Badinov*) .. 142
4.1. Spectral transparency in a homogeneous direction due to aerosol scattering and absorption .. 142
4.2. Transparency of vertical column of atmosphere due to aerosol component 147
4.3. Vertical profile of aerosol attenuation 151

5. Absorption of Radiation in Real Atmosphere (*I. Ya. Badinov*) .. 156

6. Integral Transparency of the Atmosphere (*L. V. Popova*) .. 166

7. Transparency Variation in Atmospheric Thickness (*L. V. Popova*) 170
7.1. Synoptic situation and transparency 170
7.2. Annual and diurnal variations in atmospheric transparency 172

8. Integrated Transmission Function for Longwave Radiation (*A. M. Brounshtein* and *F. N. Shekhter*) 176
8.1. Computed relation 176
8.2. Experimental data and their comparison with computations 181

Chapter 4. Albedo of Earth's Surface and Clouds (*Z. F. Mironova*) 192
Part I. Integrated Reflection Factor 192
1. Computation of Average Values of Albedo 192
2. Albedo of Different Underlying Surfaces 194
2.1. Albedo of soil surface 194
2.2. Albedo of vegetative covers 195
2.3. Albedo of snow cover 196
2.4. Albedo of ice 196
2.5. Daily variation in albedo 199
3. Albedo of Bodies of Water Basins 202
3.1. Albedo of bodies of water for direct solar radiation .. 202
3.2. Albedo of water basins for total radiation in a clear sky 203
3.3. Experimental data on albedo of water surface .. 205
3.4. Dependence of sea albedo for total radiation on cloudiness 207
3.5. Average values of albedo of water surfaces .. 208
4. Albedo of Large Areas 210
4.1. Measurements of albedo from great height .. 210
4.2. Variation in albedo with altitude 213
4.3. Seasonal variation in albedo of large areas .. 215
5. Geographic Distribution of Albedo 215
6. Albedo of Clouds 219
7. Albedo of the System : Earth's Surface-Atmosphere .. 221
7.1. Planetary albedo of the earth 221
7.2. Geographic distribution of albedo for the earth-atmosphere system 223

Part II. Spectral Albedo 226
8. Variation of Spectral Albedo Under Natural Conditions .. 226
9. Laboratory Measurements of Spectral Characteristics of Reflection from Different Surfaces 232
10. Albedo of Water Reservoirs 235
10.1. Albedo of water reservoirs for direct solar radiation .. 235
10.2. Dependence of albedo for water reservoirs on cloudiness 237
11. Spectral Albedo Measured from an Airplane 238
12. Albedo of Clouds 239

Chapter 5. Direct Solar Radiation 248
1. Spectral Composition of Solar Radiation (*G. A. Nikol'skii*) .. 248

1.1. Spectral energy distribution of solar radiation at sea level 248
1.2. Energy distribution in the spectrum of solar radiation outside the atmosphere 273
1.3. Attenuation of solar radiation in an ideal atmosphere 284
2. Integrated Flux of Direct Solar Radiation (*G. A. Nikol'skii*) .. 289
2.1. Solar constant 289
2.2. Vertical distribution of direct solar radiation .. 293
2.3. Geographic distribution (*L. N. D'yachenko*) .. 296
2.4. Incidence of direct solar radiation on an inclined surface (*M. P. Fedorova*) 311
2.5. Radiative heat flux of solar radiation 316

Chapter 6. Scattered and Reflected Radiation (*M. P. Fedorova*) 329

Part I. Scattered Radiation of the Atmosphere 329
1. Spectral Composition of Scattered Radiation (*V. S. Grishechkin*) 329
2. Angular Distribution of Intensity of Scattered Radiation .. 336
3. Flux of Scattered Radiation from Distinct Zones of the Sky 339
3.1. Zonal radiation 339
3.2. Radiation in the vicinity of the sun 343
4. Vertical Profile of the Flux of Scattered Radiation .. 344
5. Scattered Radiation on a Horizontal Surface 345
5.1. Cloudless atmosphere 345
5.2. Scattered radiation in cloudy atmosphere .. 349
5.3. Daily variations and daily aggregates of scattered radiation 351
5.4. Monthly amounts and annual course of scattered radiation 353
5.5. Contribution of scattered radiation to total radiation 353

Part II. Reflected Radiation of the Atmosphere 355
6. Angular Distribution of Intensity of Reflected Radiation .. 355
6.1. Angular distribution of integrated intensity of reflected radiation 356
6.2. Spectral characteristics of reflected radiation .. 358
6.3. Measurements of reflection characteristics from an airplane 365
7. Vertical Profile of Flux of Reflected Radiation 371

8. Flux of Scattered and Reflected Radiation 375
9. Geographic distribution of Scattered Radiation (*L. N. D'yachenko*) 381
10. Outgoing Shortwave Emission of the Earth-Atmosphere System (Results of Theoretical Computations) (*O. I. Smoktii*) .. 387
10.1. Parallel-plane model of Rayleigh's atmosphere .. 387
10.2. Parallel-plane model of a real atmosphere .. 396
10.3. Spherical model of the atmosphere 401

Chapter 7. Total Radiation (*G. N. Gaevskaya*) 415
1. Spectral Composition of Total Radiation (*V. S. Grishechkin*) .. 415
2. Total Radiation Incident on a Horizontal Surface .. 420
2.1. Dependence of total radiation on solar altitude .. 420
2.2. The effect of cloudiness on the incidence of radiation .. 425
2.3. The dependence of total radiation on the duration of sunshine 436
2.4. The effect of atmospheric turbidity on total incoming radiation 438
2.5. Variation in total radiation with albedo value of underlying surface 439
3. Variation of Total Radiation with Altitude 441
3.1. Vertical distribution of total radiation in clear sky 441
3.2. Influence of cloudiness on total radiation in a free atmosphere 446
4. Radiative Heating in the Troposphere and Stratosphere .. 446
4.1. Absorption of shortwave radiation in a free atmosphere 446
4.2. Radiative heating of the troposphere and stratosphere 451
4.3. Effect of cloudiness on radiative heat inflow .. 455
5. Incidence of Total Radiation on an Inclined Surface (*M. P. Fedorova*) 456
6. Geographic Distribution of Total Radiation 463

Chapter 8. Thermal Radiation of the Atmosphere .. 476
1. Spectral Composition of Thermal Radiation of the Atmosphere (*S. V. Ashcheulov*) 477
2. Angular Distribution of Thermal Radiation of the Earth's Surface and the Atmosphere (*K. E. Yakushevskaya*) .. 483
2.1. Downward atmospheric radiation 483

2.2. Upward emission 487
2.3. Outgoing radiation 489
2.4. Effective radiation 493
3. Vertical Profile of Radiation (*Kh. Yu. Niilisk*) 493
4. Geographic Distribution of Longwave Balance in the Atmosphere and its Components (*L. N. D'yachenko*) 504
4.1. Outgoing radiation 505
4.2. Effective radiation of the underlying surface .. 509
4.3. The longwave balance of the atmosphere .. 513
5. Fluxes of Atmospheric Thermal Radiation on Differently Oriented Planes (*M. P. Fedorova*) 520
5.1. Fluxes at the ground level 520
5.2. Flux of outgoing longwave radiation 523
6. Characteristics of Mesostructure of Thermal Radiation Field of the Earth as a Planet (*V. A. Baryshev*) 529
6.1. Statistical method of describing radiation field .. 530
6.2. Peculiarities of statistical description of the radiation field 532
6.3. Methods of determination and some results of computations of structural characteristics of the field of outgoing radiation 533

Chapter 9. Net Radiation (*G. A. Nikol'skii*) 543
1. Net Radiation and its Measurement 543
1.1. Constituents of net radiation 543
1.2. Measurement of net radiation 544
2. Net Radiation of an Underlying Surface 546
2.1. Variation of net radiation with time 546
2.2. Geographic distribution of net radiation of an underlying surface (*L. N. D'yachenko*) 549
2.3. Net radiation of slopes (*M. P. Fedorova*) 557
3. Net Radiation of the Atmosphere and the Earth-Atmosphere System 561
3.1. Incoming and diffuse components of net radiation of the atmosphere and the earth-atmosphere system .. 561
3.2. Geographic distribution of net radiation of the atmosphere and of the earth-atmosphere system (*L. N. D'yachenko*) 565
3.3. Vertical profiles of net radiation 570
3.4. Radiant influx of heat 576

NOTATION

A—integrated absorption function
A_ν—spectral absorption function
A—integral albedo
A_λ—spectral albedo
A_s—albedo of the earth's surface-atmosphere system
A_{in}—albedo of an inclined surface
B_λ—brightness of emission
B_{in}—net radiation of an inclined surface
B—net radiation of an underlying surface
B_a—net radiation of the atmosphere
B_s—radiation balance of the earth's surface-atmosphere system
B_{LW}—balance of longwave radiation
B_{SW}—balance of shortwave radiation
c—velocity of light
c_p—specific heat at constant pressure
D—flux of scattered radiation on a horizontal surface
D_{in}—flux of scattered radiation on an inclined surface
$D_{\lambda m}$—spectral flux of scattered radiation
E_λ—illumination
E_a—flux of atmospheric longwave radiation
E_s—flux of emission of the underlying surface
E_∞—flux of longwave emission of the atmosphere in space
F_0—flux of effective radiation at the earth's surface
F_{eff}—flux of effective radiation
F_∞—flux of outgoing longwave radiation
F_h—flux of effective emission of a horizontal surface
F_{in}—flux of effective emission of an inclined surface
F_λ—flux of emission at wavelength λ
F_f—flux of downward emission
F_u—flux of upward emission
g—acceleration due to gravity
H—height of ascent
H_u—height of uniform atmosphere
h—Planck's constant
$h_\odot$—height of the sun
h_c—height of clouds
I—intensity of radiation

I_λ—intensity of radiation of wavelength λ
I_D—ntensity of scattered radiation
I_G—intensity of atmospheric back radiation
I_u—intensity of upward atmospheric radiation
I_R—intensity of reflected radiation
I_{eff}—intensity of effective atmospheric radiation
I_1—intensity of singly scattered radiation
I_n—intensity of multiply scattered radiation
I_n'—intensity of multiply scattered radiation in the plane atmospheric model
k—Boltzmann constant
k_v—volume coefficient of absorption
$k_v(m)$—bulk coefficient of absorption
$k_v(\mu)$—molecular coefficient of absorption
m—atmospheric mass
m'—atmospheric mass at normal pressure
$\tilde{m}$—complex index of refraction
$\mathcal{N}$—index of turbidity
N_r—index of refraction
N_i—volume content of the i-th gas
N_i^*—content of molecules in a column of unit cross section
$\mathcal{N}(H)$—particle distribution function with respect to height
n—real part of the index of refraction
n_0—coefficient of refraction
n_c—extent of cloudiness in tenths
n_s—number of molecules in a unit volume at normal conditions
P—transmission function
P_i—transparency of the atmosphere at i-th atmospheric mass
P_λ—spectral transparency
P_p—degree of polarization
p—pressure
p_{eff}—effective pressure
Q—flux of total radiation on a horizontal surface under a clear sky
Q_g—flux of total radiation on a horizontal surface under a cloudy sky
Q_{in}—flux of total radiation on an inclined surface
q—shortwave radiation absorbed in the atmosphere
q_e—solar radiation absorbed at the earth's surface
q_s—solar radiation absorbed by the earth's surface-atmosphere system
R_0—universal gas constant
R—flux of reflected shortwave radiation
R_{in}—flux of reflected shortwave radiation on an inclined surface
r_i—mass content of the i-th gas
r_i^*—ratio of mixtures of the i-th gas

r_λ—spectral coefficient of brightness
r_λ'—spectral reflection coefficient
S—flux of direct solar radiation on a vertical surface
S_{id}—flux of direct solar radiation in an ideal atmosphere
S_h—flux of direct solar radiation on a horizontal surface
S_v—flux of direct solar radiation on a vertical surface
S_{in}—flux of direct solar radiation on an inclined surface
S_λ—spectral flux of direct solar radiation
S_0—solar constant
S_0'—solar constant for a horizontal surface
S_0^*—solar constant on a given day
$S_{0\lambda}$—spectral solar constant
S_l—intensity of a spectral line
s—actual duration of daylight
S_0—probable duration of daylight
s_M—duration of daylight in a month
$T°$ C—temperature in °C
$T°$ K—temperature in °K
T—turbidity factor
t—time
U_a—emission of an underlying surface absorbed in the atmosphere
U_{in}—longwave exchange between an inclined and a horizontal surfaces
u—amount of absorbed substance in the path of the ray
u'—total content of attenuated component (cm or g/cm^2)
u_{eff}—effective mass of absorbed substance
w_∞—amount of water vapor in a column of atmosphere of unit cross section
w_H—amount of water vapor in a layer from the earth's surface to the clouds
$\varkappa(\gamma)$—scattering function
z—vertical coordinate
α—angle of inclination of a surface relative to the horizontal surface
α_v—volume coefficient of scattering
$\alpha_v(m)$—bulk coefficient of scattering
$\alpha_v(\mu)$—molecular coefficient of scattering
$\beta_v(m)$—bulk attenuation coefficient
γ—angle of scattering
γ_1—half-width of the spectral line
Δp—pressure difference
ΔH_2O—shortwave radiation absorbed by water vapor
ΔS_{aer}—attenuation of solar radiation by aerosol
ΔS_{H_2O}—attenuation of solar radiation by water vapor
δ—emission capability

δ_h—emission capability of a horizontal surface
δ_{in}—emission capability of a vertical surface
$\delta_\odot$—inclination of the sun
$\varepsilon_\odot$—angle of sunset at the horizon
$\eta_\nu(m)$—bulk emission coefficient
$\vartheta_\odot$—zenith separation of the sun
$\varkappa$—imaginary part of the index of refraction
λ—wavelength
μ—molecular weight
$\mu_0(\gamma)$—coefficient of scattering in a given direction
ν—wave number
ρ—density of gas, air
ρ_s—density of snow
σ—Stefan-Boltzmann constant
τ—optical thickness of the atmosphere
φ—latitude of the point
ψ—azimuth angle
$\psi_\odot$—azimuth of the sun
ω—solid angle
$\mathfrak{Q}$—hourly angle of the sun

1. STRUCTURE AND COMPOSITION OF THE ATMOSPHERE

1. GENERAL TERMINOLOGY

The study of the atmosphere can be subdivided into regions based on specific criteria in accordance with the existing terminology. Thus, if we consider the molecular weight as a fundamental criterion, then we may divide the atmosphere into a homosphere with constant molecular weight and a heterosphere in which the molecular weight decreases with altitude; however, if the concentration of charged particles is to serve as a basic criterion, then a special zone, viz. the ionosphere, can be distinguished; while investigating the scattering processes of gases the scattering region in the atmosphere called the exosphere attains importance. The atmosphere can be divided into regions according to temperature ranges while examining the thermal regime as well as the radiative and dynamic processes. The lowest region (i.e. the region of convectional equilibrium) is called the troposphere. In this region the temperature drops with increasing height at a mean rate of 6° per km. Above the troposphere we find the stratosphere, in which the temperature rises with height due to the absorption of the solar radiation by ozone. The tropopause separates troposphere from stratosphere and represents an isothermal region of comparatively narrow vertical extent, depending on specific

conditions. The average height of the tropopause in polar latitudes is 10-12 km, and in equatorial latitudes between 15 and 17 km. The stratopause, being situated at an average height of 50 km, serves as the upper boundary of the stratosphere. Above the stratopause the temperature decreases once again with height up to 80 km, the corresponding region being called the mesosphere. This drop in the temperature with height comes to an end within the mesopause (80-90 km), above which lies a wide region with a positive temperature gradient, known as the thermosphere. The rise of temperature ceases between the heights of 250 and 300 km and isothermy sets in at this stage.

2. STRUCTURE OF THE ATMOSPHERE

In studying the structure of the atmosphere we usually take into consideration the vertical distribution of temperature T, pressure p and density of air ρ. These three parameters are related among themselves by two equations, viz. the equation of state and the hydrostatic equation as follows :

$$p=\frac{1}{\mu}\rho R_0 T, \tag{1.1}$$

$$\frac{dp}{dz}=-\rho g. \tag{1.2}$$

Two more parameters, depending on height, besides T, p and ρ enter into these equations, viz. the molecular weight and the acceleration due to gravity. However, it has been experimentally established that up to a height of 100 km the molecular weight remains a constant and begins to decrease only at higher altitudes. Inasmuch as the properties of the atmosphere below 100 km only will be examined in the present book, it is possible to make use of a constant value of molecular weight, viz. 28.964. The dependence on altitude of the acceleration due to gravity can be represented by the following approximate formula:

$$g(z)=g_0\frac{d^2}{(d+z)^2}, \tag{1.3}$$

where d is radius of the earth. From this equation it is clear that up to a height of 100 km one can, in practice, use a constant value of acceleration due to gravity.

Thus, for a description of the structure of the atmosphere, it is necessary to have either a third equation, connecting these very parameters,

or an experimental determination of the vertical distribution of one of the three parameters, i.e. T, p and ρ. The energy equation could be the third equation, but it usually employs new unknowns and consequently requires the use of more equations. The mathematical problem thus obtained cannot be resolved very satisfactorily. Therefore, in order to describe the structure of the atmosphere we make use of models in which one of the three parameters T, p and ρ is known on the basis of experimental data, and the remaining two are found with the help of equations (1.1) and (1.2). Such an average model for the earth representing standard atmosphere USA-1962 [27] is presented in Table 1.1. Other characteristics of the atmospheric gas besides the temperature, pressure and density are also presented in this Table. Specific vertical distributions of atmospheric parameters can differ considerably from their standard values. These deviations could be of a regular or a fluctuating nature. A large amount of experimental data, accumulated recently, has allowed us to establish with reliability the basic patterns of regular latitudinal and seasonal variations of the structural parameters of the atmosphere in the layer between 0 and 90 km. These patterns are reflected in models of atmosphere for different latitudes and seasons appended to standard atmosphere USA-1962 [27] (Table 1.2).

3. GASEOUS CONSTITUENTS OF THE ATMOSPHERE

3.1 Units of measurement of gaseous content

We make use of different units of measurement for a quantitative representation of a specific gas, whose choice depends upon the experimental methods of investigation as well as on traditions laid down during the study of a particular gas. The fundamental units of measuring gaseous contents and their definitions are presented in Table 1.3.

Besides the characteristics enumerated in Table 1.3 it is necessary to point out the often-used expression about the general contents of molecules in the form of thickness of the layer of molecules under specific conditions (for instance, at normal temperature and pressure or during transition of all the molecules into the liquid phase). In this case the unit for density of gas is cm/km and represents the quantity of gas introduced under normal conditions in a vertical column of atmosphere with a cross section of 1 cm^2 and height equal to 1 km.

This unit is most often used in the case of ozone, whose conversion from cm/km to $\mu g/m^3$ is given by the following formula :

$$1 \text{ cm/km} = 2.14 \times 10^4 \ \mu g/m^3.$$

Table 1.1 Standard atmosphere USA-1962 [27]

Altitude, km	Temperature, °K	Pressure, mb	Density, kg/m³	Collision frequency, sec⁻¹	Mean free path, m	Molecular weight	Speed of sound, m/sec	Coefficient of viscosity, kg/m . sec	Kinematic viscosity m²/sec	Thermal conductivity, kcal/ m · sec · deg
0	288.150	1.013 (3)	1.225 (0)	6.919 (9)	6.633 (—8)	28.964	340.294	1.789 (—5)	1.461 (—5)	6.053 (—6)
4	262.166	6.166 (2)	8.194 (—1)	4.414 (9)	9.917 (—8)	28.964	324.589	1.661 (—5)	2.028 (—5)	5.559 (—8)
8	236.215	3.565 (2)	5.258 (—1)	2.688 (9)	1.545 (—7)	28.964	308.105	1.527 (—5)	2.904 (—5)	5.052 (—6)
12	216.650	1.940 (2)	3.119 (—1)	1.528 (9)	2.605 (—7)	28.964	295.069	1.422 (—5)	4.557 (—5)	4.662 (—6)
16	216.650	1.035 (2)	1.665 (—1)	8.153 (8)	4.881 (—7)	28.964	295.069	1.422 (—5)	8.540 (—5)	4.662 (—6)
20	216.650	5.529 (1)	8.891 (—2)	4.355 (8)	9.139 (—7)	28.964	295.069	1.422 (—5)	1.599 (—4)	4.662 (—6)
24	220.560	2.972 (1)	4.694 (—2)	2.320 (8)	1.731 (—6)	28.964	297.720	1.443 (—5)	3.074 (—4)	4.740 (—6)
28	224.527	1.616 (1)	2.508 (—2)	1.250 (8)	3.240 (—6)	28.964	300.386	1.465 (—5)	5.841 (—4)	4.820 (—6)
32	228.490	8.891 (0)	1.356 (—2)	6.818 (7)	5.994 (—6)	28.964	303.025	1.486 (—5)	1.096 (—3)	4.899 (—6)
36	239.282	4.985 (0)	7.258 (—3)	3.736 (7)	1.120 (—5)	28.964	310.099	1.543 (—5)	2.126 (—3)	5.113 (—6)
40	250.350	2.871 (0)	3.996 (—3)	2.104 (7)	2.034 (—5)	28.964	317.189	1.601 (—5)	4.007 (—3)	5.330 (—6)
44	261.403	1.695 (0)	2.259 (—3)	1.215 (7)	3.597 (—5)	28.964	324.116	1.657 (—5)	7.337 (—3)	5.544 (—6)
48	270.650	1.023 (0)	1.317 (—3)	7.208 (6)	6.171 (—5)	28.964	329.799	1.704 (—5)	1.294 (—2)	5.721 (—6)
52	269.650	6.223 (—1)	8.010 (—4)	4.385 (6)	1.014 (—4)	28.964	327.911	1.688 (—5)	2.674 (—2)	5.662 (—6)
56	263.628	3.766 (—1)	4.976 (—4)	2.689 (6)	1.633 (—4)	28.964	325.492	1.669 (—5)	3.353 (—2)	5.587 (—6)
60	255.772	2.246 (—1)	3.659 (—4)	1.628 (6)	2.656 (—4)	28.964	320.606	1.629 (—5)	5.324 (—2)	5.435 (—6)
64	243.202	1.315 (—1)	1.884 (—4)	9.775 (5)	4.313 (—4)	28.964	312.628	1.564 (—5)	8.302 (—2)	5.190 (—6)
68	227.529	7.445 (—2)	1.140 (—4)	5.721 (5)	7.122 (—4)	28.964	302.387	1.481 (—5)	1.299 (—1)	4.886 (—6)
72	211.876	4.050 (—2)	6.659 (—5)	3.225 (5)	1.22 (—3)	28.964	291.800	1.395 (—5)	2.095 (—1)	4.565 (—6)
76	196.24	2.405 (—2)	3.736 (—5)	1.741 (5)	2.175 (—3)	28.964	280.83	1.307 (—5)	3.499 (—1)	4.247 (—6)
80	180.65	1.037 (—2)	1.999 (—5)	8.940 (4)	4.065 (—3)	28.964	269.44	1.216 (—5)	6.085 (—1)	3.925 (—6)
90	180.65	1.644 (—3)	3.170 (—6)	1.418 (4)	2.563 (—2)	28.964	269.44	1.216 (—5)	3.837 (0)	3.925 (—6)

NOTE : The number in brackets represents the power of ten.

Table 1.2 Models of atmosphere for different latitudes and seasons [27] (supplement to standard atmosphere USA-1962)

Altitude, km	15° N		30° N				45° N			
			July		January		July		January	
	T °K	p mb	T °K	p mb	T °K	p mb	T °K	p mb	T °K	p mb
0	299.65	1.01(3)	301.15	1.01(3)	287.15	1.02(3)	294.15	1.01(3)	272.15	1.02(3)
2	287.68	8.04(2)	288.17	8.05(2)	281.16	8.04(2)	285.15	8.02(2)	265.15	7.90(2)
4	276.98	6.33(2)	277.19	6.33(2)	268.20	6.27(2)	273.17	6.28(2)	255.67	6.08(2)
6	263.63	4.92(2)	266.23	4.93(2)	255.24	4.84(2)	261.19	4.87(2)	243.69	4.63(2)
8	250.29	3.78(2)	252.30	3.80(2)	242.29	3.69(2)	248.22	3.72(2)	231.71	3.47(2)
10	236.96	2.86(2)	238.35	2.87(2)	229.34	2.76(2)	235.25	2.81(2)	219.75	2.57(2)
12	223.64	2.13(2)	224.42	2.14(2)	216.40	2.63(2)	222.30	2.09(2)	218.66	1.88(2)
14	210.32	1.56(2)	210.50	1.57(2)	211.68	1.48(2)	215.65	1.53(2)	217.67	1.38(2)
16	197.02	1.12(2)	203.15	1.12(2)	205.91	1.07(2)	215.65	1.11(2)	216.67	1.01(2)
18	198.78	7.89(1)	207.38	8.08(1)	203.15	7.65(1)	216.79	8.12(1)	215.68	7.36(1)
20	206.71	5.65(1)	211.75	5.85(1)	207.93	5.50(1)	219.17	5.95(1)	215.15	5.37(1)
22	214.64	4.09(1)	215.94	4.26(1)	212.89	3.98(1)	221.56	4.37(1)	215.15	3.91(1)
24	219.23	3.00(1)	219.90	3.12(1)	216.90	2.91(1)	223.94	3.22(1)	215.15	2.86(1)
26	223.58	2.21(1)	223.87	2.30(1)	220.87	2.13(1)	226.32	2.39(1)	215.15	2.08(1)
28	227.94	1.64(1)	227.83	1.70(1)	224.83	1.57(1)	229.49	1.77(1)	215.85	1.52(1)
30	232.29	1.22(1)	231.79	1.27(1)	228.79	1.17(1)	233.65	1.32(1)	217.44	1.11(1)
32	236.63	9.15(0)	235.74	9.51(0)	232.74	8.72(0)	237.81	9.92(0)	219.02	8.16(0)
34	240.98	6.90(0)	240.40	7.16(0)	237.40	6.54(0)	242.70	7.49(0)	224.79	6.02(0)
36	245.32	5.23(0)	245.15	5.42(0)	242.15	4.94(0)	247.64	5.68(0)	230.92	4.47(0)
38	249.66	3.98(0)	249.88	4.13(0)	246.88	3.75(0)	252.59	4.34(0)	237.05	3.35(0)
40	253.99	3.05(0)	254.62	3.16(0)	251.62	2.86(0)	257.53	3.33(0)	243.18	2.53(0)

Table 1.2—*Contd.*

Altitude, km	15° N		30° N				45° N			
			July		January		July		January	
	T °K	p mb	T °K	p mb	T °K	p mb	T °K	p mb	T °K	p mb
42	258.33	2.34 (0)	259.35	2.43 (0)	256.35	2.19 (0)	262.46	2.57 (0)	249.29	1.92 (0)
44	262.66	1.81 (0)	264.08	1.88 (0)	261.08	1.69 (0)	267.40	1.99 (0)	255.41	1.47 (0)
46	266.99	1.40 (0)	268.80	1.46 (0)	265.80	1.31 (0)	272.33	1.55 (0)	261.53	1.13 (0)
48	270.15	1.09 (0)	272.15	1.14 (0)	269.15	1.02 (0)	275.65	1.21 (0)	265.65	8.80 (—1)
50	270.15	8.54 (—1)	272.15	8.91 (—1)	269.15	7.94 (—1)	275.65	9.51 (—1)	265.65	6.83 (—1)
52	269.24	6.66 (—1)	271.14	6.96 (—1)	268.14	6.19 (—1)	275.65	7.45 (—1)	265.65	5.30 (—1)
54	265.31	5.18 (—1)	267.21	5.42 (—1)	264.21	4.81 (—1)	271.79	5.83 (—1)	262.56	4.11 (—1)
56	261.39	4.02 (—1)	263.28	4.21 (—1)	260.28	3.72 (—1)	266.87	4.55 (—1)	258.63	3.18 (—1)
58	257.47	3.10 (—1)	259.36	3.26 (—1)	256.36	2.87 (—1)	261.96	3.53 (—1)	254.70	2.45 (—1)
60	253.10	2.39 (—1)	254.79	2.51 (—1)	252.04	2.21 (—1)	257.05	2.72 (—1)	250.77	1.88 (—1)
62	246.25	1.83 (—1)	247.40	1.92 (—1)	245.97	1.69 (—1)	252.15	2.09 (—1)	246.85	1.43 (—1)
64	239.40	1.39 (—1)	239.91	1.46 (—1)	239.90	1.28 (—1)	244.52	1.60 (—1)	242.93	1.09 (—1)
66	232.56	1.05 (—1)	232.47	1.10 (—1)	233.83	9.66 (—2)	235.70	1.21 (—1)	238.87	8.25 (—2)
68	225.73	7.81 (—2)	225.04	8.23 (—2)	227.77	7.23 (—2)	226.89	9.06 (—2)	234.76	6.22 (—2)
70	218.89	5.79 (—2)	217.61	6.08 (—2)	221.71	5.37 (—2)	218.08	6.71 (—2)	230.65	4.67 (—2)
72	212.06	4.25 (—2)	210.19	4.45 (—2)	215.66	3.96 (—2)	209.28	4.90 (—2)	226.54	3.48 (—2)
74	205.23	3.09 (—2)	202.77	3.22 (—2)	209.60	2.89 (—2)	200.48	3.54 (—2)	222.44	2.59 (—2)
76	198.42	2.22 (—2)	195.36	2.31 (—2)	203.56	2.09 (—2)	191.69	2.52 (—2)	218.34	1.91 (—2)
78	191.53	1.57 (—2)	187.95	1.63 (—2)	197.51	1.50 (—2)	182.91	1.76 (—2)	214.24	1.40 (—2)
80	184.78	1.11 (—2)	180.55	1.14 (—2)	191.47	1.07 (—2)	174.15	1.21 (—2)	210.15	1.03 (—2)
82	184.150	7.72 (—3)	180.15	7.85 (—3)	191.15	7.54 (—3)	174.15	8.28 (—3)	210.15	7.47 (—3)
84	184.150	5.38 (—3)	180.15	5.43 (—3)	191.15	5.32 (—3)	174.15	5.65 (—3)	210.15	5.44 (—3)
86	184.150	3.75 (—3)	180.15	3.75 (—3)	191.15	3.76 (—3)	174.15	3.86 (—3)	210.15	3.97 (—3)
88	184.150	2.62 (—3)	180.15	2.60 (—3)	191.15	2.65 (—3)	174.15	2.63 (—3)	210.15	2.89 (—3)
90	184.150	1.83 (—3)	180.15	1.80 (—3)	191.15	1.88 (—3)	174.15	1.80 (—3)	210.15	2.11 (—3)

Table 1.2—*Contd.*

Altitude, km	60° N				60° N			
	July		January		warm winter		cold winter	
	T °K	p mb	T °K	p mb	T °K	p mb	T °K	p mb
0	287.15	1.01 (3)	257.15	1.01 (3)	257.15	1.01 (3)	257.15	1.01 (3)
2	276.34	7.93 (2)	255.94	7.77 (2)	255.94	7.77 (2)	255.94	7.77 (2)
4	265.54	6.16 (2)	247.74	5.93 (2)	247.74	5.93 (2)	247.74	5.93 (2)
6	253.14	4.74 (2)	234.14	4.47 (2)	234.14	4.47 (2)	234.14	4.47 (2)
8	239.15	3.59 (2)	220.55	3.31 (2)	220.55	3.31 (2)	220.55	3.31 (2)
10	225.17	2.68 (2)	217.15	2.42 (2)	220.14	2.42 (2)	217.15	2.42 (2)
12	225.15	1.98 (2)	217.15	1.77 (2)	224.14	1.78 (2)	217.15	1.77 (2)
14	225.15	1.46 (2)	217.15	1.29 (2)	224.15	1.31 (2)	215.16	1.29 (2)
16	225.15	1.08 (2)	216.56	9.43 (1)	224.15	9.70 (1)	213.17	9.38 (1)
18	225.15	7.98 (1)	215.37	6.88 (1)	224.15	7.16 (1)	211.18	6.81 (1)
20	225.15	5.90 (1)	214.17	5.01 (1)	224.15	5.29 (1)	209.19	4.92 (1)
22	225.15	4.36 (1)	212.98	3.65 (1)	224.15	3.90 (1)	207.20	3.55 (1)
24	226.56	3.23 (1)	211.79	2.65 (1)	224.15	2.88 (1)	205.21	2.56 (1)
26	229.54	2.40 (1)	212.08	1.92 (1)	224.58	2.13 (1)	203.22	1.83 (1)
28	232.52	1.79 (1)	214.06	1.40 (1)	226.56	1.58 (1)	201.24	1.31 (1)
30	235.50	1.34 (1)	216.05	1.02 (1)	228.55	1.17 (1)	199.25	9.34 (0)
32	238.47	1.01 (1)	218.03	7.46 (0)	230.53	8.72 (0)	201.78	6.66 (0)
34	244.24	7.59 (0)	220.01	5.48 (0)	232.51	6.51 (0)	204.56	4.77 (0)
36	250.18	5.77 (0)	224.76	4.04 (0)	234.49	4.87 (0)	209.86	3.44 (0)
38	256.17	4.42 (0)	229.71	3.00 (0)	237.71	3.66 (0)	218.57	2.51 (0)
40	262.65	3.40 (0)	234.65	2.24 (0)	242.65	2.76 (0)	227.27	1.85 (0)
42	267.98	2.64 (0)	239.59	1.69 (0)	247.60	2.09 (0)	233.13	1.38 (0)

Table 1.2—*Contd.*

Altitude, km	60° N				60° N			
	July		January		warm winter		cold winter	
	T °K	p mb	T °K	p mb	T °K	p mb	T °K	p mb
44	272.48	2.06 (0)	244.54	1.28 (0)	252.54	1.60 (0)	238.66	1.04 (0)
46	274.65	1.61 (0)	249.47	9.71 (—1)	257.47	1.23 (0)	244.19	7.85 (—1)
48	276.82	1.26 (0)	254.40	7.43 (—1)	262.40	9.47 (—1)	249.71	5.97 (—1)
50	277.15	9.87 (—1)	259.33	5.72 (—1)	267.33	7.34 (—1)	255.23	4.57 (—1)
52	277.15	7.74 (—1)	260.15	4.41 (—1)	268.15	5.71 (—1)	256.15	3.52 (—1)
54	275.92	6.07 (—1)	260.15	3.41 (—1)	268.15	4.44 (—1)	256.15	2.70 (—1)
56	271.99	4.75 (—1)	257.30	2.63 (—1)	264.20	3.45 (—1)	252.04	2.08 (—1)
58	268.05	3.70 (—1)	253.76	2.02 (—1)	259.28	2.67 (—1)	246.92	1.59 (—1)
60	262.73	2.88 (—1)	250.89	1.55 (—1)	254.36	2.06 (—1)	243.67	1.21 (—1)
62	253.49	2.22 (—1)	249.91	1.18 (—1)	249.45	1.58 (—1)	245.63	9.16 (—2)
64	244.26	1.69 (—1)	248.93	9.05 (—2)	244.54	1.20 (—1)	247.59	6.98 (—2)
66	235.04	1.28 (—1)	247.95	6.9 (—2)	239.64	9.10 (—2)	249.56	5.33 (—2)
68	225.83	9.57 (—2)	246.97	5.27 (—2)	234.73	6.86 (—2)	251.52	4.08 (—2)
70	216.61	7.07 (—2)	245.69	4.02 (—2)	229.83	5.14 (—2)	253.48	3.13 (—2)
72	207.41	5.16 (—2)	242.95	3.05 (—2)	225.51	3.83 (—2)	254.58	2.40 (—2)
74	198.21	3.71 (—2)	240.21	2.32 (—2)	224.53	2.85 (—2)	250.66	1.85 (—2)
76	189.02	2.63 (—2)	237.47	1.75 (—2)	223.55	2.11 (—2)	246.75	1.41 (—2)
78	179.83	1.83 (—2)	234.73	1.32 (—2)	222.57	1.57 (—2)	242.84	1.07 (—2)
80	171.15	1.25 (—2)	232.00	9.91 (—3)	221.60	1.16 (—2)	238.93	8.14 (—3)
82	171.15	8.46 (—3)	229.27	7.42 (—3)	220.62	8.58 (—3)	235.03	6.14 (—3)
84	171.15	5.73 (—3)	226.53	5.54 (—3)	219.64	6.33 (—3)	231.13	4.61 (—3)
86	171.15	3.88 (—3)	223.80	4.12 (—3)	218.67	4.67 (—3)	227.23	3.45 (—3)
88	171.15	2.63 (—3)	221.08	3.05 (—3)	217.69	3.44 (—3)	223.33	2.57 (—3)
90	171.15	1.78 (—3)	218.35	2.26 (—3)	216.72	2.54 (—3)	219.43	1.90 (—3)

Table 1.2—*Contd.*

Altitude, km	75° N				75° N			
	July		January		warm winter		cold winter	
	T °K	p mb	T °K	p mb	T °K	p mb	T °K	p mb
0	278.15	1.01 (3)	249.15	1.01 (3)	249.15	1.01 (3)	249.15	1.01 (3)
2	272.94	7.90 (2)	250.88	7.72 (2)	250.88	7.72 (2)	250.88	7.72 (2)
4	261.86	6.12 (2)	239.87	5.84 (2)	239.87	5.84 (2)	239.87	5.84 (2)
6	248.85	4.69 (2)	228.86	4.36 (2)	228.86	4.36 (2)	228.86	4.36 (2)
8	235.85	3.53 (2)	217.86	3.21 (2)	217.86	3.21 (2)	217.86	3.21 (2)
10	226.66	2.63 (2)	214.40	2.34 (2)	219.37	2.35 (2)	212.89	2.34 (2)
12	228.65	1.95 (2)	213.25	1.70 (2)	222.15	1.72 (2)	209.89	1.69 (2)
14	230.15	1.25 (2)	211.65	1.23 (2)	222.15	1.27 (2)	206.90	1.22 (2)
16	230.15	9.27 (1)	210.05	8.93 (1)	222.15	9.37 (1)	203.95	8.80 (1)
18	230.15	6.96 (1)	208.46	6.45 (1)	222.64	6.87 (1)	201.36	6.26 (1)
20	230.15	5.13 (1)	207.65	4.65 (1)	223.64	5.06 (1)	200.16	4.46 (1)
22	230.15	3.82 (1)	207.65	3.35 (1)	224.64	3.74 (1)	198.97	3.17 (1)
24	231.90	2.85 (1)	207.65	2.41 (1)	225.63	2.76 (1)	197.77	2.25 (1)
26	234.29	2.13 (1)	207.65	1.74 (1)	227.58	2.05 (1)	197.15	1.59 (1)
28	236.67	1.59 (1)	207.65	1.25 (1)	230.56	1.52 (1)	197.15	1.13 (1)
30	239.05	1.20 (1)	207.65	9.05 (0)	233.54	1.14 (1)	197.15	8.01 (0)

NOTE : The number in brackets represents the power of ten.

Table 1.3 Characteristics of gaseous constituent

Quantitative characteristics of gas	Definition	Units	Ratio of different characteristics	Observation
n_i—absolute concentration of i^{th} gas	Number of molecules in a unit volume (depending on T and p)	cm^{-3}, m^{-3}	$n_i = \frac{p_i}{k_i}$	This characteristic is essential in photochemical computations
N_i—volumetric concentration of i^{th} gas (volume contents)	Ratio between concentration of molecules of i^{th} gas and air or ratio between molar volumes	Dimensionless	$N_i = \frac{n_i}{n} = \frac{p_i}{p} = \frac{V}{V_i}$ where n and p are the number of molecules of air and the total pressure, and V and V_i are the molar volumes	Percentages and units, representing a millionth fraction of a unit of measurements, may be often used as the unit of measurement
ρ_i—density of i^{th} gas	Mass of i^{th} gas in units of volume of air (to be used for actual T and p, and at standard values of T and p)	g/cm^3, g/m^3, microgram/m^3 ($\mu g/m^3$)	$\rho_i = \frac{\rho_i \mu_i}{RT} = \frac{n_i \mu_i}{N_0}$, where μ_i—molecular weight, N_0—Avogadro Number; R—universal gas constant	This characteristic is called "absolute humidity" when applied to water vapor (using the units g/m^3); ozone in troposphere is usually measured in $\mu g/m^3$

r_i—mass concentration of i^{th} gas (mass content)	Ratio of density of i^{th} gas to density of air (not depending on T and p)	Dimensionless	$r_i = \frac{\rho_i}{\rho} = N_i \frac{\mu_i}{\mu}$	In application to water vapor, the characteristic is called "specific humidity". It is convenient while examining processes of dynamic diffusion in gases. Units used in this case are the following; g/g, g/kg, μg/kg
r_i^*—mixing ratio	Ratio of density of the i^{th} gas to density of air without this gas (not depending on T and p)	Dimensionless	$r_i^* = \frac{\rho_i}{\rho - \rho_i} = \frac{r_i}{1 - r_i}$	There is practically no difference between mass concentration and air for secondary components
N_i^*—general molecular contents	Number of molecules above the observed level in the column of atmosphere of cross section equal to 1 cm^2	cm^{-2}	$N_i^* = \int_z^\infty n_i(t)\, dt$	Necessary for optical computations (absorption, emission, etc.)

3.2 General information about the constituents of air near the earth's surface

The basic information about the constitution of dry air near the ground is given in Table 1.4.

From the Table it is obvious that 99% of dry atmosphere consists of oxygen and nitrogen. However, the immediate role of these gases in the formation of radiative and thermal regimes in the atmosphere to a height of 70 km is comparatively unimportant and mainly lies in the creation of a medium with definite values of pressure, density, specific heat, etc. This is because of the optical insensitivity of these gases in the near-ultraviolet, visible and infrared regions of the spectrum and of the insignificant variability in time and space. The time-space distribution of water vapor, carbon dioxide and ozone is of the greatest importance in the study of radiative and thermal regimes.

3.3 Water vapor

(a) Characteristics of humidity. The possibility of transforming water vapor into the liquid state under natural conditions differentiates it from all the other gases. Thus, for the determination of the amount of water vapor in air we have to introduce other characteristics besides those enumerated in Table 1.3, viz. :

(1) water vapor pressure e, representing partial pressure;

(2) saturation vapor pressure E (i.e. maximum value of pressure at a given temperature);

(3) relative humidity f (ratio of actual vapor pressure e to saturation vapor pressure E at a given temperature, expressed as a percentage). These characteristics together with dew-point temperature (i.e. temperature at which vapor contained in air at constant partial and full pressures becomes saturated) are given in psychrometric tables.

It is necessary to know the local characteristics of humidity besides the total amount of water vapor in the path of the ray during optical investigations and computations given as follows :

$$w = \int_0^L \rho_v(l)\,dl = 2.19 \times 10^{-4} \int_0^L \frac{e\,(l)}{T\,(l)}\,dl.$$

The value of w, having units g/cm^2, numerically equals the pressure exerted on a layer of water of thickness w cm. Therefore a layer of condensed water 1 cm in thickness is used as a unit for measuring the amount of water vapor.

Table 1.4 Standard constituents of dry atmospheric air at sea level [27]

Gas	Contents in % vol.	Remarks
N_2	78.084	Dissociates in thermosphere
O_2	20.948	
Ar	0.934	
CO_2	0.003	Changes with respect to time and space
Ne	0.0018	
He	0.00052	
Kr	0.00011	
Xe	0.000087	
H_2	0.00005	Disappears during chemical reactions in thermosphere
CH_4	0.0002	Dissociates in the upper regions of mesosphere, significantly changes in space
N_2O	0.000025	Dissociates
O_3	summer, from 0 to 0.000007	Changes strongly. Forms and disappears in stratosphere and mesosphere
	winter, from 0 to 0.000002	
SO_2	from 0 to 0.0001	Changes strongly
NO_2	from 0 to 0.000002	-do-
I_2	from 0 to 0.000001	-do-

The influence of water vapor in practically all processes occurring in the troposphere, and its strong variability (volume content may change in values from nearly zero to 3-4%) has been responsible for the great interest exhibited since ancient times in the study of the peculiarities of its distribution. However, the problem of space-time distribution of moisture content remains unresolved in a significant measure. We outline the available experimental data below.

(b) Humidity at the earth's surface. The humidity of air to a considerable extent determines its temperature. The humidity at the earth's surface has a distribution similar to the temperature distribution. However, appreciable differences in the temperature and humidity distributions may be observed because of the strong influence of many other factors such as the increase in moisture due to evaporation, convectional intermixing in the atmosphere, and processes of cloud formation.

The humidity at the surface is due to a number of parameters regularly measured by a network of meteorological stations. Maps and tables of humidity of the air at the surface have been compiled as a result of many years of observations (for instance [13]). However, the actual

value of humidity can be significantly different from the average climatological magnitudes.

(c) Vertical profile of humidity. In spite of many years of investigation of the vertical profile of humidity with the help of meteorological radiosondes there are extremely scanty data even for comparatively small altitudes. It is possible to derive an approximate value of humidity at different heights by using the empirical formulas given below; these were obtained on the basis of observations [7] over a number of years.

Gann's formula

$$e=e_0\times 10^{-z/6\cdot 3}, \tag{1.4}$$

or Khrgian's formula

$$r=r_0\times 10^{-Az-Bz^2} \tag{1.5}$$

where e = water vapor pressure,
r = specific humidity and
A and B = constants depending on atmospheric conditions (mean annual values $A=0.0845$ km^{-1} and $B=0.0161$ km^{-2}).

The parameters entering into these formulas change with the geographic position of the point of observation, the season and meteorological conditions.

The humidity profile in the upper troposphere has been studied even less than at the surface of the earth. Usually magnitudes measured by a group of English investigators [16, 36] are used as provisional mean values of humidity in the upper troposphere. Besides mean profiles given in Fig. 1.1, many important though semiqualitative derivations of the pattern of variation of humidity in the upper troposphere have been obtained in the articles [28, 36].

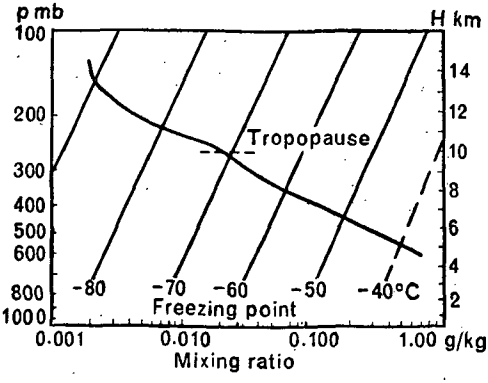

Fig. 1.1. Mean profile of humidity in upper troposphere and lower stratosphere [36].

1. Humidity in the upper troposphere has a sufficiently well-defined seasonal behavior; the air in winter is a little drier at higher altitudes than in summer. The magnitude of seasonal variation of humidity in the troposphere decreases with altitude. In the lowest layers of the stratosphere an inverse seasonal behavior of humidity may be observed.

2. Meteorological conditions and the previous history of the air mass exert considerable influence on humidity at all altitudes up to the tropopause. Thus the humidity is lower in cyclones and higher in anticyclones (high-pressure areas) than the average humidity at a fixed altitude. The warm sea air close to the tropopause appears to be more damp than the cold continental air.

Latitudinal behavior of humidity at different altitudes in the troposphere is shown in Fig. 1.2 from the results in the article [22].

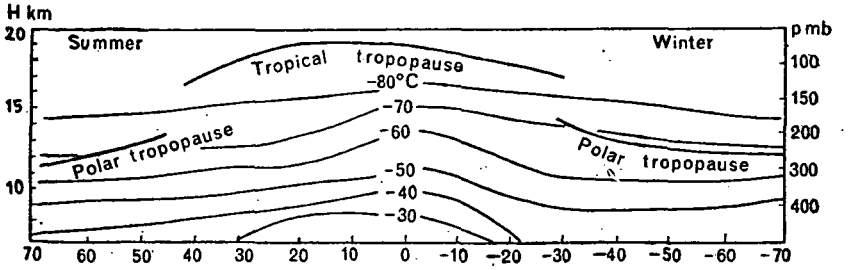

Fig. 1.2. Latitudinal distribution of dew-point temperature in stratosphere [22].

In Table 1.5, as in Table 1.2, which is a supplement to standard atmosphere USA-1962, the standard distribution of temperature, relative humidity, and virtual temperature in the troposphere are given at different latitudes and in different seasons.

The researchers encountered many difficulties in making measurements of humidity in the stratosphere. To date scientists do not agree as to the amount of water vapor contained in the atmosphere above 15 km. The experimental data which exist in profusion up to a height of 30 km are extremely contradictory. Therefore the following two extreme cases are usually accepted for different kinds of computations and study:

1. The mixing ratio of water vapor in the stratosphere is a constant and equals $(2\text{-}4) \times 10^{-6}$ g/g. This model is based chiefly on the results obtained in articles [29, 31, 32].

2. Mixing ratio reaches a minimum at the altitude of 14-15 km but again increases at higher altitudes. Several models of humidity distribution have been proposed of the type based on different experimental data [19, 33] the most prevalent of these being Gutnik's model [26].

S. F. Rohrbough [33] investigated humidity up to an altitude of

Table 1.5 Humidity characteristics of standard atmosphere [27]

z km	T °K	t virtual	Relative humidity, %
	15° N		
0	299.65	302.588	75
1	293.65	295.893	75
2	287.65	289.336	75
2.25	286.15	287.717	75
2.5	286.95	287.743	35
4	276.20	277.363	35
6	263.50	263.709	35
8	250.10	250.172	30
10	236.70	236.717	20

z km	T °K		t virtual		Relative humidity %	
	January	July	January	July	January	July
			30° N			
0	287.15	301.15	288.519	304.583	80	80
1	284.15	293.65	285.244	295.580	70	65
2	281.15	288.15	281.862	289.536	50	60
3	274.65	282.65	275.098	283.716	45	60
4	268.15	277.15	268.389	277.823	35	50
6	255.15	266.15	255.239	266.445	30	40
8	242.15	252.15	242.185	252.266	30	40
10	229.15	238.15	229.162	238.179	30	30
			45° N			
0	272.15	294.15	272.594	296.216	77	75
1	268.65	289.65	268.998	291.142	70	65
2	265.15	285.15	265.427	286.192	65	55
3	261.65	279.15	261.850	279.777	55	45
4	255.65	273.15	255.774	273.552	50	40
6	243.65	261.15	243.698	261.299	45	30
8	231.65	248.15	231.664	248.211	35	30
10	219.65	235.15	219.654	235.172	30	30
			60° N			
0	257.15	287.15	257.285	288.449	80	75
1	259.15	281.75	259.311	282.685	70	70
2	255.95	276.35	256.089	277.062	70	70
3	252.75	270.95	252.861	271.447	65	65
3.5	251.15	268.25	251.245		60	
4	247.75	265.55	247.824	265.889	60	60
5	240.95	260.15		260.376		55
6	234.15	253.15	234.170	253.277	50	50
8	220.55	239.15	220.550	239.185	40	40
10		225.15		225.155		

40 km, and suggested an empirical formula which in his opinion reliably describes the profile of humidity between the altitudes of 15 and 40 km as follows:

$$r=\frac{2.457}{p^{1.22}}. \tag{1.6}$$

The humidity remains practically uninvestigated at altitudes higher than 40 km. It is assumed that between the altitudes of 40 and 70 km it changes in the following manner:

(1) "Dry" stratosphere, i.e. constant humidity exists between the altitudes of 15 and 40 km and is preserved in the region between 40 and 70 km;

(2) "Moist" stratosphere—the increase in humidity comes to an end in the altitude range of 40-45 km; furthermore, the magnitude of the humidity remains constant between the altitudes of 45 and 50 km, but above this height it decreases, reaching the same value at an altitude of 70 km that it possessed in the "dry" model.

Above 70 km a rapid decrease in humidity occurs due to photodissociation of water vapor.

There exist practically no experimental data regarding geographic and seasonal variation of humidity in the stratosphere. It is possible to plot a graph of the seasonal behavior of the mixing ratio above the altitude of 13.7 km, based on the results of article [20], while assuming a constant mixing ratio in the stratosphere with respect to altitude. Such a graph is shown in Fig. 1.3.

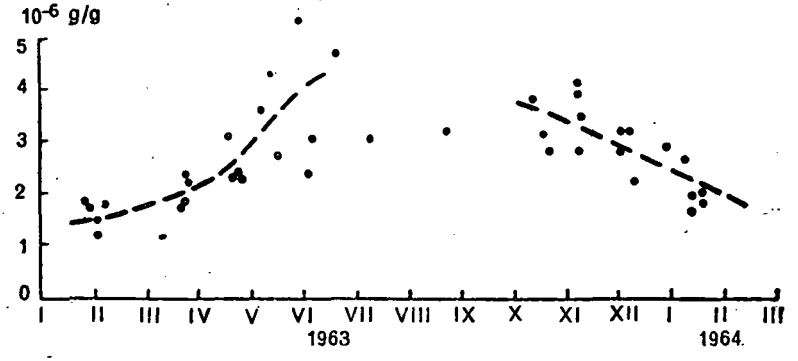

Fig. 1.3. Seasonal behavior of ratio of mixture of water vapor in atmosphere above 13 km [20].

(d) Amount of water vapor in the atmosphere. It is necessary to know the amount of water vapor in the path of a ray during optical investigations. In particular, it becomes necessary to know the amount of water vapor in a vertical column of atmosphere in most cases (sometimes this magnitude

is called moisture content in atmosphere, by which we imply moisture in the form of vapor only). The amount of water vapor in the mass of atmosphere is usually specified for a vertical column of atmosphere. Here it is assumed that it can be easily converted for different inclinations. This is not completely justified, since the atmosphere is practically never uniform in a horizontal direction.

The most significant contribution to the moisture content in the vertical column of atmosphere enters in the lowest layers of air. The contribution to layers above 12-15 km is infinitesimally small, and all ambiguity regarding the question about the distribution of humidity in the stratosphere loses its significance in this case. The vertical moisture content can be easily determined with sufficient accuracy from the data obtained by meteorological probing. The average value of vertical moisture content in moderate latitudes is a layer of condensed water of thickness 1.6-1.7 cm. However, this magnitude differs widely from place to place and from one day to another [13].

Repeated attempts have been made to relate the atmospheric moisture content to the absolute humidity at the surface of the earth (or other characteristics of humidity). In [1] it is shown that this relation can be established only for stable air masses under conditions of weakly developed convectional currents in the atmosphere. In the remaining cases the determination of some sort of uniform dependence appears impossible.

(e) Theoretical concepts of water vapor. The spatial distribution of water vapor is chiefly determined by the location and the intensity of source (evaporation) and of sink (condensation), as well as by the processes of mechanical transportation. Insofar as the intensities of source and sink depend on the temperature and the distribution of moisture and phase conversion of water influence the temperature distribution, the distribution of temperature, wind, and moisture in the troposphere appear to be mutually interrelated. Consequently the theoretical problem of the distribution of moisture in the troposphere becomes part of the more general problem of weather forecasting with the help of hydrodynamical equations. The lifetime of water vapor in the troposphere is approximately 10 days, although it can significantly differ from this value depending on climatic conditions.

In the stratosphere and mesosphere the distribution of water vapor is controlled by transfer processes through the tropopause and photodissociation which begins at an altitude of 65-75 km. It is possible that such a source of water vapor exists in the stratosphere (evaporation of water and ice occurring in the stratosphere can become such a source). Although photodissociation of water vapor probably starts with wavelengths shorter than 2400 Å, for wavelengths up to 1850 Å atmospheric H_2O remains practically

transparent. The photodissociation rate at neutral optical thickness is given by $J_\infty(H_2O)=1.5\times10^{-5}$ sec^{-1}. Approximately one third of this magnitude is due to L_α emission. The rate of formation of H_2O in the mesosphere according to the reactions

$$OH+OH \rightarrow H_2O+O$$

and

$$OH+HO_2 \rightarrow H_2O+O_2$$

is less than the rate of photodissociation, as a result of which the photochemical equilibrium for water vapor cannot take place and a constantly effective sink appears in the mesosphere. Computations of vertical distribution of water vapor have been worked out in [31] at levels above which dissociation starts taking into consideration the processes of vertical turbulent diffusion and photodissociation. Here the following approximate formula for profile of specific humidity above 70 km has been obtained:

$$r(z)=r(z_0)\exp\left[\frac{\frac{1}{H}-\sqrt{\frac{1}{H^2}+\frac{4J_\infty}{k}}}{2}(z-z_0)\right]. \qquad (1.7)$$

Here $H=\frac{kT}{mg}$ —height to which the atmosphere remains uniform,

k —coefficient of turbulent diffusion,

J_∞ —photodissociation rate of H_2O at neutral optical thickness and equals 1.5×10^{-5} sec^{-1},

z_0 —level at which dissociation sets in (approximately 70 km).

The influence of water vapor on the structure of the stratosphere and mesosphere has not been defined clearly, since its amount in these regions is not precisely determined. However, even in the case of "dry" stratosphere the role of water vapor can be significant, since it can affect the amount of ozone, which determines the thermal regime in the stratosphere and mesosphere [5, 30].

3.4 Ozone

(a) Fundamental experimental results. Ozone is the most variable of all the atmospheric constituents to be studied in detail. This accounts for the relative simplicity of the methods of measurement on the one hand,

and its important role in the thermal regime of the stratosphere and in the protection of the surface of the earth from ultraviolet radiation of the sun on the other. Recently the space-time variation of the total amount of ozone and the fundamental properties of the vertical distribution up to 70 km have been studied in sufficient detail. Most of the data about ozone are obtained at ozonometric stations (numbering 25 in the USSR alone) with the help of terrestrial optical methods. Fewer measurements, referring mainly to vertical distribution of ozone, at a level lower than its maximum concentration, have been taken with the help of optical, electrochemical and chemiluminescent ozone-probes. These distinct measurements on ozone have been carried out with the help of rockets and artificial satellites. Detailed information about the methods of measuring ozone are contained in a number of monographs and articles (for instance, [2, 3, 9, 35]).

The fundamental observations on ozone lead to the following:

(1) The mean monthly values of the overall ozone content have clearly defined latitudinal and seasonal variations, increasing from the equator to the pole, being a maximum in March and April and a minimum in September. The mean monthly values of the ozone content for different latitudes and in different months according to data from ozonometric stations participating in IQSY in 1958 are given in Table 1.6.

Table 1.6 Latitudinal and seasonal variation of ozone content (cm)

Latitude	Month											
	Jan	Feb	Mar	Apr	May	Jun	Jul	Aug	Sept	Oct	Nov	Dec
80	0.32	0.48	0.52	0.49	0.43	0.35	0.32	0.29	0.29	0.33	0.37	0.37
70	0.36	0.50	0.48	0.44	0.43	0.36	0.33	0.30	0.31	0.32	0.36	0.31
60	0.34	0.41	0.44	0.42	0.40	0.37	0.35	0.34	0.30	0.30	0.28	0.32
50	0.34	0.37	0.39	0.40	0.37	0.36	0.34	0.31	0.29	0.29	0.31	0.34
40	0.32	0.34	0.34	0.38	0.34	0.32	0.30	0.28	0.28	0.28	0.29	0.32
30	0.28	0.29	0.31	0.31	0.31	0.30	0.29	0.28	0.26	0.26	0.25	0.27
20	0.23	0.23	0.25	0.27	0.26	0.26	0.25	0.25	0.25	0.25	0.24	0.23

Thus, the mean annual values increase from the equator to the pole, but over the entire Northern Hemisphere the total ozone content has a maximum in March and a minimum in September. Typical curves are shown in Fig. 1.4.

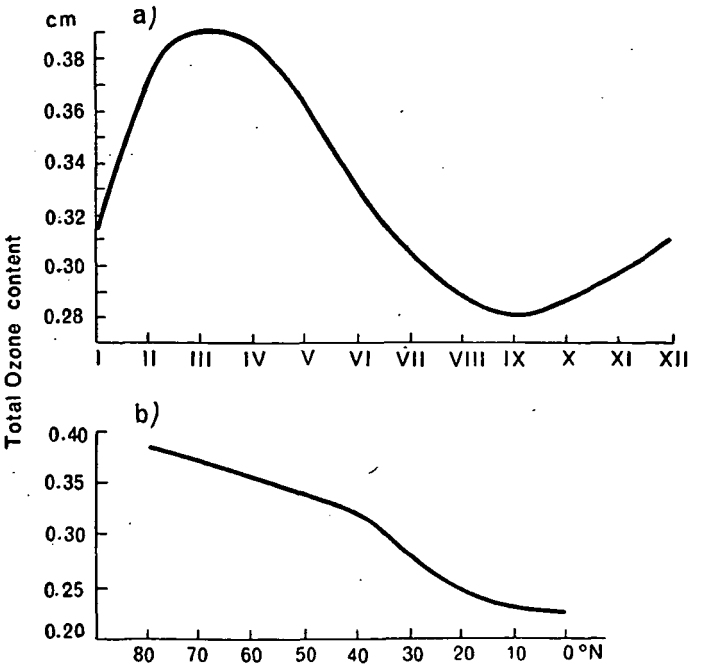

Fig. 1.4. Distribution of ozone in the atmosphere.
a—seasonal behavior of mean total ozone content in the Northern Hemisphere;
b—latitudinal behavior of mean yearly total ozone content.

(2) The total ozone content in a unit vertical atmospheric column varies considerably from day to day, sometimes even exceeding the amplitude of seasonal and latitudinal variations. Numerous correlations of these variations with temperature distribution, pressure and wind have been established. Detailed information about the relation between ozone and meteorological conditions is contained in [2, 9, 21].

(3) The variation in total ozone content in the course of a day due to the change in solar zenith angle is extremely small.

(4) Vertical distribution of ozone changes significantly. Its fundamental property is a sharp maximum of concentration, usually located at altitudes between 20 and 30 km. Another important feature is a rapid decrease in ozone concentration at the stratosphere-troposphere boundary. Results of isolated measurements of the vertical distribution of ozone by chemical methods are shown in Fig. 1.5 [35]. The mean spatial distribution of ozone at altitudes below 30 km, according to data obtained at the American ozone probing stations, is shown in Figs. 1.6 and 1.7 [27]. The results of optical measurements of ozone using rockets and artificial satellites at higher altitudes are shown in Fig. 1.8.

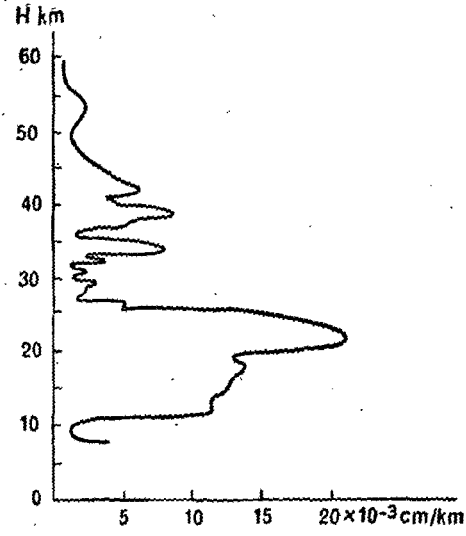

Fig. 1.5. Profile of ozone concentration obtained with the help of chemical methods during rocket probing on November 23, 1965 [35].

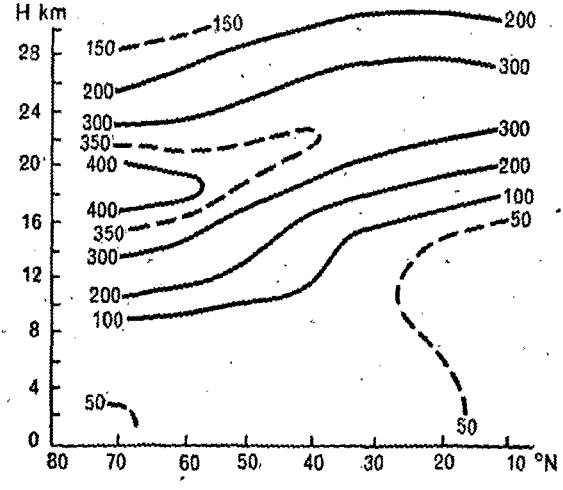

Fig. 1.6. Spatial distribution of ozone (μg/m³) in July-August, 1963 [27].

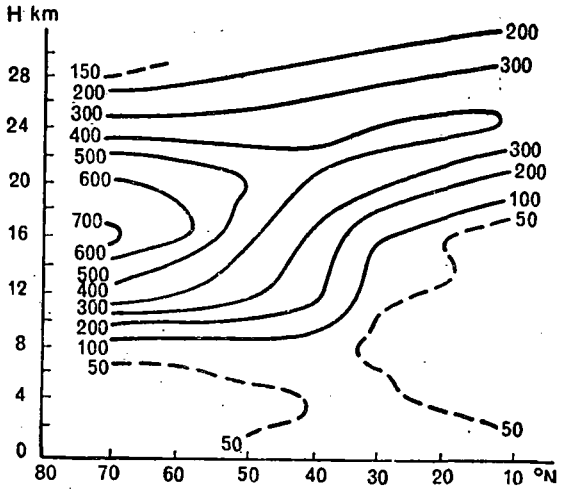

Fig. 1.7. Spatial distribution of ozone ($\mu g/m^3$) in March-April, 1963 [17].

(b) Comparison of experimental results with theory. The experimental patterns of ozone behavior in the atmosphere enumerated above are not in agreement with theory. According to the existing theory, the following photochemical processes generate ozone in the atmosphere, viz.

$$\begin{aligned} O_2+h\nu &\rightarrow O+O, \\ O+O+M &\rightarrow O_2+M, \\ O+O_2+M &\rightarrow O_3+M, \\ O_3+h\nu &\rightarrow O+O_2, \\ O+O_3 &\rightarrow 2O_2, \end{aligned} \qquad (1.8)$$

where M denotes any molecule.

The solutions of the photochemical equations, which take into consideration these processes, show a latitudinal and seasonal behavior of the total ozone content which is contrary to observations, and does not show a noticeable amount of ozone in the troposphere. The theoretical vertical distributions and the total ozone content in an infinite column differ noticeably from the experimental distribution. This is illustrated in Fig. 1.8, where computation [9, 21, 30] are compared with rockets [3] and artificial satellites [9] measurements. Computations of the time necessary to set up a photochemical equilibrium [2, 9, 21] account for a large part of the ozone (below 35 km) in a passive admixture, which does not change its concentration for any possible changes in intensity of solar radiation. Thus it is easy to interpret the relation between the ozone

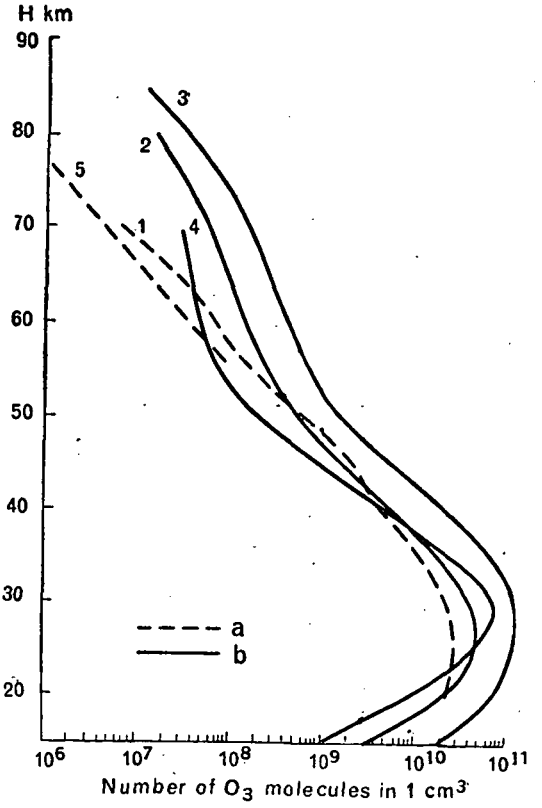

Fig. 1.8. Vertical distribution of ozone.

a) Experimental: 1—according to Johnson et al. [3];
5—according to Raucliffe et al. [9];

b) Theoretical: 2—according to London and Prabkahara [9];
3—according to Hunt [30]; 4—according to Craig [21].

content and the meteorological conditions and the absence of variation of total amount connected with the change in the solar altitude. Above 40 km the computed characteristic time is small and thus the concentration of ozone can undergo considerable variation from day to night. This is, however, not reflected in the total ozone content since only a small portion of it is situated at these altitudes. The development of the photochemical theory of ozone was conducted along two directions: by consideration of processes of actual transportation of ozone (general circulation, vertical movement and turbulent diffusion) [2, 34] and by consideration of reactions which are not included in the reaction scheme (1.8) [30]. However, none of these methods successfully explains all the observed patterns, and thus

one is led to believe that the question of formation, destruction and transportation of ozone is far from solved.

3.5 Carbon dioxide

Carbon dioxide undergoes significantly fewer time and spatial variations than water vapor and ozone. The sources and sinks of CO_2 are connected with the life activity of plants, its solubility in sea water and with industrial processes. Insofar as all these sources and sinks are situated on the surface of the earth, one can naturally expect that the variation of the CO_2 content is at its maximum at the earth's surface and decreases with altitude. The interest in the study of the behavior pattern of CO_2 at the surface of the earth is primarily connected with biological problems. Investigations made over different vegetative covers show that the deviation in the amount of CO_2 from the mean value in the course of 24 hours can reach 100% and more. However, the thickness of the layer in which the daily variation is clearly marked is less than 1 km [11]. The lifetime of CO_2 in the atmosphere is about four years. Carbon dioxide is thus well mixed in the atmosphere. In meteorological problems its volume concentration is almost always accepted as a constant equal to 3.1×10^{-2} %. This, as well as the existence of intense absorption bands, allows the use of CO_2 in problems of optical probing of the atmosphere to determine its structural parameters.

The measurement of the CO_2 content in the troposphere (with the exception of the surface layer) and in the stratosphere shows that the deviation from mean concentration does not usually exceed 3%. Fig. 1.9 shows the seasonal variations of the CO_2 content at altitudes of 5, 7, 9 and 11 km (60° N), moreover, the levels of 9 and 11 km are situated in the troposphere as well as in the stratosphere [17]. From Fig. 1.9 it is clear that the magnitude of seasonal variation decreases with altitude from 10 ppm at an altitude of 5 km to 6 ppm in the upper troposphere and to 2 ppm during transition from the troposphere to the stratosphere. Although there are no measurements of the amount of CO_2 above 30 km, it is usually supposed that the mixing ratio of CO_2 remains constant up to altitudes of the order of 100 km. At these altitudes carbon dioxide begins to dissociate under the action of ultraviolet radiation of $\lambda < 1690$ Å, with L_α providing main contribution to dissociation.

As a result of the formation of a large amount of carbon dioxide in the burning of fuel since the middle of the last century, the amount of CO_2 in the atmosphere began gradually to increase. Because CO_2 is absorbed in ocean water, the increase in the amount of CO_2 in the atmosphere is considerably less than the amount formed by artificial means. An analysis of a large number of observations shows that in our time the amount of

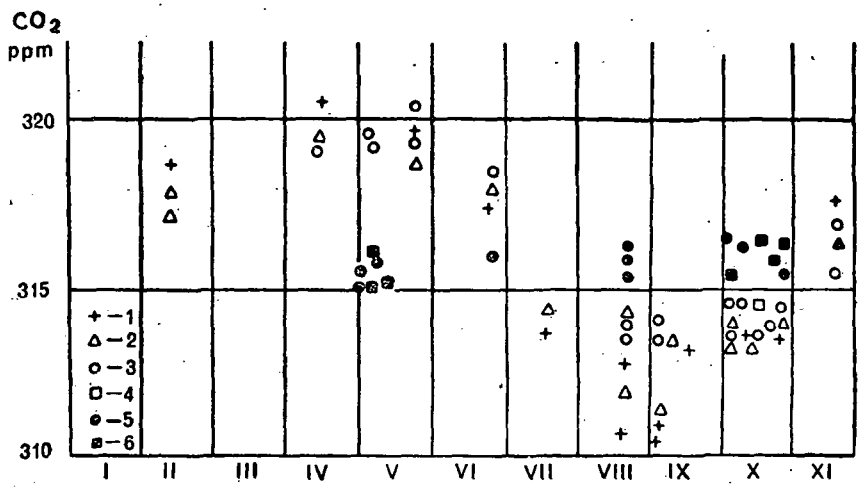

Fig. 1.9. Seasonal variation of the CO_2 content in the troposphere at altitudes of 5 km (1), 7 km (2), 9 km (3), 11 km (4) and in the stratosphere at altitudes of 9 km (5) and 11 km (6)[17].

CO_2 is increasing at the rate of 0.7 ppm in a year [11, 17] and that 20% of atmospheric CO_2 is artificial in origin [11].

3.6 Methane

Just as in the case of carbon dioxide, atmospheric methane is formed on the earth's surface. Biological reactions under anaerobic conditions, geochemical and industrial processes serve as its sources. Methane does not exert a direct influence on the structure of the atmosphere. Methane becomes a source of atomic hydrogen at altitudes higher than 70 km, where it dissociates under the action of ultraviolet radiation at $\lambda < 1450$ Å. It is possible that CH_4 plays a role in chemical processes in the troposphere and stratosphere, but it has not been determined as yet.

Spectroscopic measurements of the amount of methane in a vertical column of unit cross section show a value of 1.1-1.2 cm (under normal conditions)[24]. Volumetric content of CH_4 in the air on the earth's surface is $(1\text{-}2) \times 10^{-6}$ [18]. An analysis of the measurements of absorption of white light at different angles shows that in all probability the volumetric content of methane does not depend on the altitude [25]. Investigation on samples of air [12] obtained with the help of traps set up in balloons shows that the volumetric content of methane is almost constant in the troposphere and that it decreases rapidly at the boundary of the stratosphere. These results are shown in Fig. 1.10. Different quantities of methane in a vertical column of atmosphere with unit cross section obtained on

flights A (3.2×10^{19} mol/cm^2) and B (3.4×10^{19} mol/cm^2) make it possible to suggest that the rate of formation and destruction of methane is variable. Conclusions drawn on the basis of a comparison between the rate of formation of methane at the surface of the earth and the rate of turbulent transportation of methane through the tropopause in [12] show that the disintegration of methane occurs mainly in the tropopause. This contradicts the existing opinion that photodissociation is the fundamental mechanism of destruction of methane [15], proceeding with the coefficient of dissociation at neutral optical thickness equal to 4×10^{-7} sec^{-1} [8]. The process of destruction of methane in the troposphere is not fully understood.

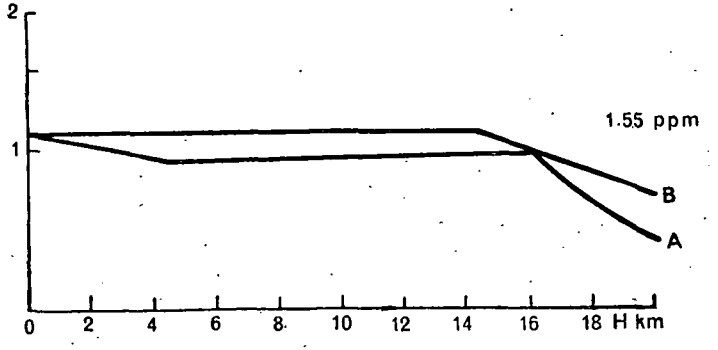

Fig. 1.10. Vertical distribution of methane for two balloon flights A and B [12]**. The concentration of methane relative to the standard (1.55 ppm) is along the ordinate.**

3.7 Oxides of nitrogen

N_2O is the most important of all the oxides of nitrogen in the lower layers of the atmosphere. A sufficiently large number of measurements on the amount of N_2O on the earth's surface give an approximate value of 2.5×10^{-7}. Table 1.7 gives several results on measurements of N_2O by different methods [14].

Table 1.7 Volumetric concentration of N_2O [14]

Method of measurement	$N\times10^7$
Solar spectrum; band 7.8 μ	2.7±0.8
Solar spectrum; *P* branch of band 4.5 μ.	1.2
Solar spectrum; line of band 3.7 μ	2.5
Absorption in horizontal path of length 760 m; *P* branch of band 4.5 μ	2.7±0.5
Mass spectrometry	5±1
Gas chromatography	3±1

Depending on the angle of the sun [25], measurements on the intensity of atmospheric emission of 2.16 μ from N_2O lead to the conclusion that the oxide of nitrogen is uniformly distributed along the vertical. There are little time and spatial variations in the N_2O content [11].

Photodissociation of N_2O starts at $\lambda=2100$ Å and can occur at altitudes of the order of 20 km. A source of formation of N_2O with a rate of production of $(2\text{-}3)\times 10^9$ cm^{-2} sec^{-1} [14] must exist in order to balance the loss.

The total volumetric concentration of all the remaining oxides of nitrogen on the surface of the earth is of the order of 10^{-8} [11]. The role of oxides of nitrogen (especially NO) is augmented in the upper atmosphere. As a result of the small ionization potential these oxides exert an influence on ionospheric processes.

4. ATMOSPHERIC AEROSOL

In meteorology the name "aerosol" is given to particles of solid or liquid substances of radii from 10 Å to 20 μ suspended in air. Aerosol is one of the optically most active, though least studied components of the atmosphere. It is present at practically all altitudes; moreover, the calculated concentration and measurements of the sizes of aerosol particles change with altitude in a complex manner.

In atmospheric optics it is most important to know the concentration and distribution of particles with radius $r\geqslant 0.2$ μ known as large or gigantic aerosol particles. It should be observed that particles of this size participate in the cloud-forming processes. Particles with $r<0.1$ μ (Aitken's nuclei and large ions) are comparatively less active optically and are of greatest interest in the investigation of electrical properties of the lower atmosphere.

4.1 Experimental investigation of vertical distribution of atmospheric aerosol

The available experimental data on the vertical distribution of atmospheric aerosol can be divided into three groups, according to the different methods of measurements:

(1) measurement of vertical profile of bulk attenuation coefficient of aerosol radiation or optical thickness of aerosol;

(2) measurement of radiation scattered in atmospheric aerosol; and

(3) measurement of particle concentration at different altitudes.

The most complete data on the vertical profile of the attenuation coefficient of radiation in aerosol are obtained with the help of projection

probing (particularly, laser) and the twilight method. A considerably smaller amount of analogous data has been obtained with the help of spectral probing of the atmosphere from aeroplanes, balloons and artificial satellites.

A sufficiently complete survey of measurements of this nature is contained in [4, 10, 11]. One can draw the following conclusions from the available experimental data on optical probing:

(a) it is always possible to have a layer of increased attenuation of aerosol at altitudes close to 20 km; volume coefficient of absorption of aerosol in this layer approaches 0.02 km^{-1};

(b) the aerosol layer below the tropopause is not always observable at altitudes between 9 and 11 km, especially in daytime;

(c) there occurs a change in the nature of the vertical behavior of aerosol attenuation in the troposphere above 5 km, in which case a layer of cloudiness can be observed at the altitude of 6 km;

(d) there exists a layer of increased aerosol attenuation in the region of mesopause (near 80 km);

(e) there is a possibility of formation of aerosol layers at altitudes between 23 and 80 km but the data on altitudes of these layers are very scanty;

(f) there exist aerosol layers above 80 km, which can be determined from scattered or emitted radiation;

(g) the layers at altitudes above 10 km probably exhibit fine structure in the vertical direction and can be distinguished by a significant spreading and uniformity in the horizontal plane; and

(h) there exist layers of aerosol attenuation with temperature inversion and isothermal layers.

The data on measurements carried out by different authors demonstrating the existence of aerosol layers are presented in Table 1.8.

The estimated concentration of large aerosol particles with $r \geqslant 0.1\ \mu$ was measured with the help of photoelectric counters, filters of impactors and airplane traps [4, 10, 11]. On the basis of these experiments it is possible to draw the following important conclusions:

(a) layers of increased concentration of large aerosol particles have been observed which coincide with layers of reduced ionic concentration;

(b) there exists a zone of increased concentration of large aerosol particles at altitudes of 17-23 km (Young's layer); probably there exists a layer below the tropopause;

(c) the aerosol layers up to an altitude of 7-8 km are unstable and may be formed under specific meteorological conditions (advection of contaminated air masses, convectional lifting of aerosol on the surface of the earth).

Table 1.8 Investigation of vertical profile of aerosol attenuation by optical methods [4]

Author	Method of measurements	Conditions of measurements	Results of measurements	Remarks
L. Elterman	Searchlight probing	Night time, 0-70 km	Layer between 18-23 km, at 10 km	Change of optical characteristics of aerosol was observed during night time
G. Klemesh, G. Kent	Laser probing			Coefficient of inverse scattering can be measured
G. V. Rosenberg et al.	Searchlight probing	In the night, 0-40 km	Layers: 11 km, 25-27 km, 43 km	
G. V. Rosenberg et al.	Twilight method	After sunset, large optical thicknesses between radiation and receiver	Layers: about 50 km & 80 km	
G. V. Rosenberg et al.	Probing with space vehicles		Layers: 18-22 km, 10-11 km	A minimum of scattered radiation between 22 and 30 km can be explained by the washing out of aerosol
N. B. Divari	Twilight method	10-150 km	Course of aerosol attenuation, without layer; estimated concentration is determined	Discrepancy between rocket and optical measurements can be explained by the low density of particles of cosmic origin
E. Bigg	Twilight method	0-40 km	Types of stratification in aerosol layers, layers: about 20 km, 25-30 km, 9-12 km	Obtained the latitudinal course of layers of aerosol attenuation

G. Fiokko et al.	Laser probing		Layers about 20 km, absence of stable layer at altitudes approaching 80 km	Observed the seasonal course of vertical profile of aerosol scattering
G. Goer and R. *Watson*	Laser probing	0-30 km		
D. Voldrem	Measurements of localized scattering function in troposphere			
B. A. Chayanov	Aerosol measurements of scattering functions in free atmosphere	0-25 km (4 flights)	Layers of increased extent of the function 2-3, 6, 8, 6-9, 10.5, 12, 15.5, 22, 25 km	
A. B. Sandomirskii et al.	Airplane measurements of scattering function in free atmosphere	0-12 km	Increase in the extent of function below tropopause: seasonal variations	
E'. A. Chayanova	Aerosol measurements of localized scattering functions	0-12 km, measurements during night (8 flights)	Increase in the extent of scattering curves at altitudes of 6.5 and 9-10 km	
G. N. Faraponova	Airplane measurements of coefficients of aerosol attenuation		Layer of aerosol attenuation, about 6 km	
I. Ya. Badinov et al.	Balloon measurements on aerosol components of spectral attenuation direct solar radiation	0-30 km, measurements in morning, anticyclone (high-pressure area)	Vertical profile of spectral coefficients of aerosol attenuation, layers 17-22 and 9-10 km	Components of aerosol attenuation are found after deduction of attenuation from molecular

Table 1.8—*Contd.*

Author	Method of measurements	Condition of measurements	Results of measurements	Remarks
			α_{18} (5000 Å)$=2\times 10^{-3}$ km^{-1} α_{9} (5000 Å)$=2\times 10^{-3}$ km^{-1}	absorption and scattering
G. A. Nikol'skii	Balloon measurements on aerosol components of overall attenuation of direct solar radiation	0-30 km, measurements in morning, anticyclone	Aerosol layers near temperature inversion and isotherms	
R. Penndorf et al.	Airplane measurements of aerosol attenuation	0-7 km	Profile of aerosol attenuation in troposphere	
F. Link	Twilight method	20-100 km		
F. Link	Lunar eclipses	80-150 km	Existence of aerosol layers above 100 km, amount of aerosol material of cosmic origin	
E. O. Fedorova et al.	Balloon measurements on luminosity of sky and scattering function in infrared region of the spectrum	0-32 km, measurements in the morning	Aerosol layers at altitudes of 3, 6, 10, 18, and above 23 km	Method of greatest sensitivity to the presence of huge aerosol particles
A. E. Mikirov	Measurements of sky brightness by rockets and artificial satellites	80-500 km	Evaluation of the amount of aerosol at altitude of 100 km (10^{-16} g/cm^3)	

G. N'yukirk et al.	Measurements on aerosol halo	0-25 km, morning, anticyclone	Aerosol layers of thickness 30 m, associated with temperature profile and the amount of ions (10.5-12, 15, 17.5, 20, 22 km)	The only optical method which allows us to determine the fine structure of vertical profile of aerosol absorption at low concentrations of aerosol
G. N'yukirk et al.	Aerosol measurements of sky brightness	0-25 km	Estimated concentration of aerosol particles at different altitudes	
Kh. Flen, D. Kh'ening	Visual observations from a plane	For several months after the eruption of Agung volcano	Layers of volcanic dust; 16.5, 12.9 ± 0.9, 25 ± 1.5, 31 km	
L. Jacobs (1954)	Visual observations from a plane		Layer above 15 km	
D. Mur	Balloon observations		Layer near 24 km	
R. Kollis, G. Ligda	Laser probing	10-60 km	Layers of increased scattering 19, 24, 34, 38-40, 47 km	
F. Rossler	Rocket photometers	Measurements in Sahara	Layers of increased brightness, 19-32 km	Latitudinal variation in altitude of Young's layer has been suggested

Table 1.9 Measurements of calculated concentration of atmospheric aerosol [4]

Author	Methods of measurements	Conditions of measurements	Results of measurements	Remarks
A. Vigand (1919)	Nuclear condensation counter on a balloon	Up to 8 km (19 flights)	Exponential drop in concentration $N_0=5\times10^4$ cm^{-3} $N_8=30$ cm^{-3}	Without considering the variation in the efficiency of the apparatus with respect to altitude
Kh. Veikman	Nuclear condensation counter			
H. Young et al.	Nuclear condensation counter on a balloon	Up to 27 km	Concentration of nuclear condensation higher than that observed by Vigand and Veikman	Data on measurements above 15 km are possibly underestimated
H. Young et al.	Airplane trap	Horizontal flights at different levels, inertial sedimentation	Layer of gigantic aerosol particles ($r\geq 1\ \mu$) above tropopause	
H. Young et al.	Balloon impactor	Measurements on concentration of large aerosol particles at several levels	Layer of large aerosol particles ($r\geq 0.1\ \mu$) of sulfurous origin from 17 to 23 km, $N=0.1$ cm^{-3} Exponential size distribution of particles with index four, in layer 17-23 km	

A. M. Borovikov, I. I. Gaivoronskii	Balloon konimeter	0-6 km	Studied the dependence of concentration of large aerosol particles on altitude and meteorological conditions
E. S. Selezneva et al.	Nuclear condensation counter	Up to a height of 6 km measurements were made by a plane	Map of geographical distribution of aerosol over the territory of the Soviet Union, influence of ground sources and meteorological conditions on the amount of nuclear condensation in the atmosphere
A. G. Laktionov	Photoelectric counter in a plane	Measurements at different times of a year at different heights (up to 8 km)	Dependence of concentration of large aerosol particles on size distribution of particles(index of power changes from −2 to−5)
D. Fre'nd et al.	Measurements from a plane	Flights on horizontal routes	Determination of chemical composition of aerosol at different altitudes and size distribution of aerosol particles

Table 1.9—*Contd.*

Author	Methods of measurements	Conditions of measurements	Results of measurements	Remarks
D. Rosen	Aerostat photoelectric counter and filter		Layerwise distribution of aerosol, concentration of large aerosol particles ($r \geqslant 0.55\ \mu$) is higher than that determined by H. Young	
L. S. Ivlev, O. M. Surikov	Balloon impactor	Flights during morning hours up to height of 30 km, anticyclone	Layers: 2.5, 6.5, 10-11, 17-19, 25 km, size distribution of particles, approaching exponential with $\nu = 3.5$	
K. Khe'menvei, P. Fullam	Collection of samples by airplane		Determination of chemical composition of atmospheric aerosol, discovery of aerosol of extraterrestrial origin	
K. Khe'menvei et al.	Collection of samples from noctilucent clouds and micrometeorites with the help of rockets		Increased concentration of aerosol at altitudes between 78 and 83 km (for large aerosol particles $N = 10^{-4}$ cm^{-3} in the absence of clouds, $N = 10^{-1}$ cm^{-3} in the presence of clouds), size distribution of particles of Young's type	

P. Khodzh et al.	Measurements from a plane	Collection of particles of extraterrestrial origin at high altitudes	Size distribution of H. Young	
S. Mossop	Airplane dust collector	Measurements after the eruption of Agung volcano at altitudes of 15-35° N	Measurement of size distribution at long intervals after the eruption of volcano	
S. Melton	Airplane filter	Horizontal flights at altitudes between 9-12 km	Studied concentration of gigantic particles (for $d > 4\,\mu$ N varies from 20 to 200 m^{-3})	Could not obtain dependence of estimated concentration upon altitude
F. Rossman	Impactor	Tropospheric measurements of vertical profile of aerosol	Exponential dependence	

As regards Aitken's nuclei, it may be observed that their estimated concentration changes with altitude rather smoothly; moreover, the vertical profile of concentration depends on the underlying surface and meteorological conditions. The rate of fall in the concentration of nuclear condensation decreases at altitudes approaching 12 km. The suggestion by Young about the absence of a layer of Aitken's nuclei between 17 and 23 km does not find sufficient support.

The results of microphysical measurements on the concentration of aerosol obtained from different investigations have been presented in Table 1.9.

4.2 Size distribution of atmospheric aerosol particles

Aerosol particles of widely different sizes are present in the atmosphere, i.e. from particles having the dimension of about 10 Å, representing a group of atoms or molecules, to the gigantic aerosol particles of the size of several microns. The equilibrium distribution of aerosol particles exists according to their dimensions, which may be determined by the equilibrium of their production and loss. The minutest particle may appear under the influence of ionization radiations on the molecules of air and disappear when coagulation occurs between these and the largest particles. The largest particles separate out under the action of gravitational force. A stability of the size distribution of atmospheric aerosol particles under specific meteorological conditions and a rapid restoration of such a distribution at the end of the perturbation to the normal state of the atmosphere have been repeatedly observed.

The distribution of aerosol particles with $r \geq 0.1\ \mu$ is described very well in the troposphere by the following exponential law, viz.

$$N(r) = \frac{c}{r^{\beta}}, \tag{1.9}$$

where $2.5 < \beta < 5$.

This law is not obeyed for an increased concentration of atmospheric aerosol and atmospheric humidity. In strongly contaminated industrial regions a bimodal distribution may be observed, whereas the highly scattered fraction possesses a normal, logarithmic, or gamma-distribution. The existence of multi-distribution of aerosol in the layer above the surface of the earth can be explained in this manner. It should be noticed that Young's distribution (1.9) can be satisfied for particles in the range $0.1\text{-}0.2\ \mu \leqslant r \leqslant 2\mu$.

The spectrum of aerosol particles changes with the altitude. The

experimental data available for the troposphere (Fig. 1.11) are extremely contradictory. Probably a change in the spectrum of aerosol occurs in the lower stratosphere (Young's layer) along with an increase in the amount of highly scattered aerosol. Above Young's layers a decrease in the portion of highly scattered aerosol can again be observed, where the index β is between 4 and 5. Such a distribution was observed in rocket samples taken in the region of noctilucent clouds.

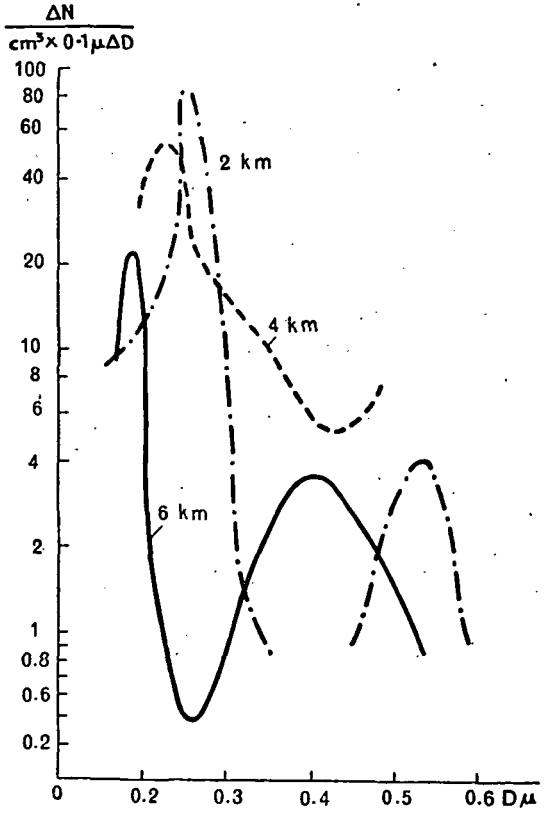

Fig. 1.11. Size distribution of aerosol at different altitudes (after Fenn) [4].

4.3 Sources of aerosol and mechanism of distribution in the atmosphere

To solve the problem of vertical distribution of aerosol in the atmosphere one needs to know only the sources of aerosol and the processes which regulate its distribution in the atmosphere.

The following gives the chief sources of aerosol in the atmosphere:

(1) cosmic dust and products of meteorite combustion;
(2) volcanic dust thrown out into the lower stratosphere during eruption;
(3) aerosol of photochemical origin;
(4) aerosol of natural, terrestrial and marine origin; and
(5) aerosol of artificial origin (industrial dust, products of combustion).

The first two sources contribute only in the stratosphere and, perhaps, in the upper troposphere, the last two only in the troposphere. The fundamental processes for the distribution of aerosol in the atmosphere are as follows:

(1) turbulent diffusion of aerosol particles;
(2) precipitation of aerosol particles;
(3) coagulation;
(4) condensation of water vapor on aerosol particles;
(5) convection current of aerosol; and
(6) washing out of aerosol.

The equation describing the distribution of atmospheric aerosol has not been formally solved. However, the problem can be simplified by dividing the atmosphere into regions, in which the action of several modes of distribution such as the following can be ignored :

(1) region in which cosmic dust decelerated (200-100 km);
(2) region of possible condensation of water vapor on particles of cosmic origin (100-75 km);
(3) region of sufficiently rapid settling of particles (75-30 km);
(4) region of possible condensation of water vapor on particles of cosmic, volcanic, and photochemical origin, advective transfer of aerosol in polar region (30-15 km); during prolonged occurrence of particles in the lower part of the zone a coagulated growth of particles is possible;
(5) region of diffusive washing of particles (15-9 km);
(6) region of washing of particles by condensation and convectional loss of particles of terrestrial origin between 9-5 km; and
(7) below 5 km the distribution of aerosol determines convection, condensation, coagulation, and terrestrial sources.

4.4 Aerosol models

The patterns of vertical distribution of atmospheric aerosol have not been established to date because of the numerous factors which determine the distribution of aerosol in the atmosphere. The proposed aerosol model of Elterman (1964) [23] attributes no significance to the estimated concentration and volume coefficient of aerosol attenuation of radiation for altitudes above 10 km. The deviation in the aerosol density between Elterman's

Table 1.10 Vertical distribution of aerosol in atmosphere [4]

z km	Particle concentration, N cm^{-3}		a km^{-1} (λ=5000 Å)	
	Aitken's nuclei	$2r>0.1\mu$	a_{min}	a_{av}
0-1	2×10^{4}	1.5×10^{2}	—	0.12
1-2	3×10^{3}	80	—	6×10^{-2}
2-3	1×10^{3}	27	—	3
3-4	5×10^{2}	20	—	1.8
4-5	3	15	—	7×10^{-3}
5-6	3	3.1	—	3
6-7	2.5	2.1	—	5
7-8	2.5	1.2	—	1.2
8-9	2.5	1.0	—	1.0
9-10	2.3	2.6	1.1×10^{-3}	2.0
10-11	2,0	0.6	2×10^{-5}	1.1
11-12	1.2	0.18	1.9	9.5×10^{-4}
12-13	7×10^{1}	0.15	2.0	8.5
13-14	2	0.15	2.1	7.5
14-15	1	0.20	3.2	7.5
15-16	8×10^{0}	0.27	5.1	1.05
16-17	3	0.3	0.1	1.35
17-18	1	0.35	6.6	2×10^{-3}
18-19	8×10^{-1}	0.45	7.4	2
19-20	7	0.42	7.3	1
20-21	7	0.4	7.0	4.5×10^{-4}
21-22	6.5	0.12	6.7	1.3×10^{-3}
22-23	6	2.2×10^{-1}	6.4	2.5×10^{-4}
23-24	6	4.5	4.6	5.0
24-25	6	4.5	2.8	5.0
25-26	0.5	2.0×10^{-1}	2.3×10^{-5}	4.0×10^{-5}
26-27	0.4	4×10^{-2}	2.0	4.0
27-28	0.3	3.6	1.8	4.0
28-29	0.3	3.6	1.7	4.0
29-30	0.3	3.6	1.6	4.0
30-35	0	5.0×10^{-1}	1.0×10^{-6}	5.5
35-40	—	1.0	0	1.2×10^{-4}
40-45	—	6.8×10^{-2}	0	7.8×10^{-5}
45-50	—	5.4	0	6.0
50-55	—	5.4	—	6.0
55-60	—	3.6	—	4.0
60-65	—	2.2	—	2.5
65-70	—	1.8	—	2.0
70-75	—	2.2×10^{-3}	—	2.5
75-80	—	4.5×10^{-4}	—	5.0×10^{-6}
80-90	—	2.4	—	2.7
90-100	—	7.2×10^{-3}	—	8×10^{-7}

model (obtained primarily on the basis of Young's experimental data) and the mean experimental values of optical measurements takes two forms. A review of the majority of data presently available permits us to obtain what is in our opinion the most characteristic vertical profiles of atmospheric aerosol. These profiles are represented in Table 1.10 and in Fig. 1.12.

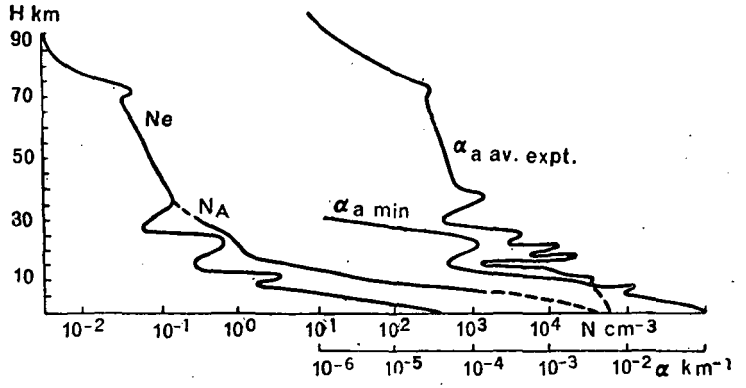

Fig. 1.12. Vertical profile of concentration of aerosol (of large nuclei N_e and Aitken's nuclei N_A) and coefficient of attenuation [4].

It should be noticed that Elterman constructed a model based on the distribution of aerosol particles (Young's distribution) with $\beta=4$. However, optical measurements of the coefficient of aerosol attenuation at altitudes greater than 6-8 km show almost neutral behavior of the coefficient of attenuation of radiation over the spectrum in the region of long waves, i.e. 0.4-1 μ, and this signifies that either in Young's distribution $\beta=3$, or that the size distribution of particles possesses a more complex nature.

REFERENCES

1. Badinov, I. Ya., C. D. Andreev and V. B. Lipatov. Nekotorye rezul'taty nazemnykh spektroskopicheskikh issledovanii vlagosoderzhaniya tolshchi atmosfery (Some results of ground spectroscopic investigations on the moisture-content of atmospheric layer). Problemy fiziki atmosfery, No. 4, Izd. LGU, 1966.
2. Dzhonson, F. S., Dzh. D. Persell and R. Tausi. Izuchenie ozonogo sloya nad N'yu—Meksiko. Raketnye issledovaniya verkhnei atmosfery (Study of ozone layer over New Mexico. Rocket investigations of upper atmosphere). IL, 1957.
3. Gushchin, G. P. Ozon i ae'rosinopticheskie usloviya v atmosfere (Ozone and aerosynoptic conditions in the atmosphere). Gidrometeoizdat, 1964.
4. Ivlev, L. S. Ae'rozol'naya model' atmosfery (Aerosol model of the atmosphere). Problemy fiziki atmosfery, No. 6, Izd. LGU, 1968.

5. Klimaticheskie karty oblachnosti severnogo polushariya, yanvar' i iyul' (period MGG i MGSS) [Climatic charts of cloudiness in the Northern Hemisphere, January and July (period of IGY and IQSY)]. GUGMS, NIIAK, Moskva, 1967.

6. Konashenok, V. N. Model' kislorodno-vodorodnoi mezosfery (Model of oxygen-hydrogen mesosphere). Fizika atmosfery i okeana 3, No. 3, 1967. Izd. AN SSSR.

7. Matveev, L. T. Osnovy obshchei meteorologii (Foundation of General Meteorology). Fizika atmosfery. Gidrometeoizdat, 1965.

8. Nikole, M. Ae'ronomiya (Aeronomy). Izd-vo "Mir", 1965.

9. Ozon v zemnoi atmosfere (Ozone in the earth's atmosphere) Collection of articles translated under the editorship of G. P. Gushchin. Gidrometeoizdat. Leningrad, 1966.

10. Selezneva, E. S. Atmosfernye ae'rozoli (Atmospheric aerosol). Gidrometeoizdat, Leningrad, 1966.

11. Yunge, Kh. Khimicheskii sostav i radioaktivnost' atmosfery (Chemical composition and radioactivity of the atmosphere). Izd-vo "Mir", 1965.

12. Bainbridge, A. E. and L. E. Heidt. Measurement of methane in the troposphere and lower stratosphere. Tellus, vol. 18, Nos. 2-3, 1966.

13. Bannon, J. K., R. Frith, and H. C. Shellard. Humidity of the upper troposphere and lower stratosphere over Southern England. Geophys. Memoirs, No. 88, MO AM, London, 1952.

14. Bannon, J. K. and L. P. Steel. Average water vapor content of the air. Geophys. Memoirs, No. 102, MO AM, London, 1960.

15. Bates, D. R. and A. E. Witherspoon. The photochemistry of some minor constituents of the earth's atmosphere. Monthly Notices Roy. Astron. Soc., vol. 112, 101, 1952.

16. Bates, D. R. and P. B. Hays. Atmospheric nitrous oxide. Planet. Space Sci., vol. 15, No. 1, 1967.

17. Bichof, W. and B. Bolin. Space and time variation of the CO_2 content of the troposphere and lower stratosphere. Tellus vol. 18, Nos. 2-3, 1966.

18. Bowman, R. L. and J. H. Shaw. The abundance of nitrous oxide, methane and carbon monoxide in ground level air. Applied Optics, vol. 2, 176, 1963.

19. Brown, J. A. and E. S. Pybus. Stratospheric water vapor soundings at McMurdo sound Antarctica : December 1960-February 1961. J. Atmos. Sci., vol. 21, No. 6, 1964.

20. Calfee, R. F. and D. M. Gates. Calculated slant-path absorption and distribution of atmospheric water vapor. Applied Optics, vol. 5, No. 2, 1966.

21. Craig, R. A. The observation and photochemistry of atmospheric ozone and their meteorological significance. Met. Monogr. Amer. Met. Soc., vol. 1, No. 2, 1950.

22. Dobson, M. B. Origin and distribution of the polyatomic molecules in the atmosphere. Proc. Roy. Soc., vol. 236, No. 1205, 1956.

23. Elterman, L. Atmospheric attenuation model 1964. Environment Res. Papers, 46, 1964.

24. Fink, V., D. H. Rank, and T. A. Wiggins. Abundance of methane in the earth's atmosphere. J. Optical Soc. Am., vol. 54, No. 4, 1964.

25. Goldberg, L. and E. A. Muller. The vertical distribution of nitrous oxide and methane in the earth's atmosphere. J. Optical Soc. Am., vol. 43, No. 11, 1953.

26. Gutnick, M. Mean atmospheric moisture profiles to 31 km for middle latitudes. Applied Optics, vol. 1, No. 5, 1962.

27. Handbook of Geophysics and Space Environments. McGraw-Hill Book Company, New York, 1966.

28. Helliwell, N. C., J. K. MacKenzie and M. J. Kerley. Some further observation from aircraft of frost point and temperature up to 50,000 ft. Quart. J. Roy. Met. Soc., vol. 83, No. 356, 1957.

29. Houghton, J. T. and J. S. Seeley. Spectroscopic observation of the water vapor content of the stratosphere. Quart. J. Roy. Met. Soc., vol. 86, No. 358, 1960.

30. Hunt, B G. Photochemistry of ozone in a moist atmosphere. J. Geophys. Res., vol. 71, No. 5, 1966.

31. Kondratyev, K. Y. et al. Stratospheric water vapor distribution and the problem of noctilucent clouds. Collection "Noctilucent Clouds". International symposium. Tallin, 1966.

32. Mustenbrook, H. I. Frost-point hydrometer measurements in the stratosphere and the problem of moisture contamination. Humidity and Moisture, vol. 11, p. 480. Reynold Publishing Corporation, New York, 1965.

33. Palmer, T. J., S. F. Rohrbough, and S. Steinberg. A stratosphere humidity experiment. Humidity and Moisture, vol. 11, p. 473. Reynold Publishing Corporation, New York, 1965.

34. Prabkahara, C. Effect of nonphotochemical processes on the meridional distribution and total amount of ozone in the atmosphere. Monthly Weather Rev., vol. 91, 411, 1963.

35. Randhawa, J. S. Ozone measurement with rocket-borne ozone zondes. J. Geophys. Res., vol. 71, No. 5, 1966.

36. Tucker, G. B. An analysis of humidity in the upper troposphere and lower stratosphere over Southern England. Meteorol. Res. Paper, No. 1052, MO AM, London, 1957.

2. OPTICAL CHARACTERISTICS OF THE ATMOSPHERE

The density and flux of the radiation, characterisitic quantities for the radiation field in atmospheric physics and astrophysics, are denoted by I_ν and F_ν respectively (in photometry, intensity and luminosity are denoted by B_ν and E_ν respectively). When radiation is propagated in a medium, particularly in the atmosphere, it interacts with the medium. The coefficients of absorption and scattering and the scattering function are employed to describe the interaction process. The following processes can be distinguished : (1) *volume coefficient of absorption* (scattering) k_ν, α_ν which are computed in units of length through unit cross-section; (2) *bulk coefficient of absorption* (scattering) $k(m)$, $\alpha(m)$, calculated in units in mass of the substance in a column of unit cross-section; (3) *coefficient of absorption* (scattering), referring to 1 cm of atmosphere or distinct component, considered at NTP; (4) *molecular coefficient of absorption* (scattering), relative to the number of molecules in a unit volume, sometimes this is called transverse cross-section of molecules and is denoted by k_ν (μ).

Table 2.1 shows the dimensions and the conversion factors for the attenuation coefficients. The sum of the coefficients of absorption and scattering is sometimes called the attenuation coefficient.

Table 2.1 Dimensions and conversion factors for attenuation coefficients [5]

	Volume coefficient of absorption k_ν cm^{-1}	Bulk coefficient of absortion k_ν (m) gm^{-1} cm^2	Molecular coefficient of absorption k_ν (μ) cm^2
k_ν	1	ρ	n^{-1}
k_ν (m)	ρ	1	m
k_ν (μ)	n	m^{-1}	1

REMARKS: ρ—density of absorbed gas (g/cm) ;
n—number of molecules in a unit volume (cm^{-3}) ;
m—mass of molecules in grams.

The scattering function $\varkappa(\gamma)$, which denotes the fraction of the radiation scattered at some angle from the incident ray, is a dimensionless quantity.

1. COEFFICIENT OF ABSORPTION OF ATMOSPHERIC GASES IN THE VISIBLE AND ULTRAVIOLET REGIONS OF SPECTRUM

Absorption spectra of gases in ultraviolet (UV), visible and infrared (IR) regions considerably differ from one another depending on their nature. Similarly the methods for the calculation of the amount of absorption also vary. In most cases it is possible to apply Bouguer's law for the computation of absorption in the UV and visible regions. Bouguer's law can be stated as follows :

$$I_\nu = I_{0\nu} e^{-k_\nu u}, \tag{2.1}$$

where $I_{0\nu}$ — intensity of radiation incident on the absorptive medium,
I_ν — intensity of radiation passing through the absorbing medium,
u — amount of absorbed gas in the path of the ray (dimension depends on selected absorption coefficient).

However, the computation of absorption in the IR region is more complex. It is therefore advisable to examine these regions of the spectrum separately.

For the determination of the amount of absorption from the formula (2.1) the knowledge of k_ν or $k_\nu(\mu)$ for different wavelengths suffices. Thus the values k_ν for different gasses will be introduced as their optical characteristics. Since it is necessary to know the ionization coefficient for the solution of many problems relating to the physics of upper atmosphere,

the value k_i or the magnitudes of ionization efficiency $\zeta = k_i/k(\mu)$ will also be given. It should be noticed that the application of formula (2.1) for the computation of absorption is not entirely justified, since the spectrum possesses sharply expressed fine structure in many cases. All values of k were obtained on the basis of formula (2.1), so that the results of various researchers do not agree since the measurements are carried out with the help of an apparatus having different resolving power.

1.1 Oxygen O_2

$^3\Sigma_g^-$ is the ground state of the molecule. The O_2 spectrum starts from 2600 Å in the ultraviolet region. A weak Hertzberg's continuum appears below 2420 Å, on account of dissociation of the molecule into O^{16} (^3P) + O^{16} (^3P) with molecular absorption coefficient of the order of 10^{-23}-10^{-24} cm^2.

Spectral range 2000-1750 Å. The Schumann-Runge's band lies in this region, brought about by the transition $^3\Sigma_g^- \rightarrow {}^3\Sigma_u^-$. Absorption coefficient is given in Fig. 2.1 [48].

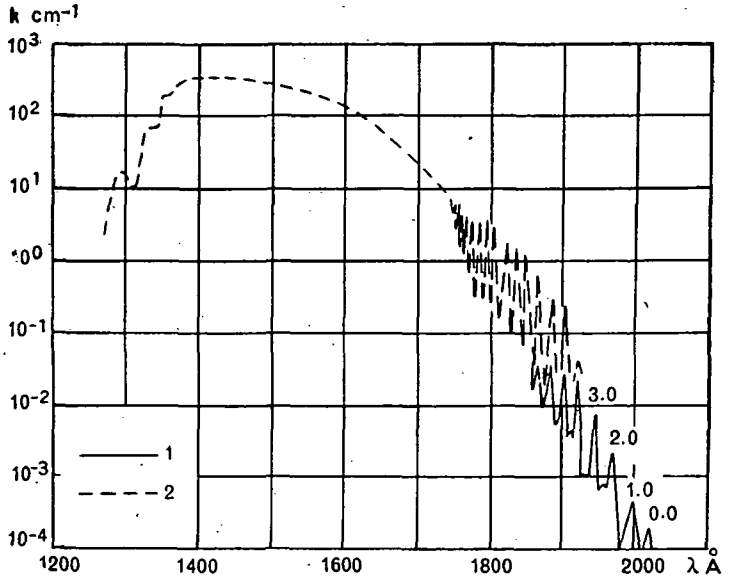

Fig. 2.1. Absorption coefficient of O_2.
1—from [48], 2—from [10].

Spectral range 1750-1250 Å. The Schumann-Runge's continuum resulting from photoionization of O_2 lies in the region is given by the following expression :

$$^3\Sigma_g^- \rightarrow O^{16}(^3P) + O^{16}(^1D).$$

The upper boundary of the continuum, determined from the convergence of the Schumann-Runge band, is sometimes assumed to be equal to 1759 Å [32]. The values of the absorption coefficient, taken from [32, 40], are presented in Table 2.2. The last column in Table 2.2 gives the values of mean square errors taken from [32]. A comparison between the results of [32] and [40] shows that probably these errors are considerably higher. The values of the mean square errors, obtained in [40], with an accuracy between 1 to 5% coincide with the results of Watanabe [10].

Table 2.2 Absorption coefficient of O_2 under normal conditions (cm^{-1}) and coefficient of molecular absorption (cm^2) of Schumann-Runge continuum [32, 40]

λ Å	k cm^{-1}	$k(\mu) \times 10^{-18}$	Error %	λ Å	k cm^{-1}	$k(\mu) \times 10^{-18}$	Error %
1272	1.4	0.05	36	1610	114	4.2	8
1287	13.0	0.48	30	1613	3.82		
1295	12.7	0.47	28	1623.5	3.28		
1300	10.9	0.41	23	1625	100	3.7	6
1310	11.0	0.41	13	1633.5	2.78		
1317	19.7	0.73	18	1640	68.9	2.6	
1325	32.0	1.2	14	1644	2.33		
1332	55.1	2.1	12	1654	1.96		
1340	53.4	2.0	11	1655	56.5		
1347	83.6	3.1	5	1663	1.67	2.1	12
1355	181	6.7	4	1670	41.6	1.55	10
1367	213	7.9	4	1671	1.44		
1370	186	6.9	—	1682	1.18		
1377	335	12.5	6	1685	35.1	1.3	9
1385	309	11.5	1	1689	1.02		
1400	329	12.2	1	1700	25.9	0.96	13
1415	339	12.6	1	1702	0.790		13
1430	366	13.6	5	1712	0.639		
1445	382	14.2	5	1715	14.5	0.54	5
1457	368	13.7	8	1722	0.510		
1475	324	12.1	2	1730	10.6	0.39	13
1490	312	11.6	2	1732	0.403		
1505	310	11.5	5	1742	0.321		
1520	261	9.7	4	1745	6.5	0.24	13
1535	257	9.6	8	1750	0.240		
1565	190	7.1	1	1755	0.110		
1580	170	6.3	4	1760	0.057		
1591	5.05			1770	0.015		
1595	138	5.1	10	1780	0.004		
1602	4.47			1790	0.001		

Spectral range 1250-1050 Å. The observable spectrum in this region has not been thoroughly analyzed. Probably a major portion of the strongest spectral lines are members of Rydberg's series which converge toward the first ionization potential at 12.063 ± 0.001 eV (1027.8 ± 0.1 Å) [32]. The values of absorption coefficient corresponding to the minimum in seven deep windows can be found in Table 2.3. The L^{α} emission occurs at $\lambda = 1215.7$ Å, when the absorption coefficient, according to various researchers, lies in the range 1×10^{-20}-8.5×10^{-21} cm^2.

Table 2.3 Absorption coefficient of O_2 in seven windows of spectrum [10]

Photoelectric method		Photographic method	
λ Å	k cm^{-1}	λ Å	k cm^{-1}
1217.3	0.60	1217.2	0.55
1216.5	0.40	1216.2	0.43
1215.7*	0.27	1215.7	0.23
1215.0	0.50	1215.0	0.64
1214.8	0.70	1214.6	0.40
1188.9	0.64	1188.8	0.48
1188.3	0.39	1188.6	0.38
1187.8	0.25	1187.5	0.43
1187.1 *	0.18	1187.0	0.35
1186.6	0.35	1186.6	0.38
1167.2	0.35	1167.3	0.30
1166.8 *	0.27	1167.0	0.28
1166.1	0.52	1166.3	0.55
1157.4	0.60	1157.5	0.50
1157.0 *	0.51	—	—
1145.3	0.70	1145.2	0.56
1144.3	0.65	1143.8	0.30
1143.0	0.33	1143.0	0.43
1142.8 *	0.26	—	—
1126.9 *	0.53	—	—
1110.5	0.48	1110.2	0.31
1109.9	0.35	1110.0	0.43
1108.9	0.25	1109.2	0.32
1108.3 *	0.11	1108.5	0.44
1107.8	0.32	—	—

NOTE : Asterisk (*) denotes approximate position of minimum absorption.

Spectral range below 1050 Å. The absorption spectrum in this region consists of bands superimposed on the continuum. For $\lambda < 700$ Å only a continuum may be observed. Many of the bands are fairly wide and in these the absorption coefficient does not depend on pressure.

Hopfield's bands are found in the region 1000-680 Å, some of which refer to vibrational series, while others belong to Rydberg's series, converging to the higher electronic states of ions O_2^+. The dissociation process occurs in this region.

The spectrum possesses a complex structure from 860 to 770 Å, probably caused by the overlapping of higher electronic states of O_2 over the fundamental state of ions O_2^+ ($X^2\Pi_g$).

A small continuum below 740 Å is brought about either by ionization of $O_2^+(A^2\Pi)$, or by the dissociative ionization process. Bands situated below 736.8 Å may be looked upon as members of Rydberg's series converging toward (0-0), (1-0) and (2-0) vibrational levels O_2^+ ($b^4\Sigma_g^-$) [(4th ionization potential at 18.17 eV (682.3 Å)]. The absorption spectrum in the given spectral region can be represented in the form of five groups of bands and five continuums.

The groups of bands are as follows : (1) up to 850 Å, (2) 850-770 Å, (3), 770-740 Å, (4) 740-683 Å, and (5) 683-580 Å.

The continuums are as follows : (1) intercepted near 842.2 Å, where the absorption coefficient is a maximum, $k=350$ cm^{-1}; (2) around 809.5 Å, $k=300$ cm^{-1}; (3) around 760 Å, $k=575$ cm^{-1}; (4) around 724.8 Å, $k=740$ cm^{-1}; (5) around 635 Å, without bands.

Coefficients of absorption and ionization are given in [25]. The values of absorption coefficient for the principal lines of solar radiation are of special interest and are given in Table 2.4 [47]. Besides those cases which have already been mentioned, the error in measurements amounts to 5%.

There is a 15% error in the determination of the absorption coefficient in the region 650-900 Å, and 20% outside; there is a spectral resolution of 0.5 Å.

Molecular absorption coefficient of the L_α emission ($\lambda=1025.7$ Å) according to [47] equals 1.82×10^{-18} cm^2, and according to [10] and [52] corresponds to 1.55×10^{-18} cm^2 and 1.59×10^{-18} cm^2.

1.2 Molecular nitrogen N_2

Ground state of the molecules is $N_2X^3\Sigma_g^+$. The ultraviolet region of the absorption spectrum begins from 1450 Å (band 0-0), belonging to the series of Lyman-Birge-Hopfield bands. Since the spectrum consists chiefly of sharp bands, the available data for N_2 are less reliable than that for O_2, so that spectral equipment of high resolution is required for measurement of nitrogen.

Spectral range 3000-1450 Å. Absorption is practically nil.

Spectral range 1450-1000 Å [10]. Absorption spectrum consists mainly of Lyman-Birge-Hopfield bands. These narrow bands can be

Table 2.4 Molecular absorption coefficient $k(\mu)$ and effective ionization efficiency ζ of O_2 in the principal lines of solar spectrum [47]

λ Å	$k(\mu)\times10^{-18}$ cm²	ζ %	λ Å	$k(\mu)\times10^{-18}$ cm²	ζ %	λ Å	$k(\mu)\times10^{-18}$ cm²	ζ %
303.781	16.6[1]	100	617.033	—	—	790.103	—	—
				24.4	97		27.7	37
429.918 OII[3]	—	—	617.051			790.203	—	—
430.041 OII	17.8[1]	100	624.617	25.3	93	832.754	—	—
430.177	—	—	625.130	24.6	96	832.927	26.3[1]	38
434.975	20.9	100	625.852	30.3	96	833.326	—	—
498.491	23.0	100	629.732	30.0	97	833.742	13.0[1]	39
507.391	—	—	684.896	26.4	100	834.462	10.6[1]	38
	23.1	97	—	—	—	—	—	—
507.683	—	—	685.513	—	—	835.096	—	—
				18.4	100			
508.182	23.7	97	685.816			835.292	9.93	37
519.610	25.2	100	686.335	22.1	100	904	10.6	
522.208	20.9	99	702.3	24.2		921.982	5.50	79
525.795	24.5	97	703.8	32.0		922.507	6.36	84
537.027	21.2	98	758.677	18.3	57	923.045		
							10.1	88
553.328	26.2	93	759.440	17.2	53	923.211		
554.074	25.5	97	760.229	28.5	49	923.669	9.15	90
554.514	26.4	97	760.445			924.274	17.8	83
555.262	26.0	97	761.130	20.3	51	930.7	27.1	
584.331	23.2	98	762.001	20.3	50	937.8	5.02	
599.598	28.4	97	764.357	17.8	60	972.537	32.0	83
608.395	24.1	94	765.140	22.9	54	977.026	3.98	
609.705			770.4	22.1		989.790	1.38	69
609.829	26.6	94	774.522	14.2	63	991.514		
							1.75	69
610.043			779.821			991.573		
				27.3	33			
610.746			779.905			1025.722	1.52	64
	28.4	96						
610.850			780.3	31.4		1031.912	1.04	1[2]
616.933	24.4	97	787.710	24.0	54	1037.613	0.78	0.1[2]

[1]Error ± 10%.

[2]Error ± 50%.

[3]OII—absorption coefficient of ionic oxygen O_2^{++}.

identified by electronic transition down to 0-14 for 1114.2 Å, but at $\lambda < 1123$ Å they overlap Tanaka's bands. The data on absorption coefficients are semiquantitative as they have been obtained with the help of an apparatus possessing low resolution. The strongest Lyman-Birge-Hopfield bands at the maximum have $k(\mu) \approx 10^{-20}$ cm^2; the other bands, $k(\mu) \approx 10^{-21}$ cm^2. At the maximum of the bands $k(\mu) \approx 6 \times 10^{-23}$-$3 \times 10^{-22}$ cm^2; for N_2 in L_α line ($\lambda = 1215.6$ Å), $k(\mu) = 6 \times 10^{-23}$ cm^2 and in L_β line ($\lambda = 1025.7$ Å), $k(\mu) = 1.1 \times 10^{-20}$-$3.7 \times 10^{-21}$ cm^2. Dissociation continuum in the case of N_2 does not exist. However, nitrogen atoms can appear as a result of dissociative recombination of ions of molecular nitrogen with electrons on account of neutral ionic reaction, as well as of dissociation of N_2 (1150-1250 Å).

Spectral range 1000-600 Å. In this region the spectrum consists of a multitude of narrow absorption bands, situated close to one another and disappearing near 750 Å, highly ionized Hopfield bands, Rydberg's series near 670 Å and a smooth ionization continuum in the region of shorter wavelengths. A strong ionization continuum is superimposed on the bands for $\lambda < 820$ Å, which decreases rapidly with the increase of wavelength. Nitrogen fluoresces strongly under the influence of the incident radiation with $\lambda = 661$ Å. Absorption bands in the region 1050-820 Å belong to the vibration series, denoted by Worli thus :—*i, j, k, l, m, n, o, p, q, h, r, s, t,* and ϑ. In addition there are eight Worli-Jenkins bands in Rydberg's series converging toward the ground state of the $N_2^+(X^2\Pi_u)$ ions for 796 Å. Several members of Rydberg's series may also be observed, converging to the first four vibrational levels $N_2^+(A^2\Pi_u)$ for lines corresponding to wavelengths 742.7; 732.1; 722.4 and 703.9 Å, which were first observed by Worli, Ogava and Tanaka.

In the region 725-650 Å five Hopfield lines of the Rydberg's series may be observed. Thus:—$N_2(X^1\Sigma_g^+) \rightarrow N_2^+(B^2\Sigma_g^+)$. A distinct continuum may be observed in the region of wavelength below 650 Å. The spectrum determined by photoionization shows that ions appear for $\lambda = 795.8$ Å, while forming a band starting from $\lambda = 795$ Å. As a result of dissociation of N_2 into atoms of N, situated mainly in the excited state, a weak continuum appears in the region 1050-800 Å. The first strong continuum appears at $\lambda = 831.5$ Å, the absorption coefficient equals 8.1 cm^{-1}, and at $\lambda = 752$ Å it reaches the value 421 cm^{-1}. The maximum value of absorption coefficient of the second continuum equals 620 cm^{-1} for $\lambda = 715.3$ Å, and the third—780 cm^{-1} for $\lambda = 620$ Å.

In the region of wavelengths 907; 856.7 and 843.5 Å a weak continuum with absorption coefficients 16.6, 41 and 30 cm^{-1} may be observed. They are overlapped by strong absorption bands. Probably a continuum exists for $\lambda = 970$ Å with $k = 5$ cm^{-1}. The values of absorption coefficients are given in [25]. The results obtained in [38] cannot be derived. In

spite of the high accuracy of the computations in [25] and [38] (10-15%), the maximum and minimum absorption coefficients differ considerably according to the data in these references. The requirement for sufficiently reliable data demands the use of an apparatus with a very high resolving power.

Table 2.5 Coefficients of molecular absorption and ionization efficiency of N_2 in the principal lines of solar spectrum [47]. Error of ± 5% in measurements

λ Å	$k(\mu)\times10^{-18}$ cm²	ζ %	λ Å	$k(\mu)\times10^{-18}$ cm²	ζ %	λ Å	$k(\mu)\times10^{-18}$ cm²	ζ %
303.781	12.1[1]	100		23.7	98		22.7	45
429.918			617.051			790.203		
430.041			624.617	24.0	97	832.754		
	21.0[1]	100	625.130	23.9	97	832.927		0
430.177			625.852	24.0	98	833.326		
434.975	23.7	100	629.732	24.2	97	833.742		0
498.491	24.2	100	684.996	24.3	95	834.462		0
507.391			685.513			835.096		
	24.3	100		24.9	95			
507.683			685.816			835.292		0
508.182	22.2	100	686.335	24.1	95	904		
519.610	25.8	98	702.3	25.6		921.982		0
522.208	23.6	97	703.8	25.6		922.507	6.3	0
525.795	26.2	98	758.677	23.9	75	923.045		0
537.024	25.2	97	759.440	11.6	86	923.211		0
553.328	24.9	96	760.229			923.669		0
554.074	25.3	93		19.8	57	924.274		0
554.514	24.6	93	760.445			930.7	4.8	
555.262	24.8	95	761.130	40.1	55	937.8	10.4	
584.331	23.1	100	762.001	27.8	46	949.7	5.2	
597.818	23.4	97	763.340	27.3	80	972.537		0
599.598	23.4	95	764.357	13.5[1]	69	977.026	0.082	0
608.395	23.4	100	765.140	85.4	77	989.790	0.167	0
609.705			770.4	15.3		991.514		
609.829	23.7	100	774.522	34.0	40		0.074	0
610.043			779.821			991.570		
610.746				12.8	65	1025.722	0.010	0
	23.3	99	779.905			1031.912	0.00074	0
610.850			780.3	18.6		1037.613	0.00074	0
616.933	23.7	98	787.710	24.0	54			
617.033			790.103					

[1]Error ± 10%.

Table 2.5 represents absorption and ionization coefficients for the principal lines of solar radiation in the region 1040-300 Å [52].

1.3 Nitric oxide NO

The ground state of the molecule of NO is $X^2\Pi$. The dissociation energy is 6.49 eV. The first ionization potential is 9.25 eV (λ=1340 Å). As the spectrum of NO has a complex structure, it has been examined less than the spectrum of N_2 and O_2, even though there is a sufficiently large number of measurements [10]. A detailed analysis of the spectrum has been carried out in [10].

Spectral range 2300-1500 Å. The data are semiquantitative. More accurate data are given in Fig. 2.2 [48] in the region 2300-1850 Å.

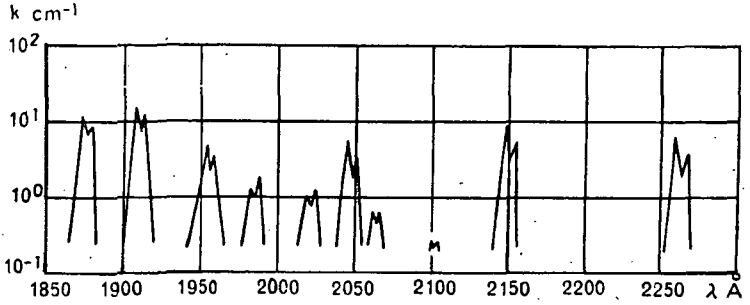

Fig. 2.2. Absorption coefficient of NO [48].

Spectral range 1500-1050 Å. The data on absorption and ionization coefficients are given in [51]. The magnitude of molecular ionization coefficient k_1 in the region of line $L\alpha$ (λ=1216 Å) had important significance for the theory of formation of the layer *D*. From [10] it is found that in this regoin $k_1=2.02\times10^{-18}$ cm².

Spectral range 1000-200 Å. Absorption and photoionization coefficients in the region of the spectrum 1350-580 Å obtained recently are given in [51].

1.4 Ozone O_3

The ionization potential is 12.8 eV. Many researchers have studied the absorption spectrum of ozone in the visible and ultraviolet regions.

Spectral range 7400-3400 Å. Chappuis bands are situated in this spectral region. The cross section of molecular absorption has a maximum value of 5×10^{-21} cm². The values of the absorption cross section are given in Fig. 2.3 [6]. In the region of the spectrum between 4500 and

3400 Å the absorption cross section is very small and a long optical path is necessary in order to obtain a measurable value of absorption.

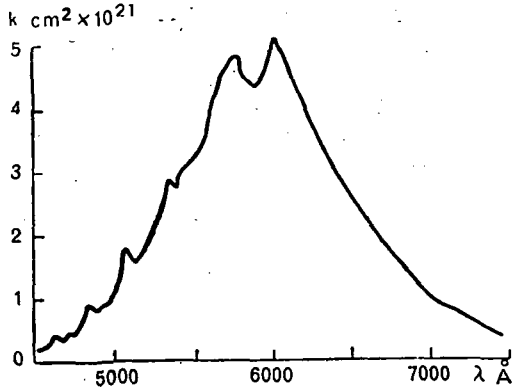

Fig. 2.3. Molecular absorption cross section of ozone in Chappuis band at 18°C, after Vigroux [6].

Spectral range 3400-2400 Å. Hartley bands with maximum absorption coefficient of 1.08×10^{-17} cm² at $\lambda = 2553$ Å are situated in this region. Hartley bands consist of a large number of weak bands, with a separation of the order of 10 Å between them, overlapping a very weak continuum. The structure is most clearly expressed in the long wavelength part of Hartley bands (Huggins' bands) in the region between 3400 and 3100 Å. Absorption in Huggins' bands depends on temperature, not on pressure. Table 2.6 [49] gives the absorption coefficient for the region 3400-3100 Å. There is a weaker dependence on temperature in the region of the spectrum 3000-2400 Å. Table 2.7 gives the values of absorption coefficient obtained with high accuracy in [35]. They are in agreement with the data in [41].

Spectral range 2200-1050 Å. Obviously there exists uninterrupted absorption in this region. It is possible to isolate several diffusion bands in the region of wavelength less than 1500 Å which are probably members of Rydberg's series. The cross sections of molecular absorption are given in Fig. 2.4 [10]. In the region of L_α line $k(\mu) = 2.4 \times 10^{-17}$ cm².

1.5 Water vapor H_2O

Measurement of absorption coefficients of water vapor were carried out by several researchers [10]. However, the data obtained by different authors differ. The chief source of discrepancy caused by its absorption along the walls of the cell probably lies in the inaccuracy of the determination of the amount of water vapor.

Table 2.6 Absorption coefficient of ozone in spectral region 3421-3037 Å [49]

λ Å	k cm^{-1}	λ Å	k cm^{-1}	λ Å	k cm^{-1}	λ Å	k cm^{-1}
3037.0	2.76	3107.2	1.01	3242.0	0.162	3319.2	0.0549
3042.3	2.56	3109.5	1.04	3245.0	0.152	3321.2	0.0424
3043.6	2.49	3110.3	1.00	3248.0	0.224	3322.2	0.0456
3044.9	2.435	3112.0		3253.0	0.171	3324.3	0.0369
3046.2	2.37	3113.0	1.03	3255.0	0.185	3325.0	0.0410
3048.9	2.21	3119.7	0.858	3256.3	0.136	3328.0	0.0350
3051.0	2.06	3120.4	0.881	3258.2	0.147	3332.0	0.0500
3053.0	2.09	3121.2	0.818	3269.0	0.092	3334.0	0.0440
3059.0	1.97	3121.7	0.842	3272.0	0.121	3338.0	0.0770
3061.0	2.01	3124.5	0.784	3275.0	0.106	3345.0	0.0381
3066.0	1.90	3130.0		3269.0	0.092	3372.0	
3075.0		3167.0	0.450	3272.0	0.121	3377.4	0.0295
3077.0	1.62	3170.0	0.490	3275.0	0.106	3378.0	0.0318
0033.0	1.46	3173.0	0.450	3279.0	0.162	3382.4	0.0143
9058.0	1.48	3176.0	0.500	3292.0	0.061	3384.6	0.0182
0330.8	1.47	3177.7	0.426	3295.0	0.066	3385.6	0.0168
3893.0	1.41	3178.4	0.443	3299.0	0.056	3388.6	0.0124
8892.0	1.35	3181.8	0.359	3303.0	0.094	3391.0	0.0140
ε094.7	1.225	3182.3	0.377	3309.0	0.078	3395.0	0.0220
3095.4	1.25	3185.0	0.334	3312.0	0.108	3398.0	0.0170
3098.0	1.16	3186.2	0.350	3303.0	0.0940	3401.0	0.0280
3100.0		3190.0		3309.0	0.0780	3408.4	0.0120
3104.5	1.04	3226.0	0.293	3312.0	0.108	3417.0	0.0078
3106.7	1.07	3239.0	0.140	3318.7	0.0530	3421.0	0.0090

Table 2.7 Absorption coefficient of O_3 in ultraviolet region of spectrum [35]

λ Å	k cm^{-1}	$k(\mu) \times 10^{-19}$ cm^2
2536.5	133.9	114.7
2893.6	17.2	14.7
2967.3	6.969	5.971
3021.5	3.340	2.860
3341.5	0.0498	0.0427
5769.6	0.0555	0.0476

Spectral range 2000-1450 Å. This region mainly consists of a continuum, starting around 2000 Å and possessing a maximum around 1650 Å. The dependence of molecular absorption coefficient on wavelength is given in Fig. 2.5 [48]. The results obtained in [48] are in close agreement with the earlier data obtained by Watanabe [10].

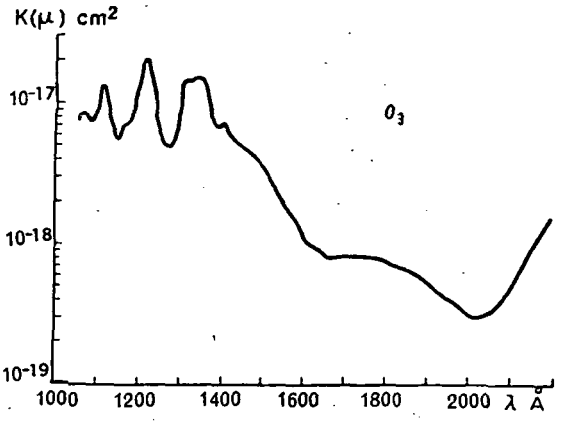

Fig. 2.4. Cross section of molecular absorption of ozone in the region of the spectrum 1050-2200 Å [10].

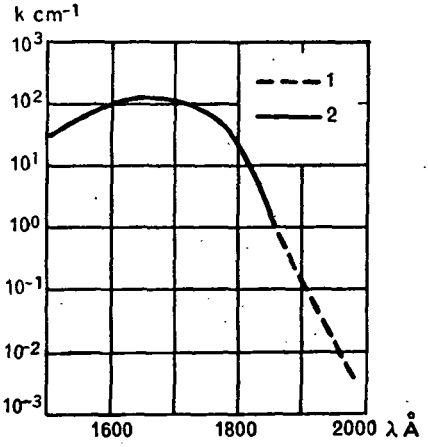

Fig. 2.5. Absorption coefficient of H_2O [48].
1—from [10]; 2—from [48].

Spectral range 1450-1050 Å. The spectrum consists of absorption bands, identified as members of the Rydberg series, superimposed on the continuum. The continuum stretches almost up to $\lambda=1150$ Å. Figs. 2.6 and 2.7 [10] present molecular absorption coefficients in this region. The molecular absorption coefficient in the region of the line L_α varies, according to the data of different authors, from 1.34×10^{-17} to 1.45×10^{-17} cm².

Spectral range below 1050 Å. Figs. 2.8 and 2.9 [10] present the dependence of coefficient on wavelength.

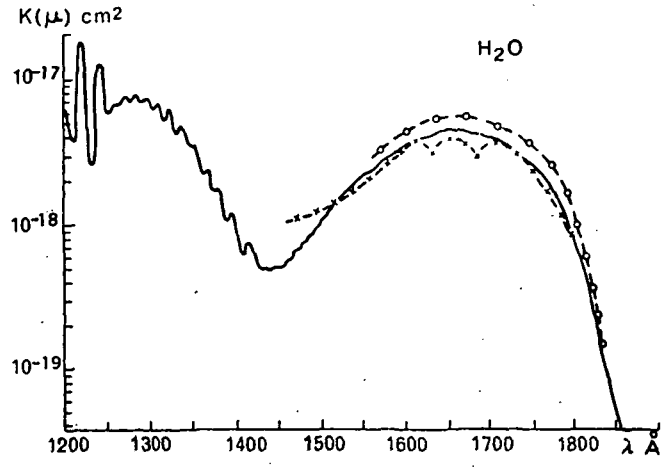

Fig. 2.6. Cross section of molecular absorption of water vapor in the region 1200-1850 Å [10].

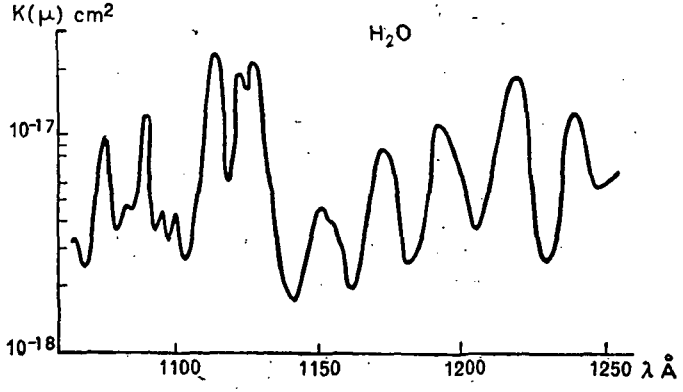

Fig. 2.7. Cross section of molecular absorption coefficient of water vapor in the region of the spectrum from 1050 to 1250 Å [10].

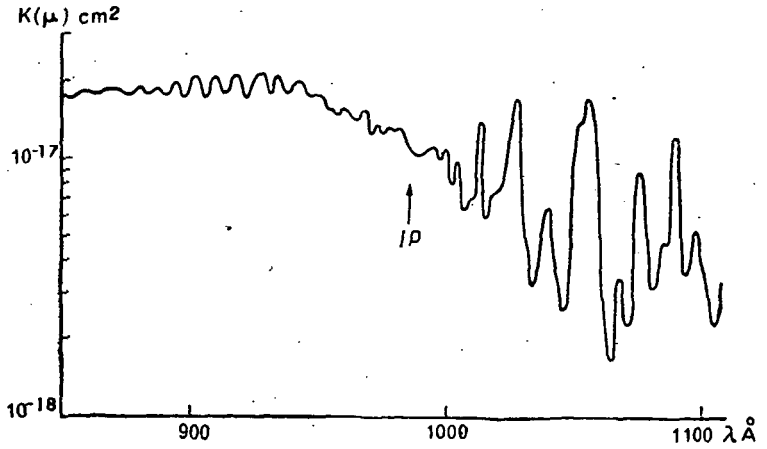

Fig. 2.8. Cross section of molecular absorption of water vapor in the region of spectrum from 850 to 1100 Å [10].

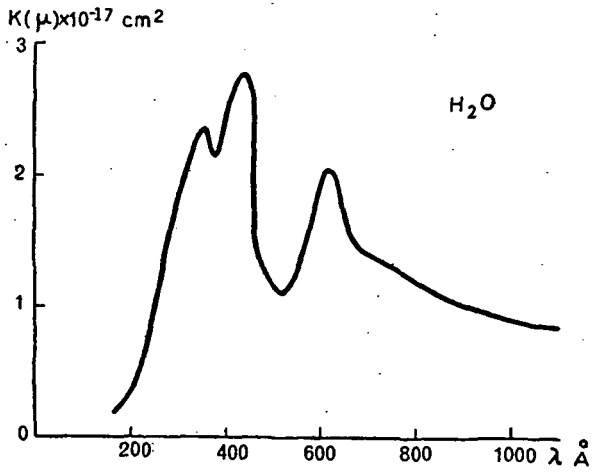

Fig. 2.9 Cross section of molecular absorption of water vapor in the region of spectrum from 150 to 1100 Å [10].

1.6 Remaining gases

Absorption plays a minor role in the radiation processes in the atmosphere in the visible and ultraviolet regions of the spectra of gases such as CO_2, CO, N_2O, NH_3 and others. Therefore the discussion is restricted to results for these gases in the region between 4000 and 1850 Å. Absorption coefficients are given in Figs. 2.10–2.13 [48].

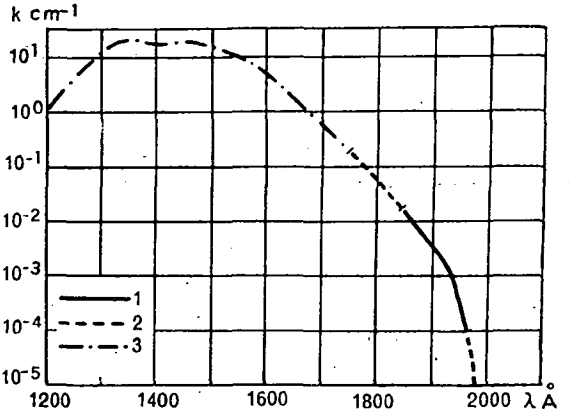

Fig. 2.10. Absorption coefficient of CO_2.
1—from [48] ; 2—from the results of extrapolation ; 3—from [10].

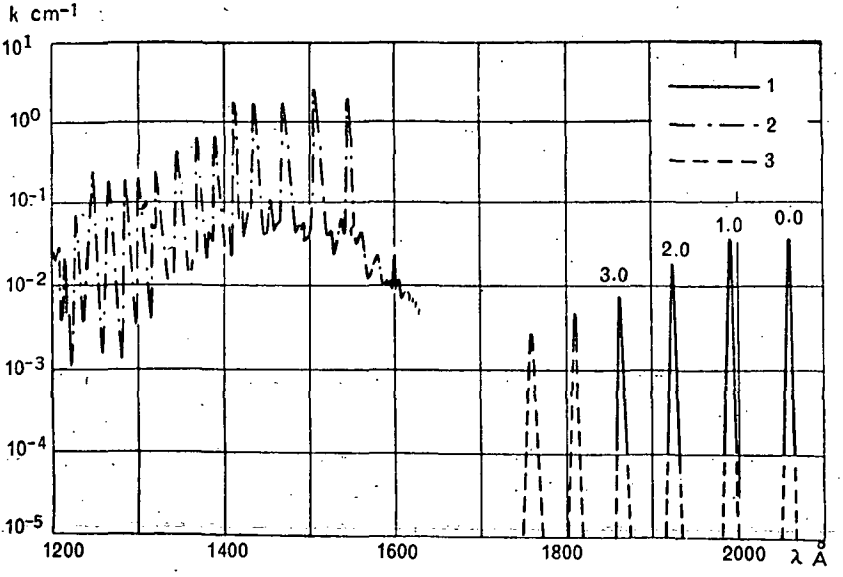

Fig. 2.11. Absorption coefficient of CO.
1—from [48] ; 2—from [10] ; 3—from the results of extrapolation.

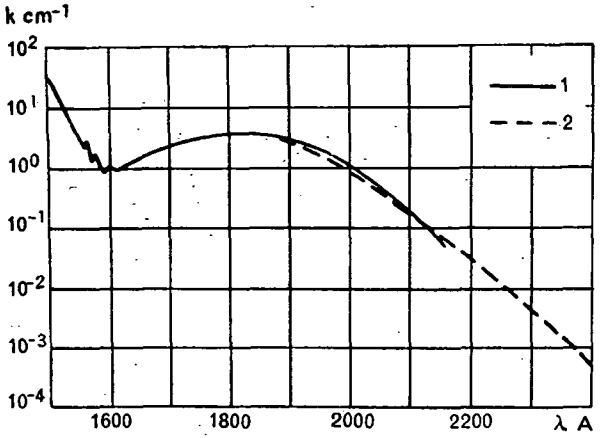

Fig. 2.12. Absorption coefficient of N_2O.
1—from [10] ; 2—from [48].

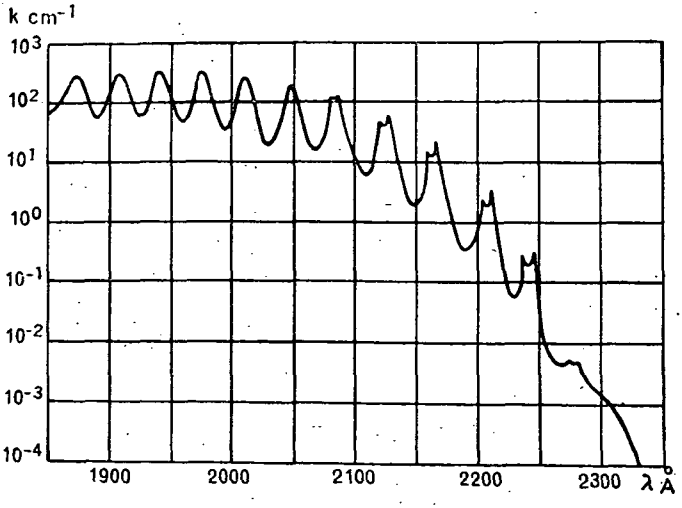

Fig. 2.13. Absorption coefficient of NH_3 [48].

2. OPTICAL CHARACTERISTICS OF ATMOSPHERIC GASES IN THE ULTRAVIOLET REGION OF THE SPECTRUM

The absorption spectrum of molecules in the infrared and microwave regions, which is caused by vibrational and rotational transitions, consists of a very large number of spectral lines. For computations of absorption it is necessary to know the intensity S, halfwidth γ and position of the center ν_0 of spectral lines. Then the absorption function for the spectral interval $\Delta\nu$ is given by the following expression:

$$A=\frac{1}{\Delta\nu}\int_{\nu\Delta}\left\{1-\exp\left[-u\sum_{i=1}^{n}S_i b\ (\nu,\ \nu_{0i}\gamma_i)\right]\right\}, \qquad (2.2)$$

where $b\ (\nu, \nu_0, \gamma)$—contour of spectral line.

Summation in the exponential is carried over all the lines which contribute toward absorption in the interval $\Delta\nu$.

In the absence of exhaustive material on S, γ and ν_0 for the computation of absorption either the model of absorption bands or empirical functions based on experiments may be used. From [6, 12], it is known that for Elsasser's model the absorption function has the following form:

$$A=\sinh\beta\int_0^y \exp\ (-y\cosh\beta)\ \mathcal{J}_0\ (y)dy, \qquad (2.3)$$

where $$y=\frac{S}{d}\frac{u}{\sinh\beta},\quad \beta=\frac{2\pi\gamma}{d},$$

d—average separation between lines;

$\mathcal{J}_0(y)$—Bessel's function of zero order for a purely imaginary argument.

In the limiting cases the following equations are used in place of (2.3):

$$A=1-\exp\left(-\frac{Su}{d}\right)\quad y\ll 1, \qquad (2.4)$$

$$A=\Phi\left(\frac{1}{d}\sqrt{Su\pi\gamma}\right)\quad y\gg 1, \qquad (2.5)$$

where $\Phi(x)=\frac{1}{\sqrt{\pi}}\int_0^x e^{-x^2}dx$ is the errror integral. The absorption func-

tion for the statistical model has the form :

$$A=1-\exp\left[-\frac{1}{\Delta\nu}\sum_{i=1}^{n}A_i\right], \tag{2.6}$$

where A_i =absorption of the i-th isolated line
n =number of lines.

If specific distribution of intensity of spectral lines is to be determined, then in place of (2.6) we have the following equation:

$$A=1-\exp\left\{-xe^{-x/\beta}\left[I_0\left(\frac{x}{\beta}\right)+I_1\left(\frac{x}{\beta}\right)\right]\right\} \tag{2.7}$$

for the case of lines with equal intensity and

$$A=1-\exp\left\{-\frac{x}{\sqrt{1+\frac{2x}{\beta}}}\right\} \tag{2.8}$$

for the case of exponential distribution of intensity of lines where $x=Su/d$.

At $\frac{x}{\beta}\ll 1$ expressions (2.7) and (2.8) change into (2.4), at $\frac{x}{\beta}\gg 1$ the following is used instead of (2.7) :

$$A=1-\exp\left(-\sqrt{\frac{\beta x}{\pi}}\right), \tag{2.9}$$

and in place of (2.8) we have

$$A=1-\exp\left(-\sqrt{\frac{\beta x}{2}}\right). \tag{2.10}$$

One can find absorption functions for other types of intensity distribution of lines in the literature [4]. However, here we do not introduce them. As a rule, the parameters S/d and β in the above-mentioned expressions are determined experimentally. Formulas (2.3), (2.7) and (2.8) are valid only for narrow spectral intervals.

An analytic expression for the absorption function is absent in the case of quasistatic model.

The existing empirical formulas make it possible to compute absorption for all absorption bands or narrow spectral segments. Often the empirical formulas of Howard, Birch and Williams are employed for the computation of absorption dependent upon the entire band; thus for the case of weak absorption

$$\int A_\nu\, d\nu = cu^a p_{\text{eff}}^k, \tag{2.11}$$

for the case of strong absorption

$$\int A_\nu d\nu = C + D \log u - K \log p_{eff}, \qquad (2.12)$$

where c, C, d, D, k, K, are constants, p_{eff}—effective pressure in mm of Hg, u in cm of condensed H_2O and in cm of atmosphere for CO_2.

In the narrow spectral intervals transmission is often defined according to a formula of the type given in [5], viz.

$$P = 1 - A = \exp\left[-\beta(\nu) u^m p_{eff}^n\right], \qquad (2.13)$$

where m, n and $\beta(\nu)$ are the experimentally determined parameters, $P_{eff} = p_a + Bp_{ab}$; p_a—pressure of extraneous gas and p_{ab}—pressure of absorbent gas, and B—coefficient equal to 6 and 2 for H_2O and CO_2 respectively. For H_2O, u is taken in cm, for CO_2 in atm · cm, and for p_{eff}—in atmospheres.

2.1 Water vapor

There exists a large collection of material in which experimental data obtained with the help of statistical models for different spectral resolutions are given. However, the numerical values of the parameters entering into formulas (2.7) and (2.8) are generally not derived except in [29].

Table 2.8 Absorption bands of H_2O for 1.87 μ ($m=0.53$; $n=0.80$) [5]

ν cm^{-1}	β	ν cm^{-1}	β	ν cm^{-1}	β	ν cm^{-1}	β
4950	0.040	5220	3.27	5385	3.79	5550	1.17
5000	0.110	5230	3.57	5390	3.73	5560	0.910
5050	0.163	5240	3.35	5400	3.88	5570	0.661
5055	0.204	5250	3.84	5408	4.04	5580	0.551
5060	0.204	5255	4.04	5409	3.92	5590	0.388
5070	0.204	5260	3.74	5420	3.88	5600	0.388
5080	0.319	5270	3.00	5430	3.89	5610	0.359
5090	0.323	5280	2.51	5440	4.57	5620	0.286
5100	0.567	5290	2.62	5442	4.70	5630	0.245
5110	0.815	5300	2.39	5450	4.45	5640	0.204
5120	0.836	5305	2.37	5460	3.35	5650	0.114
5130	1.02	5310	2.52	5470	2.82	5660	0.130
5140	1.30	5320	3.06	5480	2.37	5670	0.130
5150	1.69	5330	4.29	5485	2.29	5680	0.114
5160	1.88	5340	5.81	5490	2.37	5690	0.098
5170	1.88	5350	5.23	5500	2.22	5700	0.0815
5180	2.08	5360	3.53	5510	1.98	5750	0.0408
5190	2.40	5364	3.33	5520	1.81		
5200	2.40	5370	3.35	5530	1.53		
5210	2.83	5380	3.73	5540	1.26		

Table 2.9 Absorption bands of H_2O for 2.7 μ ($m=0.53$; $n=0.99$) [5]

ν cm^{-1}	β	ν cm^{-1}	β	ν cm^{-1}	β	ν cm^{-1}	β
3010	0.540	3245	1.330	3510	5.500	3830	22.800
3015	1.520	3250	0.430	3516	3.380	3840	14.500
3022	0.295	3257	1.240	3523	9.600	3850	20.700
3025	0.750	3260	0.905	3534	3.900	3854	16.100
3027	0.750	3266	0.850	3537	4.400	3860	18.500
3029	0.650	3269	0.656	3540	4.570	3862	18.700
3032	1.950	3275	1.890	3545	10.300	3870	11.900
3045	0.135	3282	1.050	3550	7.850	3872	11.800
3053	0.863	3286	0.998	3556	6.280	3880	13.900
3055	0.400	3288	0.655	3566	14.200	3882	12.700
3060	1.180	3292	1.520	3574	7.800	3890	12.200
3062	0.730	3303	0.535	3580	8.400	3895	11.300
3070	1.600	3310	1.605	3590	17.800	3900	14.400
3075	0.220	3320	0.580	3597	14.700	3910	4.340
3082	1.660	3327	1.200	3600	16.600	3915	7.150
3096	0.112	3330	0.595	3605	14.700	3920	7.600
3098	0.320	3337	1.100	3615	24.000	3923	7.300
3105	2.000	3341	0.320	3620	18.200	3930	4.300
3110	0.870	3352	1.310	3626	21.500	3935	4.500
3120	2.000	3354	1.390	3635	10.900	3945	5.300
3123	1.530	3360	2.120	3645	22.500	3951	3.350
3128	1.610	3370	0.465	3650	21.000	3956	3.300
3133	0.610	3380	1.360	3663	9.650	3960	1.140
3138	1.000	3386	0.820	3673	21.800	3970	3.150
3140	0.350	3390	1.380	3680	12.300	3975	1.660
3145	0.350	3400	1.200	3688	20.100	3980	1.450
3150	0.175	3403	1.120	3695	11.900	3984	1.600
3155	0.327	3408	0.508	3710	20.750	3988	1.450
3160	0.078	3410	0.685	3715	17.150	3990	1.040
3170	0.500	3418	2.450	3724	22.100	3997	0.833
3175	0.305	3425	0.980	3729	21.300	4000	1.350
3180	1.050	3430	1.300	3732	28.500	4005	1.323
3185	0.610	3435	1.040	3740	30.000	4008	1.270
3190	1.050	3442	2.580	3745	32.000	4010	1.230
3193	0.490	3452	0.815	3750	28.500	4018	0.810
3203	1.505	3463	2.360	3760	13.900	4027	0.440
3207	0.345	3470	2.200	3765	14.750	4035	0.950
3210	1.088	3474	2.900	3770	8.600	4040	0.290
3212	2.088	3478	2.300	3773	8.500	4045	0.440
3215	1.410	3482	4.130	3778	10.400	4052	0.187
3220	1.300	3485	3.750	3788	7.700	4060	0.600
3223	1.540	3490	3.630	3800	19.200	4065	0.620
3225	0.765	3495	2.660	3810	12.100	4070	0.480
3230	1.370	3500	7.900	3815	22.000	4075	0.220
3240	0.980	3507	5.700	3822	16.700	4080	0.153

ν cm^{-1}	β	ν cm^{-1}	β	ν cm^{-1}	β	ν cm^{-1}	β
4090	0.530	4125	0.177	4180	0.105	4240	0.053
4092	0.610	4130	0.137	4182	0.100	4250	0.330
4100	0.033	4140	0.083	4190	0.100	4260	0.050
4107	0.143	4150	0.110	4200	0.093	4280	0.000
4110	0.400	4160	0.145	4210	0.033		
4115	0.433	4167	0.150	4220	0.053		
4120	0.330	4170	0.145	4230	0.100		

Table 2.10 Absorption bands of H_2O for 6.3 μ (m=0.5 ; n=0.86) [5]

ν cm^{-1}	β	ν cm^{-1}	β	ν cm^{-1}	β	ν cm^{-1}	β
1210	0	1370	3.02	1540	20.6	1785	6.22
1220	0.43	1380	4.98	1550	13.9	1795	6.86
1225	0.14	1385	2.42	1555	17.45	1805	5.06
1230	0.466	1390	4.34	1560	16.8	1812	3.18
1234	0.0703	1392	4.70	1568	9.75	1835	4.62
1239	0.0703	1400	7.52	1573	9.0	1840	4.1
1245	0.488	1402	5.06	1590	3.02	1850	3.5
1252	0.25	1410	2.87	1600	3.7	1860	2.42
1255	0.179	1415	5.25	1612	6.22	1870	3.02
1260	0.25	1420	7.98	1620	9.47	1880	1.83
1265	0.90	1430	5.06	1630	8.46	1890	1.9
1270	0.82	1435	6.74	1640	10.6	1908	1.77
1274	2.20	1445	3.34	1655	15.5	1920	2.27
1280	0.98	1450	7.86	1660	15.0	1940	1.28
1285	0.30	1456	12.8	1670	9.2	1950	1.51
1287	0.70	1460	12.0	1680	13.5	1970	1.01
1294	1.48	1468	7.53	1685	14.3	1985	0.62
1300	0.44	1475	11.9	1692	14.1	2005	1.0
1310	1.22	1480	8.46	1700	15.5	2020	0.674
1318	2.94	1485	6.03	1715	11.6	2030	0.738
1320	2.82	1490	8.45	1725	8.45	2050	0.446
1325	0.745	1495	11.2	1740	11.9	2070	0.33
1330	2.72	1500	11.2	1750	11.0	2080	0.347
1335	5.06	1510	18.5	1760	9.0	2090	0.29
1346	1.15	1518	17.45	1762	8.2	2110	0.179
1352	2.72	1525	20.9	1770	8.7	2114	0.105
1360	4.34	1530	14.6	1780	7.0		

Table 2.11 Absorption bands of H_2O for 15-40 μ

ν cm^{-1}	*m*	*n*	β	ν cm^{-1}	*m*	*n*	β
248	0.705	0.640	222	358	0.607	0.599	37.6
250.5	0.941	0.807	519	360	0.594	0.541	14.9
252	0.591	0.635	93.7	362	1.002	0.294	19.8
253.5	0.627	0.550	157	366	0.942	0.507	11.1
255	0.653	0.597	112	368	0.955	0.530	15.1
257	0.804	0.704	110	371	0.523	0.500	12.4
259	1.08	0.834	184	373	0.672	0.568	15.4
261	1.09	0.870	138	376	0.455	0.455	16.1
263	0.948	0.749	95.8	380	0.924	0.578	13.6
265	0.705	0.613	57.4	386	0.510	0.498	12.6
266.5	0.682	0.568	62.2	390	1.03	0.530	96.7
268	0.797	0.608	57.6	395	0.517	0.554	8.52
270	1.11	0.855	146	399	0.437	0.456	14.9
272	0.944	0.729	91.5	402	0.637	0.485	12.6
275	0.714	0.625	63.7	404	1.02	0.471	10.4
278	0.638	0.555	136	410	1.277	0.497	9.46
280	0.682	0.637	227	416	0.687	0.539	5.78
283	0.627	0.515	72.2	420	0.423	0.443	11.8
286	0.901	0.756	138	422	0.538	0.477	13.7
288	0.679	0.609	63.7	426	0.631	0.561	11.5
289.5	0.616	0.555	59.4	430	0.832	0.563	7.02
292	0.771	0.637	53.9	437	0.801	0.566	9.36
295	1.100	0.838	122	440	0.805	0.498	6.11
300	0.661	0.602	52.2	444	0.576	0.496	7.47
302.5	0.526	0.464	42.0	450	0.700	0.411	4.24
305	0.659	0.558	42.5	459	0.478	0.449	6.77
310	0.992	0.757	69.9	466	0.808	0.456	3.94
312	0.825	0.694	41.5	474	0.597	0.437	7.30
315	0.631	0.546	25.3	480	0.946	0.464	4.42
318.5	1.08	0.780	83.0	486	0.835	0.556	19.5
322	0.693	0.564	36.1	490	0.760	0.486	3.49
326	0.669	0.586	77.4	503	0.482	0.538	7.64
330	0.688	0.540	32.2	505	0.648	0.574	6.13
332	0.891	0.771	59.1	507	0.509	0.480	5.69
335	0.607	0.541	26.7	509	0.549	0.578	3.33
339	0.738	0.597	30.8	511	0.577	0.435	3.69
342	0.713	0.609	37.7	513	0.729	0.437	3.25
345	0.802	0.635	35.8	515	0.681	0.582	7.71
346	0.771	0.671	23.4	517	0.479	0.461	8.07
348	0.695	0.688	26.6	520	0.506	0.411	3.89
350	0.537	0.605	32.8	523	0.737	0.654	3.69
352	0.534	0.607	45.8	526	0.571	0.476	6.48
354	0.533	0.614	45.8	528	0.503	0.423	1.94
355	0.523	0.550	34.0	531	0.929	0.300	2.14
357	0.601	0.637	38.5	537	0.500	0.375	2.47

ν cm^{-1}	m	n	β	ν cm^{-1}	m	n	β
539	0.806	0.267	2.54	576	0.493	0.448	3.23
541	0.502	0.613	2.26	578	0.632	0.366	2.58
543	0.493	0.424	1.39	581	0.556	0.393	3.94
546	0.527	0.528	5.61	583	0.680	0.301	2.91
548	0.561	0.419	3.97	585	0.685	0.361	3.15
550	0.477	0.468	2.86	588	0.993	0.201	3.30
552	0.621	0.317	1.65	592	0.611	0.394	4.97
555	0.687	0.429	2.82	597	0.717	0.317	2.63
560	0.763	0.293	1.63	600	0.622	0.415	3.17
563	0.668	0.368	2.30	603	0.666	0.399	2.52
564	0.652	0.313	2.11	605	0.829	0.207	2.75
569	0.541	0.475	4.48	610	0.601	0.192	1.34
573	0.899	0.292	3.51	615	0.626	0.288	3.20

Emission in the bands of water vapor of 1.87, 2.7, 6.3 and 15-40 μ can be similarly calculated with the help of formula (13). The parameters entering into this formula are given in Tables 2.8-2.11 [5]. Parameters entering into formulas (2.11) and (2.12) are given in Table 2.12.

Table 2.12 Empirical constants in Howard-Birch-Williams formulas for water vapor ($d = \frac{1}{2}$, $B = 1$) [24]

Band, μ	Limits of the bands, cm^{-1}	c	k	C	D	K	$\int A_\nu d\nu$
6.3	1150-2050	356	0.30	302	218	157	160
3.2	2800-3340	40.2	0.30				500
2.7	3340-4400	316	0.32	337	246	150	200
1.87	4800-5200	152	0.30	127	232	144	275
1.38	6500-8000	163	0.30	202	460	198	350
1.1	8300-9300	31	0.26				200
0.94		38	0.27				200
3.7[1]	2670-2770	0.325	0.37				

NOTE : The last graph gives the value below which weak absorption occurs, and above which three is strong absorption.

[1]HDO isotope band.

2.2 Carbon dioxide CO_2

Elsasser's model, i.e. formula (3) or its limiting expressions, is usually employed for the description of absorption caused by carbon dioxide.

Computation of emission in the bands of CO_2 of 2, 2.7, 4.3, 4.8, 9-12 and 15 μ may be carried out similarly according to formula (2.13). The parameters of computation are presented in Tables 2.13-2.18 [5]. The parameters entering into formulas (2.11) and (2.12) for a computation of absorption brought about by the entire band are given in Table 2.19.

Table 2.13 Absorption bands of CO_2 for 2 μ (m=0.64 ; n=0.45) [5]

ν cm^{-1}	β	ν cm^{-1}	β	ν cm^{-1}	β
4674	0	4878	5.5×10^{-3}	5026	0.92×10^{-3}
4714	0.25×10^{-3}	4899	2.03	5036	3.1
4754	0.58	4917	4.8	5059	12.1
4797	2.67	4938	15.9	5080	19.5
4817	5.95	4959	32.8	5094	10.9
4838	11.4	4973	54.0	5115	0.29
4850	13.1	4998	16.4	5133	0.83
4865	11.0	5014	3.4	5163	

Table 2.14 Absorption band of CO_2 for 2.7 μ (m=0.64 ; n=0.45) [5]

ν cm^{-1}	$\beta\times10^{-2}$	ν cm^{-1}	β	ν cm^{-1}	β	ν cm^{-1}	β
3480	0.09	3565	0.0896	3630	0.47	3700	0.516
3485	0.157	3570	0.100	3635	0.397	3705	0.496
3490	0.224	3575	0.114	3637	0.330	3710	0.384
3495	0.280	3580	0.155	3638	0.270	3715	0.320
3500	0.386	3585	0.248	3640	0.205	3720	0.560
3505	0.490	3590	0.294	3645	0.090	3725	0.670
3510	0.560	3595	0.360	3650	0.055	3730	0.650
3515	0.670	3600	0.433	3655	0.031	3735	0.560
3520	0.740	3605	0.398	3660	0.028	3740	0.426
3525	0.806	3610	0.222	3665	0.042	3745	0.290
3530	0.850	3613	0.196	3670	0.058	3750	0.155
3535	1.03	3615	0.206	3675	0.167	3755	0.044
3540	1.61	3617	0.270	3680	0.189	3760	0.044
3545	2.36	3620	0.360	3685	0.270	3762	0.023
3550	3.14	3622	0.476	3690	0.360	3765	0.014
3555	3.90	3625	0.504	3695	0.430	3770	0.004
3560	5.56	3627	0.48				

Table 2.15 Absorption band of CO_2 for 4.3 μ [5]

ν cm^{-1}	β	ν cm^{-1}	β	ν cm^{-1}	β	ν cm^{-1}	β
			$m=0.64$; $n=0.45$; $u^m p_{eff}^n > 0.7$				
2250	0.07	2290	0.43	2325	4.4	2360	6.6
2255	0.117	2295	0.72	2330	4.6	2565	6.4
2260	0.187	2300	1.08	2335	4.4	2370	4.6
2265	0.25	2305	1.58	2340	4.9	2375	3.25
2270	0.295	2310	2.12	2343	5.2	2380	1.78
2275	0.28	2315	2.4	2345	4.4	2385	0.36
2280	0.25	2320	2.6	2350	3.17	2390	0.15
2285	0.19	2323	4.25	2355	4.6	2395	0.10
			$m=0.5$; $n=0.48$; $u^m p_{eff}^n < 0.7$				
2179	4×10^{-4}	2223	2.6×10^{-2}	2270	40×10^{-2}	2390	18.6×10^{-2}
2181	5.7	2225	4	2275	44	2395	4.55
2185	9.3	2227	6	2280	44	2400	2.8
2188	1.2×10^{-3}	2230	8.1	2284	37	2405	1.65
2193	1.76	2233	10.5	2290	85	2411	1.3
2196	2.5	2237	12	2295	135	2416	9.1×10^{-2}
2199	3.3	2238	14.5	2300	158	2421	6
2201	4.6	2240	15.6	2305	231	2426	3.4
2206	5.9	2246	20.1	2372	359	3431	2.5
2210	7.3	2253	28.6	2377	207	2436	1.6
2214	9.1	2260	33	2382	108	2441	1
2216	1.1×10^{-2}	2265	37.5	2386	37.8	2446	4×10^{-4}
2219	1.5						

Table 2.16 Absorption band of CO_2 for 4.8 μ ($m = 0.64$; $n = 0.45$) [5]

ν cm^{-1}	β	ν cm^{-1}	β	ν cm^{-1}	β
2170.6	1.27×10^{-4}	2108.6	1.89×10^{-3}	2073.3	11.34×10^{-3}
2158.2	3.10	2106.7	2.76	2065.2	9.20
2145.8	5.95	2102.4	5.31	2057.1	5.07
2139.6	1.47×10^{-3}	2098.7	3.22	2052.2	3.40
2135.9	2.85	2096.2	4.19	2040.4	1.88
2132.2	1.52	2093.1	6.80	2035.4	1.68
2129.1	1.62	2090.0	15.36	2031.1	2.16
2124.1	2.28	2086.9	10.55	2028.0	1.66
2121.0	2.48	2085.0	7.77	2021.8	1.06
2117.3	2.44	2080.7	10.05	2015.6	0.61
2111.7	1.97	2078.0	11.12	2009.4	0.29

Table 2.17 Absorption band of CO_2 for 9-12 μ ($m = 0.84$) [5]

ν cm^{-1}	n	ν cm^{-1}	n	ν cm^{-1}	$\beta \times 10^4$	ν cm^1	$\beta \times 10^4$
1100	0.230	970	0.360	1100	0.5	956	6.4
1091	0.280	969	0.340	1090	7	948	9
1085	0.366	967	0.300	1085	12	943	8
1075	0.434	965	0.249	1076	16	935	4
1070	0.360	963	0.220	1070	12	925	2
1068	0.300	958	0.230	1067	8	915	1.2
1063	0.243	956	0.250	1063	5.8	900	0.8
1050	0.356	954	0.280	1058	8	875	0.4
1036	0.364	952	0.312	1055	10.4	866	0.4
1025	0.320	947	0.324	1050	12	862	0.7
1020	0.292	935	0.308	1045	10.4	860	0.5
1017	0.274	925	0.280	1042	8	850	0.5
1014	0.258	914	0.264	1038	6.3	837	0.9
1010	0.240	900	0.220	1022	2	830	1.5
1007	0.223	877	0.170	1010	0.5	825	2.4
1000	0.202	866	0.186	1000	0.25	822	2
995	0.210	860	0.220	993	1.8	812	4.7
990	0.240	850	0.262	983	8	802	8
988	0.270	825	0.280	975	10	798	7.6
987	0.300	800	0.276	971	8	792	12
986	0.320	792	0.298	968	4.8	787	6.4
985	0.345	786	0.252	963	3	770	22.4
984	0.366	782	0.298				
983	0.390	766	0.300				
975	0.438	755	0.280				
971	0.423						

Table 2.18 Absorption band of CO_2 for 15 μ ($m = 0.64$) [5]

ν cm^{-1}	β	n	ν cm^{-1}	β	n
575	0.480×10^{-2}	0.170	600	0.799×10^{-1}	0.224
580	0.957×10^{-2}	0.170	605	0.914×10^{-1}	0.230
585	0.214×10	0.172	607.5	0.959×10^{-1}	0.228
590	0.339×10^{-1}	0.170	610	0.961×10^{-1}	0.224
595	0.633×10^{-1}	0.168	612.5	0.968×10^{-1}	0.220
598	0.108	0.180	615	0.118	0.200

ν cm^{-1}	β	n	ν cm^{-1}	β	n
617.5	0.300	0.166	685	1.062	0.428
620	0.110	0.250	690	0.806	0.408
625	0.197	0.256	692.5	0.706	0.394
630	0.324	0.315	695	0.629	0.382
635	0.462	0.344	697.5	0.542	0.370
640	0.625	0.360	700	0.469	0.354
642.5	0.719	0.367	703	0.395	0.346
645	0.862	0.374	705	0.332	0.338
647	1.035	0.340	710	0.224	0.314
648	1.078	0.326	715	0.161	0.270
650	1.087	0.384	717.5	0.209	0.200
655	1.111	0.398	720	0.243	0.132
657.5	1.108	0.400	722	0.156	0.180
660	1.082	0.396	723	0.099	0.252
662	1.062	0.389	725	0.075	0.256
663	1.074	0.384	730	0.091	0.253
665	1.332	0.330	735	0.095	0.252
667.5	2.352	0.238	740	0.100	0.252
670	1.309	0.310	745	0.062	0.254
672	1.250	0.440	750	0.037	0.254
675	1.266	0.446	755	0.023	0.253
667.5	1.258	0.442	758	0.012	0.254
680	1.188	0.440			

Table 2.19 Empirical constants in formulas of Howard-Birch-Williams for carbon dioxide [24]

Bands, μ	Boundaries, cm^{-1}	c	d	k	C	D	K	$\int A_\nu \, d\nu$
15	550-800	3.16	0.5	0.44	—68	55	47	50
10.4	750-1000	0.016	0.78	0.20				35
9.4	1000-1110	0.023	0.75	0.23				40
5.2	1870-1980	0.024	0.5	0.40				30
4.8	1980-2160	0.12	0.5	0.37				60
4.3	2160-2500	15.0	0.54	0.41	27.5	34	31.5	50
2.7	3480-3800	3.15	0.58	0.43	—137	77	68	50
2.0	4750-5200	0.492	0.50	0.39	—536	138	114	80
1.6	6000-6550	0.063	0.50	0.38				80
1.4	6650-7250	0.058	0.50	0.41				80

2.3 Ozone O_3

The most significant of all the absorption bands of ozone is 9.6 μ, being studied in [3, 43, 50]. The model of this band has not been definitely established to date. The expression (2.5) has been employed in [44] for the description of absorption of O_3 as follows :

$$A = \Phi\left(\frac{1}{d}\sqrt{Su\pi\gamma}\right) y \gg 1,$$

where $\frac{1}{d}\sqrt{Su\pi\gamma} = k$ (k—absorption coefficient in $mm^{-\frac{1}{2}}$, u—ozone layer in mm). The values of k are given in Table 2.20.

Table 2.20 Absorption coefficient of ozone [44]

λ, μ	k, $mm^{-\frac{1}{2}}$	λ, μ	k, $mm^{-\frac{1}{2}}$	λ, μ	k, $mm^{-\frac{1}{2}}$
8.6	0.0	12.2	0.0	14.2	0.03
8.8	0.04	12.4	0.01	14.6	0.03
9.0	0.11	12.6	0.01	14.8	0.03
9.2	0.07	12.8	0.01	15.0	0.02
9.4	0.39	13.0	0.02	15.2	0.02
9.6	0.48	13.2	0.03	15.4	0.02
9.8	0.39	13.4	0.06	15.6	0.01
10.0	0.20	13.6	0.07	15.8	0.01
10.2	0.06	13.8	0.04	16.0	0.01
10.4	0.0	14.0	0.03	16.2	0.0

It is possible to compute absorption, determined by the entire band 9.6 μ according to the empirical formula [50].

$$\int A_\nu \, d\nu = 138\left(1 - 10^{-u\xi f(\varphi)}\right), \tag{2.14}$$

where

$$\varphi = \frac{u\xi\,(u)^{2.11}}{p}$$

$$f(\varphi) = 1.185\,(1 + 734\varphi)^{-\frac{1}{2}}\,\eta\,(\varphi),$$

$$\xi\,(u) = \begin{cases} \dfrac{1 + 0.1025u}{1 + 1.161u} & u \leqslant 0.1 \\ 0.984 \times 10^{-0.53u} & 0.1 \leqslant u \leqslant 0.4 \\ 0.317u^{-0.74} & u \geqslant 0.4 \end{cases}$$

log φ −4.0; −3.9; −3.8; −3.7; −3.6; −3.5; −3.4: −3.3; −3.2; −3.1
η(φ) 1; 0.998; 0.995; 0.993: 0.989; 0.984; 0.982; 0.980; 0.977; 0.974
log(φ) −3.0; −2.9; −2.8; −2.7; −2.6; −2.5; −2.4; −2.3; −2.2; −2.1;
η(φ) 0.977; 0.979; 0.982; 0.989; 1.002; 1.016; 1.030; 1.045; 1.057; 1.069; log φ −2.0
η(φ) 1.079.

2.4 Minor components of the atmosphere: CH_4, N_2O and CO

Although the amount of CH_4, N_2O and CO is small in the atmosphere, it is necessary to account for them in many problems of atmospheric optics. Formula (13) may be employed for the computation of absorption in the narrow spectral segments brought about by these gases. Parameters entering into this case are given in Tables 2.21-2.26 [5]. Absorption for the entire band may be computed according to formulas (11) and (12), the necessary parameters being given in Table 2.27 [24]. The effective pressure $p_{\text{eff}} = p_a + Bp_{ab}$ has been used in place of p in formulas (11) and (12). The values of coefficient of resonance B are given in Table 2.28.

Table 2.21 Absorption band of CH_4, 3.3 μ (m=0.58) [5]

ν cm^{-1}	β	n	ν cm^{-1}	β	n
1120	0.002	0.125	1350	0.503	0.450
1135	0.005	0.130	1365	0.358	0.427
1160	0.010	0.137	1380	0.182	0.395
1180	0.020	0.170	1390	0.100	0.358
1186	0.030	0.190	1400	0.055	0.225
1190	0.020	0.208	1410	0.028	0.158
1200	0.055	0.312	1426	0.030	0.190
1206	0.040	0.338	1440	0.030	0.210
1220	0.175	0.350	1460	0.023	0.190
1230	0.143	0.360	1480	0.018	0.175
1247	0.335	0.403	1500	0.010	0.210
1250	0.278	0.418	1520	0.005	0.241
1260	0.400	0.500	1536	0.025	0.270
1265	0.500	0.475	1547	0.070	0.283
1275	0.380	0.450	1560	0.015	0.265
1290	0.516	0.460	1580	0.005	0.243
1305	0.786	0.290	1600	0.005	0.235
1314	0.412	0.412	1620	0.012	0.300
1320	0.208	0.533	1640	0.010	0.313
1330	0.320	0.460	1660	0.005	0.325
1340	0.423	0.450			

Table 2.22. Absorption band of CH_2, 7.6 μ (m=0.58) [5]

ν cm^{-1}	β	n	ν cm^{-1}	β	n
2530	0.010		2938	0.190	0.268
2560	0.014	0.098	2948	0.220	0.276
2600	0.018	0.098	2960	0.247	0.324
2620	0.021	0.098	2970	0.270	0.342
2640	0.022	0.098	2986	0.262	0.334
2660	0.026	0.110	3000	0.250	0.322
2680	0.028	0.148	3015	0.320	0.266
2700	0.032	0.184	3026	0.375	0.222
2720	0.034	0.196	3038	0.375	0.250
2740	0.040	0.216	3043	0.370	0.300
2750	0.045	0.222	3050	0.290	0.378
2760	0.050	0.218	3060	0.212	0.440
2780	0.060	0.202	3068	0.232	0.460
2800	0.070	0.190	3075	0.255	0.482
2814	0.074	0.244	3088	0.320	0.500
2830	0.082	0.300	3100	0.290	0.407
2853	0.103	0.294	3115	0.254	0.378
2862	0.082	0.242	3126	0.220	0.360
2875	0.112	0.221	3150	0.154	0.336
2890	0.145	0.236	3176	0.100	0.310
2916	0.160	0.252	3200	0.040	0.278
2928	0.174	0.260	3218	0.025	0.232

Table 2.23 Absorption band of N_2O, 4.5 μ (m = 0.6) [5]

ν cm^{-1}	β	n
2125	0	0.170
2138	0.015	0.170
2150	0.050	0.170
2157	0.08	0.175
2162	0.13	0.174
2170	0.20	0.176
2175	0.28	0.190
2182	0.48	0.230
2188	0.80	0.310
2194	1.33	0.355
2200	1.80	0.410
2206	2.26	0.430
2212	2.45	0.450
2218	2.24	0.434

ν cm^{-1}	β	n
2224	1.90	0.400
2230	2.46	0.445
2237	2.94	0.475
2244	2.65	0.460
2250	1.92	0.450
2256	0.80	0.427
2263	0.28	0.283
2268	0.12	0.25
2275	0.05	0.25
2287	0	0.25

Table 2.24 Absorption band of N_2O, 7.8 μ ($m = 0.6$) [5]

ν cm^{-1}	β	n
1206	0	0.30
1213	0.04	0.30
1225	0.06	0.30
1231	0.12	0.30
1240	0.32	0.33
1245	0.58	0.36
1254	1.10	0.38
1257	1.44	0.42
1262	1.74	0.43
1267	1.98	0.44
1276	1.72	0.45
1283	1.46	0.46
1287	1.75	0.46
1290	2.18	0.47
1295	2.70	0.47
1302	2.00	0.44
1307	1.44	0.42
1310	0.90	0.39
1315	0.64	0.36
1324	0.37	0.32
1331	0.18	0.31
1342	0	0.30

Table 2.25 Absorption band of N_2O, 15 μ ($m = 0.6$). [5]

ν cm^{-1}	β	n	ν cm^{-1}	β	n
525	0	0.078	615	0.280	0.280
535	0.008	0.078	620	0.190	0.375
540	0.025	0.080	625	0.112	0.500
545	0.058	0.078	630	0.070	0.566
550	0.092	0.260	635	0.046	0.600
555	0.124	0.300	640	0.020	0.500
558	0.192	0.310	645	0.006	0.310
560	0.289	0.340	650	0.003	0.240
565	0.440	0.387	660	0.004	0.180
570	0.435	0.410	670	0.007	0.226
574	0.420	0.337	685	0.012	0.255
578	0.404	0.273	689	0.027	0.235
581	0.390	0.305	692	0.048	0.220
585	0.377	0.336	694	0.027	0.225
590	0.374	0.365	696	0.012	0.226
592	0.548	0.392	699	0.015	0.400
595	0.568	0.400	701	0.012	0.355
600	0.529	0.440	706	0.015	0.406
605	0.635	0.460	715	0.008	0.580
610	0.400	0.377	735		0.500

Table 2.26 Absorption band of CO, 3.7 μ ($n = 0.45$; $m = 0.58$) [5]

ν cm^{-1}	β	ν cm^{-1}	β	ν cm^{-1}	β
2000	0.0202	2100	0.394	2180	0.454
2012	0.038	2112	0.504	2190	0.350
2025	0.0564	2125	0.462	2200	0.292
2037	0.085	2132	0.380	2212	0.195
2050	0.128	2140	0.289	2225	0.086
2062	0.185	2150	0.374	2237	0.044
2075	0.247	2160	0.462	2250	0.0096
2087	0.320	2170	0.552		

Table 2.27 Empirical constants for formulas (11) and (12) [24]

Absorbing gas	Center of band, cm^{-1}	Boundaries, cm^{-1}	c	d	k	C	D	K	p, mm of Hg	$\int A_\nu d\nu$, cm^{-1}
N_2O	2224	2100-2300	18.0	0.53	0.371				10-25	10-45
						15	40	28	10-760	45-120
CO	2143	1975-2275	2.75	0.55	0.44				20-250	4-40
			2.75	0.55	0.44				20-760	10-40
			3.20	0.43	0.43				20-760	40-120
						—106	61	61	20-3000	120-200
CH_4	3020	2300-3400	15.5	0.55	0.22				10-760	15-250
						—375	272	108.8	10-3000	250-500
CH_4	1306	1050-1535	7.3	0.45	0.27				10-760	20-130
CH_4	1550	1535-1800	Not obtained							

Table 2.28 Coefficient of resonance for different gases [24]

Absorbing gas	Absorption band	Coefficient of resonance
H_2O	5332, 3756, 1595 cm^{-1} 20 μ line 4025.4 cm^{-1}	5 ± 1.5 6-11 increases linearly with increase of absorption
CO_2	3716, 3609, 2356, 1064, 961 cm^{-1} and 875-495 cm^{-1}	1.30 ± 0.08
CO	2143 cm^{-1} 4260 cm^{-1}	1.02 ± 0.06 1.08 ± 0.06
CH_4	3020 cm^{-1} 1306 cm^{-1} 1550 cm^{-1}	1.30 ± 0.08 1.38 ± 0.08 1.38
N_2O	2224, 1285, 1167 cm^{-1}	1.12 ± 0.07

3. CHARACTERISTICS OF SCATTERING OF VISIBLE AND INFRARED RADIATION BY AEROSOL PARTICLES AND AIR MOLECULES

Inasmuch as the phenomenon of scattered radiation of the atmosphere is complex and varied, one is limited by certain factors while studying the scattering characteristics of radiation in the atmosphere. It is assumed that the scattered radiation always possesses the same frequency as the incident radiation, i.e. there is no quantum transition; scattering occurs on clearly bounded, distinct and independent particles, i.e. there exists no correlation between the phases of radiation scattered by different particles; besides only characteristics of single scattering are to be examined. Mie's general theory is applicable to scattering of radiation by particles when these conditions are fulfilled, and makes it possible to solve direct as well as indirect problems of atmospheric optics, such as the enumeration of optical characteristics of the medium according to the data on the composition of the scattering medium and the stating of its microphysical properties from optical measurements.

The fundamental properties of molecular scattering and aerosol attenuation (scattering and absorption) of radiative fluxes in the atmosphere as well as the volume coefficient of molecular and aerosol scattering and aerosol absorption can be expressed through sums of coefficients corresponding to single particles as follows:

$$k_{\nu a} = k_\nu + \alpha_\nu = \sum_{i=1}^{N} k_{\nu a}^{(i)}(\mu), \tag{2.15a}$$

$$\alpha_{\nu a} = \sum_{i=1}^{N} \alpha_{\nu a}^{(i)}(\mu), \tag{2.15b}$$

$$k_\nu = \sum_{i=1}^{N} k_\nu^{(i)}(\mu), \tag{2.15c}$$

$$\alpha_\nu = \sum_{i=1}^{N} k_\nu^{(i)}(\mu), \tag{2.15d}$$

where $k_{\nu a}$ —volume coefficient of aerosol attenuation and is equal to the sum of volume coefficients of scattering α_ν and absorption k_ν, and α_ν —volume coefficient of molecular scattering $k_a^{(i)}(\mu)$, $\alpha_{\nu a}^{(i)}(\mu)$, $k_\nu^{(i)}(\mu)$ —attenuation, scattering and absorption coefficients for the i^{th} particle

respectively; N—number of aerosol particles in a unit volume (calculated concentration) and n_i—number of molecules in a unit volume. The ratio of these coefficients to the geometric cross section of the particle, called the effective attenuation factor K, scattering factor K_s and absorption factor K_a, depend on the chemical constitution and structure of aerosol particles and the medium (primarily the indices of refraction) as well as the relation between the size of the particle and the wavelength of radiation. For spherical particles we have the following :

$$K = \frac{k_a(\mu)}{\pi a^2}, \tag{2.16a}$$

$$K_s = \frac{\alpha_{\nu a}(\mu)}{\pi a^2}, \tag{2.16b}$$

$$K_a = \frac{k_\nu(\mu)}{\pi a^2}, \tag{2.16c}$$

the relative size of particles $\bar{\rho} = \frac{a\pi 2}{\lambda}$ and relative index of refraction $\tilde{m} = n + i\varkappa = \frac{\tilde{m}_m}{\tilde{m}_p}$, where $\tilde{m}_p$ and $\tilde{m}_m$ are complex indices of refraction of the particle and the medium respectively, n—usual refractive index, $\varkappa$—index of absorption for the material of the particle, a—radius of particle and λ—wavelength of incident radiation. The introduction of the supplementary condition of sphericity for the scattering particle in most cases does not lead to a large error in the computation since the scattering particle in the atmosphere possesses a form which does not differ basically from the spherical and is, moreover, oriented in a random manner.

The concept of the scattering coefficient of a particle in a given direction may be introduced for the characterization of the scattering properties of the particle at different angles from the direction of the incident wave. In practice a spatial picture of scattering of the incident radiation may be obtained by applying the concept of scattering function $\varkappa(\gamma)$ or the angular function of scattering which represents the ratio of intensity of radiation, fraction scattered in a given direction, to the flow of energy scattered in all directions as follows :

$$\varkappa(\gamma) = \frac{I_\nu(\gamma)}{\int\limits_{4\pi} I_\nu(\gamma)\, d\omega}, \tag{2.17}$$

where $I_\nu(\gamma)$—intensity of light scattered by a particle in the direction of angle γ and $d\omega$—element of solid angle.

The scattering function depends on the direction of polarization of the radiation, which in turn may change the polarization characteristics of the scattered radiation. The extent of polarization of scattered radiation is determined by the following expression, viz.

$$p_p = \frac{I_1 - I_2}{I_1 + I_2},$$

where I_1—intensity of radiation when the vibrations of the electric field vector are perpendicular to the plane of propagation of radiation and I_2—parallel to the plane of propagation of radiation.

A characterization of scattering properties of real atmosphere is of significance in the investigation of molecules of air and aerosol particles of relatively very small size ($\bar{\rho} \ll 1$), and for particles of a size comparable to the wavelength of the incident radiation. The scattering theory and the computation of characteristics of radiation scattered by these particles have been executed in detail in [6, 18, 20]. The fundamental derivations obtained in these references will be briefly considered.

3.1 Small particles and molecules of air

In order to obtain the asymptotic formulas for K and K_s in the case of particles with $\bar{\rho} \ll 1$, the expansions of Bessel's and Hankel's functions in powers of $\bar{\rho}$ entering into the expression for K and K_s can be employed. Since the index of refraction for the scattering particles $\tilde{m}$ is small in air, the inequality $|\tilde{m}|\bar{\rho} < 1$ holds and the appropriate expression for the effective attenuation factor is given by

$$K(\bar{\rho}, \tilde{m}) = \sum_{i}^{s} P_i \bar{\rho}^i, \tag{2.18}$$

where

$$P_1 = 4 \operatorname{Im}\left(\frac{1-\tilde{m}^2}{\tilde{m}^2+2}\right),$$

$$P_2 = 0,$$

$$P_3 = 2 \operatorname{Im}\left[\frac{-2(\tilde{m}^2-1)(\tilde{m}^2-2)}{(\tilde{m}^2+2)^2} + \frac{\tilde{m}^2-1}{15} - \frac{\tilde{m}^2-1}{3(2\tilde{m}^2+3)}\right],$$

$$P_4 = \frac{8}{3}\operatorname{Re}\left(\frac{\tilde{m}^2-1}{\tilde{m}^2+2}\right)^2,$$

$$P_5 = 2 \operatorname{Im}\left[\frac{3}{175}\frac{\tilde{m}^2-1}{\tilde{m}^2+2}\frac{\tilde{m}^6+20\tilde{m}^4-200\tilde{m}^2+200}{\tilde{m}^2-2} - \frac{1}{56}\frac{\tilde{m}^2-1}{3\tilde{m}^2+4} - \frac{(\tilde{m}^2-1)(2\tilde{m}^2-3)}{315}\right].$$

If the particle is transparent, then $\varkappa = 0$ and $\rho \ll 1$, so that the following equation holds, viz.

$$K(\bar{\rho}, \tilde{m}) = K_s(\bar{\rho}, \tilde{m}) = \frac{8}{3}\bar{\rho}^4\left(\frac{\tilde{m}^2-1}{\tilde{m}^2+2}\right)^2. \tag{2.19}$$

This expression is valid for Rayleigh's particles. The volume scattering coefficient for these particles is similarly inversely proportional to the fourth power of wavelength of the incident radiation and is directly proportional to the square of the volume of the scattering particle. The first member of the expansion in (2.18) will determine the magnitude of the effective attenuation factor in the case of absorbent particles. In this case the radiation attenuation coefficient is inversely proportional to the wavelength of the incident radiation. The following expression holds for the scattering function of small particles

$$\varkappa(\gamma) = \frac{4}{3}\bar{\rho}^4\left(\frac{\tilde{m}^2-1}{\tilde{m}^2+2}\right)^2 (1+\cos^2\gamma), \tag{2.20}$$

i.e. scattering is identical in the forward and backward directions.

The extent of polarization is determined by the following expression:

$$p_D = \frac{\sin^2\gamma}{1+\cos^2\gamma} \tag{2.21}$$

The numerical values of coefficients of molecular scattering have been derived in [46], and are given in Table 2.29 of the same article.

3.2 Large particles

Radiation attenuation and scattering functions of particles with $\bar{\rho} \gg 1$ may be looked upon as arising from geometrical optics and diffraction of incident radiation on the contours of particles. For the case of absorbent particles we have:

$$K(\bar{\rho}, \tilde{m}) = \frac{2-8\sqrt{n^2-\varkappa^2}}{(n+1)^2+\varkappa^2}\,\frac{n}{n+1}\,\frac{e^{-2\bar{\rho}\varkappa}}{\bar{\rho}} \times \sin 2\bar{\rho}(n-1)$$

$$-2\tan^{-1}\frac{\sqrt{n^2+\varkappa^2}}{\sqrt{n^2+\varkappa^2}+1}\,\frac{\varkappa}{\sqrt{n^2+\varkappa^2}+n}. \tag{2.22}$$

Table 2.29 Efficiency factor and molecular scattering coefficient at $T = 0°C$ and $p = 1013.25$ millibars [46]

$\lambda\ \mu$	k_λ (μ) cm^2	k_λ (m) cm^2.g^{-1}	$k_\lambda \times 10^8$ cm^{-1}	$\lambda\ \mu$	k_λ (μ) cm^2	k_λ (m) cm^2.g^{-1}	$k_\lambda \times 10^8$ cm^{-1}
0.20	3.551×10^{-25}	7.382×10^{-3}	954.2	0.48	7.961	1.655	21.40
0.21	2.802	5.826	753.1	0.49	7.316	1.521	19.66
0.22	2.244	4.666	603.1	0.50	6.735×10^{-27}	1.400×10^{-4}	18.10
0.23	1.836	3.818	493.4	0.51	6.211	1.291	16.69
0.24	1.511	3.142	406.1	0.52	5.736	1.193	15.42
0.25	1.258	2.616	338.2	0.53	5.307	1.103	14.26
0.26	1.057	2.199	284.2	0.54	4.917	1.022	13.21
0.27	8.959×10^{-26}	1.863	240.8	0.55	4.563×10^{-27}	9.486×10^{-5}	12.26
0.28	7.645	1.590	205.5	0.56	4.239	8.814	11.39
0.29	6.568	1.367	176.5	0.57	3.945	8.201	10.60
0.30	5.676	1.180	152.5	0.58	3.675	7.641	9.876
0.31	4.933	1.026	132.6	0.59	3.428	7.127	9.212
0.32	4.309	8.859×10^{-4}	115.8	0.60	3.202	6.657	8.604
0.33	3.782	7.863	101.6	0.61	2.994	6.224	8.045
0.34	3.334	6.931	89.59	0.62	2.802	5.826	7.531
0.35	2.951	6.135	79.29	0.63	2.626	5.460	7.057
0.36	2.622	5.450	70.45	0.64	2.464	5.122	6.620
0.37	2.337	4.860	62.82	0.65	2.313	4.810	6.217
0.38	2.091	4.348	56.20	0.66	2.175	4.521	5.844
0.39	1.877	3.902	50.43	0.67	2.046	4.254	5.498
0.40	1.689	3.512	45.40	0.68	1.927	4.006	5.178
0.41	1.525	3.170	40.98	0.69	1.816	3.776	4.881
0.42	1.380	2.869	37.08	0.70	1.713	3.562	4.605
0.43	1.252	2.603	33.65	0.71	1.618	3.364	4.348
0.44	1.139	2.368	30.60	0.72	1.529	3.179	4.109
0.45	1.038	2.158	27.89	0.73	1.446	3.006	3.886
0.46	9.482×10^{-27}	1.972	25.48	0.74	1.369	2.845	3.678
0.47	8.680	1.805	23.33	0.75	1.296	2.695	3.484

Table 2.29—*Contd.*

$\lambda\,\mu$	k_λ (μ) cm^2	k_λ (m) cm^2.g^{-1}	$k_\lambda \times 10^8$ cm^{-1}	$\lambda\,\mu$	k_λ (μ) cm^2	k_λ (m) cm^2.g^{-1}	$k_\lambda \times 10^8$ cm^{-1}
0.76	1.229	2.555	3.302	5.0	6.434×10^{-31}	1.338×10^{-9}	1.729×10^{-11}
0.77	1.166	2.423	3.132	5.5	4.394	9.136×10^{-9}	1.181
0.78	1.106	2.300	2.973	6.0	3.102	6.450	8.337×10^{-12}
0.79	1.051	2.185	2.824	6.5	2.252	4.683	6.053
0.80	9.989×10^{-28}	2.077×10^{-5}	2.684	7.0	1.582	3.289	4.251
0.90	6.212	1.292	1.670	7.5	1.271	2.642	3.414
1.00	4.065	8.452×10^{-6}	1.092	8.0	9.815×10^{-32}	2.041	2.637
1.10	2.771	5.761	0.7447	8.5	7.701	1.601	2.069
1.20	1.954	4.062	0.5250	9.0	6.127	1.274	1.647
1.30	1.417	2.946	0.3807	9.5	4.935	1.026	1.326
1.40	1.052	2.188	0.2828	10.0	4.020	8.358×10^{-10}	1.080
1.50	7.979×10^{-29}	1.659	0.2144	11.0	2.746	5.708	7.378×10^{-13}
1.60	6.160	1.281	0.1655	12.0	1.938	4.030	5.209
1.70	4.831	1.005	0.1298	13.0	1.407	2.926	3.782
1.80	3.842	7.988×10^{-7}	0.1033	14.0	1.046	2.175	2.812
1.90	3.094	6.432	0.08314	15.0	7.940×10^{-33}	1.651	2.134
2.0	2.519	5.238	0.06770	16.0	6.133	1.275	1.648
2.5	1.031	2.143	0.02770	17.0	4.813	1.001	1.293
3.0	4.968×10^{-30}	1.033	0.01335	18.0	3.829	7.961×10^{-11}	1.029
3.5	2.681	5.574×10^{-8}	0.007204	19.0	3.084	6.413	8.288×10^{-14}
4.0	1.571	3.267	0.004222	20.0	2.512	5.223	6.751
4.5	9.807×10^{-31}	2.039	0.002636				

If the particle is transparent, then the following equation holds, viz:

$$K_s(\bar{\rho}, \tilde{m}) = 2 - \frac{8n^2}{\bar{\rho}(n+1)^2(n-1)} \sin 2\bar{\rho}(n-1). \qquad (2.23)$$

The following simple expression for the effective attenuation factor of a large particle with complex index of refraction can be obtained for the case of "soft" particles, when $|\tilde{m}-1| \to 0$, from the following :

$$K(\bar{\rho}, \tilde{m}) = 2 - 4e^{-\bar{\rho}' \tan\beta} \frac{\cos\beta}{\bar{\rho}'} \sin(\bar{\rho}'-\beta) - 4e^{-\bar{\rho} \tan\beta} \left(\frac{\cos\beta}{\bar{\rho}'}\right)^2$$

$$\times \cos(\rho'-2\beta) + 4\left(\frac{\cos\beta}{\beta}\right)^2 \cos^2\beta, \qquad (2.24)$$

where $\bar{\rho}' = 2\bar{\rho}(n-1)$, $\tan\beta = \frac{\varkappa}{n-1}$.

The expression $K_s(\bar{\rho}, \tilde{m})$ for transparent "soft" particles is given by the following equation, viz:

$$K_p(\bar{\rho}, \tilde{m}) = 2 - \frac{4}{\bar{\rho}'} \sin\bar{\rho}' - \frac{4}{\bar{\rho}'^2}(1-\cos\bar{\rho}'). \qquad (2.25)$$

The computations for scattering functions for large transparent particles were carried out by K. S. Shifrin. Large particles with a wide range of values of $\bar{\rho}$ produce strong intensification in the scattering function, which may be expressed by the approximate formula:

$$\varkappa(\gamma) = \frac{1}{2}\left[\frac{\varkappa'(\gamma)}{2} + \bar{\rho}^2(1+\cos\gamma)^2 \frac{J_1^2(\bar{\rho}\sin\gamma)}{z(\bar{\rho}\sin\gamma)^2}\right], \qquad (2.26)$$

where $\varkappa'(\gamma)$ is part of the function determined by a pencil of light obeying the laws of geometrical optics, and which has been computed in [20] in steps of 5° for spheres with $\tilde{m}=1.33$ and J_1 is Bessel's function.

A large amount of computed material on the scattering function in the case of water particles is contained in [41].

Optical phenomena such as the rainbow and glory can be explained by the scattering of light by large transparent particles. The high degree of polarization of dispersed light in rainbows should be noted.

3.3 Transparent particles of different sizes

The solution of problems on scattered radiation of particles of non-absorbent substances in the general form is no simpler than for particles with a complex index of refraction. However, considerable simplification may be achieved in this case when the following inequalities hold :

$$\bar{\rho} \ll 1 \text{ or } \bar{\rho} \gg 1,$$
$$\tilde{m}-1 \ll 1 \text{ or } \tilde{m}-1 \gg 1,$$
$$\bar{\rho}(\tilde{m}-1) \ll 1 \text{ or } \bar{\rho}(\tilde{m}-1) \gg 1.$$

The computations of effective scattering factors (attenuation) for transparent particles are quite simple. Fig. 2.14 shows the curves for effective attenuation factors of scattering for several indices of refraction, whereas Table 2.30 gives the analogous characteristics for water in the visible region of the radiation spectrum ($\tilde{m}=1.33$), computed by Houghton and Chalker [37]. The computations for scattering functions are far more laborious. In atmospheric optics the computations for water particles and particles possessing an index of refraction equal to the mean index of refraction of atmospheric aerosol are of practical interest (20, 27, 31, 42]. Fig. 2.15 and Table 2.31 present these data for the visible part of the spectrum.

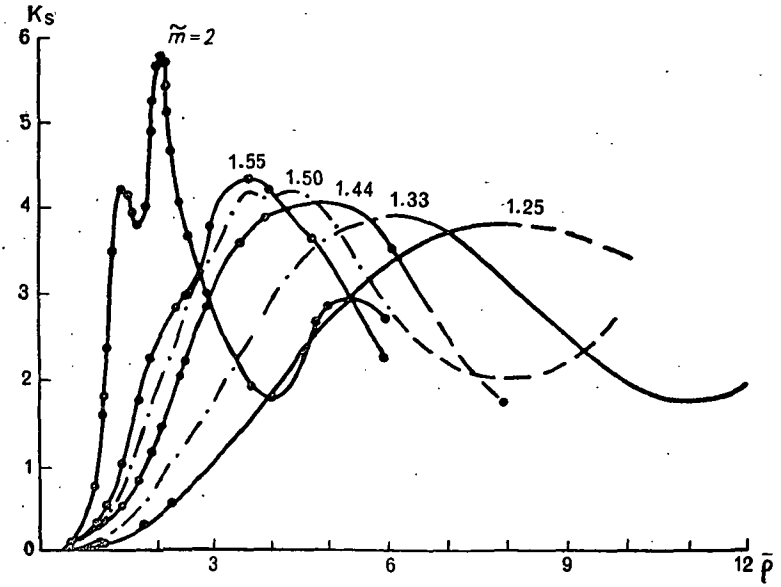

Fig. 2.14. Effective scattering factors for transparent particles with different indices of refraction [6].

Table 2.30 Effective attenuation of radiation for particles with $\tilde{m}=1.33$ [37]

$\tilde{\rho}$	K	$\tilde{\rho}$	K	$\tilde{\rho}$	K	$\tilde{\rho}$	K
0.5	0.00676	9.0	2.738	12.250	1.892	17.125	2.704
0.6	0.0138	9.5	2.394	12.333	1.936	17.25	2.822
1.0	0.0938	10.0	2.152	12.5	1.938	17.375	2.820
1.2	0.171	10.25	2.052	12.6	1.822	17.5	2.738
1.5	0.322	10.5	1.886	12.75	1.850	18.0	2.598
1.8	0.522	10.625	1.918	13.0	2.012	18.5	2.432
2.0	0.710	10.75	1.930	13.5	2.192	19.0	2.218
2.4	1.126	10.875	1.832	14.0	2.474	19.25	2.090
2.5	1.212	11.0	1.740	14.5	2.528	19.5	1.998
3.0	1.754	11.125	1.728	15.0	2.744	19.75	1.976
3.6	2.376	11.333	1.734	15.5	2.740	20.0	2.092
4.8	3.490	11.4	1.768	16.0	2.870	20.25	2.180
5.0	3.592	11.5	1.858	16.25	2.872	20.5	2.078
6.0	3.888	11.75	1.758	16.5	2.850	21.0	1.834
7.0	3.722	12.0	1.670	16.75	2.810	22.0	1.922
8.0	3.282	12.125	1.776	17.0	2.632	24.0	2.438

3.4 Particles with complex index of refraction

In the actual atmosphere other particles besides transparent aerosol particles may be present. It is possible to completely disregard the absorbent properties of atmospheric aerosol even in the visible region of the solar spectrum. It is more true in the case of the infrared region. Thus, the computation of effective attenuation, scattering and absorption factors, as of the scattering function for particles with a complex index of refraction, is of great interest. At present no data are available on the mean index of refraction of atmospheric aerosol in the infrared region. Assuming that the majority of aerosol particles may be either water particles or particles covered with a fine aqueous layer, the application of complex

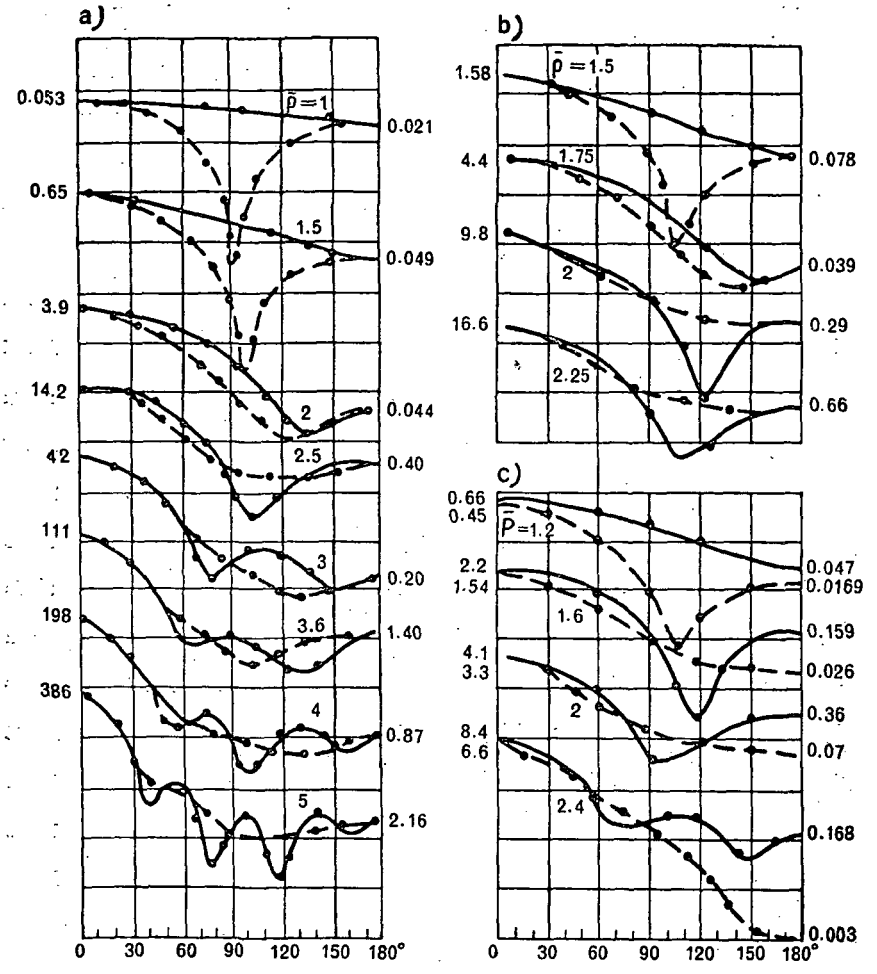

Fig. 2.15. Scattering functions for particles of different sizes

a) $\tilde{m}=1.3$, sphere ; b) $\tilde{m}=1.50$, sphere ; c) $\tilde{m}=1.50$, cylinder ;

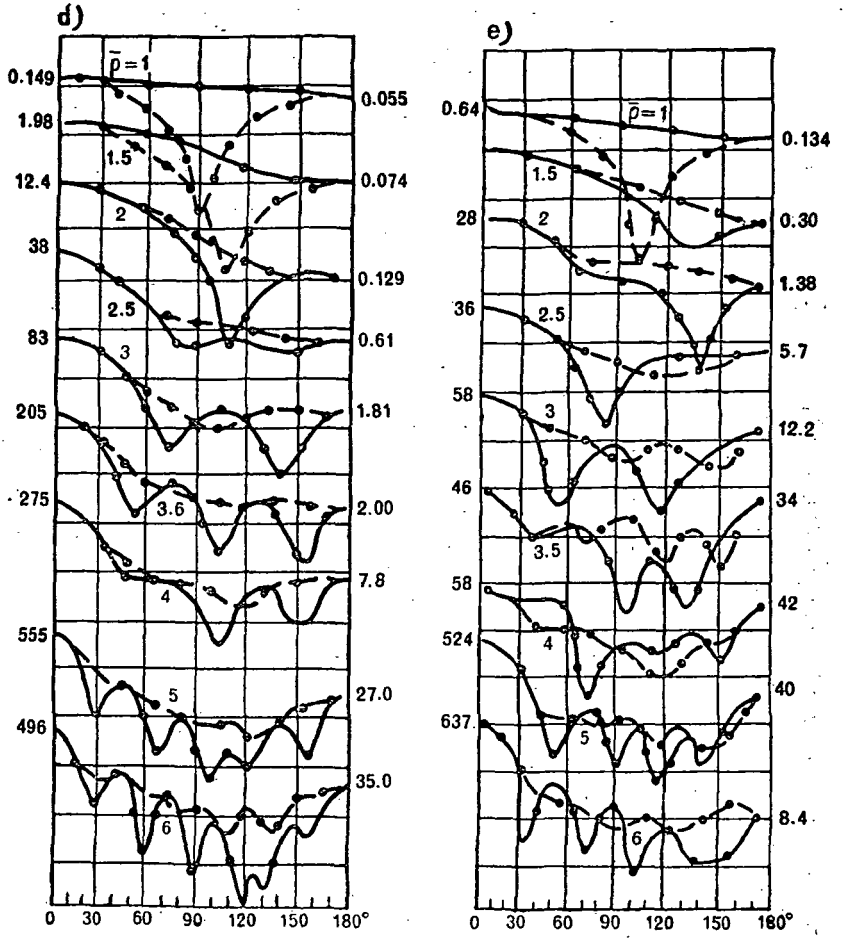

and with different indices of refraction.

d) $\tilde{m}=1.55$, sphere ; e) $\tilde{m}=2$, sphere [20]

Table 2.31 Scattering functions of water droplets $\varkappa(\gamma)$ and p_p [20]

$\gamma°$	$\tilde{\rho}$									
	0.1		1.5		3		4		6	
	$\varkappa$	p_p	$\varkappa$	p_p	$\varkappa$	p_p	$\varkappa$	p_p	$\varkappa$	p_p
0	0.4252	0.000	0.6606	0.000	42.519	0.000	125.240	0.00	1237.15	0
10	0.4188	0.0152	0.6426	0.0125	39.455	0.0070	114.645	− 0.08	908.35	0.4
20	0.4002	0.0614	0.5916	0.0507	31.459	0.0271	80.273	− 1.30	343.15	− 3.1
30	0.3719	0.1422	0.5664	0.1163	21.402	0.0568	44.255	− 3.60	56.82	−25.8
40							18.853	−10.30	28.22	−11.6
45	0.3188	0.3326	0.3840	0.2711	8.618	0.0945				
50							6.549	−15.40	27.88	9.2
60	0.02654	0.5989	0.2606	0.4948	2.134	−0.0095	2.005	− 2.71	4.51	−64.2
70	0.02372	0.7892	0.1950	0.6706	0.658	−0.3866	2.522	−20.95	4.16	−45.4
80	0.2187	0.9405	0.1451	0.8409	0.332	−0.4821	0.533	81.36	6.05	29.7
90	0.2120	1.000	0.1098	0.9645	0.408	0.2095	1.622	68.17	3.46	1.2
100	0.2180	0.9426	0.0863	0.9974	0.497	0.5714	0.841	−15.18		
110	0.2363	0.7922	0.0714	0.9205	0.477	0.7161	1.277	−95.63	3.15	45.7
120	0.2644	0.6015	0.0624	0.7552	0.363	0.7538	0.771	−13.95		
130							0.612	−13.45	0.20	71.7
135	0.3171	0.3343	0.0551	0.4557	0.184	0.5934				
140							0.654	14.47		
150	0.3699	0.1437	0.0516	0.2032	0.169	0.0695	1.429	34.02	5.24	26.9
160	0.3982	0.0625	0.0504	0.0896	0.147	−0.0520	3.462	21.21		
170	0.04164	0.0151	0.0498	0.0222	0.190	−0.0020	5.416	5.06	2.26	−15.1
180	0.4227	0.000	0.0496	0.000	0.210	0.000	7.350	0.00		

γ°	$\tilde{\rho}$									
	8		10		15		20		30	
	$\varkappa$	p_p	$\varkappa$	p_p	$\varkappa$	p_p	$\varkappa$	p_p	$\varkappa$	p_p
0	2922.05	0.00	2768.31	0	22781.35	0.00	45871.00	0.00	195719	0.00
10	1499.30	− 5.6	635.98	− 2.2	4036.17	11.0	1210.00	−26.5	9560.58	7.1
20	358.81	− 8.0	237.20	−16.6	228.66	31.2	685.04	− 6.3		
30	145.22	9.4	164.26	− 6.2	16.070	−14.6	226.03	−51.9	1034.20	− 0.8
40	66.48	−36.8	82.28	−28.9	227.08	−12.3	157.72	−72.7		
50	28.68	15.8	62.03	18.8	104.57	10.8	128.51	82.7	333.09	−10.6
60	59.81	−17.3	36.12	−41.4	44.04	−20.0	67.03	−76.2	97.90	−81.9
70	15.71	−89.3	22.94	55.3	59.34	−92.4	22.76	−68.0		
80	3.48	−20.4	31.75	−63.9	27.54	−70.6	16.42	−85.8	34.30	−81.4
90	7.58	35.3	4.87	8.6			29.92	−85.8	24.20	25.1
100	3.03	−43.0	18.50	−94.6	16.88	−42.4	23.88	−81.5	7.25	−37.1
110	8.77	−75.4	8.78	−22.3	12.64	−26.8	4.03	−27.1		
120	12.77	−18.1	22.57	45.3	15.40	−11.0	18.07	33.2	23.75	25.1
130	14.53	−81.5	2.73	− 7.8	8.82	−36.6	58.13	−16.2	39.25	−15.2
140	4.55	−18.0	44.95	35.3	27.47	−99.2	48.48	−20.4		
150	8.31	46.2	33.28	−88.5	13.14	75.4	34.50	88.6	97.91	43.7
160	11.38	59.1	49.23	58.7	24.44	−48.3	108.71	−10.6		
170	5.63	−25.2	16.94	66.6	136.74	−57.2	223.92	−90.6	173.30	58.4
180	38.20	0.00	19.99	0.00						

index of refraction of water is sufficiently justified. The complex index of refraction of water has been measured by many researchers [11, 13, 29]. Table 2.32 gives these values.

Table 2.32 Complex index of refraction and absorption coefficient of water [11, 13, 29]

λ_μ	n	k	$\varkappa$	λ_μ	n	k	$\varkappa$
0.20	1.424	8.0×10^{-2}	1.3×10^{-7}	1.20	1.323	1.020	9.74
0.25	1.377	3.0	6.0×10^{-8}	1.25	1.322	0.890	8.85
0.30	1.359	1.5	3.6	1.258	1.322	0.88	8.80
0.35	1.349	3.0×10^{-3}	8.0×10^{-9}	1.30	1.321	1.08	11.17
0.40	1.343	1.0	3.0	1.35	1.320	2.70	29.00
0.45	1.339	2.0×10^{-4}	7.0	1.40	1.320	13.00	14.48×10^{-5}
0.50	1.336	2.5	8.0	1.45	1.319	26.0	3.00×10^{-4}
0.55	1.334	3.5	1.5×10^{-9}	1.50	1.318	17.3	2.065
0.60	1.332	1.5×10^{-3}	7.0	1.55	1.317	9.6	1.184
0.65	1.331	2.5	1.3×10^{-8}	1.60	1.316	6.2	7.89×10^{-5}
0.70	1.330	6.0	3.3	1.65	1.316	5.1	6.70
0.75	1.329	2.5	1.49×10^{-7}	1.66	1.315	5.0	6.6×10^{-5}
0.76	1.329	2.6×10^{-2}	1.50	1.70	1.315	5.15	6.97
0.80	1.328	2.1	1.34	1.75	1.314	6.4	8.91
0.806	1.328	2.0	1.20	1.80	1.312	8.0	1.146×10^{-4}
0.85	1.327	4.1	2.77	1.85	1.311	9.5	1.399
0.90	1.328	6.7	4.80	1.90	1.309	80.5	1.217×10^{-3}
0.95	1.327	3.65×10^{-1}	2.76×10^{-6}	1.94	1.307	114.0	1.76
0.97	1.327	4.3	3.55	1.95	1.307	110.0	1.707
1.00	1.326	3.55	2.82	2.00	1.304	68.0	1.082
1.05	1.325	1.31	1.10	2.05	1.302	41.0	6.689×10^{-4}
1.06	1.325	1.28	1.07	2.10	1.300	26.0	4.345
1.10	1.324	1.90	1.66	2.15	1.296	19.0	3.25
1.15	1.3235	8.00	7.32	2.20	1.293	16.0	2.8
1.19	1.323	1.05×10^{0}	9.90	2.21	1.292	15.5	2.72

Table 2.32—*Contd.*

λ_μ	n	k	$\varkappa$	λ_μ	n	k	$\varkappa$
2.25	1.290	17.0	3.04×10^{-4}	8.00	1.293	566	3.603×10^{-2}
2.30	1.286	23.0	4.21	8.50	1.286	557	3.768
2.35	1.282	30.0	5.61	9.00	1.269	566	4.054
2.40	1.276	42.0	8.02	9.50	1.245	579	4.377
2.45	1.270	61.0	1.189×10^{-3}	10.00	1.214	668	5.316
2.50	1.246	83.0	1.651	10.50	1.185	826	6.900
2.55	1.213	97.0	1.968	11.00	1.151	1165	1.021×10^{-1}
2.60	1.180	99.0	2.048	11.50	1.145	1672	1.53
2.625	1.160	109.0	2.277	12.00	1.160	2191	2.092
2.65	1.140	131.0	2.763	12.50	1.19	2451	2.438
2.70	1.134	235.0	5.049	13.0	1.220	2821	2.918
2.75	1.133	1.100	2.401×10^{-2}	13.5	1.245	2980	3.202
2.80	1.232	4.212	9.361	14.0	1.275	3215	3.582
2.90	1.310	10.580	2.435×10^{-1}	15.0	1.330	3601	4.298
2.95	1.325	11.700	2.740	16.0	1.400	3211	4.088
3.00	1.351	10.860	2.586	17.5	1.485	2840	3.955
3.10	1.426	7.430	1.826	18.0	1.535	2750	3.939
3.20	1.509	3.700	9.422×10^{-2}	18.5	1.606		
3.30	1.470	1.650	4.333	19.0	1.681		
3.40	1.449	698.0	1.888	20.0	1.722	2450	3.899
3.50	1.423	334.0	9.300×10^{-3}	25.0	1.690	1877	3.734
3.60	1.402	198.0	5.670	30.0	1.652	1411	3.368
3.75	1.372	119	3.55×10^{-3}	33.0	1.636		
3.83	1.358	111	3.38	35.0	1.615	1211	3.373
4.00	1.349	151	4.81	40.0	1.577	1194	3.8007
4.50	1.341	411	1.472×10^{-2}	42.0	1.567	1211	4.0476
4.66	1.338	468	1.736	50.0	1.590	1298	5.1647
4.80	1.336	431	1.647	52.0	1.609		
5.00	1.331	308	1.225	60.0	1.670	1245	5.9446
5.26	1.318	229	9.59×10^{-3}	63.0	1.696		
5.50	1.303	276	1.208×10^{-2}	75.0	1.760	939	5.6044
5.80	1.266	699	3.226	83.0	1.801	800	5.284
6.00	1.313	2138	1.028×10^{-1}	100.0	1.878	665	5.292
6.05	1.324	2328	1.1208	117.0	1.942	540	5.025
6.40	1.347	852	4.339×10^{-2}	150.0	1.995	412	4.9187
6.50	1.338	794	4.107	152.0	1.996		
7.00	1.323	618	3.443	200.0	2.025	326	0.51886
7.50	1.303	579	3.456				

Effective attenuation, scattering and absorption factors for water particles as computed by Deirmendjian, Herman, Shifrin and others [9, 20, 26, 36] are given in Figs. 2.16 and 2.17.

Deirmendjian selected an approximate expression valid for different values of $\bar{\rho}$ and complex $\tilde{m}$ satisfying the condition $|\tilde{m}|<2$ for the computation of $K(\bar{\rho}, \tilde{m})$ as follows :

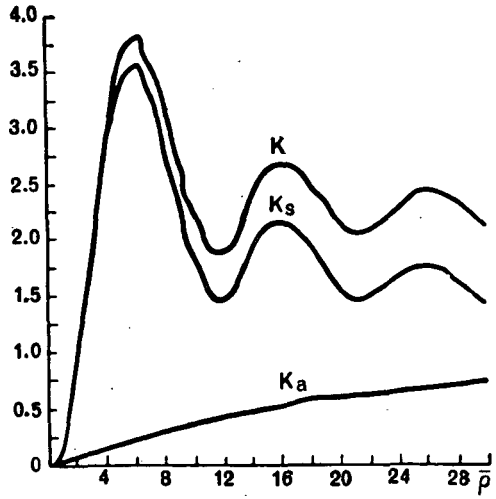

Fig. 2.16. Effective attenuation scattering and absorption factors for water aerosol at $\lambda=5\ \mu$, $\tilde{m}=1.330$, $(1\text{-}0.0074\ i)$ [36].

$$K\ (\bar{\rho},\ \tilde{m})=(1+D)\ F, \tag{2.27a}$$

where F is determined from formula (2.24), obtained by Van der Hulst for large "soft" particles, and $(1+D)$—an approximate factor given by the following :

$$D\ (\bar{\rho},\ \tilde{m})=D_1=\frac{n-1}{2n}\ \frac{5(n-1)}{4.08}\ [f(\beta)+1]\ -\ \frac{5\ (n-1)-\bar{\rho}'}{5\ (n-1)\ f(\beta)}\ , \tag{2.27b}$$

for the region

$$\bar{\rho}'\leqslant 5\ (n-1)\leqslant\ \frac{4.08}{1+3\ \tan\ \beta}$$

$$D\ (\bar{\rho},\ \tilde{m})=D_2=\frac{n-1}{2n}\ [f(\beta)+1]\ \ \frac{\bar{\rho}'}{4.08}\ , \tag{2.27c}$$

for the region

$$5\ (n-1)\leqslant \bar{\rho}'\leqslant\ \frac{4.08}{1+3\ \tan\beta}$$

$$D\ (\bar{\rho},\ \tilde{m})=D_3=\ \frac{n-1}{2n}\ \frac{f(\beta)+1}{1+3\ \tan\ \beta}\ , \tag{2.27d}$$

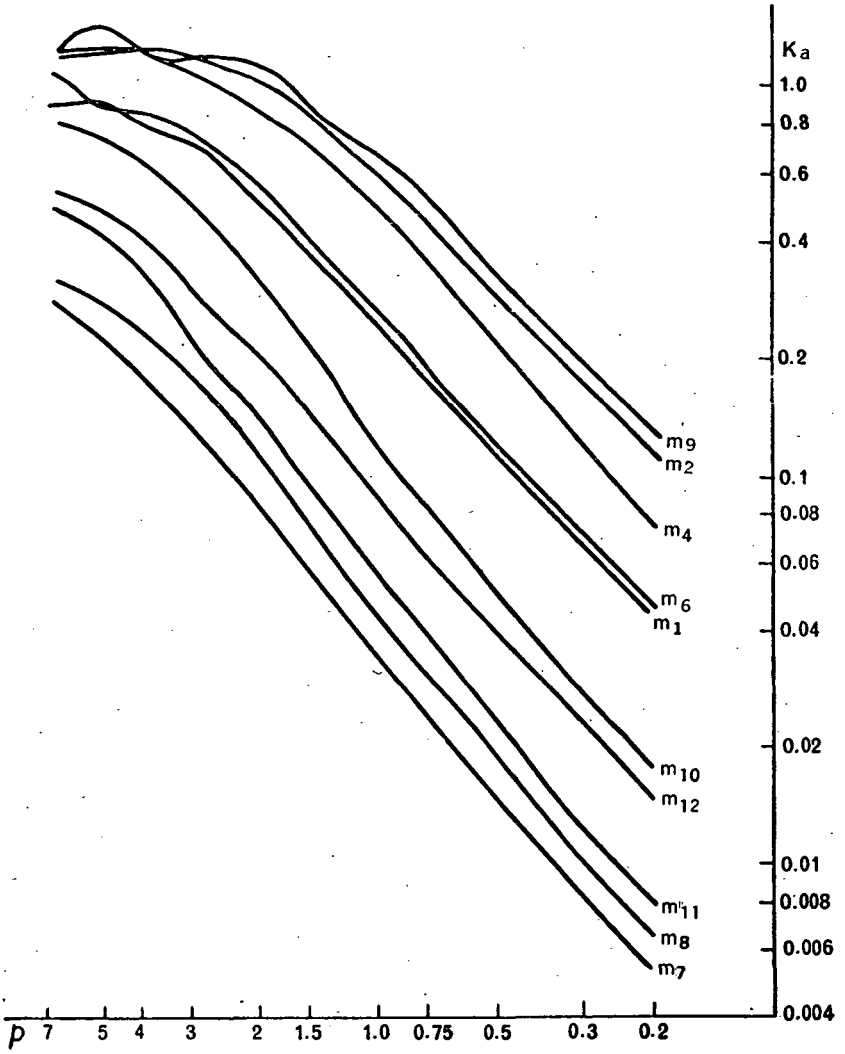

Fig. 2.17. Effective absorption factor $K_a(\rho)$ for particles with different complex indices of refraction ($m_1=1.23-0.094\,i$; $m_2=1.31-0.244\,i$: $m_4=1.43-0.183\,i$; $m_6=1.31-0.1\,i$; $m_7=1.33-0.012\,i$; $m_8=1.34-0.015\,i$; $m_9=1.33-0.274\,i$; $m_{10}=1.47-0.019\,i$; $m_{11}=1.45-0.019\,i$; $m_{12}=1.27-0.0326\,i$) [9].

for the region

$$\frac{4.08}{1+3\tan\beta} \leqslant \bar{\rho}' \leqslant \frac{4.08}{1+\tan\beta}$$

$$\Gamma(\bar{\rho}, \tilde{m}) = D_4 = \frac{n-1}{2n} \frac{f(\beta)+1}{f(\beta} \frac{4.08}{\bar{\rho}'}, \qquad (2.27e)$$

when $\bar{\rho}' > \dfrac{4.08}{1+\tan\beta}$,

where $f(\beta)=(1+\tan\beta)\,(1+3\tan\beta)$, and $\bar{\rho}'$ and β have been defined earlier for the formula (24).

The difference between the computations made from the exact formulas of Mie and from Deirmendjian's approximate expressions does not exceed 4%.

A complete characterization of the scattering properties of aerosol particles of varying chemical compositions and different sizes is given in the tables of Shifrin and Zel'manovich : cross section of absorption and scattering and absorption of particles with $\bar{\rho}$, from 0.5 to 100 and with different complex refractive indices, all components of scattering matrices for twelve values of refractive indices corresponding to these values of $\bar{\rho}$ as well as the electric vector which may be employed for the computation of scattering functions for different aerosol particles [22].

3.5 Polydispersional aerosol

For systems of polydispersional aerosol particles the volume attenuation coefficient k_{va} depends on the estimated particle concentration N, distribution functions of particles according to size and the effective attenuation factor $K(\bar{\rho}, \tilde{m})$ for each particle, whereas the scattering function for a system of particles will be determined by the size distribution functions of particles and the scattering function of each particle as follows:

$$k_{va} = \int_0^\infty \pi a^2 K(\bar{\rho}, \tilde{m})\, Nf(a)\, da, \tag{2.28}$$

where $f(a)$—normalized size distribution function of particles.

The magnitude representing the ratio of the volume attenuation coefficient to the area of cross section of all particles in a unit of volume of polydispersional aerosol will be called the mean effective attenuation factor (this value coincides with effective attenuation for monodispersional aerosol) and is given by the following:

$$\overline{K}(\tilde{m}, \bar{a}) = \frac{\displaystyle\int_0^\infty \pi a^2 K(\bar{\rho}, \tilde{m})\, Nf(a)\, da}{\displaystyle\int_0^\infty \pi a^2 f(a)\, da}. \tag{2.29}$$

For the computation of $k_{\nu a}$, $\overline{K}$ and scattering function of polydispersional aerosol, which best describe the true composition of atmospheric aerosol, it is necessary to know the function expressing size distribution of the particles. In storms and clouds the size distribution of particles is described satisfactorily by the following logarithmic normalized function:

$$f(a) = \frac{1}{\sqrt{\pi}\, t} \frac{1}{r} e^{-\frac{t}{4} - \frac{1}{t} (\ln \xi)^2} \tag{2.30}$$

(where $\xi = \frac{a}{r}$, r is most probable radius, t—parameter) and Gamma function

$$f(a) = \frac{1}{\Gamma(\mu + 1)} \mu^{\mu+1} \frac{a^{\mu}}{r^{\mu+1}} e^{-\mu \frac{a}{r}}, \tag{2.31}$$

where $\Gamma(\mu + 1)$ is the Gamma function, equal to $\mu!$ for all μ; r and μ—parameters.

Gamma distribution may be a particular case of Khrgian-Mazin distribution as follows:

$$f(a) = Aa^2 e^{-ba}, \tag{2.32}$$

which is obtained on the basis of numerous experimental data on the spectrum of cloud particles.

It is shown in [7] that the computations of mean effective attenuation factors with the application of the first two distributions coincide within 1-3%. The particle distribution of atmospheric aerosol in the layer above the ground can be satisfactorily described by Young's power function

$$f(a) = Ce^{-b_1 a}, \tag{2.33}$$

where the power b_1 may change from 2 to 6.

A more detailed study of the size distribution of particles shows that there exists a minimum concentration of particles in the range of 0.2-0.6 μ [8, 28]. However, the majority of calculations for coefficient of aerosol attenuation of radiation and scattering function are made for Young's distribution [21, 23]. Several researchers have employed Rokar's and Best's distribution for their computations besides the sums of different gamma distributions [21, 37]. The scattering function of aerosol at the ground (Table 2.33), obtained in [21] for particles with refractive indices 1.33; 1.44; 1.50 and 2.05 for Young's distribution are of practical

Table 2.33 Scattering functions for radiation in polydispersional aerosol with particle size distribution according to Young's measurements [21]

γ°	$\tilde{m} = 1.33$, $\tilde{\rho}_{max} = 80$								
	$b_1 = 4$			$b_1 = 5$			$b_1 = 6$		
	$\tilde{\rho}_{min} = 0.5$ $\tilde{\rho}_{av} = 0.75$	$\tilde{\rho}_{min} = 1$ $\tilde{\rho}_{av} = 1.5$	$\tilde{\rho}_{min} = 2$ $\tilde{\rho}_{av} = 3$	$\tilde{\rho}_{min} = 0.5$ $\tilde{\rho}_{av} = 0.66$	$\tilde{\rho}_{min} = 1$ $\tilde{\rho}_{av} = 1.33$	$\tilde{\rho}_{min} = 2$ $\tilde{\rho}_{av} = 2.7$	$\tilde{\rho}_{min} = 0.5$ $\tilde{\rho}_{av} = 0.62$	$\tilde{\rho}_{min} = 1$ $\tilde{\rho}_{av} = 1.25$	$\tilde{\rho}_{min} = 2$ $\tilde{\rho}_{av} = 2.5$
0	7.470	7.630	8.233	1.696	1.820	2.436	0.6486	0.7969	1.328
1	5.300	5.300	5.800	1.500	1.600	2.200	0.6300	0.7750	1.300
2	3.500	3.550	3.900	1.350	1.450	2.000	0.6150	0.7600	1.280
3	2.700	2.750	2.800	1.200	1.300	1.800	0.6000	0.7400	1.250
4	2.200	2.250	2.300	1.100	1.150	1.650	0.5900	0.7250	1.230
5	1.850	1.900	2.000	1.000	1.050	1.500	0.5800	0.7050	1.190
6	1.600	1.650	1.700	0.9500	1.000	1.400	0.5650	0.6900	1.150
7	1.400	1.500	1.550	0.9200	0.9500	1.300	0.5550	0.6750	1.120
8	1.300	1.350	1.400	0.9100	0.9300	1.250	0.5400	0.6550	1.080
9	1.250	1.300	1.350	0.9000	0.9200	1.200	0.5300	0.6450	1.040
10	1.210	1.232	1.297	0.8590	0.9127	1.167	0.5174	0.6247	0.9917
20	0.05762	0.5850	0.5986	0.5078	0.5335	0.6446	0.3716	0.4335	0.6340
30	0.2981	0.3011	0.2959	0.3004	0.3101	0.3453	0.2569	0.2889	0.3737
40	0.1599	0.1602	0.1493	0.1780	0.1794	0.1783	0.1753	0.1869	0.2041

Table 2.33—*Contd.*

γ°	$\tilde{m} = 1.33$, $\tilde{\rho}_{max} = 80$								
	$b_1 = 4$			$b_1 = 5$			$b_1 = 6$		
	$\tilde{\rho}_{min} = 0.5$ $\tilde{\rho}_{av} = 0.75$	$\tilde{\rho}_{min} = 1$ $\tilde{\rho}_{av} = 1.5$	$\tilde{\rho}_{min} = 2$ $\tilde{\rho}_{av} = 3$	$\tilde{\rho}_{min} = 0.5$ $\tilde{\rho}_{av} = 0.66$	$\tilde{\rho}_{min} = 1$ $\tilde{\rho}_{av} = 1.33$	$\tilde{\rho}_{min} = 2$ $\tilde{\rho}_{av} = 2.7$	$\tilde{\rho}_{min} = 0.5$ $\tilde{\rho}_{av} = 0.62$	$\tilde{\rho}_{min} = 1$ $\tilde{\rho}_{av} = 1.25$	$\tilde{\rho}_{min} = 2$ $\tilde{\rho}_{av} = 2.5$
50	0.08519	0.08435	0.07267	0.1066	0.1039	0.08844	0.1204	0.1205	0.1065
60	0.04734	0.04610	0.03590	0.06653	0.06223	0.04430	0.08478	0.07918	0.05550
70	0.02575	0.2441	0.01919	0.04483	0.04025	0.02478	0.06240	0.05439	0.03132
80	0.02161	0.02044	0.01493	0.03333	0.02893	0.01725	0.04830	0.03920	0.01974
90	0.01522	0.01405	0.09917	0.02382	0.02021	0.01067	0.03899	0.02886	0.01177
100	0.01002	0.008820	0.005449	0.01926	0.01452	0.006205	0.03386	0.02260	0.007044
110	0.01044	0.009268	0.006630	0.01792	0.01318	0.006282	0.03158	0.02008	0.006070
120	0.009452	0.008146	0.005765	0.01756	0.01215	0.005750	0.03295	0.01904	0.005594
130	0.01038	0.008986	0.006799	0.01811	0.01218	0.006046	0.03463	0.01902	0.005647
140	0.01213	0.01065	0.008604	0.01934	0.01289	0.006919	0.03698	0.01970	0.006240
150	0.01128	0.01034	0.008938	0.02062	0.01370	0.007776	0.03952	0.02077	0.007326
160	0.01544	0.01382	0.01192	0.02244	0.01521	0.009592	0.04178	0.02192	0.008629
170	0.01682	0.01517	0.01332	0.02315	0.01566	0.01003	0.04323	0.02264	0.009368
180	0.02092	0.01934	0.01783	0.02451	0.01704	0.01188	0.04399	0.02321	0.01029

Table 2.33—*Contd.*

$\tilde{m} = 1\ 50$, $\tilde{\rho}_{max} = 150$

γ°	$b_1 = 3$				$b_1 = 4$				$b_1 = 5$	
	$\tilde{\rho}_{min} = 0.2$ $\tilde{\rho}_{av} = 0.4$	$\tilde{\rho}_{min} = 0.6$ $\tilde{\rho}_{av} = 1.2$	$\tilde{\rho}_{min} = 1$ $\tilde{\rho}_{av} = 2$	$\tilde{\rho}_{min} = 2$ $\tilde{\rho}_{av} = 4$	$\tilde{\rho}_{min} = 0.2$ $\tilde{\rho}_{av} = 0.3$	$\tilde{\rho}_{min} = 0.6$ $\tilde{\rho}_{av} = 0.9$	$\tilde{\rho}_{min} = 1$ $\tilde{\rho}_{av} = 1.5$	$\tilde{\rho}_{min} = 2$ $\tilde{\rho}_{av} = 3$	$\tilde{\rho}_{min} = 0.2$ $\tilde{\rho}_{av} = 0.27$	$\tilde{\rho}_{min} = 0.6$ $\tilde{\rho}_{av} = 0.8$
0	89.42	89.50	89.89	94.26	8.191	8.260	8.537	10.37	1.032	1.083
1	39.69	39.72	39.89	41.82	5.335	5.350	5.528	6.652	0.9496	0.9955
2	11.91	11.92	11.97	12.54	3.129	3.156	3.258	3.796	0.8574	0.8981
3	5.868	5.873	5.899	6.170	2.321	2.339	2.414	2.751	0.7986	0.8360
4	3.603	3.605	3.619	3.779	1.916	1.934	1.995	2.278	0.7799	0.8163
5	2.488	2.491	2.500	2.606	1.625	1.639	1.327	1.899	0.7188	0.7517
6	1.839	1.841	1.849	1.922	1.437	1.449	1.493	1.658	0.6878	0.7192
7	1.465	1.467	1.473	1.528	1.299	1.309	1.348	1.480	0.6601	0.6898
8	1.248	1.248	1.253	1.298	1.194	1.203	1.239	1.345	0.6337	0.6630
9	1.047	1.048	1.052	1.088	1.104	1.112	1.145	1.229	0.6104	0.6375
10	0.8829	0.8835	0.8867	0.9142	1.026	1.0339	1.063	1.130	0.5871	0.6128
20	0.3783	0.3786	0.3795	0.3837	0.6077	0.6118	0.5913	0.6084	0.3972	0.4126
30	0.2177	0.2177	0.2182	0.2164	0.4026	0.4050	0.4141	0.3705	0.2706	0.2793
40	0.1353	0.1353	0.1354	0.1319	0.2758	0.2769	0.2827	0.2368	0.1848	0.1798
50	0.08050	0.08050	0.08040	0.07655	0.1792	0.1799	0.1826	0.1415	0.1218	0.1236
60	0.04916	0.04914	0.04896	0.04561	0.1167	0.1170	0.1180	0.08605	0.08147	0.08161

Table 2.33—*Contd.*

	$\tilde{m} = 1.50$, $\tilde{\rho}_{max} = 150$									
γ°	$b_1 = 3$				$b_1 = 4$				$b_1 = 5$	
	$\tilde{\rho}_{min} = 0.2$ $\tilde{\rho}_{av} = 0.4$	$\tilde{\rho}_{min} = 0.2$ $\tilde{\rho}_{av} = 1.2$	$\tilde{\rho}_{min} = 1$ $\tilde{\rho}_{av} = 2$	$\tilde{\rho}_{min} = 2$ $\tilde{\rho}_{av} = 4$	$\tilde{\rho}_{min} = 0.2$ $\tilde{\rho}_{av} = 0.3$	$\tilde{\rho}_{min} = 0.6$ $\tilde{\rho}_{av} = 0.9$	$\tilde{\rho}_{min} = 1$ $\tilde{\rho}_{av} = 1.5$	$\tilde{\rho}_{min} = 2$ $\tilde{\rho}_{av} = 3$	$\tilde{\rho}_{min} = 0.2$ $\tilde{\rho}_{av} = 0.27$	$\tilde{\rho}_{min} = 0.6$ $\tilde{\rho}_{av} = 0.8$
70	0.03312	0.03310	0.03292	0.03043	0.07684	0.04184	0.07699	0.05442	0.05644	0.05571
80	0.02077	0.02073	0.02053	0.01871	0.04949	0.04969	0.04921	0.03391	0.03877	0.03960
90	0.01491	0.01488	0.01468	0.01344	0.03423	0.03397	0.03316	0.02346	0.03192	0.03037
100	0.01012	0.01021	0.01050	0.009118	0.02420	0.02386	0.02279	0.01656	0.02665	0.02478
110	0.008269	0.008200	0.007958	0.007316	0.01950	0.01878	0.01720	0.01308	0.02667	0.02320
120	0.007854	0.007783	0.007555	0.007080	0.01676	0.01626	0.01481	0.01178	0.02316	0.02052
130	0.007444	0.007393	0.007146	0.006730	0.01643	0.01236	0.01424	0.01149	0.02355	0.02054
140	0.01071	0.009809	0.009548	0.009257	0.01883	0.01819	0.01648	0.01398	0.02509	0.01191
150	0.01436	0.01430	0.01404	0.01394	0.02234	0.02206	0.02031	0.01797	0.02520	0.02344
160	0.04135	0.04127	0.04113	0.04229	0.03024	0.02958	0.02795	0.02666	0.02973	0.02568
170	0.04687	0.04685	0.04671	0.04812	0.03500	0.03434	0.03278	0.03206	0.03215	0.02879
180	0.05349	0.05347	0.05335	0.05508	0.04232	0.04171	0.04037	0.04130	0.03545	0.03138

Table 2.33—*Contd.*

$\tilde{m} = 1.50$, $\tilde{\rho}_{max} = 150$

$\gamma°$	$b_1 = 5$		$b_1 = 6$				$b_1 = 8$			
	$\tilde{\rho}_{min} = 1$ $\tilde{\rho}_{av} = 1.33$	$\tilde{\rho}_{min} = 2$ $\tilde{\rho}_{av} = 2.7$	$\tilde{\rho}_{min} = 0.2$ $\tilde{\rho}_{av} = 0.25$	$\tilde{\rho}_{min} = 0.6$ $\rho_{av} = 0.75$	$\tilde{\rho}_{min} = 1$ $\tilde{\rho}_{av} = 1.25$	$\tilde{\rho}_{min} = 2$ $\tilde{\rho}_{av} = 2.5$	$\tilde{\rho}_{min} = 0.2$ $\tilde{\rho}_{av} = 0.23$	$\tilde{\rho}_{min} = 0.6$ $\tilde{\rho}_{av} = 0.7$	$\tilde{\rho}_{min} = 1$ $\tilde{\rho}_{av} = 1.2$	$\tilde{\rho}_{min} = 2$ $\tilde{\rho}_{av} = 2.3$
0	1.195	1.746	0.4012	0.4637	0.5616	0.9336	0.1461	0.2202	0.3215	0.5762
1	1.095	1.587	0.3991	0.4627	0.5626	0.9306	0.1461	0.2202	0.3213	0.6741
2	0.9876	1.393	0.3947	0.4599	0.5590	0.9223	0.1460	0.2199	0.3209	0.6723
3	0.9177	1.298	0.3901	0.4554	0.5531	0.9093	0.1458	0.2195	0.3201	0.6692
4	0.8959	1.263	0.3850	0.4490	0.5460	0.8940	0.1461	0.2212	0.3248	0.7011
5	0.8235	1.147	0.3800	0.4432	0.5370	0.8733	0.1453	0.2182	0.3178	0.6595
6	0.7868	1.088	0.3738	0.4360	0.5275	0.8526	0.1449	0.2174	0.3160	0.6530
7	0.7540	1.036	0.3677	0.4284	0.5176	0.8308	0.1445	0.2164	0.3142	0.6456
8	0.7240	0.9877	0.3613	0.4205	0.5072	0.8083	0.1441	0.2153	0.3121	0.6372
9	0.6954	0.9428	0.3548	0.4124	0.4967	0.7855	0.1435	0.2141	0.3096	0.6281
10	0.6677	0.8990	0.3481	0.4041	0.4858	0.7621	0.1429	0.2128	0.3071	0.6180
20	0.6677	0.8990	0.3481	0.4041	0.4858	0.7621	0.1429	0.2128	0.3071	0.6180
30	0.2964	0.3360	0.2141	0.2399	0.2744	0.3428	0.1221	0.1684	0.2257	0.3476
40	0.1977	0.2011	0.1617	0.1770	0.1960	0.2104	0.1080	0.1413	0.1796	0.2262
50	0.1260	0.1106	0.1194	0.1270	0.1349	0.1193	0.09349	0.1152	0.07493	0.1355
60	0.08077	0.05870	0.08830	0.09082	0.09193	0.06539	0.08027	0.09259	0.1028	0.07675

Table 2.33—*Contd.*

γ°	$\tilde{m} = 1.50$, $\tilde{\rho}_{max} = 150$									
	$b_1 = 5$		$b_1 = 6$				$b_1 = 8$			
	$\tilde{\rho}_{min} = 1$ $\tilde{\rho}_{av} = 1.33$	$\tilde{\rho}_{min} = 2$ $\tilde{\rho}_{av} = 2.7$	$\tilde{\rho}_{min} = 0.2$ $\tilde{\rho}_{av} = 0.25$	$\tilde{\rho}_{min} = 0.6$ $\tilde{\rho}_{av} = 0.75$	$\tilde{\rho}_{min} = 1$ $\tilde{\rho}_{av} = 1.25$	$\tilde{\rho}_{min} = 2$ $\tilde{\rho}_{av} = 2.5$	$\tilde{\rho}_{min} = 0.2$ $\tilde{\rho}_{av} = 0.23$	$\tilde{\rho}_{min} = 0.6$ $\tilde{\rho}_{av} = 0.7$	$\tilde{\rho}_{min} = 1$ $\tilde{\rho}_{av} = 1.2$	$\tilde{\rho}_{min} = 2$ $\tilde{\rho}_{av} = 2.3$
70	0.05338	0.03493	0.06669	0.06603	0.06328	0.03676	0.07008	0.07467	0.07634	0.04314
80	0.03652	0.02197	0.05235	0.04970	0.04479	0.02278	0.06216	0.06168	0.05738	0.02604
90	0.02692	0.01653	0.04373	0.03965	0.03331	0.01662	0.05849	0.02858	0.04464	0.01799
100	0.02092	0.01345	0.03923	0.03380	0.02622	0.01353	0.05854	0.04936	0.03670	0.01405
110	0.01747	0.01181	0.03820	0.03521	0.02209	0.01176	0.06935	0.06513	0.03231	0.01174
120	0.01551	0.01085	0.03856	0.03025	0.01990	0.01053	0.06799	0.05039	0.03037	0.01015
130	0.01496	0.01053	0.04083	0.03094	0.01913	0.009988	0.07580	0.05370	0.03005	0.009316
140	0.01599	0.01152	0.04401	0.03262	0.01947	0.01037	0.08421	0.05778	0.03079	0.009381
150	0.01699	0.01333	0.04736	0.03467	0.02041	0.01144	0.09215	0.06181	0.03199	0.01030
160	0.01899	0.01605	0.05036	0.03670	0.02165	0.01307	0.09860	0.06519	0.03326	0.01192
170	0.02126	0.01926	0.05277	0.03857	0.02319	0.01570	0.1029	0.06753	0.03431	0.01396
180	0.02496	0.02511	0.05402	0.03979	0.02448	0.01840	0.1043	0.06827	0.03460	0.01435

Table 2.33—*Contd.*

γ°	$\tilde{m} = 2.105$, $\tilde{\rho}_{max} = 15$						
	$b_1 = 4$				$b_1 = 5$		
	$\tilde{\rho}_{min} = 0.2$ $\tilde{\rho}_{av} = 0.3$	$\tilde{\rho}_{min} = 1$ $\tilde{\rho}_{av} = 1.5$	$\tilde{\rho}_{min} = 1.4$ $\tilde{\rho}_{av} = 2.1$	$\tilde{\rho}_{min} = 2.2$ $\tilde{\rho}_{av} = 3.3$	$\tilde{\rho}_{min} = 0.2$ $\tilde{\rho}_{av} = 0.26$	$\tilde{\rho}_{min} = 1$ $\tilde{\rho}_{av} = 1.33$	$\tilde{\rho}_{min} = 1.4$ $\tilde{\rho}_{av} = 1.86$
0	0.7134	0.7682	0.9100	1.426	0.2732	0.3008	0.3312
10	0.4422	0.4710	0.5336	0.7350	0.2412	0.2660	0.2814
20	0.2745	0.2855	0.3018	0.3295	0.2114	0.2256	0.2276
30	0.1940	0.1979	0.1966	0.1702	0.1790	0.1880	0.1816
40	0.1462	0.1473	0.1392	0.1028	0.1481	0.1533	0.1425
50	0.1114	0.1110	0.1008	0.06756	0.1191	0.1210	0.1081
60	0.08730	0.08495	0.07549	0.04959	0.1015	0.09356	0.0810
70	0.06800	0.06673	0.05939	0.04204	0.07444	0.07336	0.06348
80	0.05498	0.05375	0.04901	0.03667	0.05916	0.05724	0.05030
90	0.04581	0.04328	0.03891	0.02864	0.05146	0.04702	0.03980
100	0.03316	0.03018	0.03138	0.02321	0.03836	0.03424	0.03126
110	0.03083	0.02890	0.02870	0.02554	0.03260	0.02716	0.02526
120	0.02691	0.02451	0.02477	0.02423	0.02946	0.02264	0.02132
130	0.02529	0.02243	0.02303	0.02506	0.02764	0.01930	0.01779
140	0.02637	0.02323	0.02441	0.02923	0.02840	0.01898	0.01782
150	0.03167	0.02866	0.03132	0.04139	0.03026	0.02002	0.01933
160	0.04602	0.04411	0.05082	0.07666	0.03536	0.02556	0.03846
170	0.06854	0.06875	0.08197	0.1315	0.03884	0.02908	0.04376
180	0.08787	0.08988	0.1089	0.1807	0.04098	0.03152	0.04744

Table 2.33—*Contd.*

γ°	$\tilde{m} = 2.105$, $\tilde{\rho}_{max} = 15$					$\tilde{m} = 1.44$, $\tilde{\rho}_{max} = 6$	
	$b_1 = 5$	$b_1 = 6$				$b_1 = 4$	
	$\tilde{\rho}_{min} = 2.2$ $\tilde{\rho}_{av} = 2.93$	$\tilde{\rho}_{min} = 0.2$ $\tilde{\rho}_{av} = 0.25$	$\tilde{\rho}_{min} = 1$ $\tilde{\rho}_{av} = 1.25$	$\tilde{\rho}_{min} = 1.4$ $\tilde{\rho}_{av} = 1.75$	$\tilde{\rho}_{min} = 2.2$ $\tilde{\rho}_{av} = 2.75$	$\tilde{\rho}_{min} = 0.5$ $\tilde{\rho}_{av} = 0.75$	$\tilde{\rho}_{min} = 1$ $\tilde{\rho}_{av} = 1.5$
0	0.3912	0.2490	0.3141	0.3768	0.7048	1.041	1.076
10	0.2640	0.2276	0.2933	0.3430	0.5747	0.8143	0.8399
20	0.1597	0.2099	0.2547	0.2846	0.3894	0.5408	0.5554
30	0.1001	0.1795	0.2113	0.2229	0.2283	0.2980	0.3032
40	0.06792	0.1502	0.1717	0.1718	0.1347	0.1743	0.1753
50	0.04429	0.1231	0.1367	0.1308	0.08281	0.1016	0.1005
60	0.02840	0.09976	0.1077	0.1004	0.05977	0.06235	0.06044
70	0.02554	0.0859	0.08438	0.07835	0.05091	0.04103	0.03892
80	0.02215	0.06538	0.06563	0.06162	0.04363	0.02794	0.02579
90	0.01761	0.05886	0.05482	0.04797	0.03374	0.02042	0.01828
100	0.01341	0.04594	0.03904	0.03748	0.02740	0.01650	0.01433
110	0.01316	0.04154	0.03103	0.02997	0.02697	0.01422	0.01189
120	0.01531	0.03991	0.02580	0.02471	0.02982	0.01337	0.01084
130	0.01435	0.04026	0.02266	0.02112	0.03116	0.01352	0.01075
140	0.01858	0.04243	0.02198	0.02044	0.03700	0.01408	0.01107
150	0.02239	0.04632	0.02436	0.02443	0.05676	0.01511	0.01188
160	0.04238	0.05201	0.03029	0.03448	0.1006	0.01401	0.01051
170	0.05339	0.05722	0.03714	0.04623	0.1521	0.01575	0.01220
180	0.06191	0.05776	0.04061	0.05226	0.1790	0.01788	0.01788

interest. The distributions are limited as there are no lower and upper limits to the size of the particles. The first boundary condition effectively influences the result only when $b_1 > 5$ and the second boundary condition is connected with computational difficulties and is confirmed by the low concentration of large aerosol particles.

4. LOCALIZED SCATTERING FUNCTION IN REAL ATMOSPHERE

The concept of scattering coefficient along a given direction in the following form has been introduced for the characterization of angular dependence of scattering so that the following equation holds:

$$\mu_0(\gamma) = \frac{dF}{Ed\omega dv}, \tag{2.34}$$

where dF—flux of scattered light in the direction γ from volume dV in a solid angle $d\omega$, E—area of illumination perpendicular to direct rays.

The quantity $\mu_0(\gamma)$ is also called the localized scattering function. The function $\mu_0(\gamma)$ may be experimentally determined from projection and turbidity measurements. It is impossible to obtain this value through direct measurements of the brightness of the sky. In this case a quantity $\mu_0(\gamma)$ may be introduced which is defined as the scattering coefficient in a given direction computed over the entire atmospheric layer.

$$\mu_1(\gamma) = \int_0^\infty \mu_0(\gamma)\, dz.$$

Through direct measurements one can obtain the scattering coefficient in a given direction, calculated for the entire thickness of atmosphere, while taking into account the influence of multiple scattering, reflection from the ground and absorption. Over a period of many years E. V. Piaskowskaya-Fesenkova and collaborators carried out observations on the scattering function over the entire thickness of atmosphere in the vicinity of Alma-Ata and in other places [14, 15, 16].

In these works the functions $\mu(\gamma)$ can be determined through observations on the brightness of the sky in solar almucanthorat. The brightness of the screen illuminated by solar radiation in a plane perpendicular to its direction can be determined at the beginning and end of the series of measurements.

The function $\mu(\gamma)$ can be found from the following expression:

$$\mu(\gamma)=\frac{B_n(\gamma)}{B_s}\frac{A}{\pi}\frac{1}{m}, \tag{2.35}$$

where B_s —brightness of the screen;
A —albedo of the screen;
m —atmospheric mass in the direction of the sun; and
B_n —brightness of sky.

Measurements show that the form of function changes significantly from day to day for angles $\gamma<40°$ and varies very little within the limits $40<\gamma<120°$. A strong forward projection of the scattering function is characteristic in this region.

It has been established by E. V. Piaskowskaya-Fesenkova [16] that all functions for equal transparency of the atmosphere intersect around a point in the interval of γ from 55 to 60°.

The elimination of the influence of multiple scattering, reflection of light from the underlying surface and perfect absorption appears to be the most difficult task during the construction of scattering functions in a real atmosphere.

The following expression for the computation of $\mu_1(\gamma)$ has been suggested by G. Sh. Lifshits [14]:

$$\mu_1(\gamma)=\frac{B_s(\gamma)}{Em}-\left[\frac{B_s(\gamma_0)}{Em}-\frac{\tau B_s(\gamma_0)}{4\pi\left(\frac{Em}{4\pi}+B_2(\gamma_0)+B_q(\gamma)\right)}\right]\times\frac{B_2(\gamma)+B_q(\gamma)}{B_2(\gamma_0)+B_q(\gamma_0)}, \tag{2.36}$$

where τ —optical thickness of atmosphere determined by Bouguer's lines;
$B_s(\gamma_0)$—brightness of sky observed at a special point $\gamma_0\cong57°$;
$B_2(\gamma)$—theoretical value of brightness of sky due to multiple scattering;
$B_q(\gamma)$—theoretical values of sky brightness theoretically computed at a special point.
$B_2(\gamma_0)$ and $B_q(\gamma_0)$—the same value of sky brightness computed theoretically at a special point.

Values of $\mu(\gamma)$ and $\mu_1(\gamma)$ for optical thicknesses $\tau=0.1$, 0.2 and 0.3 are given in Table 2.34 which is taken from [14]. From this table it is obvious that even for the smallest optical thickness ($\tau=0.1$) $\mu(\gamma)$ and

Table 2.34 Functions $\mu(\gamma)$ and $\mu_1(\gamma)$ [14]

τ	$\lambda\mu$	γ°									
		10		15		20		30		45	
		μ	μ_1	μ	μ_1	μ	μ_1	μ	μ_1	μ	μ_1
0.1	704	0.1059	0.1044	0.0457	0.0442	0.0329	0.0314	0.0254	0.0240	0.0106	0.0092
0.2	491	0.1343	0.1289	0.0656	0.0604	0.0547	0.0495	0.0390	0.0338	0.0331	0.0279
0.3	440	0.1189	0.1043	0.0842	0.0698	0.0690	0.0544	0.0573	0.0432	0.0511	0.0378

τ	$\lambda\mu$	γ°									
		60		80		90		100		120	
		μ	μ_1	μ	μ_1	μ	μ_1	μ	μ_1	μ	μ_1
0.1	740	0.0091	0.0077	0.0045	0.0031	0.0050	0.0036	0.0045	0.0030	0.0050	0.0031
0.2	491	0.0176	0.0125	0.0114	0.0064	0.0109	0.0059	0.0109	0.0059	0.0109	0.0060
0.3	440	0.0319	0.0191	0.0205	0.0088	0.0200	0.0089	0.0200	0.0094	0.0209	0.0114

$\mu_1(\gamma)$ differ significantly, especially for large scattering angles, since the first order scattering is extremely large for small angles.

More detailed measurements on scattering coefficient of layers of atmosphere on the ground, $\mu_a(\gamma)$ were carried out by Foitzik and Zshaeck [30] using the projection method and by Barteneva [2], who employed turbiditimeter IF-14 for measurements of scattering functions of air above the ground.

Barteneva's results are based on the measurements of 1020 functions obtained under different meteorological and geographic conditions with changes in meteorological visual range from D_0=0.2 km to D_0=220 km.

In order to analyze the characteristic parameters of the family of curves representing the scattering function of light under different conditions, Barteneva considered the asymmetry coefficient of light flux C, i.e. the ratio of scattering flux in the anterior hemisphere F_1 to the scattering flux in the posterior hemisphere F_2 as follows :

$$C=\frac{F_1}{F_2}=\frac{\int_0^{\pi/2}\mu_0(\gamma)\sin\gamma\,d\gamma}{\int_{\pi/2}^{\pi}\mu_0(\gamma)\sin\gamma\,d\gamma}. \tag{2.37}$$

All the functions possessing similar values of parameter C are grouped together and form a single class. Scattering functions which differ in the value of C by one and a half times are included in distinct classes. In all 10 classes of scattering functions have been identified. Two types of functions can be identified along with the classes : viz. gently sloping and steep with a deep minimum at γ=110-120°.

Fig. 2.18 shows the curves corresponding to different classes of functions [2]. Scattering angles in degrees are marked along the abscissa and values of normalized scattering functions along the ordinate.

$$\overset{*}{\mu o}(\gamma)=\frac{\mu_0(\gamma)}{2\pi\int_0^{\pi}\mu_0(\gamma)\sin\gamma\,d\gamma}. \tag{2.38}$$

In agreement with the normalizing condition,

$$\int_{4\pi}\overset{*}{\mu_0}(\gamma)\,d\omega=1.$$

The curve corresponding to the value of $C=1$ in Fig. 2.18 is obtained as the mean for 13 functions, measured at different times on the night of September 21-22, 1957 at Mt. Terskol at a height of $D_0=220$ km. Curve 1 is close to Rayleigh's functions (curve 1*a*). Functions of one sloping type alone are included in classes 1-4 for $C\leqslant 3.5$. The functions for $C>3.5$ may be looked on as sloping as well as of the steep type (curves 5, 6, etc). For $C>5.6$ (i.e. class 6) curves of the steep type have a maximum close to $\gamma=140°$, which is maintained up to class 10 but decreases somewhat along the ordinate.

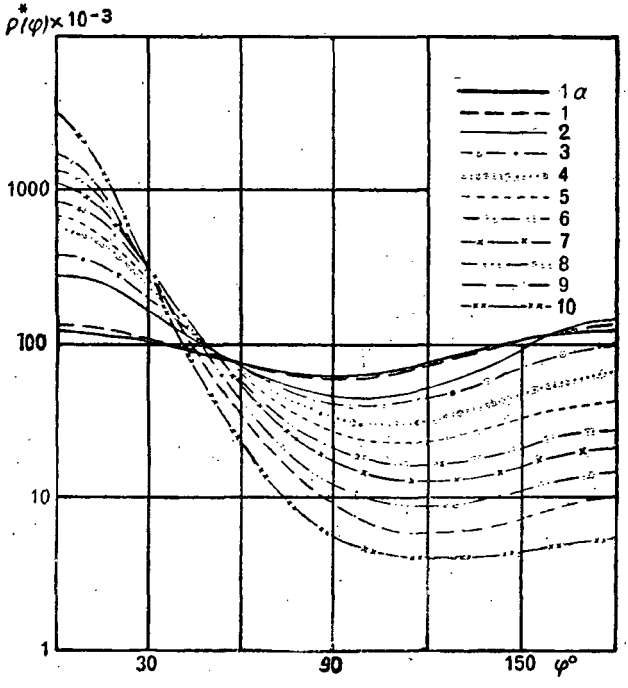

Fig. 2.18. Scattering function of light in air (sloping type) [2].
1) results obtained in El'brus ; 1*a*) Rayleigh function for pure dry air ; 2) class 2, sloping type ; 3) class 3, sloping type, etc.

The function projects forward with the increase of parameter C. The division of the functions into two types has been brought about by the existence of two different types of aerosol in the atmosphere. The functions of a sloping type have been observed under continental conditions in the presence of persistent mist. The appearance of scattering functions of the steep type (curves 5-9) is caused by the presence of huge droplets in air with diameters up to 20 μ. Such functions may be obtained above oceans and seas. The functions of the steep type (curves 7, 8, 9) can

be observed under continental conditions before formation of mist at the time of scattering.

The form of scattering functions in mist differs considerably from the form of those in fog. Scattering functions of a steep type with a maximum close to $\gamma=140°$ have been included in classes 6, 7, 8, 9 and 10.

This type is represented by curves 6″, 7″, 8″, 9″ and 10″ in Fig. 2.19.

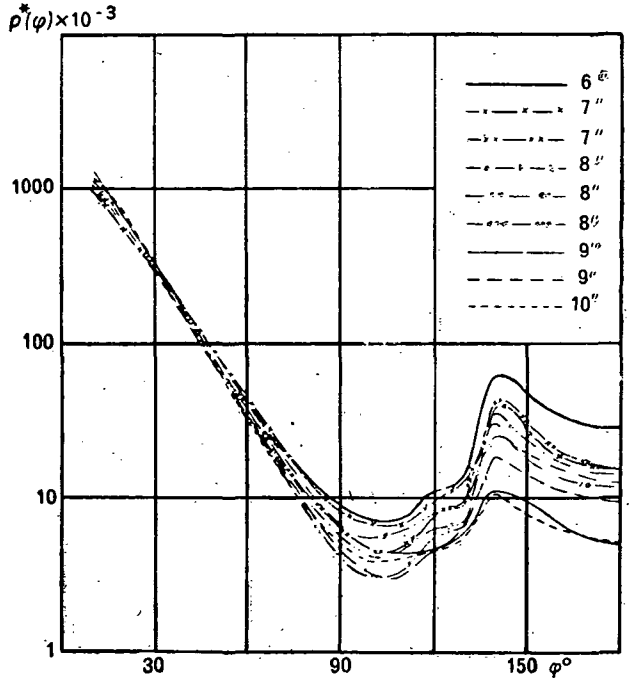

Fig. 2.19. Scattering curves of light on air (steep type with a maximum in the neighborhood of $\varphi=140°$) [2].

6″—class 6, steep type with a maximum ; 7″—class 7, steep type with a maximum, etc.

The region of the first rainbow corresponds to a maximum in the neighborhood of $\gamma=140°$, and the steps of curves observed in classes 6″, 7″ and 8″ for $\gamma=120°$-$130°$ correspond to the region of the second rainbow. The values of these maxima depends on the relative proportion of huge droplets in the overall ensemble of particles suspended in the air.

The point of interaction of the functions observed for a given transparency depends on the atmospheric transparency. The functions observed for a high transparency intersect in the vicinity of $\gamma=60°$. In proportion to the increase in turbidity in the atmosphere the point of intersection of the functions starts shifting toward smaller angles. The

functions for strongly turbid atmosphere intersect in the vicinity of 30° or 20°.

Fig. 2.20 represents the dependence of the point of intersection of the functions on atmospheric transparency.

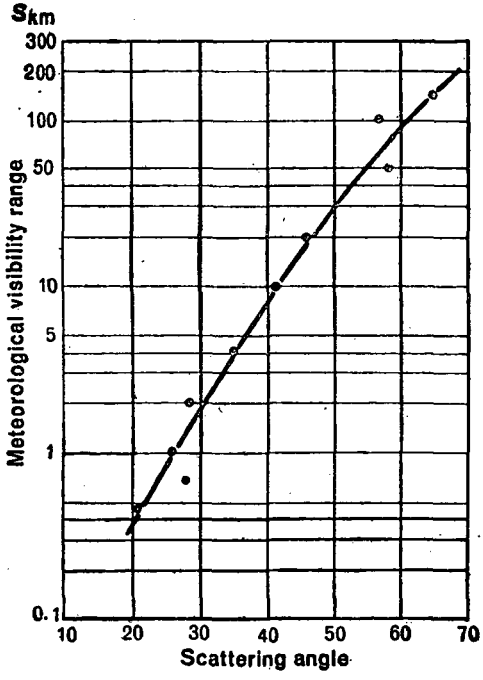

Fig. 2.20. Dependence of the position of the point of intersection of scattering functions in light on atmospheric transparency [2].

With the exception of two extreme cases—almost ideal atmosphere and fog close to mist—the main mass of functions intersect in the neighborhood of $\gamma=45°$.

During measurements on scattering functions from the observations on brightness of the sky, Pyaskovskaya-Fesenkova was concerned with measurements at very large atmospheric transparency, so that the point of intersection of the functions in her case lay close to $\gamma=60°$.

The dotted line in Fig. 2.20 represents scattering functions of classes 3-9 according to Barteneva's classification. The functions, drawn in points, were obtained by Foitzik and Zshaeck, and correspond to a specific class of the given classification. The slightly increased values of $\mu_0^*(\gamma)$ in the region of angles 90-130° for classes 3, 5, 6 and 7 in the case of Foitzik as compared to the data of Barteneva can be explained by

Table 2.35 Classes and types of functions [2]

	Classes (types)								
	1		2	3	4	5	5′	6	6′
γ°	(Sloping)								
	Rayleigh's theoretical	Experimental	(Sloping)	(Sloping)	(Sloping)	(Sloping)	(Steep)	(Sloping)	(Steep)
0	119×10^{-3}	130×10^{-3}	282×10^{-3}	385×10^{-3}	564×10^{-3}	681×10^{-3}	820×10^{-3}	834×10^{-3}	900×10^{-3}
10	118	126	270	350	499	594	712	727	792
20	112	114	216	272	354	410	445	498	598
30	104	105	162	196	234	269	280	295	324
40	94.7	94	123	139	152	168	163	171	172
50	84.4	84	87.7	98.0	101	106	97.3	98.8	91.0
60	74.6	75	69.0	71.4	70.0	68.4	56.7	58.8	51.3
70	66.7	65	55.4	54.8	50.5	45.8	35.3	38.1	31.0
80	61.5	61	48.5	45.1	39.6	34.0	22.9	26.9	19.7
90	59.7	60	46.7	40.9	34.2	26.9	17.3	20.6	14.5
100	61.5	62	46.7	40.0	32	24.1	15.2	17.8	12.2
110	66.7	67	49.0	41.3	31.8	23.2	15.7	16.7	12.0
120	74.6	72	53.4	44.5	33.2	23.6	17.6	16.7	13.0
130	84.4	80	61.2	50.0	36.2	25.4	22.0	17.4	15.8
140	94.7	92	74.0	57.9	41.4	28.7	30.1	18.4	22.2
150	104	104	94.0	66.3	46.7	31.7	46.5	20.6	33.0
160	112	115	115	77.8	54.3	35.8	69.5	23.4	48.0
170	118	126	133	91.0	62.4	40.6	91.2	27.0	67.7
180	119	130	139	96.0	65.3	42.6	99.0	28.0	73.5

Table 2.35—*Contd.*

	Classes (types)								
	6″	7	7′	7″		8	8′	8″	
γ°	(Steep with a maximum)	(Sloping)	(Steep)	(Steep with a maximum)		(Sloping)	(Steep)	(Sharp with a maximum)	
				Rayleigh's theoretical	Experimental			Rayleigh's theoretical	Experimental
0		1100×10^{-3}	1519×10^{-3}			1320×10^{-3}	1545×10^{-3}		
10	1095×10^{-3}	935	1185	1041×10^{-3}	1126×10^{-3}	1080	1201	1079×10^{-3}	1185×10^{-3}
20	504	548	610	560	600	587	551	602	597
30	278	299	274	310	310	302	278	324	309
40	144	161	143	161	155	150	143	164	158
50	82.0	90.6	76.8	85.0	78.2	78.7	78.7	83.5	80.4
60	42.6	53.1	41.6	44.0	39.2	42.8	40.4	42.2	40.0
70	23.6	33.1	25.8	23.5	19.6	25.6	23.7	21.2	19.4
80	13.4	22.6	17.2	13.3	10.8	16.8	14.9	10.8	10.0
90	8.9	16.9	12.3	8.6	6.6	12.5	10.5	6.6	5.9
100	7.2	14.1	10.2	6.9	4.8	10.1	8.5	5.5	4.3
110	7.5	12.9	9.4	6.9	4.8	9.3	7.7	6.2	4.6
120	11.2	12.8	10.1	9.5	7.8	9.1	7.8	8.3	6.4
130	13.4	13.4	11.9	12.3	9.4	9.4	8.7	8.9	7.0
140	64.3	14.0	15.7	39.6	43.6	10.2	10.6	24.7	31.4
150	49.1	15.9	20.1	30.5	30.4	11.5	13.2	19.5	19.4
160	36.0	18.4	26.8	18.8	20.6	12.9	17.0	16.0	14.4
170	29.7	20.7	35.3	16.3	17.2	14.3	20.9	14.1	12.4
180		21.3	38.3			15.0	21.9		

Table 2.35—*Contd.*

$\gamma°$	Classes (types)						
	8	9	9′	9″		10	10′
				(Steep with a maximum)			
	(Steep with a maximum)	(Sloping)	(Steep)	Rayleigh's theoretical	Experimental	(Sloping)	(Steep with a maximum)
0		1760×10^{-3}	1924×10^{-3}			2500×10^{-3}	
10	1286×10^{-3}	1380	1470	1381×10^{-3}	1183×10^{-3}	1600	1199×10^{-3}
20	594	618	596	649	642	700	702
30	303	284	268	287	328	280	334
40	151	134	128	138	161	100	162
50	72.5	67.0	63.9	67.5	76.1	46.0	63.0
60	31.4	35.0	35.8	34.8	36.8	22.0	32.5
70	16.3	20.2	18.8	19.0	18.0	12.0	15.8
80	7.9	12.7	11.1	10.6	8.7	7.2	8.6
90	4.4	9.1	7.6	6.8	4.8	5.3	5.3
100	3.2	7.1	6.0	5.0	3.3	4.5	4.0
110	3.3	6.2	5.3	4.4	3.2	4.2	4.1
120	5.7	5.9	5.3	4.7	4.7	4.0	4.6
130	6.5	6.1	6.1	6.0	6.0	4.0	5.4
140	37.4	6.6	7.1	11.6	18.8	4.2	10.3
150	23.6	7.5	8.8	9.8	15.0	4.4	8.4
160	17.8	8.5	11.0	6.8	12.0	4.8	6.7
170	15.3	9.8	13.0	5.5	10.4	5.3	5.6
180		10.2	13.7			5.5	

the fact that in Foitzik's experiments the observations of light scattering were carried out against the background of a hill covered with a forest, whose inherent brightness in the region of a minimum of the function could substantially increase the value of $\mu_0^*(\gamma)$. During measurements the background served as a perfectly black body.

Normalized scattering functions $\mu_0^*(\gamma)$ for different classes through 10° intervals are given in Table 2.35 [2].

There exists only a correlational dependence between the form of functions, characterized by the magnitude of parameter C, and meteorological visual range, and, in turn, the attenuation index of the atmosphere. For any transparency the value K_{va} can change two and a half times, i.e. include three different classes of protruded curves ; moreover the limits of vibrations increase with increasing atmospheric turbidity.

The form of scattering functions is independent of geographical position.

In obtaining scattering functions μ_0 (γ) the data in Table 2.35 have to be multiplied by the corresponding attenuation index for which the given function is observed.

REFERENCES

1. Atroshenko, V. S. et al. Raschet yarkosti sveta v atmosfere pri anizotropnom rasseyanii (Computation of luminosity of light in atmosphere for anisotropic scattering). Trudy IFA, part II, No. 3, 1962.
2. Barteneva, O. D., E. N. Dovgyallo and E. A. Polyakova. E'ksperimentaly'nye issledovaniya opticheskikh svoistv prizemnogo sloya atmosfery (Experimental study of optical properties of layer of atmosphere at the earth's surface). Trudy GGO, vyp. 220, 1967.
3. Gal'tsev, A. P. Issledovanie polosy pogloshcheniya ozona 9.6 mkm v iskusstvennoi atmosfere (Study of the absorption bands of ozone 9.6 μ in artificial atmosphere). Problemy fiziki atmosphery, vyp. 5, Izd. LGU, 1967.
4. Gal'tsev, A. P. Funktsii pogloshcheniya s uchetom izmeneniya intensivnosti i polushiriny spektral'nykh linii v polose (Absorption functions considering changes in intensity and halfwidth of spectral lines in a band). Optika i spektroskopiya, t. 11, vyp. 2, 1966.
5. Golubitskii, B. M. and N. I. Moskalenko. Funktsii spektral'nogo propuskaniya v polosakh parov H_2O i CO_2. Ismereniya i raschet spektral'nogo propuskaniya v polosakh N_2O v blizhnei infrakrasnoi oblasti (Spectral emission functions in bands of H_2O and CO_2 vapor. Measurements and computations of spectral emission in N_2O bands in the near infrared region). Izv. AN SSSR, FAO, 4, No. 3, 1958.
6. Gudi, R. Atmosfernaya radiatsiya (Atmospheric Radiation). Izd-vo "Mir", Moskva, 1966.
7. Zuev, V. E. Prozrachnost' atmosfery dlya vidimykh i infrakrasnykh luchei (Atmospheric transparency for visible and infrared rays). Izd-vo "Sov. Radio", Moskva, 1966.
8. Ivlev, L. S. Ae'rozol'naya model' atmosfery (Aerosol model of atmosphere). Problemy fiziki atmosphery, vyp. 7. Izd. LGU, 1969.

9. Ivlev, L. S. and E. L. Yanchenko. Opticheskie kharakteristiki vodnogo ae'rozolya (Optical properties of aqueous aerosol). Problemy fiziki atmosphery, No. 8, LGU, 1969.

10. Issledovaniya verkhnei atmosfery s pomoshch'yu raket i sputnikov (Study of upper atmosphere with the help of rockets and artificial satellites) Edited by D. Ratkliff. IL, Moskva, 1961.

11. Kislovskii, L. D. Opticheskie kharakteristiki vody i l'da v infrakrasnom i mikrovolnovom diapazone spektra (Optical characteristics of water and ice in infrared and microwave spectral frequencies). Optika i spektroskopiya, t. 7, 201, 1959.

12. Kondrat'ev, K. Ya. Actinometriya (Actinometry). Gidrometeoizdat, Leningrad, 1965.

13. Kondrat'ev, K. Ya. et al. Infrakrasnyi spektr pogloshcheniya vody (Infrared absorption spectrum of water) Coll. "Problemy fiziki atmosfery", vyp. 2, Izd. LGU, 1963.

14. Lifshits, G. Sh. Rasseyanie sveta v atmosfere (Scattering of light in atmosphere) Izd-vo "Nauka", Alma-Ata, 1965.

15. Pavlov, V. E. Atmosfernaya indikatrisa rasseyaniya v vidimoi i ul'trafioletovoi oblastyakh (Atmospheric scattering functions in visible and ultraviolet regions). Astr. zhurn., t. XVI, vyp. 3, 546, 1966.

16. Pyaskovskaya-Fesenkova, E. V. Issledovanie rasseyaniya sveta v zemnoi atmosfere (Study on scattering of light at the earth's atmosphere). Izd. AN SSSR, Moskva, 1957.

17. Feigel'son, E. M. Raschet yarkosti sveta v atmosfere pri anizotropnom rasseyanii (Consideration of luminosity of light in the atmosphere for anistropic scattering). Trudy IFA, Part I, No. 1, 1958.

18. Van de Khyulst. Rasseyanie sveta malymi chastitsami (Scattering of light by small particles). IL, Moskva, 1961.

19. Shifrin, K. S. and V. F. Raskin. K teorii indikatrisy Rokara (Theory of Rokar's coefficients). Trudy GGO, vyp. 100, 1960.

20. Shifrin, K. S. Rasseyanie sveta v mutnoi srede (Scattering of light in a turbid medium). Gostekhizdat, Moskva-Leningrad, 1951.

21. Shifrin, K. S. and E'. A. Chayanova. Indikatrisy dlya raspredelenii Yunge i tipa Yunge (Functions for Young's distribution and Young type distribution). Trudy GGO, vyp. 170, 1965.

22. Shifrin, K. S. and I. L. Zel'manovich. Tablitsy po svetorasseyaniyu (Tables on scattering of light). Gidrometeoizdat, Leningrad, 1965.

23. de Bary, E., B. Braun and K. Bullrich. Tables Related to Light Scattering in a Turbid Atmosphere. AFCRL, Sp. Rept., 23, 1965.

24. Burch D. et al. Infrared Absorption by Carbon Dioxide, Water Vapor, and Minor Atmospheric Constituents. Res. Rept. AFCRL, AFI9 (604)—2633, 1962.

25. Cook, J. and P. Metzger. Photoionization and Absorption Cross Sections of O_2 and N_2 in the 600 to 1000 Å Region. Journ. Chem. Phys., 41, 2, 1964.

26. Deirmendjian, D., R. Clasen and W. Viezee. Mie Scattering with Complex Index of Refraction. JOSA, 51, 6, 1961.

27. Deirmendjian, D. Scattering and Polarization Properties of Water Clouds in Visible and Infrared. Appl. Opt. 3, 2, 1964.

28. Fenn, R. Aerosolverteilungen und atmospherisches Streulicht. Beitr. Phys. Atmosph., 37, 2, 1964.

29. Ferriso, C., C. Ludwig and A. Thomson. Empirically Determinated Infrared Absorption Coefficients of H_2O from 300 to 3000°K. J. Q. S. R. T. 6, 3, 1966.
30. Foitzik, L. und H. Zshaeck. Messungen der spektralen Zerstreuungsfunktion bodennaher Luft bei guter Sicht, Dunst und Nebel. Zeitschrift für Meteorologie, Band 7, 1, 1953.
31. Giese, R. et al. Tabellen der streufuntkionen $i_1(\gamma)$, $i_2(\gamma)$ und des streuguerschnittes $k(\alpha, m)$, Homogener Kugelchen nach der Mie-schen Theorie. Ak. Verb., Berlin, 1962.
32. Goldstein, R. and F. Mastrap. Absorption Coefficients of the O_2 Shuman-Runge Continuum from 1270-1745 Å using a New-Continuum Source. JOSA, 56, 6, 1966.
33. Gumprecht, R. et al. Angular Distribution of Intensity of Light Scattered by Large Droplets of Water. JOSA, 42, 2, 1952.
34. Harrison, A., B. Cedernolen and E. Coffin. Technical Report, Mount Holyoke College, Holyoke, Mass., 1951.
35. Hearn, A. The Absorption of Ozone in the Ultraviolet and Visible Regions of the Spectrum. Proc. Phys. Soc., A78, 1961.
36. Herman, B. Infra-red Absorption, Scattering and Total Attenuation Cross Sections for Water Spheres. Q. J. R. M. S., 88, 376, 1962.
37. Houghton, H. and W. Chalker. The Scattering Cross Section of Water Drops in air for Visible Light. JOSA, 39, 2, 1949.
38. Huffman, R., J. Larabee and Y. Tanaka. Absorption Coefficients of Nitrogen in the 1000-580 Å wavelengths region. Journ. Chem. Phys., 39, 4, 1963.
39. Huffman, R., J. Larabee and Y. Tanaka. Nitrogen and Oxygen Absorption Cross Section in the Vacuum Ultraviolet. Disc. Farad. Soc., No. 37, 1964.
40. Hudson, R. et al. An Investigation of the Effect of Temperature on the Shuman-Runge Absorption Continuum of Oxygen 1580-1950 Å. Journ. Geoph. Res. 71, 9, 1966.
41. Jin, E. and Y. Tanaka. Absorption Coefficient of Ozone in the Ultraviolet and Visible Regions. JOSA, 43, 6, 1953.
42. Lowan, A. Tables of Scattering Function for Spherical Particles. Nat. Bur. Stand. Appl. Math., Ser. 4. Wash., 1948.
43. McCaa, D. and J. Shaw. The Infrared Absorption Bands of Ozone. Contr. AF 19 (628)—3806, 1967.
44. McGee, R. Transmission Tables for H_2O, CO_2 and O_3. Proc. IRIS, 7, 2, 1962.
45. Mie, G. Beitrag Zur Optic trüber Medien. Ann. Phys. 25, 4, 1908.
46. Penndorf, R. Tables of the Refractive Index for Standard Air and the Rayleigh Scattering Coefficient for the Spectral Region between 0.2 and 20.0 mc and their Application to Atmospheric Optics. JOSA, 47, 2, 1957.
47. Samson, J. and R. Cairns. Absorption and Photoionization Cross-Sections of O_2 and N_2 at Intense Solar Emission. Journ. Geoph. Res., 69, 21, 1964.
48. Thompson, B., P. Hartek and R. Reeves. Ultraviolet Absorption Coefficients of CO_2, CO, O_2, H_2O, N_2O, NH_3, NO, SO_2 and CH_4 between 1850 and 4000 Å. Journ. Geoph. Res., 68, 24, 1963.
49. Vigroux, E. Dètermination des coefficients moyens d'absorption de l'ozone en vue des observations concernant l'ozone atmosphérique à l'aide du spectromètre Dobson. Ann. Phys., t. 2, 1967.
50. Walshaw, C. Integrated Absorption by the 9.6 mc Band of Ozone. Q. J. R. M. S., 83, 315, 1957.
51. Watanabe, K., F. Matsunage and H. Sakai. Absorption Coefficients and Photoionization Yield of NO in the Region 580-1350 Å. Appl. Opt., 6, 3, 1967.
52. Weissler, G. and P. Lee. Absolute Absorption Coefficients of Oxygen in the Vacuum Ultraviolet. JOSA, 42, 2, 1952.

3. SPECTRAL TRANSPARENCY OF REAL ATMOSPHERE

The absorption and scattering mechanisms of electromagnetic waves with frequencies in the optical range give rise to an emission spectrum of the atmosphere. The spectral transparency of the real atmosphere, brought about by the mutually overlapping emission spectra of selected optically active components, is a complex function of the frequency, concentration and partial pressure of the components, pressure and temperature of the medium in the optical path (cf. Ch. 2). The energy of solar radiation penetrating through the atmosphere in turn affects the chemical composition and the physical state of the atmosphere (i.e. its transparency).

The main gases in the atmosphere, i.e. nitrogen and oxygen, determine the existing radiative attenuation caused by molecular scattering in ultraviolet and visible regions of the spectrum. Triatomic gases, which are generally found in the atmosphere in the form of small mixtures, such as water vapor, carbon dioxide and ozone, play an important role in the selective absorption of radiation. Secondary gaseous components such as hydrocarbons and oxides of nitrogen (cf. Chs. 1 and 2) which are optically active make an appreciable contribution to the absorption of

infrared radiation.

Variability in the concentration of water vapor and ozone, and the concentration and the optical characteristics of aerosol under the influence of various interaction processes of the solar radiation field, atmosphere and underlying surface lead to fluctuations in spectral transparency. Phase transitions in water cause the most vital changes in the transparency of the troposphere (of the order of 10^6). Turbidity in the atmosphere, which increases sharply with dew point (formation of mist), also changes at temperatures other than the saturation temperatures (moist fog), because of the presence of hydroscopic aerosol particles in the atmosphere.

Changes in the turbidity of the atmosphere may occur under conditions of low relative humidity when dry aerosol particles of different origins are accumulated in the atmosphere.

Variations in the chemical constitution, concentration and distribution of aerosol particles, together with a special "sensitivity" of transparency changes in the relative concentration of particles whose size is comparable to the wavelength, lead to changes in the spectral nature of transparency in the visible and near-infrared regions of the spectrum. The absence of reliable methods of standardizing the microphysical parameters of aerosol without destroying its natural state (especially hygroscopic particles) allows only a qualitative systematization of spectral measurements.

A significant amount of information on aerosol attenuation at different altitudes has been obtained through observations on intensity of the scattered radiation of natural and artificial sources of light (rocket research methods of search-light or laser probing, observation on brightness of the horizon from space ships, and methods of twilight observation). These methods may be comparable but are very sensitive to the presence of aerosol components (which is important during the study of the upper layers of atmosphere).

The inadequate resolving power of the spectroscopes is the chief obstacle in the study of selective transmission of radiation using atmospheric gases, and limits the means of obtaining information on the attenuation patterns of monochromatic radiation in the lines of the vibrational and rotational absorption bands of the optically active components.

Results of investigations on unresolved emission spectra (averaged over spectral intervals), obtained under natural as well as laboratory conditions, are widely used. Even though the patterns obtained (emission function) do not in reality describe the processes of selective transmission, they nonetheless permit us to solve a wide range of pure and applied problems connected with transfer of radiation in spectral intervals of different widths (cf. Ch. 2).

Because of the small extent and complexity of spectral investigations

in practice use is made of a method of evaluating atmospheric transparency with a simple actinometric apparatus widely distributed in the network of the Hydrometeorological Service. The application of integrated apparatus is associated with the ambiguity in the values of spectral transparency, but data of statistical significance have been obtained.

The fundamental problems connected with atmospheric transparency have been discussed in [15, 17, 24, 27, 30, 33, 47, 62].

Table 3.1 Index of refraction n of standard atmosphere for several values of temperature [112]

λ, μ	T°C				
	—30	—15	0	15	30
0.20	1.00038406	1.00036174	1.00034187	1.00032408	1.00030802
0.23	36526	34403	32514	30821	29294
0.26	35422	33363	31530	29889	28408
0.30	34552	32544	30756	29156	27711
0.35	33907	31936	30182	28611	27194
0.40	33509	31561	29828	28276	26875
0.45	33245	31312	29592	28052	26662
0.50	33060	31138	29428	27896	26514
0.55	32995	31011	29308	27783	26406
0.60	32824	30915	29218	27697	26325
0.65	32746	30842	29148	27631	26262
0.70	32684	30784	29093	27579	26213
0.75	32634	30737	29049	27537	26173
0.80	32594	30699	29013	27503	26140
0.90	32533	30641	28959	27451	26091
1.00	32489	30600	28920	27415	26056
1.50	32387	30504	28829	27329	25974
2.00	32351	30470	28797	27298	25940
3.00	32326	30447	28775	27277	25925
4.00	32317	30438	28767	27270	25918
5.00	32314	30435	28763	27267	25915
6.00	32311	30432	28761	27264	25913
7.00	32309	30431	28760	27263	25912
8.00	32309	30430	28759	27262	25912
10.0	32308	30429	28758	27262	25911
15.0	32307	30498	28757	27261	25910
20.0	32306	30428	28757	27260	25910

1. ATTENUATION OF MONOCHROMATIC RADIATION AT VARIOUS INCLINATIONS IN THE ATMOSPHERE. OPTICAL MASS

Attenuation of monochromatic radiation at various inclinations during its passage through the entire atmosphere (not considering the influence of radiation and the form of scattering on the intensity of direct radiation) may be given by the following formula:

$$J_\nu = J_{\nu 0} e^{-\int \beta_\nu \rho \, dl}, \tag{3.1}$$

where the integration is carried over along the contour and $\beta_\nu = k_\nu + \alpha_\nu$ — bulk attenuation factor determined by absorption and scattering.

The quantity $\int \beta_\nu \rho dl = \tau_{\nu \odot \text{total}}$, which is the optical thickness of the atmosphere in the direction of the source of light ;

and

$$\tau_{\nu \odot \text{ total}} = \sum_{i=1}^{n} \tau_{\nu \odot i},$$

where $\tau_{\nu \odot i}$—optical thickness of i-th component of the atmosphere.

In order to compute optical thickness at various inclinations it is convenient to determine the optical thickness $\tau_{\nu \text{ total}}$ for the vertical direction and then to recalculate it for any zenith angle $\vartheta_\odot$ with the help of the table giving the values $\tau_{\nu \odot \text{total}}/\tau_{\nu \text{total}} = m_\nu (\vartheta_\odot)$.

The quantity $m_\nu (\vartheta_\odot)$ is the optical mass of the atmosphere and gives the ratio of the optical thickness of the atmosphere along an inclination to the vertical optical thickness, which is equivalent to the ratio of the lengths of optical contours along these directions.

The dependence of m_ν upon frequency is determined by the frequency dependence of the refractive index of atmosphere n, whose computation in real atmosphere is complicated by the changes in its composition, temperature and pressure at different altitudes.

The dependence of refractive index (refractive index N_r) upon wavelength and atmospheric characteristics may be expressed numerically in the following form [112] :

$$N_r = (n-1) \times 10^6 = C(\lambda) G(p, T, e, p_0, \lambda), \tag{3.2}$$

with the condition

$$C(\lambda) = 272.729 + \frac{1}{\lambda^2} 1.4814 + \frac{1}{\lambda^4} 0.2039,$$

$$G = \frac{p\,[1 + (1.049 - 0.0157T)\ p \times 10^{-6}]}{720.883\ (1 + 0.003661\,T)} - \frac{p}{p_0 C\,(\lambda)} \frac{e\left(0.0624 - \frac{1}{\lambda^2} 0.00068\right)}{1 + 0.003661\,T}.$$

where λ = wavelength in μ ($\lambda = \frac{10{,}000}{\nu}$, if ν is in cm^{-1}), p=pressure at the given altitude in mm of Hg, p_0 = pressure at ground level in mm of Hg, T—temperature at the given altitude in °C, e—pressure of water vapor at the given altitude in mm of Hg.

The values of the limits of variation of refractive index for $\lambda = 0.3\,\mu$, where refraction is most noticeable, show that

$N_{r\ max} = 376$ (at $e=0$, $T=-50°C$, $p=800$ cm of Hg)

$N_{r\ min} = 227$ (at $e=96$ mm of H_g, $T=+50°C$, $p=650$ mm of Hg).

The values of N_r between 200 and 400 are taken for the computation.

In order to compute optical masses for the visible region of the spectrum it is usually possible to neglect the dependence of the refractive index on wavelength and the variation of N_r with atmospheric conditions and to use $N_r = 293.2$ and compute refractive index n for white light from the following expression :

$$n^2 = 1 + 2a\frac{\rho}{\rho_0}, \tag{3.3}$$

where $a = N_r \times 10^{-6}$, ρ—density of the atmosphere at the given altitude, ρ_0—density at the earth's surface.

The dependence of the optical mass of the atmosphere upon the zenith angle $\vartheta_\odot$ for the spherical earth's atmosphere is given by the approximate expression :

$$dm = \frac{1}{an_0 \sin \vartheta_\odot} \frac{r+H}{r} n^3 a\ \mathrm{Refr}, \tag{3.4}$$

where n_0 — refractive index at ground level,

r — radius of earth,

H — altitude above the ground, and

$$\mathrm{Refr} = \int_1^{n_0} \frac{\frac{r}{r+H}\frac{n_0}{n} \sin \vartheta_\odot\, dn}{\sqrt{1 - \left(\frac{r}{r+H}\frac{n_0}{n}\right)^2 \sin^2 \vartheta_\odot}}. \tag{3.5}$$

The results of computations for the entire atmosphere show that the following holds :

1. For $\vartheta_\odot < 60°$ it is possible to neglect refraction and consider the atmosphere to be made up of parallel plane layers, when

$$m = \sec \vartheta_\odot. \tag{3.6}$$

2. For $60 < \vartheta_\odot < 80°$ it is possible to neglect refraction, but it is necessary to consider the curvature of the earth's atmosphere

$$m = \frac{\sqrt{r^2 \cos^2 \vartheta_\odot + 2rH_0 + H_0^2} - r \cos \vartheta_\odot}{H_0}, \tag{3.7}$$

where H_0—height of uniform atmosphere ($H_0 = \int_0^\infty \frac{\rho}{\rho_0} dH = \frac{p}{\rho_0 g}$, g—acceleration due to gravity).

The following formula can be employed to a sufficient degree of accuracy:

$$m = \sec \vartheta_\odot - \frac{2.8}{(90 - \vartheta_\odot)^2}. \tag{3.8}$$

3. For $\vartheta_\odot > 80°$ atmospheric refraction becomes substantial. Computations of optical masses considering refraction for standard atmosphere ($p_0 = 1000$ mb, $T_0 = 0°$C) have been carried out by Bemporad [66]. Results of these calculations are given in Table 3.2.

Table 3.2 Optical masses for different zenith angles $\vartheta_\odot$ [66]

$\vartheta_\odot$	$m_\odot$	$\vartheta_\odot$	$m_\odot$	$\vartheta_\odot$	$m_\odot$	$\vartheta_\odot$	$m_\odot$
0°	1.000	18°	1.052	36°	1.235	54°	1.698
1	1.000	19	1.058	37	1.251	55	1.740
2	1.001	20	1.064	38	1.267	56	1.784
3	1.002	21	1.071	39	1.285	57	1.831
4	1.002	22	1.078	40	1.304	58	1.882
5	1.004	23	1.086	41	1.324	59	1.937
6	1.005	24	1.094	42	1.344	60	1.995
7	1.007	25	1.103	43	1.366	60°.1	2.001
8	1.010	26	1.112	44	1.389	60 .2	2.007
9	1.012	27	1.122	45	1.413	60 .3	2.013
10	1.015	28	1.132	46	1.438	60 .4	2.019
11	1.018	29	1.143	47	1.464	60 .5	2.025
12	1.022	30	1.154	48	1.492	60 .6	2.031
13	1.026	31	1.166	49	1.522	60 .7	2.037
14	1.030	32	1.178	50	1.553	60 .8	2.044
15	1.035	33	1.191	51	1.586	60 .9	2.050
16	1.040	34	1.205	52	1.621	61 .0	2.056
17	1.046	35	1.220	53	1.658	61 .1	2.062

Table 3.2—*Contd.*

$\vartheta_\odot$	$m_\odot$	$\vartheta_\odot$	$m_\odot$	$\vartheta_\odot$	$m_\odot$	$\vartheta_\odot$	$m_\odot$
61°.2	2.069	65°.9	2.437	70°.6	2.989	75°.3	3.890
61 .3	2.076	66 .0	2.447	70 .7	3.004	75 .4	3.915
61 .4	2.083	66 .1	2.456	70 .8	3.019	75 .5	3.941
61 .5	2.089	66 .2	2.466	70 .9	3.034	75 .6	3.967
61 .6	2.096	66 .3	2.476	71 .0	3.049	75 .7	3.993
61 .7	2.102	66 .4	2.486	71 .1	3.064	75 .8	4.020
61 .8	2.109	66 .5	2.496	71 .2	3.079	75 .9	4.047
61 .9	2.116	66 .6	2.506	71 .3	3.095	76 .0	4.075
62 .0	2.123	66 .7	2.516	71 .4	3.110	76 .1	4.103
62 .1	2.130	66 .8	2.526	71 .5	3.126	76 .2	4.131
62 .2	2.137	66 .9	2.536	71 .6	3.142	76 .3	4.159
62 .3	2.144	67 .0	2.546	71 .7	3.159	76 .4	4.188
62 .4	2.151	67 .1	2.556	71 .8	3.175	76 .5	4.218
62 .5	2.158	67 .2	2.567	71 .9	3.192	76 .6	4.248
62 .6	2.165	67 .3	2.577	72 .0	3.209	76 .7	4.278
62 .7	2.172	67 .4	2.588	72 .1	3.226	76 .8	4.309
62 .8	2.180	67 .5	2.599	72 .2	3.243	76 .9	4.340
62 .9	2.187	67 .6	2.610	72 .3	3.260	77 .0	4.372
63 .0	2.195	67 .7	2.621	72 .4	3.278	77 .1	4.404
63 .1	2.203	67 .8	2.632	72 .5	3.296	77 .2	4.436
63 .2	2.211	67 .9	2.643	72 .6	3.314	77 .3	4.469
63 .3	2.218	68 .0	2.654	72 .7	3.332	77 .4	4.503
63 .4	2.226	68 .1	2.665	72 .8	3.340	77 .5	4.537
63 .5	2.234	68 .2	2.677	72 .9	3.369	77 .6	4.572
63 .6	2.242	68 .3	2.688	73 .0	3.388	77 .7	4.607
63 .7	2.250	68 .4	2.700	73 .1	3.407	77 .8	4.643
63 .8	2.258	68 .5	2.712	73 .2	3.426	77 .9	4.679
63 .9	2.266	68 .6	2.724	73 .3	3.445	78 .0	4.716
64 .0	2.274	68 .7	2.736	73 .4	3.465	78 .1	4.753
64 .1	2.282	68 .8	2.748	73 .5	3.485	78 .2	4.792
64 .2	2.290	68 .9	2.760	73 .6	3.505	78 .3	4.831
64 .3	2.298	69 .0	2.773	73 .7	3.526	78 .4	4.870
64 .4	2.306	69 .1	2.773	73 .8	3.546	78 .5	4.910
64 .5	2.314	69 .2	2.798	73 .9	3.567	78 .6	4.950
64 .6	2.322	69 .3	2.811	74 .0	3.588	78 .7	4.992
64 .7	2.330	69 .4	2.824	74 .1	3.610	78 .8	5.034
64 .8	2.339	69 .5	2.837	74 .2	3.632	78 .9	5.077
64 .9	2.348	69 .6	2.850	74 .3	3.654	79 .0	5.120
65 .0	2.357	69 .7	2.863	74 .4	3.676	79 .1	5.164
65 .1	2.365	69 .8	2.877	74 .5	3.699	79 .2	5.210
65 .2	2.374	69 .9	2.880	74 .6	3.722	79 .3	5.256
65 .3	2.383	70 .0	2.904	74 .7	3.745	79 .4	5.303
65 .4	2.392	70 .1	2.918	74 .8	3.768	79 .5	5.531
65 .5	2.401	70 .2	2.932	74 .9	3.792	79 .6	5.399
65 .6	2.410	70 .3	2.946	75 .0	3.816	79 .7	5.448
65 .7	2.419	70 .4	2.960	75 .1	3.840	79 .8	5.498
65 .8	2.428	70 .5	2.975	75 .2	3.865	79 .9	5.549

Table 3.2—*Contd.*

$\vartheta_\odot$	$m_\odot$	$\vartheta_\odot$	$m_\odot$	$\vartheta_\odot$	$m_\odot$	$\vartheta_\odot$	$m_\odot$
80°.0	5.600	84°7′	9.054	84°54′	10.225	85°41′	11.717
80 .1	5.652	8	9.076	55	10.253	42	11.753
80 .2	5.705	9	9.098	56	10.281	43	11.790
80 .3	5.760	10	9.121	57	10.310	44	11.826
80 .4	5.816	11	9.143	58	10.338	45	11.863
80 .5	5.873	12	9.166	59	10.367	46	11.900
80 .6	5.932	13	9.189	85°0′	10.395	47	11.937
80 .7	5.992	14	9.212	1	10.424	48	11.974
80 .8	6.053	15	9.235	2	10.453	49	12.012
80 .9	6.114	16	9.258	3	10.483	50	12.050
81 .0	6.177	17	9.281	4	10.512	51	12.088
81 .1	6.241	18	9.304	5	10.542	52	12.126
81 .2	6.306	19	9.328	6	10.571	53	12.164
81 .3	6.373	20	9.351	7	10.601	54	12.202
81 .4	6.442	21	9.375	8	10.631	55	12.241
81 .5	6.512	22	9.399	9	10.661	56	12.280
81 .6	6.583	23	9.423	10	10.691	57	12.320
81 .7	6.656	24	9.447	11	10.722	58	12.359
81 .8	6.730	25	9.471	12	10.752	59	12.399
81 .9	6.806	26	9.495	13	10.783	86°0′	12.439
82 .0	6.884	27	9.520	14	10.814	1	12.480
82 .1	6.964	28	9.544	15	10.845	2	12.520
82 .2	7.045	29	9.569	16	10.876	3	12.561
82 .3	7.128	30	9.593	17	10.908	4	12.602
82 .4	7.213	31	9.618	18	10.939	5	12.643
82 .5	7.300	32	9.643	19	10.971	6	12.685
82 .6	7.389	33	9.668	20	11.003	7	12.727
82 .7	7.481	34	9.694	21	11.035	8	12.769
82 .8	7.574	35	9.719	22	11.068	9	12.811
82 .9	7.670	36	9.744	23	11.100	10	12.854
83 .0	7.768	37	9.770	24	11.133	11	12.897
83 .1	7.869	38	9.796	25	11.166	12	12.940
83 .2	7.972	39	9.822	26	11.199	13	12.983
83 .3	8.078	40	9.848	27	11.232	14	13.027
83 .4	8.186	41	9.874	28	11.266	15	13.071
83 .5	8.298	42	9.900	29	11.299	16	13.115
83 .6	8.412	43	9.926	30	11.333	17	13.160
83 .7	8.529	44	9.953	31	11.367	18	13.204
83 .8	8.650	45	9.979	32	11.401	19	13.249
83 .9	8.773	46	10.006	33	11.435	20	13.294
84° 0′	8.900	47	10.033	34	11.470	21	13.340
1	8.922	48	10.060	35	11.505	22	13.386
2	8.944	49	10.087	36	11.540	23	13.432
3	8.966	50	10.114	37	11.575	24	13.478
4	8.988	51	10.142	38	11.610	25	13.525
5	9.010	52	10.169	39	11.615	26	13.572
6	9.032	53	10.197	40	11.681	27	13.619

Table 3.2—*Contd.*

$\vartheta_\odot$	$m_\odot$	$\vartheta_\odot$	$m_\odot$	$\vartheta_\odot$	$m_\odot$	$\vartheta_\odot$	$m_\odot$
86°28′	13.667	87°7′	15.787	87°46′	18.571	88°25′	22.331
29	13.715	8	15.849	47	18.653	26	22.445
30	13.763	9	15.912	48	18.736	27	22.559
31	13.812	10	15.975	49	18.820	28	22.674
32	13.860	11	16.038	50	18.905	29	22.790
33	13.909	12	16.102	51	18.990	30	22.980
34	13.959	13	16.166	52	19.076	31	23.026
35	14.009	14	16.231	53	19.162	32	23.146
36	14.059	15	16.296	54	19.249	33	23.266
37	14.109	16	16.362	55	19.337	34	23.387
38	14.160	17	16.428	56	19 426	35	23.510
39	14.211	18	16.494	57	19.515	36	23.633
40	14.262	19	16.561	58	19.605	37	23.758
41	14.314	20	16.629	59	19 696	38	23.884
42	14.366	21	16.697	88°0′	19.787	39	24.011
43	14.419	22	16.765	1	19.879	40	24.139
44	14.471	23	16.834	2	19.971	41	24.268
45	14.524	24	16.903	3	20.065	42	24.398
46	14.578	25	16.973	4	20.160	43	24.529
47	14.432	26	17.044	5	20.255	44	24.662
48	14.686	27	17.115	6	20.351	45	24.796
49	14.740	28	17.187	7	20.448	46	24.931
50	14.805	29	17.259	8	20.545	47	25.068
51	14.860	30	17.331	9	20.643	48	25.205
52	14.906	31	17.404	10	20.742	49	25.343
53	14.962	32	17.478	11	20.842	50	25.483
54	15.018	33	17.552	12	20.943	51	25.625
55	15.075	34	17.627	13	21.045	52	25.767
56	15.132	35	17.702	14	21.147	53	25.911
57	15.190	36	17.778	15	21.250	54	26.057
58	15.248	37	17.855	16	21.355	55	26.203
59	15.306	38	17.932	17	21.460	56	26.351
87°0′	15.365	39	18.010	18	21.566	57	26.501
1	15.424	40	18.088	19	21.672	58	26.652
2	15.483	41	18.167	20	21.779	59	26.805
3	15.543	42	18.247	21	21.888	89°0′	26.959
4	15.603	43	18.327	22	21.997		
5	15.664	44	18.408	23	22.108		
6	15.725	45	18.489	24	22.219		

For the computation of optical thickness of a spherical shell, located at an altitude H above ground level, the following expression may be used:

$$m(\vartheta_\odot)=\frac{1}{x}\int_{H_1}^{H_2}\frac{\rho' dH}{\sqrt{1-\left(\frac{r}{r+H}\times\frac{n_0}{n}\right)^2\sin^2\vartheta_\odot}}, \tag{3.9}$$

where $x=\int_{H_1}^{H_2}\rho' dH$ (ρ'—concentration of the substance, attenuating radiation).

For $\vartheta_\odot<60°$ formula (3.9) leads to the relation

$$m(\vartheta_\odot)=\sec\vartheta_\odot \tag{3.10}$$

For $60<\vartheta_\odot<80°$ consideration of curvature of the atmosphere alone leads to the following

$$m(\vartheta_\odot)=\frac{1}{\sqrt{1-\frac{\sin^2\vartheta_\odot}{\left(1+\frac{H_1}{r}\right)^2}}}. \tag{3.11}$$

where H_1—height of the lower boundary of the layer.

For the ozone layer computations of the function $m(h_\odot)$ are given in Table 3.3 [18].

"Absolute" optical masses are also used in actinometry besides relative optical masses m and $m(\vartheta_\odot)$ defined by

$$m'=\frac{p}{p_0}m, \tag{3.12}$$

where $p_0=1000$ mb.

It should be noticed that the introduction of optical thickness at normal pressure can be justified only in the case of a direct relation of the attenuation factor (e.g. caused by molecular scattering) to pressure, as well as in the consideration of an exponential distribution of attenuating components.

Table 3.3 Optical mass of spherical (ozone) layer $m_\odot$ ($h_\odot$) depending on apparent solar altitude $h_\odot{}^\circ$ [18]

$h_\odot$	$m_\odot$	$h_\odot$	$m_\odot$	$h_\odot$	$m_\odot$	$h_\odot$	$m_\odot$
5.0	8.238	9.5	5.402	14.0	3.915	18.5	3.056
5.1	8.157	9.6	5.361	14.1	3.889	18.6	3.041
5.2	8.071	9.7	5.316	14.2	3.864	18.7	3.026
5.3	7.988	9.8	5.272	14.3	3.843	18.8	3.011
5.4	7.912	9.9	5.233	14.4	3.818	18.9	2.996
5.5	7.831	10.0	5.186	14.5	3.794	19.0	2.982
5.6	7.752	10.1	5.148	14.6	3.774	19.1	2.969
5.7	7.672	10.2	5.107	14.7	3.750	19.2	2.954
5.8	7.597	10.3	5.066	14.8	3.726	19.3	2.940
5.9	7.523	10.4	5.026	14.9	3.707	19.4	2.926
6.0	7.447	10.5	4.987	15.0	3.684	19.5	2.912
6.1	7.373	10.6	4.952	15.1	3.661	19.6	2.901
6.2	7.298	10.7	4.910	15.2	3.639	19.7	2.887
6.3	7.227	10.8	4.876	15.3	3.619	19.8	2.873
6.4	7.155	10.9	4.839	15.4	3.599	19.9	2.860
6.5	7.087	11.0	4.803	15.5	3.577	20.0	2.847
6.6	7.018	11.1	4.764	15.6	3.556	20.1	2.833
6.7	6.950	11.2	4.732	15.7	3.538	20.2	2.822
6.8	6.884	11.3	4.694	15.8	3.517	20.3	2.809
6.9	6.816	11.4	4.663	15.9	3.497	20.4	2.797
7.0	6.752	11.5	4.626	16.0	3.476	20.5	2.784
7.1	6.689	11.6	4.598	16.1	3.460	20.6	2.772
7.2	6.626	11.7	4.560	16.2	3.440	20.7	2.761
7.3	6.563	11.8	4.531	16.3	3.420	20.8	2.749
7.4	6.502	11.9	4.496	16.4	3.404	20.9	2.737
7.5	6.442	12.0	4.468	16.5	3.385	21.0	2.724
7.6	6.383	12.1	4.434	16.6	3.366	21.1	2.712
7.7	6.323	12.2	4.406	16.7	3.350	21.2	2.700
7.8	6.266	12.3	4.374	16.8	3.332	21.3	2.691
7.9	6.208	12.4	4.344	16.9	3.313	21.4	2.679
8.0	6.155	12.5	4.315	17.0	3.295	21.5	2.667
8.1	6.091	12.6	4.284	17.1	3.277	21.6	2.656
8.2	6.038	12.7	4.258	17.2	3.262	21.7	2.645
8.3	5.986	12.8	4.227	17.3	3.245	21.8	2.633
8.4	5.935	12.9	4.202	17.4	3.227	21.9	2.622
8.5	5.885	13.0	4.172	17.5	3.210	22.0	2.613
8.6	5.836	13.1	4.143	17.6	3.193	22.1	2.602
8.7	5.778	13.2	4.119	17.7	3.179	22.2	2.591
8.8	5.730	13.3	4.091	17.8	3.162	22.3	2.580
8.9	5.684	13.4	4.062	17.9	3.146	22.4	2.570
9.0	5.638	13.5	4.039	18.0	3.130	22.5	2.559
9.1	5.584	13.6	4.012	18.1	3.116	22.6	2.549
9.2	5.539	13.7	3.989	18.2	3.100	22.7	2.540
9.3	5.496	13.8	3.963	18.3	3.085	22.8	2.530
9.4	5.445	13.9	3.936	18.4	3.069	22.9	2.520

Table 3.3—*Contd.*

$h_\odot$	$m_\odot$	$h_\odot$	$m_\odot$	$h_\odot$	$m_\odot$	$h_\odot$	$m_\odot$
23.0	2.509	27.6	2.130	32.2	1.859	36.8	1.658
23.1	2.499	27.7	2.123	32.3	1.854	36.9	1.655
23.2	2.489	27.8	2.117	32.4	1.850	37.0	1.651
23.3	2.480	27.9	2.110	32.5	1.845	37.1	1.648
23.4	2.471	28.0	2.104	32.6	1.840	37.2	1.644
23.5	2.462	28.1	2.097	32.7	1.835	37.3	1.640
23.6	2.452	28.2	2.090	32.8	1.830	37.4	1.636
23.7	2.443	28.3	2.083	32.9	1.825	37.5	1.633
23.8	2.433	28.4	2.077	33.0	1.821	37.6	1.629
23.9	2.424	28.5	2.070	33.1	1.816	37.7	1.625
24.0	2.414	28.6	2.064	33.2	1.811	37.8	1.621
24.1	2.406	28.7	2.058	33.3	1.806	37.9	1.618
24.2	2.398	28.8	2.052	33.4	1.801	38.0	1.615
24.3	2.389	28.9	2.045	33.5	1.797	38.1	1.611
24.4	2.380	29.0	2.039	33.6	1.792	38.2	1.607
24.5	2.371	29.1	2.033	33.7	1.787	38.3	1.604
24.6	2.362	29.2	2.027	33.3	1.784	38.4	1.600
24.7	2.353	29.3	2.020	33.9	1.779	38.5	1.597
24.8	2.344	29.4	2.014	34.0	1.774	38.6	1.594
24.9	2.336	29.5	2.008	34.1	1.770	38.7	1.591
25.0	2.328	29.6	2.002	34.2	1.765	38.8	1.587
25.1	2.320	29.7	1.996	34.3	1.761	38.9	1.584
25.2	2.311	29.8	1.990	34.4	1.756	39.0	1.580
25.3	2.303	29.9	1.985	34.5	1.752	39.1	1.577
25.4	2.295	30.0	1.979	34.6	1.748	39.2	1.574
25.5	2.287	30.1	1.973	34.7	1.743	39.3	1.570
25.6	2.278	30.2	1.967	34.8	1.739	39.4	1.567
25.7	2.270	30.3	1.961	34.9	1.735	39.5	1.564
25.8	2.263	30.4	1.956	35.0	1.730	39.6	1.561
25.9	2.256	30.5	1.950	35.1	1.726	39.7	1.557
26.0	2.248	30.6	1.944	35.2	1.722	39.8	1.554
26.1	2.240	30.7	1.938	35.3	1.718	39.9	1.551
26.2	2.232	30.8	1.933	35.4	1.714	40.0	1.548
26.3	2.224	30.9	1.927	35.5	1.710	40.1	1.544
26.4	2.217	31.0	1.922	35.6	1.706	40.2	1.141
26.5	2.209	31.1	1.917	35.7	1.702	40.3	1.538
26.6	2.201	31.2	1.912	35.8	1.698	40.4	1.535
26.7	2.194	31.3	1.907	35.9	1.694	40.5	1.532
26.8	2.188	31.4	1.901	36.0	1.690	40.6	1.529
26.9	2.180	31.5	1.896	36.1	1.686	40.7	1.526
27.0	2.173	31.6	1.891	36.2	1.682	40.8	1.523
27.1	2.166	31.7	1.885	36.3	1.678	40.9	1.520
27.2	2.158	31.8	1.880	36.4	1.674	41.0	1.517
27.3	2.151	31.9	1.875	36.5	1.670	41.1	1.514
27.4	2.144	32.0	1.870	36.6	1.666	41.2	1.511
27.5	2.137	32.1	1.864	36.7	1.662	41.3	1.508

Table 3.3—*Contd.*

$h_\odot$	$m_\odot$	$h_\odot$	$m_\odot$	$h_\odot$	$m_\odot$	$h_\odot$	$m_\odot$
41.4	1.505	46.0	1.385	50.6	1.291	55.2	1.215
41.5	1.502	46.1	1.383	50.7	1.289	55.3	1.214
41.6	1.499	46.2	1.381	50.8	1.287	55.4	1.212
41.7	1.496	46.3	1.379	50.9	1.285	55.5	1.211
41.8	1.493	46.4	1.376	51.0	1.284	55.6	1.210
41.9	1.490	46.5	1.374	51.1	1.282	55.7	1.208
42.0	1.487	46.6	1.372	51.2	1.280	55.8	1.207
42.1	1.484	46.7	1.369	51.3	1.278	55.9	1.206
42.2	1.482	46.8	1.367	51.4	1.277	56.0	1.204
42.3	1.479	46.9	1.365	51.5	1.275	56.1	1.203
42.4	1.476	47.0	1.363	51.6	1.273	56.2	1.201
42.5	1.473	47.1	1.361	51.7	1.271	56.3	1.200
42.6	1.471	47.2	1.359	51.8	1.269	56.4	1.199
42.7	1.468	47.3	1.357	51.9	1.268	56.5	1.197
42.8	1.465	47.4	1.354	52.0	1.266	56.6	1.196
42.9	1.463	47.5	1.352	52.1	1.264	56.7	1.194
43.0	1.460	47.6	1.350	52.2	1.263	56.8	1.193
43.1	1.457	47.7	1.348	52.3	1.261	56.9	1.192
43.2	1.454	47.8	1.346	52.4	1.259	57.0	1.190
43.3	1.452	47.9	1.344	52.5	1.258	57.1	1.189
43.4	1.449	48.0	1.342	52.6	1.256	57.2	1.188
43.5	1.446	48.1	1.340	52.7	1.254	57.3	1.186
43.6	1.444	48.2	1.338	52.8	1.253	57.4	1.185
43.7	1.441	48.3	1.335	52.9	1.251	57.5	1.184
43.8	1.439	48.4	1.333	53.0	1.250	57.6	1.182
43.9	1.436	48.5	1.331	53.1	1.248	57.7	1.181
44.0	1.434	48.6	1.329	53.2	1.246	57.8	1.180
44.1	1.431	48.7	1.327	53.3	1.245	57.9	1.179
44.2	1.429	48.8	1.325	53.4	1.243	58.0	1.177
44.3	1.426	48.9	1.323	53.5	1.242	58.1	1.176
44.4	1.424	49.0	1.321	53.6	1.240	58.2	1.175
44.5	1.421	49.1	1.319	53.7	1.238	58.3	1.173
44.6	1.419	49.2	1.317	53.8	1.237	58.4	1.172
44.7	1.416	49.3	1.315	53.9	1.235	58.5	1.171
44.8	1.414	49.4	1.313	54.0	1.234	58.6	1.169
44.9	1.412	49.5	1.311	54.1	1.232	58.7	1.168
45.0	1.409	49.6	1.310	54.2	1.231	58.8	1.167
45.1	1.407	49.7	1.308	54.3	1.229	58.9	1.166
45.2	1.404	49.8	1.306	54.4	1.227	59.0	1.165
45.3	1.402	49.9	1.304	54.5	1.226	59.1	1.164
45.4	1.400	50.0	1.302	54.6	1.224	59.2	1.163
45.5	1.397	50.1	1.300	54.7	1.223	59.3	1.161
45.6	1.395	50.2	1.298	54.8	1.221	59.4	1.160
45.7	1.392	50.3	1.296	54.9	1.220	59.5	1.159
45.8	1.390	50.4	1.295	55.0	1.218	59.6	1.158
45.9	1.388	50.5	1.293	55.1	1.217	59.7	1.157

Table 3.3—*Contd.*

$h_\odot$	$m_\odot$	$h_\odot$	$m_\odot$	$h_\odot$	$m_\odot$	$h_\odot$	$m_\odot$
59.8	1.155	63.7	1.114	67.6	1.081	71.5	1.054
59.9	1.154	63.8	1.113	67.7	1.080	71.6	1.053
60.0	1.153	63.9	1.112	67.8	1.079	71.7	1.053
60.1	1.152	64.0	1.111	67.9	1.078	71.8	1.052
60.2	1.151	64.1	1.111	68.0	1.078	71.9	1.051
60.3	1.150	64.2	1.110	68.1	1.077	72.0	1.051
60.4	1.149	64.3	1.108	68.2	1.076	72.1	1.050
60.5	1.147	64.4	1.107	68.3	1.075	72.2	1.050
60.6	1.146	64.5	1.107	68.4	1.075	72.3	1.049
60.7	1.145	64.6	1.106	68.5	1.074	72.4	1.049
60.8	1.144	64.7	1.105	68.6	1.073	72.5	1.048
60.9	1.143	64.8	1.104	68.7	1.073	72.6	1.047
61.0	1.142	64.9	1.103	68.8	1.072	72.7	1.047
61.1	1.141	65.0	1.102	68.9	1.071	72.8	1.046
61.2	1.140	65.1	1.101	69.0	1.070	72.9	1.046
61.3	1.139	65.2	1.101	69.1	1.070	73.0	1.045
61.4	1.138	65.3	1.100	69.2	1.069	73.1	1.044
61.5	1.137	65.4	1.099	69.3	1.068	73.2	1.044
61.6	1.135	65.5	1.098	69.4	1.068	73.3	1.043
61.7	1.134	65.6	1.097	69.5	1.067	73.4	1.043
61.8	1.133	65.7	1.096	69.6	1.066	73.5	1.042
61.9	1.132	65.8	1.095	69.7	1.065	73.6	1.042
62.0	1.131	65.9	1.095	69.8	1.065	73.7	1.041
62.1	1.130	66.0	1.094	69.9	1.064	73.8	1.041
62.2	1.129	66.1	1.093	70.0	1.063	73.9	1.040
62.3	1.128	66.2	1.092	70.1	1.063	74.0	1.039
62.4	1.127	66.3	1.091	70.2	1.062	74.1	1.039
62.5	1.126	66.4	1.090	70.3	1.062	74.2	1.038
62.6	1.125	66.5	1.090	70.4	1.061	74.3	1.038
62.7	1.124	66.6	1.089	70.5	1.060	74.4	1.038
62.8	1.123	66.7	1.088	70.6	1.060	74.5	1.037
62.9	1.122	66.8	1.087	70.7	1.059	74.6	1.037
63.0	1.121	66.9	1.086	70.8	1.058	74.7	1.036
63.1	1.120	67.0	1.085	70.9	1.058	74.8	1.036
63.2	1.119	67.1	1.085	71.0	1.057	74.9	1.035
63.3	1.118	67.2	1.084	71.1	1.056	75.0	1.034
63.4	1.117	67.3	1.083	71.2	1.056		
63.5	1.116	67.4	1.082	71.3	1.055		
63.6	1.115	67.5	1.082	71.4	1.055		

2. SELECTIVE ABSORPTION IN CASE OF INHOMOGENEOUS ATMOSPHERE

2.1 Method of reduced absorbent masses

The computation of absorption (cf. Ch. 2) in a nonuniform direction while introducing a somewhat reduced (effective) mass of absorbent gas u_{eff} possessing equivalent absorption in the case of homogeneous direction with fixed p and T can be accomplished, if the absorption coefficient $k_\nu\ (pT)$ is represented in the form

$$k_\nu\ (p,\ T)=\psi\ (p,\ T)\ \psi\ (\nu)=S_\lambda\ (T)\ p\ (p)\ \psi\ (\nu), \tag{3.13}$$

although this is not possible in the general case of a Lorentzian contour. Then the amount of absorption is determined not as a function of these parameters but as a single parameter u_{eff} and the optical thickness of the nonuniform path $\tau(\nu)$ may be expressed as follows :

$$\tilde{\tau}(\nu)=u_{eff}\ Q\ (p_0,\ T_0,\ \nu), \tag{3.14}$$

where Q—absorption function under standard conditions of p_0 and T_0 and u_{eff} is expressed as a function of p and T as follows :

$$u_{eff}=\sec\vartheta_\odot \int_{H_n}^{H_{n+1}} \rho_\alpha\ (H) \left(\frac{p\ (\vartheta_\odot)}{p_0}\right)^m \left(\frac{T_0}{T\ (H)}\right)^n dH. \tag{3.15}$$

The value of the parameter m depends upon the amount of absorption. In weak absorption, when the spectral lines do not overlap, total absorption is proportional to the quantity of the substance and does not depend upon pressure, and in this case $m=0$. The values of m and n for distinct bands are given in Ch. 2.

2.2 Approximation with two parameters

The method of two-parameter approximation is based on the selection of mean pressure and the amount of absorbent gas in the equivalent homogeneous path. Not only the intensity but the width of absorption lines are selected in such a manner that the most accurate results can be obtained in the regions where the approximation of weak and strong lines is justified. Because of this the transitional regions can be studied more accurately [17].

A nonuniform layer may be substituted by a homogeneous one to be found at constant weighted mean pressure p_{eff} and temperature T_0.

Optical thickness in a nonuniform course $\tau(\nu)$ can be replaced by the following expression:

$$\bar{\tau}(\nu) = u'_{eff}\, Q(p_{eff}, \nu), \tag{3.16}$$

where

$$\mu_{eff} = \sec \vartheta_{\odot} \int_{H_n}^{H_{n+1}} \rho_{\alpha}(H)\, dH, \tag{3.17}$$

$$p_{eff} = \frac{\int_{H_n}^{H_{n+1}} f(T)\, \rho_{\alpha}(H)\, p(H)\, dH}{\int_{H_n}^{H_{n+1}} \rho_{\alpha}(H)\, dH}, \tag{3.18}$$

function $f(T)$ represents the dependence of absorption upon temperature (cf. Ch. 2).

In [17] the conditions of the application of two-parameter approximation to real atmosphere for a statistical absorption model have been examined. It has been found that the application of this approximation is not suitable when a large part of the absorbent gas (e.g. ozone) lies under low pressure. For cases where the mixing ratio decreases with altitude as well as when the mixing ratio is constant (assuming stratification), this approximation is in close agreement with accurate numerical computations of ratio of mixtures and pressure within a wide range. Reference [24] demonstrates the applicability of the method of weighted mean pressure in the interval between regions where the approximation of weak and strong lines is justified in narrow (0.1 μ) as well as in wide segments of the spectrum.

3. ATMOSPHERIC TRANSPARENCY CAUSED BY MOLECULAR SCATTERING

It is possible to express optical thickness of dry and pure atmosphere considering molecular scattering in the following manner:

$$\tau_{\lambda\,mol} = mf \int_{H}^{\infty} \beta_{\lambda\,mol}(H)\, dH, \tag{3.19}$$

where $\beta_{\lambda mol}$—volume attenuation coefficient caused by molecular scattering : $f=\frac{6+3\,\rho_n}{6-7\,\rho_n}$ is the anisotropy coefficient approximately equal to 1.061 (ρ_n—depolarization factor, whose mean value for atmosphere $\rho_n=0.037$).

Optical thickness for a vertical column of uniform atmosphere may be expressed as follows :

$$\tau_{\lambda\ mol}=\frac{f\beta_{0\lambda\ mol}p_0}{\rho_0 g}=fH_0\sigma_{0\lambda\ mol}, \tag{3.20}$$

where p_0 and ρ_0 are the pressure and density of the layer of the atmosphere near the earth's surface, respectively, g—acceleration due to gravity ; H_0—altitude of homogeneous atmosphere.

Considering the explicit dependence of optical thickness on wavelength, F. Linke gave an approximate expression for the optical thickness of a vertical column of dry and pure atmosphere as follows :

$$\tau_{\lambda mol}=0.00879\ \lambda^{-4.09}, \tag{3.21}$$

where λ—wavelength in micrometers.

Table 3.4 gives computed values of optical thickness $\tau_{\lambda\ mol}$ of a vertical column of dry and pure atmosphere in the spectral range 0.28-2.17 μ, which were used in the 1968 model [79]. Computations were carried out for a layer of 80 km.

Table 3.4 Spectral transparency in vertical thickness of dry and pure atmosphere [79]

λ, μ	$\tau_{\lambda_{mol}}$	λ, μ	$\tau_{\lambda_{mol}}$
0.28	1.545	0.60	0.069
0.30	1.222	0.65	0.050
0.32	0.927	0.70	0.037
0.34	0.717	0.80	0.021
0.36	0.564	0.90	0.013
0.38	0.450	1.06	0.007
0.40	0.364	1.26	0.003
0.45	0.223	1.67	0.001
0.50	0.145	2.17	0.000
0.55	0.098		

Table 3.5 Values of $\tau_{\lambda mol}$ at different altitudes in NO_2 atmosphere [76]

h km	$\lambda=0.375\,\mu$	$\lambda=0.520\,\mu$	$\lambda=0.835\,\mu$
0	0.4542	0.1181	0.017315
2	0.3566	0.0927	0.01360
4	0.2770	0.0720	0.01056
6	0.2127	0.0553	0.00811
8	0.1608	0.0418	0.00613
10	0.1196	0.0311	0.00456
12	0.0879	0.02285	0.00335
16	0.0473	0.0123	0.001805
20	0.0255	0.00663	0.000972
24	0.0138	0.00358	0.000524
30	0.00546	0.00142	0.000209
50	0.00043	0.00011	0.000017
70	0.000037	0.0000095	0.0000014
100	0.00000022	0.000000058	0.0000000085

Optical thicknesses of NO_2 atmosphere at different altitudes between 0 and 100 km have been computed for three wavelengths : 0.375, 0.520, 0.835 μ and are given in Table 3.5 [76].

There is a change in the value of $\tau_{\lambda mol}$ comprising 1% at ground level and 4-6% at an altitude of 8 km [76] brought about by the variation in parameters which determine optical thickness, (magnitude of $\tau_{\lambda mol}$ has a maximum value in summer). The values of optical thickness of atmosphere for altitudes ranging from 0-30 km in the interval of wavelength 0.3-1.3 μ are given in [109, 110].

Table 3.6 gives the value of volume attenuation coefficient $\tau_{\lambda mol}$ in the range 0.27-4 μ computed for layers of atmosphere of width 1 km up to an altitude of 50 km [79].

In actual practice the solid angle of sensitivity of any radiation receiver is $\triangle\omega\neq 0$, so that not only direct attenuated radiation but also radiation scattered by the medium fall on the receiving plane. The scheme of the scattering process is given in Fig. 3.1. The amount of contribution from scattering is of interest in this case. The contribution of double-scattering of light to the intensity of direct attenuated radiation

depends upon wavelength, albedo, incident angle $\vartheta_\odot$ of radiation with intensity $I_{0\lambda}$, falling on a layer of atmosphere of optical thickness $\tau_{\lambda mol}$. The scattered radiation I_m and I_a enter the receiver along with direct radiation I_d attenuated by the medium. The equation of monochromatic radiative transition in this case has the following form :

$$F_\lambda = F_{\lambda_0} \exp\left[\left(-\frac{\tau_\lambda}{\cos\vartheta_\odot}\right) + (I_{\lambda_m} + I_{\lambda a}) \triangle \omega\right], \qquad (3.22)$$

where $F_{\lambda_0} = \pi I_{\lambda_0}$—flux of monochromatic radiation on the boundary of the layer.

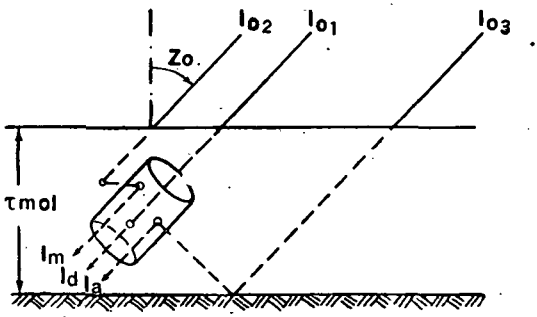

Fig. 3.1. Contribution of multiple scattering to the flux of direction radiation.

D. Deirmendjian and Z. Sekera [71] carried out computations at $1 \geqslant \cos\vartheta_\odot \geqslant 0.2$ for wavelength $0.809\,\mu \geqslant \lambda \geqslant 0.312\,\mu$, uniquely connected with optical thickness $0.02 \leqslant \tau_{\lambda mol} \leqslant 1.00$. Two values : 0.25 and 0.8 of albedo were considered. Selected results of the computations for the limiting parameters are given in Table 3.7. The magnitude of flux F_0 is normalized to unity.

Recently a lot of research work has been published in connection with effects playing a secondary role in the process of molecular attenuation. Thus in [73] the values of scattering up to the 13th order ($\lambda = 0.3120\,\mu$) have been derived. The problems of multiple scattering, influences of temperature on molecular attenuation and effects of absorption in molecular atmosphere have been investigated in [72, 73, 82, 96].

Table 3.6 Distribution of attenuation coefficient $\beta_{\lambda mol}$ km^{-1}

H km	λ, μ				
	0.27	0.28	0.30	0.32	0.34
0	2.282×10^{-1}	1.948×10^{-1}	1.446×10^{-1}	1.098×10^{-1}	8.492×10^{-2}
2	1.875	1.600	1.188	9.020×10^{-2}	6.979
4	1.527	1.303	9.672×10^{-2}	7.342	5.680
6	1.230	1.050	7.792	5.915	4.576
8	9.795×10^{-2}	8.359×10^{-2}	6.207	4.712	3.645
10	7.703	6.574	4.881	3.705	2.867
12	5.811	4.959	3.682	2.795	2.162
14	4.245	3.623	2.690	2.042	1.580
16	3.101	2.647	1.965	1.492	1.154
18	2.266	1.934	1.436	1.090	8.433×10^{-3}
20	1.656	1.413	1.049	7.966	6.164
22	1.202	1.026	7.614×10^{-3}	5.780	4.472
24	8.744×10^{-3}	7.461×10^{-3}	5.540	4.205	3.254
26	6.381	5.446	4.043	3.069	2.375
28	4.671	3.986	2.960	2.247	1.738
30	3.430	2.927	2.173	1.649	1.276
32	2.525	2.155	1.600	1.214	9.397×10^{-4}
34	1.842	1.572	1.167	8.859×10^{-4}	6.854
36	1.352	1.154	8.566×10^{-4}	6.503	5.031
38	9.997×10^{-4}	8.531×10^{-4}	6.334	4.808	3.720
40	7.443	6.352	4.716	3.580	2.770
42	5.579	4.761	3.534	2.683	2.076
44	4.208	3.591	2.666	2.024	1.566
46	3.193	3.725	2.023	1.536	1.188
48	2.453	2.093	1.554	1.180	9.128×10^{-5}
50	1.913	1.632	1.212	9.201×10^{-5}	7.119

with altitude, caused by molecular scattering [79]

λ, μ					
0.36	0.38	0.40	0.45	0.50	0.55
6.678×10^{-2}	5.327×10^{-2}	4.303×10^{-2}	2.644×10^{-2}	1.716×10^{-2}	1.162×10^{-2}
5.487	4.377	3.536	2.173	1.410	9.552×10^{-3}
4.467	3.563	2.878	1.769	1.148	7.775
3.599	2.871	2.319	1.425	9.246×10^{-3}	6.264
2.866	2.286	1.847	1.135	7.364	4.989
2.254	1.798	1.452	8.926×10^{-3}	5.792	3.924
1.701	1.356	1.096	6.734	4.369	2.960
1.242	9.908×10^{-3}	8.003×10^{-3}	4.919	3.191	2.162
9.075×10^{-3}	7.239	5.847	3.593	2.332	1.580
6.632	5.290	4.273	2.626	1.704	1.154
4.847	3.866	3.122	1.919	1.245	8.436×10^{-4}
3.517	2.805	2.266	1.392	9.034×10^{-4}	6.121
2.559	2.041	1.648	1.013	6.573	4.453
1.868	1.489	1.203	7.394×10^{-4}	4.797	3.250
1.367	1.090	8.807×10^{-4}	5.412	3.512	2.379
1.004	8.004×10^{-4}	6.465	3.973	2.578	1.747
7.390×10^{-4}	5.893	4.760	2.926	1.898	1.286
5.391	4.299	3.472	2.134	1.385	9.381×10^{-5}
3.957	3.156	2.549	1.566	1.016	6.886
2.926	2.333	1.885	1.158	7.516×10^{-5}	5.092
2.178	1.737	1.403	8.624	5.596	3.791
1.633	1.302	1.052	6.464	4.194	2.841
1.232	9.821×10^{-5}	7.933×10^{-5}	4.875	3.163	2.143
9.345×10^{-5}	7.453	6.020	3.700	2.400	1.626
7.179	5.725	4.624	2.842	1.844	1.249
5.598	4.465	3.606	2.216	1.438	9.746×10^{-6}

Table 3.6—*Contd.*

H km	λ, μ				
	0.60	0.65	0.70	0.80	0.90
0	8.157×10^{-3}	5.893×10^{-3}	4.364×10^{-3}	2.545×10^{-3}	1.583×10^{-3}
2	6.703	4.842	3.586	2.091	1.300
4	5.456	3.941	2.919	1.702	1.058
6	4.396	3.175	2.352	1.371	8.528×10^{-4}
8	3.501	2.529	1.873	1.092	6.792
10	2.753	1.989	1.473	8.590×10^{-4}	5.342
12	2.077	1.500	1.111	6.480	4.030
14	1.517	1.096	8.117×10^{-4}	4.733	2.944
16	1.109	8.007×10^{-4}	5.930	3.458	2.151
18	8.100×10^{-4}	5.851	4.334	2.527	1.572
20	5.920	4.276	3.167	1.847	1.148
22	4.295	3.103	2.298	1.340	8.333×10^{-5}
24	3.125	2.257	1.672	9.749×10^{-5}	6.063
26	2.281	1.648	1.220	7.115	4.425
28	1.670	1.206	8.932×10^{-5}	5.208	3.239
30	1.226	8.854×10^{-5}	6.557	3.824	2.378
32	9.025	6.519	4.828	2.815	1.751
34	6.583	4.755	3.522	2.054	1.277
35	4.832	3.491	2.585	1.507	9.375×10^{-6}
38	3.573	2.581	1.912	1.115	6.932
40	2.660	1.922	1.423	8.299×10^{-6}	5.161
42	1.994	1.440	1.067	6.220	3.868
44	1.504	1.086	8.046×10^{-6}	4.692	2.918
46	1.141	8.244×10^{-6}	6.105	3.560	2.214
48	8.766×10^{-6}	6.333	4.690	2.735	2.214
50	6.837	4.939	3.658	2.133	1.326

Table 3.6—*Contd.*

λ, μ					
1.06	1.26	1.67	2.17	3.50	4.00
8.458×10^{-4}	4.076×10^{-4}	1.327×10^{-4}	4.586×10^{-5}	6.830×10^{-6}	4.002×10^{-6}
6.950	3.349	1.091	3.768	5.612	3.289
5.657	2.726	8.877×10^{-5}	3.067	4.568	2.677
4.558	2.196	7.152	2.471	3.680	2.157
3.630	1.749	5.697	1.968	2.931	1.718
2.855	1.376	4.480	1.548	2.305	1.351
2.154	1.038	3.380	1.168	1.739	1.019
1.573	7.582×10^{-5}	2.469	8.529×10^{-6}	1.270	7.444×10^{-7}
1.149	5.539	1.804	6.231	9.281×10^{-7}	5.439
8.399×10^{-5}	4.048	1.318	4.554	6.782	3.974
6.138	2.958	9.632×10^{-6}	3.328	4.956	2.904
4.453	2.146	6.989	2.415	3.596	2.107
3.240	1.562	5.085	1.757	2.617	1.533
2.365	1.140	3.711	1.282	1.910	1.119
1.731	8.343×10^{-6}	2.717	9.385×10^{-7}	1.398	8.191×10^{-8}
1.271	6.125	1.994	6.890	1.026	6.014
9.357×10^{-6}	4.510	1.468	5.073	8.803×10^{-8}	4.428
6.826	3.289	1.071	3.701	6.452	3.230
5.010	2.415	7.862×10^{-7}	2.716	4.718	2.371
3.705	1.785	5.814	2.009	2.992	1.753
2.758	1.329	4.329	1.495	2.227	1.305
2.067	9.963×10^{-7}	3.244	1.121	1.669	9.783×10^{-9}
1.559	7.515	2.447	8.454×10^{-8}	1.259	7.379
1.183	5.703	1.857	6.416	9.556×10^{-9}	5.599
9.089×10^{-7}	4.380	1.426	4.928	7.340	4.301
7.089	3.416	1.112	3.843	5.724	3.354

Table 3.7 Contribution of second order scattering to radiation flux $\pi I_d = F$, preceding layer in a plane parallel to molecular atmosphere (limiting values) [71]

Radiation flux	Albedo	$\cos \vartheta_{\odot_0}$	$\lambda = 0.809\ \mu$	$\lambda = 0.312\ \mu$
			$\tau = 0.02$	$\tau = 1.00$
I_m	—	1	0.024	0.0979
	—	0.2	0.0129	0.0242
πI_d	—	1	0.9802	0.3679
	—	0.2	0.9048	0.0067
$I_m/\pi I_d$	—	1	0.0025	0.2661
	—	0.2	0.0142	3.5982
$I_a/\pi I_d$	0.25	1	0.0008	0.0547
		0.2	0.0008	0.6045
	0.80	1	0.026	0.2419
		0.2	0.0026	0.6749

4. AEROSOL ATTENUATION IN REAL ATMOSPHERE

4.1 Spectral transparency in a homogeneous direction due to aerosol scattering and absorption

Insufficient investigation of the microphysical parameters of aerosol in the case of less turbid atmosphere and the variation of these parameters show that the results of aerosol attenuation obtained on the basis of an approximate model of systems of aerosol particles (cf. Ch. 2) can be used only for a qualitative evaluation of the spectral transparency in a real atmosphere. The main volume of quantitative information has so far been based on direct optical investigation of spectral transparency of real atmosphere, although a specification of localized conditions makes the task of generalization of data difficult.

Aerosol attenuation is determined not only by its scattering but also by its absorbing properties. As distinct from the attenuation patterns in water droplets (cf. Ch. 2), the absorptive properties of dry aerosol of

varying chemical composition have been studied even less [74, 99, 113]. The ambiguity of the question shows that the absorption of atmospheric aerosol in the visible region of the spectrum is normally not taken into consideration (scattering coefficient α_{aer} is formally equated to attenuation coefficient β_{aer}) or else is evaluated arbitrarily, although it follows, for instance, from Table 3.8, that the contribution of absorption can be quite considerable.

Table 3.8 Dependence on the wavelength of the ratio of optical thickness of aerosol absorption to the total optical thickness [34]

Substance	Wavelength, μ				
	0.398	0.496	0.556	0.696	0.977
Meteorite "Elenovka"	0.021	0.027	0.033	0.024	0.030
Meteorite "Saratov"	0.053	0.080	0.048	0.046	0.055
Lava (red)	0.039	0.075	0.192	0.030	0.018
Lava (gray)	0.039	0.088	0.078	0.096	0.074
Graphite	0.409	0.320	0.383	0.378	0.537
Soot	0.518*	0.503	0.458	0.415	0.314
Coal slag	0.311*	0.331	0.294	0.249	0.289
Room dust	0.134*	0.099	0.056	0.080	0.026
Cement	0.095*	0.144	0.055	0.055	0.041
Clay	0.071*	0.039	0.041	0.034	0.025
Sand	0.101*	0.130	0.130	0.061	0.044

REMARKS: Asterisks denote magnitudes relating to $\lambda = 0.405$ μ.

Table 3.8, taken from [34], shows the results of laboratory investigation on absorption of aerosol from various origins in the range 398-977 nm. In [34] it was observed that a systematic error in the computation of the optical path in the scattering medium allows us to evaluate only the upper limit of the ratio of the optical thickness of aerosol absorption to the total optical thickness caused by scattering and absorption.

In spite of the wide variation in the optical density of the atmospheric layer at the earth's surface, primarily determined by the condensation processes ($10^{-2} < \beta_{\lambda aer} < 10^{4}$ km^{-1}), many problems require the evaluation of mean values $\beta_{\lambda aer}$ of semiturbid atmosphere.

Table 3.9 gives the magnitude of $\beta_{\lambda aer}$ at sea level for the atmospheric layer above the ground in the region 0.27-4.0 μ for a mean meteorological visual range of 25 km (model of 1968) [79].

The complicated investigation of optical characteristics of the atmosphere above the ground in the region of Zvenigorod (near Moscow)

Table 3.9 Aerosol attenuation coefficient $\beta_{\lambda aer}$ at sea level in atmospheric layer above the ground for mean meteorological visual range $S_m = 25$ km [79]

λ, μ	0.27	0.28	0.29	0.30	0.32	0.34	0.36	0.38	0.40	0.45	0.50
$\beta_{\lambda aer}$ km^{-1}	0.29	0.27	0.26	0.25	0.24	0.24	0.23	0.20	0.180	0.167	0.158
λ, μ	0.55	0.60	0.70	0.80	0.90	1.06	1.26	1.67	2.17	3.50	4.00
$\beta_{\lambda aer}$ km^{-1}	0.150	0.142	0.135	0.127	0.120	0.113	0.108	0.098	0.083	0.070	0.063

for visual range 0.1-130 km and in a wide range of variations of relative humidity [16, 53] shows that it is possible to distinguish many types of of optical "weather" in the optical states of atmosphere.

The following are the main types of optical states of air :

1. *Haze.* Caused by a rise in the concentration of dry aerosol of different origins in the atmosphere (smoke, dust and aerosol of volcanic origin) ; this has been insufficiently studied.

2. *Dry haze.* Most often occurs in the atmosphere immediately above the earth's surface (probability 90%). The visual range is not less than 3-5 km. In case of relative humidity up to 30% the optical density of fog ($\beta_{aer} \leqslant 0.05$ km^{-1}) can be determined by the dry portion of aerosol, whereas an expansion of particles occurs in case of higher values of humidity (probably a mixing of the upper boundary of the size distribution of particles varying in dimension from 0.07-0.08 μ to 0.2-0.25 μ).

3. *Misty fog.* Visual range 1-5 km. It may be observed at relative humidity 80-99%, caused by condensational growth of large (obviously, hygroscopic) particles, exhibiting a wide spectrum of size distribution with a maximum in the region 1-5 μ. There probably occurs a simultaneous growth in fog particles (supposedly Aitken's nuclei). It is characterized by different spectral dependecies of $\beta_{\lambda aer}$ in the visible and near-infrared region of the spectrum and by a wide range of changes in optical density.

4. *Fog* (clouds). Visual range does not exceed 1-2 km. Fog is caused by intense growth in drops of water in the region of dew point. The effective size of particles of fog varies from 5-6 up to 30 μ depending on conditions. The spectrum of $\beta_{\lambda aer}$ does not depend on wavelength in the visible region. The transitional processes between misty fog and heavy fog are unstable. Fog is characterized by a significant fluctuation of optical density.

5. *Haze with drizzle.* It is haze impregnated with drizzle falling from the clouds lying above. The meteorological visibility range can be different—from 1 to 10 km : It possesses the same optical properties as fog, or large drops of water (rainbow, halo). Effective radius of the drops exceeds 50 μ.

Fig. 3.2 shows the spectral relations of $\beta_{\lambda aer}$ which are characteristic for different types of optical weather. The variation of atmospheric transparency with time and with respect to wavelength (in particular the development of misty fog) is traced.

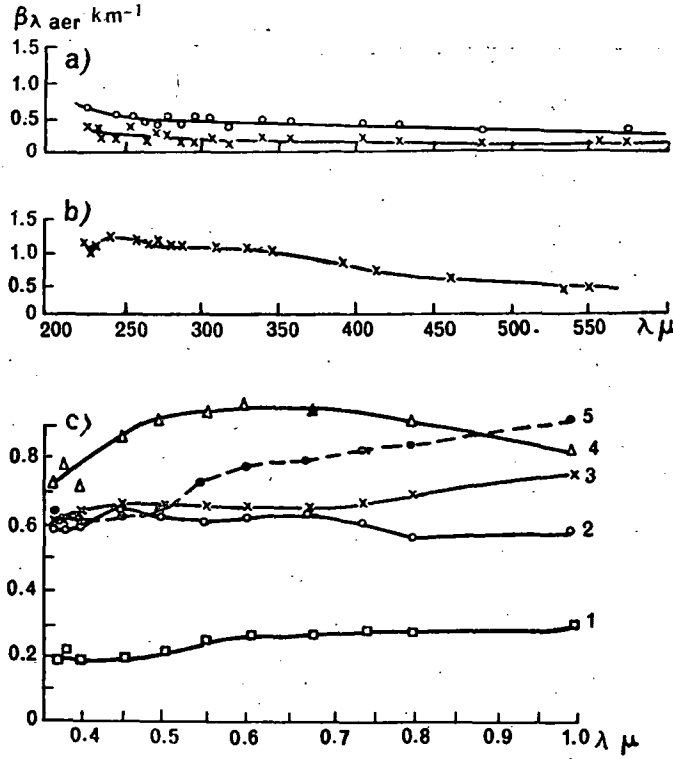

Fig. 3.2. Spectral relations of $\beta_{\lambda aer}$, characteristic for different types of optical weather. Zvenigorod [53].

a) moist haze; b) misty fog; c) sample of variation of $\beta_{\lambda aer}$ in time. October 30-31, 1965. Relative humidity 92-97%, 1—15 hrs 29 min, 2—19 hrs 30 min, 3—21 hrs 30 min. 4—3 hrs 30 min, 5—7 hrs 00 min.

Direct measurements of optical thickness of aerosol in the long wavelength region of the spectrum ($\lambda > 1\ \mu$) are possible only in selected ranges of transparency windows while considering absorption fringes of neighboring bands, as well as in the range of continuous absorption by the fringe of the rotational band of water vapor. The predominant role of selective absorption in polyatomic gases introduces difficulty in the study of the continuous spectrum of aerosol attenuation under low turbidity conditions for a sufficiently extended optical path. Measurements on

infrared transparency of semitransparent clouds and artificial mist possessing high optical density are simpler.

Fig. 3.3 shows the spectral dependence of transmission of incident radiation in the upper cloud level Ci (vertical thickness) obtained from measurements on attenuation of solar radiation [5, 90]. It is seen from Fig. 3.3 that the transmission of clouds in the visible range of the spectrum, as well as in the window 8-12 μ, may be considered.

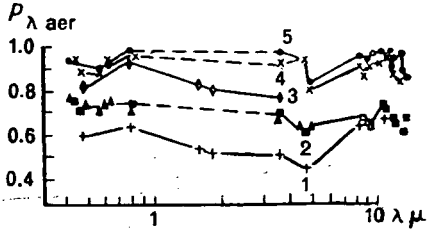

Fig. 3.3. Spectral transmission of radiation in upper cloud level of Ci in the region 0.35-13 μ; 1, 3—according to [90]; 2, 4, 5—according to [5].

Transmission of fog containing liquid droplets in the visible region of the spectrum is also neutral. Transparency of fog in the infrared region may be determined by the size distribution function of fog particles and by the complex coefficient of absorption of aqueous aeorosl (cf. Ch. 2). Results of the investigations on spectral transparency of artificial mist of liquid drops of different density have been discussed in detail [24, 25].

It is possible to consider the spectral transparency of rain as in the entire optical range to a sufficient degree of accuracy, from [46] $\beta_r = 0.22\ I_r^{0.71}\ km^{-1}$, where I_r—intensity of rainfall in nm/hr.

Although the complex microphysical structure of haze has been inadequately studied, attempts have been made to compute the continuous transmission spectrum of haze employing methods worked out for the computation of the spectral transparency of fog with liquid drops.

Thus, for the evaluation of emission in the infrared region of the spectrum use is made of the relative spectral coefficients of aerosol attenuation $\beta'(\lambda) = \frac{\beta(\lambda)}{\beta_{0.55}}$ for the wavelength 0.55 μ.

Fig. 3.4 shows curves of $\beta'(\lambda)$ computed in [25a] allowing for the complexity of the refractive index using Young's size distribution functions for particles (cf. Ch. 2); $\beta_s = 3, 4, 5$; upper boundary of particle distribution having $a = 3$ μ. Index of refraction of water is taken from [29].

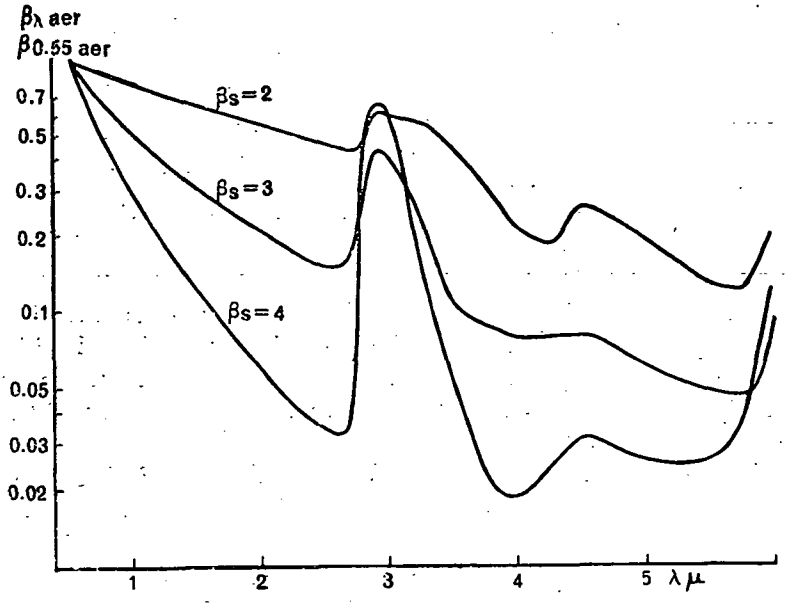

Fig. 3.4. Spectral dependence of relative coefficient of aerosol attenuation calculated for particles of aqueous aerosol allowing for the complexity of refractive index in Young's distribution with different indices β_S. Limiting values for particle distribution : $a_1 = 0.05\ \mu$, $a_2 = 3\ \mu$ [25a].

The quantity β_S accepts different values for various meteorological visual ranges S_M. Thus for $S_M \geq 50$ km, $\beta_S=5$, for S_M 20 km, $\beta_S=4$, and for $S_M<20$ km, $\beta_S=3$. Attenuation coefficient for $\beta_{0.55}$ is found either with the help of experimental spectral measurements or from S_M. For mean visual range $S_M=25$ km, $\beta_{0.55}=0.150$ and correspondingly

$$\tau_{\lambda aer}=0.150\,\beta'(\lambda)l, \qquad (3.23)$$

where l—length of the path of ray in kilometers.

4.2 Transparency of vertical column of atmosphere due to aerosol component

Table 3.10 gives mean values of $\tau_{\lambda aer}$ of a vertical column of cloudless atmosphere at sea level in the spectral region 0.27-4.00 μ for terrestrial $S_M=25$ km, as suggested in the model of 1968 [79].

Table 3.10 Optical thickness of vertical column of atmosphere caused by aerosol attenuation [79]

Meteorological visual range $S_m = 25$ km. H above sea level $m = 0$

λ, μ	0.27	0.28	0.30	0.32	0.34	0.36	0.38	0.40	0.45	0.50	0.55
τ_{aer}	0.458	0.427	0.411	0.395	0.379	0.379	0.364	0.316	0.285	0.264	0.250
λ, μ	0.60	0.65	0.70	0.80	0.90	1.06	1.26	1.67	2.17	3.50	4.0
τ_{aer}	0.237	0.224	0.213	0.201	0.190	0.179	0.171	0.155	0.134	0.111	0.100

The optical thickness of a vertical column of atmosphere in the infrared region of the spectrum can be approximately evaluated with the help of the curve in Fig. 3.4 for $\beta_s=4$. The values taken from the curve are multiplied by $\tau_{(0\cdot55)}=0.25$. The latter quantity is characteristic for cloudless atmosphere.

The computation of optical thickness of a vertical column of atmosphere involves greater error than that of transmission in terrestrial paths as a result of the inhomogeneity of the atmosphere according to altitude and the absence of information about localized optical characteristics in the layers situated at different levels. The magnitude S_M determined under surface conditions can be correlated with the optical thickness of the vertical column of atmosphere. An experimental determination of the magnitude of optical thickness provides a most reliable index.

The method of spectral investigation of attenuation in direct radiation is simple

$$\tau_{total}=\sum\tau_{\lambda i},$$

where $\tau_{\lambda i}$—optical thickness of distinct components and can be determined by attenuation in direct radiation from sources of light beyond the atmosphere (usually the sun) for different $m_\odot$. The "long" method of Bouguer [47] permits one to determine τ_λ in two or more measurements of $\ln I_\lambda(m.)$. The aerosol component outside the absorption band can be determined after deducting general optical thickness caused by molecular attenuation, absorption of ozone and other gases, which are determined by the usual methods of computation.

Accuracy in measurement is enhanced due to the repeated determination of $I_\lambda\ (\vartheta_\odot)$ (while plotting Bouguer's lines). The quantity $\tau_{\lambda\,total}$ represents the calculation of relative magnitudes of intensity $I_{\lambda o}$ beyond the atmosphere. In future the value $I_{\lambda o}$ can be used for the determination of $\tau_{\lambda total}$ under different conditions of turbidity in the atmosphere for the unique measurement of $I_\lambda\ (\vartheta_\odot)$. In reality the "long" method loses its significance during changes of $\tau_{\lambda total}$ in the course of a cycle of measurements often observed in real atmosphere.

The method of evaluating errors caused by aerosol scattering at small angles, and the conditions under which Bouguer's law is applicable, are given in [14, 24, 25, 47, 49, 50, 58, 93]. The method of determining the optical thickness of the atmosphere through observations on the intensity of radiation scattered in solar almucanthorat and the method of optical stability control in atmosphere have been investigated in [33, 47].

The method of investigating aerosol attenuation with the help of the integral actinometric apparatus requires consideration of optical characteristics of aerosol attenuation and absorption of gaseous components. Thus, according to Ångström [64, 102, 106, 111], aerosol attenuation in atmospheric thickness can be approximately computed from the assumption that

$$\tau_{\lambda aer}=\gamma\lambda^{-b}. \tag{3.24}$$

While measuring the integral flux of solar radiation reaching the earth's surface $S(m)$ and taking into consideration the solar spectral constant $S_{0\lambda}$ it is possible to compute the turbidity coefficient $\gamma=\int_0^\infty \gamma_H\, dH$ from the expression

$$S(m)=S'(m)\triangle S=\int_0^\infty S_{\lambda o}\exp\left(-m\tau_{\lambda real}-m\gamma\lambda^{-b}\right)d\lambda-\triangle S, \tag{3.25}$$

where $\triangle S$—amount of flux of absorbent gaseous components, which may be determined in different ways.

Ångström took $b=1$, 3, but an analysis of possible values of b [102] showed that depending upon p and $\tilde{m}$ of the particles, the magnitude of the parameter can change within the limits $2\leqslant b\leqslant 4$. For Young's type of particle distribution (cf. Ch. 2) $b=\beta_S-2$ and changes in β_S are evaluated within the limits 1.7-5.0, which indicates that a variation in the value of b is inevitable.

V. Shyuepp [89, 116, 117] generalized Ångström's method, by suggesting the application of two parameters : β_S and b. On the basis of actinometric observation found in [64, 89, 102] the values of parameters b and β_S are given in real atmosphere for the case of Young's particle distribution of aerosol over the continental region. Evidently the variation in parameters introduced above is caused by the variation in the spectral nature of aerosol attenuation.

In actual fact an investigation on spectral transparency in the visible and near-infrared regions of spectrum shows that as in the case of terrestrial measurements, spectral variation of $\tau_{\lambda aer}$ can differ considerably from computed variations when the distribution function of aerosol particles remains stationary with height. The results of researches [19, 48, 57, 98] show that with decreasing $\tau_{\lambda aer}$ and increasing wavelength a neutral course of $\tau_{aer}(\lambda)$ may be observed with a maximum in the region of the spectrum 0.380-0.550 μ. The parameter b can change with respect to wavelength and according to data obtained by different authors the values of b lie within the limits $0 \leqslant b \leqslant 3.3$.

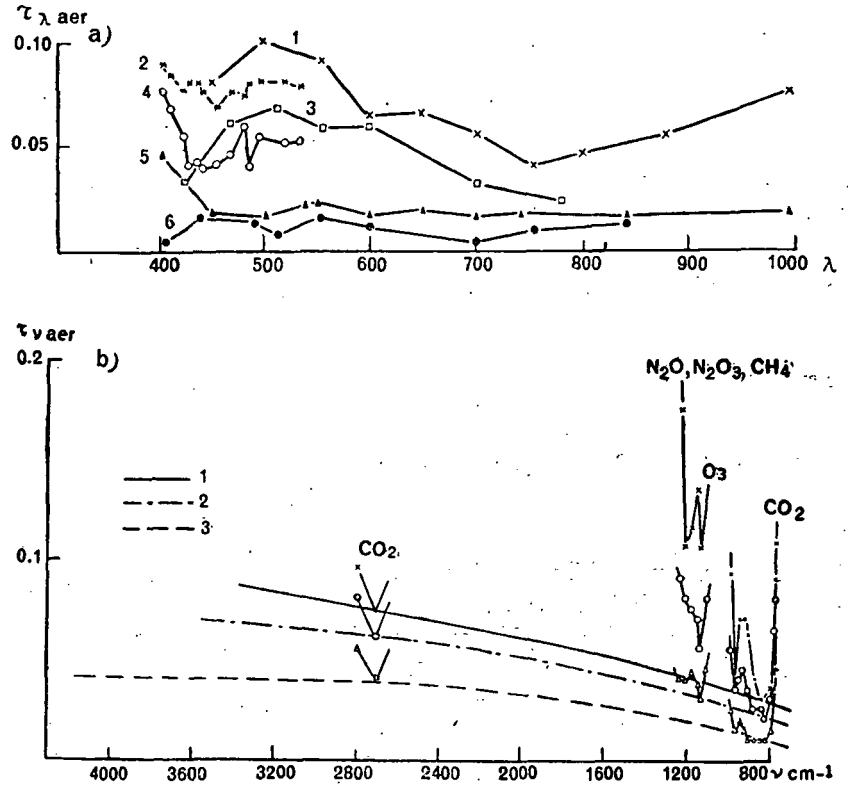

Fig. 3.5. Optical thickness of a vertical column of atmosphere due to aerosol attenuation.

a) Examples of changes in spectral dependency of the visible region of spectrum [75, 98] :

1—45 m above sea level; 2—2800 m; 3.6—3100 m; 4—3410 m; 5—3700 m;

b) infrared region of the spectrum (700-4000 cm^{-1}) [3] :

1—Leningrad, spring of 1963; 2—Mineral'nye Vody, autumn of 1962; 3—Terskol Peak (El'brus) 2100 m above sea level, summer of 1962; λ is given in manometers.

Fig. 3.5a [98] illustrates the significant variation in $\tau_{\lambda aer}$ even during high altitude observations. Although the nature of dependence is irregular, there is an obvious tendency of decrease in $\tau_{\lambda aer}$ with increasing λ. In an attempt to simplify the computation of transparency which does not demand high accuracy, several researchers assigned a fixed value to the parameter b. Thus, while examining the dependence of overall optical thickness on wavelength caused by molecular and aerosol attenuation of the type $\tau_{\lambda total}=a\lambda^{-4}+b'\lambda^{-b'}+c$, the authors of [63] accepted the value $b'=1$. In [41] a neutral course of $\tau_{\lambda aer}(\lambda)$ has been used for conditions of low turbidity with $\tau_{\lambda total}=a\lambda^{-4}+c$.

The contribution of aerosol in attenuation of infrared radiation in a vertical column of atmosphere has not been studied in detail. Qualitative values of the contribution of aerosol attenuation are given in [107]. The values of $\tau_{\lambda aer}$ in selected ranges of windows in the region of spectrum 3-13 μ have been obtained in [3], these segments being free from noticeable selective absorption by the gases. The mean values $\tau_{\lambda aer}$ are connected by a smooth curve (dotted line in Fig. 3.5 b). These values can be distinguished from the unbroken continuum, mainly determined by the fringe of the rotational absorption band of water vapor. The mean parameter b' as defined by the curve τ_{aer} (λ) equals 0.6-0.8 which is in agreement with the results discussed in [24], obtained for horizontal direction with $b'=0.7$.

As shown from computations, the large "spacing" of measurements, which is unavoidable in the infrared region of the spectrum, does not permit one to determine the variation of b' with wavelength although it is evident that the existence of water drops in the atmosphere must lead to an oscillatory dependence of $\tau_{aer}(\lambda)$ in the short wavelength region under investigation.

4.3 Vertical profile of aerosol attenuation

Information about the vertical profile of aerosol attenuation has been accumulated with the help of many optical methods, direct or otherwise, a sufficiently complete review of which is given in [53]. In the troposphere the *direct method* is convenient for the determination of the spectral attenuation coefficient $\beta_{\lambda aer}(H)$ km^{-1} from the mass of observations on attenuation of direct solar radiation, carried out at different heights, viz.

$$\beta_{\lambda aer}(H)=\frac{\Delta\tau_{H_1-H_2\,aer}}{\Delta z}.$$

The method is not so sensitive for lower values of $\beta_{\lambda aer}$ so that it is not possible to examine the fine structure of the profile by employing the usual technique of registering the quantities being measured.

The *indirect methods* are usually employed at high altitudes—which involve measurements of intensity of scattered solar light or of artificial sources of light at different angles [33, 40, 50, 60].

Recently, data on the profile of aerosol dispersion, determined from intensity of scattered solar radiation, have been obtained from space ships [51, 52, 50]. Methods of projection probing [19, 80, 81] as well as

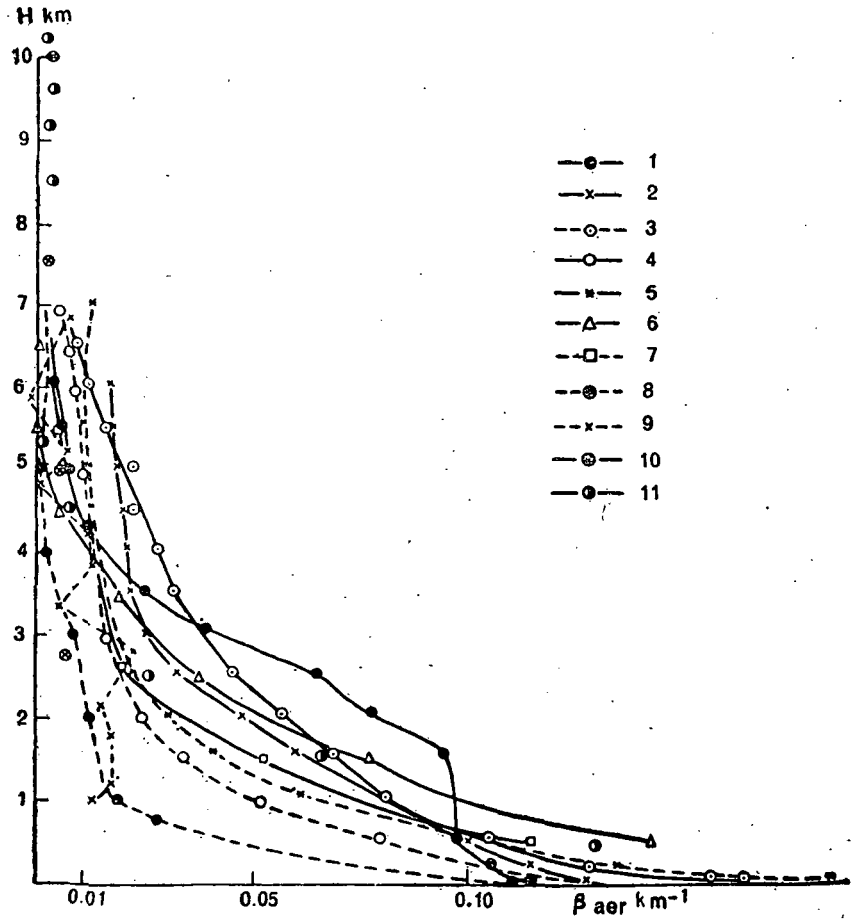

Fig. 3.6. Variation in profile of attenuation coefficient in the troposphere according to data of different researchers : 1, 2, 3, 4, 5 are obtained from [55]; 6, 7, 11 from [99]; 8 from [59]; 9 from [42] and 10 from [80].

methods of twilight observation [54] have also been employed and methods of laser probing are being developed [77, 86].

Experimental investigation on $\beta_{\lambda aer}(H)$ indicates the important role of aerosol attenuation in a wide range of altitudes. Stratification of aerosol attenuation components is characteristic. The position of aerosol layers is usually connected with regions of temperature inversion.

Often for various reasons it is not possible to carry out an investigation on the optical density of atmosphere at different altitudes with the help of spectral equipment. Thus measurements are carried out at small spectral intervals usually separated by light filters. The spectral interval selected in the section 0.5 μ lying in the region of maximum spectral distribution of solar radiation is of greatest interest.

Fig. 3.6 shows the relation between altitude and the aerosol attenuation coefficient obtained by many researchers [42, 55, 59, 80]. It is evident from Fig. 3.6 that the lower tropospheric layer plays a fundamental role in the variation of optical thickness in a vertical column of atmosphere, even though a variation in the attenuation coefficient $\beta_{\lambda aer}$ may be observed at all altitudes.

A systematic investigation of aerosol attenuation with the help of projection probing has been described in [80, 81].

Measurements were carried out in mountainous conditions at an altitude of 2.76 km (Sacramento Peak, New Mexico.).

From Fig. 3.7a it is evident that there is a considerable variation in the limits of $\beta_{\lambda aer}$ (H) at all altitudes.

Diurnal variation of $\beta_{\lambda aer}$ km^{-1} [81] is given in Fig. 3.7b. Increase in optical thickness of troposphere from evening to night is obviously caused by the influence of condensation processes [8].

With the improvement in the methods of investigating atmospheric aerosol and the accumulation of information regarding the optical structure of the atmosphere, the significant role of aerosol in the formation of radiation regime of the atmosphere [86, 99] becomes obvious. Data obtained in recent years allowed L. Elterman [79] to revise the aerosol attenuation model suggested by him (1964 model). Fig. 3.8a shows a comparison of the earlier model with the aerosol attenuation model of 1968 (λ=0.55 μ). Data obtained from space ships [52] (Fig. 3.8b) were used for the construction of this model which permitted the raising of the "ceiling" of the model to 50 km.

The spectral dependence of a $\beta_{\lambda aer}$ at different levels of atmosphere has practically not been studied. Sporadic investigations on aerosol attenuation from balloons [99] shows that a selective variation of $\beta_{\lambda aer}$ with a maximum in the region 0.4-0.5 μ may be observed in special cases (Fig. 3.9).

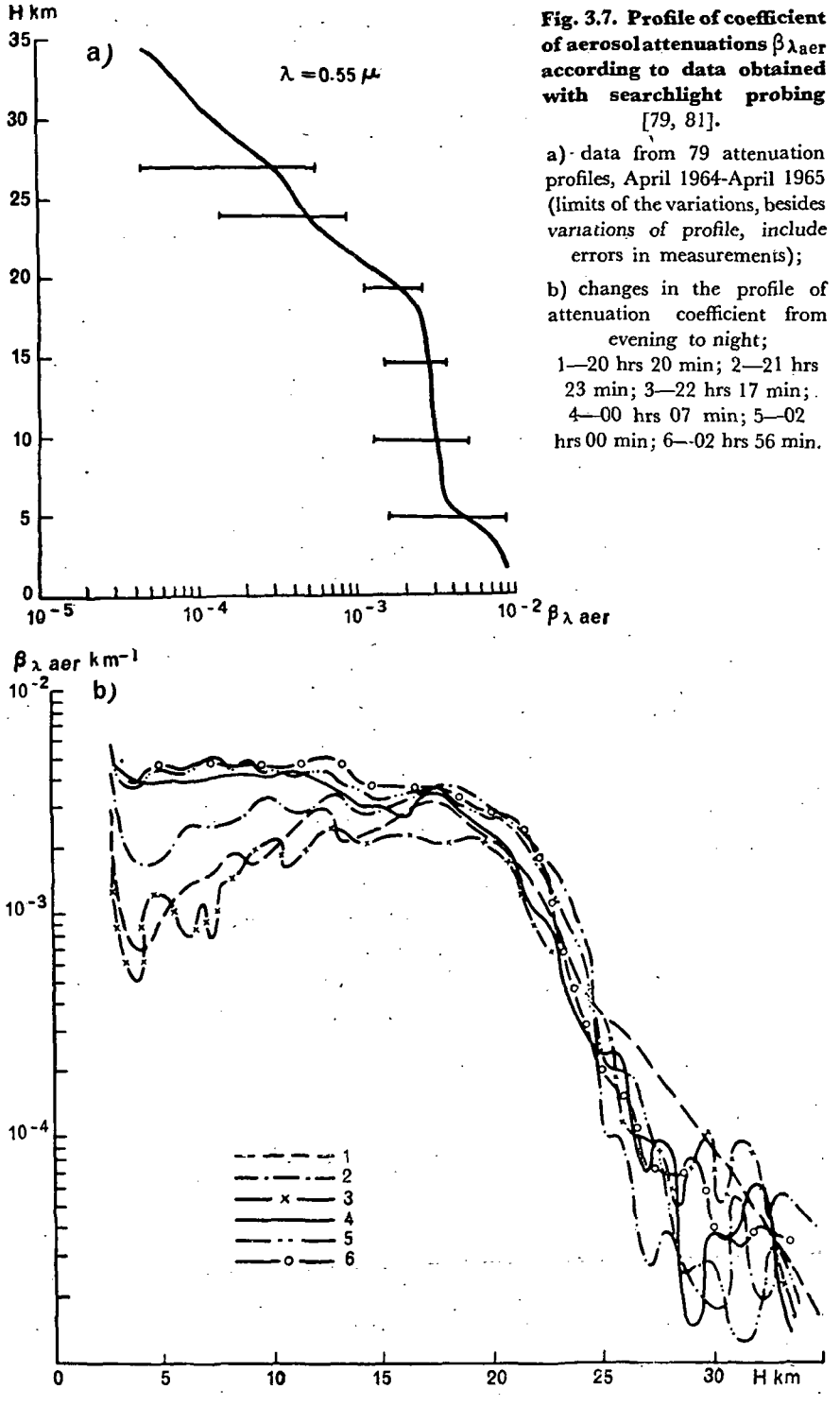

Fig. 3.7. Profile of coefficient of aerosol attenuations $\beta_{\lambda aer}$ according to data obtained with searchlight probing [79, 81].

a) data from 79 attenuation profiles, April 1964-April 1965 (limits of the variations, besides variations of profile, include errors in measurements);

b) changes in the profile of attenuation coefficient from evening to night; 1—20 hrs 20 min; 2—21 hrs 23 min; 3—22 hrs 17 min; 4—00 hrs 07 min; 5—02 hrs 00 min; 6—02 hrs 56 min.

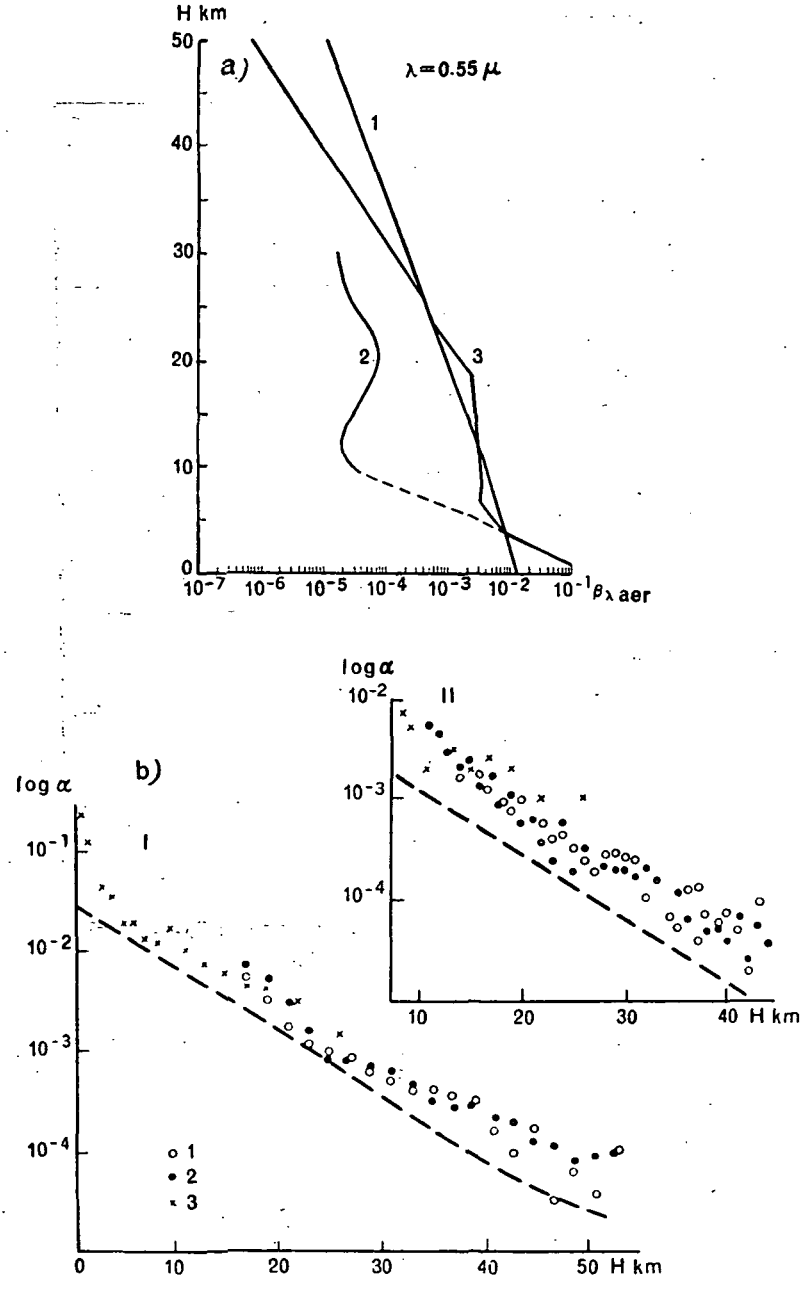

Fig. 3.8. Contribution of aerosol and molecular scattering to optical density of atmosphere [52, 79].

a) 1—Level of molecular scattering; 2—Elterman model 1964; 3—Elterman model 1968. b) variation in coefficient with altitude; I for $\lambda=0.6\mu$; II for $\lambda=0.4\mu$; 1-2—according to [52], 3—according to [99].

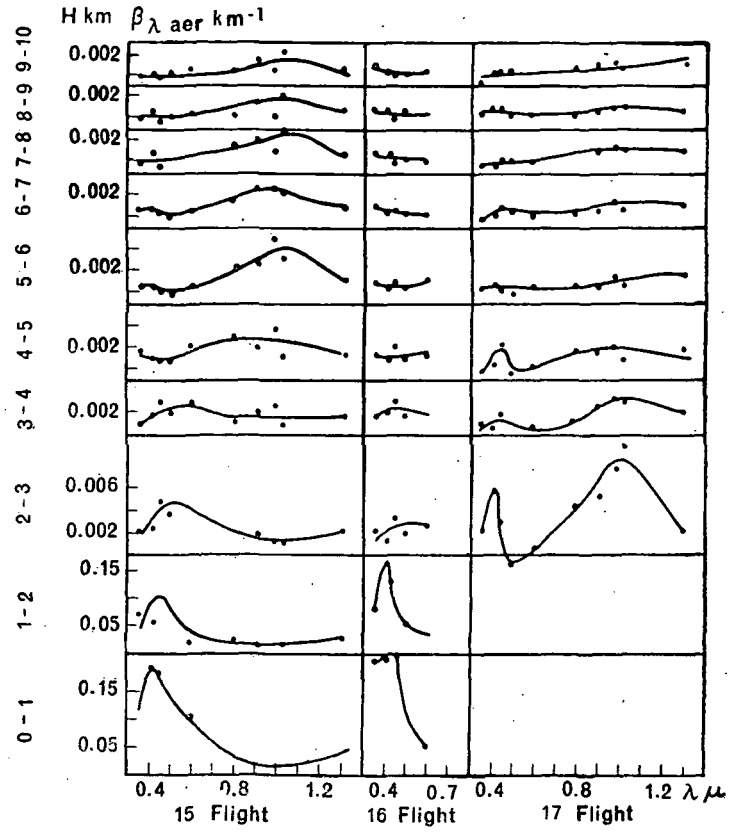

Fig. 3.9. Examples of spectral dependence of $\beta_{\lambda aer}$ km^{-1} at different altitudes [99].

The profile of aerosol attenuation in the region 0.27-4.00 μ recommended by the authors of [79] as the 1968 model is given in Table 3.11.

5. ABSORPTION OF RADIATION IN REAL ATMOSPHERE

Mutually overlapping systems of bands of vapors of H_2O, CO_2, O_3, CH_4, N_2O and other gaseous components of the atmosphere divide the absorption spectrum of atmosphere into many segments (transparency windows), in which selective absorption is less intense (Fig. 3.10). Considerable unbroken (continuous) absorption takes place in these segments; this is caused by the fringes of distant bands. (Mainly of rotational bands of H_2O vapor with the center at $\lambda=50$ μ).

Table 3.11 Vertical profile of coefficients of aerosol attenuation $\beta_{\lambda aer}$ km^{-1} in the spectral region 0.27-4.00 μ (1968 model) [79]

H km	0.27	0.28	0.30	0.32	0.34	0.36	0.38	0.40	0.45	0.50	0.55
0	2.90×10^{-1}	2.70×10^{-1}	2.60×10^{-1}	2.50×10^{-1}	2.40×10^{-1}	2.40×10^{-1}	2.30×10^{-1}	2.00×10^{-1}	1.80×10^{-1}	1.67×10^{-1}	1.58×10^{-1}
2	5.51×10^{-2}	5.13×10^{-2}	4.94×10^{-2}	4.75×10^{-2}	4.56×10^{-2}	4.56×10^{-2}	4.37×10^{-2}	3.80×10^{-2}	3.42×10^{-2}	3.17×10^{-2}	3.00×10^{-2}
4	1.22×10^{-2}	1.14×10^{-2}	1.10×10^{-2}	1.05×10^{-2}	0.01×10^{-2}	0.01×10^{-3}	9.69×10^{-3}	8.43×10^{-3}	7.59×10^{-3}	7.04×10^{-3}	6.66×10^{-3}
6	6.50×10^{-3}	6.05×10^{-3}	5.83×10^{-3}	5.60×10^{-3}	5.38×10^{-3}	5.38×10^{-3}	5.15×10^{-3}	4.48×10^{-3}	4.03×10^{-3}	3.74×10^{-3}	3.54×10^{-3}
8	6.22	5.79	5.58	5.36	5.15	5.15	4.93	4.29	3.86	3.58	3.39
10	5.82	5.42	5.22	5.02	4.82	4.82	4.61	4.01	3.61	3.35	3.17
12	5.73	5.33	5.13	4.94	4.74	4.74	4.54	3.95	3.55	3.30	3.12
14	5.18	4.82	4.60	4.46	4.28	4.28	4.11	3.57	3.21	2.98	2.82
16	4.63	4.31	4.15	3.99	3.83	3.83	3.67	3.19	2.87	2.66	2.52
18	4.42	4.12	3.97	3.81	3.66	3.66	3.51	3.05	2.75	2.55	2.41
20	2.73	2.55	2.45	2.36	2.26	2.26	2.17	3.05	1.70	1.57	1.49
22	1.49	1.39	1.34	1.29	1.23	1.23	1.18	1.03	9.26×10^{-4}	8.59×10^{-4}	8.13×10^{-4}
24	9.05×10^{-4}	8.42×10^{-4}	8.11×10^{-4}	7.80×10^{-4}	7.49×10^{-4}	7.49×10^{-4}	7.18×10^{-4}	6.24×10^{-4}	5.62	5.21	4.93
26	6.64	6.19	5.96	5.73	5.50	5.50	5.27	4.58	4.12	3.83	3.62
28	3.89	3.62	3.49	3.35	3.22	3.22	3.09	2.68	2.42	2.24	2.12
30	2.29	2.14	2.06	1.98	1.90	1.90	1.82	1.58	1.42	1.32	1.25
32	1.34	1.25	1.20	1.16	1.11	1.11	1.06	9.25×10^{-5}	8.33×10^{-5}	7.73×10^{-5}	7.31×10^{-5}
34	7.87×10^{-5}	7.33×10^{-5}	7.06×10^{-5}	6.79×10^{-5}	6.52×10^{-5}	6.52×10^{-5}	6.24×10^{-5}	5.43	4.89	4.53	4.29
36	4.63	4.31	4.15	3.99	3.83	3.83	3.67	3.19	2.87	2.66	2.52
38	2.72	2.53	2.44	2.34	2.25	2.25	2.15	1.87	1.69	1.56	1.48
40	1.59	1.48	1.43	1.37	1.32	1.32	1.26	1.10	9.87×10^{-6}	9.15×10^{-6}	8.66×10^{-6}
42	9.32×10^{-6}	8.68×10^{-6}	8.36×10^{-6}	8.04×10^{-6}	7.72×10^{-6}	7.72×10^{-6}	7.39×10^{-6}	6.43×10^{-6}	5.79	5.37	5.08
44	5.47	5.09	4.90	4.72	4.53	5.91	4.34	3.77	3.39	3.15	2.98
46	3.21	2.99	2.88	2.77	2.66	2.66	2.55	2.22	1.99	1.85	1.75
48	1.89	1.76	1.69	1.63	1.56	1.56	1.50	1.30	1.17	1.09	1.03
50	1.10	1.03	9.91×10^{-7}	9.53×10^{-7}	9.14×19^{-7}	9.14×10^{-7}	8.76×10^{-7}	$7.62\cdot10^{-7}$	6.86×10^{-7}	6.36×10^{-7}	6.02×10^{-7}

Table 3.11—*Contd.*

H km	0.60	0.65	0.70	0.80	0.90	1.06	1.26	1.67	2.17	3.50	4.00
0	1.50×10^{-1}	1.42×10^{-1}	1.35×10^{-1}	1.27×10^{-1}	1.20×10^{-1}	1.13×10^{-1}	1.08×10^{-1}	9.80×10^{-2}	8.50×10^{-2}	7.00×10^{-2}	6.30×10^{-2}
2	2.85×10^{-2}	2.79×10^{-2}	2.56×10^{-2}	2.41×10^{-2}	2.28×10^{-2}	2.15×10^{-2}	2.05×10^{-2}	1.86×10^{-2}	1.61×10^{-2}	1.33×10^{-2}	1.20×10^{-2}
4	6.32×10^{-3}	5.99×10^{-3}	5.69×10^{-3}	5.35×10^{-3}	5.06×10^{-3}	4.76×10^{-3}	4.55×10^{-3}	4.13×10^{-3}	3.58×10^{-3}	2.95×10^{-3}	2.66×10^{-3}
6	3.36	3.18	3.02	2.85	2.69	2.58	2.42	2.20	1.90	1.57	1.41
8	3.22	3.05	2.90	2.72	2.57	2.42	2.32	2.10	1.82	1.50	1.35
10	3.01	2.85	2.71	2.55	2.41	2.27	2.17	1.97	1.71	1.40	1.26
12	2.96	2.80	2.67	2.51	2.37	2.23	2.13	1.94	1.68	1.38	1.24
14	2.68	2.53	2.41	2.27	2.14	2.23	2.13	1.75	1.52	1.25	1.12
16	2.39	2.26	2.15	2.03	1.91	1.80	1.72	1.56	1.36	1.12	1.00
18	2.29	2.17	2.06	1.94	1.83	1.72	1.65	1.49	1.30	1.07	9.61×10^{-4}
20	1.41	1.34	1.27	1.20	1.13	1.72	1.65	1.49	8.02×10^{-4}	6.60×10^{-4}	5.94
22	7.72×10^{-4}	7.35×10^{-4}	6.95×10^{-4}	6.53×10^{-4}	6.17×10^{-4}	5.81×10^{-4}	5.56×10^{-4}	5.04×10^{-4}	4.37	3.60	1.24
24	4.68	4.43	4.21	3.96	3.74	3.53	3.37	3.06	2.65	2.18	1.97
26	3.44	3.25	3.09	2.91	2.75	2.59	2.47	2.26	1.95	1.60	1.44
28	2.01	1.91	1.81	1.70	1.61	1.52	1.45	1.31	1.14	9.39×10^{-5}	8.45×10^{-5}
30	1.19	1.12	1.07	1.00	9.49×10^{-5}	8.94×10^{-5}	8.54×10^{-5}	7.75×10^{-5}	6.72×10^{-5}	5.54	4.98
32	6.94×10^{-5}	6.57×10^{-5}	6.25×10^{-5}	5.88×10^{-5}	5.55	5.23	5.00	4.53	5.90	3.24	2.91
34	4.07	3.86	3.67	3.45	3.26	3.07	2.93	2.56	2.31	1.90	1.71
36	2.39	2.26	2.15	2.03	1.91	1.80	1.72	1.56	1.36	1.12	1.00
38	1.41	1.33	1.26	1.19	1.12	1.06	1.01	9.18×10^{-6}	7.96×10^{-6}	6.56×10^{-6}	5.90×10^{-6}
40	8.22×10^{-6}	7.78×10^{-6}	7.40×10^{-6}	6.96×10^{-6}	6.58×10^{-6}	6.19×10^{-6}	5.92×10^{-6}	5.37	4.66	3.84	3.45
42	4.82	4.57	4.34	4.08	3.86	3.63	3.47	3.15	2.73	2.25	2.03
44	2.83	2.68	2.55	2.40	2.26	2.13	2.04	1.85	1.60	1.32	1.19
46	1.66	1.57	1.50	1.41	1.33	1.25	1.20	1.09	9.41×10^{-7}	7.75×10^{-7}	6.98×10^{-7}
48	9.78×10^{-7}	9.26×10^{-7}	8.80×10^{-7}	8.28×10^{-7}	7.82×10^{-7}	7.37×10^{-7}	7.04×10^{-7}	6.39×10^{-7}	5.54	4.56	4.11
50	5.72	5.41	5.14	4.84	4.57	4.31	4.11	3.73	3.24	2.67	2.40

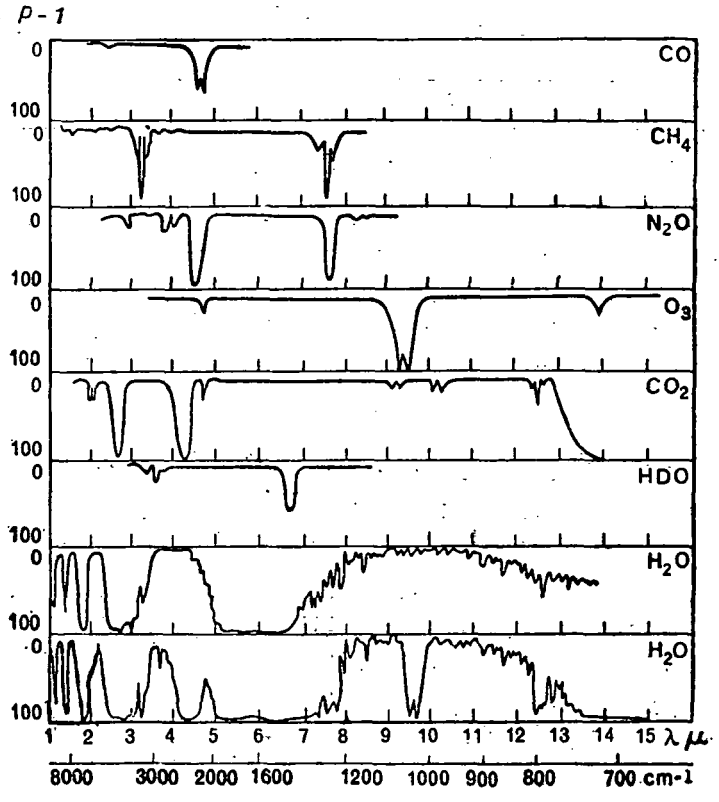

Fig. 3.10. Selective transmission of individual optical components.

Data about spectral transmission of real atmosphere can be divided into three groups.

High resolution spectra in wide spectral intervals for the purpose of identification of absorption lines of gaseous components belong to the first group.

The results of measurements are given in the form of atlases. The data of investigations on solar spectrum in the region of the spectrum 0.2-1.2016 μ are published in [65a, 69a, 77a, 77b, 100a, 100b, 101a]. Data on selective absorption of radiation in the interval 0.8465-2.5242 μ are given in [101b]. Solar spectra recorded with a resolution of 0.02 cm^{-1} in the region 2.8-23.7 μ are given in an atlas [101]. In atlas [85] we find solar registograms in the region from 7-400 μ recorded with a slightly poorer resolution ($\sim$1 cm^{-1}).

Table 3.12 Height distribution of absorption coefficient of ozone in the ultra-

H km	λ, μ							
	0.27	0.28	0.30	0.32	0.34	0.36	0.38	0.40
0	7.48×10^{-1}	3.77×10^{-1}	3.60×10^{-2}	3.20×10^{-3}	2.28×10^{-4}	6.41×10^{-6}	0	0
2	6.15	3.11	2.96	2.63	1.88	5.27	0	0
4	4.75	2.40	2.28	2.03	1.45	4.07	0	0
6	4.54	2.29	2.18	1.94	1.38	3.89	0	0
8	4.79	2.42	2.30	2.05	1.46	4.10	0	0
10	7.35	3.71	3.53	3.14	2.24	6.30	0	0
12	1.30×10^{0}	6.58	6.27	5.58	3.97	1.12×10^{-5}	0	0
14	2.01	1.01×10^{0}	9.67	8.59	6.12	1.72	0	0
16	2.16	1.09	1.04×10^{-1}	9.25	6.59	1.85	0	0
18	2.56	1.29	1.23	1.10×10^{-2}	7.81	2.20	0	0
20	3.44	1.74	1.66	1.47	1.05×10^{-3}	2.95	0	0
22	4.14	2.09	1.99	1.77	1.26	3.55	0	0
24	4.05	2.05	1.95	1.73	1.24	3.47	0	0
26	3.42	1.73	1.65	1.46	1.04	2.93	0	0
28	2.58	1.30	1.24	1.10	7.87×10^{-4}	2.21	0	0
30	1.90	9.57×10^{-1}	9.12×10^{-2}	8.11×10^{-3}	5.78	1.63	0	0
32	1.43	7.23	6.89	6.12	4.36	1.23	0	0
34	1.01	5.12×10^{-1}	4.88	4.34	3.09	8.69×10^{-6}	0	0
36	7.58×10^{-1}	3.83	3.65	3.24	2.31	6.50	0	0
38	5.31	2.68	2.56	2.27	1.62	4.55	0	0
40	3.91	1.97	1.88	1.67	1.19	3.35	0	0
42	2.50	1.26	1.20	1.07	7.62×10^{-5}	2.14	0	0
44	1.56	7.89×10^{-4}	7.51×10^{-4}	6.68×10^{-4}	4.76	1.34	0	0
46	9.37×10^{-2}	4.73	4.50	4.01	2.85	8.03×10^{-7}	0	0
48	5.86	2.96	2.82	2.51	1.79	5.02	0	0
50	3.91	1.97	1.88	1.67	1.19	3.35	0	0

violet and visible regions of spectrum, from [79] (overall content 0.3 cm)

λ, μ							
0.45	0.50	5.55	0.60	0.65	0.70	0.80	0.90
1.25×10^{-5}	1.23×10^{-4}	3.28×10^{-4}	4.70×10^{-4}	2.21×10^{-4}	8.19×10^{-7}	3.56×10^{-5}	0
1.09	1.01	2.70	3.87	1.82	6.74	2.93	0
7.91×10^{-6}	7.80×10^{-5}	2.08	2.98	1.40	5.20	2.26	0
7.56	7.45	1.99	2.85	1.34	4.97	2.16	0
7.98	7.87	2.10	3.01	1.41	5.24	2.28	0
1.22×10^{-5}	1.21×10^{-4}	3.22	4.62	2.17	8.05	3.50	0
2.17×10^{-5}	2.14	5.71	8.20	3.85	1.43×10^{-4}	6.21	0
3.35	3.30	8.80	1.26×10^{-3}	5.93	2.20	9.57	0
3.60	3.55	9.48	1.36	6.39	2.37	1.03×10^{-4}	0
4.27	4.21	1.12×10^{-3}	1.61	7.56	2.81	1.22	0
5.74	5.66	1.51	2.16	1.02×10^{-3}	3.77	1.64	0
6.90	6.80	1.81	2.60	1.22	4.53	1.97	0
6.76	6.66	1.78	2.55	1.20	4.44	1.93	0
5.70	5.62	1.50	2.15	1.01	3.75	1.63	0
4.31	4.24	1.13	1.62	7.63×10^{-4}	2.83	1.23	0
3.16	3.12	8.31×10^{-4}	1.19	5.60	2.08	9.03×10^{-5}	0
2.39	2.35	6.27	9.00×10^{-4}	4.23	1.57	6.82	0
1.69	1.67	4.44	6.38	2.99	1.11	4.83	0
1.26	1.25	3.32	4.77	2.24	8.30×10^{-5}	3.61	0
8.86×10^{-6}	8.73×10^{-5}	2.33	3.34	1.57	5.82	2.53	0
6.51	6.42	1.71	2.46	1.15	4.28	1.86	0
4.16	4.11	1.09	1.57	7.38×10^{-5}	2.74	1.19	0
2.60	2.57	6.84×10^{-5}	9.82×10^{-5}	4.61	1.71	7.44×10^{-6}	0
1.56	1.54	4.10	5.89	2.77	1.03	4.46	0
9.77×10^{-7}	9.63×10^{-6}	2.57	3.68	1.73	6.42×10^{-6}	2.79	0
6.51	6.42	1.71	2.46	1.15	4.28	1.86	0

Recordings of solar spectra obtained from an airplane with resolution of 1 cm^{-1} in the region 1.0-6.5 μ up to an altitude of 15 km are shown in an atlas [92].

Results of measurements of absorption of radiation from an artificial source in the near-infrared region on a horizontal contour of 25 km in the layer of atmosphere near ground level have been published in [114].

The second group of data includes information obtained through computation made with the help of theoretical and laboratory investigations on the patterns of selective absorption and height distribution models of absorptive components (cf. Chs. 1 and 2). Some of the information of practical importance has been given below.

Absorption coefficients of O_3 in the ultraviolet and visible regions of the spectrum (Hartley and Chappuis bands), computed for different altitudes considering standard distribution of O_3 with altitude, are shown in Table 3.12 [79].

Computations on spectral transparency based on data from investigations in the laboratory on forbidden bands of fundamental and secondary gaseous components (cf. Ch. 2) have wide application. From Fig. 3.11 it is possible to evaluate the spectral transparency of the troposphere along different directions in the spectral range of 1-6 μ determined by the selective absorption in optically active fundamental gases.

The family of curves (*a*) permits us to determine transmission of water vapor for different values of effective mass u_{eff} (see 3.2). With the help of the family of curves (*b*) it is possible to determine transmission of dry air, consisting of optically active gases, whose concentration may be considered invariable. The effective mass of CO_2 is taken as the effective mass of dry air. Using both families of curves it is possible to compute the emission spectrum of the atmosphere for paths of different lengths and inclinations for varying humidity contents in the course of the path. There is an error of about 10-15% in the determination of transparency. For the construction of the curves use is made of data obtained in the laboratory regarding the laws of absorption of the following distinct components, viz. H_2O, N_2O, CH_4, CO, CO_3 (cf. Ch. 2). For the distribution models of optically active components see Ch. 1.

It is necessary to mention the tables of transmission functions of H_2O and CO_2, published in [108, 115]. Computation of transmission of water vapor for a quasistatic model with resolution of 5, 20, 50 and 100 cm^{-1} was carried out by considering all bands up to 1000 cm^{-1}. (Continuous attenuation caused by rotational bands of $\lambda=200$ cm^{-1} was not considered. See [22] for computation on the absorption from rotational band of H_2O.)

The third group of data includes quantitative measurements on transmission of radiation in a real atmosphere as well as outside the

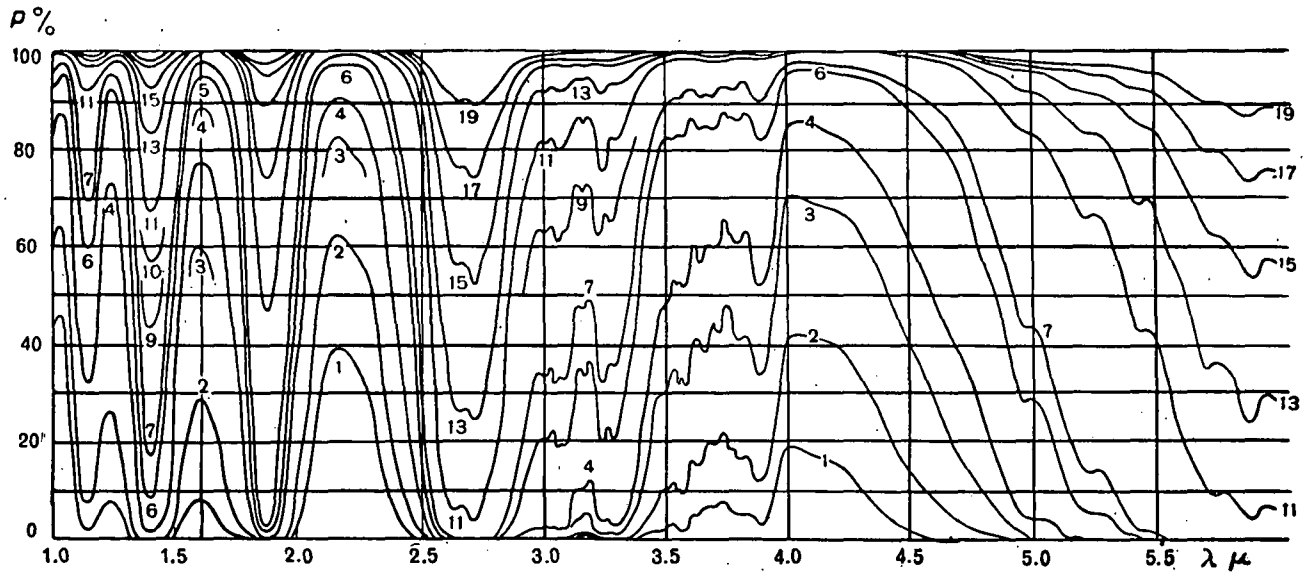

Fig. 3.11a. Selective transmission of optically active gases of atmosphere in the region 1-6 μ (spectral resolution $\Delta\lambda = 0.05$ μ, the instrumental function is an approximation through a triangle).

Transmission of water vapor for different values of effective mass u_{eff} (in cm of precipitated water).

1) 100 cm, 2) 50 cm, 3) 20 cm, 4) 10 cm, 5) 5 cm, 6) 2 cm, 7) 1 cm, 8) 0.5 cm, 9) 0.2 cm, 10) 0.1 cm, 11) 0.05 cm, 12) 0.02 cm, 13) 0.01 cm, 14) 0.005 cm, 15) 0.002 cm, 16) 0.001 cm, 17) 0.0005 cm, 18) 0.0002 cm, 19) 0.0001 cm.

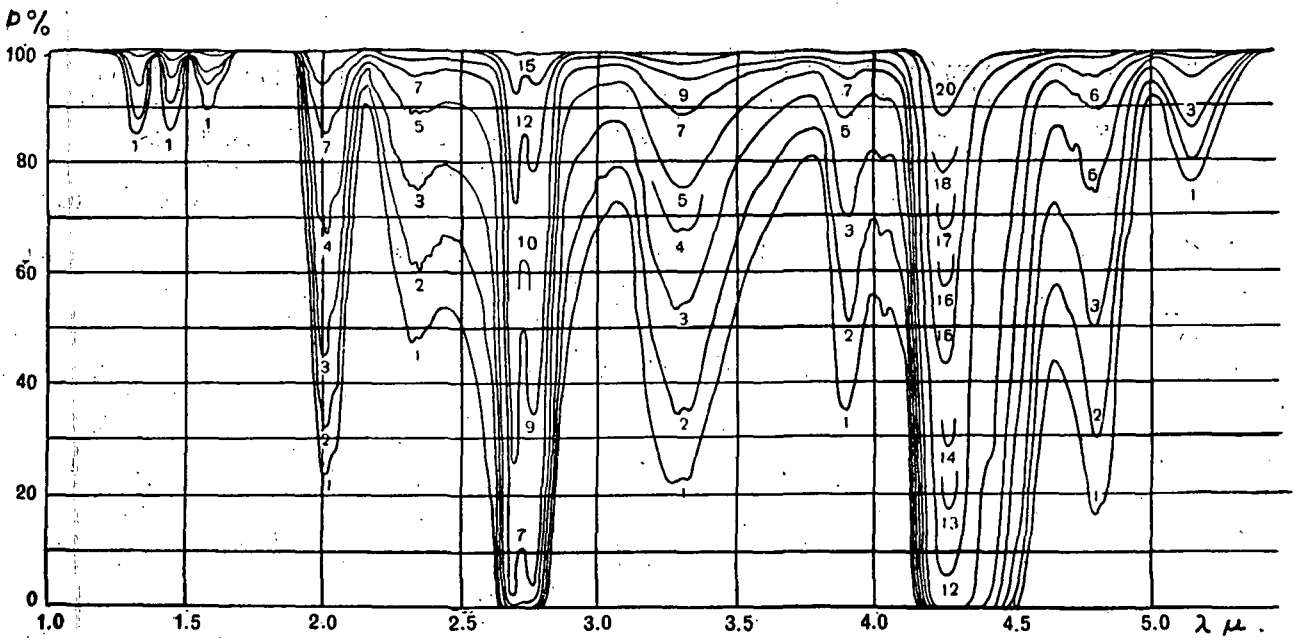

Fig. 3.11b. Selective transmission of optically active atmospheric gases in range 1-6 μ (spectral resolution $\Delta\lambda = 0.05\ \mu$ the instrumental function is an approximation through triangle).

Transmission of optically active and stable atmospheric gases (CO_2, CH_4, N_2O, CO) at different values of effective mass :

1) 3200 atm × cm, 2) 1600 atm × cm, 3) 640 atm × cm, 4) 320 atm × cm, 5) 160 atm × cm, 6) 64 atm × cm, 7) 32 atm × cm, 8) 16 atm × cm, 9) 6.4 atm × cm, 10) 3.2 atm × cm, 11) 1.6 atm × cm, 12) 0.64 atm × cm, 13) 0.32 atm × cm, 14) 0.16 atm × cm, 15) 0.064 atm × cm, 16) 0.032 atm × cm, 17) 0.016 atm × cm, 18) 0.0064 atm × cm, 19) 0.0032 atm × cm, 20) 0.0016 atm × cm.

absorption bands. A large accumulation of data on these measurements is lacking. Methodological difficulties in the separation of absorption due to mutually overlapping unresolved bands of polyatomic gases does not permit the determination of the mode of attenuation in intersecting bands for variations of optical mass and the amount of water vapor in the path of the ray. For instance, the authors of [90a] attempted to establish the relationships which satisfy different model representations for each of the 203 spectral regions into which the transmission spectrum of the atmosphere at oblique incidences from 1 to 12.5 μ can be divided. Practical application of the results obtained in [90a] proved to be difficult because of complications in the interpretation of data for different conditions and with different spectral resolutions. Investigations on attenuation in distinct segment of spectrum in regions of transparency windows, more or less free from selective absorption, are more reliable even though incomplete.

Fig. 3.12 shows the spectral variation of continuous absorption coefficients obtained in [22, 31, 69, 98] for measurements on absorption and emission of radiation in the window 8-12 μ. From the diagram it is obvious that the fringe of a rotational band of water vapor can have an effect on transmission of transparency windows having wavelength shorter than 8-12 μ.

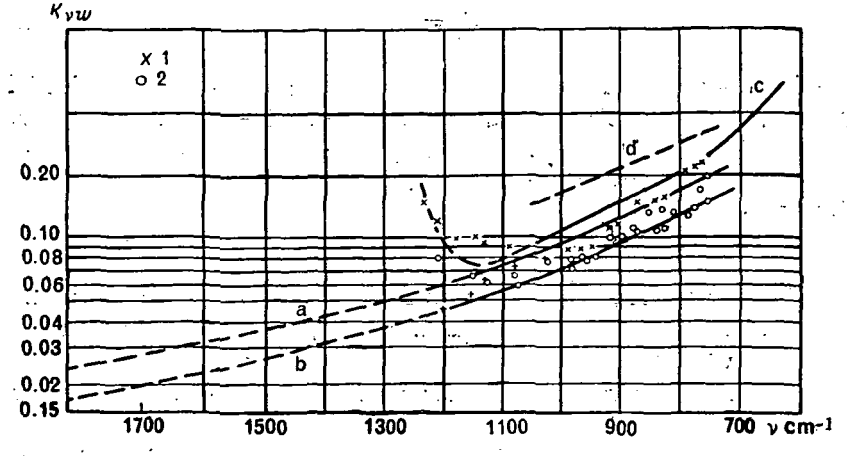

Fig. 3.12. Spectral course of continuous absorption of water vapor in the region 1200-750 cm^{-1}, computed in 1 cm of precipitated water, from observations by different authors.

(a) background of fringe of rotational band normalized to the value $\nu = 850$ cm^{-1} at $P_{eff} = 0.860$ atm; (b) background of fringe of rotational band, normalized to the value $\nu = 850$ cm^{-1} at $P_{eff} = 0.640$ atm; (c) from [69]; (d) from [22] 1—from [31] at $P_{eff} = 0.860$ atm; 2—at $P_{eff} = 0.640$ atm.

6. INTEGRAL TRANSPARENCY OF THE ATMOSPHERE

Depending on the conditions the transparency of an atmospheric column can vary considerably in different segments of the spectrum, as is obvious from the previous sections of Ch. 3. While measuring the integral flux of direct solar radiation attenuated by the atmospheric column, it is impossible to determine unequivocally the effect caused by the observed attenuation. Nevertheless it is necessary to evaluate atmospheric transparency.

For the meteorological purposes several modes of evaluating integral atmospheric transparency have been developed that employ semi-empirical methods based on measurement of the attenuation of solar radiation flux by means of integral actinometric apparatus [23, 27, 37, 38, 39].

The following are the basic requirements reflecting the characteristics of transparency: (1) sensitivity with respect to a variation in atmospheric transparency ; (2) independence from changes in optical mass of atmosphere ; (3) simplicity and clarity ; (4) simplicity in the method of computation.

The properties given below are most convenient for application. Transparency coefficient P can be computed from the following formula :

$$S_{30}=S_0P^m, \tag{3.26}$$

where S_{30}—measured intensity from direct solar radiation, given in Table 3.13 for the solar altitude of 30° ($m=2$), $S_0=1.98$ cal/cm² · min.

For $m=2$, $P=\sqrt{\frac{S_{30}}{S_0}}$.

The transparency coefficient can be easily computed with the help of Table 3.14 (corrections of measured intensity at a distance from the sun are given in Ch. 4).

Table 3.14 gives values of P for solar altitudes of 18-50° and values of $S=1.00$-1.29 cal/cm² · min.

The turbidity factor T suggested by Linke determines the ratio of observed transparency to the transparency of the ideal atmosphere free of water vapor or aerosol particles in suspension.

Turbidity factor T is determined from the formula :

$$T=\frac{\log P}{\log P_i}=\frac{\log S_0-\log S}{\log S_0-\log S_i}, \tag{3.27}$$

Table 3.13 Dependence of magnitude $S_\odot$ cal/cm² · min on solar altitude [38]

Altitude of sun, deg																					
18	19	20	21	22	23	24	25	26	27	28	30	32	34	36	38	40	42	44	46	48	50
0.79	0.81	0.83	0.85	0.87	0.89	0.90	0.92	0.94	0.96	0.97	1.00	1.03	1.05	1.08	1.10	1.12	1.13	1.15	1.16	1.17	1.19
0.80	0.82	0.84	0.86	0.88	0.90	0.91	0.93	0.95	0.97	0.98	1.01	1.04	1.06	1.09	1.11	1.13	1.14	1.16	1.17	1.18	1.20
0.81	0.83	0.85	0.87	0.89	0.91	0.92	0.94	0.96	0.98	0.99	1.02	1.05	1.07	1.10	1.12	1.14	1.15	1.17	1.18	1.19	1.21
0.82	0.84	0.86	0.88	0.90	0.92	0.93	0.95	0.97	0.99	1.00	1.03	1.06	1.08	1.11	1.13	1.15	1.16	1.17	1.18	1.20	1.21
0.83	0.85	0.87	0.89	0.91	0.93	0.94	0.96	0.98	1.00	1.01	1.04	1.07	1.09	1.12	1.14	1.16	1.17	1.18	1.19	1.21	1.22
0.84	0.86	0.88	0.90	0.92	0.94	0.96	0.97	0.99	1.01	1.02	1.05	1.08	1.10	1.12	1.14	1.16	1.17	1.19	1.20	1.21	1.23
0.85	0.87	0.89	0.91	0.93	0.95	0.97	0.98	1.00	1.02	1.03	1.06	1.09	1.11	1.13	1.15	1.17	1.18	1.20	1.21	1.22	1.24
0.86	0.88	0.90	0.92	0.94	0.96	0.98	0.99	1.01	1.03	1.04	1.07	1.10	1.12	1.14	1.16	1.18	1.19	1.20	1.21	1.23	1.24
0.87	0.89	0.91	0.93	0.95	0.97	0.99	1.00	1.02	1.04	1.05	1.08	1.11	1.13	1.15	1.17	1.19	1.20	1.21	1.22	1.24	1.25
0.88	0.90	0.92	0.94	0.96	0.98	1.00	1.01	1.03	1.05	1.06	1.09	1.12	1.14	1.16	1.18	1.20	1.21	1.22	1.23	1.25	1.26
0.89	0.91	0.93	0.95	0.97	0.99	1.01	1.02	1.04	1.06	1.07	1.10	1.13	1.15	1.17	1.19	1.21	1.22	1.23	1.25	1.26	1.27
0.90	0.92	0.94	0.96	0.98	1.00	1.02	1.03	1.05	1.07	1.08	1.11	1.14	1.16	1.18	1.20	1.22	1.23	1.24	1.26	1.27	1.28
0.91	0.93	0.95	0.97	0.99	1.01	1.03	1.04	1.06	1.08	1.09	1.12	1.15	1.17	1.19	1.21	1.23	1.24	1.25	1.27	1.28	1.29
0.92	0.94	0.96	0.98	1.00	1.02	1.04	1.05	1.07	1.09	1.10	1.13	1.16	1.18	1.20	1.22	1.24	1.25	1.26	1.28	1.29	1.30
0.93	0.95	0.97	0.99	1.01	1.03	1.05	1.06	1.08	1.10	1.11	1.14	1.17	1.19	1.21	1.23	1.25	1.26	1.27	1.29	1.29	1.31
0.94	0.96	0.99	1.01	1.03	1.05	1.06	1.08	1.10	1.11	1.13	1.15	1.18	1.20	1.22	1.24	1.25	1.26	1.27	1.29	1.30	1.31

Table 3.13—*Contd.*

Altitude of sun, deg																					
18	19	20	21	22	23	24	25	26	27	28	30	32	34	36	38	40	42	44	46	48	50
0.95	0.98	1.00	1.02	1.04	1.06	1.07	1.09	1.11	1.12	1.14	1.16	1.19	1.21	1.23	1.24	1.26	1.27	1.28	1.30	1.31	1.32
0.96	0.99	1.01	1.03	1.05	1.07	1.08	1.10	1.12	1.13	1.15	1.17	1.20	1.22	1.24	1.25	1.27	1.28	1.29	1.31	1.32	1.33
0.97	1.00	1.02	1.04	1.06	1.08	1.09	1.11	1.13	1.14	1.16	1.18	1.21	1.23	1.25	1.26	1.28	1.29	1.30	1.32	1.33	1.34
0.98	1.01	1.03	1.05	1.07	1.09	1.10	1.12	1.14	1.15	1.17	1.19	1.22	1.24	1.26	1.27	1.29	1.30	1.31	1.33	1.34	1.35
0.99	1.02	1.04	1.06	1.08	1.10	1.11	1.13	1.15	1.16	1.18	1.20	1.23	1.25	1.27	1.28	1.30	1.31	1.32	1.34	1.35	1.36
1.00	1.03	1.05	1.07	1.09	1.11	1.12	1.14	1.16	1.17	1.19	1.21	1.24	1.26	1.28	1.29	1.31	1.32	1.33	1.35	1.36	1.37
1.01	1.04	1.06	1.08	1.10	1.12	1.13	1.15	1.17	1.18	1.20	1.22	1.25	1.27	1.29	1.30	1.32	1.33	1.34	1.35	1.36	1.37
1.02	1.05	1.07	1.09	1.11	1.13	1.14	1.16	1.18	1.19	1.21	1.23	1.26	1.28	1.29	1.31	1.32	1.33	1.34	1.35	1.37	1.38
1.03	1.06	1.08	1.10	1.12	1.14	1.15	1.17	1.19	1.20	1.22	1.24	1.27	1.29	1.30	1.32	1.33	1.34	1.35	1.37	1.38	1.39
1.05	1.07	1.09	1.11	1.13	1.15	1.17	1.19	1.20	1.21	1.23	1.25	1.27	1.29	1.31	1.32	1.34	1.35	1.36	1.38	1.39	1.40
1.06	1.08	1.10	1.12	1.14	1.16	1.18	1.20	1.21	1.22	1.24	1.26	1.28	1.30	1.32	1.33	1.35	1.36	1.37	1.38	1.39	1.40
1.07	1.09	1.11	1.13	1.15	1.17	1.19	1.21	1.22	1.23	1.25	1.27	1.29	1.31	1.33	1.34	1.36	1.37	1.38	1.39	1.40	1.41
1.08	1.11	1.13	1.15	1.17	1.18	1.20	1.22	1.23	1.24	1.26	1.28	1.30	1.32	1.33	1.35	1.36	1.37	1.39	1.40	1.41	1.42
1.09	1.12	1.14	1.16	1.18	1.19	1.21	1.23	1.24	1.25	1.27	1.29	1.31	1.33	1.34	1.36	1.37	1.38	1.39	1.40	1.41	1.42

Table 3.14 Dependence of transparency coefficient of atmospheric P on magnitude of $S_{30} \cdot S_0 = 1.98$ cal/cm² · min [38]

S_{30} cal/cm² · min	One hundredth part of S_{30} cal/cm² · min									
	0	1	2	3	4	5	6	7	8	9
1.00	0.711	0.714	0.718	0.721	0.725	0.728	0.732	0.735	0.739	0.742
1.10	0.746	0.749	0.752	0.756	0.759	0.762	0.765	0.769	0.772	0.776
1.20	0.779	0.782	0.785	0.789	0.792	0.795	0.798	0.801	0.804	0.807

where P and P_i are transparencies in real and ideal atmosphere respectiveyl, S_i—intensity of radiation in ideal (dry and clear) atmosphere. For solar altitude 30° $S_{i,m=2}=1.62$ cal/cm² · min. Then

$$T=11.5\log\frac{S_0}{S_{30}}\,. \tag{3.28}$$

The computed values of T for different values of S_{30} according to this formula are given in Table 3.15.

Table 3.15 Dependence of turbidity factor of atmosphere T on magnitude of S_{30}

S_{30} cal/cm² · min	Hundredth fraction of S_{30} cal/cm² · min									
	0.00	0.01	0.02	0.03	0.04	0.05	0.06	0.07	0.08	0.09
1.00	3.41	3.36	3.31	3.27	3.22	3.17	3.12	3.08	3.03	2.99
1.10	2.94	2.89	2.85	2.80	2.76	2.71	2.66	2.62	2.58	2.54
1.20	2.50	2.46	2.42	2.38	2.34	2.30	2.26	2.22	2.18	2.14

L. G. Makhotkin [37, 39] suggested the index of turbidity N as a characteristic of atmospheric transparency which shows the amount of normal atmosphere to be taken so as to obtain the observed value of intensity for a given altitude of the sun. N is determined by the following relation :

$$N=\frac{m^*}{m}\,, \tag{3.29}$$

where m—optical mass, for which the intensity S is measured ; m^*—mass, introduced at normal atmosphere assuming $S=S^*$ (S^*—the intensity of solar radiation in normal atmosphere).

The rationality of this characteristic is indicated in [23, 39] and it is widely applied in actinometry [20, 23].

Makhotkin's turbidity factor N can be easily determined from the nomographs composed by Myurk [39] and shown in Fig. 3.13.

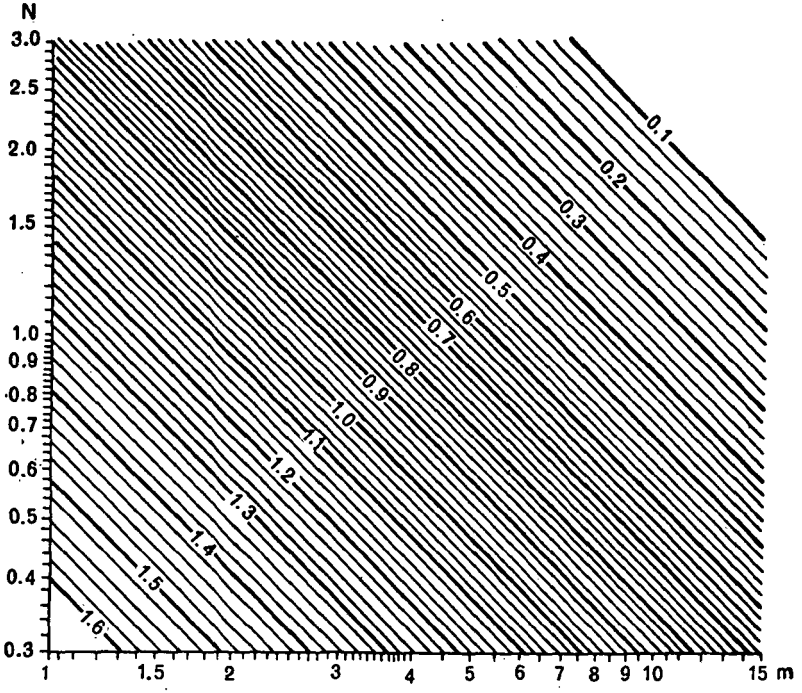

Fig. 3.13. Myurk's nomograph for the determination of turbidity factor N of Makhotkin (39).

$S = 0.1\text{-}1.6$ cal/cm² · mm;

m = mass of atmosphere at the time of observation.

Myurk in [36] suggested the characteristic of turbidity N_M, to be determined from the relation

$$S_m = S_0 P^m m^{N_{M,m}} \tag{3.30}$$

where P—coefficient of transparency for $m=1$. N_M is determined from the nomograph, introduced in [39].

7. TRANSPARENCY VARIATION IN ATMOSPHERIC THICKNESS

7.1 Synoptic situation and transparency

Transparency variations in the atmosphere are caused by changes

in the synoptic situation such as the shifting and transformation of masses of air, transmission through frontal zones, appearance and development of inversion, clouds and mists [23, 43, 118, 123]. The amount of humidity in the incoming mass of air is a very important parameter. The two fundamental types of air masses, viz. the arctic and the tropical, possess opposite optical properties. The arctic air is distinguished because of the absence of moisture and dust whereas the tropical air is very humid and dusty. Thus the exchange of an arctic air mass in the tropics leads to a decrease in transparency.

The magnitudes of the turbidity factor of Linke T and of Schüpp N_{sh} depending on the type of air masses are given in Table 3.16, which is borrowed from [121].

Table 3.16 Mean values of integral turbidity for different air masses according to measurements by different authors [121]

Type of air mass	T				$N_{sh} \times 10^3$
	After Foitsik and Heinspeter	After Mamontova and Khromov	After Ditts	After Barashkova	After Zempleni
Continental arctic air	2.20	2.4	2.8	—	7.9
Arctic sea air	2.10	—	—	2.8	—
Continental temperate air	2.89	—	—	—	8.2
Temperate sea air	2.85	—	—	—	11.0
Continental tropical air	3.76	3.5	3.9	3.2	16.8
Tropical sea air	3.66	—	—	—	15.5

The manner in which the coefficient of spectral transparency in an atmospheric column P_λ and its aeorosl component $P_{\lambda aer}$ change during transformation of a cold arctic air mass can be seen from the data in Table 3.17 [43] obtained from measurements in the Sosnovo region of Leningrad during the prevalence of an arctic air mass.

The value of P_λ diminishes by 5-10% with the warming up of a cold arctic air mass. The greatest stability of optical characteristics in the course of a day may be observed for arctic masses.

Table 3.17 Spectral coefficient of transparency in thickness of atmosphere P_λ and aerosol componment $P_{\lambda aer}$ for arctic air mass. Leningrad region [43]

Date	λ, μ							
	372		406		464		532	
	P_λ	$P_{\lambda aer}$	P_λ	$P_{\lambda aer}$	P_λ	$P_{\lambda aer}$	P_λ	$P_{\lambda aer}$
Sept. 8	0.613	0.943	0.689	0.946	0.792	0.952	0.857	0.952
Sept. 9	0.615	0.946	0.692	0.950	0.786	0.944	0.855	0.950
Sept. 10	0.613	0.943	0.685	0.941	0.787	0.945	0.850	0.944
Sept. 11[1]	0.595	0.907	0.664	0.912	0.760	0.919	0.834	0.927
Sept. 23	0.618	0.942	0.683	9.939	0.783	0.940	0.848	0.942
Oct. 12[1]	0.595	0.907	0.658	0.903	0.766	0.919	0.834	0.927
Oct. 26	0.621	0.947	0.688	0.945	0.788	0.946	0.855	0.948
Oct. 27	0.613	0.935	0.690	0.948	0.787	0.945	0.857	0.952

Date	λ, μ							
	615		650		715		805	
	P_λ	$P_{\lambda aer}$	P_λ	$P_{\lambda aer}$	P_λ	$P_{\lambda aer}$	P_λ	$P_{\lambda aer}$
Sept. 8	0.867	0.952	0.913	0.955	0.920	0.950	0.939	0.958
Sept. 9	0.867	0.952	0.904	0.947	0.924	0.954	0.935	0.954
Sept. 10	0.860	0.945	0.900	0.943	0.920	0.950	0.931	0.950
Sept. 11[1]	0.850	0.934	0.893	0.935	0.913	0.942	0.929	0.948
Sept. 23	0.863	0.949	0.897	0.940	0.916	0.945	0.936	0.954
Oct. 12[1]	0.850	0.934	0.894	0.936	0.913	0.942	0.931	0.950
Oct. 26	0.872	0.956	0.908	0.950	0.929	0.959		
Oct. 27	0.863	0.946	0.905	0.948	0.922	0.951	0.937	0.956

[1]Days of transformation of air masses

7.2 Annual and diurnal variations in atmospheric transparency

The influence of the height above sea level of the place of observation, of geographic latitude and other factors leads (within limits of observation) to wide variations of transparency (Fig. 3.14). The mean monthly values of optical thickness of the entire column of atmosphere from the articles

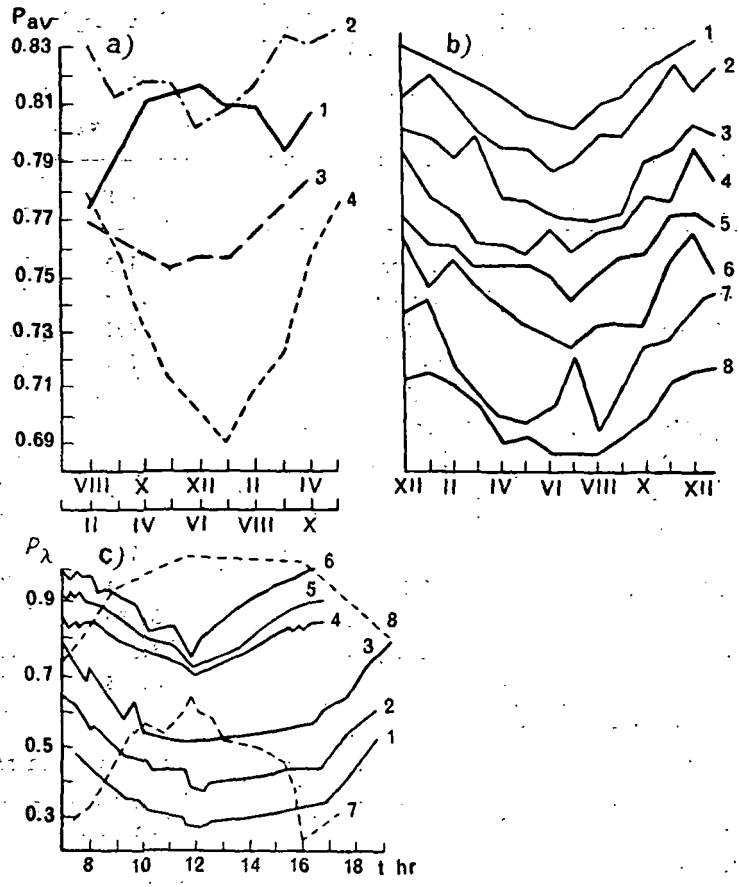

Fig. 3.14. Annual and diurnal variation of integral atmospheric transparency.

a) annual variation [23] : 1, 2—Antarctica; 3—Arctic; 4—Pavlovsk;
b) Annual variation [27]: 1—Pavlovsk; 2—Moscow; 3—Kursk; 4—Feodosiya; 5—Tbilisi; 6—Tashkent; 7—Baku; 8—Samarkand;
c) daily variation in transparency of vertical column of atmosphere during summer in Odessa (1, 2, 3) and at top of Mt. Terskol (4, 5, 6) and humidity content of atmospheric column in Odessa (8) and at the top of Mt. Terskol (7).

[20, 75] are given in Table 3.18 for points situated at different heights up to 4000 m, and for this purpose the entire visible region of the spectrum may be provisionally divided into two sections, viz. 0.4 μ and 0.5-0.7 μ.

Numerous observations on spectral and integral transparency in different geographic regions of the European Territory of the USSR, in mountain regions, and in Siberia [21, 23, 27 ; 30, 35, 56] show that there exists a definite daily variation of transparency in the presence of a stable mass of air.

Table 3.18 Observed values of optical thickness of atmosphere (mean values) [20, 75]

Point (height above sea level)	Month and Year	τ_λ total	
		0.4 μ	0.5-0.7 μ
Karadag	September, 1959	0.300	0.100
Leningrad (30 m)	May, 1963	0.730	0.330
Sablino (30 m)	April, 1960	0.400	0.150
	May, 1960	0.400	0.200
	September, 1960	0.300	0.060
Mineral'nye Vody (310 m)	October, 1962	0.400	0.100
Tucson (760 m)	1931	0.386	0.248
Klaimaks (1735 m)	1939	0.297	0.094
Mt. Sacramento (2800 m)	1934	0.269	0.105
		0.346	0.164
Mt. Terskol (3100 m)	July, 1962	0.300	0.100
	September, 1962	0.250	0.050
Ledovaya Basa (3700 m)	September, 1960	0.300	0.030
		0.316	0.130

Rising convection and, consequently, contamination of atmosphere around noon time, as well as the increase in the amount of humidity at midday, are the reasons for the minimal daily variation of transparency in continental regions (Mineral'nye Vody, Aktyubin, Nal'chik and others). Circulation of sea breezes (Odessa, Leningrad) and daily variations of winds in the mountains and valleys (El'brus) determine the nature and daily course of turbid atmosphere in corresponding regions.

The annual variation of transparency in the thickness of the atmosphere follows a similar course.

Investigations [2, 21] show that the daily and annual variations of horizontal atmospheric transparency contradict the variation of vertical transparency coefficients [20, 27, 36].

Tables 3.19 and 3.20 show the yearly course of Linke's turbidity factor (mean monthly and seasonal values) for thickness of atmosphere (above 200, 500 m, etc.) and for layers up to 30 km in the region of the Austrian Alps [105].

The maximum values of turbidity in summer are characteristic for the annual variation even in the region of the Alps and in El'brus.

A continuous rise in turbidity from morning to evening has been observed in the daily variation in mountain regions (June-August).

Table 3.19 Yearly course of turbidity factor T in Austrian Alps [105]

Month	Height, m				
	200	500	1000	2000	3000
Jan	3.0	2.7	2.2	1.8	1.7
Feb	2.8	2.5	2.1	1.8	1.7
Mar	3.2	2.9	2.6	2.1	1.9
Apr	3.6	3.3	2.8	2.2	2.1
May	3.8	3.6	3.2	2.5	2.2
Jun	3.8	3.5	3.2	2.6	2.2
Jul	3.9	3.7	3.3	2.6	2.2
Aug	3.8	3.4	3.1	2.6	2.2
Sep	3.3	3.0	2.8	2.3	2.0
Oct	3.2	2.8	2.5	2.0	1.9
Nov	2.7	2.4	2.2	1.8	1.8
Dec	2.6	2.4	2.1	1.7	1.7

Table 3.20 Turbidity factor T at different heights in Austrian Alps [105]

Season	Layer, km			
	0.2-1.0	1.0-1.5	1.5-2.0	2.0-3.0
Winter	11.0	6.1	4.7	2.2
Spring	10.7	10.3	6.8	4.0
Summer	11.1	9.5	7.6	5.7
Autumn	9.6	8.2	5.4	3.0

Strong evaporation of moisture and contrasts between frozen and thawed surfaces play an important role in promoting an increase in turbulence. A daily variation with minimum transparency at noon is typical for mountain regions during autumn and spring months. Condensation turbidity is a determining factor in the polar regions [23].

C-3

8. INTEGRATED TRANSMISSION FUNCTION FOR LONGWAVE RADIATION

8.1 Computed relation

In meteorology the term "longwave radiation" implies the type of radiation that is emitted by the natural underlying surface or atmosphere (the entire atmosphere or its distinct layers, in particular clouds).

The characteristic emission of these objects possesses a spectral composition which is distinct from the radiation of a perfectly black body. The emission from air is especially distinguishable because of its complex spectral composition—radiation from clouds and different surface layers—because of a spectral composition close to black-body emission. In spite of the difference between the spectral composition of naturally warm radiation and perfect black-body emission, approximate methods for the computation of longwave fluxes of radiation in the atmosphere have been successfully established [17, 28]. These methods are based on the application of the so-called *integrated transmission functions of longwave radiation* which determine the transparency of homogeneous layers of air for perfect black-body emission.

The integrated transmission function of longwave radiation A is the fraction of black-body emission at a specific temperature T, which is transmitted through a homogeneous column or layer of air of thickness l with absolute humidity a and temperature T_a at total pressure p. The magnitude A changes from 0 to 1.

The indicated parameters (l, a, p, T_a) determine the amount of precipitated water u_{H_2O} and the quantity of CO_2—u_{CO_2} in layer l. The influence of T_a on the transmission function is found to be insignificant.

Thus
$$A = A\,(u_{H_2O},\ u_{CO_2},\ p,\ T_p,\ T_a). \qquad (3.31)$$

Similarly the absorption in ozone should be considered for computation of the transmission function for the upper layers of the atmosphere. For clouds and mists it is necessary to take into consideration attenuation of radiation by water droplets.

Emission from a black body, corresponding to mean temperature on the earth's surface and in the atmosphere—taken as equal to 288° K (15°C), possesses a maximum* in the energy distribution over the

*The maximum occurs at $\lambda = 10\mu$, if the energy distribution in the spectrum is carried out on the scale of wavelength ($\Delta\lambda = \text{const}$). In the scale of wave number ($\Delta\nu = \text{const}$) the distribution curve is deformed and the maximum shifts to $\lambda = 17.7\ \mu$ or $\nu = 565\ \text{cm}^{-1}$.

spectral range of 10 or 1000 cm^{-1}. Ninety-four per cent of the entire black-body emission for the indicated temperature lies in the region of wavelengths between 4 and 40 μ, whereas 99.3% lies in the region 4-100 μ [1, 9].

Insofar as the integrated transmission function relates to a wide interval of the spectrum, it cannot be represented exponentially because of the complex structure of the absorption spectrum of atmospheric gases.

The integrated function A for a parallel beam of black-body radiation can be determined in two ways : (1) by direct measurements of the emission of black-body radiation by layers of atmosphere with specific values of the indicated parameters or (2) by computations based on the application of spectral recordings on absorption of radiation by water vapor, CO_2 and O_3.

Direct measurements of A are associated with noticeable experimental difficulties so that such measurements are few in number and the range of u_{H_2O}, u_{CO_2} is comparatively narrow. The computational method allows one to cover wide ranges of values of the parameters, but gives non-singularity and fragmentation in the original experimental data, and is full of errors due to the inevitable simplifications of a complex structure of the absorption spectra of atmospheric gases. Thus a noticeable disparity still exists between computations and experimental data.

The integrated transmission function may be expressed through spectral emission functions in the following manner :

$$P(u, T)=\int_0^\infty \frac{E_\lambda(T)}{E(T)} P_\lambda(u)\, d\lambda, \tag{3.32}$$

where $P_\lambda(u)$—transmission function for wavelength λ; E_λ/E—fraction of emission from a perfect black body, entering a unit interval of wavelength with center at λ ; u—mass of absorbing substance ; T—temperature of black-body emission.

It is necessary to know the following function in computing transmission of radiation in atmosphere :

$$\Phi(u, T)=\frac{\int_0^\infty \frac{dE_\lambda}{dT} P_\lambda(u)\, d\lambda}{\frac{dE}{dT}}, \tag{3.33}$$

where the functions $\Phi(u, T)$ and $P(u, T)$ are connected by the following relation :

Table 3.21 Values of $P(u, T)$ at different temperatures of the source of radiation

T°C	u_{H_2O}										
	0.0001	0.0003	0.001	0.003	0.01	0.03	0.1	0.3	1	3	10
—80	0.884	0.857	0.798	0.718	0.620	0.526	0.426	0.341	0.242	0.129	0.027
—60	0.907	0.884	0.832	0.758	0.668	0.578	0.480	0.392	0.284	0.154	0.034
—40	0.924	0.904	0.857	0.790	0.705	0.620	0.524	0.433	0.317	0.176	0.040
—20	0.937	0.919	0.877	0.814	0.734	0.651	0.557	0.464	0.342	0.193	0.045
0	0.947	0.931	0.892	0.832	0.754	0.673	0.581	0.488	0.361	0.206	0.049
20	0.955	0.941	0.904	0.846	0.770	0.690	0.598	0.504	0.373	0.214	0.052
40	0.962	0.948	0.913	0.856	0.780	0.700	0.610	0.514	0.380	0.219	0.055
60	0.967	0.954	0.920	0.863	0.787	0.707	0.617	0.519	0.383	0.222	0.056

Table 3.22 Values of $\Phi(u, T)$ at different temperatures of the source of radiation

T°C	u_{H_2O}										
	0.0001	0.0003	0.001	0.003	0.01	0.03	0.1	0.3	1	3	10
—150	0.841	0.805	0.727	0.623	0.503	0.393	0.286	0.208	0.137	0.064	0.011
—120	0.906	0.880	0.822	0.740	0.641	0.543	0.436	0.345	0.243	0.126	0.025
—90	0.940	0.921	0.877	0.812	0.730	0.644	0.545	0.450	0.329	0.181	0.040
—60	0.959	0.945	0.909	0.854	0.780	0.702	0.610	0.515	0.383	0.218	0.051
—30	0.971	0.959	0.928	0.876	0.806	0.703	0.642	0.545	0.408	0.236	0.058
0	0.978	0.967	0.938	0.886	0.815	0.739	0.652	0.554	0.412	0.241	0.062
30	0.982	0.972	0.943	0.889	0.815	0.736	0.648	0.548	0.404	0.237	0.062
60	0.985	0.975	0.945	0.887	0.810	0.728	0.637	0.534	0.390	0.228	0.061

Table 3.23 Values of $\Delta A\ (u_{H_2O},\ u)$ and $\Delta\Phi\ (u_{H_2O},\ u)$ for computation of absorption in carbon dioxide

$[\Delta A\ (u_{H_2O},\ u)=\Delta\Phi\ (u_{H_2O},\ u)]$

u	u_{H_2O}										
	0.0001	0.0003	0.001	0.003	0.01	0.03	0.1	0.3	1	3	10
0.01	0.001	0.001	0.001	0.001	0.001	0.001	0.001	0.001	0.001	0.000	0.000
0.03	0.006	0.006	0.006	0.006	0.006	0.006	0.006	0.005	0.004	0.002	0.000
0.1	0.013	0.013	0.013	0.013	0.013	0.012	0.012	0.011	0.008	0.005	0.000
0.3	0.022	0.022	0.022	0.022	0.021	0.021	0.020	0.018	0.013	0.006	0.001
1	0.039	0.039	0.039	0.039	0.038	0.038	0.036	0.032	0.023	0.012	0.002
3	0.071	0.071	0.071	0.070	0.070	0.069	0.065	0.058	0.042	0.021	0.003
10	0.101	0.101	0.101	0.100	0.100	0.098	0.093	0.083	0.061	0.029	0.004
30	0.124	0.124	0.124	0.123	0.122	0.120	0.114	0.101	0.074	0.036	0.005
100	0.147	0.147	0.147	0.146	0.145	0.142	0.135	0.121	0.088	0.043	0.006
300	0.166	0.166	0.166	0.165	0.164	0.162	0.154	0.137	0.100	0.055	0.007
1000	0.184	0.184	0.184	0.183	0.182	0.178	0.170	0.151	0.101	0.054	0.007

Table 3.24 Values of $\Delta A\ (m)$ $\Delta\Phi\ (m)$ for computation of absorption in ozone

m	0.001	0.003	0.01	0.03	0.10	0.30	1.00
ΔA	0.000	0.000	0.001	0.004	0.011	0.022	0.030
$\Delta\Phi$	0.000	0.001	0.002	0.007	0.020	0.040	0.055

$$\Phi(u, T)=P(u, T)+\frac{T}{4}\frac{\partial P(u, T)}{\partial T}. \quad (3.34)$$

The values of functions P and Φ computed on the basis of spectral data on absorption of radiation in water vapor, carbon dioxide and ozone are given in Tables 3.21 and 3.22.

The contributions of carbon dioxide and ozone to the functions P and Φ are represented for convenience in the form of corrections to A and Φ caused by absorption of water vapor alone (Tables 3.23 and 3.24). In this manner we have the following relations :

$$P(u_{H_2O}, u_{CO_2}, u_{O_3}, T)=P(u_{H_2O}, T)-\Delta P(u_{H_2O}, u_{CO_2})-\Delta P(u_{O_3}); \quad (3.35)$$

$$\Phi(u_{H_2O}, u_{CO_2}, u_{O_3}, T)=\Phi(u_{H_2O}, T)-\Delta\Phi(u_{H_2O}, u_{CO_2})-\Delta\Phi(u_{O_3}). \quad (3.36)$$

Here $P(u_{H_2O}, T)$—integral emission function for water vapor ; $\Delta P(u_{H_2O}, u_{CO_2})$—correction for carbon dioxide gas ; $\triangle P(u_{O_3})$—correction in ozone ; u_{H_2O}, u_{CO_2}, u_{O_3}—masses of water vapor, carbon dioxide and ozone respectively. Similarly all the above-mentioned quantities refer to the function $\Phi(u_{H_2O}, u_{CO_2}, u_{O_3}, T)$.

All the magnitudes in Tables 3.21-3.24 are given for normal pressure and temperature of absorbing gas, viz. 10-20°C. The corrections for carbon dioxide and ozone are averaged over the range of emission temperatures from −80 to +60°C and from −80 to −20°C. Besides the correction on ozone is averaged over masses of water vapor from 0 to 1 cm.

The magnitudes of u_{H_2O} are expressed in cm of precipitated water, u_{CO_2}, u_{O_3}—in atm.

The values of the functions P, Φ, $\triangle P$, $\triangle\Phi$ in Tables 3.21-3.24 are computed for direct radiation. The values of these functions for diffuse radiation are connected with the values for direct radiation by the following relation :

$$f^*(u)=\int_0^{\pi/2} f\left(\frac{u}{\cos\vartheta}\right)\sin 2\vartheta\, d\vartheta, \quad (3.37)$$

where $f\left(\frac{u}{\cos\vartheta}\right)$ implies any of the functions P, Φ, $\triangle P$, $\triangle\Phi$; $f^*(u)$—corresponding function for diffuse radiation; ϑ—incident angle of radiation. For sufficiently accurate computation in atmosphere the following approximate relation may be similarly applied, viz.:

$$f^*(u)=f(1.66u). \quad (3.38)$$

In case of approximate computation not requiring the consideration of the dependence of emission function of temperature of the source, it is possible to make use of functions $P(u_{H_2O}; u_{CO_2}; u_{O_3})$ and $P^*(u_{H_2O}; u_{CO_2}; u_{O_3})$ found in the tables taken from [44, 45].

For computations of radiation on flux as well as incident fluxes in the boundary layer of the atmosphere in the absence of any large temperature gradient it is possible to employ average emission functions, which are independent of temperature and automatically take into consideration the influence of carbon dioxide [30] ; thus

$$P^*(u_{H_2O}) = 0.461 \exp\left(-0.674\sqrt{u_{H_2O}}\right) + 0.539 \exp\left(-7.75\sqrt{u_{H_2O}}\right). \tag{3.39}$$

The formula (3.39) is applicable for diffuse emission.

To determine the changes of pressure in the atmosphere with altitude it is necessary to make use of the effective absorbing masses $u_{eff} = \int \left(\frac{p}{p_0}\right)^m du$, where p—pressure, p_0—standard atmospheric pressure. The power m accepts the following values ; for water $m = 0.60$; for carbon dioxide $m = 0.86$ and for ozone $m = 0.30$.

The computation [61] of functions $P(u_{H_2O}; u_{CO_2}; u_{O_3}; T)$ and $\Phi(u_{H_2O}; u_{CO_2}; u_{O_3}; T)$ was carried out by using the following experimental and theoretical data : range of 3-5 μ [87]; range of 5-9 μ [87, 91, 94] ; range of 9-12 μ [65, 91] ; range of 12-13μ [65, 87, 91] ; range of 13-20 μ [83, 97, 119] ; range of 20-25 μ [104]; CO_2—[67, 84, 95]; O_3—[120].

8.2 Experimental data and their comparison with computations

1. *Methods of measurement.* A comparatively simpler scheme (single channel)—perfect black body at a specific temperature and removed from an inactive receiver with a single receiving surface (for example, [32, 88]) —provides for two successive measurements of a single source (the second at a different temperature) and the detection of two signals. A more precise and less ambiguous case is the double channel scheme, with two sources at different temperatures and a receiving set with two receiving surfaces for automatic detection of signals; the rotation of the receiver along with the shield through 180° eliminates interference and leads to detection of useful signals against the background of interference.

For both the schemes, which are based on the method of heated emitter, the measured signal I^* is proportional to the following expression

$$I^* \sim P_1 T_1^4 - P_2 T_2^4. \tag{3.40}$$

in which the values of emission function P_1 and P_2 correspond to those for a black-body radiation from sources at temperatures T_1 and T_2, respectively. If these temperatures differ from 273° K by some 40 or 50 degrees, then both the functions (P_1 and P_2) are comparable. For convenience in working out the results of measurements, it is necessary to assume that P is independent of T, i. e. to assume $P_1=P_2=P$. Then

$$\tilde{P} \sim \frac{I^*}{T_1^4 - T_2^4}. \tag{3.41}$$

By neglecting the dependence of P upon T we introduce a systematic error, leading to a higher value of P compared to original values of transmission function P_1 and P_2, and the following relation is found to hold [7] :

$$\tilde{P}(T_1, T_2) = \frac{P_1 T_1^4 - P_2 T_2^4}{T_1^4 - T_2^4}. \tag{3.42}$$

The method of heated emitters also does not investigate the relation $P(T)$ for the range of atmospheric temperatures.

For sources at high temperature (several hundred degrees C) the systematic error becomes insignificant [13, 24, 32].

It is possible to eliminate the systematic error for radiation at low temperatures by using highly chilled plates (radiation screen) [7, 12] in place of one of the heated sources. In this case $T_2 \ll T_1$, $I^* \sim P T_1^4$, $\tilde{P}(T_1, T_2) = P(T_1)$ and the measurements give values of emission functions closer to the original; while changing the temperature T, of the emitter it is possible to study the function $P(T)$ in the zone of atmospheric temperatures.

2. *Results of measurements.* The results of measurements of P with the help of a heated emitter and radiation screen on a horizontal receiving track for emission temperatures of 15 and 80°C and for distances of 59.7, 93.6 and 247.4 m [11] and the computed curves are shown in Fig. 3.15. Measurements were carried out in pure atmosphere (visual range greater than 10 km).

The values of P obtained from experimental data are smaller than those obtained through computation. Similarly the dependence of the source and thickness of layer on temperature is more sharply brought out. The values of $\tilde{P}$ obtained by the method of two emitters [10] are considerably greater than the original values of P, which is explained by the significant dependence of P on T.

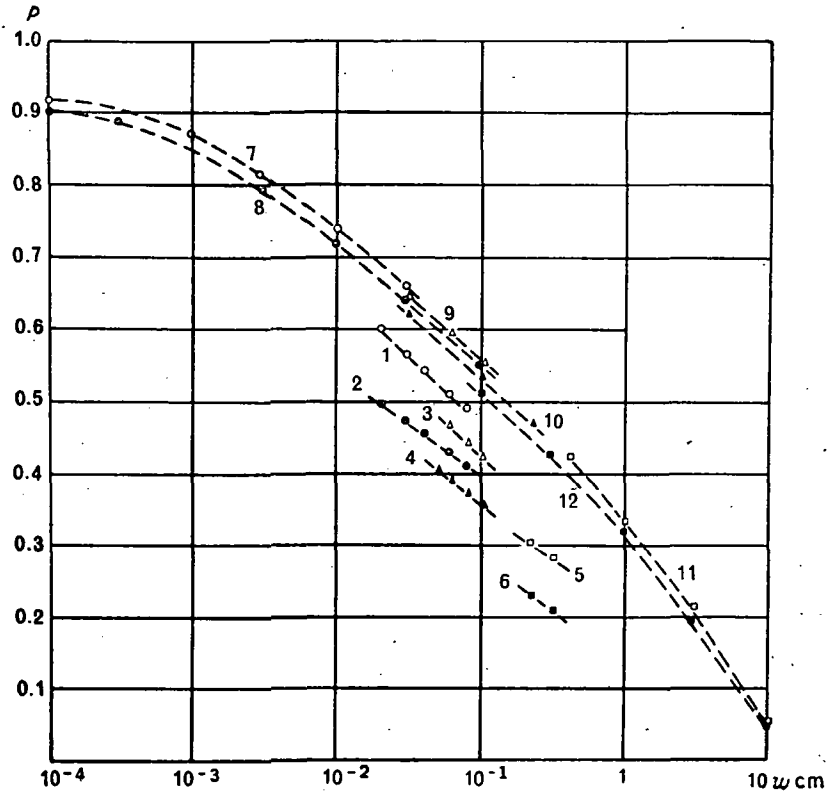

Fig. 3.15 Comparison of computed and experimental determinations of integrated transmission function in horizontal tracks of different lengths (59.7, 93.6, 247.4 m) at emission temperatures 20 and 80°C and S_M=10 km.

Experimental curves : 1) 59.7 m, 80°; 2) 59.7 m, 20°; 3) 93.6 m, 80°; 4) 93.6 m, 20°; 5) 247.4 m, 80°; 6) 247.4, 20°;

Computed curves : 7) 60 m, 80°; 8) 60 m, 20°; 9) 90 m, 80°; 10) 90 m, 20° ; 11) 250 m, 80°; 12) 250 m, 20°.

REFERENCES

1. Ananasevich, P.A. and V.S. Aizenshdadt. Tablitsy raspredaleniya e'nergii i fotonov v spektre ravnovesnogo izlucheniya (Tables on distribution of energy and photons in the spectrum of radiation equilibrium). Izd-vo AN SSSR, Minsk, 1961.
2. Barteneva, O. D., E. N. Dovgyallo and E. A. Polyakova. E'ksperimental'nye issledovaniya opticheskikh svoistv prizemnogo sloya atmosfery (Experimental study of optical properties of layer of atmosphere near the earth's surface). Trudy GGO, vyp. 220, 1967.
3. Badinov, I. Ya and S. D. Andreev. Prozrachnost' zemnoi atmosfery i razdelenie opticheskoi tolshchiny na komponenty v infrakrasnoi oblasti spektra 8-13 mkm. (Transparency of earth's atmosphere and division of optical thickness into components in the infrared region of the spectrum 8-13 μ). Problemy fiziki Atmosfery, vyp. 3, Izd. LGU, 1965.
4. Badinov, I. Ya., S. D. Andreev and V. B. Lipatov. Nekotorye resul'ty nazemnykh spektrometricheskikh issledovanii vlagosoderzhaniya tolshchi atmosfery (Some results on surface spectrometric investigations of moisture-content of the thickness of atmosphere). Problemy fiziki Atmosfery, vyp. 4, Izd. LGU, 1966.
5. Badinov, I. Ya., and L. V. Popova. O nekotorykh resul'tatakh izmerenii spektral'noi prozrachhosti atmosfery v usloviyakh oblachnosti verkhnogo yarusa (Some results on measurements of spectral transparency of atmosphere for cloudiness of upper stratum). Problemy fiziki Atmosfery, vyp. 5, Izd. LGU, 1967.
6. Barashkova, E. P. Mutnost' atmosfery v Karadage (Turbidity of atmosphere at Karadag). Trudy GGO, vyp. 80, 1959.
7. Beritashvili, B. A., A. M. Brounshtein and K. V. Kazakova. O zavisimosti integral'noi funktsii propuskaniya atmosphery ot temperatury chernogo izlucheniya (The relation between integrated emission function in atmosphere and temperature of black-body radiation). Trudy GGO, vyp. 114, 1966.
8. Badinov, I. Ya and L. V. Popova. O svyazi spektral'noi opticheskoi tolshchi atmosphery (0.36-1.03 mkm) s nekotorymi meteorologicheskimi kharakteristikami (The relation between spectral optical thickness of atmosphere (0.36-1.03 μ) and some meteorological characteristics). Problemy fiziki Atmosphery, vyp. 7, Izd. LGU, 1969.
9. Bramson, M. A. Spravochnye tablitsy po infrakrasnomu izlucheniyu nagretykh tel (Reference Tables on infrared radiation of heated bodies). Izd-vo "Nauka", Moskva, 1964.
10. Brounshtein A. M. and K. V. Kazakova. Ob ogranichenii sloev vozdukha dlya issledovaniya ikh sobstvennogo izlucheniya (On the limitations of air while studying their intrinsic radiation). Trudy GGO, vyp. 213, 1968.
11. Brounshtein, A. M. and K. V. Kazakova. Issledovanie integral'noi funktsii propuskaniya dlinnovolnovoi radiatsii s ispol'zovaniem radiatsionnogo e'krana (Investigation on integral emission function of longwave radiation with the application of a radiation screen). Trudy GGO, vyp. 223, 1968.
12. Brounshtein, A. M. and K. V. Kazakova. E'kspeiimental'noe issledovanie integral'noi funktsii propuskaniya. III. Result'aty izmerenii dlya srednikh vlazhnostei vozdukha (Experimental study of emission functions. III. Results of measurements on average moisture of air). Aktinometriya i atmosfernaya optika. Trudy V mezhvedomst vennogo soveshchaniya, June 1963, Izd-vo "Nauka", Moskva, 1964.
13. Blokh, A. G. Osnovy teploobmena islucheniem (Fundamentals of heat exchange in radiation). Gose'nergoizdat, 1962.

14. Vavilov, S. I. Sobranie cochinenii (Collection of essays). t. 2. Izd. AN SSSR, 1952.

15. Van de Khyulst. Rasseyanie sveta malymi chastitsami (Scattering of light by small particles). IL, 1961.

16. Gorchakov, G. I. E'ksperimental'noe issledovanie matritsy rasseyaniya sveta prizemnym vozdukhom i nekotorye svoistva atmosfernoi dymki (Experimental study of matrices of light scattering by the surface air and some properties of atmospheric mist). Avtoreferat dissertatsii, Moskva, 1967.

17. Gudi, R. M. Atmosfernaya radiatsiya (Atmospheric radiation). Moskva, 1966.

18. Gushchin, G.P. Issledovanie atmosfernogo ozona (Study of atmospheric ozone). Gidrometeoizdat, Leningrad, 1963.

19. Geogrievskii, Yu. S. et al. Prozhektornyi luch v atmosfere (Projected ray in atmosphere). Izd. AN SSSR, Moskva, 1960.

20. Daeva, L. V. K voprosu ob opredelenii spektral'nykh koe'ffitsientov prozrachnosti real'noi zamutnennoi atmosfery v oblasti spektra 0.4-1 mkm. (On the determination of spectral coefficients of transparency of naturally turbid atmosphere in the region of the spectrum 0.4-1 μ). Coll. 'Aktinometriya i optika atmosferry', Izd-vo "Nauka" Moskva, 1964.

21. Dovgyallo, E. P. Prozrachnost' atmosfery v gorizontal'nom i vertikal'nom napravleniyakh (Atmospheric transparency in horizontal and vertical directions). Trudy GGO, vyp. 169, 1965.

22. Zhevakin, S. A. and A. P. Naumov. O koe'ffitsiente pogloshcheniya e'lektromagnitnykh voln vodyanymi parami v diapazone 10 mkm-2 cm (Absorption coefficient of electromagnetic waves in water vapor in the range 10 μ-2 cm.) Izd. VUZov, ser. radiofizika, VI, 4, 1963.

23. Zvereva, S. V. Prozrachnost' atmosfery v polyarnykh raionakh (Atmospheric transparency in polar regions). Avtoreferat dissertatsii, LGMI, Leningrad, 1967.

24. Zuev, V. E. Prozrachnost' atmosfery dlya vidimykh i infrakrasnykh luchei (Atmospheric transparency for visible and infrared rays). Izd-vo "Sovetskoe radio", Moskva, 1966.

25. Zuev, V. E., V. V. Sokolov and S. D. Tvorogov. Spektral'naya prozrachnost' i mikrostruktura iskusstvennykh tumanov (Spectral transparency and microstructure of artificial mists). Izv. VUZov, ser. fizika, No. 3, 1966.

25a. Ivlev, L. S. and E. L. Yanchenko. Ob'emnye koeffitsienty rasseyaniya dlya razlichnykh modelei atmosfernogo ae'rozolya (Volume coefficients of scattering for different models of atmospheric aerosol). Izv. VUZov, ser. fizika, 1969.

26. Kovaleva, E. D. and F. N. Shekhter. Vliyanie stratifikatsii atmosfery na radiatsionnyi pritok tepla (The effect of atmospheric stratification on radiative heat influx). Trudy GGO, vyp. 187, 1967.

27. Kondrat'ev, K. Ya. Luchistaya e'nergiya Solntsa (Radiant energy of the sun). Gidrometeoizdat, Leningrad, 1954.

28. Kondrat'ev, K. Ya. Luchistyi teploobmen v atmosfere (Radiative heat exchange in atmosphere). Gidrometeoizdat, Leningrad, 1956.

29. Kondrat'ev, K. Ya., M. P. Burgova and G. A. Totunova. Pogloshcheniye vody v infrakrasnoi oblasti spektra (Absorption of water in the infrared region of the spectrum). Problemy fiziki atmosfery, vyp. 2, Izd. LGU, 1963.

30. Kondrat'ev, K. Ya. Aktinometriya (Actinometry). Gidrometeoizdat, Leningrad, 1965.

31. Kondrat'ev, K. Ya. et al. Nekotorye resul'taty nazemnykh issledovanni infrakrasnogo spektra pogloshcheniya i teplovogo izlucheniya atmosfery (Some results of terrestrial investigations on infrared spectrum of absorption and thermal radiation of atmosphere). Izv. AN SSSR. Ser. fizika atmosfery i okeana, t. 1, 4, 1965.

32. Kozyrev. B. P. and A. A. Buznikov. Apparatura i metodika issledovaniya pogloshcheniya atmosfernoi radiatsii slabo nagretogo absolyutno chernogo izlychatelya (Apparatus and investigation method of absorption of atmospheric radiation in a weakly heated absolutely black body). Izv. LE'TI named after V. L. UI'yanov (Lenin), vyp. 55, Leningrad, 1966.

33. Livshits, G. Sh. Rasseyaniye sveta v atmosfere (Scattering of light in atmosphere). Part I. Izd-vo "Nauka", Alma-Ata, 1965.

34. Lifshits, G. Sh., V. E. Pavlov and S. N. Milyutin. O pogloshchenii sveta atmosfernymi ae'rozolyami (Absorption of light in atmospheric aerosol). Trudy Astrofizicheskovo in-ta AN Kazakh SSR, t. VII, 1966.

35. Makhon'ko K. P. Sutochnye izmeneniya zapylennosti prizemnogo sloya atmosfery. Sb. "Voprosy yadernoi meteorologii" (Diurnal variation of dust in the surface layer of atmosphere. Coll. "Problems of Nuclear Meteorology"). Gosatomizdat, Moskva, 1962.

36. Myurk, Kh. Yu. O novoi formule intensivnosti izlucheniya i o novykh kharakteristikakh prozrachnosti atmosfery (On the new formula for intensity of radiation and new characteristics of atmospheric transparency). Issledovaniya po fizike atmosfery, vyp. 1. Izd. AN E'SSR, 1959.

37. Makhotkin, L. G. Pryamaya radiatsiya i prozrachnost' atmosfery (Direct radiation and atmospheric transparency). Izv. AN SSSR, ser. geofizicheskaya, No. 5, 1957.

38. Metodicheskie ukazaniya po opredeleniyu kharakteristik prozrachnosti atmosfery dlya aktinometricheskikh otdelov (grupp) gidrometeoobservatorii UGMS (Instructions for the determination of characteristics of atmospheric transparency for actinometric sections [groups] of hydro-meteorological observatories of UGMS). Izd. GGO, Leningrad, 1965.

39. Myurk, Kh. Yu. O ratsional'nosti indeksa Makhotkina (Makhotkin's efficiency index). Issledovaniya no fizike atmosfery IFA AN E'SSR, 1, 1959.

40. Mikirov, A. E. O malykh uglakh indikatrisy passeyaniya (Small angle scattering functions). Izv. AN SSSR, ser. geofiz., 2, 1959.

41. Mirzoyan, L. V. Ob atmosfernoi e'kstinktsii (Atmospheric extinction). Izv. AN Arm SSR, No. 2, 1953.

42. Myukhkyurya, V. I. K voprosu o vertikal'nom raspredelenii ae'rozol'noi ostavlyayushchei pokazatelya oslableniya solnechnogo sveta v atmosfere (On the vertical distribution of aerosol constituting attenuation characteristics of sunlight in atmosphere). Trudy GGO, vyp. 105, 1960.

43. Nikitinskaya, N. I. Osobennosti opticheskikh kharakteristik arkticheskikh mass vozdukha (Peculiarities of optical characteristics of masses of air in the Artic regions). Trudy GGO, vyp. 118, 1961.

44. Niilisk, Kh. Yu. Ob opredelenii intensivnosti dlinnovolnovoi radiatsii v atmosfere (Determination of intensity of longwave radiation in the atmosphere). Issledovaniya po fizike atmosfery, vyp. 3, Izd. AN E'SSR, 1962.

45. Niilisk, Kh. Yu. Novaya radiatsionnaya nomogramma (New radiative nomogram). Izv. AN E'SSR, ser. fiz.-mat. I tekhn. nauk, No. 4. 1961.

46. Polyakova, E. A. Dal'nost' vidimosti v zone dozhdya (Visual range in a rainy zone). Meteorologlya i gidrologiya, No. 8, 1956.

47. Pyaskovskaya-Fesenkova, E. V. Issledovaniye rasseyaniya sveta v zemnoi atmosfere (Study of scattering light in terrestrial atmosphere). Izd. AN SSSR, Moskva, 1957.

48. Rodionov, S. F. Prozrachnost' atmosfery v ul'trafioletovoi oblasti spektra (Atmospheric transparency in the ultraviolet region of the spectrum). Izv. AN SSSR, ser. geogr. i geofiz., No. 4. 1950.

49. Rozenberg, G. V. O granitsakh primenimosti zakona Bugera i ob effektakh obrashcheniya anomal'noi i selektivnoi prozrachnosti atmosfery (The limits of applicability of Bouguer's law and the effect of inversion on anomalous and selective atmospheric transparency). DAN SSSR, 145, No. 6, 1962.

50. Rozenberg, G. V. and Yu. S. Lyobovtseva. E'ksperimental'nyi metod ucheta vliyaniya oreola pri izmereniyakh koe'ffitsientov ekstinktsii i rasseyaniya (Experimental method of considering the effect of halo on measuring the coefficients of extinction and scattering). Izv. AN SSSR, fizika atmosfery i okeana, t. III, No. 2, 1967.

51. Rozenberg, G. V. and V. V. Tereshkova. Stratosfernyi ae'rozol' po izmereniyam s kosmicheskogo korablya (Stratospheric aerosol according to measurements from space ship). Izv. AN SSSR, fizika atmosfery i okeana, t. I, No. 4, 1965.

52. Rozenberg, G. V. and A. B. Sandomirskii. Opredeleniye vysotnogo khoda koe'ffitsienta rasseyaniya po fotografiyam dnevnogo gorizonta Zemli, poluchennym s kosmicheskogo korablya "Voskhod" (Determination of the altitudinal course of the scattering coefficient from photographs of daily horizon of the earth obtained from the space ship "Voskhod"). Izv. AN SSSR, fizika atmosfery i okeana, t. III, No. 2, 1967.

53. Rozenberg, G. V. Opticheskie issledovaniya atmosfernogo aérozolya (Optical study of atmospheric aerosol). UFN, t. 95, No. 5, 1968.

54. Rozenberg, G. V. Sumerki (Twilight). Fizmatgiz, Moskva, 1963.

55. Rabinovich, Yu. I. Vertikal'noe raspredelenie ae'rozol'nogo oslableniya v troposfere (Vertical distribution of aerosol attenuation in troposphere). Trudy GGO, vyp. 118, 1961.

56. Rabinovich, Yu. I and L. N. Guseva. E'ksperimental'nye issledovaniya spektral'noi prozachnosti atmosfery (Experimental investigation on spectral transparency of atmosphere). Trudy, GGO, vyp. 118, 1961.

57. Toropova, T. P. K voprosy o roli razhlichnykh faktorov v oslablenii sveta zemnoi atmosferoi (The role of different factors in light attenuation at the earth's surface). Izv. Astrofizicheskogo in-ta Kazakh. SSR, t. VI, 1958.

58. Fabrikant, V. A. O zakone Bugera (Bouguer's law). Izv. AN SSSR, ser. fizicheskaya, t. 26, No. 1. 1962.

59. Faraponova, G. P. Izmerenie oslableniya solnechnogo sveta v svobodnoi atmosfere (Measurement of attenuation of sunlight in free atmosphere). Trudy TsAO, vyp. 32, 1959.

60. Chayanova, E'. A. Opredelenie spektra chastits po indikatrise rasseyaniya (Determination of spectrum of particles from the scattering function). Izv. AN SSSR, fizika atmosfery i okeana, t. 2, No. 2, 1966.

61. Shekhter, F. N. Spektral'nye i integral'nye funktsii propuskaniya dlinnovolnovoi radiatsii (Spectral and integral emission functions for longwave radiation). Trudy GGO, vyp. 184, 1966.

62. Shifrin, K. S. Rasseyanie sveta v mutnoi srede (Scattering of light in a turbid medium). Gostekhizdat, 1951.

63. Shifrin, K. S. and I. N. Minin. Teoriya negorizontal'noi vidimosti (Theory of nonhorizontal visibility). Trudy GGO, vyp. 68, 1957.

64. Ångström, A. Techniques of determining the turbidity of the atmosphere. Tellus, 13. No. 2, 1961.

65. Adel, A. Lampland atmospheric absorption of infrared solar radiation of the Lowell observatory. Astroph. J., v. 91, No. 1, 5, 1940.

65a. Babcock, H. D. and C. E. Moore. The solar spectrum λ 6600 to λ 13495 Å. Carnegie Institution of Washington, Publication No. 579, 1947.

66. Bemporad, A. Mitteilungen der Grossh. Sternwartezy Heidelberg. (Astrometrisches Institut). V. 1. 1904. Karlsruhe. Zur Theorie der Extinktion des Lichtes.

67. Burch, D. E. and D. Gryvnak. Infrared absorption by dioxide, water vapor and minor atmospheric constituents. Res. Rep., July 1962.

68. Bignel, K., F. Saiedy and P. A. Sheppard. On the atmospheric infrared continuum J. Opt. Soc. America, 53, No. 4, 1963.

69. Bolle, H. J., H. Quenzel and W. Zdunkowski. Geofisicia e Meteorologia, v. 11, 1963.

69a. Brückner, G. Photometrischer Atlas des nahen ultravioletten Sonnenspectrums 2988–3629 Å. Göttingen, Vandenhoeck and Rupecht, 1960.

70. Chaco, O. and V. Desikan. Atmospheric turbidity measurements over India. Indian J. Meteorol. and Geophys., 16, No. 4, 1965.

71. Deirmendjian, D. and Z. Sekera. Quantitive evaluation of multiply scattered and diffusely reflected light in the direction of a stellar source in a Rayleigh atmosphere. J. Opt. Soc. of America, v. 43, No. 12, 1953.

72. Deirmendjian, D. and Z. Sekera. Global radiation resulting from multiple scattering in a Rayleigh atmosphere. Tellus, vol. 6, 1954.

73. Dave, J. V. Multiple scattering in a nonhomogeneous Rayleigh atmosphere. J. Atm. Sci., v. 22, No. 3, May 1965.

74. Danzer, K. H. and K. Bullrich. The influence of absorption on the extinction of solar and sky radiation. Applied Optics, v. 4, No. 11, 1965.

75. Deirmendjian, D. and Z. Sekera. Atmospheric turbidity and the transmission of ultraviolet sunlight. J. Optic. Soc. Am. v. 46, No. 8, 1956.

76. Deirmendjian, D. The optical thickness of the molecular atmosphere. Archives Meteor., Geophys. and Bioklim., Serie B, v. 6, 1955.

77. Deirmendjian, D. Note on lazer detection of atmospheric dust layers. Journ. of Geoph. Res., 70, p. 743, 1965.

77a. Delbouille, L. and G. Roland. Atlas photométrique du spectre solaire de λ 7498 à λ 2016 Å. Liège, 1963.

77b. Delbouille, L., et al. The solar spectrum in the 5577 and 6300 Å regions. Oxford, 1967.

78. Dessens, H. Sur l'équilibre radiatif des particules atmosphériques. J. Rech. Atmosp., 2, Nos 2-3, 1966, 159-163.

79. Elterman, L. Ultraviolet, Visible and Infrared Attenuation for altitudes to 50 km, 1968. Environmental Research Papers, No. 285, April, 1968.

80. Elterman, L. Aerosol measurements in the troposphere and stratosphere. Appl. Opt., v. 5, No. 11, 1966.

81. Elterman, L. An atlas of aerosol attenuation and extinction profiles for the troposphere and stratosphere. Environmental Research Papers, No. 241. AFCRL-66-828, Dec. 1966.

82. de Bary, E. and K. Bullrich. Effects of higher-order scattering in a molecular atmosphere. J. Opt. Soc. Am., v. 54, No. 12, 1964.

83. Elsasser, W. M. Note on atmospheric absorption caused by rotational water band. Phys. Rev., v. 53, No. 9, 1938.

84. Edwards, D. K. Absorption by infrared bands of carbon dioxide at elevated pressures and temperatures. J. Opt. Soc. Am., v. 50, No. 6, 1960.

85. Farmer, C. B. and P. J. Key. A study of the solar spectrum from 7 to 400 microns. Report No. DMP 2160, 1965.

86. Fiocco, G. Observations of the aerosol layer at the 20 km by optical radar. J. Atm. Sci., 21, 1964, p. 323.

87. Fowle. Water vapor transparency to low-temperature radiation. Smiths. Misc. Collections, v. 68, No. 8, 1917.

88. Falckenberg, G. Expérimentelles zur Absorption dünner Luftschichten für infrarote Strahlung. Met. Z., B. 53, Heft 5, 1936.

89. Galindo, I. "Turbidometric estimations in Mexico City using the Volz Sun photometer. Pure and Applied Geophysics, 60, No. 1, 1965, 189-196.

90. Gates, D. M. and C. Shaw. Infrared transmission of clouds. J. Opt. Soc. Am., v. 50, No. 9, 1960.

90a. Gates, D. M. and W. J. Harrop. Infrared transmission of the atmosphere to solar radiation. Appl. Opt., v. 2, No. 9, 1963.

91. Gebbie, H. A. Atmospheric transmission in the 1 to 14 mkm region. Proc. Roy. Soc., A. v. 206, 1951.

92. Houghton, J. T. et al. An atlas of the infrared solar spectrum from 1 to 6.5 mkm. Philos. Trans. Roy. Soc. London, Ser. A., 1961, v. 254, No. 1037.

93. Hughes, H. K. Beer's law and the optimum transmittance in absorption measurements. Appl. Opt. Spectroscopic Instrumentations, v. 2, No. 9, 1963.

94. Howard, J. N., D. E. Burch and D. Williams. Near-infrared transmission through synthetic atmosphere. Geoph. Res. Pap. No. 40, 1955.

95. Hottel, Mangelsdorf. Heat transmission by radiation. Experimental study of CO_2. Trans. Am. Inst. Chem. Eng., v. 31, 3, 1935.

96. Herman, B. M. and D. N. Jarger. The effect of absorption on a Rayleigh atmosphere. J. Atm. Sci. v. 22, No. 6, 1965.

97. Yamomoto, G. and G. Onishi. Absorption coefficient of water vapor in the far infrared region. The Sc. Rep. Tohoku Univ. 5th ser., Geophysics, v. 1 No. 1, 1949.

98. Kondratyev, K. Y. et al. Atmospheric optics investigations on Mt. Elbrus. Applied Optics, v. 4, No. 9, 1965, 1069-1076.

99. Kondratyev, K. Y. et al. Aerosol structure of the troposphere and stratosphere. Thesis of the Symposium on Radiation, including Satellite Techniques at Bergen (Aug. 22-28. 1968).

100. Leupolt, A. Determination of aerosol absorption from spectral sky radiation measurements. Symposium on radiation processes in the atmosphere. Leningrad, 1964. Paris, Monographie No. 28, 1965.

100a. Mac Alister. A preliminary photometric Atlas of the solar u.v. spectrum. Colorado, 1960.

100b. Mehltreter, J. P. Absolute spectral photometric Atlas in Ultraviolett zwishen 2000 und 3000 Å. Heidelberg, 1962.

110. Migeotte, M., L. Neven, and I. Swenson. The solar spectrum from 2.8 to 23.7 microns Univers. of Liège. Final Report., pt. 1, 1956; pt., 2, 1957.

101a. Minnaert, M., G. F. W. Mulders and J. Hovgast. Photometric atlas of the solar spectrum, from λ 3612 to λ 8771 Å, with an appendix from λ 3332 to 3637 λ Å. Amsterdam, 1940.

101b. Mohler, O. C., A. K. Pierce, R. R. McMath and L. Goldberg. Photometric atlas of the near infrared solar spectrum λ 8465 to λ 25242 Å. University of Michigan Press, 1950.

102. Puchalsky, S. Okreslenie parametrow jungowskiego roskladu aerosolu za pomoca pomiarow dwoch monochomatycnych współczy nników ekstynkcji. Mater i prace. Zakl. geofiz RAN, No. 13, 1966, 61-69.

103. Penndorf, R. B. Tables of the refractive index for standard air and the Rayleigh scattering coefficients for the spectral region between 0.2 and 20.0 μ and their application to atmospheric optics. J. Opt. Soc. Am., 47, No. 2, 1957.

104. Palmer, C. H. Experimental transmission functions for the pure rotation band of water vapor. J. Opt. Soc. Am., 50, No. 12, 1960.

105. Robinson. Solar radiation. 1966.

106. Ruzicková, B. Photoelektrische Messungen der atmosphärischen Extinktion in Ondrejov., 11, No. 6, 242-247, 1960.

107. Roach, W. T. and R. M. Goody. Absorption and emission in the atmosphere window from 770 to 1250 cm^{-1}. Q.J.R.M.S., v. 84, No. 362, 1958.

108. Stull, V. R., P. Y. Wyatt and G. N. Plass. The infrared absorption of water vapor. Report SSD-TDR-62-127, v. 11, 1962.

109. Sekera, Z. and G. Blanch. Tables relating to Rayleigh scattering of light in the atmosphere. Sci. Rept. No. 3, Contract AF 19 (122)—239. Air Force Cambridge Res. Center, 1952.

110. Sekera, Z. and E. V. Ashburn. Tables relating to Rayleigh scattering of light in the atmosphere. NAVORD Rept. 2061 U.S. Naval Ordnance Test Station, Inyokern, Calif., 1953.

111. Schulman, E. Filter measurement of solar radiation at Blue Hill Obs. Harv. Meteor. Stud., No. 7, 1943.

112. Simon, G. W. A practical solution of the atmospheric dispersion problem. The Astronomical J., v. 71, No. 3, 1966.

113. Sekinara, K. and Murai Keizo. On the absorption properties of atmospheric dust particles as considered from various kinds of ground level observations. Symposium on Radiation Processes in the Atmosphere. Leningrad, 1964. Paris, Mon. 28, 1965.

114. Street, Y. L., Y. H. Taylor and S. L. Ball. Near infrared atmospheric absorption over a 25 km sea level. Appl. Opt. March 1967.

115. Stull, V. R., P. J. Wyatt and G. N. Plass. The infrared absorption of carbon dioxide. Report SSD-TDR-62-127, v. 111, 1962.

116. Valko, P. Vereinfachtes Answerteverfahren für die Schüppsche Methode zur Bestimmung der atmosphärischen Trübung. Arch. Meteor. Geophys und Biokl., Bd 11, No. 1, 1961.

117. Valko, P. Trübungsbestimmung im Alpengebiet auf aktinometrischen und photometrischen Wege. Geofis. e meterorol., 11, 1963.

118. Williams, P., Jr. Air pollution potential over the Salt Lake valley of Utah as related to stability and wind speed. J. Appl. Meteorol., v. 3, No. 1, 1964.

119. Weber, L. R. and H. M. Randall. The absorption spectra of H_2O beyond 10 mkm. Phys. Rev., v. 40, 1932.

120. Walshaw, C. D. Integrated absorption by the 9.6 mkm band of ozone. Q.J. Roy. Met. Soc., v. 83, No. 357, 1957.

121. Zempleinyi, S. Some characteristics of urban turbidity as determined by actinometric measurements. Symposium on Radiation Processes. Leningrad, 1964. Paris. Monogr. No. 28, 1965.

4. ALBEDO OF EARTH'S SURFACE AND CLOUDS

PART I. INTEGRATED REFLECTION FACTOR

1. COMPUTATION OF AVERAGE VALUES OF ALBEDO

Reflective properties of the earth's surface can be characterized by the magnitude of albedo, defined as the ratio of radiation flux reflected from a given surface in all directions to the flux incident on this surface. Integrated albedo A (or simply albedo) can be determined from the following expression :

$$A = \frac{\int_0^\infty A_\lambda \, (S_{\lambda m} + D_{\lambda m}) \, d\lambda}{(S+D)_m}, \tag{4.1}$$

where A_λ—spectral albedo ; $(S+D)_m$—flux of total (direct solar S and scattered D) radiation incident on a horizontal surface for a mass of atmosphere m; $(S_{\lambda m}+D_{\lambda m})$—monochromatic flux of total radiation incident on a horizontal surface for a mass of atmosphere m.

Since all the observations made so far have been mainly obtained by means of thermoelectric pyranometers (in the USSR—by a pyranometer

devised by Yu. D. Yanishevskii), whose spectral sensitivity covers the spectral range 0.4-3.0 μ [19, 39], it is necessary to consider measurements of integral albedo as related to this part of the spectrum.

Ground measurements of albedo are usually carried out from a height of 1-2 m above the level of the underlying surface and consequently characterize the reflective properties of small territorial areas. Albedo can be computed from measurements of reflected and incident radiation at three intervals daily in the network of meteorological stations, viz. 9 hrs 30 min, 12 hrs 30 min, 15 hrs 30 min (mean local time).

The mean daily albedo may be considered as the arithmetic average determined over these intervals. The reflection factor computed in this manner does not precisely define the average value of albedo in a day. The difference can be significant over the long stretch of a day and especially in the case of those surfaces for which wide changes are characteristic in the course of a day. For a more accurate computation it is necessary to consider the mean daily albedo $\bar{A}$ or the ratio of total fluxes of reflected radiation $\sum R$ to the total incident radiation $\sum Q$ $\left(\bar{A}=\sum R/\sum Q\right)$. A comparison of mean values of albedo in a day evaluated as the ratio $\sum R/\sum Q$, with mean values computed as the arithmetic average of observations for several intervals (more than three), has been made in [8, 18].

The mean value of albedo over a month is usually computed as the arithmetic mean of the average albedo values over a month for each interval of observation as follows :

$$A_{\text{mon}}=\frac{\sum A_{9\ 30}}{n_1}+\frac{\sum A_{12\ 30}}{n_2}+\frac{\sum A_{15\ 30}}{n_3}, \qquad (4.2)$$

where n_1, n_2, n_3—number of measurements at intervals over a month.

Average albedo over a season or a year may be defined as the arithmetic mean of average monthly values of albedo.

The most precise method of computing average values of albedo over a month, season or year includes the determination of weighted mean values of albedo using weights equal to the ratio of the total incident radiation in an interval during which several changed values of albedo have been observed, to the total amount of incident radiation in the entire period. For instance, mean seasonal albedo can be computed from the following formula :

$$A_{\text{seas}}=\frac{A_1Q_1+A_2Q_2+A_3Q_3}{Q_{\text{seas}}}$$

Indices 1, 2 and 3 indicate those three months of the season to which the given value refers. The average yearly albedo can be determined from the formula :

$$A_{yr} = \frac{A_w Q_w + A_{sp} Q_{sp} + A_{su} Q_{su} + A_a Q_a}{Q_{yr}}, \qquad (4.4)$$

where the indices *w, sp, su, a* denote values corresponding to the winter, spring, summer and autumn seasons, respectively.

2. ALBEDO OF DIFFERENT UNDERLYING SURFACES

It is convenient to use the classification of surfaces suggested by E. L. Krinov while analyzing albedo, according to which soil and exposed rocks belong to the first class, vegetative covers to the second, snow and glacial surfaces to the third and water surface to the fourth.

2.1 Albedo of soil surface

The albedo of a specific type of soil can change considerably depending on its color, structure and dampness. The albedo of soil decreases with increasing moisture (Table 4.1). The sharpest decrease in albedo occurs during an increase in humidity from 1 to 15% ; the value of albedo changes little with a further increase in humidity. Thus for example $A=26\%$ for sand with a humidity of 5%, $A=16\%$ for a humidity of 15%, $A=14\%$ for humidity of 25% (values are taken from the chart) [21].

Table 4.1 Albedo (%) for moist and dry soil covers [3]

Soil characteristic	Even surface		Tilled surface	
	dry	moist	dry	moist
Chernozem of dark gray color	13	8	8	4
Light chestnut soil of gray color	18	10	14	6
Chestnut soil of grayish red color	20	12	15	7
Gray sandy soil	25	18	20	11
White sand	40	20	—	—
Dark blue clay	23	16	—	—

The dependence of the albedo of soil on the roughness, for instance, in the case of white clay soil at the foot of the mountains, is clearly illustrated in Table 4.2 (observations were carried out during identical conditions of illumination). Values of albedo given in the Table for different surfaces considered show that albedo increases with decreasing roughness ; thus, for example, for a freshly tilled field albedo equals 17%, and for a leveled surface it is 30-31%.

Table 4.2 Albedo of clayey white soil at the foot of a mountain [47]

Surface characteristic	Albedo, %
Leveled	30-31
Silt covered	28
Covered by mulch as a result of tilling after wetting	27
Covered by fine clods	25
Covered by huge clods	30
Freshly tilled field	17

2.2 Albedo of vegetative covers

Albedo of vegetative covers differs with respect to the type of plants. For the same type of plants albedo depends on the condition of the surface (which is connected with variations in dampness) and the stage of vegetation (characterized by different heights of plants, by the density of grass stand, by color, by the amount of tilling, etc.).

Table 4.3 shows that albedo increases for plants which change color (color becomes yellow) but do not change volume in the ripening process (corn, cereal crops).

Table 4.3 Albedo changes in vegetative covers with respect to the stage of vegetation [5, 37, 55]

Characteristic of vegetative cover	Albedo, %	$h^\circ_\odot$
Potato		
Height of plant 40-50 cm, coverage of earth less than 50%, green color	18	63
Bulk coloring	16	71
End of coloring	15	71
Start of wilting of stems	13	72
Wilting stem, coverage of earth 50%	11	71
Corn		
Height of plant 15-20 cm, coverage of earth 40-50%	16	69
Height of plant 40-50 cm, coverage 70-75%	18	70
Height of plant 140-200 cm, in green corn, coverage 80%	20	70
Height of plant 200-250 cm, complete agricultural maturity	23	69
Grass		
Green meadow grass, height 25 cm	18	30
Meadow grass in the wilting stage	13	30
Winter crop of wheat		
Milky ripeness, light green	13	41.7
Ceraceous maturity, yellow	17	41.7
Complete maturity, light yellow	21	41.7

2.3 Albedo of snow cover

The physical properties of a snow cover are determined in the first place by the structure and the state of the snow, which continuously changes under the influence of weather conditions and many other factors. This accounts for the various types of snow surfaces as well as the large variation in albedo (Tables 4.4 and 4.5).

From data given in Tables 4.4 and 4.5 it is clear that there are wide changes in the albedo of snow surfaces, viz. between 28 and 98% taking into consideration the density, structure and moisture of the snow cover. Special albedometric measurements were carried out in VNIGL* [29] to establish a relation between the pattern of these variations of albedo. The observations were made under identical conditions of incident radiation, so that the results of measurements could be compared among themselves. The following conclusions could be drawn on the basis of these investigations; for dry snow (freshly fallen, average-sized grains changing into huge-sized grains) the important variations in albedo occur in the range in low density snow ρ_s from 0.16 to 0.28 g/m^3 during which albedo decreases by approximately 12%. However, albedo remains practically stationary with an increase in density from 0.28 to 0.32 g/m^3.

On an average albedo decreases by 33% for moist snow within the range of variation in density from 0.28 to 0.44 g/m^3 and in dampness from 0 to 19%. This change in albedo is brought about not only by the difference in density and dampness but also by the extent of impurity.

2.4 Albedo of ice

Investigations on ice surfaces, carried out in the Antarctic and on glaciers, indicate the wide variation of albedo as a result of the appearance and the melting of snow as well as its contamination. The average values of snow albedo in the Arctic region are shown in Table 4.6. The albedo of ice floes is somewhat less than that of pack ice. The existence of snow in ice increases albedo by 11-16% and the appearance of snowflakes sharply decreases albedo by 42% (Table 4.7). Results of air reconnaissance of ice carried out over the Davis Sea and over the adjoining part of the Indian Ocean show that different types of ice possess different values of albedo—from 2 to 20% (dark glass ice) up to 90-95% (shelf ice) (Table 4.8). The flight was conducted at an altitude of 250 m. A striated-cumulus cloudiness of 9-10 pts prevailed over the sea.

*VNIGL—Valdaiskaya nauchno-issledovatel'skaya gidrologicheskaya laboratoriya (Valday Scientific Research Hydrological Laboratory).

Table 4.4 Mean values of albedo for different types of snow according to observations made in the Moscow region in 1955 [29]

Condition of snow	Albedo, %	
	field	forest
Freshly fallen, dry or wet	82	82
Fine grained, wet	73	65
Medium-sized wet grain	64	56
Large-sized wet grain	55	47
Mottled region	47	39
Distinct spots of snow	36	31

Table 4.5 Albedo of snow surface, according to data from drifting stations SP-4, SP-6 and SP-7 [6]

Structure	State of dampness and color	Albedo, %		
		mean	maximum	minimum
Freshly fallen snow	Dry, pure, shining white	88	98	72
	Moist, shining white	80	85	80
Freshly drifted snow	Dry, clean, weakly compressed	85	96	70
	Moist, grayish white	77	81	59
Snow which fell or drifted 2-5 days before	Dry, clean	80	86	75
	Moist, grayish-white	75	80	56
Dense snow	Dry, clean	77	80	66
	Moist, grayish-white	70	75	61
Recrystallized snow	Moist	63	75	52
Snow and ice	Dry, grayish-white	65	70	58
Snow saturated with water (snow at the time of thawing)	Light green	35	—	28

The mean values of albedo characteristic of glacial surfaces in the Caucasus and Alps are given in Table 4.9. The value of albedo may change between 26 and 54% depending on the condition of the ice surface.

Table 4.6 Albedo of ice in Arctic region [59]

Surface characteristic	Albedo, %			Condition of surface color
	mean	maximum	minimum	
Ice floe without snow	45	50	40	Green, dry (in spring)
Melting ice floe	50	55	45	Gray, moist
Melting packed ice without snow	56	67	49	Gray, moist (knobby)
Frozen snowflakes (naslud, fresh pool ice)	44	50	42	Gray

Table 4.7 Albedo of icy surface in June-August, 1957, at the station "Severnyi Polyus-7" [59]

Period	Surface	Mean albedo over a day, % ($h_\odot$=10-30°)
June (last ten days)	Ice, partial snow	72
July	Melting ice	61
August	Ice, partial snow	70
August	Ice with snow	77
July	Snowflakes	35

Table 4.8 Albedo of ice surface in Antarctic region [1]

Type of snow	Cohesion, pts	Snow encrustation	Albedo, %
Dark glass ice	9-10	—	2-20
Gray glass pancake ice	8-9	—	20-50
Gray ice	9	—	50-70
Grayish white and white ice including year old ice	7-8	1-2	60-70
	9-10	1-2	70-80
	9	2-3	80-90
Ice floe	9-10	2	80
Shelf ice	—	2-3	80
Shelf glacier	—	—	90-95
Glacial domes	—	—	90

Table 4.9 Albedo of glacial surface in the region of El'brus and in the Alps (Hintereisferner) [8, 70]

Surface	Albedo, %
Clear, moist névé	50-54
Contaminated névé	46
Pure ice, and ice covered by soft hail	39-41
Contaminated melting ice	26-33

2.5 Daily variation in albedo

Overall roughness in the surface and the condition of illumination exert an influence on the daily variation of albedo (for the term "roughness" see [60]). The altitude of the sun, the relation between scattered and total radiations (or between direct and scattered radiations), as well as the change in spectral composition of the incident radiation, constitute the conditions of illumination. The last factor affects the daily variation of albedo of soils and vegetative surfaces (0.1-0.5% when $\triangle h_{\odot}=10°$) less than the change in roughness ($\sim$1% for $\triangle h_{\odot}=10°$) [15]. The albedo of soils (Table 4.10) and of vegetative surfaces (Fig. 4.1) possesses a minimum value at midday in the majority of observations under conditions of cloudless atmosphere, whereas with decreasing altitude of the sun their albedo rises. This fact has been reaffirmed by theoretical computation also [40, 60]. It should be observed that there exists an asymmetry in the value of albedo for vegetative covers in the course of a day with respect to midday [13, 37, 53]. The cause of this asymmetry has not been finally understood. The physiological properties of plants [53] may be considered as one of the causes.

Table 4.10 Dependence of albedo of soils (%) on altitude of sun in clear weather [2]

Surface	Altitude of sun, deg						
	10	20	30	40	50	60	65
Stony dry soil	22	16	14	13	12	12	11
Clayey dry soil	34	29	21	20	19	18	17
Grayish-green soil, dry	—	30	27	26	25	24	23

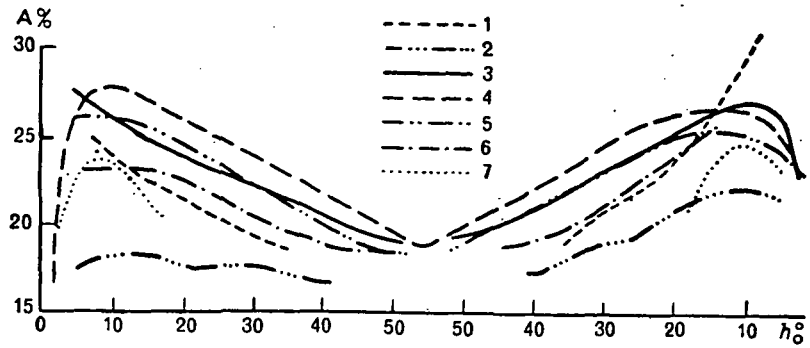

Fig. 4.1. Dependence of albedo of grass cover on solar altitude [53].
1—dry last year's grass; 2—damp last year's grass; 3—new grass; 4—grass cover (mean value for 12 days, June, 1959); 5—grass cover (mean value for 7 days, July, 1959) ; 6—grassy cover (mean value for 7 days, August, 1959); 7—old grass (September 30, 1959).

A nonuniform variation of albedo (Table 4.11) has been observed for vegetative surfaces of different roughness during changes in solar altitude by 1°. The dependence of the albedo of grass on solar altitude becomes more noticeable with a thick herbage (grass—May, June). This dependence is clearly expressed for "basaltiform" surfaces (sunflower). There exists practically no change in albedo within the limits of solar altitude between 10-50° for bushy growths, sparsely seeded (potato).

Table 4.11 Variation in albedo (%) for 1° solar altitude for vegetative surface [13, 37]

Surface	Solar altitude, deg			
	10-20	20-30	30-40	40-50
Grass				
May	0.15	0.10	0.13	0.12
June	0.25	0.18	0.12	0.05
Meadow grass (thick herbage)	0.46	0.35	0.20	0.15
Sunflower	0.30	0.30	0.15	0.13
Potato field	0.07	0.04	0.03	—

The dependence of albedo on the ratios D/Q and S/D has been studied by many authors [13, 53]. A nomograph for the determination of albedo for different ratios D/Q (Fig. 4.2) has been established from the data of numerous measurements taken in the course of seven years for grassy surfaces.

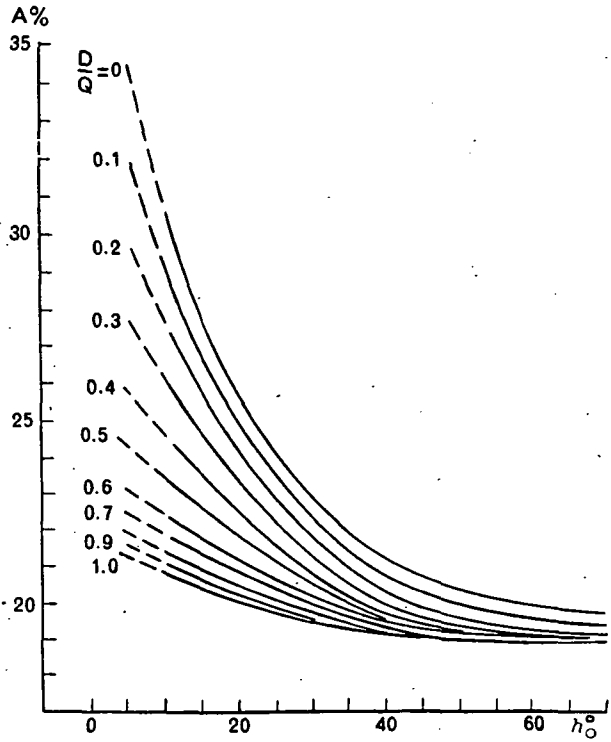

Fig. 4.2. The dependence of albedo of grass cover A on solar altitude $h_\odot$ for different values of the ratio of scattered radiation to the total radiation D/Q [13].

The top curve shows the dependence of albedo on solar altitude for direct radiation. The curve is determined by extrapolation of correlational dependence of A on D/Q. The nomogram shows that the variation in albedo of grass covers with solar altitude possesses a nonlinear character for values of D/Q. The value of albedo at a given solar altitude decreases as the portion of scattered radiation in the total flux increases. Many researchers [37, 53] have indicated an analogous dependence in the range of solar altitude from 10 to 40°. A different dependence has been observed for solar altitudes above 40°, viz. albedo increases with an increase in the portion of scattered radiation in the total flux [53]. However, in both these cases the variation in albedo does not exceed 1-1.5%, during a change from 0.1 to 1.0 in D/Q or S/Q. In case of dense cloudiness (lower curve) the daily course of albedo possesses a level character.

The condition of a snow surface is a determining factor in the daily course of its albedo.

Albedo has a minimum value around midday for dry pure snow in the presence of a clear sky, the amplitude of variation being 9% ($h_\odot$= 10-45°) [41]. However, an inverse dependence with maximum value of albedo at midday [20, 53] exists along with the indicated variation. Thus the following results were obtained for observations on March 21, 1961, for different masses of atmosphere *m*, viz.

m	2	3	4	5
A%	90.5	89.0	87.2	86.6

Variation in albedo has also been observed in the course of a day [53] for freshly fallen snow.

The albedo for "scintillating" snow and snow cover on ice dome, for air temperatures below 0°, exhibits a clearly marked daily course with a maximum value at noontime.

According to data in [6], the albedo of "scintillating" clear snow for $h_\odot = 30°$ equals 85%, whereas for $h_\odot$ = 5-10°, A = 90-93%.

The differences in the daily variations of the albedo of a snow surface can be explained by the dependence of the reflective properties of a surface on the angle of incident radiation and by the change in the spectral composition of the incident flux of direct solar radiation with respect to solar altitude.

When the change in the properties of a surface is caused by a change in the temperature of the air, the daily course of albedo for thawed snow can be expressed in gradually decreasing values of A in the course of a day, from morning hours to evening, or by some increase of albedo in the afternoon, when the temperature of the air falls again. For instance, albedo for a spring snow which is thawing and contaminated (March) decreases from 53 to 40% for a rise in temperature of air from −8.3 to +2.5°. During subsequent decrease in temperature to −0.5°, the albedo increases again to 52% ($h_\odot$ changed from 32 to 13°) [53].

3. ALBEDO OF BODIES OF WATER BASINS

3.1 Albedo of bodies of water for direct solar radiation

Since water in its pure form is a dielectric, the albedo of its surface for unpolarized light can be expressed by Fresnel's formula. The results of theoretical computations indicate a considerable dependence of the albedo on the angle of incident radiation (Table 4.12).

The albedo of water surface may be computed for direct solar radiation in the presence of perturbation by using Fresnel's formula ; in which case it is necessary to know the wave profile (Table 4.13).

Table 4.12 Dependence of albedo (%) of water surface on the incident angle of direct radiation [44]

Angle of incidence	0	1	2	3	4	5	6	7	8	9
0	2.1	2.1	2.1	2.1	2.1	2.1	2.1	2.1	2.1	2.1
10	2.1	2.1	2.1	2.1	2.1	2.1	2.1	2.1	2.1	2.1
20	2.1	2.1	2.1	2.1	2.1	2.2	2.2	2.2	2.2	2.2
30	2.2	2.3	2.3	2.3	2.3	2.4	2.4	2.4	2.4	2.5
40	2.5	2.5	2.6	2.7	2.8	2.9	3.0	3.1	3.2	3.4
50	3.5	3.6	3.8	4.0	4.2	4.4	4.7	5.0	5.4	5.8
60	6.2	6.6	7.0	7.5	8.2	8.8	9.6	10.4	11.4	12.4
70	13.6	14.8	16.2	17.8	19.6	21.5	23.8	26.0	28.8	31.4
80	35.0	38.6	42.8	47.6	52.9	58.6	65.0	72.0	80.6	89.6
90	100.0									

Table 4.13 Albedo (%) of water surface for direct radiation in perturbation [48]

Average curvature of wave	Altitude of sun, deg			
	10	30	50	90
10	18.4	6.9	2.9	2.0
7.3	23.0	6.7	2.7	2.0
6	25.7	6.5	2.6	2.0
Calm	34.9	6.0	2.4	2.0

The angles of incidence of solar radiation vary considerably with respect to wavefront in the presence of disturbance, which leads to a definite dependence of the albedo on the amount of disturbance. This dependence is most clearly evident in the case of a low solar altitude ($h_\odot = 10°$), when albedo decreases with an increase in the average curvature of the wave (angle of inclination of wavefront relative to the horizontal plane). For higher solar altitudes albedo rises with increasing disturbance, although this effect is negligible.

3.2 Albedo of water basins for total radiation in a clear sky

The albedo of water surface for total radiation in a clear sky is given in Table 4.14. The computation is carried out by considering the actual

intensity distribution of scattered radiation over the sky for different solar altitudes. The nature of the dependence of the albedo of a water surface on the extent of disturbance obtained in this case is the same as for direct solar radiation. However, the values of albedo for direct and total radiations differ considerably for lower altitudes of the sun (Tables 4.13 and 4.14).

Table 4.14 Albedo of water surface (%) for total radiation in clear sky [48]

Average curvature of wave, deg	Solar altitude, deg						
	10	15	20	30	40	50	70
10	14.0	12.0	10.0	7.0	5.0	3.5	2.8
7.3	17.0	12.0	10.0	7.0	5.0	3.4	2.7
6	19.0	13.0	10.0	6.8	4.8	3.4	2.7
Calm	24.0	17.0	12.0	6.7	4.5	3.4	2.7

The values of albedo for solar altitude in the range 5-90° have been given in Table 4.15 as a supplement to Table 4.14. The wind velocity v m/sec is taken as the parameter of disturbance. The computation was carried out for total radiation in an optical thickness of atmosphere equal to 0.3, horizontal visual range of 20 km and albedo=10%.

Table 4.15 Albedo of sea (%) for total radiation [32]

v m/sec	Altitude of sun, deg					
	5	10	30	50	70	90
2	16.0	18.4	9.4	5.9	5.3	5.3
5	13.5	14.9	8.7	5.8	5.2	5.1
10	13.1	14.3	8.7	6.5	5.4	5.2
15	11.5	12.9	8.1	6.6	5.6	5.1

The computations carried out show that the albedo decreases for altitudes of sun below 10°. It is possible to explain this decrease in albedo on account of the predominant contribution of scattered radiation to the total flux (albedo of water surface is considerably lower for scattered radiation than for direct radiation [51]).

3.3 Experimental data on albedo of water surface

The experimental data for determination of the albedo of a water surface for total radiation has been qualitatively confirmed by theoretical computations. Thus, for instance, the dependence of the albedo of a sea surface for total radiation on solar altitude in a cloudless sky (Fig. 4.3) has been investigated in [14] for the case of no disturbance (curve 2) and for disturbance of 1-2 points (curve 1). Curve 3, obtained for a smooth surface from Fresnel's formula, has been introduced so as to compare experimental data with the computations in Fig. 4.3. From the measurements it follows that there is a close correspondence between experimental and theoretical data in cloudless weather for the range of solar altitude between 40 and 70°. The computed values of albedo are considerably below the observed values for $h_\odot < 40°$. The deviations in the actual properties of a water surface from the ideal properties assumed for com-

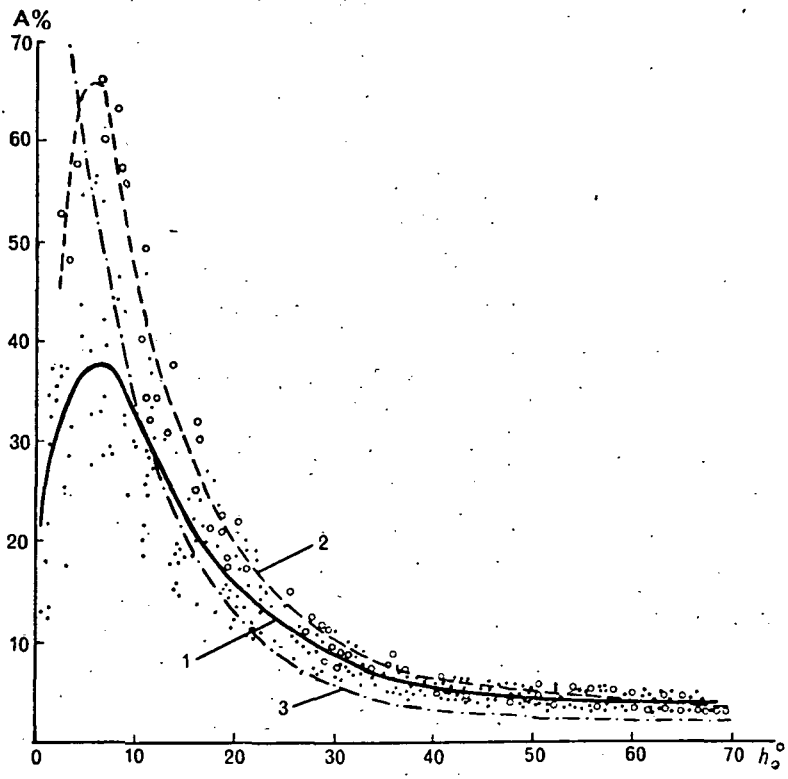

Fig. 4.3. Dependence of albedo of sea on solar altitude [14].

1—In the presence of disturbance of 1-2 pts; 2—absence of disturbance; 3—computed curve.

putations using Fresnel's formula explain the above disparity. A sharp decrease in albedo has been observed for very small solar altitudes (beginning with 5°), a result which has also been confirmed by theoretical computations [31].

An analogous dependence of albedo on solar altitude has been observed for other bodies of water in the altitude range between 10 and 60° (Table 4.16).

Table 4.16. Dependence of albedo for water surface (%) on solar altitude in a clear sky [11, 43, 46]

Regions	Solar altitude, deg						
	10	15	20	30	40	50	60
Black Sea							
shallow-water region	41		16	12	9	7	6
deep-water region	36		12	10	6	5	4
Norwegian Sea		18.0	11.0	7.0	4.0	—	—
Kara-Kum water reservoir		24.4	19.8	14.4	11.7	10.5	10.0

There is a characteristic low value of albedo in the deep-water region of the Black Sea, which occurs on account of the high transparency of water and in the complete absence of any influence from the bottom.

The measurements in the Norwegian Sea were carried out during moderate disturbance (height of cave 0.27-0.75 m). Mean monthly values of albedo are given in the case of the Kara-Kum water reservoirs. The higher values of albedo in the case of reservoirs can be caused by the high turbidity of water in comparison with the Norwegian Sea.

The presence of disturbance in the water surface causes a decrease in the value of albedo, especially at low solar altitudes (Fig. 4.3) [14]. As already indicated, the variation in the angle of incidence of the radiation relative to the wave surface could be considered as the chief reason for this effect. If the disturbance in the water surface causes a decrease in transparency (which is characteristic for water reservoirs), then the albedo of this surface rises (Table 4.17). Data for the following range of solar altitude, viz. 30-60°, are given in this Table.

The dependence of the albedo for water reservoirs on the transparency of the water is given in Table 4.18.

Table 4.17 Dependence of albedo on roughness for Volgograd water reservoir [17]

Roughness, points	0	1	2	3	4
Albedo, %	5	7	7	8	9

Table 4.18 Dependence of albedo on transparency of water, $h_\odot = 40\text{-}56°$ [42]

Fishing reservoirs		All reservoirs examined	
Transparency, m	Albedo, %	Transparency, m	Albedo, %
20-40	5.4	20-40	6.0
41-80	4.6	41-80	5.3
81-100	4.1	81-100	4.7
101-120	3.9	101-120	4.2
121-140	3.8	121-140	4.1
141-160	3.8	141-160	4.0
161-210	4.3	161-180	4.5
		181-230	4.1

3.4 Dependence of sea albedo for total radiation on cloudiness

The albedo of total radiation has been computed for varying cloudiness from data on actinometric observations over total radiation in a clear sky and over dense clouds considering observed values of the albedo of the sea (Table 4.19).

Table. 4.19 Albedo (%) of water surface for total radiation in varying degrees of cloudiness of the lower stratum (roughness of 1-3 points, transparency of water 8-12 m taken from Sekki's plate) [51]

$h^\circ_\odot$	Cloudiness in tenths						
	0	2	4	6	8	9	10
5	27.4	26.3	24.8	22.3	17.8	13.8	7.0
10	26.0	25.2	23.8	21.6	17.5	13.8	7.0
15	19.4	18.7	17.6	16.0	13.3	10.9	7.0
20	13.5	13.1	12.6	11.7	10.2	9.0	7.0
30	8.1	8.0	7.9	7.8	7.6	7.3	7.0
40	5.8	5.9	6.0	6.2	6.4	6.6	7.0
50	4.9	5.0	5.2	5.5	5.9	6.4	7.0
60	4.0	4.2	4.4	4.7	5.4	6.0	7.0
70	3.7	3.9	4.1	4.5	5.2	5.8	7.0

In the range of solar altitudes 5-20° the dependence of albedo on the degree of cloudiness bears a non-linear relation. Beginning with a cloudiness of 6 points the variation in albedo is most noticeable. The dependence of albedo on cloudiness is almost absent at a solar altitude of 30°.

Similarly the experimental data indicate a dependence of the albedo of water on cloudiness [14, 17, 59]. For instance, the dependence of the albedo of a water surface (mean values) on solar altitude for the Kara Sea is given in Table 4.20. In this case the values of albedo in a clear and hazy sky coincide in the range of altitude of the sun between 25 and 35°. The albedo under a clear sky is significantly higher than the albedo under a cloudy sky for a lower altitude of the sun (5-10°).

Table 4.20 Albedo (%) of water surface of Kara Sea on clear or cloudy days (June-October) [59]

	Altitude of sun, deg						
	5	10	15	20	25	30	35
Clear	22	15	13	12	10	10	10
Cloudy (intermediate conditions)	17	13	12	10	9	10	10

The varying transparency of water is one of the reasons for the different values of the albedo of water reservoirs under identical conditions of observation. The values of the albedo given in Table 4.18 for many water reservoirs (rivers, lakes) indicate an increase in albedo with decreasing transparency of water.

3.5 Average values of albedo of water surfaces

The annual variation in average monthly values of the albedo of water surfaces at different latitudes under a cloudless sky is determined by the solar altitude and the condition of the surface (Table 4.21). The table shows the results of computations in which average values of the albedo for a day computed for the midday altitude of the sun at different altitudes have been employed.

N. E. Ter-Markarayan computed the values of albedo in different degrees of cloudiness through interpolation from values of albedo of a water surface, these values being characteristic under the condition of clear as well as under an overcast sky. Computations were carried out for

Table 4.21 Annual variation of mean monthly values of albedo (%) for a water surface at different latitudes under clear sky [45]

Latitude, deg	Jan	Feb	Mar	Apr	May	Jun	Jul	Aug	Sep	Oct	Nov	Dec
80	—	—	50	22	12	10	11	17	34	—	—	—
70	—	54	25	12	8	7	7	10	18	38	—	—
60	47	26	13	7	6	5	5	6	10	20	38	55
50	23	14	8	5	5	4	4	5	7	11	20	27
40	12	8	6	5	4	4	4	4	5	7	11	14
30	8	6	5	4	4	4	4	4	4	5	7	8
20	6	5	4	4	4	4	4	4	4	4	5	6
10	5	4	4	4	4	4	4	4	4	4	4	5
0	4	4	4	4	4	4	4	4	4	4	4	4

cloudiness in the lower stratum at different altitudes (Table 4.22). There is a linear dependence of albedo on the degree of cloudiness. The dependence of values of albedo on cloudiness is shown to be considerably weaker in the summer months at lower and intermediate latitudes than in the winter months at higher latitudes.

Table 4.22 Mean values of albedo (%) of a water surface for total radiation under varying degrees of cloudiness of lower stratum (roughness 1-3 pts, transparency 8-12 m) [49]

Cloudiness in tenths	Jan	Feb	Mar	Apr	May	Jun	Jul	Aug	Sep	Oct	Nov	Dec
						$\varphi=30°$						
0	9.3	7.7	6.7	5.7	5.8	5.6	5.6	5.6	6.3	5.8	8.2	9.7
2	9.2	7.6	6.7	5.8	5.8	5.7	5.7	5.6	6.4	5.8	8.1	9.5
4	8.9	7.5	6.7	5.9	5.9	5.8	5.8	5.7	6.4	5.9	8.0	9.3
6	8.6	7.5	6.8	6.0	6.1	5.9	6.0	5.9	6.5	6.0	7.8	8.9
8	8.0	7.2	6.8	6.4	6.3	6.2	6.3	6.2	6.6	6.4	7.6	8.3
9	7.7	7.0	6.8	6.6	6.6	6.5	6.5	6.5	6.8	6.6	7.4	7.8
10	7.0	7.0	7.0	7.0	7.0	7.0	7.0	7.0	7.0	7.0	7.0	7.0
						$\varphi=40°$						
0	12.6	9.1	7.5	6.3	6.1	5.7	5.7	6.4	8.1	10.7	11.4	13.3
2	12.2	9.0	7.5	6.3	6.1	5.7	5.8	6.4	8.0	10.6	11.1	13.0
4	11.7	8.8	7.4	6.4	6.2	5.8	5.9	6.4	8.0	10.2	10.8	12.4
6	11.0	8.5	7.4	6.5	6.4	6.0	6.0	6.5	7.9	9.7	10.1	11.6

8	9.7	8.0	7.4	6.6	6.5	6.2	6.4	6.7	7.5	8.9	9.1	10.1
9	8.6	7.6	7.2	6.8	6.7	6.6	6.6	6.8	7.3	8.1	8.3	8.9
10	7.0	7.0	7.0	7.0	7.0	7.0	7.0	7.0	7.0	7.0	7.0	7.0
						$\varphi=50°$						
0	18.0	14.2	9.6	7.7	7.2	6.7	6.6	6.2	8.1	11.0	16.0	22.1
2	17.2	13.8	9.5	7.7	7.2	6.7	6.7	6.9	8.0	10.7	15.3	21.4
4	16.3	13.2	9.2	7.6	7.1	6.7	6.7	6.9	7.9	10.5	14.7	20.0
6	14.9	12.2	8.9	7.5	7.1	6.8	6.8	6.9	7.8	9.9	13.6	18.3
8	12.4	10.5	8.3	7.3	7.1	6.8	6.8	7.0	7.5	9.0	11.4	15.0
9	10.3	9.1	7.8	7.2	7.0	7.0	6.9	7.0	7.3	8.2	9.7	12.5
10	7.0	7.0	7.0	7.0	7.0	7.0	7.0	7.0	7.0	7.0	7.0	7.0
						$\varphi=60°$						
0	27.0	20.3	13.0	8.9	7.4	7.4	7.7	8.0	10.2	16.8	25.6	27.4
2	25.8	19.4	12.8	8.7	7.3	7.3	7.6	8.0	10.0	16.2	24.8	26.3
4	24.1	18.3	12.1	8.6	7.3	7.3	7.6	7.9	9.7	15.4	23.1	24.6
6	21.5	16.7	11.3	8.3	7.2	7.2	7.5	7.8	9.4	14.2	20.8	22.1
8	17.0	13.8	9.9	7.9	7.2	7.2	7.3	7.6	8.6	11.9	16.6	17.6
9	13.1	11.2	8.8	7.5	7.2	7.1	7.2	7.4	7.9	10.0	12.8	13.7
10	7.0	7.0	7.0	7.0	7.0	7.0	7.0	7.0	7.0	7.0	7.0	7.0
						$\varphi=70°$						
0	—	27.1	20.3	12.5	10.0	8.9	9.2	10.5	15.8	25.6	24.3	—
2	—	25.8	19.6	11.7	9.8	8.8	9.1	10.3	15.3	24.6	23.4	—
4	—	23.8	18.3	11.6	9.5	8.6	8.9	10.0	14.5	23.1	21.5	—
6	—	20.3	16.7	10.9	9.1	8.3	8.6	9.5	13.8	20.8	18.8	—
8	—	16.1	13.6	9.7	8.5	7.9	8.1	8.8	11.6	16.6	14.6	—
9	—	12.4	11.1	8.6	7.9	7.6	7.7	8.0	9.6	13.1	11.3	—
10	—	7.0	7.0	7.0	7.0	7.0	7.0	7.0	7.0	7.0	7.0	—

4. ALBEDO OF LARGE AREAS

4.1 Measurements of albedo from great height

Direct measurements of the albedo of large territories are of practical value. Such measurements may be accomplished through pyranometric observations from an airplane or a balloon. A similar method is described in [24, 57] in detail. Airplane measurements of albedo, carried out over territories of several continents, gave practically identical values [64, 79] of the albedo for similar surfaces (under identical conditions of observation). The most prolonged measurements on albedo from an airplane were conducted by V. L. Gaevskii (in the course of five years). Observations were made from a height of almost 500 m. A catalog of values of albedo for the Soviet Union Territory, which is partially reproduced in Table 4.23, was composed from the data obtained where the limits in the values of albedo for many types of surfaces have been derived (altitude of sun is indicated).

Table 4.23 Albedo of natural surfaces, measured from an airplane over the Soviet Union Territory [2]

Surface	Month	$h_\odot°$	A %
Tundras	Aug	24-36	11-23
Swamps	Aug	28-38	10-18
Forest (without leaves)	Mar	34	11
Coniferous forest (against background of freshly fallen snow)	Mar	19-23	35-40
Forest (leafy, coniferous)	Jun	39-55	14-17
	Aug	30-41	12-16
	Sep	26-38	19-20
Leafy forest, covered by freshly fallen snow	Nov		
Steppe	Dec	12-25	48-55
	Jul		
	Aug	40-52	17-29
Semidesert and desert			
Yellowish-gray sand	Aug	56	25
Light yellow sand	Aug	50	37
Gray sand	Sep	36-45	20-28
Soils			
Chernozem (moist)	May	41-45	5-6
Chernozem (dry)	Jun	41-48	10-15
Podzolic light gray soil	Jul	40	25-28
Podzolic gray soil	Jul	41	18
Freshly fallen dry snow	Feb	15	81-88
Moist, porous, light gray snow	Mar	18	43

The albedo of icy seas, depending on the thickness of the ice, is given in Table 4.24 (average values of albedo for summer periods are indicated). A significant rise in the albedo for a marine surface was observed with the appearance of ice (for open sea as well as for water in proximity to shoreline).

Table 4.24 Albedo (%) of surface of icy seas for different thicknesses of pack ice (summer months) [59]

Place of observation	Iciness in pts										
	0	1	2	3	4	5	6	7	8	9	10
Coastal water	6	7	11	15	20	24	28	32	36	40	44
Open sea	8	12	18	22	28	33	40	46	53	63	73

Data obtained from artificial satellites, just like those obtained from an airplane, indicate a considerable variation of albedo according to territory (Table 4.25).

Table 4.25 Albedo of different surfaces, measurements obtained from artificial satellite [66]

Surface	Albedo, %
Sands (White Sands, New Mexico, USA)	60
Sands (valleys, plains, slopes)	27
Sands and bushes	17
Coniferous woods	12
Lakes (Great Salt Lake, USA)	9
Mexican Gulf	9
Pacific Ocean	7
Snow 3-7 days old, covering forest laden slopes of mountains	59

It is necessary to take into consideration the inhomogeneity of the underlying surface during measurements of albedo from a height. Albedo changes most sharply at the boundary of two media possessing different values, for example at the boundary of land and water. It follows from observations carried out by a helicopter over the Black Sea that for a flight at 30 m the apparatus will receive reflected radiation of dry land or water beginning at a distance of 600-700 m in any direction from the dividing line (Table 4.26).

Table 4.26 Albedo of sea (%) at different distances from the coast [16]

Flight No.	Date	Time, hrs min	Land	Reduced value	Distance from coast, km				Condition of surface
					0.5	1	3	8	
1	Sept 15	14 45	24.9	12.2	—	5.5	5.4	5.4	Ripple; weak fleecy clouds
2	Sept 16	16 15	21.8	11.8	—	5.6	5.4	5.6	—do—
3	Sept 16	10 30	21.2	11.8	4.4	4.4	4.5	4.5	Calm sea

4.2 Variation in albedo with altitude

Variation in albedo with the altitude is determined by the optical properties of the atmospheric layer situated at different distances from the ground. The albedo of the underlying surface is an important factor in the variation of albedo for layers with identical optical characteristics. Theoretical [31, 60] and experimental data [30; 38, 87] show that the albedo of the earth's surface-atmosphere system increases with altitude under a clear sky for low values of albedo of the earth's surface, whereas it decreases for higher values of albedo (above 30%). For instance, the values of a vertical gradient of albedo ($\xi = A/100$ m), obtained under a clear sky over surfaces showing different values of albedo A_0, are shown in Table 4.27.

Table 4.27 Vertical gradient of albedo under a clear sky [9, 38]

Surface	$A_\odot$%	$h^\circ_\odot$	Thickness of atmospheric layer, m			
			0-500	500-1000	1000-2000	
Snow (Jan, Feb)	83	11-14	0.4	0.3	0.1	<0 [38]
Snow (Apr)	34	41.6	0.58	0.11	0.10	<0 [38]
Water (Jun)	3-4	>45	0.04-0.12	0.02-0.08	0.13-0.20	>0 [38]
Steppe (Jul)	26	>50	0.4	0.06	0.06	>0 [9]

The determination of albedo up to altitudes of the order of 30 km was accomplished with the help of balloon probings [23]. The profiles of vertical distribution of albedo for different meteorological conditions and seasons are shown in Fig. 4.4.

The variation in albedo up to an altitude of 6-8 km recorded with balloon probings is determined by the degree of homogeneity of albedo in the underlying surfaces ; thus, for instance, in the case of profiles 2, 3 and 5 (Fig. 4.4) the nature of the underlying surface showed sharp changes in view of the movement of the balloon along an inclined trajectory.

In the case of transparent atmospheric masses albedo remains practically stationary with altitude for clear weather so that $A = 21\%$ (profile 1, underlying surface—harvested and tilled fields). Turbidity of atmospheric masses may lead either to some increase in albedo, viz. from 13% at an altitude of 6 km to 15% at a level of 27 km (the case of low values for albedo of underlying surface, profile 2), or to some decrease in albedo with altitude, viz. from 73% at 13 km to 63% at 22 km (profile 3, underlying surface being snow).

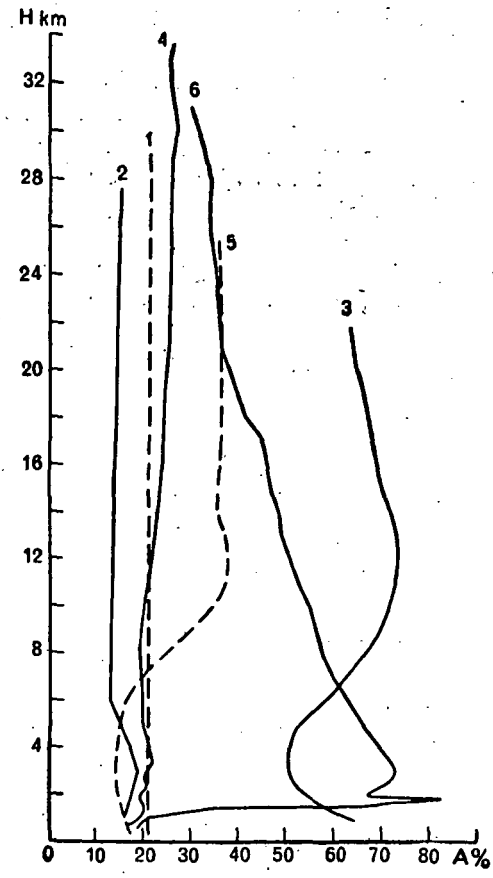

Fig 4.4 Vertical profiles of albedo [23].
Under clear sky : 1) $h_{\odot}=17°35'$, November 1962; 2) $h_{\odot}=55°30'$-$58°30'$, May 1962; 3) $h_{\odot}=19°$, November 1961; 4) $h_{\odot}=24°$-$27°$, October 1965. Under cloudy sky : 5) $h_{\odot}=58°48'$, July 1862; 6) $h_{\odot}=26°21'$-$22°36'$, October 1964 [1].

The significantly turbid stratosphere (profile 4) leads to a change in albedo from 19% at 9 km to 25% at 32 km. The presence of clouds in the intermediate and upper strata (profile 5) increases albedo (the value 38% corresponds to a fine layer of cirrus cloud, located at an altitude of 10-11 km).

Profile 6 represents an especially strong influence of tropospheric mist. A turbid atmospheric mass is situated directly over a cloudy layer, and a decrease in albedo from 73 to 45% at 17 km results from the action of mist on the reflected shortwave radiation. A further decrease of albedo is caused by a change in the number of clouds under a balloon.

4.3 Seasonal variation in albedo of large areas

The seasonal variation in the albedo of large territories is determined primarily by a change in the condition of the underlying surface in the course of a year. Sharp changes in albedo are connected with the appearance and vanishing of snow cover. For instance, Fig. 4.5 represents the seasonal variation of albedo for a water surface (Ladaga Lake) and for bushes. Large changes in albedo, from 50 to 85%, may be observed in winter on account of snowfall and thawing.

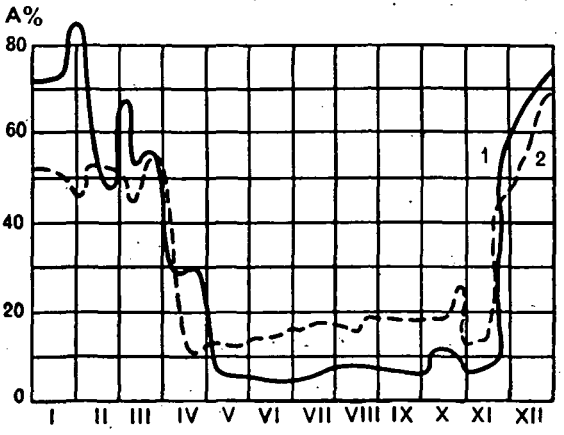

Fig. 4.5. Annual course of the albedo of (1) Ladaga Lake and (2) bushes [38].

V. V. Mukhenberg composed a Table of the annual course of albedo of the main zones of Soviet Union Territory for a complete climatological description of large territories (Table 4.28).

5. GEOGRAPHIC DISTRIBUTION OF ALBEDO

It is necessary to determine the mean values of albedo for large sections of an underlying surface over a long interval of time (month, year) in order to describe the geographic distribution of albedo. The material accumulated from surface as well as airplane measurements enables the construction of the distribution charts of albedo over many territories; thus, for example, the seasonal charts of albedo for the Territory of the Soviet Union [34], North America [79], Labrador region of Newfoundland [67], as well as albedo charts for the earth's hemispheres [33, 82] were obtained. Mukhenberg suggested a computational method for the determination of average albedo of different zones of the earth [33].

Table 4.28 Annual variation of albedo (%) [33]

Type of underlying surface	Jan	Feb	Mar	Apr	May	Jun	Jul	Aug	Sep	Oct	Nov	Dec
Tundras	80	80	80	80	80	32	18	18	45	79	80	80
Forest region	46	46	46	45	14	14	14	14	14	37	46	46
Steppe	70	70	70	31	18	18	18	18	18	20	51	70
Desert	44	44	24	27	28	28	28	28	28	28	28	34
Western regions of European Territory of USSR with unstable snow cover	66	66	46	16	18	18	18	18	18	18	35	50

Albedo charts of land surface of the earth for January and July are shown in Figs. 4.6 and 4.7. In these charts the mountainous regions are not elucidated on account of the absence of original data (regions of high mountains are shaded).

A large change in albedo over the earth, viz. from 18 to 80%, is characteristic for the month of January (Fig. 4.6) [34]. The highest value of albedo, viz. 80%, is observed in high latitudes of the Northern Hemisphere, where the snowy surface remains uncontaminated because of the low quantity of dust in the atmosphere and where there are practically no forests. Albedo in the southern regions, with increasing coverage of the territory by forest, decreases, reaching a value of 45% in the region of dense forest. Approaching the area of the Steppes in the continental region albedo again rises and in the Steppes achieves a value of 70%. In regions of sea climate, where a stable snow cover is not formed, albedo attains a value of 44 and 25% for arid and forest regions respectively ; a further decrease in the value of albedo with latitude is caused by the varying state of snow cover. In the southern latitudes of the Northern Hemisphere and in the continents of the Southern Hemisphere (for which January is a summer month), with no snow cover at all (apart from Antarctica), albedo attains a value of 18 or 24% respectively, depending on whether January is a wet or dry month. In desert regions albedo equals 28%.

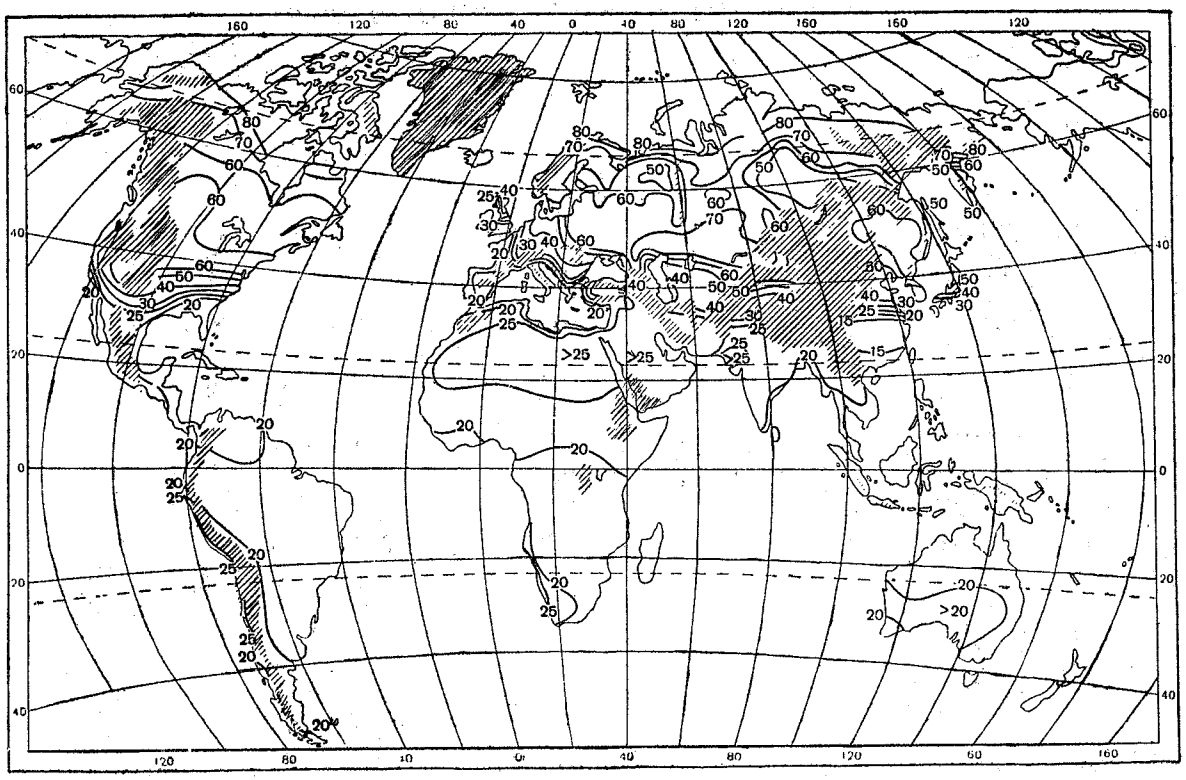

Fig. 4.6. Albedo (%) of land surface of the earth. January. [34].

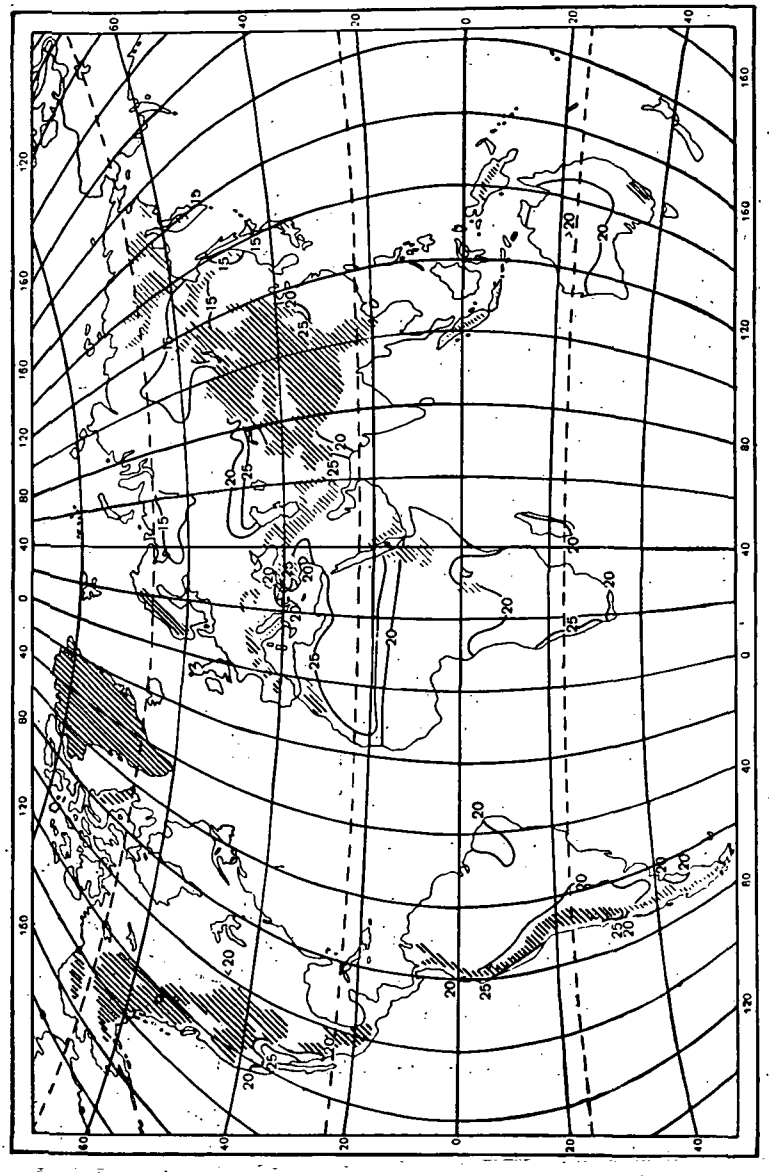

Fig. 4.7. Albedo (%) of land surface of the earth. July. [34].

In June (Fig. 4.7) a snow cover was absent in all the territories surveyed. Variation in albedo with the territory is insignificant. In forest regions covered with the coniferous variety of trees, albedo has a value of 14-15%. In the Steppes and forest covered with leaves it is 18-20%, in dry Steppes and semidesert areas 22-24%, and in deserts it is 28%.

6. ALBEDO OF CLOUDS

Investigations carried out from airplanes, balloons and artificial satellites, for the determination of the albedo of clouds show its dependence on the thickness and form of clouds and solar altitude, whereas for clouds of low density, it depends on the albedo of the underlying surface. For instance, the mean values of albedo of clouds may be found in the experimental data [24] where a value of $A=68\%$ was obtained for dense cloudiness of Sc, St, Ns types. The value of albedo becomes 70-75% [52] for clouds of thickness 1.5 km with an underlying surface of any type.

Observations made by N. I. Chel'tsov in the Moscow and Arkhan-

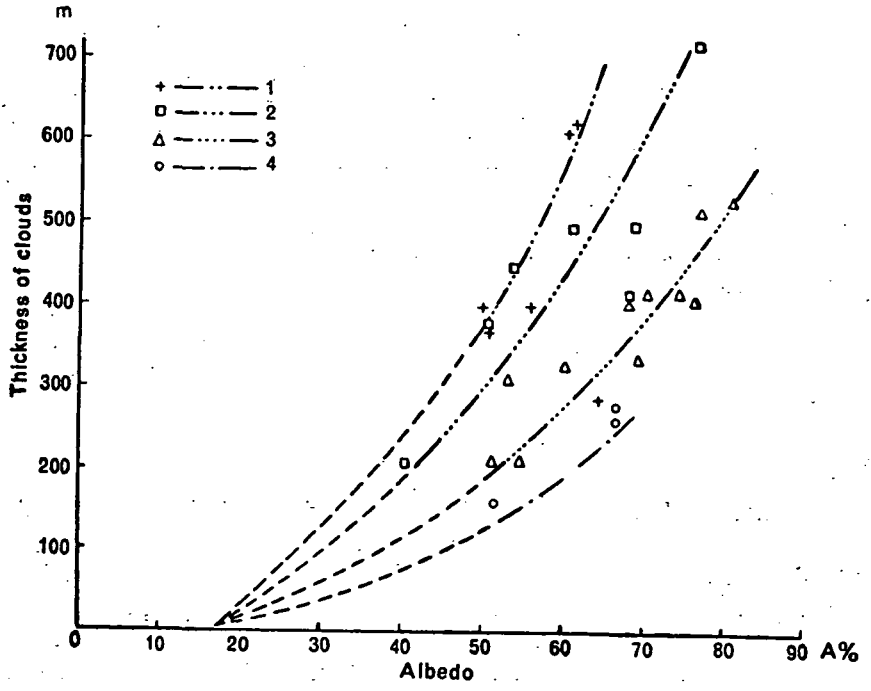

Fig. 4.8. Dependence of albedo of clouds on thickness, from data obtained during flights. Arkhangelsk 1949-1950 [57].

1) Sc, 10 tenths, transilluminating; 2) Sc, Cu, 10 tenths; 3) Sc, 10 tenths; 4) Ac, 10 tenths.

gelsk regions showed that the albedo of clouds substantially depends on their vertical thickness. The results of these investigations are shown in Fig. 4.8. The graphs indicate an uneven growth of albedo with decreasing thickness of clouds. Albedo increases most rapidly in relatively thin layers of cloud (to 200-300 m) and significantly slowly for a further increase in thickness. The nature of the dependence of albedo on the thickness of clouds is identical for all types of clouds examined, with a change in the value of albedo alone. Analogous values of albedo were obtained in [4] for layers of clouds of thickness 200-300 m.

For clouds of lesser thickness, as well as for transilluminating clouds, the albedo of the underlying surface plays a significant role (Table 4.29). Results of measurements given in this Table refer to clouds of the lower stratum ; moreover the clouds are provisionally divided into dense (underlying surface is not illuminated), intermediate (dense clouds with transparent gaps), and translucent. The widest variations in albedo, connected with a change in thickness of clouds, refer to observations over surfaces with small values of albedo (water, tundras).

Table 4.29 Albedo (%) of clouds of lower stratum with different density for various types of underlying surface [52]

Underlying surface	Breaking of snow, tenths	Clouds			Clear sky
		dense	inter-mediate	translucent	
Snow, 9-10 tenths	0	86	83	79	79
	1	82	76	70	70
	1-2	73	67	58	57
	2-3	71	61	51	45
Tundra	—	61	46	30	17
Water	—	58	45	25	8

N. I. Goisa [12] studied the dependence of the albedo of stratiformis and stratocumulus clouds on the solar altitude for different water reserves and thicknesses of clouds. The values of albedo indicated in Table 4.30 refer only to cloudy cover, since the influence of the underlying surface has been excluded, and the values of relative transmission of radiation in the clouds have been taken into consideration. Albedo of St and Sc rises with the increase in thickness of the cloud as well as with the increase of the water-content. The dependence of the albedo of clouds on solar altitude is most clearly manifested in the low values of thickness (120-210 m) and water content (0-20 g/m^2) of clouds.

Table 4.30 Dependence of albedo (%) of stratiformis and stratocumulus clouds on solar altitude for different water content and thickness of clouds [12]

$h^\circ_\odot$	Water content of cloud, g/m²				Thickness of cloud, m				
	0-20	20-40	60-80	130-170	120-210	190-340	340-440	500-660	600-760
10	64	74	81	87	62	72	76	82	85
20	56	68	75	81.5	60	70	75	80	83
30	51	64	71	78	56	66	75	78	82
40	46	64	69.5	77	52	60	73	74	81
50	43	64	68	—	47	—	70	70	—

The albedo of clouds, computed from data collected by artificial satellite, changes within a wide range, from 29% to 86% (Table 4.31).

Table 4.31 Mean albedo for different types of cloudiness, measured from brightness of television pictures of cloudy covers [66]

Cloudiness	Albedo, %
Cumulus-rainy clouds	86
Cumulus fair weather clouds over dry land, more than 8 tenths	29
Cumulus and stratocumulus clouds over land, more than 8 tenths	69
Stratocumulus clouds over land, more than 8 tenths	68
Stratiformis, dense clouds at an altitude of 500 m over ocean	64
Stratocumulus clouds, continuous mass over the ocean	60
Stratiformis transilluminating clouds over the ocean	42
Cirrus-stratiformis dense clouds	74
Cirrus clouds over dry land	36
Cirrus-stratiformis clouds over dry land	32

7. ALBEDO OF THE SYSTEM: EARTH'S SURFACE-ATMOSPHERE

7.1 Planetary albedo of the earth

The albedo of the earth's surface-atmosphere system can be determined as the ratio of radiative flux reaching the upper boundary of the atmosphere in the form of reflected radiation from the earth's surface and radiation scattered in the atmosphere, to the incident radiative flux entering this boundary.

Theoretical computations of planetary albedo for the Northern Hemisphere (Table 4.32) enable us to determine the contribution to the albedo of solar radiation which is scattered by the cloudless part of the atmosphere and reflected from the ground. It follows from this Table that in the case of a clear sky the value of albedo changes mainly because of the variable reflective power of the earth's surface (depending on the season), whereas the contribution due to atmospheric dispersion is almost stationary. A small variation in the contribution of back scattering to planetary albedo may be explained by the insignificant dependence of the optical thickness of the atmosphere on the season and the latitude. The mean planetary albedo of the Northern Hemisphere in a cloudless atmosphere reaches a value of 14.7% whereas considering cloudiness it is 35%. A small seasonal variation in albedo may be observed in this case ; 35.6% for winter and 36.3% for summer [80]. According to data from many theoretical computations the planetary albedo of the earth, considering cloudiness, becomes 35% [7, 75, 77]. Experimental measurements of albedo, besides theoretical computations, are of great interest.

Table 4.32. Seasonal distribution of the components of average planetary albedo (%) for clear sky (Northern Hemisphere [80])

Component of albedo	Winter	Spring	Summer	Autumn
Reflection from earth's surface	9.0	7.4	5.0	6.0
Scattering in atmosphere	8.3	7.6	8.5	7.4
Complete planetary albedo	17.3	15.0	13.5	13.2

An indirect method of measuring albedo based on photometric measurements of ashen light on the moon in also known. Recent investigations in this direction have provided the following data [63] ; for $\lambda = 0.554\,\mu$; $A_\lambda = 40\%$ (average for 10 years), mean annual value of albedo changes within the following limiting values, viz. $37 < A < 44\%$; for other sections of the spectrum

$\lambda\,\mu$	0.467	0.544	0.606
A_λ %	48	39	31.5

Direct measurements of reflected radiation from artificial satellites with the help of radiometers permit the computaion of planetary albedo (Table 4.33).

The values of albedo for the entire earth's surface (including polar region) for the period of May and June change imperceptibly from 29.5 to 30.5%.

Table 4.33 Planetary albedo, according to data from artificial satellite [62, 83, 85]

Satellite	Spectral range, μ	Range of latitudes	Month	Albedo, %	Month	Albedo, %
"Tairos-IV"	0.2-5.0	60° N	Feb-Jun	31		
[85]		60°				
"Tairos-VII"	0.55-0.75	63.5°	Jun-Aug	28.4	Dec-Feb	32.9
[62]		63.5°	Sep-Nov	35.8	Mar-May	31.3
"Nimbus-II"	0.2-4.0	Polar	May, 16-31	30.4	Jul, 1-15	30.2
[83]		orbit	Jun, 1-15	30.5	Jul, 16-28	29.5

7.2 Geographic distribution of albedo for the earth-atmosphere system

The data on geographic distribution of albedo for the earth-atmosphere system are of practical importance.

According to computations [7], the year-to-year values of albedo for intermediate latitudes in the illuminated part of the earth change within the limits of 32-43% (Table 4.34).

Table 4.34 Year-to-year values of albedo for the earth-atmosphere system in the intermediate latitudes % [7]

Latitude	*A* %	Latitude	*A* %
70-60°N	43	0-10°S	33
60-50	40	10-20	33
50-40	37	20-30	33
40-30	35	30-40	35
30-20	33	40-50	38
20-10	32	Entire	
10-0°	33	earth	35

Direct measurements carried out from artificial satellites permit an evaluation of albedo under real conditions. The latitudinal variation of albedo (Fig. 4.9) was computed from the data of satellite "Tairos-VII". The dotted curve was plotted by considering the theoretical values obtained in [80]. The geographic distribution of surface albedo for the first half of June, 1966, is given in Fig. 4.10 [83].

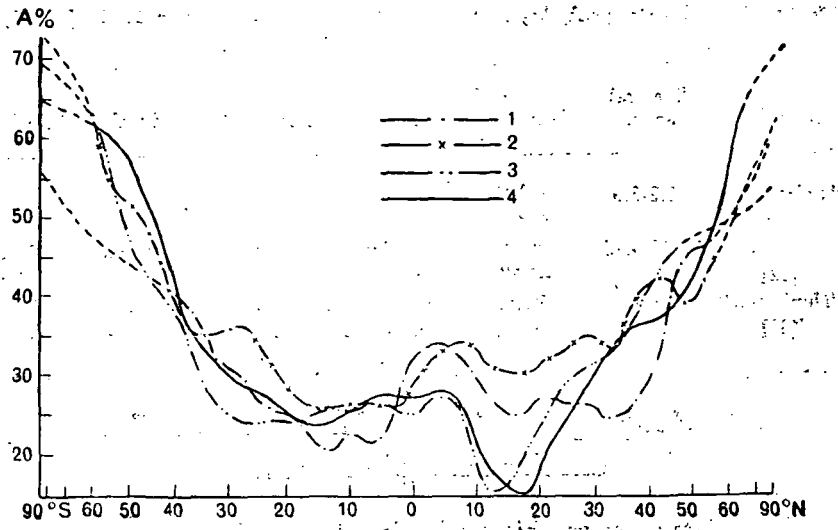

Fig. 4.9. Latitudinal distribution of planetary albedo [63].
1—Jun-Jul-Aug 1963; 2-Sept-Oct-Nov 1963; 3-Dec-Jan-Feb 1964; 4—Mar-Apr-May 1964.

While analyzing the data from the satellite one notices several peculiarities of the albedo distribution over the earth's surface.

On an average albedo increases as we move from the lower to the higher latitudes. A minimum for albedo may be observed in the subtropical and equatorial zones (regions of minimum cloudiness). The greatest variation in albedo (from 15 to 33%) may be observed in the Northern Hemisphere for the latitudes 10-20° (Fig 4.9).

There exist characteristic values of albedo, 10-20%, for oceans with a minimum of cloudy cover. The influence of cloudiness (Fig. 4.10) explains the higher values of albedo in latitudes north of 50° N and south of 40° S. A characteristic high value of albedo is found for the polar region of the Northern Hemisphere starting from 70° N, which is caused by the presence of snow and ice surfaces as well as by a rapid decrease in solar altitude as we move toward the North.

The longitudinal characteristics of albedo (see Fig. 4.10 and [88]) for the latitudes $\pm$ 45°, $\pm$ 20° and 0° show a more noticeable variation in albedo in the Northern as compared to the Sourthern Hemisphere. As shown in Table 4.35, there is little change in albedo for the entire Northern Hemisphere in the period May-June, the mean value being 32%. A higher mean value of albedo (36.3%) obtained through theoretical computations for the summer period [80], can obviously be attributed to the fact that the real distribution of cloudiness does not correspond to the distribution of cloudiness considered for theoretical computations.

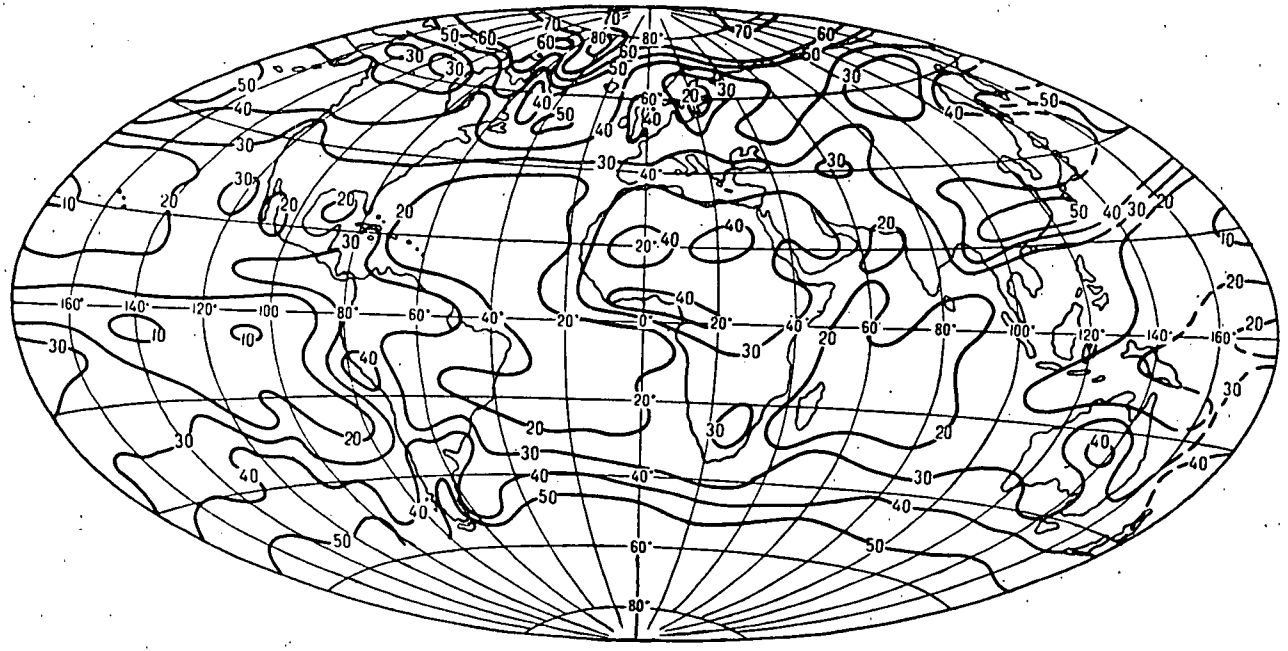

Fig. 4.10. Geographic distribution of albedo for the earth-atmosphere system over the surface (data from satellite "Nimbus II", first half of June 1966) [83].

Table 4.35 Mean zonal value of albedo (%) for the Northern Hemisphere [84]

Latitude	May 16-31	June 1-15	June 16-30	July 1-16	July 16-28
65°N	47.8	39.9	39.3	41.1	40.7
70	60.3	52.3	47.2	45.7	44.9
75	67.7	64.6	58.9	55.8	48.8
80	68.9	67.9	61.6	57.7	56.1
85	66.3	65.7	61.9	56.6	55.2
Northern Hemisphere	32.8	32.8	32.2	31.5	30.9

PART II. SPECTRAL ALBEDO

8. VARIATION OF SPECTRAL ALBEDO UNDER NATURAL CONDITIONS

Spectral albedo A_λ is the ratio of the amount of radiation flux in a specific interval of wavelength reflected by a given surface in all directions in the hemisphere, to the flux of radiation energy incident on this surface.

The evaluation of albedo for many surfaces in the visible region of the spectrum (0.36-0.76 μ) was carried out with the help of a selenium photoelement (Table 4.36). The values of integrated albedo are also given in this Table.

Table 4.36 Integral albedo A and albedo in the visible region of the spectrum $A_{0.36\text{-}0.76\mu}$ ($h_\odot$=30-60°, clear) [71]

Surface	A, %	$A_{0.36\text{-}0.76\ \mu}$, %
Fresh snow	70	78
Old snow	58	66
Limestone	57	46
Sand	31	24
Green vegetation	23	8.4

The difference in the values of integrated albedo and albedo in the visible region of the spectrum is caused by the reflection peculiarities of spectral properties of the surfaces.

The continuous movement of albedo over the spectrum with a resolving power of the order of several nanometers can be determined through measurements on albedo by the spectrophotometric method.

The Department of Physics of the Atmosphere, Leningrad State University [22, 78] was the first to conduct these measurements under natural conditions. The monochrometers UM-2 and DMR-4 were employed as dispersive devices, whereas a spherical photometer served as the receiver for radiation.

The values of albedo for the surfaces investigated in a clear sky are given in Table 4.37. A graphical representation of the spectral characteristics of albedo in the interval of wavelength 350-1000 nm is given in Fig. 4.11.

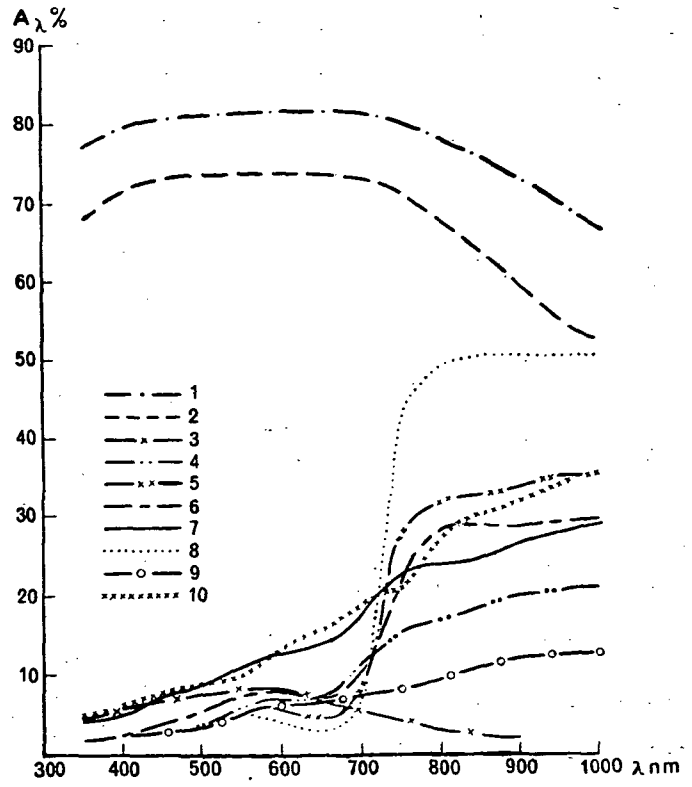

Fig. 4.11. Spectral albedo of different natural underlying surfaces [22].
1—snow with ice-crust, $h_\odot = 38°$; 2—large grained wet snow, $h_\odot = 37°$; 3—water surface of a lake, $h_\odot = 56°$; 4—soil after thawed snow, $h_\odot = 24°30'$; 5—silage corn, $h_\odot = 54°$; 6—tall green corn, $h_\odot = 56°$; 7—yellow corn, $h_\odot = 46°$; 8—sudan grass, $h_\odot = 52°$; 9—chernozem, $h_\odot = 40°$; 10—stubble of cereals, $h_\odot = 35°$.

There is a monotonic increase in the albedo with a rise in wavelength (from 400 to 1000 nm) in the visible and near-infrared regions of the spectrum for soils and road cover (class 1) (Table 4.37, Nos. 1-7; Fig. 4.11, curve 9).

For the vegetative covers (class 2) the value of spectral albedo shows

Table 4.37 Spectral albedo of natural

No.	Surface	$h_\odot$, deg	Wavelength, nm			
			400	450	500	550
						Soils and
1	White sand (river)	47	—	—	34.0	37.0
2	Chernozem	48	2.1	2.4	3.3	5.2
3	Asphalt road	48	—	—	—	13.2
4	Concrete road	47	—	—	12.4	13.6
5	Concrete in the form of light slabs	50	—	—	13.0	22.0
6	Dirt road (dry)	50	—	—	8.0	10.0
7	Dirt road (wet)	50	—	—	7.0	8.8
						Vegetative
8	Sudan grass	52	2.0	2.8	2.8	5.0
9	Alfalfa (June)	56	1.8	2.0	3.5	6.5
10	Cabbage	50	5.0	5.8	6.8	8.0
11	Green thick grass	56	2.0	2.8	3.6	5.2
12	Tomato	53	—	3.2	4.6	7.2
13	Alfalfa (July)	53	1.8	2.0	2.8	4.2
14	Clover	55	1.8	2.0	2.4	4.2
15	Maple sapling	50	1.5	2.0	2.0	3.0
16	Millet	57	—	—	—	8.0
17	Thin grass	50	—	3.0	5.6	7.0
18	Bulgarian pepper	46	—	4.7	5.2	6.0
19	Biennial vineyard	50	2.3	2.9	3.3	5.0
20	Fruit-bearing wineyard	42	—	2.4	2.7	5.2
21	Silage corn	54	2.0	2.3	3.0	5.8
22	Tall green maize	56	—	3.8	5.0	7.6
23	Yellow corn	46	5.0	7.0	8.0	10.6
24	Sunflower	52	1.5	2.0	2.5	7.9
25	Stubble of cereals (thick)	35	6.0	7.6	8.2	10.2
26	Straw	56	6.0	8.0	11.0	14.4
27	Mowed silage corn	52	4.2	5.6	7.0	8.0
28	Dry grass	28	3.5	4.5	5.6	7.0
29	Annual wineyard	50	3.0	3.3	4.1	5.2
30	Seedling of winter wheat	48	4.0	4.3	5.0	6.6
31	Soil after thawing of snow	24	2.0	2.5	4.0	5.8
						Snow
32	Dry freshly fallen snow	30	85	87	90	90
33	Wet freshly fallen snow	30	83	85	87	87
34	Wet snow	38	62	66	67	67

surfaces in a clear sky [22]

600	650	700	750	800	850	900	950	1000
road covers								
40.0	44.0	46.0	48.0	49.0	50.0	54.0	—	—
5.3	5.8	6.8	7.9	9.3	10.7	12.0	12.7	13.0
16.5	18.2	19.2	19.8	20.4	20.9	22.0	22.0	24.0
15.3	15.1	16.6	20.4	22.3	22.8	22.9	23.2	25.0
29.0	34.0	38.0	39.0	40.0	40.0	40.0		
12.0	13.0	15.0	20.0	22.0	24.0	26.0	26.0	—
9.0	9.6	12.0	16.8	19.4	20.8	21.6	21.6	—
covers								
3.8	3.0	6.0	43.0	50.0	51.0	51.0	51.0	—
5.2	4.8	11.7	35.0	40.0	42.0	42.0	42.0	41.0
9.4	7.6	13.0	37.0	42.0	44.0	44.0	41.0	—
6.2	5.8	5.6	23.0	39.6	40.0	39.2	38.5	37.7
7.4	6.4	13.0	26.0	30.0	32.0	32.0	—	—
3.5	6.0	9.2	24.0	28.0	30.0	30.0	30.0	30.0
4.4	3.8	8.0	23.0	30.0	32.0	33.0	34.0	—
3.2	3.1	6.0	20.0	23.6	24.0	24.0	24.0	—
9.6	10.0	12.6	27.0	30.0	32.0	35.0	36.0	—
5.0	4.5	8.4	19.0	27.0	28.0	29.0	29.0	30.0
7.0	7.2	14.0	22.0	26.0	28.0	31.0	—	—
5.2	5.0	14.0	22.0	25.0	27.0	28.0	29.0	29.0
4.3	4.0	4.0	18.0	26.0	28.0	29.0	29.0	29.0
5.4	4.2	8.0	28.0	32.0	33.0	34.0	35.0	35.0
7.6	7.3	10.8	24.0	29.0	28.0	29.0	30.0	30.0
11.8	13.0	16.4	22.4	24.0	25.0	27.0	28.0	29.0
7.1	6.5	10.0	21.8	25.0	27.0	28.0	29.0	29.0
12.9	15.5	18.6	20.3	28.0	30.5	32.5	33.2	33.9
20.6	26.0	30.0	36.0	38.0	40.0	43.0	43.0	—
7.6	7.4	9.0	14.0	15.2	15.8	19.9	20.4	21.1
8.7	11.0	13.6	16.5	19.3	21.0	22.5	23.5	24.0
6.2	6.0	8.3	10.5	12.0	13.0	13.6	14.2	14.5
7.2	7.2	10.4	14.0	17.2	19.4	21.0	21.8	22.6
7.0	6.8	11.0	15.5	16.7	17.8	20.1	20.8	20.8
cover								
90	90	90	90	89	87	86	81	78
87	86	86	86	86	84	82	76	70
69	68	67	65	62	58	51	46	42

a slight rise with increase in wavelength from 350 to 550 nm. The observed decrease in the value of the albedo for further increase in wavelength is caused by the presence of the fundamental absorption band of chlorophyll (650-680 nm). There is a sharp increase in albedo starting from the wavelength $\lambda = 700$ nm. It attains a maximum value in the segment of the spectrum 800-1000 nm. In this region albedo may either remain stationary or decrease slightly in the range 850-1000 nm. Albedo exhibits a different value for each type of vegetative cover. High albedo values for plants of a bright green color are characteristic in the infrared region of the spectrum (40-50%) and the absorption band of chlorophyll is clearly expressed (Fig. 4.11, curve 8 and Table 4.37, Nos. 8-11).

Similarly the absorption band of chlorophyll for grass covers in the later stages of growth (color of surface—dark green) is clearly expressed, but albedo in the infrared region of the spectrum is lower than in the first case, being equal to 30-32% (Fig. 4.11, curve 5; Table 4.37, Nos. 12-14, 21). Surfaces with vegetation in the form of bushes possess analogous albedo characteristics (Table 4.37, Nos. 15, 19, 20).

Surfaces with sparsely planted and undeveloped vegetation exhibit all the peculiarities shown by thick green herbage which is rather weakly expressed. The contour of absorption bands of chlorophyll is blurred (Fig. 4.11, curve 4 ; Table 4.37, Nos. 29-31).

The variation of spectral albedo with respect to the phase of vegetation can be followed, for instance, from the development of corn (Table 4.37, Nos. 21-23; Fig. 4.11, curves 5-7). According to the growth of the plant, i.e., during transition from silo to tall green corn, the profile of the absorption band of chlorophyll changes (it becomes less explicit) and in the segment of the spectrum 450-700 nm albedo increases by 2-3%. In the range of wavelength 750-1000 nm the value decreases by 2-5%. When corn ripens (when it turns yellow) albedo increases in the region 400-700 nm and the absorption band of chlorophyll disappears. A further increase in albedo occurs in the region 600-1000 nm for grain stubble.

The spectral properties of plants (leaves of different plants, lichens, desert plants, coniferous plants) [73] have been investigated in the laboratory for the region of spectrum 0.4-2.0 μ. The data from these measurements qualitatively confirm the results for albedo obtained under natural conditions [22].

The spectral albedo of snow cover, as opposed to the albedo of other surfaces, is widely changeable in magnitude because of variations in the nature of the snow cover. All snow covers investigated possess fully determined spectral characteristics, especially a slight decrease in albedo on the side of short wavelengths and a stronger decrease on the side of wavelengths with respect to a smooth maximum in the region 500-700 nm, where selectivity of reflection is almost absent (Table 4.37, Nos. 32-34 ;

Fig. 4.11, curves 1, 2). A further decrease in albedo occurs as the wavelength changes from 1.0 to 1.65 μ. Such a movement of albedo for snow and ice surfaces was obtained during experimental investigations, the measurements being made under natural conditions with the help of interference filters. The data from measurements (taken from the graph) are shown in Table 4.38.

Table 4.38 Spectral albedo (%) of snow and névé [69]

Wavelength, nm	450	500	550	600	650	700	
Snow	77.5	79.5	80.0	80.0	80.0	80.0	
Névé	65.0	66.0	67.5	68.0	70.0	70.0	
Wavelength, nm	750	800	850	900	950	1000	
Snow	80.0	78.5	75.0	72.5	71.5	70.0	
Névé	70.0	70.0	66.5	64.0	60.0	50.0	
Wavelength, nm	1050	1100	1150	1200	1250	1300	
Snow	70.0	68.5	65.0	60.0	57.5	52.5	
Névé	50.0	45.0	41.5	34.0	26.5	23.5	
Wavelength, nm	1350	1400	1450	1500	1550	1600	1650
Snow	52.5	50.0	34.5	20.0	20.0	18.0	20.0
Névé	20.0	16.0	7.5	4.5	2.5	2.5	2.8

The spectral albedo of water surfaces, measured over a lake of depth 60-70 cm (bottom covered by a seaweed) is shown in Fig. 4.11, curve 3. Small values of albedo in the entire range of wavelengths investigated between 428-850 nm are characteristic for the given water surface. According to the spectrum the variation in albedo does not exceed 4%.

There exists a maximum value of albedo at midday in the range of wavelengths 400-1000 nm for all the surfaces investigated (similarly for integral albedo). The coefficient K obtained from the data in [22] defines the dependence of albedo on the altitude of the sun. The coefficient K is equal to the ratio of albedo for given solar altitude to its value at the altitude $h_\odot = 50°$, which is taken as a unit. The values of K, averaged over wavelengths 400-1000 nm, are given in Table 4.39. The values of K are primarily determined by the structure of the surface. Thus, for instance, for chernozem at $h_\odot = 18°$, $K = 1.13$, and for mowed silage corn (column-type surface) for the same altitude of the sun $K = 2.00$. The greatest variation in albedo with respect to midday values corresponds to $h_\odot < 35°$.

Table 4.39 The dependence of conversion factor K upon solar altitude in a clear sky [22]

Surface	Solar altitude, deg							
	50	45	40	35	30	25	20	18
Chernozem	1.00	1.00	1.02	1.04	1.06	1.08	1.10	1.13
Sparse grass	1.00	1.00	1.03	1.08	1.16	1.22	1.24	1.27
Green thick grass	1.00	1.03	1.07	1.14	1.19	1.25	1.29	1.32
Silage corn	1.00	1.04	1.07	1.12	1.21	1.32	1.42	1.45
Yellow corn	1.00	1.05	1.09	1.20	1.37	1.54	1.69	1.76
Mowed silage corn	1.00	1.00	1.07	1.15	1.33	1.59	1.89	2.00

9. LABORATORY MEASUREMENTS OF SPECTRAL CHARACTERISTICS OF REFLECTION FROM DIFFERENT SURFACES

The spectral characteristics of surfaces in the farther region of the spectrum, viz. 0.7-2.3 μ, obtained on the basis of laboratory measurements, are given in Table 4.40. The values of the coefficient of brightness measured on the spectrogonio-photometer for different angles of incident radiation i and reflection θ' are given in the Table. Fig. 4.12 presents the spectral coefficients of brightness for different surfaces derived from [26, 68, 72]. For vegetative covers there is a little change in the coefficient of brightness in the region of the spectrum 0.7-1.3 μ with a maximum value as compared with the visible segment and a spectral range of 1.4-2.2 μ. Absorption bands of water are situated in the region 1.5 and 2.0 μ which disappear in proportion to the desiccation of plants.

There exists a characteristically monotonic decrease in coefficients of brightness in the region from 0.4 to 2.3 μ for snow-covered surfaces along with the presence of an absorption band in the regions 1.0, 1.3, 1.5 and 2.0 μ. Theoretical computations of spectral coefficients of brightness of snow [72] obtained for crystals of different sizes (Fig. 4.12, graph 7) confirm the results of laboratory investigations [26, 68].

The spectral characteristics of building materials and dry sand in the infrared region possess an identical movement but differ considerably in values. The dependence of coefficient of brightness of soil samples upon the humidity content is evident in the case of silty loam (Fig. 4.13). Thus, for instance, for $\lambda \approx 1.9$ μ the coefficient of brightness decreases from 58.9 to 13.6% when the humidity content of the soil changes from 0.8 to 20.2% respectively. The spectral coefficient of reflection for different

Table 4.40 Spectral coefficients of luminosity [26]

λ μ	$i = 0°, \theta' = 15°$, MS-14 (GGO)	$i = 40°, \theta' = 60°$, fresh meadow grass	$i = 5°, \theta' = 5°$							
			lilac leaf		dry birch leaf	brown turf		black dry turf	red brick	silica brick
			fresh	dry		moist	dry			
0.70	0.99	0.25	0.28	0.12	0.31	—	—	—	0.62	0.41
0.75	1.01	0.36	0.49	0.36	0.47	0.05	—	—	0.65	0.38
0.80	1.03	0.40	0.51	0.42	0.52	0.10	0.12	0.06	0.56	0.41
0.85	1.01	0.43	0.43	0.48	0.51	0.12	0.22	0.13	0.60	0.36
0.90	0.98	0.44	0.49	0.54	0.53	0.22	0.21	0.20	0.58	0.39
0.95	0.95	0.46	0.45	0.56	0.53	0.27	0.25	0.26	0.59	0.40
1.00	0.92	0.46	0.43	0.54	0.56	0.30	0.29	0.27	0.62	0.40
1.05	0.91	0.47	0.43	0.52	0.55	0.32	0.31	0.30	0.63	0.37
1.10	0.91	0.46	0.45	0.54	0.55	0.36	0.33	0.33	0.66	0.39
1.15	0.91	0.43	0.44	0.54	0.54	0.37	0.35	0.34	0.67	0.38
1.20	0.92	0.41	0.42	0.53	0.53	0.40	0.37	0.36	0.66	0.38
1.25	0.93	0.40	0.40	0.52	0.53	0.41	0.40	0.36	0.61	0.37
1.30	0.93	0.39	0.37	0.50	0.52	0.42	0.41	0.37	0.69	0.36
1.35	0.94	0.35	0.34	0.49	0.51	0.40	0.40	0.38	0.69	0.35
1.40	0.94	0.25	0.19	0.49	0.49	0.34	0.41	0.37	0.70	0.36
1.45	0.95	0.12	0.13	0.44	0.45	0.27	0.38	0.35	0.69	0.35
1.50	0.95	0.11	0.15	0.43	0.44	0.27	0.39	0.36	0.70	0.34
1.55	0.95	0.15	0.21	0.43	0.45	0.30	0.41	0.38	0.69	0.33
1.60	0.95	0.19	0.25	0.43	0.46	0.34	0.42	0.39	0.69	0.33
1.65	0.95	0.23	0.27	0.44	0.46	0.37	0.42	0.39	0.71	0.33
1.70	0.95	0.24	0.26	0.41	0.45	0.37	0.41	0.38	0.69	0.33
1.75	0.95	0.24	0.24	0.39	0.44	0.36	0.39	0.37	0.64	0.32
1.80	0.95	0.22	0.22	0.38	0.43	0.34	0.39	0.37	0.70	0.32
1.85	0.95	0.19	0.21	0.39	0.44	0.34	0.40	0.37	0.66	0.33
1.90	0.95	0.10	0.10	0.38	0.43	0.27	0.36	0.36	0.63	0.31
1.95	0.95	0.03	0.04	0.30	0.34	0.12	0.29	0.29	0.62	0.27
2.00	0.94	0.02	0.05	0.31	0.33	0.13	0.31	0.31	0.63	0.28
2.05	0.94	0.03	0.07	0.31	0.33	0.15	0.31	0.32	0.65	0.29
2.10	0.94	0.04	0.08	0.33	0.30	0.18	0.29	0.30	0.61	0.29
2.15	0.94	0.06	0.08	0.26	0.29	0.20	0.28	0.30	0.50	0.29
2.20	0.94	0.07	0.06	0.23	0.28	0.21	0.27	0.30	0.58	0.26
2.25	—	0.09	0.07	0.21	0.26	0.21	0.23	0.26	0.66	0.22
2.30	—	0.08	0.06	0.20	0.23	0.17	0.23	0.24	0.64	0.21

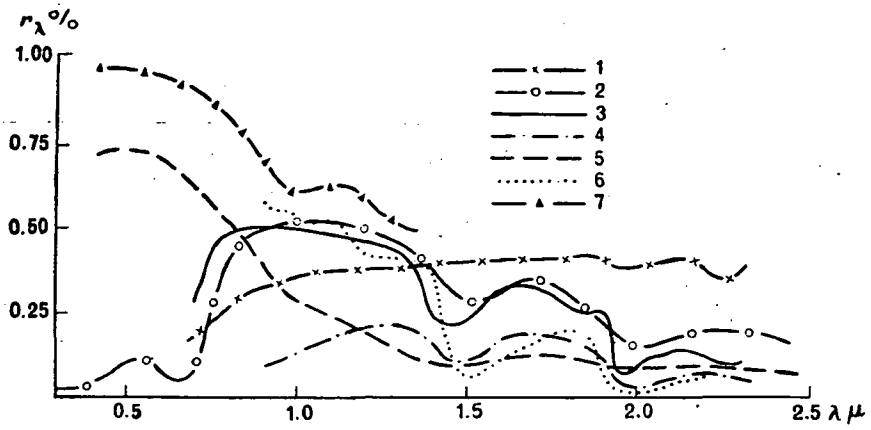

Fig. 4.12. Coefficients of brightness for different surfaces [62, 68, 72].
1—fine sand [26]; 2—plant leaves [68]; 3—birch leaves (freshly collected) [26]; 4—black turf (moist) [26]; 5—snow (old) [68]; 6—snow (freshly fallen) [26]; 7—snow (the graph is computed for particles of size 2.54 mm) [72].

samples in the distant region of spectrum, viz. 0.7-100 μ, is given in Fig. 4.14 as well as in Table 4.41 (data are taken from the graph). These measurements were accomplished through the method of mirror-like hemisphere. All the indicated spectral characteristics of samples possess the minimum value of reflection coefficient in the absorption bands of water of about 3 μ and in the wide band with center at 6.25 μ.

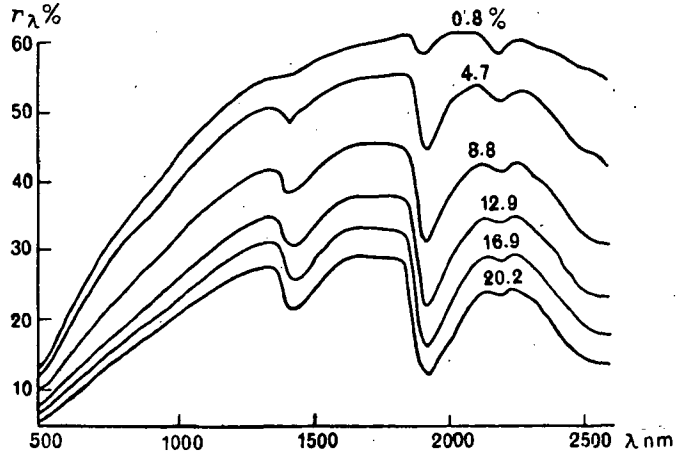

Fig. 4.13. Dependence of coefficient of brightness of silty loam on wavelength for different humidity contents [65].

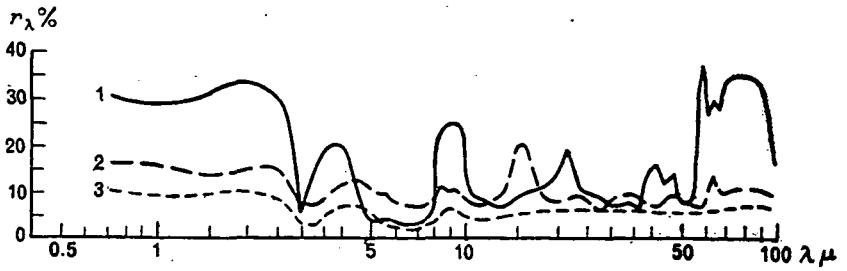

Fig. 4.14. Spectral coefficients of water reflection for different samples in the region 0.7-100 μ [28].
1—sand; 2—soil; 3—asphalt.

Table 4.41 Spectral coefficient of reflection (%) for different samples in the region of spectrum 0.7-100 μ [28]

λ μ	Green leaf of indoor lemon	Brick	Concrete	λ μ	Green leaf of indoor lemon	Brick	Concrete
0.7	41.2	50.0	21.2	10	4.7	11.8	5.9
1.0	41.8	40.0	21.2	15	5.9	28.2	7.1
1.5	37.6	54.7	24.7	20	5.3	6.5	4.7
2.0	22.9	52.3	29.4	30	4.7	10.6	4.7
2.5	12.9	48.2	26.5	40	5.9	9.4	5.9
3.0	4.7	21.8	4.1	50	5.9	8.2	7.3
4.0	12.0	44.7	12.9	60	5.3	—	—
5.0	10.6	18.8	12.9	70	—	—	—
6.0	10.6	10.6	5.9	80	—	37.4	15.3
7.0	6.5	8.2	2.9	90	—	38.8	15.9
8.0	4.1	8.2	5.9	100	—	40.6	18.8
9.0	4.1	11.8	4.7				

An analogous character of reflection for samples of mountain rocks for the region 0.5-22 μ has been obtained in [76]. The similar character of reflection for sand, soil, asphalt and concrete is accounted for by the generality of their chemical structure.

10. ALBEDO OF WATER RESERVOIRS

10.1 Albedo of water reservoirs for direct solar radiation

Albedo of a water surface, computed for direct solar radiation (from Fresnel's formula), in the limits of wavelength 0.214-1.256 μ decreases

monotonically with increasing wavelengths, especially for large angles of incidence of radiation (Table 4.42). The dependence of the albedo of water surface on wavelength can be determined as the refractive index of water in the region of the spectrum being examined.

Table 4.42 Albedo of aqueous surface for direct radiation for 0.214-1.256 μ [50]

Angle of incidence, deg	Wavelength, μ									
	0.214	0.303	0.405	0.486	0.589	0.671	0.768	1.028	1.256	
	Refractive index									
	1.403	1.358	1.343	1.337	1.333	1.331	1.329	1.324	1.321	$A_{0.214-1.256}$
0	2.80	2.30	2.10	2.08	2.04	2.01	2.00	1.95	1.91	2.10
10	2.90	2.30	2.16	2.09	2.05	2.05	2.00	2.00	1.91	2.14
20	2.90	2.32	2.19	2.10	2.05	2.05	2.03	2.02	1.94	2.18
30	2.97	2.42	2.25	2.16	2.16	2.10	2.10	2.06	2.04	2.26
40	3.32	2.72	2.50	2.49	2.46	2.42	2.40	2.32	2.30	2.52
50	4.36	3.74	3.52	3.45	3.35	3.30	3.30	3.22	3.19	3.46
60	7.25	6.40	6.15	6.00	5.95	5.92	5.85	5.80	5.75	6.12
70	15.1	14.0	13.5	13.5	13.3	13.3	13.3	13.1	13.0	13.7
75	23.2	22.0	21.5	21.5	21.2	21.2	21.1	20.9	20.9	21.7
80	36.8	35.6	35.1	34.8	34.8	34.7	34.8	34.4	34.4	35.6
85	60.0	58.1	58.5	58.5	58.4	58.4	58.4	58.2	58.2	59.6
90	100	100	100	100	100	100	100	100	100	100

The albedo of an even water surface for the spectral range 1.5-314.0 μ with respect to the angle of incidence of the radiation is given in Table 4.43. Evaluation was carried out according to Fresnel's formula by considering absorption of radiation in water. For the section of the spectrum 1.5-12 μ the albedo of water possesses a lower value as compared to the region 12-314 μ, which may be caused by the different spectral properties of water in the indicated region of the spectrum. Laboratory measurements of the coefficient of spectral reflection r_λ of water in the region of the spectrum 1-40 μ for different angles of incidence point to an analogous spectral dependence [81]. The coefficient of reflection rapidly rises with an increase in the incident angle i, especially above $i=70°$. Thus, for instance, for $\lambda=9$ μ, $r'_\lambda=3\%$ when $i=50°$ and $r'_\lambda=58\%$ for $i=80°$. For an increase in the angle of incidence from 50 to 80° the intensity of the absorption bands decreases and the spectral course becomes smooth.

Table 4.43 Albedo of an even water surface for wavelength 1.5-314 μ with respect to incident angle of radiation [36]

λ μ	i°								
	10	20	30	40	50	60	70	80	85
1.5	1.95	1.95	2.04	2.33	3.21	5.75	13.0	34.4	58.1
2.0	1.74	1.76	1.83	2.11	2.96	5.45	12.4	33.6	57.6
3.0	3.40	3.41	3.53	3.94	5.20	8.35	16.6	38.6	61.4
3.2	4.12	4.13	4.26	4.71	5.95	9.20	17.5	39.4	61.8
3.4	3.25	3.28	3.39	3.78	4.88	7.90	15.9	37.6	60.5
4.5	2.14	2.16	2.24	2.57	3.49	6.25	14.2	35.2	58.6
5.47	1.68	1.69	1.77	2.04	2.85	5.30	12.3	33.5	57.3
6.0	2.00	2.02	2.11	2.37	3.32	6.00	14.4	35.1	58.6
7.0	2.00	2.02	2.12	2.45	3.33	5.90	13.3	34.8	58.4
8.0	1.68	1.68	1.76	2.04	2.87	5.25	12.3	33.6	57.5
9.0	1.44	1.46	1.53	1.79	2.55	4.84	11.6	32.6	56.6
10.0	0.95	0.98	1.01	1.21	1.82	3.70	9.75	29.8	54.2
11.0	0.80	0.81	0.85	1.20	1.53	3.21	9.00	28.9	53.5
12.0	2.00	2.15	2.16	2.51	3.65	6.80	15.6	38.3	61.5
13.0	3.08	3.11	3.25	3.91	5.10	8.55	17.6	40.5	63.0
15.0	5.30	5.40	5.50	6.13	7.80	11.9	21.5	44.1	65.6
18.0	6.70	6.80	6.90	7.40	9.05	12.9	21.9	44.2	65.0
52.0	7.95	8.00	8.20	8.80	10.4	14.3	23.3	44.4	65.5
63.0	10.8	10.8	11.0	11.5	13.0	16.5	24.4	44.8	65.0
83.0	11.8	11.8	12.0	12.5	13.9	17.2	25.0	44.4	64.4
100.0	12.3	12.3	12.5	13.0	14.3	17.4	24.8	43.7	63.7
117.0	12.8	12.8	13.0	13.5	14.8	17.8	25.0	43.6	63.5
152.0	13.4	13.4	13.5	14.1	15.3	18.3	25.5	43.9	63.6
314.0	15.1	15.2	15.3	15.7	17.0	20.1	27.1	45.2	64.5

The spectral course of albedo for a water surface in the visible region of the spectrum, computed for total radiation at high solar altitudes, is similar to the spectral movement of albedo for direct solar radiation [20].

10.2 Dependence of albedo for water reservoirs on cloudiness

The influence of cloudiness on the value of albedo for a water surface has been computed for the region of the spectrum 1.5-83 μ (Table 4.44). For the computation they used calculated coefficients of reflection of water

and measured angular distribution of intensity of atmospheric back-radiation over the sky when it is clear and in the presence of dense cloudiness for different amounts of water vapor in the atmosphere. From the Table it is evident that during calm weather cloudiness exerts an insignificant influence on the value of albedo for a water surface.

Table 4.44 Albedo (%) of a water surface under a clear sky, and under cloud, for wavelengths 1.5-83.0 μ [36]

Condition of sky	Wavelength, μ							
	1.5	2.0	3.0	3.2	4.5	5.5	6.0	8.0
Clear $w_\infty = 0.41$ g/cm²	6.4	6.1	8.7	9.4	6.9	6.1	6.7	6.0
Cloudy $w_H = 0.34$ g/cm²	6.1	5.8	8.2	9.0	6.6	5.8	6.3	5.7

Condition of sky	Wavelength, μ							
	9.0	10.0	11.0	12.0	15.0	18.0	52.0	83.0
Clear $w_\infty = 0.41$ g/cm²	5.6	4.6	4.3	7.5	11.6	12.7	13.9	17.0
Cloudy $w_H = 0.34$ g/cm²	5.3	4.4	4.0	7.0	11.4	12.2	13.5	16.6

NOTE : w_∞ —amount of water vapor in a column of atmosphere of unit cross section, w_H—amount of water vapor in a layer of air from the ground to the clouds (column of unit cross section).

11. SPECTRAL ALBEDO MEASURED FROM AN AIRPLANE

Direct measurements of spectral albedo from an airplane or a balloon are lacking. Only in [66] one finds measurements on the spectral albedo of lower undergrowth and an eroded sand surface from an altitude of 300 m. Interference filters and spherical photometers for the reception of radiation (region of spectrum 400-650 nm) were used for the monochromatization of radiation.

The dependence of albedo upon solar altitude for this surface is shown in Table 4.45 (data taken from the graph). A decrease in albedo for

lower solar altitudes starting from $h_{\odot}=10°$ is characteristic, and this agrees with the data of [53].

Table 4.45 Dependence of albedo (%) upon solar altitude for lower undergrowth and eroded sand surface [61]

λ nm	Solar altitude, deg							
	60	50	40	30	20	15	10	5
400	11.3	11.3	11.6	11.8	12.6	12.9	13.3	11.6
500	15.3	15.5	15.9	16.1	18.8	21.2	25.3	22.5
600	24.0	22.9	23.0	25.1	35.4	42.2	43.5	38.6

12. ALBEDO OF CLOUDS

The albedo of clouds in the visible range of the spectrum, viz. 0.4-0.7 μ, does not depend on wavelength, as shown from theoretical computations in [35, 54]. The values of albedo for water-bearing clouds of stratiformis type are given in Table 4.46. Computations accomplished for fixed wavelengths 0.40 ; 0.55 and 0.70 μ can be carried over for the entire visible range of the spectrum.

Table 4.46 Albedo (%) of clouds of different forms with respect to the zenith distance of sun [54]

Form of cloud	Zenith angle of sun, deg		
	30	50	70
St	59	63	69
Sc	68	72	76
Ns-As	68	88	90
As	63	68	73

Albedo of clouds possesses a selective dependence upon wavelength [54, 74] in the infrared region of the spectrum, viz. 0.7-3 μ. Table 4.47 gives the values of albedo for spectral range 0.7-2.19 μ computed over distinct spectral intervals as well as for the fundamental absorption bands of water vapor. Calculations are conducted for water-bearing clouds of thickness 0.25 and 1 km with the upper boundary at the 2 km level ("low"

clouds) for average cloud temperature of 0°C and average water content of 0.2 g/m³ and for a "high" cloud, situated in the layer $4 \leqslant H \leqslant 5$ km, for a temperature of −15°C and water content 0.2 g/m³. The spectral albedo of clouds remains stationary up to approximately $\lambda = 0.08\,\mu$, and then albedo in the infrared range of the spectrum decreases to 2.5 μ, which is caused mainly by the absorption bands of water vapor. As a result of this the integral albedo of cloud appears to be less than the albedo in the visible region of the spectrum. Thus for instance for layer $\tau_{tot} = 30$ when $\vartheta_\odot = 30°$ albedo in the visible range of the spectrum $A_v = 76\%$, integrated albedo $A = 67\%$, for $\vartheta_\odot = 60°$, $A_v = 81\%$ and $A = 74\%$ [54]. According to computations in [86], the mean values of albedo for clouds in the

Table 4.47 Albedo of cloud for different optical thickness and zenith distance of sun [54]

$\Delta\lambda\,\mu$	Low cloud	High cloud	Spectral band	Low cloud			
				$\tau_{tot} = 6$		$\tau_{tot} = 30$	
	$\tau_{tot} = 30$	$\vartheta_\odot = 30°$		$\vartheta_\odot = 30°$	$\vartheta_\odot = 60°$	$\vartheta_\odot = 30°$	$\vartheta_\odot = 60°$
0.700-0.719	66	66					
0.719-0.721	59	63	*a*	33	50	67	78
0.721-0.740	66	66					
0.740-0.790	65	65					
0.790-0.814	66	66					
0.814-0.816	55	62	0.8 μ	33	50	65	77
0.816-0.840	66	66					
0.840-0.860	66	66					
0.860-0.915	65	65					
0.915-0.935	45	57	$\rho\sigma\tau$	33	54	64	75
0.935-0.990	65	66					
0.990-1.030	66	66					
1.030-1.112	66	66					
1.112-1.148	46	57	Φ	32	50	64	75
1.148-1.230	62	63					
1.230-1.240	64	64					
1.240-1.321	62	63					
1.321-1.449	25	40	ψ	24	42	48	55
1.449-1.530	37	37					
1.530-1.755	46	48					
1.755-1.965	18	24	Ω	24	37	41	45
1.965-2.190	34	34					

infrared range of the spectrum is 45%, and in the visible and ultraviolet ranges it is about 85%.

Direct measurements of brightness of clouds, accomplished during airplane surveys in the range 0.6-2.5 μ [56], as well as laboratory measurements on coefficients of brightness for model of ice-bearing clouds and frost (Fig. 4.15) qualitatively confirm theoretical calculations [54, 74]. The albedo of a cloud in the spectral range 3-4 μ depends on the temperature and the water content of the layer of clouds (Table 4.48). From the data in the Table it follows that the albedo of cloud decreases slightly with an increase in the temperature.

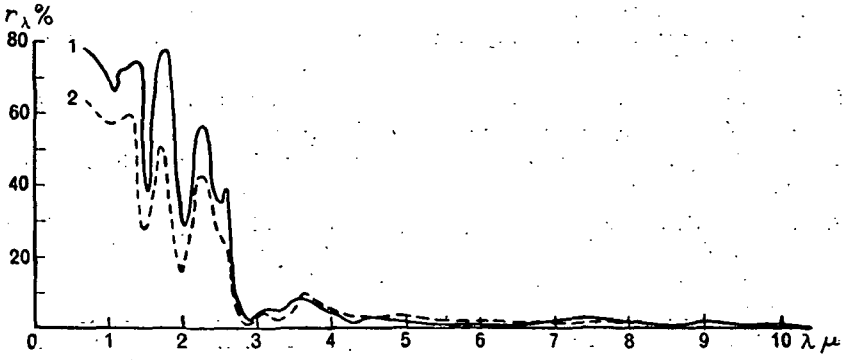

Fig. 4.15. Spectral coefficient of brightness for model of ice-bearing cloud and frost [89].

1—ice-bearing clouds; 2—frost.

Table 4.48 Albedo (%) of cloud in the range 3-4 μ at different temperatures and water content of 0.2 g/m³ [54]

λ μ	T_{tot}, °C		
	−15	−5	+15
3.0	9	6	5
3.4	12	12	11
4.0	24	22	21

Experimental data for investigation of the spectral albedo of clouds are lacking. Indirect determination of the albedo of stratiformis clouds for spectral range 8-12 μ provides mean values of albedo for water-bearing clouds of 3-4%; for mixed clouds it is 8-9%. The albedo was computed from data of measurements on radiation temperature of the upper surface of clouds and temperature of the air.

REFERENCES

1. Babarykin, V. K. et al. Al'bedo poverkhnosti antarkticheskikh l'dov (Albedo of Antarctic snow surface). Inform. byull. Sovetskoi Antarkticheskoi e'kspeditsii No. 48. Gidrometoizdat, Leningrad, 1964.
2. Barashkova, E.P. et al. Radiatsionnyi rezhim territori SSSR. (Radiational regime of Soviet territory). Gidrometeoizdat, Leningrad, 1961.
3. Beletskii, F. A. Al'bedo podstilayushchei poverkhnosti territori Povolzh'ya (Albedo of underlying surface of territory around Volga). Trudy Saratovskogo in-ta mekhanizatsii s/kh, vyp. 38, 1965.
4. Belov, V. F. Al'bedo podstilayushchei poverkhnosti i nekotorykh form oblakov v raione Antarkticheskogo sklona i morya Devisa (Albedo of underlying surface and several forms of clouds in the region of Antarctic slope and Davis Sea). Trudy TsAO, vyp. 37, 1960.
5. Berezina, L. S. Al'bedo nekotorykh cel'skokhozyaistvennykh kul'tur (Albedo of agricultural farms). Trudy Ukr. NIGMI, vyp. 8, 1957.
6. Bryazgin, N. M. K voprosy ob al'bedo poverkhnostei dreifuyushchikh l'dov (Albedo of surfaces of ice-drifts). Problemy Arktiki i Antarktiki, No. 1, 1959.
7. Vinnikov, K. Ya. Al'bedo sistemy zemlya-atmosphera i pole ykhodyashchei korotkovolnovoi radiatsii (Albedo of earth-atmosphere system and the field of outgoing shortwave radiation). Trudy GGO, vyp. 170, 1965.
8. Voloshina, A. P. Teplovoi balans poverkhnosti vysokogornykh lednikov v letnii period (Thermal balance of snow surface in high mountains during summer). Izd-vo "Nauka", Moskva, 1966.
9. Gaevskii, V. L. K voprosy o roli al'bedo v formirovanii radiatsionnogo rezhima poverkhnosti (The role of albedo in the formation of radiational regime of surface). Trudy GGO, vyp. 39 (101), 1953.
10. Gaevskii. V. L., Yu. I. Rabinovich and A. I. Reshetnikov. Nekotorye resul'taty izmerenii al'bedo sloistykh oblakov v oblasti spektra 8-12 mkm (Some results on albedo measurements of stratiformis clouds in the spectral range 8-12 μ). Trudy, GGO, vyp. 196, 1966.
11. Girdyuk, G. V. Nekotorye resul'taty nablyudenii za e'ffektivnym izlucheniem i al'bedo v Norvezhskom more (Some results of observations on effective radiation and albedo in the Norwegian Sea). Aktinometriya i atmosfernaya optika, Gidrometeoizdat, Leningrad, 1961.
12. Goisa, N. I. O vliyanii moshchnosti i vodnosti sloistoobraznykh oblakov na otrazhenie, propuskanie i nogloshchenie korotkovolnovoi radiatsii (The effect of thickness and water content of stratiformis clouds on reflection, emission and absorption of shortwave radiation). Trudy Ukr. NIGMI, vyp. 70, 1968.
13. Goisa, N. I. Nekotorye zakonomernosti sutochnogo i godovogo khoda radiatsionnogo balansa podstilayushchei poverkhnosti i ego sostavlyayushchikh (Some patterns of diurnal and annual variations of net radiation of the underlying surface and its constituents). Trudy Ukr. NIGMI, vyp. 31, 1962.
14. Grishchenko, D. L. Zavisimost' al'bedo morya ot vysoty Solntsa i volneniya morskoi poverkhnosti (Dependence of albedo of sea on solar altitude and waves on the sea surface). Trudy GGO, vyp. 80, 1959.

15. Kastrov, V. G. K voprosy o dnevnom khode al'bedo zemnoi poverkhnosti (Daily variation in albedo of earth's surface). Trudy TsAO, vyp. 14, 1955.

16. Kirillova, T. V. and S. P. Malevskii-Malevich. Ob izmerenii al'bedo morya s vertoleta (Measurement of sea albedo from a helicopter). Trudy GGO, vyp. 150, 1964.

17. Kirillova, T. V. and A. Ya. Myl'nikova. Radiatsionnyi balans Volgogradskogo vodokhranilishcha (Net radiation of Volgagrad water reservoir). Meteorologiya i gidrologiya, No. 9, 1965.

18. Kirillova, T. V. and T. A. Ogneva. Osobennosti teplovogo balansa vodnoi poverkhnosti (Properties of thermal balance of water surface). Meterologiya i gidrologiya, No. 4, 1956.

19. Kozyrev, B. P. and V. A. Bunchikov. Izmereniya spektral'noi chuvstvitel'nosti piranometrov i balancomerov (Measurements on spectral sensitivity of pyranometers and balancemeters). Izy. AN SSSR, fizika atmosfery i okeana, 2, No. 5, 1966.

20. Kondrat'ev, K. Ya. Aktinometriya (Actinometry). Gidrometeoizdat, Leningrad, 1965.

21. Kondrat'ev, K. Ya. Luchistaya e'nergiya Solntsa (Radiant energy of the sun). Gidrometeoizdat, Leningrad, 1954.

22. Kondrat'ev, K. Ya., Z. F. Mironova and A. N. Otto. Spektral'noe al'bedo estestvennykh podstilayushchikh poverkhnostei (Spectral albedo of natural underlying surfaces). Problemy fiziki atmosfery, 3, 1965.

23. Kondrat'ev, K. Ya., G. A. Nikol'skii and E. N. Esipova. Ae'rostatnye issledovaniya radiatsionnykh potokov v svobodnoi atmosfere (Balloon investigations on radiative flux in free atmosphere). Isv. AN SSSR, fizika atmosfery i okeana, No. 4, 1966.

24. Koptev, A. P. Al'bedo oblakov, vody i snezhno-ledyanoi poverkhnosti. Radiatsionnyi i teplovoi balans Arktiki (Albedo of clouds, water and snow or ice surfaces. Radiative and thermal balance of Arctic region). Trudy AANII, t. 229. 1961.

25. Koptev, A. P. Metodika aktinometricheskikh nablyudenii s samoleta v Arktike (Method of actinometric observations from an airplane in the Arctic region). Trudy AANII, t. 239. Izd-vo "Morskoi transport", Leningrad, 1962.

26. Korzov, V. I. and L. B. Krasil'shchikov. Nekotorye resul'taty izmerenii spektral'nykh koe'ffitsientov yarkosti v oblasti 0.7-2.5 mkm (Some results of measuring spectral coefficients of luminosity in the range 0.7-2.5 μ). Trudy GGO, vyp. 183, 1966.

27. Krinov, E. L. Spektral'naya otrazhatel'naya sposobnost' prirodnykh obrazovanii (Spectral reflection properties of natural formations). Moskva-Leningrad, 1947.

28. Kropotkin, M. A. and B. P. Kozyrev. Issledovanie spektrov otrazheniya prirodnykh i iskysstvenykh materialov v oblasti dlin voln 0.7-100 mkm (Investigation on reflection spectra of natural and artificial materials in the range of wavelengths 0.7-100 μ). Optika i spektroskopiya, t. XVII, vyp. 2, 1964.

29. Kyz'min, P. P. Fizicheskie svoistva snezhnogo pokrova (Physical properties of snow cover). Gidrometeoizdat, Leningrad, 1957.

30. Lopukhin, E. A. Issledovaniya raspredelenii sostavlyayushchikh radiatsionnogo balansa nad Srednei Aziei (Investigation on distribution of components of net radiation above Central Asia). Trudy SANIGMI, vyp. 16, 1963.

31. Malkevich, M. S. Vliyanie gorizontal'nykh izmenenii al'bedo podstilayushchei poverkhnosti na rasscyanie sveta v odnorodnoi atmosfere (The effect of horizontal variation

of albedo of underlying surface on the scattering of light in homogeneous atmosphere). Izv. AN SSSR, ser. geofiz., No. 8, 1958.

32. Mullamaa, Yu. A. R. Atlas opticheskikh kharakteristik vzvolnovannoi poverkhnosti morya (Atlas of optical characteristics of perturbed sea surface). Tartu, 1964.

33. Mukhenberg, V. V. Al'bedo poverkhnosti sushi severnogo polushariya (Albedo of land in the Northern Hemisphere). Nauchnye soobshcheniya in-ta geologii i geografii. AN Lit. SSSR, t. XIII, 1962.

34. Mukhenberg, V. V. Albedo poverkhnosti sushi zemnogo shara (Albedo of land on the earth). Trudy GGO, vyp. 193, 1967.

35. Novosel'tsev, E. P. Spektral'naya otrazhatel'naya sposobnost' oblakov (Spectral reflective properties of clouds). Trudy GGO, vyp. 152, 1964.

36. Novosel'tsev, E. P. and N. E. Ter-Markaryants. Ob otrazhenii dlinnovolnovoi radiatsii vodnoi poverkhnosti (Reflection of longwave radiation by water surface). Trudy GGO, vyp. 125, 1962.

37. Pleshkova, T. T. Al'bedo rastitel'nogo pokrova (Albedo of vegetative cover). Trudy GGO, vyp. 49, 1955.

38. Pyatovskaya, N. P. Izmereniya albedo a samoleta (Measurement of albedo from an airplane). Trudy GGO, vyp. 109, 1961.

39. Ross, Yu. K. Ob izmerenii radiatsii piranometrom Yanishevskogo (Measurements of radiation by Yanishevskii's pyranometer). Izv. AN E'SSR, No. 1, 1957.

40. Ross, Yu. K. K teorii al'bedo rastitel'nogo pokrova (Theory of albedo of vegetative cover). Nauchnoe soobshchenie in-ta geologii i geografii AN Lit.SSR., t. XIII, vyp. 1, 1962.

41. Rusin, N. P. Meteorologicheskii i radiatsionnyi rezhim Antarktiki (Meterological and radiative regime in the Antarctic region). Gidrometeoizdat, 1964.

42. Rutkovskaya, V. A. Kharakteristika nekotorykh radiatsionnykh svoistv ozer, vodokhranilishch i morei (Characteristics of the radiative properties of lakes, water-reservoirs and seas). Trudy in-ta okeanografii AN SSSR, t. LVII, 1962.

43. Sakali, L. I. and G. I. Zorina. Sravnitel'naya kharakteristika radiatsionnogo balansa podstilayushchei poverkhnosti sushi i morya v pribrezhnoi polose (Comparative characteristic of radiative balance of underlying surface of land and sea in coastal region). Aktinometriya i atmosfernaya optika. Gidrometeoizdat, Leningrad, 1961.

44. Sivkov, S. I. O vychislenii summ radiatsii, otrazhennoi ot vodnoi poverkhnosti (Computation of the amount of radiation reflected from a water surface). Meteorologiya i gidrologiya, No. 3, 1951.

45. Sivkov, S. I. Geograficheskoe raspredelenie e'ffektivnykh velichin al'bedo vodnoi poverknosti (Geographic distribution of effective values of albedo of water surface). Izv. VGO, t. 84, vyp. 2, 1952.

46. Sitnikova, M. V. Al'bedo nekotorykh podstilayushchikh poverkhnostei (Albedo of several underlying surfaces). Trudy SANIGMI, vyp. 16, 1963.

47. Skvortsov, A. A. K voprosy o klimate o azisai pustyni i nekotorykh osobennostyakh ikh teplovogo balansa (The climate in oasis and desert and some properties of their thermal balance). Trudy po s.-kh. meteor., t. XX, 1928.

48. Ter-Markaryants, N. E. Al'bedo morya. Avtoreferat dissertatsii (Sea albedo—Author's abstract of dissertation). GGO, Leningrad, 1958.

49. Ter-Markaryants, N. E. O srednykh dnevnykh velichinakh al'bedo morya (Mean daily values of sea albedo). Trudy GGO, vyp. 100, 1960.

50. Ter-Markaryants, N. E. Zavisimost' koe'ffitsienta otrazheniya vody ot dliny volny padayushchego sveta (The dependence of reflection coefficient of water on wavelength of incident light). Trudy GGO, vyp. 68, 1957.

51. Ter-Markaryants, N. E. Otrazhenie radiatsii morem (Reflection of radiation by sea). Aktinometriya i atmosfernaya optika. Gidrometeoizdat, Leningrad, 1961.

52. Timerev, A. A. Summarnaya radiatsii i al'bedo po nablyudeniyam s samoleta v Arktike v 1963 g (Total radiation and albedo according to observations from airplanes in the Arctic region in 1963). Trudy AANII, t. 273, Gidrometeoizdat, Leningrad, 1965.

53. Tooming, Kh. Dnevnye i sezonnye izmeneniya al'bedo nekotorykh estestvennykh poverkhnostei E'stonskoi SSR (Daily and seasonal variations in albedo of some natural surfaces of the Estonian Republic). Issledovaniya po fizike atmosfery, 2, Tartu, 1960.

54. Feigel'son, E. M. Radiatsionnye protsessy v sloistoobraznykh oblakakh (Radiative processes in stratiformis clouds). Izd-vo "Nauka", Moskva, 1964.

55. Tsutskiridze, Ya. A. Albedo nekotorykh kyl'turnykh rastenii i drugikh estestvennykh poverkhnosti (Albedo of some agricultural growths and other natural surfaces). Trudy Tbil. NIGMI, vyp. 8, 1963.

56. Chapurskii, L. I. E'ksperimental'nye issledovaniya spektral'nykh yarkostnykh kharakteristik oblakov, atmosfery i podstilayushchei poverkhnosti v intervale dlin voln 0.3-2.5 mkm (Experimental investigation on spectral and luminosity characteristics of clouds, atmosphere and underlying surface in wavelengths between 0.3 and 2.5 μ). Trudy GGO, vyp. 196, 1966.

57. Chel'tsov, N. I. Issledovanie otrazheniya, propuskaniya i pogloshcheniya solnechnoi radiatsii oblakami nekotorykh form (A study of reflection, emission and absorption of solar radiation by clouds of several forms). Trudy TsAO, vyp. 6, 1952.

58. Chernigovskii, N. T. O radiatsionnykh svoistvakh snezhnogo pokrova i l'da arkticheskikh morei (Radiative properties of snow and ice covers of Arctic seas). Problemy Arktiki, No. 6, 1939.

59. Chernigovskii, N. T. and M. S. Marshunova. Klimat Sovetskoi Arktiki (radiatsionnyi rezhim) [Climate of Soviet Arctic region (radiational regime)]. Gidrometeoizdat, Leningrad, 1965.

60. Shifrin, K. S. K teorii al'bedo (On the theory of albedo). Trudy GGO, vyp. 39 (101), 1953.

61. Ashburn, E. V. and R. G. Weldon. Spectral diffuse reflectance of desert surface. JOSA, 46, No. 8, 1956.

62. Bandeen, W. R., M. Halev and I. Strange. A radiation climatology in the visible and infrared from the TIROS meteorological satellites. NASA TND-2534, National Aeronautics and Space Admin., Washington, D. C., 1965.

63. Bartman, F. L. The reflectance and scattering of solar radiation by the Earth. Technical Report. NASA Contract No. NASr-54(03), Washington, D. C., 1967.

64. Bauer, K. G. and J. A. Dutton. Albedo variations measured from an airplane over several types of surfaces. J. Geophys. Res., 67, No. 6, 1962.

65. Bowers, S. A. and R. J. Haks. Reflection of radiant energy from soils. Son. Science, v. 100, No. 2, 1965.

66. Conover, J. H. Cloud and terrestrial albedo determinations from TIROS satellite pictures. J. Appl. Meteor., v. 4, No. 3, 1965.

67. Davis, J. A. Albedo investigations in Labrador. Ungava. Archiv für Meteor. Geophys. und Bioklim. Ser. B 13, No. 1, 1963.

68. Dirmhirn, J. Zur spektralen Verteilung der Reflexion natürlicher Medien. Wetter und Leben. Bd 9 H-3-5, 1957.

69. Dirmhirm, J. Ergebnisse von Albedountersuchungen in Sonnblickgebiet. Wetter und Leben Sondernheft, IX, 1961.

70. Dirmhirm, J. and E. Trojer. Albedoundersuchungen auf dem Hintereisferner. Archiv Meteorol., Geophys. u. Bioklimatol., Ser. B, Bd. 6, H. 4, 1955.

71. Dirmhirm, J. On the applicability of silicon cells in atmospheric radiation studies. Atmospheric Science Paper, No. 113, 1967. Department of Atmospheric Science, Colorado State University, Fort Collins, Colorado.

72. Dunckle, R. V. and J. T. Bewans. An approximate analysis of the solar reflectance and transmittance of a snow-cover. J. Meteorol., v. 13, No. 2, 1956.

73. Gates, D. M. et al. Spectral properties of plants. Applied Optics, v. 4, No. 1, 1965.

74. Fritz, S. Absorption and scattering of solar energy in clouds of "large water drops", J. Meteorol., v. 15, No. 1. 1958.

75. Fritz, S. The albedo of the planet Earth and of clouds. J. Meteorol., v. 6, No. 4, 1949.

76. Hovis, W. A. et al. Infrared reflectance spectra of igneous rocks, tuffs and red sandstone from 0.5 to 22 mkm. JOSA, 56, No. 5, 1966.

77. Katayama, A. On the radiation budget of the troposphere over the Northern Hemisphere. II: Hemispheric distribution, III: Zonal cross section and energy consideration. J. Met. Soc. of Japan, ser. II, v. 45, No. 1, Febr. 1967.

78. Kondratyev, K. Ya., Z. F. Mironova and A. N. Otto. Spectral albedo of natural surfaces. Pure and Applied Geophysics, v. 59, 1964.

79. Kung, E. C., R. S. Bryson and D. H. Lenschow. Study of a continental surface albedo on the basis of flight measurements and structure of the Earth's surface cover over North America. Monthly Weather Review, v. 92, No. 12. 1964.

80. London, J. A study of atmospheric heat balance, Final report, Contract No. AF 19 (122)—165, 1957.

81. Pohtier, L. and C. Dechambenoy. Détermination des constants optiques de l'eau liquide entre 1 et 40 mk. Application en calcul. de son pouvoir reflecture et de son émission. Analles de géophys., 22, No. 4, 1966.

82. Posey, J. W. and F. F. Clapp. Distribution global de l'albedo normal de superificie. Geophys. internat., No. 4, 1964.

83. Raschke, E. and M. Pasternak. The global radiation balance of the earth-atmosphere system obtained from radiation data of the meterological satellite Nimbus II. The University of Munich, 1967.

84. Raschke, E., F. Moller and W. R. Bandeen. The radiation balance of the earth-atmosphere system over both polar regions obtained from radiation measurements of the Nimbus II. Meteorological Satellite X-622-67-460. Goddord Space Flight Center, Greenbelt, Maryland, September 1967.

85. Rasool, S. I. and C. Prabhakara. Radiation studies from meteorological satellites. New York Univ., Geophys. Sci. Lab. Rep. No. 65-1, Jan. 1965.

86. Robinson, G. D. Some observations from aircraft of surface albedo and the albedo and absorption of cloud. Archiv für Meteorol. Geoph. and Bioklimat., Ser. B, Bd 9, No. 1, 1958.

87. Spano, A. F. Results of an airborne albedo program in Antarctica, 1963. Monthly Weather Rev., v. 93, No. 11, 1965.

88. Winston, J. S. Planetary-scale characteristics of monthly mean longwave radiation and albedo and year-to-year variations. Monthly Weather Review., v. 95, No. 5, May 1967 (235-256).

89. Zander, R. Spectral scattering properties of ice clouds and hoarfrost. J. of Geophys. Res., v. 71, No. 2, 1966.

5. DIRECT SOLAR RADIATION

1. SPECTRAL COMPOSITION OF SOLAR RADIATION

1.1 Spectral energy distribution of solar radiation at sea level

Direct solar radiation implies a continuum of electromagnetic emission, arriving directly from the sun and comprising energy of wavelengths ranging from 100 Å to several microns.

Radiation of wavelengths from 200 nm to 25 μ has a practical significance for actinometry and atmospheric optics. Usually this range can be divided into five regions, viz. ultraviolet ($\lambda<400$ nm), visible ($400>\lambda>750$ nm) ; infrared ($3<\lambda<25\ \mu$), far infrared ($\lambda>25\ \mu$) and near infrared (750 nm $<\lambda<3\ \mu$).

The division of the solar energy spectrum into many regions is carried out in different ways by different authors. Thus, for example, in the American literature the longwave boundary of the ultraviolet region is often considered to be 380 nm. There is a still greater discrepancy in the determination of the boundary of the near infrared region, viz. from 1500 to 3000 nm. This situation indicates that the location of the boundaries of the spectral regions is more or less arbitrary. With respect to the energy distribution the solar radiation is almost completely (99.65%) included within the range 220-7000 nm. Recently the solar constant has been determined in this range of wavelengths.

The following notation has been accepted for different regions of the solar spectrum :

Spectral range, nm	Notation	Spectral range, nm	Notation	Spectral range, μ	Notation
200-400	UV	400-750	S	0.75-25	IR
200-280	UV-C	400-520	S-A	0.75-1.4	IR-A
280-320	UV-B	520-620	S-B	1.40-3.0	IR-B
320-400	UV-A	620-750	S-C	3.0-25	IR-C

Different units were used until recently for the measurement of wavelengths of electromagnetic radiation, viz. 1 (micrometer) = 1 μ (micron) = 10^{-3} mm = 10^{-4} cm = 10^{4} Å ; 1 millimicron = 10^{-6} mm = 10^{-7} cm = 10 Å ; Greek letters are often used for the notation of these units as follows : μ—micron ; mμ—millimicron (1 μ = 1000 mμ = 10,000 Å).

The International System of Units (SI) was introduced in 1963, in accordance with which the application of the terms nanometer and micrometer were suggested for measuring wavelengths in the optical frequencies (1 nm = 10^{-9} m = 10^{-6} nm and 1 μ = 10^{3} nm).

In some cases the frequency scale may be used instead of the wavelength scale (scale of wave numbers). The quantity that is the inverse of wavelength λ is called the wave number ν. The unit in the scale of wave numbers is cm^{-1}. The application of the wave number scale provides a more detailed picture of the spectral energy distribution in the shortwave region of the spectrum being examined.

In order to obtain the quantitative characteristics of the radiation field in SI units the use of *energy luminosity* has been suggested, which was earlier known as the *intensity of emission* (cal/cm^2·min·ster) as well as the *surface density of radiation flux*, which in actinometry corresponds to radiation flux or intensity of radiation.

In SI units the radiation flux is measured in W/m^2, but it is convenient to use this unit for the measurement of the spectral flux in narrow section of the spectrum.

The World Meteorological Organization recommended the use of large units in actinometry such as 1 milliwatt/cm^2 (mW/cm^2 = 10 W/m^2). Obviously the earlier unit of flux will be in use for some time and 1 cal/cm^2·min = 69.76 mW/cm^2 = 10^{3} cal/cm^2·min.

In foreign literature use is often made of a quantity equal to 1 cal/cm^2, called "langley" and denoted as "ly".

If a high resolution solar spectrum is observed beyond the limits of the atmosphere, then it appears that solar radiation consists of a collec-

tion of emission lines and Fraunhofer absorption lines, in the radiation continuum. Although solar radiation varies significantly in distinct spectral regions, it is assumed that the general integrated flux changes only a little ($\pm$ 3%).

During transmission of radiation through the atmosphere the spectral distribution changes radically in all regions of the spectrum, except in distinct narrow segments.

The energy distribution of solar radiation as a function of wave numbers is given in Fig. 5.1 [32] beyond the atmosphere (1) and at sea level (2), tracing the energy distributions in the spectrum of scattered radiation for a clear (4) and cloudy (3) sky.

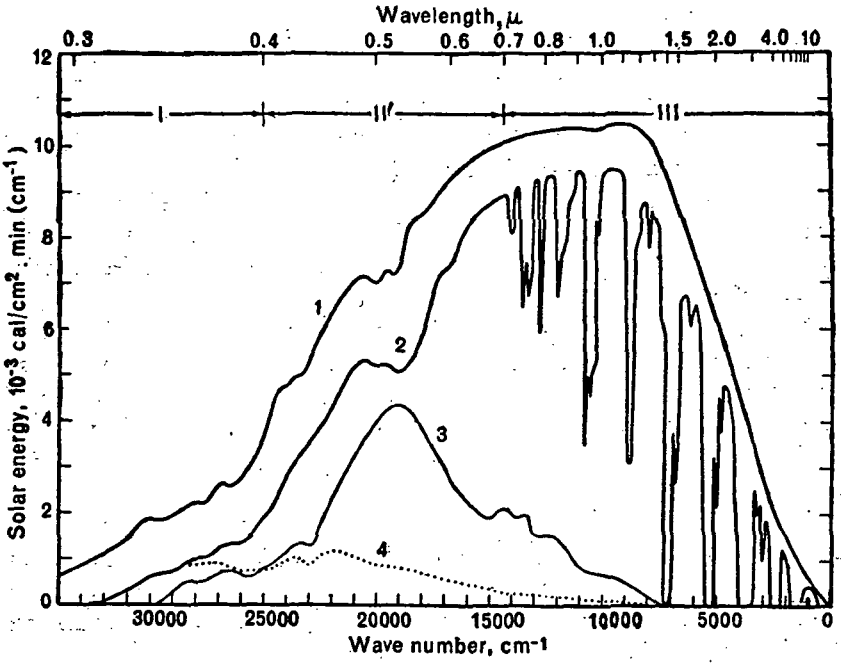

Fig. 5.1. Energy distribution in the spectrum of solar radiation in wave numbers beyond the atmosphere (1), at sea level (2), in the spectrum of scattered radiation of a cloudy (3) and clear (4) sky [21].

The spectral distribution in the frequency scale differs from the usual form of the intensity distribution curve of radiation in the wavelength scale. The maximum spectral intensity of solar radiation can be identified for different wavelengths in these cases. The width of the maximum in spectral distributions is likewise different. However, the same amount of energy is included within a specific wavelength interval and the interval of wave numbers corresponding to it. This situation allows us to use in

practice either form of spectral distribution. It should be mentioned that yet another form of spectral distribution can be used. In this case the intensity of radiation can be determined for identical intervals of dimensionless quantities $\frac{d\lambda}{\lambda} = \frac{d\nu}{\nu}$ [13].

As already stated, direct solar radiation reaches sea level considerably weakened and with its energy distribution greatly changed. The change in the composition of solar radiation may be caused chiefly by the following three factors :

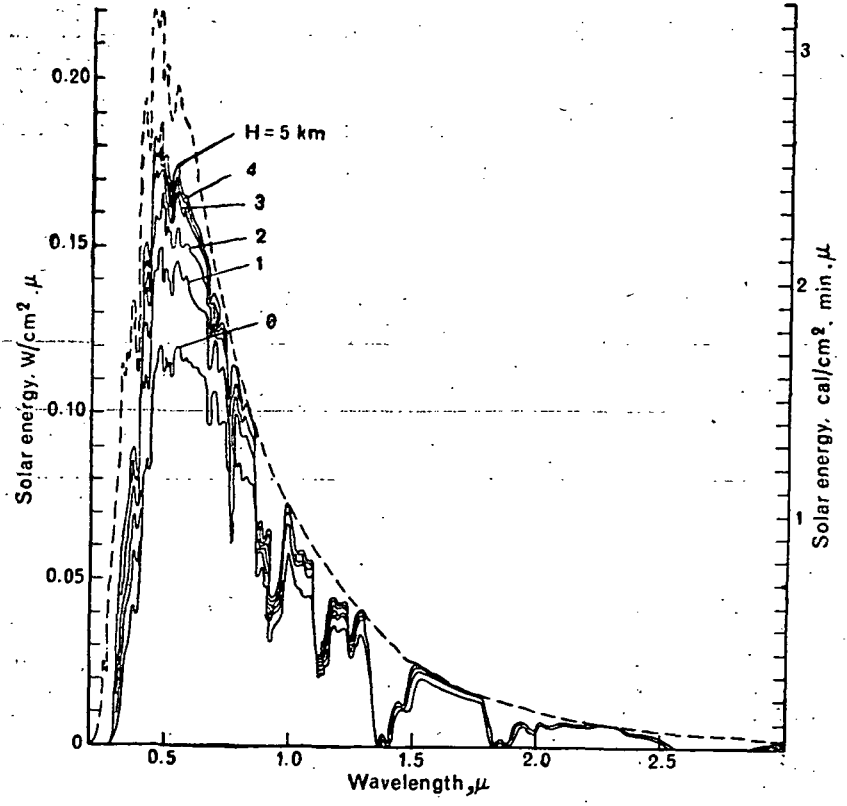

Fig. 5.2. Spectral distribution of direct solar radiation outside the atmosphere and at several levels in the troposphere for air mass $m = 1.5$ containing 10 mm of precipitated water, 0.35 cm of ozone, aerosol concentration of 200 cm^{-3} at the earth's surface [38]. Integrated flux outside the atmosphere equals 2.00 cal/cm² · min, at the altitude of 5 km—1.51 cal/cm² · min; at the altitude of 4 km—1.48 cal/cm² · min; at the altitude of 3 km—1.45 cal/cm² · min; at the altitude of 2 km—1.38 cal/cm² . min; at the altitude of 1 km—1.28 cal/cm² . min; and at sea level—1.07 cal/cm² . min.

(1) molecular scattering ;
(2) aerosol scattering by large particles ; and
(3) selective absorption in water vapor and ozone.

The variations in spectral fluxes of direct solar radiation for penetration in the atmosphere are shown in Fig. 5.2 [38]. These values were obtained through computations based on Elterman's attenuation model [36].

The computations of the values of spectral fluxes (in millicalories) for different atmospheric masses at heights of 0.5 ; 3.0 ; 6.5 ; 9.0 and 20.0 km are given in Table 5.1 [1]. The data were obtained from computations carried out for a model with parallel planes which is closer to average real atmosphere τ_0 $(\lambda_0)=0.3$; $\lambda_0=550$ nm, $u'_{H_2O}=2.1$ cm] ; $u'_{CO_2}=264$ cm ; $u'_{O_3}=0.25$ cm, visual range D $(\lambda_0=20$ km). Such a model has been named the mean standard radiation model of the atmosphere. Results of calculations for this model show close correspondence to average experimental values.

Table 5.1 Energy distribution in the spectrum of direct solar radiation at different levels in mcal/cm² · min in the case of standard radiation model of atmosphere [τ_0 $(\lambda_0)=0.3$, $u'=2.1$ cm]

λ_1-λ_2, μ	m						
	1.0	1.5	2.0	2.5	3.0	4.0	6.0
			$H=0.5$ km				
0.29-0.30	0.0	0.0	0.0	0.0	0.0	0.0	0.0
0.30-0.32	3.2	1.2	0.5	0.0	0.0	0.0	0.0
0.32-0.34	11.0	6.5	3.9	2.3	1.4	0.5	0.0
0.34-0.36	15.2	10.3	6.9	4.7	3.2	1.4	0.2
0.36-0.38	18.9	13.6	9.8	7.0	5.1	2.6	0.7
0.38-0.40	20.0	15.2	11.5	8.8	6.6	3.8	1.3
0.29-0.40	68.3	46.8	32.6	22.8	16.3	8.3	2.2
0.40-0.44	69.1	55.4	44.4	35.6	28.5	18.4	7.6
0.44-0.48	87.5	73.6	61.8	52.0	43.7	30.8	15.3
0.48-0.52	85.5	74.1	64.2	55.6	48.2	36.2	20.4
0.52-0.56	86.1	75.9	66.8	58.7	51.8	40.2	24.2
0.56-0.60	85.7	76.2	67.8	60.5	53.8	42.7	26.8
0.60-0.64	80.0	72.3	68.9	59.1	53.5	43.6	29.1
0.64-0.68	78.0	71.4	65.8	60.4	55.6	47.0	33.6
0.68-0.70	37.0	34.5	31.9	29.7	27.6	23.8	17.7
0.40-0.70	608.9	533.4	471.6	411.6	362.7	282.7	174.7
0.70-0.74	65.3	60.3	55.7	51.5	47.7	41.0	30.4
0.74-0.79	78.0	73.5	69.2	65.2	61.4	54.5	42.8
0.79-0.84	65.9	61.7	57.8	54.2	50.9	45.0	35.3

Table 5.1—*Contd.*

λ_1-λ_2, μ	m						
	1.0	1.5	2.0	2.5	3.0	4.0	6.0
			H=0.5 km				
0.84-0.86	24.4	23.2	22.1	21.0	19.9	18.0	14.7
0.86-0.99	121.3	111.2	102.2	94.8	88.0	76.2	57.9
0.99-1.03	37.8	36.3	34.9	33.5	32.2	29.7	25.2
1.03-1.23	127.4	117.6	109.4	102.1	95.5	84.0	66.2
1.23-1.25	13.1	12.7	12.3	12.0	11.6	10.8	9.6
1.25-1.38	29.1	24.6	21.6	19.1	17.1	14.0	9.8
1.38-1.50	20.7	17.5	15.4	13.7	12.3	10.0	7.1
1.50-1.53	4.5	3.8	3.3	2.9	2.7	2.2	1.5
1.53-1.54	1.6	1.4	1.2	1.1	1.0	0.8	0.5
1.54-1.67	38.4	37.5	36.6	35.6	34.7	33.1	30.0
1.67-1.70	7.6	7.5	7.3	7.1	7.0	6.7	6.1
1.70-1.92	21.7	19.5	18.1	16.8	15.8	14.0	11.6
1.92-2.08	9.6	8.1	7.1	6.4	5.7	4.8	3.7
2.08-2.10	2.4	2.2	2.1	1.9	1.8	1.7	1.5
2.10-2.27	19.4	19.0	18.7	18.4	18.1	17.5	16.4
2.27-2.63	6.9	5.6	4.7	4.1	3.5	2.7	1.5
2.63-2.87	1.0	0.7	0.6	0.4	0.4	0.2	0.1
2.87-3.00	1.2	1.0	0.9	0.8	0.6	0.5	0.3
3.00-3.57	5.8	3.5	1.6	0.0	0.0	0.0	0.0
3.57-4.00	6.9	6.8	6.7	6.7	6.6	6.5	6.2
0.70-4.00	710.0	655.2	609.5	569.3	534.5	473.9	378.4
0.29-4.00	1387	1235	1114	1004	914	765	555
			H=3.0 km				
0.29-0.30	0.1	0.0	0.0	0.0	0.0	0.0	0.0
0.30-0.32	4.8	2.4	1.1	0.6	0.3	0.1	0.0
0.32-0.34	15.2	10.6	7.5	5.3	3.7	1.8	0.5
0.34-0.36	19.9	15.4	11.9	9.2	7.1	4.2	1.5
0.36-0.38	23.9	19.3	15.7	12.7	10.3	6.8	2.9
0.38-0.40	24.6	20.6	17.4	14.8	12.2	8.7	4.3
0.29-0.40	88.5	68.3	53.6	42.6	33.6	21.6	9.2
0.40-0.44	82.0	71.6	62.6	54.6	47.7	36.3	21.2
0.44-0.48	100.7	90.6	81.6	73.6	66.3	53.7	35.3
0.48-0.52	96.4	88.7	81.7	75.1	69.1	58.4	41.8
0.52-0.56	95.6	88.6	82.3	76.4	70.8	60.9	45.2
0.56-0.60	94.0	87.6	81.6	76.1	70.9	61.7	46.6
0.60-0.64	87.2	82.4	77.5	73.1	69.0	61.4	48.5
0.64-0.68	83.8	80.0	76.4	72.9	69.6	63.4	52.6
0.68-0.70	39.7	38.3	36.8	35.4	34.0	31.5	26.9
0.40-0.70	679.4	627.8	580.5	537.2	497.4	427.3	318.1
0.70-0.74	71.3	68.8	65.9	63.7	61.3	56.8	48.8
0.74-0.79	83.0	80.6	78.2	75.9	73.7	69.5	61.8

Table 5.1—*Contd.*

λ_1-λ_2, μ	*m*						
	1.0	1.5	2.0	2.5	3.0	4.0	6.0
0.79-0.84	72.0	69.6	67.1	65.4	63.4	59.7	53.2
0.84-0.86	25.7	25.1	24.5	23.9	23.4	22.3	20.2
0.86-0.99	139.5	133.8	126.1	124.2	120.2	112.0	98.7
0.99-1.03	39.5	38.8	38.1	37.4	36.7	35.3	32.8
1.03-1.23	145.6	140.6	133.7	131.5	127.6	120.6	108.5
1.23-1.25	13.6	13.4	13.2	13.0	12.8	12.5	11.8
1.25-1.38	42.9	38.6	35.4	33.0	31.0	27.8	23.2
1.38-1.50	30.3	27.2	23.5	23.2	21.7	19.6	16.3
1.50-1.53	6.4	5.8	5.1	5.0	4.7	4.2	3.6
1.53-1.54	2.3	2.1	1.8	1.8	1.7	1.5	1.2
1.54-1.67	39.6	39.1	38.6	38.1	37.7	36.8	35.1
1.67-1.70	7.8	7.8	7.7	7.6	7.5	7.4	7.1
1.70-1.92	29.3	26.1	23.8	23.6	22.6	21.1	18.9
1.92-2.08	13.7	11.8	10.8	9.8	9.1	8.1	6.6
2.08-2.10	2.6	2.4	2.3	2.2	2.2	2.1	1.8
2.10-2.27	19.7	19.6	19.4	19.3	19.2	18.9	18.4
2.27-2.63	11.0	10.2	8.3	7.7	7.0	6.2	4.9
2.63-2.87	1.9	1.6	1.3	1.1	0.9	0.8	0.5
2.87-3.00	1.9	1.8	1.6	1.5	1.4	1.2	0.9
3.00-3.57	10.8	9.7	8.6	7.8	7.0	5.7	3.4
3.57-4.00	6.9	6.9	6.9	6.9	6.8	6.8	6.7
0.70-4.00	817.3	781.4	741.9	723.6	699.6	656.9	584.4
0.29-4.00	1585	1478	1376	1303	1231	1106	912
			H=6.5 km				
0.29-0.30	0.1	0.0	0.0	0.0	0.0	0.0	0.0
0.30-0.32	6.7	3.9	2.2	1.2	0.7	0.2	0.0
0.32-0.34	19.2	15.2	12.0	9.5	7.5	4.7	1.8
0.34-0.36	24.0	20.4	17.4	14.8	12.5	9.1	4.7
0.36-0.38	27.9	24.5	21.4	18.8	16.5	12.6	7.4
0.38-0.40	27.9	25.1	22.4	20.1	18.0	14.5	9.4
0.29-0.40	105.8	89.1	75.4	64.4	55.2	41.1	23.3
0.40-0.44	90.8	83.5	76.9	70.6	64.9	54.9	39.2
0.44-0.48	109.0	102.1	95.5	89.6	83.9	73.7	56.9
0.48-0.52	102.7	97.3	92.4	87.7	83.3	74.8	60.7
0.52-0.56	100.7	95.8	91.3	87.2	83.0	75.3	62.0
0.56-0.60	98.2	93.6	89.3	85.1	81.2	73.8	61.0
0.60-0.64	90.4	87.0	83.5	80.3	77.1	71.2	60.7
0.64-0.68	86.7	84.0	81.6	79.2	76.8	72.4	64.1
0.68-0.70	40.9	40.0	39.0	38.1	37.2	35.4	32.2
0.40-0.70	719.4	683.3	649.5	617.8	587.4	531.5	436.8
0.70-0.74	75.2	73.5	71.9	70.3	68.8	65.9	60.6
0.74-0.79	85.0	83.5	82.0	80.6	79.2	76.5	71.4

Table 5.1—*Contd.*

λ_1-λ_2, μ	*m*						
	1.0	1.5	2.0	2.5	3.0	4.0	6.0
				H=6.5 km			
0.79-0.84	74.9	73.6	72.5	71.2	70.1	67.8	63.7
0.84-0.86	26.3	25.9	25.6	25.2	24.9	24.2	23.0
0.86-0.99	150.2	147.3	144.6	142.1	139.6	135.0	126.7
0.99-1.03	40.1	39.7	39.3	38.9	38.5	37.7	36.2
1.03-1.23	156.7	154.0	151.8	149.9	147.6	143.6	136.4
1.23-1.25	13.8	13.7	13.6	13.5	13.3	13.1	12.7
1.25-1.38	59.6	56.0	53.8	51.5	49.0	46.4	41.4
1.38-1.50	42.0	39.6	37.9	36.3	34.5	32.9	29.1
1.50-1.53	9.0	8.4	8.1	7.7	7.4	7.1	6.3
1.53-1.54	3.2	3.0	2.9	2.8	2.7	2.5	2.2
1.54-1.67	40.2	39.9	39.5	39.3	39.0	38.4	37.4
1.67-1.70	7.9	7.9	7.8	7.8	7.8	7.7	7.5
1.70-1.92	36.5	34.7	33.3	32.2	31.2	29.8	27.4
1.92-2.08	17.8	16.6	15.9	15.0	14.4	13.2	11.4
2.08-2.10	2.8	2.7	2.7	2.5	2.5	2.4	2.2
2.10-2.27	19.8	19.8	19.7	19.6	19.5	19.4	19.1
2.27-2.63	16.8	15.4	14.6	13.9	13.3	12.3	11.0
2.63-2.87	3.5	3.0	2.6	2.4	2.2	1.9	1.4
2.87-3.00	2.9	2.7	2.6	2.5	2.4	2.1	1.9
3.00-3.57	14.0	13.5	13.2	12.8	12.5	11.9	11.0
3.57-4.00	7.0	6.9	6.9	6.9	6.9	6.9	6.8
0.70-4.00	905.2	881.3	862.8	844.9	827.3	798.7	746.8
0.29-4.00	1730	1654	1588	1527	1470	1371	1207
				H=9.0 km			
0.29-0.30	0.2	0.0	0.0	0.0	0.0	0.0	0.0
0.30-0.32	8.0	5.0	3.1	1.9	1.2	0.5	0.0
0.32-0.34	21.8	18.3	15.4	12.9	10.9	7.7	3.9
0.34-0.36	26.7	23.8	21.2	19.0	17.0	13.5	8.6
0.36-0.38	30.4	27.7	25.3	23.2	21.1	17.7	12.3
0.38-0.40	30.0	27.9	25.9	24.1	22.4	19.3	14.4
0.29-0.40	117.1	102.7	90.9	81.1	72.6	58.7	39.2
0.40-0.44	96.1	91.1	86.1	81.4	77.1	68.9	55.3
0.44-0.48	113.9	109.2	104.7	100.3	96.1	88.2	74.4
0.48-0.52	106.3	102.7	99.1	95.6	92.3	86.1	74.8
0.52-0.56	103.9	100.6	97.3	94.1	91.0	85.3	74.7
0.56-0.60	100.9	97.6	94.0	91.1	88.0	82.3	71.8
0.60-0.64	92.6	89.9	87.4	85.0	82.6	78.0	69.6
0.64-0.68	88.2	86.5	84.7	83.0	81.3	77.8	71.9
0.68-0.70	41.7	41.2	40.6	40.0	39.4	38.3	36.2
0.40-0.70	743.6	718.8	693.9	670.5	647.8	604.9	528.7
0.70-0.74	76.9	75.9	74.9	74.0	73.1	71.3	68.0

Table 5.1—*Contd.*

λ_1-λ_2, μ	m						
	1.0	1.5	2.0	2.5	3.0	4.0	6.0
			H=9.0 km				
0.74-0.79	86.4	85.6	84.9	84.1	83.3	81.9	79.0
0.79-0.84	76.4	75.8	75.1	74.4	73.9	72.6	70.4
0.84-0.86	26.6	26.4	26.2	26.1	25.9	25.5	24.8
0.86-0.99	154.2	153.0	151.8	150.5	149.3	146.9	142.4
0.99-1.03	40.5	40.3	40.1	39.9	39.7	39.2	38.4
1.03-1.23	160.4	159.2	158.3	157.4	156.1	154.0	150.0
1.23-1.25	13.9	13.9	13.8	13.7	13.7	13.6	13.4
1.25-1.38	66.3	63.8	62.7	61.5	60.4	59.1	55.6
1.38-1.50	47.0	45.2	44.4	43.4	42.6	41.7	39.3
1.50-1.53	10.0	9.6	9.5	9.3	9.2	9.0	8.4
1.53-1.54	3.6	3.5	3.5	3.4	3.3	3.2	3.0
1.54-1.67	40.6	40.5	40.2	40.1	40.0	39.7	39.2
1.67-1.70	8.0	7.9	7.9	7.9	7.9	7.8	7.8
1.70-1.92	41.7	40.8	39.7	38.8	37.9	36.5	34.7
1.92-2.08	20.9	20.1	19.3	18.7	18.1	17.1	15.8
2.08-2.10	2.8	2.8	2.7	2.7	2.7	2.6	2.4
2.10-2.27	19.9	19.9	19.8	19.8	19.8	19.7	19.5
2.27-2.63	21.7	20.0	19.1	18.4	17.8	16.9	15.6
2.63-2.87	5.2	4.4	3.9	3.8	3.4	3.0	2.5
2.87-3.00	3.8	3.5	3.3	3.2	3.1	2.9	2.7
3.00-3.57	15.1	14.8	14.6	14.4	14.3	13.9	13.5
3.57-4.00	7.0	7.0	7.0	7.0	7.0	6.9	6.9
0.70-4.00	948.9	933.9	922.7	912.5	902.5	885.0	853.3
0.29-4.00	1810	1755	1708	1664	1623	1549	1421
			H=20.0 km				
0.29-0.30	0.4	0.0	0.0	0.0	0.0	0.0	0.0
0.30-0.32	11.7	8.8	6.6	5.0	3.8	2.2	0.7
0.32-0.34	27.3	25.8	24.3	22.8	21.6	19.2	15.1
0.34-0.36	31.6	30.8	29.9	29.2	28.4	26.9	24.1
0.36-0.38	34.9	34.2	33.5	32.9	32.2	30.9	28.5
0.38 0.40	33.7	33.1	32.6	32.1	31.5	30.5	28.5
0.29-0.40	139.6	132.7	126.9	122.0	117.5	109.7	96.9
0.40-0.44	104.9	103.7	102.4	101.3	100.1	97.6	93.1
0.44-0.48	121.5	120.3	119.2	117.9	116.7	114.4	110.0
0.48-0.52	111.9	110.9	110.0	108.9	108.0	106.0	102.4
0.52-0.56	108.4	107.0	105.7	104.6	103.2	100.9	96.1
0.56-0.60	104.7	103.0	101.5	99.9	98.5	95.4	89.7
0.60-0.64	95.6	94.3	93.2	92.1	90.9	88.6	84.4
0.64-0.68	90.6	89.8	89.3	88.5	88.0	86.6	84.1
0.68-0.70	42.7	42.5	42.3	42.1	42.0	41.7	40.9
0.40-0.70	780.3	771.5	763.6	755.3	747.4	731.2	700.7

Table 5.1—*Contd.*

λ_1-λ_2, μ	*m*						
	1.0	1.5	2.0	2.5	3 0	4.0	6.0
			H=20.0 km				
0.70-0.74	78.8	78.7	78.5	78.4	78.3	78.1	77.6
0.74-0.79	87.8	87.7	87.6	87.6	87.5	87.3	86.9
0.79-0.84	77.8	77.8	77.7	77.6	77.5	77.4	77.1
0.84-0.86	27.0	26.9	26.9	26.9	26.9	26.8	26.7
0.86-0.99	158.8	158.7	158.7	158.7	158.5	157.7	157.1
0.99-1.03	41.0	40.9	40.9	40.9	40.9	40.7	40.5
1.03-1.23	164.1	163.9	163.7	163.7	163.3	163.0	162.4
1.23-1.25	14.0	14.0	14.0	14.0	14.0	14.0	14.0
1.25-1.38	71.4	71.2	70.8	70.4	70.2	69.9	69.1
1.38-1.50	50.6	50.4	50.2	49.9	49.7	49.3	48.7
1.50-1.53	10.8	10.7	10.7	10.6	10.6	10.5	10.4
1.53-1.54	3.9	3.9	3.9	3.8	3.8	3.8	3.7
1.54-1.67	40.8	40.8	40.8	40.8	40.7	40.7	40.6
1.67-1.70	8.0	8.0	8.0	8.0	8.0	8.0	8.0
1.70-1.92	45.7	45.4	45.2	44.9	44.7	44.4	43.8
1.92-2.08	23.4	23.0	22.7	22.5	22.2	21.8	21.1
2.08-2.10	2.9	2.9	2.8	2.8	2.8	2.8	2.7
2.10-2.27	20.0	20.0	20.0	20.0	20.0	20.0	20.0
2.27-2.63	27.2	26.9	26.5	26.1	25.9	25.4	24.6
2.63-2.87	7.6	7.0	6.5	6.2	5.9	5.4	4.8
2.87-3.00	4.7	4.6	4.6	4.5	4.5	4.4	4.2
3.00-3.57	15.8	15.7	15.7	15.6	15.6	15.5	15.3
3.57-4.00	7.0	7.0	7.0	7.0	7.0	7.0	7.0
0.70-4:00	989.1	986.1	983.4	980.9	978.5	973.9	966.3
0.29-4.00	1909	1890	1874	1858	1843	1815	1764

Spectral flux, measured at sea level, to a great extent depends on the state of the mass of air and on the length of the optical path of solar rays. The influence of the varying atmospheric mass is illustrated in Figs. 5.3 and 5.4.

The effect of aerosol on the spectral distribution of flux of direct solar radiation for unit air mass containing 10 mm of precipitated water and 0.35 cm of ozone is shown in Fig. 5.5.

The computed values of spectral fluxes from solar emission at sea level for the mean standard radiation model of the atmosphere are given in Table 5.2 [1].

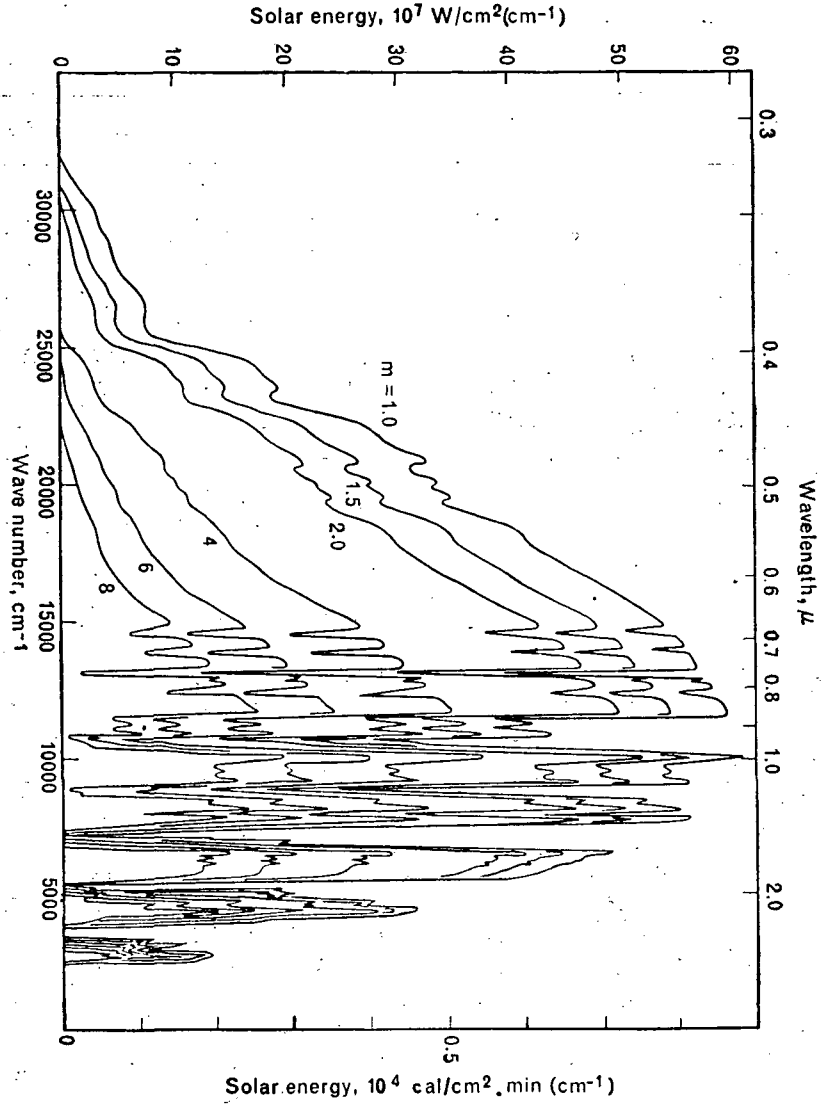

Fig. 5.3. Spectral energy distribution of direct solar radiation at sea level for different atmospheric masses in the scale of wave numbers [38].
For $m=1$ the integrated flux $S=1.24$ cal/cm^2 · min; for $m=1.5$, $S=1.08$ cal/cm^2 · min; for $m=2$, $S=0.917$ cal/cm^2 · min; for $m=4$, $S=0.533$ cal/cm^2 · min; for $m=6$, $S=0.344$ cal/cm^2 · min; and for $m=8$, $S=0.218$ cal/cm^2 · min.

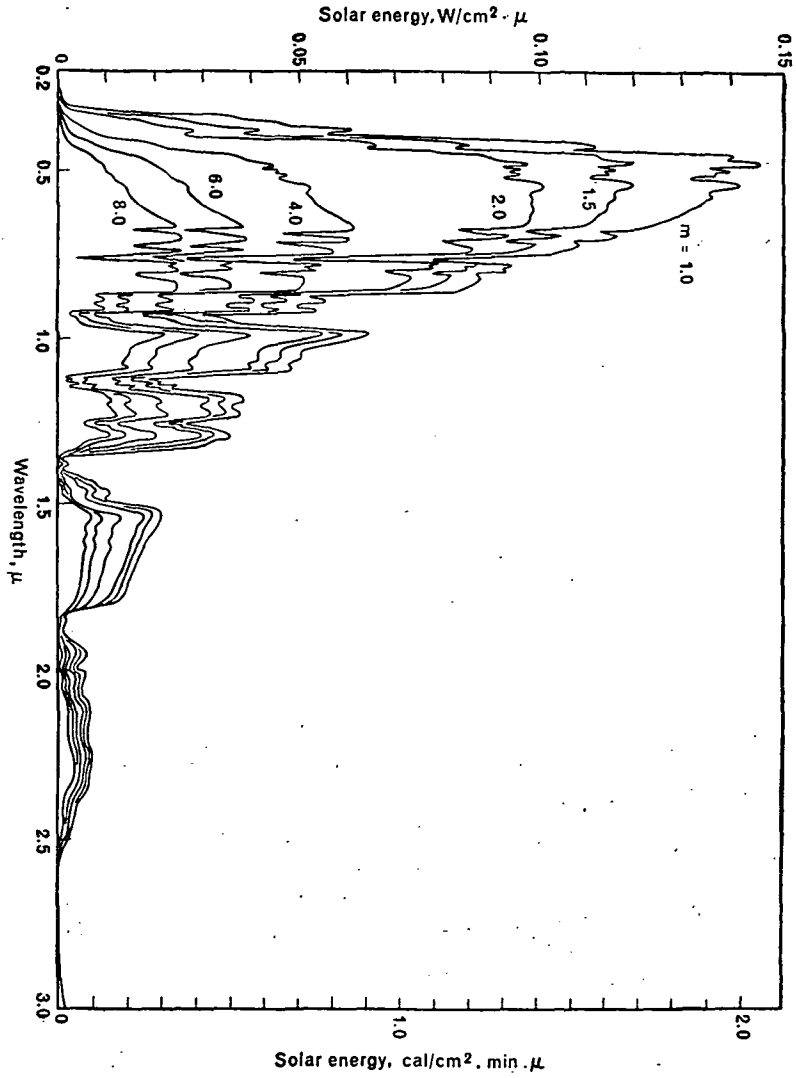

Fig. 5.4. Spectral energy distribution of direct solar radiation depending on atmospheric mass (in the scale of wavelength) [38].

Amount of attenuating components is similar to that indicated in Fig. 5.2.

For notation see Fig. 5.3.

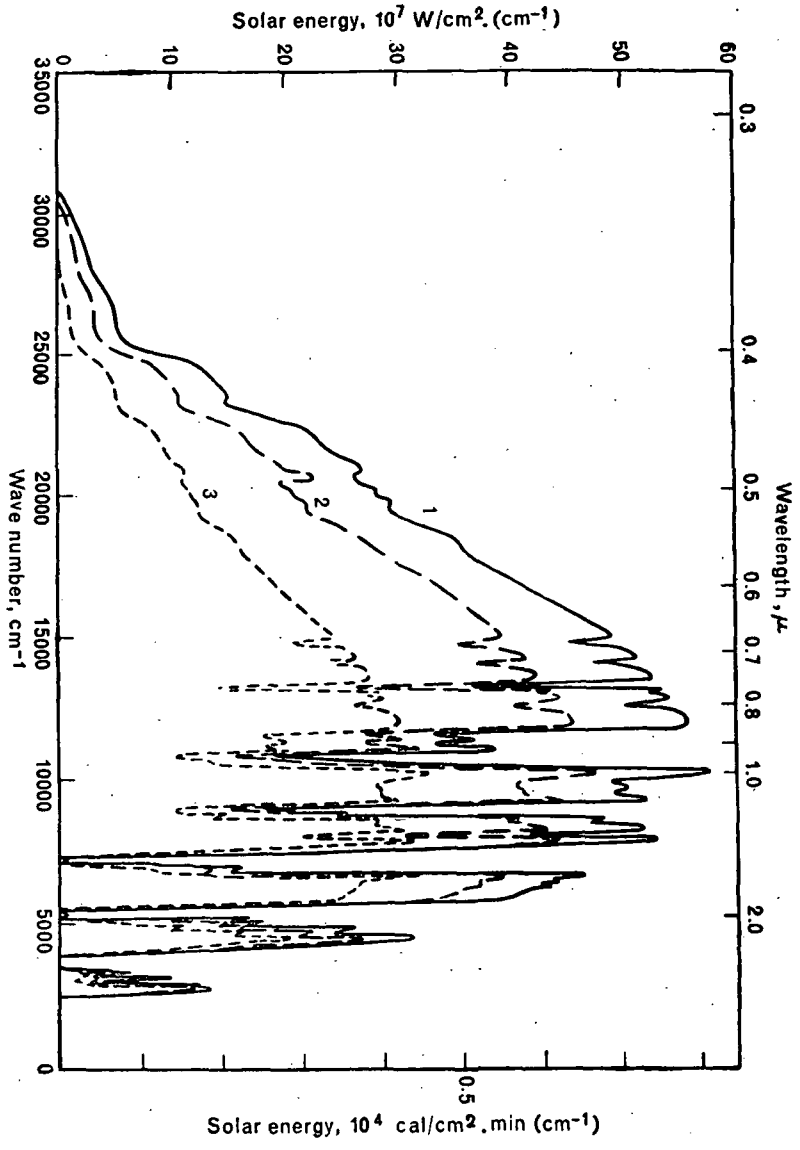

Fig. 5.5. The effect of aerosol on spectral flux of direct solar radiation (in the scale of wave numbers).

For the path of ray $m=1.5$. The amount of attenuating components is similar to that indicated in Fig. 5.2.

1) $N=200$ cm^{-3}, $S=1.08$ cal/cm^2 · min; 2) $N=400$ cm^{-3}, $S=0.847$ cal/cm^2 · min; and 3) $N=800$ cm^{-3}, $S=0.536$ cal/cm^2 · min.

Table 5.2 Spectral energy distribution of direct solar radiation at the earth's surface : (mcal/cm² . min) in case of mean standard radiation model of atmosphere depending on atmospheric mass [1]

λ_1-λ_2, μ	m						
	1.0	1.5	2.0	2.5	3.0	4.0	6.0
	$\tau_0(\lambda_0) = 0.3$, $u' = 2.1$ cm						
0.29-0.30	0.0	0.0	0.0	0.0	0.0	0.0	0.0
0.30-0.32	2.6	0.9	0.3	0.1	0.0	0.0	0.0
0.32-0.34	9.2	5.0	2.8	1.5	0.8	0.2	0.0
0.34-0.36	13.1	8.2	5.1	3.2	2.0	0.8	0.1
0.36-0.38	16.5	11.1	7.4	5.0	3.4	1.5	0.3
0.38-0.40	17.6	12.6	8.9	6.4	4.5	2.3	0.6
0.29-0.40	59.0	37.8	24.5	16.2	10.7	4.8	1.0
0.40-0.44	61.8	46.9	35.5	26.9	20.4	11.7	3.9
0.44-0.48	79.3	63.5	50.7	40.5	32.5	20.8	8.5
0.48-0.52	78.4	65.0	53.9	44.8	37.1	25.5	12.2
0.52-0.56	79.6	67.5	57.1	48.4	41.0	29.4	15.2
0.56-0.60	79.6	68.3	58.7	50.4	43.3	31.9	17.4
0.60-0.64	74.9	65.5	57.3	50.0	43.7	33.4	19.5
0.64-0.68	73.0	64.9	57.8	51.5	45.8	36.4	22.9
0.68-0.70	35.0	31.5	28.4	25.6	23.0	18.8	12.4
0.40-0.70	561.6	473.1	399.4	338.1	286.8	207.9	112.0
0.70-0.74	74.0	67.6	49.3	45.2	40.0	32.4	21.6
0.74-0.79	73.9	67.8	62.1	56.9	52.2	43.9	31.0
0.79-0.84	62.1	56.5	51.5	47.1	43.0	36.0	25.5
0.84-0.86	23.3	21.6	20.1	18.7	17.3	14.9	11.1
0.86-0.99	112.6	100.4	89.9	81.2	72.8	59.8	40.7
0.99-1.03	36.2	34.0	31.9	30.0	28.2	24.9	19.4
1.03-1.23	119.2	107.2	97.4	88.7	81.0	68.0	48.8
1.23-1.25	12.7	12.2	11.6	11.0	10.5	9.6	7.9
1.25-1.38	25.7	21.4	18.1	15.6	13.7	10.5	6.7
1.38-1.50	18.2	15.1	12.8	11.1	9.8	7.5	4.8
1.50-1.53	3.9	3.3	2.8	2.4	2.1	1.7	1.1
1.53-1.54	1.4	1.2	1.0	0.8	0.8	0.6	0.4
1.54-1.67	37.5	36.0	34.7	33.4	32.2	29.8	25.7
1.67-1.70	7.5	7.2	7.0	6.8	6.5	6.1	5.3
1.70-1.92	20.0	17.7	16.1	14.7	13.6	11.9	8.9
1.92-2.08	8.7	7.2	6.2	5.4	4.9	4.0	3.0
2.08-2.10	2.3	2.1	2.0	1.8	1.7	1.5	1.2

Table 5.2—*Contd.*

λ_1-λ_2, μ	m						
	1.0	1.5	2.0	2.5	3.0	4.0	6.0
	$\tau_0(\lambda_0)=0.3$, $\mu'=2$-1 em						
2.10-2.27	19.0	18.5	18.1	17.6	17.2	16.3	14.7
2.27-2.63	5.9	4.7	3.8	3.1	2.6	1.7	0.8
2.63-2.87	0.9	0.6	0.5	0.4	0.3	0.2	0.1
2.87-3.00	1.1	0.9	0.6	0.5	0.4	0.3	0.2
3.00-3.57	4.2	1.5	0.0	0.0	0.0	0.0	0.0
3.57-4.00	6.8	6.7	6.6	6.5	6.4	6.2	5.8
0.70-4.00	664.5	598.8	544.1	498.9	457.2	387.8	284.7
0.29-4.00	1285	1110	968	853	755	600	398
$f_3(m)\frac{S_m}{S_{id}}$	7	7	8	7	6	6	5
S_m	1278	1103	960	846	749	594	383

REMARKS: $f_3(m)\frac{S_m}{S_{id}}$ —correction in the absorption by permanent gases; S_m — integral flux of solar radiation in the region 0.29-4.00 μ.

The data on spectral fluxes of direct solar radiation at sea level, represented in Figs. 5.3 and 5.4 and in Table 5.2, were obtained on the basis of computations for any model of the atmosphere. However, the values of spectral fluxes of direct solar radiation under natural conditions may vary considerably from mean theoretical magnitudes, especially in the ultraviolet and infrared spectral ranges being examined (0.29-3.00 μ). N. N. Kalitin, E. A. Lapukhin and M. P. Garadzhi [7, 11, 19] experimentally investigated the most characteristic optical states of the atmosphere while studying the spectral distribution of direct solar radiation.

The measurements of points of direct solar fluxes given in the ultraviolet region of the spectrum (300-400 nm) are given in Table 5.3 [7]. Measurements were conducted in all seasons of the period 1962-1965. The data on spectral fluxes, obtained through experiments, were divided into four groups, in agreement with the four ranges of values for coefficients

Table 5.3 Mean values of direct ultraviolet radiation (W/m^2) for different coefficients of atmospheric transparency ($\Delta\lambda=10$ nm) [7]

Altitude of the sun, deg	Coefficient of transparency P_3											
	0.45-0.55	0.55-0.65	0.65-0.75	0.75-0.85	0.45-0.55	0.55-0.65	0.65-0.75	0.75-0.85	0.45-0.55	0.55-0.65	0.65-0.75	0.75-0.85
	$\lambda=310$ nm				$\lambda=320$ nm				$\lambda=330$ nm			
5	0	0	0	0	0	0	0	0	0	0	0	0
10	0	0	0	0	0	0	0	0.014	0	0	0	0.070
15	0	0	0	0.007	0	0	0.042	0.12	0	0	0.10	0.35
20	0	0	0	0.042	0	0.007	0.14	0.24	0	0.070	0.35	0.59
25	0	0	0.035	0.084	0	0.084	0.25	0.38	0	0.24	0.56	0.87
30	0	0.035	0.077	0.14	0	0.17	0.37	0.59	0	0.38	0.80	1.18
35	0	0.070	0.13	0.21	0.007	0.26	0.50	0.82	0.14	0.59	1.05	1.50
40	0.014	0.10	0.17	0.28	0.105	0.36	0.66	1.09	0.28	0.77	1.32	1.85
45	0.056	0.15	0.24	0.36	0.20	0.48	0.85	1.30	0.45	0.98	1.64	2.23
50	0.084	0.19	0.32	0.47	0.31	0.61	1.07	1.45	0.63	1.18	1.99	2.68
55	0.12	0.23	0.43	0.52	0.43	0.75	1.32	1.54	0.80	1.39	2.37	3.21
	$\lambda=340$ nm				$\lambda=350$ nm				$\lambda=360$ nm			
5	0	0	0	0	0	0	0	0	0	0	0	0
10	0	0	0	0.24	0	0	0.07	0.28	0	0	0.10	0.42
15	0	0	0.21	0.59	0	0	0.35	0.66	0	0	0.56	0.98
20	0	0.070	0.49	0.94	0	0.24	0.66	1.12	0	0.28	0.98	1.53
25	0	0.31	0.77	1.36	0	0.49	1.05	1.64	0	0.59	1.38	2.09
30	0	0.59	1.12	1.78	0.17	0.77	1.46	2.16	0.24	0.91	1.78	2.68
35	0.21	0.87	1.50	2.20	0.31	1.08	1.88	2.72	0.45	1.25	2.23	3.28
40	0.42	1.15	1.88	2.65	0.49	1.39	2.30	3.24	0.70	1.57	2.65	3.83
45	0.63	1.39	2.30	3.07	0.73	1.67	2.79	3.73	0.91	1.95	3.14	4.36
50	0.84	1.67	2.79	3.48	0.94	1.95	3.31	4.18	1.15	2.33	3.66	4.74
55	1.05	1.88	3.28	3.80	1.18	2.20	3.87	4.53	1.39	2.75	4.32	5.05

Table 5.3—*Contd.*

Altitude of the sun, deg	Coefficient of transparency P_2							
	0.45-0.55	0.55-0.65	0.65-0.75	0.75-0.85	0.45-0.55	0.55-0.65	0.65-0.75	0.75-0.85
	λ=370 nm				λ=380 nm			
5	0	0	0	0.03	0	0	0	0.07
10	0	0	0.24	0.66	0	0	0.31	0.73
15	0	0.035	0.73	1.29	0	0.10	0.80	1.46
20	0	0.38	1.22	1.92	0	0.45	1.36	2.23
25	0.07	0.73	1.74	2.51	0	0.87	1.88	2.96
30	0.31	1.08	2.27	3.10	0.24	1.25	2.44	3.66
35	0.56	1.43	2.82	3.66	0.56	1.71	3.00	4.29
40	0.80	1.78	3.38	4.29	0.87	2.13	3.55	4.88
45	1.05	2.13	3.97	4.81	1.18	2.54	4.11	5.40
50	1.29	2.47	4.50	5.37	1.46	2.93	4.67	5.85
55	1.53	2.79	5.02	5.79	1.78	3.42	5.19	6.17
	λ=390 nm				λ=400 mm			
5	0	0	0	0.31	0	0	0	0.59
10	0	0	0.52	1.32	0	0	0.49	1.43
15	0	0.24	1.22	2.23	0	0.31	1.32	2.37
20	0	0.63	1.85	3.00	0	0.84	2.16	3.31
25	0.28	1.05	2.51	3.73	0.03	1.46	2.96	4.21
30	0.56	1.57	3.14	4.39	0.38	2.06	3.73	5.35
35	0.87	2.09	3.76	5.02	0.91	2.68	4.50	6.03
40	1.18	2.61	4.39	5.65	1.36	3.28	5.23	6.76
45	1.46	3.07	5.05	6.25	1.88	3.87	5.96	7.49
50	1.74	3.52	5.72	6.76	2.44	4.39	6.69	8.00
55	2.20	3.87	6.38	7.21	2.96	4.84	7.39	8.57

of atmospheric transparency P_2 at the time of measurements (0.45-0.55 ; 0.55-0.65 ; 0.65-0.75 ; 0.75-0.85) ; P_2 is the transparency for the mass of atmosphere, and is equal to 2.

The largest variations in spectral fluxes occur during transparency variation at low solar altitude, with a maximum change taking place in the short wavelength segment of the ultraviolet region.

The values of fluxes obtained experimentally were compared with the computed values taken from [1] for suitable optical thicknesses.

A comparison of the results of computations and experiments shows that (except for spectral range 300-320 nm) the computed data exceed the experimental on an average by 20% (Table 5.4).

Table 5.4 Spectral flux of direct solar radiation (W/m^2) in ultraviolet region according to data from observations and computations ($m=2$)

Spectral range, nm	Computations			Observations		
	$\tau_0(\lambda_0)=0.5$	$\tau_0(\lambda_0)=0.3$	$\tau_0(\lambda_0)=0.2$	$P_2=0.60$	$P_2=0.70$	$P_2=0.80$
300-320	0.14	0.21	0.35	0.14	0.28	0.42
320-340	0.98	1.95	2.72	0.77	1.46	2.38
340-360	1.88	3.56	4.88	1.53	2.93	4.40
360-380	2.86	5.16	6.97	2.16	4.40	6.27

Experimental data on the spectral structure of direct solar radiation, obtained during measurements in mountainous and plain regions of Central Asia in 1961, are given in Tables 5.4 and 5.5.

Table 5.5 shows the relative variability in solar fluxes for the four spectral ranges as a function of the solar altitude and the optical properties of air masses (six types). These types of states of air masses are characterized by different values of vapor pressure of water 'e' in millibars at the earth's surface and by the absorption coefficient of solar radiation in aerosol to that of water vapor j. The magnitude of j may be evaluated from the formula :

$$j=\frac{S_{\mathrm{Id}}-\Delta S_{\mathrm{H_2O}}-S}{\Delta S_{\mathrm{H_2O}}}\ , \tag{5.1}$$

Table 5.5 Spectral composition of direct solar radiation in a plain for different humidities and different aerosol attenuation

$h_\odot$	S cal/cm² . min	% of total radiation at λ nm				S cal/cm² . min	% of total radiation at λ nm			
		290-380	290-520	520-606	> 606		290-380	290-520	520-606	> 606
		Type I					Type II			
		n=27; j=0.67; e=6.0 mb					n=25; j=0.77; e=11.7 mb			
2	0.162	0.10	5.9	10.5	83.6	0.104	0.83	3.7	11.3	85.0
5	0.304	0.20	7.2	10.7	82.1	0.384	1.00	5.6	11.6	82.8
10	0.732	0.61	8.9	11.3	79.8	0.695	1.23	8.2	12.1	79.7
15	0.857	1.00	10.5	11.8	77.7	0.801	1.45	10.0	12.7	77.3
20	1.000	1.33	11.9	12.4	75.7	0.967	1.68	11.2	13.2	75.6
25	1.095	1.57	13.1	13.1	73.8	1.079	1.89	12.4	13.4	74.2
30	1.163	1.78	14.3	13.6	72.1	1.187	2.04	13.4	13.8	72.8
35	1.222	1.95	15.1	14.1	70.8	1.240	2.20	14.1	14.1	71.8
40	1.272	2.10	15.6	14.4	70.0	1.274	2.33	14.6	14.4	71.0
45	1.313	2.25	16.0	14.7	69.3	1.308	2.46	15.2	14.5	70.3
50	1.351	2.37	16.3	15.0	68.7	1.338	2.58	15.6	14.6	69.8
55	1.374	2.50	16.6	15.1	68.3	1.358	2.70	16.0	14.7	69.3
60	1.392	2.61	16.9	15.2	67.9	1.376	2.81	16.3	14.8	68.9
65	1.406	2.70	17.2	15.3	67.5	1.385	2.91	16.5	14.9	68.6
70	1.417	2.80	17.3	15.4	67.3	1.397	3.00	16.8	15.0	68.2
		Type III					Type IV			
		n=32; j=1.16; e=8.6 mb					n=33; j=1.15; e=17.8 mb			
2	0.100	0.37	5.9	11.8	82.3	0.026	0.51	6.1	12.9	81.0
5	0.316	0.48	7.0	12.1	81.9	0.162	0.61	7.0	13.7	79.3
10	0.571	0.69	8.6	12.6	78.8	0.407	0.82	8.5	14.8	76.7
15	0.763	0.90	10.0	13.0	75.0	0.645	1.06	10.0	15.8	74.2
20	0.905	1.15	11.4	13.4	74.2	0.794	1.31	11.8	16.4	71.2
25	1.000	1.41	12.6	13.8	73.6	0.913	1.53	13.1	16.8	70.1
30	1.091	1.68	13.8	14.1	72.1	0.995	1.72	14.0	17.0	69.0

Table 5.5—*Contd.*

$h_\odot$	S cal/cm² . min	% of total radiation at λ nm				S cal/cm² . min	% of total radiation at λ nm			
		290-380	290-520	520-606	> 606		290-380	290-520	520-606	> 606
35	1.155	1.91	14.6	14.3	71.1	1.058	1.90	14.6	17.2	68.2
40	1.206	2.12	15.2	14.5	70.3	1.108	2.08	14.8	17.5	67.7
45	1.243	2.30	15.8	14.6	69.6	1.148	2.23	15.1	17.5	67.4
50	1.278	2.45	16.1	14.7	69.2	1.179	2.39	15.3	17.5	67.2
55	1.299	2.70	16.5	14.8	68.7	1.204	2.51	15.6	17.6	66.8
60	1.322	2.72	16.8	14.8	68.4	1.227	2.61	15.9	17.6	66.5
65	1.335	2.83	17.0	14.9	68.1	1.241	2.71	16.0	17.7	66.3
70	1.346	2.93	17.2	15.0	67.8	1.256	2.80	16.2	17.8	66.0
		Type V					Type VI			
		n=18; j=1.97; e=6.5 mb					n=46; j=1.95; e=10.6 mb			
2	0.033	0.84	5.5	13.2	81.3	—	0.20	1.6	12.8	—
5	0.217	0.99	6.8	13.2	80.0	0.185	0.31	3.4	13.1	83.5
10	0.476	1.27	8.9	13.3	77.8	0.438	0.57	6.9	13.4	78.7
15	0.682	1.58	10.6	13.4	76.0	0.580	0.84	8.0	13.8	78.2
20	0.824	1.81	12.0	13.5	74.5	0.768	1.08	10.0	14.0	76.0
25	0.927	2.01	13.2	13.5	73.3	0.877	1.32	11.7	14.2	74.1
30	1.022	2.19	14.4	13.6	72.0	0.962	1.51	12.9	14.5	72.6
35	1.081	2.36	15.1	13.7	71.2	1.026	1.71	13.9	14.7	71.4
40	1.144	2.51	15.6	13.8	70.6	1.082	1.89	15.0	14.8	70.2
45	1.183	2.65	16.1	13.8	70.1	1.123	2.04	15.5	14.9	69.6
50	1.218	2.77	16.4	13.9	69.7	1.156	2.15	15.9	15.1	69.0
55	1.247	2.86	16.6	14.0	69.4	1.185	2.27	16.2	15.3	68.5
60	1,272	2.96	16.9	14.1	68.0	1.207	2.37	16.6	15.4	68.0
65	1.286	3.02	17.1	13.2	68.7	1.223	2.44	16.9	15.5	67.6
70	1.300	3.07	17.2	14.3	68.5	1.234	2.55	17.0	15.7	67.3

REMARKS: The number of cases n and the ratio of attenuation in aerosol to attenuation in vapor j, and the vapor pressure of water e are given for each type of state of aqueous mass.

Table 5.6 Spectral composition of direct solar radiation in mountains

$h_\odot$	Type I			Type II				Type III				Type IV			
	S cal/cm². min	% of overall radiation at λ nm		S cal/cm². min	% of overall radiation at λ nm			S cal/cm². min	% of overall radiation at λ nm			S cal/cm². min	% of overall radiation at λ nm		
		290-520	520-600		290-380	380-410	>550		290-380	380-410	>550		290-520	520-620	>625
2	0.25	7.7	13.9	0.430	2.10	6.4	85.7	—	1.36	4.6	84.2	—	—	—	—
5	0.66	8.9	13.8	0.640	2.30	6.8	84.9	—	1.58	4.8	83.4	0.41	10.3	11.5	78.2
10	1.02	11.2	13.7	0.930	2.60	7.3	83.1	0.736	1.82	5.2	82.0	0.63	11.4	12.0	76.6
15	1.20	13.3	13.5	1.075		7.7	82.0	0.935		5.5	80.8	0.78	12.2	12.4	75.4
20	1.30	14.9	13.3	1.175	2.96	8.1	80.7	1.080	2.17	5.7	79.9	0.92	13.0	12.6	74.4
25	1.38	16.2	13.2	1.244		8.4	79.9	1.175		6.1	78.8				
30	1.42	17.2	13.2	1.246	3.17	8.7	79.2	1.220	2.47	6.3	78.0	1.11	14.6	12.8	72.6
35	1.46	18.1	13.1	1.325		9.0	78.6	1.250		6.5	77.2				
40	1.49	18.9	13.1	1.350	3.34	9.3	78.1	1.263	2.58	6.6	76.4	1.21	17.1	13.5	69.4
45	1.52	19.5	13.1	1.357		9.6	77.7	1.280		6.7	76.0				
50	1.54	20.1	13.1	1.380	3.62	9.7	77.3	1.306	2.70	6.8	75.6	1.27	19.6	13.9	60.5
55	1.56	20.4	13.0	1.400		9.9	76.9	1.320		6.9	75.3				
60	1.57	20.7	13.0	1.420	3.88	10.2	76.6	1.330	2.78	7.00	75.0	1.35	21.2	14.3	64.5
65	1.58	21.0	13.0	1.422	4.00	10.3	76.3	1.336		7.05	74.8				
70	1.59	21.3	13.0	1.424	4.10	10.5	76.0	1.340	2.80	7.10	74.7	1.37	—	—	—

Table 5.6—*Contd.*

$h_\odot$	Type V				Type VI				Type VII			
	S cal/cm² . min	% of overall radiation at λ nm			S cal/cm² . min	% of overall radiation at λ nm			S cal/cm² . min	% of overall radiation at λ nm		
		290-520	520-625	>625		290-380	380-410	>550		290-520	520-620	>625
2	—	—	—	—	—	1.92	3.6	82.5	—	—	—	—
5	0.38	18.0	13.7	68.3	—	2.22	3.8	38.9	0.68	7.4	19.0	73.6
10	0.57	18.6	13.3	68.1	0.482	2.56	4.2	80.8	0.93	9.4	16.9	73.5
15	0.72	19.1	13.0	67.9	0.693	—	4.8	79.8	1.04	11.3	16.3	73.4
20	0.80	19.6	12.8	67.6	0.835	3.02	5.3	78.8	1.13	12.7	15.8	71.5
25					0.944		5.7	77.9		13.8	15.7	70.5
30	0.98	20.6	12.1	67.3	1.046	3.42	6.3	77.0	1.25	14.9	15.6	69.5
35					1.130		6.7	76.1		15.6	15.6	68.8
40	1.12	21.4	11.7	66.9	1.176	3.73	7.1	75.6	1.33	16.3	15.5	68.2
45					1.216		7.4	75.1		16.9	15.5	67.6
50	1.23	22.2	11.2	66.6	1.242	4.03	7.8	74.7	1.38	17.5	15.4	67.1
55					1.260		8.2	74.4		18.0	15.3	66.7
60	1.32	22.8	11.1	66.2	1.270	4.33	8.4	74.2	1.42	18.5	15.2	66.3
65					1.278		8.6	74.0		18.8	15.1	66.1
70	1.39	23.2	10.8	66.0	1.281	4.52	8.7	73.8	1.45	19.1	15.0	65.9

REMARKS: The proposed seven types of air masses occurring in mountainous conditions being characterized by the following parameters: Type I : j=0.52, e=5.0; Type II : j=0.82, e=9.6; Type III : j=1.23, e=5.00; Type IV : j=1.4, e=10.0; Type V : j=1.77, e=10.0; Type VI : j=1.72, e=10.0; Type VII : j=2.0.

where S_{id} = flux of direct solar radiation in ideal atmosphere,

ΔS_{H_2O} = direct solar radiation absorbed by water vapor,

and S = measured flux of direct solar radiation.

E. A. Lopukhin suggested seven types of optical condition in atmosphere over mountainous regions [19] for the characterization of the state of air masses. Data on the relative spectral composition of solar radiation for three sections of the spectrum are given in Table 5.6. The measurements were carried out with the help of glass filters, so that the boundaries of the spectral ranges were defined rather arbitrarily. The types of state of air masses are described in [19] though not completely. However, the data obtained by Lopukhin encompass large ranges of solar altitudes and weather conditions and practically the entire wavelength band of the solar radiation reaching sea level. A comparison of values presented in [7] and measured by Garadzha and Lopukhin with results of the computations for the mean radiation model [1] showed (Table 5.7) that in the ultraviolet region (290-380 nm) the discrepancy between experimental and theoretical data is most noticeable for smaller solar altitudes. From the solar altitude of 30° onward there is complete agreement between the data. Lopukhin's data provide somewhat higher values of ultraviolet radiation fluxes as compared with the theoretical data and those measured in Moscow [7]. This may have been caused by the different composition of aerosol components in the region of Moscow and in Central Asia.

Table 5.7 The relation between fluxes of direct solar radiation in the spectral range 300-380 nm and integral fluxes of solar radiation (%) at different atmospheric turbidities [7]

Solar altitude, deg	Data by M. P. Garadzhi (Moscow)			Data by E. A. Lopukhin (Tashkent)		Solar altitude, deg	Computed data [1]		
	$p=0.6$	$p=0.7$	$p=0.8$	type I	type II		$\tau_0=0.5$	$\tau_0=0.3$	$\tau_0=0.2$
10	0	0.19	0.60	0.61	1.23	9.3	0.05	0.10	0.21
20	0.30	0.69	1.24	1.33	1.68	19.3	0.50	0.82	1.05
30	0.77	1.28	1.80	1.78	2.04	30.0	1.17	1.61	1.90
40	1.30	1.88	2.30	2.10	2.33	41.7	1.78	2.28	2.56
50	1.83	2.46	2.73	2.37	2.58	—	—	—	—
55	2.09	2.70	2.92	2.50	2.70	—	—	—	—

Variations in the amount of ozone and aerosol strongly influence the fluxes of direct solar radiation in the ultraviolet region. It is possible to derive the amount of the expected variations in spectral fluxes from the data on calculations of radiation models of atmosphere in the ultraviolet region of the spectrum obtained in [5]. Table 5.8 shows the variation in spectral fluxes of solar radiation in UV—B ($\lambda<315$ nm) and UV—A+B ($\lambda<400$ nm) regions depending on the average amount of ozone u'_{O_3} and the turbidity of the atmosphere b.

Table 5.8 Spectral fluxes of direct solar radiation for different amounts of ozone and turbidity (mcal/cm² . min)

Spectral region	Ozone content and turbidity		Solar altitude, deg					
	u'_{O_3}	b	75	60	45	30	15	10
B	0.30	0.025	1.69	1.38	0.85	0.30	0	0
	0.30	0.050	1.52	1.18	0.73	0.23	0	0
	0.30	0.100	1.21	0.92	0.52	0.14	0	0
	0.30	0.150	0.95	0.70	0.37	0.11	0	0
	0.30	0.200	0.75	0.55	0.27	0.06	0	0
	0.40	0.025	1.32	1.03	0.62	0.20	0	0
	0.40	0.050	1.18	0.92	0.52	0.16	0	0
	0.40	0.100	0.93	0.72	0.39	0.03	0	0
	0.50	0.025	1.03	0.83	0.47	0.14	0	0
	0.50	0.050	0.93	0.72	0.40	0.11	0	0
	0.50	0.100	0.75	0.55	0.30	0.07	0	0
B+A	0.30	0.025	70.5	65.0	54.5	37.1	12.1	4.3
	0.30	0.050	64.2	58.2	47.8	30.7	8.5	2.6
	0.30	0.100	52.7	47.0	36.7	21.3	4.3	1.0
	0.30	0.150	43.5	37.9	28.1	14.8	2.1	0.4
	0.30	0.200	35.8	30.6	21.7	10.3	1.8	0.1

There is complete agreement between the computations and the results of observations made by researchers [5] in the Caucasus and in the Crimea for $h_\odot=30°$.

Table 5.9 [5] gives the variation of ultraviolet radiation in the regions B and B+A for changes in the altitude above the sea level for average ozone content. To each of the five levels the most probable variation of the turbidity factor b may be assigned.

Table 5.9 Spectral fluxes of direct solar radiation at different altitudes for average ozone content (mcal/cm² · min)

Altitude, km	b	$h_\odot = 75°$		$h_\odot = 30°$	
		B	B+A	B	B+A
1	0.040	1.75	69.8	0.32	37.0
	0.080	1.46	60.6	0.23	27.3
	0.120	1.38	51.8	0.17	20.4
2	0.030	2.10	72.3	0.43	44.4
	0.060	1.84	69.5	0.35	35.5
	0.090	1.59	61.8	0.29	28.5
3	0.020	2.47	87.2	0.57	53.4
	0.040	2.23	79.8	0.49	46.0
	0.060	2.04	73.7	0.40	39.5
4	0.015	2.81	83.4	0.75	61.9
	0.030	2.61	88.2	0.64	55.5
	0.045	2.44	83.1	0.56	49.7
5	0.010	3.22	100.9	0.95	71.9
	0.020	3.04	57.5	0.86	65.7
	0.030	2.90	93.6	0.75	61.9

The position of the shortwave boundary of the solar spectrum (λ_{min}) significantly influences the amount of ultraviolet radiation. It thus follows from the experimental data that λ_{min} largely depends on the length of the optical path in the atmosphere and the turbidity of the air mass, so that the ultraviolet radiation exhibits clearly marked daily and annual behavior (Table 5.10).

Table 5.10 Variation of λ_{min} nm depending on solar altitude and time of year [13]

Time of year	Altitude of sun, deg					
	10	20	30	40	50	60
Spring	316	308	304	302	298	298
Summer	319	310	306	301	299	298
Autumn	312	305	302	300	—	—
Winter	314	308	307	—	—	—
Year	316	308	304	302	299	298

C-4

There is practically no variation in λ_{min} with a change in altitude above sea level (in the troposphere and in lower stratosphere), insofar as the cause of constraint in the spectrum, viz. ozone, is situated mainly above 15 km.

A comparison of the dependence of the relation of the infrared solar radiation and the integral flux of the direct solar radiation S_{IR}/S on the altitude of the sun, from the data obtained by Lopukhin (Tashkent) and Kalitin (Pavlovsk) [11], shows that these relations vary in a different manner in Pavlovsk and Tashkent for $h_\odot > 10°$ (Table 5.11).

Table 5.11 Dependence of S_{IR}/S on solar altitude

Location	Altitude of the sun, deg					
	2	5	10	15	20	
Pavlovsk	0.80	0.79	0.71	0.69	0.64	
Tashkent (type IV)	0.81	0.79	0.767	0.742	0.712	
Location	Altitude of the sun, deg					
	25	30	35	40	45	50
Pavlovsk	0.62	0.61	0.60	0.59	0.58	0.57
Tashkent (type IV)	0.701	0.69	0.682	0.677	0.674	0.672

The ratio S_{IR}/S reaches a maximum in those seasons which show high transparency in an annual course, i. e. in the south in winter and spring, and in the north in spring.

1.2 Energy distribution in the spectrum of solar radiation outside the atmosphere

Energy distribution in the spectrum of solar radiation is a necessary factor for the solution of a majority of the direct and related problems of atmospheric optics as well as a wide range of problems in actinometry and climatology. Availability of accurate data on the solar flux outside the atmosphere is essential for the computation of the thermal and radiation regimes of space ships and artificial satellites.

The energy distribution of solar emission outside the atmosphere can be obtained either through direct measurements of spectral distribution at altitudes above 80 km or through extrapolation of data from terrestrial spectrobolometric measurements at altitudes beyond the atmosphere. Direct measurements have thus far been carried out with rockets for specific spectral ranges [44], as well as for the integrated flux of solar radiation [34].

The measurement of energy distribution for the entire spectrum of solar radiation is a considerably more complex problem which will be solved in the near future with the help of artificial satellites. Abbot and Foyle developed the method of extrapolation of terrestrial measurements to the boundary of the atmosphere for practical application. The dependence of incident solar flux in any spectral range upon the magnitude of the atmospheric mass (i.e. measurements for different solar altitudes) was determined through terrestrial measurements from high altitude peaks with the help of special spectrometers. For a steady optical state of the atmosphere there is a linear relation between the logarithm of intensity of solar radiation and atmospheric mass m. Bouguer-Lambert's law gives the relation between intensity of radiation and the path length of the incident ray in an attenuating medium in the following relation, viz.

$$I_{\lambda m}=I_{\lambda 0}\rho^{m}{}_{\lambda} \text{ or } \log I_{\lambda m}=\log I_{\lambda 0}+m\log \rho_{\lambda}, \tag{5.2}$$

where $I_{\lambda 0}$ and $I_{\lambda m}$ denote the fluxes of radiation of wavelength λ before and after passage through attenuating mass m respectively, and ρ_{λ}—the spectral transparency coefficient for wavelength λ and unit mass.

The extrapolation of relations obtained for the boundary of the atmosphere, i.e. for value $m=0$, determines the spectral distribution of solar radiation outside the atmosphere for the spectrometric range of wavelengths. The distribution thus obtained is more accurate since optics has a specific transmission range when applied to spectral equipment (for the optical glass of the Smithsonian spectrometer this is 346-2440 nm). Since spectral measurements are accompanied by the simultaneous measurements of the absolute values of integrated solar radiation flux, then the area under measured spectral energy distribution, and consequently under distribution obtained through extrapolation, will be expressed in absolute units on the scale of the calibrating instrument.

When this distribution is supplemented in the ultraviolet ($\lambda<296$ nm) and infrared ($\lambda>2500$ nm) regions to take into account the solar radiation being fully absorbed in the higher atmospheric layers, the distribution finally obtained is a graphical representation of the solar constant for the day on which the observation was made. In order to obtain the value of the solar constant, it is neccessary to introduce from astrophysical computation the value of the solar constant on the given

day with respect to the average distance between the earth and the sun (see second section of this chapter).

The introduction of corrections in the distribution measured on the surface and obtained through extrapolation is well illustrated by the expression for the determination of the solar constant [50] as follows:

$$S_0 = S\frac{\sum E_{0\lambda} + \Delta E_{0\lambda}\,(\mathrm{UV}) + \Delta E_{0\lambda}\,(\mathrm{IR})}{\sum E_{\lambda} + \Delta E_{\lambda}\,(\mathrm{UV}) + \Delta E_{\lambda}\,(\mathrm{IR})}, \qquad (5.3)$$

Here $\Delta E_{0\lambda}$ (UV) is the correction for the range of wavelengths from 346 nm to the minimum wavelength for which the solar emission is being considered; $\Delta E_{0\lambda}$ (IR)—the correction for the range of wavelengths from 2440 nm to the maximum wavelength for which solar radiation in the upper atmosphere may be considered; ΔE_{λ} (UV) is correction for range 346-296 nm; ΔE_{λ} (IR)—correction for range between 2440 nm and the maximum wavelength for which solar radiation can be measured on the earth's surface.

The most appropriate spectral distribution was suggested by Johnson and Nicolet [42, 47, 48] (Fig. 5.6). Ninety-nine per cent of the entire radiative energy of the sun is concentrated in the range of wavelengths from 200 nm to 4.0 μ. Integration of the distribution curve shown in Fig. 5.6 gives the following values of the solar constant, viz. 2.002 and 1.98 cal/cm²·min.

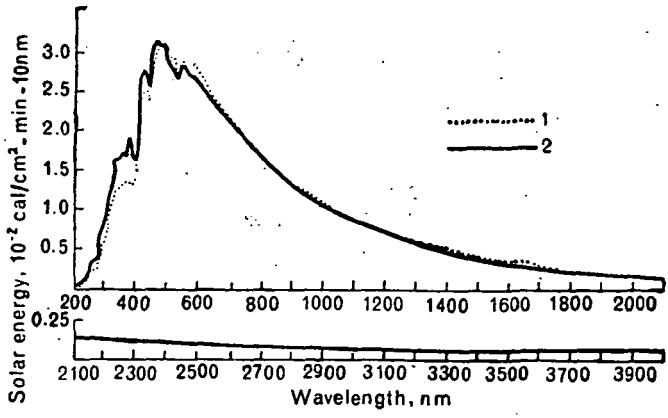

Fig. 5.6. Energy distribution in solar spectrum outside the atmosphere.
1—according to Nicolet; 2—according to Johnson.

The mean values of intensities of the solar emission in narrow spectral ranges as well as the percentage ratio with respect to integral flux are given in Table 5.12. These magnitudes were obtained on the basis of the energy distribution in the spectrum of solar radiation given by Johnson.

Table 5.12 Energy distribution in the solar spectrum at the upper boundary of the atmosphere at $h_{\odot}=90^{\circ}_{0}$, $m=0$

Δλ nm	S_λ		Δλ nm	S_λ	
	W/m²	%		W/m²	%
0-100	0.01	0.001	345-350	5.82	0.42
100-220	0.27	0.02			
220-225	0.14	0.01	325-350	28.32	2.03
0-225	0.41	0.03	350-355	5.90	0.42
			355-360	5.85	0.42
225-230	0.26	0.02	360-365	6.15	0.44
230-235	0.27	0.02	365-370	6.35	0.45
235-240	0.28	0.02	370-375	6.62	0.47
240-245	0.29	0.02			
245-250	0.30	0.02	350-375	30.87	2.20
225-250	1.40	0.10	375-380	6.18	0.44
			380-385	6.00	0.43
250-255	0.38	0.03	385-390	5.63	0.40
255-260	0.53	0.04	390-395	5.73	0.41
260-265	0.95	0.07	395-400	7.00	0.50
265-270	1.20	0.09			
270-275	1.14	0.08	375-400	30.54	2.19
250-275	4.20	0.30	400-405	8.71	0.62
			405-410	9.48	0.68
275-280	1.09	0.08	410-415	9.60	0.69
230-285	1.56	0.11	415-420	9.67	0.69
285-290	2.42	0.17	420-425	9.47	0.68
290-295	3.08	0.22			
295-300	3.02	0.22	400-425	46.93	3.36
275-300	11.17	0.80	425-430	8.80	0.63
			430-435	8.70	0.62
300-305	3.00	0.21	435-440	9.40	0.67
305-310	3.50	0.25	440-445	10.40	0.74
310-315	3.90	0.28	445-450	10.70	0.77
315-320	4.05	0.29			
320-325	4.65	0.33	425-450	48.00	3.44
300-325	19.10	1.37	450-455	10.89	0.78
			455-460	10.89	0.78
325-330	5.50	0.39	460-465	10.75	0.77
330-335	5.60	0.40	465-470	10.89	0.78
335-340	5.60	0.40	470-475	10.70	0.77
340-345	5.80	0.42			

Table 5.12—*Contd.*

Δλ nm	S_λ		Δλ nm	S_λ	
	W/m²	%		W/m²	%
450-475	54.12	3.88	610-620	17.64	1.26
			620-630	17.32	1.24
475-480	10.80	0.77	630-640	16.90	1.21
480-485	10.47	0.75	640-650	16.61	1.19
485-490	10.00	0.72			
490-495	10.20	0.73	600-650	86.49	6.19
495-500	10.30	0.74			
			650-660	16.38	1.17
475-500	51.77	3.71	660-670	16.25	1.16
			670-680	15.81	1.13
500-505	9.80	0.70	680-690	15.39	1.10
505-510	9.80	0.70	690-700	14.95	1.07
510-515	9.65	0.69			
515-520	9.60	0.69	650-700	78.78	5.64
520-525	9.65	0.69			
			700-710	15.04	1.08
500-525	48.50	3.47	710-720	14.41	1.03
			720-730	14.20	1.02
525-530	9.75	0.70	730-740	13.90	1.00
530-535	9.85	0.71	740-750	13.47	0.97
535-540	9.90	0.71			
540-545	9.90	0.71	700-750	71.02	5.09
545-550	9.75	0.70			
			750-760	13.59	0.97
525-550	49.15	3.52	760-770	12.98	0.93
			770-780	12.53	0.90
550-555	9.74	0.70	780-790	12.38	0.89
555-560	9.58	0.69	790-800	12.08	0.87
560-565	9.52	0.68			
565-570	9.50	0.68	750-800	63.56	4.55
570-575	9.57	0.69			
			800-810	11.90	0.85
550-575	47.91	3.43	810-820	11.58	0.83
			820-830	11.45	0.82
575-580	9.57	0.69	830-840	11.01	0.79
580-585	9.52	0.68	840-850	10.71	0.77
585-590	9.52	0.68			
590-595	9.48	0.68	800-850	56.65	4.06
595-600	9.35	0.67			
			850-860	10.51	0.75
575-600	47.44	3.40	860-870	10.21	0.73
			870-880	10.08	0.42
600-610	18.02	1.29	880-890	9.93	0.71
			890-900	9.63	0.69

Table 5.12—*Contd.*

Δλ nm	S_λ		Δλ nm	S_λ	
	W/m²	%		W/m²	%
850-900	50.36	3.61	1700-1800	15.55	1.11
			1800-1900	13.02	0.93
900-910	9.27	0.66	1900-2000	10.98	0.79
910-920	9.14	0.65			
920-930	8.99	0.64	1500-2000	80.90	5.80
930-940	8.77	0.63			
940-950	8.55	0.61	2000-2100	9.31	0.67
			2100-2200	7.95	0.57
900-950	44.72	3.20	2200-2300	6.82	0.49
			2300-2400	5.89	0.42
950-960	8.25	0.59	2400-2500	5.10	0.37
960-970	8.15	0.58			
970-980	8.09	0.58	2000-2500	35.07	2.51
980-990	7.68	0.55			
990-1000	7.54	0.54	2500-2600	4.46	0.32
			2600-2700	3.90	0.28
950-1000	39.71	2.84	2700-2800	3.42	0.24
			2800-2900	3.01	0.22
1000-1010	7.30	0.52	2900-3000	2.66	0.19
1010-1020	7.15	0.51			
1020-1030	7.02	0.50	2500-3000	17.45	1.25
1030-1040	6.87	0.49			
1040-1050	6.73	0.48	3000-3100	2.41	0.17
			3100-3200	2.06	0.15
1000-1050	35.07	2.51	3200-3300	1.91	0.14
			3300-3400	1.71	0.12
1050-1060	6.60	0.47	3400-3500	1.53	0.11
1060-1070	6.46	0.46			
1070-1080	6.33	0.45	3000-3500	9.62	0.69
1080-1090	6.19	0.44			
1090-1100	6.05	0.43	3500-3600	1.38	0.10
			3600-3700	1.24	0.09
1050-1100	31.63	2.27	3700-3800	1.12	0.08
			3800-3900	1.02	0.07
1100-1200	52.92	3.79	3900-4000	0.92	0.07
1200-1300	42.29	3.03			
1300-1400	34.06	2.44	3500-4000	5.68	0.41
1400-1500	27.68	1.98			
			4000-4100	0.885	0.06
1100-1500	156.95	11.24	4100-4200	0.806	0.06
			4200-4300	0.736	0.05
1500-1600	22.65	1.62	4300-4400	0.677	0.05
1600-1700	18.70	1.34	4400-4500	0.617	0.04

Table 5.12—*Contd.*

$\Delta\lambda$ nm	S_λ		$\Delta\lambda$ nm	S_λ	
	W/m²	%		W/m²	%
4000-4500	3.721	0.27	4500-5000	2.279	0.16
4500-4600	0.557	0.04	5000-6000	2.79	0.20
4600-4700	0.448	0.03			
4700-4800	0.438	0.03	6000-7000	1.47	0.11
4800-4900	0.428	0.03	7000- ∞	2.65	0.19
4900-5000	0.408	0.03			

REMARKS: $S_\lambda\ \% = 100\frac{S_\lambda}{S_0}$, where S_0—solar constant, equal to 1396.4 W·cm^{-2} or 2.002 cal/cm²·min^{-1}.

Table 5.13 Energy distribution in the solar spectrum at the upper boundary of atmosphere in the region $\lambda = 0$ to λ_i for normally incident rays

λ_i nm	$\sum_\lambda S_\lambda$		λ_i nm	$\sum_\lambda S_\lambda$	
	W/cm	%		W/cm	%
100	0.001	0.001	285	8.7	0.62
220	0.3	0.02	290	11.1	0.79
225	0.4	0.03	295	14.2	1.01
230	0.7	0.05	300	17.2	1.23
235	0.9	0.07	305	20.2	1.44
240	1.2	0.09	310	23.7	1.70
245	1.5	0.11	315	27.6	1.97
250	1.8	0.13	320	31.6	2.26
255	2.2	0.16	325	36.3	2.60
660	2.7	0.19	330	41.8	2.99
265	3.7	0.26	335	47.4	3.39
270	4.9	0.35	340	53.0	3.79
275	6.0	0.43	345	58.8	4.21
280	7.1	0.51	350	64.6	4.63

Table 5.12—*Contd.*

λ_1 nm	$\sum_\lambda S_\lambda$		λ_1 nm	$\sum_\lambda S_\lambda$	
	W/cm	×		W/cm	%
355	70.5	5.05	525	375.3	26.88
360	76.4	5.47	530	385.1	27.58
365	82.5	5.91	535	394.9	28.28
370	88.9	6.36	540	404.8	28.99
375	95.5	6.84	545	414.7	29.70
380	101.7	7.28	550	424.5	30.40
385	107.7	7.71	555	434.2	31.10
390	113.3	8.11	560	443.8	31.78
395	119.0	8.52	565	453.3	32.46
400	126.0	9.02	570	462.8	33.14
405	134.7	9.65	575	472.4	33.83
410	144.2	10.33	580	482.0	34.51
415	153.8	11.01	585	491.5	35.20
420	163.5	11.71	590	501.0	35.88
425	172.9	12.38	595	510.5	36.56
430	181.7	13.01	600	519.8	37.23
435	190.4	13.64	610	537.9	38.52
440	199.8	14.31	620	555.5	39.78
445	210.2	15.06	630	572.8	41.02
450	220.9	15.82	640	589.7	42.23
455	231.8	16.60	650	606.3	43.42
460	242.7	17.38	660	622.7	44.59
465	253.5	18.15	670	639.0	45.76
470	264.4	18.93	680	654.8	46.89
475	275.1	19.70	690	670.2	47.99
480	285.9	20.47	700	685.1	49.06
485	296.3	21.22	710	700.1	50.14
490	306.3	21.94	720	714.6	51.17
495	316.5	22.67	730	728.8	52.19
500	326.8	23.40	740	742.7	53.18
505	336.6	24.11	750	756.1	54.15
510	345.4	27.81	760	769.7	55.12
515	356.1	25.50	770	782.7	56.05
520	365.7	26.19	780	795.2	56.95

Table 5.13—*Contd.*

λ_i nm	$\sum_\lambda S_\lambda$ W/cm	%	λ_i nm	$\sum_\lambda S_\lambda$ W/cm	%
790	807.6	57.83	1800	1291.7	92.50
800	819.7	58.70	1900	1304.7	93.43
810	831.6	59.55	2000	1315.7	94.22
820	843.2	60.38	2100	1325.0	94.89
830	854.6	61.20	2200	1332.9	95.45
840	865.6	61.99	2300	1339.8	95.94
850	876.3	62.76	2400	1345.6	96.36
860	886.8	63.51	2500	1350.7	96.73
870	897.1	64.24	2600	1355.2	97.05
880	907.1	64.96	2700	1359.1	97.33
890	917.1	65.67	2800	1362.5	97.57
900	926.7	66.36	2900	1365.5	97.79
910	936.0	67.03	3000	1368.2	97.98
920	945.1	67.68	3100	1370.6	98.15
930	954.1	68.32	3200	1372.7	98.30
940	962.9	68.95	3300	1374.6	98.44
950	971.4	69.57	3400	1376.3	98.56
960	979.7	70.16	3500	1377.8	98.67
970	987.8	70.74	3600	1379.2	98.77
980	995.9	71.32	3700	1380.4	98.86
990	1003.6	71.87	3800	1381.6	98.94
1000	1011.1	72.41	3900	1382.6	99.01
1010	1018.4	72.93	4000	1383.5	99.08
1020	1025.6	73.44	4100	1384.4	99.14
1030	1032.6	73.95	4200	1385.2	99.20
1040	1039.5	74.44	4300	1385.9	99.25
1050	1046.2	74.92	4400	1386.6	99.30
1060	1052.8	75.39	4500	1387.2	99.34
1070	1059.3	75.86	4600	1387.8	99.38
1080	1065.6	76.31	4700	1388.2	99.41
1090	1071.8	76.75	4800	1388.7	99.45
1100	1077.8	77.19	4900	1389.1	99.48
1200	1130.7	80.98	5000	1389.5	99.50
1300	1173.0	84.00	6000	1392.3	99.70
1400	1207.1	86.44	7000	1393.8	99.81
1500	1234.8	88.42	∞ (S_0)	1396.4	100.00
1600	1257.4	90.05		cal/cm² · min	
1700	1276.1	91.39	∞ (S_0)	2.002	100.00

REMARKS: $\sum_\lambda S_\lambda = \sum_{\lambda=0}^{\lambda=\lambda_i} S_\lambda$ W/m², $\sum_\lambda S_\lambda$ (%) $= 100 \dfrac{\sum_\lambda S_\lambda}{S_0}$

The energy distribution in the spectral range, increasing from λ_0 to λ_i, is given in Table 5.13. The apparent disparity in the values of S_λ given in Tables 5.12 and 5.13 occurs on account of the rounding off of the values S_λ. Both tables were compiled for mean distance of the earth from the sun.

A more detailed distribution of energy outside the atmosphere for the ultraviolet region of the solar spectrum is shown in Fig. 5.7. The data were obtained from spectrographs in rockets attaining an altitude of almost 235 km.

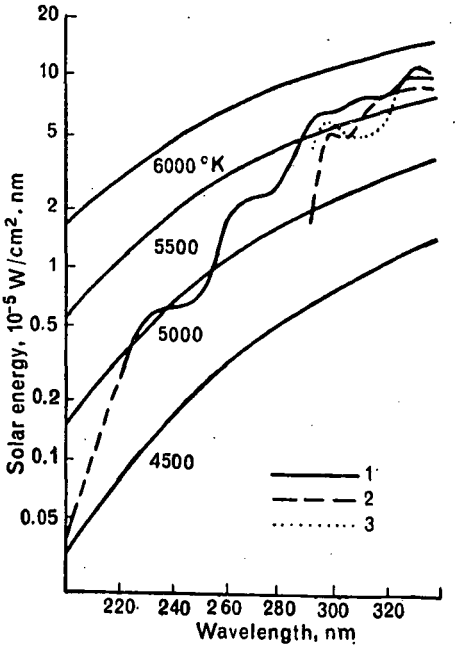

Fig. 5.7. Energy distribution in the solar spectrum outside the atmosphere for the ultraviolet region [29].
1—after Steer; 2—after Petit; 3—after Johnson.

Energy distribution in the region 80-260 nm is given in detail in Fig. 5.8 and in Table 5.14 for wavelengths corresponding to the centers of the intervals. These magnitudes refer to the average distance between the earth and the sun.

L. Dunkelman and R. Scolnik [35] have suggested the most dependable distribution for the visible region of the spectrum obtained through extrapolation of ground data. The data of Dunkelman have been compared with those of Petit, Steer and Johnson (1955) in Fig. 5.9. The

Table 5.14 Energy distribution in the spectrum of the sun outside the atmosphere in the region of wavelengths 85-260 nm ($\Delta\lambda$=5.0 nm)

λ nm	S_o erg/cm² . sec	λ nm	S_o erg/cm² . sec
260	700	170	8.2
255	560	165	5.0
250	380	160	3.2
245	390	155	1.7
240	340	150	0.95
235	320	145	0.50
230	360	140	0.26
225	350	135	0.26
220	310	130	0.18
215	240	125	0.15
210	145	120	5.7
205	90	115	0.08
200	70	110	0.06
195	55	105	0.10
190	41	100	0.18
185	28	95	0.15
180	19	90	0.25
175	12	85	0.11

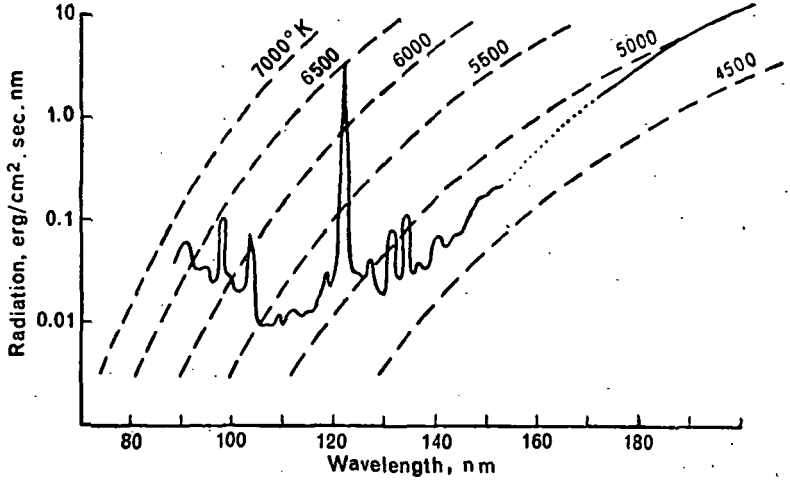

Fig. 5.8. Spectral distribution of solar radiation in the region of wavelengths 80-200 nm.

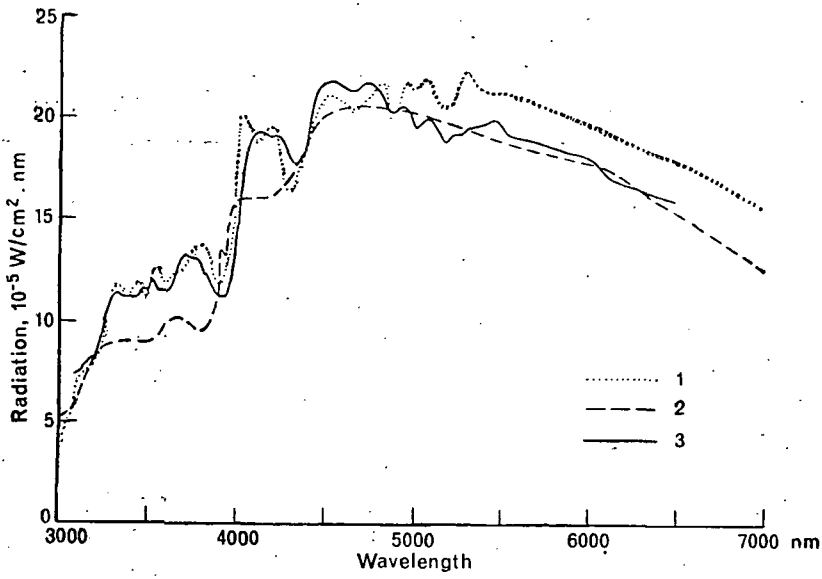

Fig. 5.9. Energy distribution in the spectrum of solar radiation in the visible range.

1—data of Steer and Johnson; 2—data of Petit; 3—data of Dunkelman and Scolnik.

data of Petit differ considerably from data obtained later in the region of the spectrum with $\lambda < 450$ nm.

The data obtained for the ultraviolet region of the spectrum contain noticeable errors : thus for the range 140-200 nm there is an error of $\pm 20\%$ and for the region with $\lambda < 140$ nm the error is several times higher. Low accuracy and large variations of ultraviolet radiation indicate the necessity of further investigation in the future.

1.3 Attenuation of solar radiation in an ideal atmosphere

There is wide interest in obtaining accurate data on the energy distribution of solar radiation at different altitudes in an ideal atmosphere (in the absence of water vapor and aerosol). It is necessary to know the amount of attenuation of direct solar radiation in an ideal atmosphere in order to study the radiation characteristics of the atmosphere as well as for the solution of related problems.

Many investigators have computed fluxes of solar radiation in an ideal atmosphere. The data obtained by Kastrov (1928), Foisner and Dubois (1930) are the most accurate among the earlier observations.

The results of several computations are given in chronological order in Table 5.15, upto the taken from [25]. The results of Kastrov, Foisner and Dubois agree which is second decimal place.

Table 5.15 Intensity of direct solar radiation at sea level in ideal atmosphere (cal/cm² . min), according to data of different researchers [25]

$S_{s\cdot 0}$—subzonal value of flux of solar radiation

Author	Year	$S_{s\cdot 0}$ ($m=1$)	Number of optical masses					
			1	2	3	4	6	8
V. G. Kastrov	1928	—	1.73	1.60	1.50	1.41	1.28	1.18
Foisner and Dubois	1930	—	1.73	1.60	1.50	1.41	1.28	1.18
Linke	1939	—	1.75	1.64	1.54	1.47	1.34	1.26
N. G. Kastrov	1956	1.94	1.75	1.61	1.51	1.43	1.30	—
K.S. Shifrin and A. A. Avaste	1960-1962	1.93	1.76	1.62	1.52	1.44	1.31	—
M. S. Averkiev	1963	—	1.78	1.65	—	—	—	—
S. I. Sivkov	1964	1.93	1.75	1.62	1.51	1.43	1.30	—

The results of computations obtained over a period of 50 years are based on the accurate data of Nicolet (1950-51) and Johnson (1956) about the solar constant and the spectral distribution of solar radiation outside the atmosphere. In addition, the coefficients of absorption in ozone given by Vigroux were used instead of the higher coefficients of Ny and Choong (1932) [46].

A comparison of values of the solar radiation flux on the surface of the earth as obtained by different authors shows the existence of a small discrepancy caused by the difference in the original data.

The computations made by S. I. Sivkov [25], who conducted a thorough analysis of original values and applied methods of calculation, may be considered the most authentic and complete to date.

The results of Sivkov's computations for the spectral range 220-7000 nm and masses from 1 to 10 are given in Table 5.16. The magnitude of solar constant, used in the computations, was taken as $S_0 = 1.98$ cal/cm² . min. The spectral transparency coefficients for ozone P_{O_3} and pure dry air P_a as well as the subzonal values of fluxes of direct solar radiation $S_{s\cdot 0}$ are given in this Table.

Table 5.16 Spectral composition of direct solar radiation in ideal atmosphere at the level of 1000 mb ($S_0 = 1980$ mcal/cm² · min)

$\Delta\lambda$ μ	$\Delta S_0, \lambda$		$P_{O_3}(\lambda)$	$S_{s,0}(\lambda)$	$P_a(\lambda)$	Number of optical masses							
	in % of S_0	mcal/cm² · min				1	2	3	4	5	6	8	10
0.22	0.02	0.4	—	—	—								
0.22-0.24	0.07	1.4	—	—	—								
0.24-0.26	0.11	2.2	—	—	—								
0.26-0.28	0.31	6.1	—	—	—								
0.28-0.30	0.72	14.3	0.007	0.1	0.249	0							
0.30-0.32	1.03	20.4	0.524	10.7	0.351	3.8	0.7	0.1	0.0	0.0	0.0	0.0	0.0
0.32-0.34	1.54	30.5	0.905	27.6	0.448	12.4	5.0	2.0	0.8	0.3	0.1	0.0	0.0
0.34-0.36	1.67	33.1	0.997	33.0	0.534	17.6	9.3	5.0	2.7	1.4	0.7	0.2	0.1
0.36-0.38	1.82	36.0	1.000	36.0	0.609	21.9	13.3	8.1	4.9	3.0	1.8	0.7	0.2
0.38-0.40	1.74	34.5	1.000	34.5	0.671	23.1	15.5	10.4	7.0	4.7	3.2	1.4	0.6
0.22-0.40	9.03	178.9		141.9		78.8	43.8	25.6	15.4	9.4	5.8	2.3	0.9
0.40-0.42	2.67	52.9	1.000	52.9	0.723	38.2	27.6	20.0	14.5	10.5	7.6	4.0	2.1
0.42-0.44	2.7	53.5	1.000	53.5	0.767	41.0	31.4	24.1	18.5	14.2	10.9	6.4	3.8
0.44-0.46	3.1	61.4	0.998	61.3	0.803	49.2	39.4	31.6	25.3	20.3	16.3	10.5	6.7
0.46-0.48	3.1	61.4	0.996	61.2	0.833	51.0	42.3	35.1	29.2	24.2	20.1	13.8	9.5
0.48-0.50	2.9	57.4	0.993	57.0	0.857	48.8	41.6	35.4	30.2	25.7	21.9	15.9	11.5
0.50-0.52	2.8	55.4	0.988	54.7	0.877	48.0	41.6	36.0	31.2	27.0	23.4	17.6	13.2
0.52-0.54	2.7	53.5	0.980	52.4	0.893	46.8	41.0	35.9	31.4	27.5	24.1	18.5	14.2

Table 5.16—*Contd.*

0.54-0.56	2.8	55.4	0.975	54.0	0.908	49.0	43.4	38.4	34.0	30.1	26.6	20.8	16.3
0.56-0.58	2.7	53.5	0.964	51.6	0.919	47.4	42.0	37.2	33.0	29.2	25.9	20.3	15.9
0.58-0.60	2.7	53.5	0.966	51.7	0.930	48.1	43.2	38.8	34.9	31.3	28.1	22.6	18.2
0.60-0.62	2.5	49.5	0.964	47.7	0.938	44.7	40.4	36.5	33.0	29.8	26.9	22.0	18.0
0.62-0.64	2.4	47.5	0.973	46.2	0.947	43.8	40.4	37.2	34.3	31.6	29.1	24.7	20.9
0.64-0.66	2.4	47.5	0.980	46.6	0.951	44.3	41.3	38.5	35.9	33.5	31.2	27.1	23.5
0.66-0.68	2.2	43.6	0.986	43.0	0.958	41.2	38.9	36.8	34.8	32.9	31.1	27.8	24.8
0.68-0.70	2.1	41.6	0.991	41.2	0.962	39.6	37.7	36.0	34.3	32.7	31.2	28.3	25.7
0.40-0.70		787.6		775.0		681.1	592.3	517.5	454.5	400.5	354.4	280.3	224.3
0.70-0.72	2.0	39.6	0.993	39.3	0.965	37.9	36.3	34.7	33.3	31.9	30.6	28.1	25.8
0.72-0.74	1.9	37.6	0.995	37.4	0.970	36.3	35.0	33.8	32.6	31.5	30.4	28.3	26.3
0.74-0.76	1.8	35.6	1.000	35.6	0.973	34.6	33.7	32.8	31.9	31.0	30.2	28.6	27.1
0.76-0.78	1.7	33.7	1.000	33.7	0.975	32.9	32.1	31.3	30.5	29.7	29.0	27.6	26.2
0.78-0.80	1.7	33.7	1.000	33.7	0.977	32.9	32.1	31.4	30.7	30.0	29.3	28.0	26.7
0.70-0.80	48.9	967.8		954.7		855.7	761.5	681.5	613.5	554.6	503.9	420.9	356.4
0.80-0.85	3.8	75.2	1.000	75.2	0.981	73.8	72.4	71.0	69.7	68.4	67.1	64.6	62.1
0.85-0.90	3.4	67.3	1.000	67.3	0.985	66.3	65.3	64.3	63.3	62.4	61.5	59.7	57.9
0.90-0.95	3.0	59.4	1.000	59.4	0.988	58.7	58.0	57.3	56.6	55.9	55.2	53.9	52.6
0.95-1.00	2.8	55.4	1.000	55.4	0.990	54.8	54.3	53.8	53.3	52.8	52.3	51.3	50.3

Table 5.16—*Contd.*

$\Delta\lambda\ \mu$	$\Delta S_0, \lambda$		$P_{O_3}(\lambda)$	$S_{s,0}(\lambda)$	$P_a(\lambda)$	Number of optical masses							
	in % of S_0	mcal/cm² · min				1	2	3	4	5	6	8	10
1.0-1.5	16.7	330.7	1.000	330.7	0.996	329.4	328.1	326.8	325.5	324.2	322.9	320.3	317.7
1.5-2.0	6.27	124.1	1.000	124.1	0.999	124.0	123.9	123.7	123.6	123.6	123.5	123.2	123.0
2.0-2.5	2.70	53.5	1.000	53.5	1.000	53.5	53.5	53.5	53.5	53.5	53.5	53.5	53.5
2.5-3.0	1.33	26.3	1.000	26.3	1.000	26.3	26.3	26.3	26.3	26.3	26.3	26.3	26.3
3.0-3.5	0.73	14.5	1.000	14.5	1.000	14.5	14.5	14.5	14.5	14.5	14.5	14.5	14.5
3.5-4.0	0.42	8.3	1.000	8.3	1.000	8.3	8.3	8.3	8·3	8.3	8.3	8.3	8.3
4.0-5.0	0.45	8.9	1.000	8.9	1.000	8.9	8.9	8.9	8.9	8.9	8.9	8.9	8.9
5.0-6.0	0.23	4.6	1.000	4.6	1.000	4.6	4.6	4.6	4.6	4.6	4.6	4.6	4.6
6.0-7.0	0.12	2.4	1.000	2.4	1.000	2.4	2.4	2.4	2.4	2.4	2.4	2.4	2.4
7.0	0.14	2.8	1.000	2.8	1.000	2.8	2.8	2.8	2.8	2.8	2.8	2.8	2.8
0.80-7.0	42.12	833.4		333.4		828.3	823.3	818.4	813.4	808.6	803.8	794.3	784.9
0.22-7.0	100.02	1980.1		1930.0		1762.8	1628.6	1525.4	1442.3	1372.6	1313.5	1217.5	1114.2
Absorption in permanent gases						10.0	12.0	13.0	14.0	15.0	16.0	18.0	19.0
Intensity of radiation (mcal/cm² · min) 1000 mb						1752.8	1616.6	1512.4	1428.3	1357.6	1297.5	1199.5	1095.2

2. INTEGRATED FLUX OF DIRECT SOLAR RADIATION

2.1 Solar constant

At great distances from the sun (for instance, in planetary orbits) the electromagnetic radiation is propagated in parallel rays. Since the distance between the sun and the earth changes continuously in the course of a year the amount of solar energy incident on the earth's surface will change accordingly. The maximum amplitude of variation comprises $\pm 3.4\%$ of the mean value of the flux of direct solar radiation. The maximum value of flux occurs toward the end of December and January whereas the minimum value takes places in July. The earth is situated at its mean distance from the sun on October 4 and April 3. The values of the coefficients for derivation of magnitudes of direct solar radiation with respect to average distance are given in Table 5.17.

Table 5.17 Coefficients for derivation of magnitudes of direct solar radiation with respect to mean distance between sun and earth

Number	Month					
	Jan	Feb	Mar	Apr	May	Jun
1	0.9667	0.9708	0.9819	0.9986	1.0154	1.0284
5	0.9669	0.9723	0.9842	1.0013	1.0177	1.0296
10	0.9671	0.9738	0.9864	1.0040	1.0199	1.0308
15	0.9677	0.9757	0.9892	1.0056	1.0220	1.0317
20	0.9682	0.9777	0.9920	1.0096	1.0241	1.0327
25	0.9694	0.9798	0.9950	1.01254	1.0261	1.0332

Number	Month					
	Jul	Aug	Sep	Oct	Nov	Dec
1	1.0337	1.0300	1.0183	1.0022	0.9849	0.9722
5	1.0337	1.0288	1.0161	1.000	0.9827	0.9710
10	1.0337	1.0276	1.0138	0.9970	0.9805	0.9698
15	1.0331	1.0257	1.0111	0.9942	0.9783	0.9688
20	1.0325	1.0237	1.0084	0.9914	0.9761	0.9679
25	1.0313	1.0212	1.0053	0.9884	0.9742	0.9673

The solar constant S_0 is the quantity of radiant energy of the sun arriving per unit time on a unit area perpendicular to the incident radiation and at the mean distance between the sun and the earth. In other words, the solar constant is the flux of radiant energy of the sun on a surface outside the atmosphere placed perpendicular to the rays for mean distance between the earth and the sun. The solar constants for other planets can be obtained by using the law of inverse proportionality of the square of distances, thus :

$$S_{\oplus} = \frac{R_m^2}{R^2} S_o, \tag{5.4}$$

where R_m is mean distance between the sun and the earth and R—mean distance between the sun and a planet.

Strictly speaking, the solar constant is not a constant quantity. Recent data confirm the suggestion that the solar constant varies within small limits with time. Thus the Smithsonian Institute has established during investigations through 30 years (1923-1952) that the annual average value of the solar constant changes only by $\pm 0.1\%$, whereas the maximum change reaches a value of 3%. Hardy and Giclas [40] showed that solar radiation does not change more than 1% in the visible range of the spectrum independently of the number of solar spots. Evidently, the change in the solar constant occurs mainly because of the intensity variation in ultraviolet and partly because of the blue region of the spectrum. Thus the ultraviolet emission from the sun doubled in the period from 1933 (minimum activity of the sun) to 1937 (maximum). The investigations of Aldrich and Hoover [29] showed that the solar constant rose by 0.6% from 1944 (minimum activity of sun) to 1948 (maximum). According to the data of Johnson and Iriante [43] it rose by 2% from 1953 (minimum) to 1959.

Although scientists attempted to determine the solar constant even in the 19th century, only in 1932 did they undertake the investigations which later provided sufficiently reliable values of the solar constant. Abbot's group at the Smithsonian Institute performed significant work for the determination of the magnitude of the solar constant and its steadiness. The magnitudes of S_0 obtained by different authors at different times are given in Table 5.18 [33].

The evaluation of the value of the solar constant is related to a precise determination of the magnitude of "ultraviolet" and "infrared" corrections. As already stated above, these corrections take into consideration radiation energy which could not be observed on the ground because of complete absorption of radiation in ozone in the region of the spectrum $\lambda < 296$ nm and in water vapor in the region of the spectrum $\lambda > 2.5\ \mu$ as well as radiation in the region of 296-346 nm and above 2440 nm as a

Table 5.18 Variation of values of the solar constant through 34 years [33]

Years	Author	S_0 cal/cm² · min	Radiation scale
1932-1952	Abbot	1.94	Smithsonian scale of 1932
1932	Linke	1.94	—do—
1934-1935	Mulders	1.95	Black body
1938	Ansold	1.90	Smithsonian scale of 1932
1950	Kvirk	1.99	—do—
1951	Nicolet	1.98±5%	—do—
1951	Allen	1.97±0.01	—do—
1954	Johnson	2.00±2%	—do—
1955	Ansold	1.96	—do—
1956	Steer, Johnston	2.05±5%	Scale of National Bureau of Standards, USA
1958	Allen	1.99±1%	Smithsonian scale of 1932
1966	Sitnik	2.076±3.5%	Black body

consequence of the limitations on the spectral range of the Smithsonian spectrobolograph (346-2440 nm). The values of the corrections obtained by different authors are given in Table 5.19 [27].

Table 5.19 Magnitudes of "ultraviolet" and "infrared" corrections (cal/cm² · min) according to various researchers [27]

Spectral range	Abbot	Nicolet	Johnson	Steer and Johnston	Sitnik
ΔS (UV, $\lambda<346$ nm)	0.061	0.062	0.085	0.074	0.059
ΔS (IR, $\lambda>2440$ nm)	0.038	0.064	0.076	0.068	0.073
ΔS ($346<\lambda<2440$ nm)	1.835	1.855	1.841	1.908	1.944

The variation in the value of the solar constant is also connected with the variation in the scale of the radiation calibrators used in the determination of relative energy distribution for the spectrum of solar radiation with respect to absolute values of flux of direct solar radiation. Thus the Smithsonian scale (based on the water-jet pyrheliometer), which was established in 1913, was corrected by 2.5% in 1932 and this correction was carried into the value of the solar constant, but the remaining American

recordings on radiation were made on the earlier scale so as not to impair an array of observations. In order to introduce the International Pyrheliometric Scale (IPS-1956) the data on the Smithsonian scale of 1913 had to be reduced by 2% (the relation between the scales is shown in Fig. 5.10). The European scale, based on the Ångström Pyrheliometer A-70, also required alteration. An estimate of the systematic errors of the pyrheliometer, carried out in 1948, showed that Ångström's scale is undervalued by 1.3%. Moreover, it was established (1958) that the understanding on an average works out at 2%. It was necessary to increase the observation recorded by 1.5% in order to switch over from the earlier Ångström scale to IPS-1956.

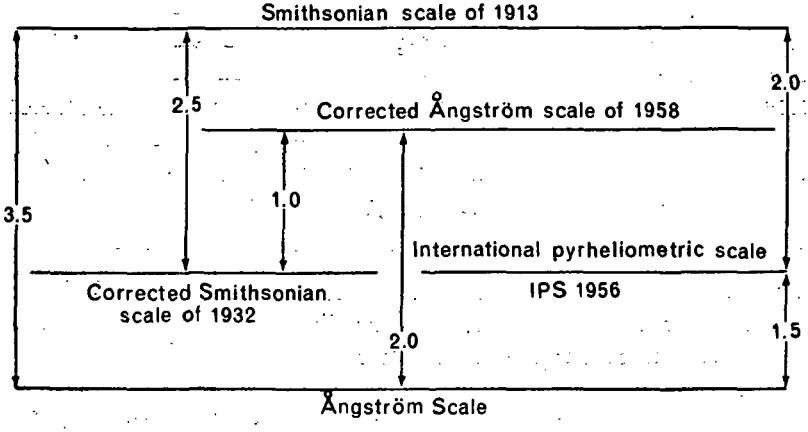

Fig. 5.10. Relation between fundamental pyrheliometric scales [22].

Complete agreement between the Smithsonian and the Ångström scales could not be achieved, and there remains a discrepancy of 1%.

The International Pyrheliometric scale, introduced on January 1, 1957, represents (within an accuracy of 1%) the absolute radiation scale, expressed in cal/cm² · min or ly/min.

Unless specifically stated, all data on radiation fluxes published since 1957 in the Soviet Union or Europe (and some in America) are expressed in IPS-1956 units. Up to 1957 Ångström's scale was utilized in Europe and the Smithsonian scale in America.

The International Commission on Radiation recommended the acceptance of the following standard value for the solar constant in 1957; viz. 1.98 cal/cm² · min according to the International Pyrheliometric scale.

A value of 2.0 cal/cm² · min for the solar constant is usually accepted for computations of radiative attenuation in the atmosphere. This magnitude could be considered as the mean estimate over the last 15 years. Recent (Oct. 1967) experimental measurements on the flux of direct solar

radiation at 84.5 km [34] gave a value of the solar constant equal to 1.95 cal/cm² · min; i. e. 2.5% lower than that of Johnson (2.00 cal/cm² · min); whereas spectral measurements showed that in the shortwave region the energy distribution in the spectrum of solar radiation is higher than that obtained by Johnson by approximately 7%. Extrapolation of balloon data on direct solar radiation at the boundary of the atmosphere also leads to the value $S_0 \approx 1.94$ cal/cm² · min [45].

These values of the solar constant are not final insofar as the possible existence of a variation in S_0 of 2% demands further investigation. The value of the constant, viz. $S_0 = 1.98$ cal/cm² · min accepted in 1957, remains unchanged to date.

The empirical formulas into which the solar constant S_0 enters are used for the evaluation of the daily movement of the flux of solar radiation with respect to a specific atmospheric mass in actinometric applications. Since solar radiation with wavelengths lying outside the limits of spectral range 346-2440 nm does not exceed 2-3% at ground level, there is no need to use S_0 obtained for the spectral interval 200-7000 nm in the formulas. For similar computations Georgi (1951) suggested the use of the Meteorological Solar Constant S_{0m} for which a value of 1.80 cal/cm² · min is adopted. While studying the empirical formula for the relation between the flux of solar radiation and the atmospheric mass Sivkov [26] arrived at the conclusion that the application of the value $S_{0\,m} = 1.80$ cal/cm² · min leads to a value of the flux of solar radiation which is closer to its real value.

However, the data of other authors (see Table 5.19) on the flux of the solar radiation entering the upper boundary of the atmosphere in the range of wavelengths 346-2440 nm differ considerably from the magnitude suggested by Georgi.

2.2 Vertical distribution of direct solar radiation

The profiles of direct solar radiation up to an altitude of 25 to 33 km were first obtained during balloon probings in 1962 [15]. Measurements of direct solar radiation in free-atmosphere, conducted by Leningrad State University, besides the investigations surveyed here, were accomplished only sporadically up to an altitude of 7 km [28]. An inadequate collection of data is the result of technical difficulties arising out of measurements of the flux of direct radiation from a moving aircraft (airplane, balloon). The use of an automatic solar tracking system alone could ensure the possibility of such measurements. Two actinometers, one of which was hermetically sealed, were installed in the Leningrad State University's tracking system. In this case light entering through a square window falls on a sensitive element. There is an accuracy of the order

of 2.0-2.5% [18] in the balloon measurements of absolute values of the flux of direct solar radiation.

The data on direct solar radiation, continuously registered at the time of the ascent and brief drift of the balloon, contain a significant amount of important information. Using these profiles, it is possible to evaluate heat flux due to absorption of solar radiation in the atmospheric layer of thickness varying from several hundred meters to 30 km. It also enables us to investigate the structure of the atmospheric layer probed, the reasons for anomalous variations in transparency in the layers probed and those lying above as well as the evaluation of the magnitude and the variation of the solar constant from a sufficient collection of data on the flux of direct solar radiation S on the roof of the probing.

Fig. 5.11 shows profiles which characterize different attenuating properties of air masses in the area of probing (intermediate region of the European part of the USSR). The magnitudes of direct solar radiation are given in IPS-1956 for the mean distance between the earth and the sun. More detailed information about profiles of solar radiation can be found in [16].

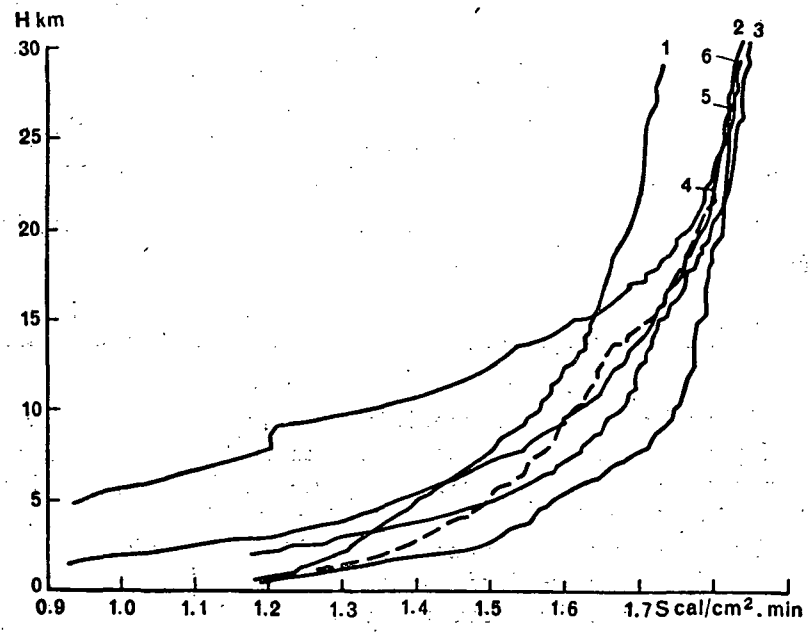

Fig 5.11. Vertical profiles of direct solar radiation obtained in the period 1962-1967.

1—November 22, 1962; 2—July 11, 1964; 3—October 23, 1964; 4—October 21, 1964; 5—June 23, 1967; July, 7, 1962.

Profile 1 gives the variation of the direct solar radiation flux around midday in summer when S usually attains a maximum value in the troposphere as well as the stratosphere. It is easily noticed that attenuation of S occurs mainly in the troposphere, so that the profile is sharply curved. Profile 1 can be accepted as the mean for midday during the summer seasons in 1962-1965. The values of the flux of direct solar radiation for this flight are given in Table 5.20.

Table 5.20 Experimental values for flux of direct solar radiation up to the altitude of 29 km for noon hours when $h_{\odot} \approx 50°$

H km	S_R cal/cm² . min	H km	S_R cal/cm² . min
0	1.087	15000	1.792
500	1.185	16000	1.793
1000	1.275	17000	1.798
2000	1.454	18000	1.800
3000	1.516	19000	1.804
4000	1.563	20000	1.817
5000	1.590	21000	1.820
6000	1.645	22000	1.820
7000	1.681	23000	1.822
8000	1.717	24000	1.823
9000	1.735	25000	1.825
10000	1.752	26000	1.830
11000	1.762	27000	1.832
12000	1.774	28000	1.835
13000	1.778	29000	1.838
14000	1.780		

REMARKS: S_R is the value of the flux of direct solar radiation derived for the average distance between the sun and the earth.

Profiles 2 and 3, which correspond to maximum values S in the troposphere (3) and the stratosphere (2), characterize the course of S at lower solar altitudes. The profiles are rather flat, i.e. attenuation of S occurs more smoothly than at greater solar altitudes. From here it follows that in autumn and winter the upper stratosphere and mesosphere are warmer than in summer. Of course, the difference in the values of S on account of different distances between the sun and the earth is added to this. At any rate these two facts evidently explain the warmer mesosphere during autumn and winter.

The similar though highly transient influence of the changing altitude of the rising sun in summer should provide the morning wave of heating, moving toward the west, in the upper stratosphere.

Of all the balloon probings given, profile 2 describes the case of minimum turbidity of the air mass. Profiles 4 and 5 represent possible variations in S in the troposphere and stratosphere under identical external conditions (time of year, time of day, area of probing), although in different years. The profiles clearly resemble each other above 15 km, but at lesser heights the difference in the attenuating properties of air masses leads to a difference in the profile structure. The above example illustrates the difficulties in assessing the attenuation characteristics of the upper troposphere and even more so of the stratosphere from the ground measurements alone.

A systematic change of all profiles is most clearly expressed at altitudes between 8-22 km. This behavior of profiles implies the continuous existence of a laminar structure in the distribution of aerosol and ozone in the stratosphere and of aerosol and water vapor in the troposphere.

Profile 6, along with the five remaining profiles, gives an estimate of the change in S in the vicinity of the peak probe altitude in the period 1962-1967, i.e. from the minimum activity of the sun to a maximum. The data obtained show that there is a variation of 2-2.5% in the integrated flux of solar radiation with respect to solar activity. As a result of the extrapolation of the high-altitude data on S through 1964-1967 at the boundary of the atmosphere and the introduction of the corrresponding corrections, many values of S_0^{extrap} were obtained which varied from 1.896 to 1.938 cal/cm^2 · min depending on the solar activity.

2.3 Geographic distribution

The most significant data characterizing the incidence of solar radiation on the ground and describing the geographic distribution of direct solar radiation over the earth will be surveyed in this section.

This information is necessary for meteorology and astronomy as well as for the solution of an array of applied problems.

For the purpose of analyzing the space-time distribution of direct solar radiation one must differentiate between the flux incident on a surface perpendicular to the solar radiation and that flux which is incident on the ground level, i.e. on an idealized underlying surface, or on a surface oriented at different angles to the rays.

It is possible to evaluate the flux S of direct solar radiation entering a surface perpendicular to the rays of the sun through direct actinometric observation. The incidence of direct solar radiation on a horizontal

surface is equally important for the characteristics of the radiative regime and may be computed from the following formula :

$$S_r = S \sin h_\odot, \qquad (5.5)$$

where $h_\odot$ is altitude of sun at the time of observation.

The duration of sunshine is an interesting and useful characteristic which qualitatively reflects the fundamental properties of the geographic distribution of the incident solar radiation. It indicates the time for which the sun is situated at a given point above the horizon when it is not hidden behind clouds, haze or mist.

The relative magnitude of the duration of sunshine or the ratio of the observed duration of sunshine to the possible (as a percentage) serves as the second representative characteristic. Relevant data for all the months in a year may be found in "Handbook on Climate of the USSR", Part I.

There is a considerably greater collection of data on the duration of sunshine than on other characteristics of solar radiation, so that this data can be used for various extents of solar radiation or for replacement of insufficient data at several stations. Thus, for instance, in the North, North-East of the USSR and in the Far East region of the Soviet Union there is a network of actinometric stations so that the duration of sunshine is taken into consideration while drawing isolines for the chart of direct solar radiation.

The planetary distribution of the sunshine duration in hours as obtained by T. G. Berlyand and V. Ya. Danil'chenko [6] is given in Fig. 5.12.

The duration of sunshine over a year changes from 500 to 4000 h over the entire earth; moreover, the minimum has been observed in the region of the Southern Orkney Islands (60°44′ S, 44°4′ W) and comprises magnitudes of 483 h, whereas the maximum is found in the Sahara Desert in the region of Aswan (of the order of 3700 h).

The subtropical deserts and semideserts are the sunniest, whereas the Western and Northern coasts of Eurasia and the Western coast of Canada appear to be the cloudiest.

High values of radiation flux have been observed in Antarctica. According to data collected by N. P. Rusin [24] the maximum value of direct vertical radiation incident on Antarctica is about 1.67 cal/cm² · min. This value noticeably exceeds the corresponding values registered at other points of the earth's surface. The same can be said about the possible daily amounts (relative to a clear sky) of solar radiation on a horizontal surface. The probable daily amount of solar radiation reaches a value of 850-900 cal/cm² at the highest points of a glacial plateau.

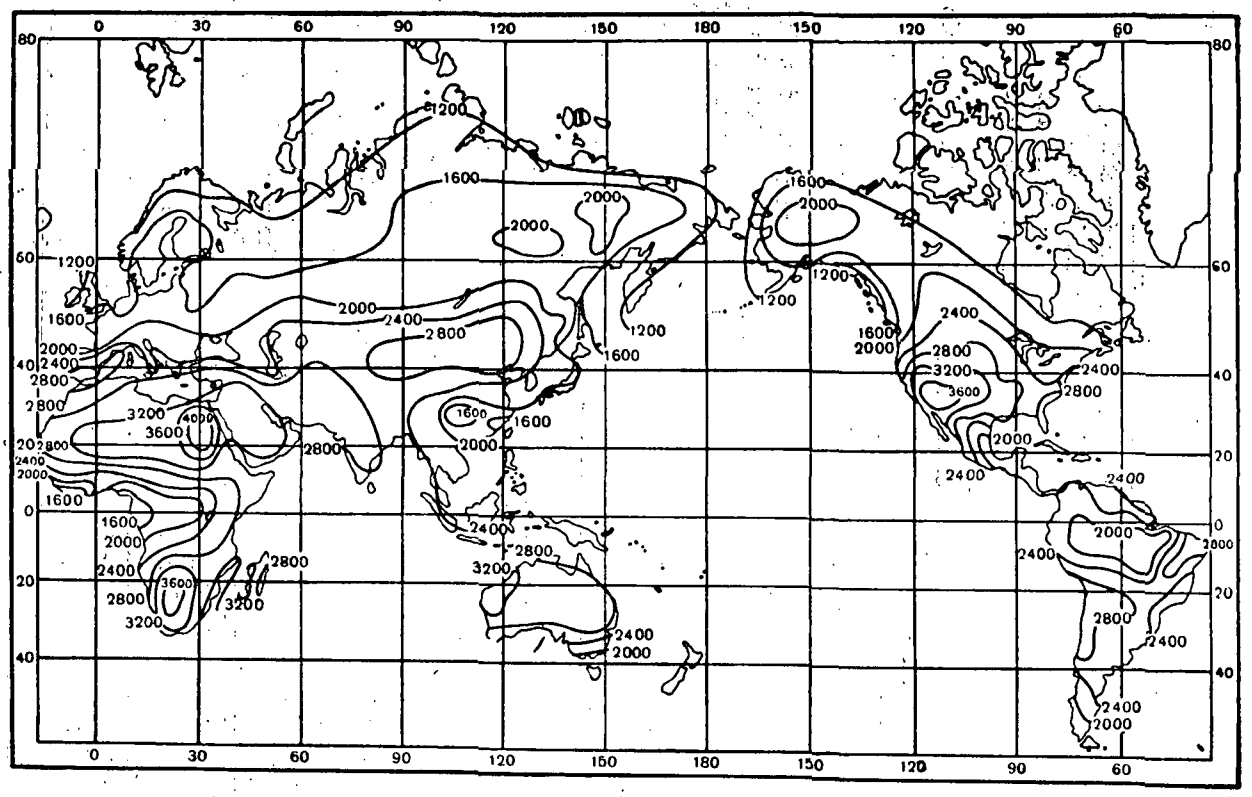

Fig. 5.12. Planetary distribution of duration of sunshine over a year (in hrs.).

Table 5.21 Probable amounts of direct solar radiation on a perpendicular surface (kcal/cm²)

Latitude	Jan	Feb	Mar	Apr	May	Jun	Jul	Aug	Sep	Oct	Nov	Dec	Year
38°N	19.0	19.6	24.4	25.4	27.4	26.6	26.1	25.1	22.8	22.4	17.7	17.7	274.2
40	17.3	19.1	24.6	25.0	27.4	26.9	26.3	25.3	22.7	21.8	17.3	17.2	270.9
42	17.5	18.3	25.0	24.9	27.8	27.2	26.5	25.2	22.8	21.3	17.1	16.5	270.1
44	16.3	17.6	24.5	24.7	27.7	27.5	26.9	24.9	22.7	20.9	16.6	15.3	265.4
46	14.8	17.0	23.8	24.6	27.9	26.5	27.1	24.7	22.7	20.3	15.9	14.0	260.6
48	13.8	16.4	23.8	24.4	27.9	27.7	27.4	24.5	22.6	19.7	14.9	12.6	255.7
50	13.0	15.4	23.8	25.0	28.6	28.0	28.0	24.9	22.6	19.3	14.2	11.8	254.6
52	12.1	14.8	23.8	25.3	28.8	29.0	28.8	25.4	22.4	18.8	13.5	10.6	253.3
54	11.2	14.4	23.6	26.4	29.0	29.4	29.3	26.0	22.3	18.2	12.8	9.3	251.9
56	10.4	14.0	23.2	26.1	29.8	29.9	30.0	26.1	21.4	17.2	11.9	8.2	248.2
58	9.1	13.3	23.0	26.1	30.6	31.2	30.6	26.4	22.3	16.2	10.8	7.1	246.7
60	7.8	12.4	22.5	26.4	31.6	32.3	32.0	26.6	23.0	15.9	9.6	5.7	245.8
62	5.8	11.4	22.2	26.8	32.6	33.3	32.6	26.7	23.2	15.6	8.8	4.4	244.4
64	5.3	10.4	22.2	26.6	34.1	34.8	33.6	28.7	22.7	15.7	6.8	0	241.0
66	3.6	9.5	21.9	27.0	35.6	40.0	35.9	29.9	23.2	15.6	5.9	0	248.1
68	3.0	8.7	17.0	28.1	36.7	40.5	40.0	31.9	22.6	12.5	4.8	0	245.8

The problem about the distribution of the monthly and annual amounts of direct solar radiation on a perpendicular surface for the territory of the USSR was studied in detail by Z. I. Pivovarova [20].

The monthly and annual amounts of direct solar radiation, determined by the trapezoid method of quick observations carried out at the network of meteostations, are given in Table 5.21.

Material from observations at 105 actinometric stations was employed for the plotting of the chart of direct solar radiation on a perpendicular surface. Mountainous regions (stations above the height of 1000 m) were not examined for lack of sufficient data on recordings. The stations are distributed rather evenly in the territories surveyed, where the network of stations is infrequent (North-North-East of the USSR and the Far East). The duration of sunshine was taken into consideration while plotting isolines (dotted).

Isolines on the yearly chart are plotted through intervals of 10 kcal/cm², (in monthly charts—through 2 kcal/cm²) which accurately determine the amounts of direct radiation for 10-year periods and its variation in space.

It is obvious from the charts plotted by Pivovarova [20] that the annual amount of solar heat incident on a perpendicular surface on the coast of the Arctic Ocean adds up to 60-70 kcal/cm². This amount increases toward the south, reaching a value of 170 kcal/cm² and above in Central Asia.

Although the astronomical factor determines direct solar radiation, cloudiness changes the latitudinal distribution of the solar radiation to a significant degree. This is especially in evidence in the European Territory of the USSR where the isolines are directed from SW to NE. A decrease in the number of hours of sunshine causes some decrease in radiation as compared with the surrounding regions.

The charts characterizing the influence of cloudiness on the incidence of direct solar radiation in warm and cold periods for June and December are given in Figs. 5.13 and 5.14.

Data on recordings from the stations of actinometric networks over intervals with marked bright sun ($\odot^2$) and general cloudiness of 0 to 2 tenths were used for the characterization of the radiative conditions during clear weather. Material from 150 stations (height below 800 m) over the period 1952-1958 (monsoon region being excluded) was treated and tables of radiation flux on perpendicular surface on clear days [23] were computed. Table 5.22 contains the mean values (over many years) for different latitudes of the Northern Hemisphere, averaged over intervals of 12 months of the year.

Analogous data on solar radiation on horizontal surface for clear days are given in Table 5.23.

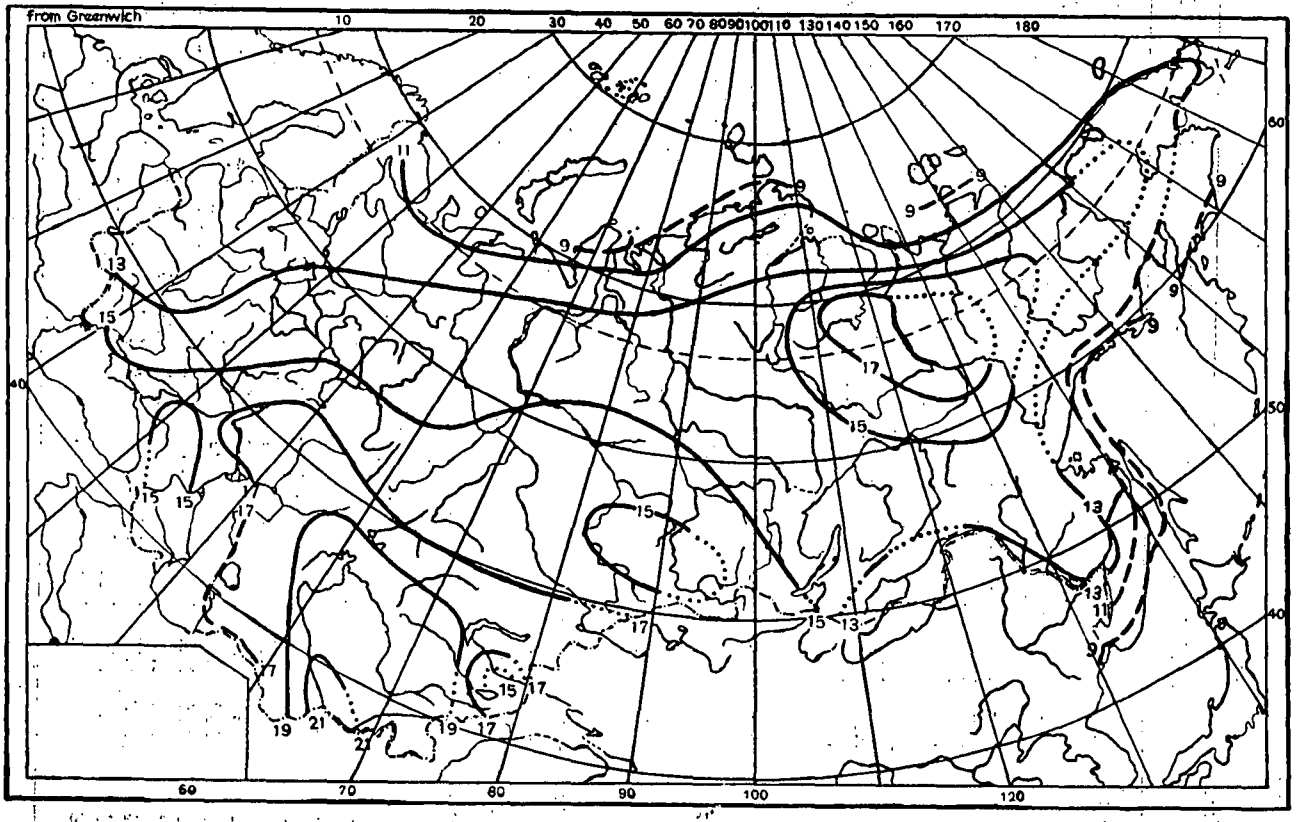

Fig. 5.13. Direct solar radiation on a perpendicular surface (kcal/cm² · mon), July.

Table 5.22 Direct solar radiation (cal/cm² · min) on perpen-

Latitude	Jan			Feb			Mar					
	9:30	12:30	15:30	9:30	12:30	15:30	6:30	9:30	12:30	15:30	6:30	9:30
38°N	1.18	1.32	0.97	1.23	1.36	1.13	0.46	1.27	1.35	1.15	0.70	1.21
40	1.12	1.28	0.94	1.20	1.35	1.08	—	1.24	1.33	1.14	0.70	1.20
42	1.06	1.26	0.90	1.16	1.31	1.03	0.51	1.23	1.32	1.13	0.71	1.19
44	1.01	1.20	0.82	1.11	1.27	0.99	0.51	1.21	1.30	1.11	0.72	1.17
46	0.94	1.13	0.73	1.05	1.23	0.93	0.52	1.20	1.29	1.09	0.72	1.15
48	0.86	1.10	0.65	1.01	1.20	0.88	0.52	1.19	1.28	1.07	0.73	1.16
50	0.82	1.06	0.60	1.00	1.18	0.85	0.52	1.19	1.26	1.06	0.75	1.17
52	0.77	1.02	0.55	0.98	1.15	0.82	0.52	1.18	1.26	1.05	0.78	1.20
54	0.73	0.98	0.50	0.96	1.13	0.80	0.51	1.16	1.26	1.04	0.80	1.23
56	0.67	0.94	0.45	0.94	1.10	0.78	0.49	1.14	1.26	1.03	0.81	1.25
58	0.60	0.88	0.38	0.88	1.08	0.75	0.48	1.12	1.23	1.00	0.83	1.23
60	0.52	0.78	0.31	0.82	1.05	0.67	0.49	1.07	1.21	0.97	0.83	1.20
62	0.42	0.71	—	0.74	1.02	0.60	0.50	1.04	1.19	0.94	0.83	1.19
64	—	0.60	—	0.68	0.96	0.55	0.53	1.01	1.15	0.90	0.83	1.19
66	—	0.49	—	0.65	0.89	0.51	0.55	0.99	1.10	0.85	0.83	1.19
68	—	0.47	—	0.64	0.84	0.44	—	0.93	1.02	0.83	0.86	1.20

Latitude	Jul					Aug						
	6:30	9:30	12:30	15:30	18:30	6:30	9:30	12:30	15:30	18:30	6:30	9:30
38°N	0.69	1.10	1.18	1.02	—	0.64	1.14	1.22	1.08	—	0.59	1.19
40	0.73	1.12	1.19	1.05	0.40	0.66	1.14	1.22	1.08	1.24	0.59	1.19
42	0.78	1.14	1.20	1.08	0.47	0.69	1.13	1.21	1.07	0.27	0.60	1.18
44	0.80	1.14	1.20	1.10	0.52	0.71	1.12	1.20	1.06	0.32	0.61	1.17
46	0.81	1.14	1.20	1.10	0.57	0.73	1.11	1.19	1.05	0.36	0.61	1.16
48	0.83	1.14	1.20	1.10	0.61	0.74	1.10	1.19	1.05	0.37	0.61	1.15
50	0.86	1.14	1.21	1.10	0.64	0.75	1.10	1.19	1.04	0.40	0.60	1.15
52	0.88	1.15	1.22	1.11	0.69	0.76	1.10	1.19	1.04	0.43	0.62	1.14
54	0.90	1.16	1.23	1.12	0.73	0.79	1.10	1.20	1.05	0.47	0.62	1.13
56	0.92	1.16	1.24	1.13	0.75	0.81	1.10	1.20	1.05	0.50	0.62	1.12
60	0.95	1.16	1.25	1.13	0.79	0.84	1.12	1.20	1.07	0.60	0.67	1.14
62	0.96	1.16	1.25	1.15	0.81	0.86	1.14	1.20	1.09	0.65	0.69	1.15
64	1.00	1.18	1.25	1.16	0.84	0.89	1.15	1.20	1.11	0.70	0.70	1.15
66	1.03	1.20	1.26	1.18	0.91	0.92	1.17	1.21	1.12	0.73	0.71	1.12
68	1.03	1.22	1.28	1.19	0.94	1.00	1.22	1.25	1.12	0.80	0.80	1.10

dicular surface on clear days (average over many years) [23]

Apr					May					Jun		
12:30	15:30	18:30	6:30	9:30	12:30	15:30	18:30	6:30	9:30	12:30	15:30	18:30
1.28	1.09	—	0.83	1.20	1.25	1.10	0.29	0.84	1.20	1.25	1.12	0.44
1.30	1.09	—	0.85	1.20	1.25	1.12	0.34	0.85	1.20	1.25	1.12	0.49
1.30	1.10	—	0.86	1.19	1.25	1.14	0.38	0.86	1.20	1.25	1.12	0.53
1.29	1.10	—	0.87	1.19	1.25	1.13	0.42	0.88	1.19	1.24	1.12	0.56
1.24	1.09	0.21	0.88	1.18	1.26	1.12	0.44	0.89	1.18	1.23	1.11	0.59
1.22	1.07	0.22	0.89	0.17	1.26	1.12	0.48	0.90	1.17	1.23	1.10	0.62
1.23	1.07	0.24	0.89	1.17	1.26	1.12	0.52	0.92	1.17	1.23	1.11	0.65
1.26	1.08	1.29	0.90	1.18	1.26	1.14	0.56	0.94	1.17	1.23	1.12	0.68
1.30	1.11	0.37	0.92	1.20	1.27	1.15	0.60	0.95	1.17	1.23	1.13	0.71
1.31	1.14	0.44	0.94	1.20	1.28	1.15	0.63	0.96	1.17	1.22	1.13	0.74
1.30	1.14	0.48	0.96	1.20	1.29	1.15	0.66	0.97	1.18	1.22	1.13	0.77
1.28	1.12	0.50	0.99	1.20	1.29	1.15	0.70	0.98	1.18	1.22	1.13	0.80
1.25	1.10	0.50	1.00	1.22	1.30	1.15	0.75	1.01	1.20	1.23	1.14	0.85
1.25	1.10	0.51	1.01	1.23	1.31	1.16	0.79	1.03	1.21	1.25	1.14	0.90
1.25	1.10	0.54	1.03	1.24	1.32	1.18	0.83	1.06	1.22	1.26	1.15	0.93
1.25	1.11	0.60	1.06	1.25	1.34	1.20	0.86	1.08	1.22	1.28	1.16	0.96

Sept		Oct				Nov			Dec		
12:30	15:30	6:30	9:30	12:30	15:30	9:30	12:30	15:30	9:30	12:30	15:30
1.25	1.04	0.44	1.20	1.26	0.98	1.14	1.24	0.80	1.17	1.27	0.77
1.25	1.03	0.44	1.18	1.25	0.97	1.13	1.24	0.80	1.11	1.25	0.76
1.24	1.02	0.43	1.16	1.24	0.95	1.13	1.23	0.78	1.08	1.21	0.75
1.23	1.02	0.42	1.14	1.23	0.93	1.13	1.22	0.74	1.03	1.16	0.65
1.21	1.01	0.41	1.11	1.22	0.90	1.09	1.20	0.69	0.95	1.10	0.55
1.21	1.00	0.38	1.10	1.20	0.86	1.04	1.15	0.62	0.89	1.05	0.43
1.20	1.00	0.37	1.08	1.19	0.84	1.00	1.12	0.57	0.84	1.02	0.37
1.20	0.99	0.37	1.07	1.18	0.82	0.97	1.09	0.53	0.78	0.99	0.26
1.20	0.99	0.37	1.06	1.16	0.80	0.92	1.06	0.50	0.73	0.95	—
1.20	1.00	—	1.05	1.15	0.77	0.86	1.00	0.47	0.68	0.88	—
1.21	1.05	—	1.03	1.12	0.73	0.75	0.85	0.31	0.49	0.74	—
1.23	1.05	—	1.02	1.11	0.73	0.70	0.80	0.30	0.44	0.57	—
1.24	1.05	—	0.98	1.10	0.72	0.64	0.75	—	—	—	—
1.22	1.04	—	0.90	1.06	0.69	0.52	0.75	—	—	—	—
1.20	0.99	—	0.82	0.95	0.60	0.42	0.70	—	—	—	—

Table 5.23 Direct solar radiation (cal/cm² · min) on horizontal

Latitude	Jan			Feb			Mar					
	9:30	12:30	15:30	9:30	12:30	15:30	6:30	9:30	12:30	15:30	6:30	9:30
38°N	0.40	0.64	0.23	0.55	0.82	0.37	0.06	0.73	0.99	0.52	0.15	0.88
40	0.37	0.59	0.18	0.51	0.78	0.34	0.06	0.71	0.97	0.51	0.15	0.85
42	0.32	0.56	0.13	0.47	0.74	0.32	0.05	0.69	0.94	0.50	0.15	0.82
44	0.28	0.50	0.09	0.43	0.69	0.29	0.05	0.65	0.90	0.48	0.16	0.80
46	0.23	0.44	0.08	0.38	0.64	0.26	0.05	0.61	0.86	0.44	0.16	0.77
48	0.20	0.38	0.06	0.34	0.61	0.23	0.04	0.58	0.83	0.42	0.16	0.76
50	0.17	0.36	0.05	0.31	0.54	0.21	0.04	0.56	0.79	0.40	0.18	0.75
52	0.13	0.31	0.04	0.29	0.48	0.18	0.04	0.54	0.75	0.38	0.18	0.72
54	0.10	0.26	0.01	0.27	0.44	0.16	0.04	0.51	0.71	0.36	0.19	0.71
56	0.08	0.21	—	0.24	0.41	0.14	0.04	0.47	0.66	0.33	0.19	0.70
58	0.06	0.16	—	0.19	0.37	0.13	0.04	0.43	0.62	0.31	0.19	0.67
60	0.03	0.12	—	0.16	0.32	0.11	0.04	0.41	0.57	0.29	0.19	0.64
62	0.03	0.09	—	0.14	0.27	0.09	0.04	0.37	0.53	0.26	0.19	0.62
64	—	0.08	—	0.12	0.24	0.08	0.03	0.35	0.48	0.24	0.18	0.58
66	—	0.07	—	0.11	0.23	0.07	0.02	0.33	0.43	0.22	0.18	0.56
68	—	—	—	0.08	0.21	0.05	—	0.27	0.37	0.19	0.18	0.54

Latitude	Jul					Aug						
	6:30	9:30	12:30	15:30	18:30	6:30	9:30	12:30	15:30	18:30	6:30	9:30
38°N	0.23	0.91	1.15	0.74	0.07	0.18	0.86	1.11	0.66	0.03	0.08	0.78
40	0.24	0.91	1.13	0.73	0.08	0.18	0.86	1.10	0.64	0.03	0.08	0.76
42	0.25	0.90	1.11	0.73	0.10	0.18	0.84	1.08	0.63	0.03	0.09	0.74
44	0.26	0.89	1.09	0.73	0.11	0.18	0.80	1.03	0.62	0.03	0.10	0.73
46	0.28	0.87	1.07	0.72	0.13	0.19	0.77	0.97	0.61	0.04	0.11	0.70
48	0.30	0.85	1.05	0.71	0.13	0.19	0.75	0.94	0.59	0.05	0.09	0.67
50	0.31	0.84	1.04	0.71	0.15	0.21	0.74	0.92	0.58	0.05	0.09	0.64
52	0.32	0.84	1.03	0.71	0.17	0.21	0.73	0.91	0.57	0.06	0.08	0.62
54	0.32	0.83	1.02	0.70	0.19	0.22	0.73	0.88	0.57	0.07	0.09	0.59
56	0.34	0.82	0.99	0.69	0.20	0.23	0.70	0.85	0.56	0.08	0.09	0.56
58	0.35	0.81	0.96	0.67	0.22	0.24	0.68	0.82	0.53	0.09	0.09	0.53
60	0.36	0.78	0.95	0.67	0.23	0.24	0.66	0.79	0.51	0.10	0.11	0.51
62	0.36	0.76	0.93	0.67	0.23	0.24	0.64	0.78	0.51	0.11	0.11	0.48
64	0.37	0.75	0.90	0.67	0.25	0.24	0.64	0.75	0.51	0.12	0.11	0.45
66	0.38	0.75	0.88	0.66	0.28	0.25	0.64	0.72	0.51	0.14	0.12	0.42
68	0.39	0.75	0.87	0.66	0.31	0.27	0.64	0.71	0.51	0.16	0.13	0.39

surface for clear days (average over many years) [23]

Apr			May					Jun				
12:30	15:30	18:30	6:30	9:30	12:30	15:30	18:30	6:30	9:30	12:30	15:30	18:30
1.14	0.65	—	0.27	0.97	1.20	0.73	0.03	0.29	0.99	1.20	0.76	0.05
1.09	0.62	—	0.28	0.96	1.17	0.71	0.04	0.31	0.98	1.18	0.75	0.07
1.06	0.60	—	0.29	0.95	1.15	0.70	0.05	0.33	0.97	1.17	0.75	0.09
1.02	0.58	—	0.29	0.93	1.12	0.69	0.06	0.34	0.94	1.16	0.75	0.11
0.99	0.56	—	0.30	0.89	1.10	0.68	0.06	0.34	0.92	1.12	0.73	0.12
0.95	0.55	0.01	0.31	0.88	1.06	0.68	0.07	0.35	0.91	1.09	0.72	0.13
0.93	0.54	0.01	0.31	0.88	1.04	0.68	0.08	0.36	0.90	1.07	0.71	0.13
0.91	0.54	0.02	0.32	0.86	1.02	0.68	0.09	0.37	0.89	1.07	0.71	0.15
0.91	0.53	0.03	0.33	0.84	0.99	0.67	0.11	0.38	0.87	1.05	0.71	0.17
0.86	0.51	0.04	0.33	0.83	0.97	0.66	0.11	0.38	0.86	1.02	0.71	0.18
0.81	0.50	0.05	0.34	0.82	0.95	0.65	0.13	0.39	0.86	1.00	0.71	0.20
0.78	0.48	0.05	0.35	0.81	0.93	0.63	0.15	0.41	0.84	0.99	0.69	0.22
0.75	0.47	0.05	0.37	0.80	0.91	0.62	0.16	0.41	0.83	0.96	0.69	0.24
0.72	0.45	0.05	0.37	0.80	0.89	0.61	0.17	0.42	0.82	0.92	0.68	0.26
0.69	0.43	0.06	0.38	0.78	0.87	0.60	0.18	0.44	0.82	0.90	0.67	0.28
0.67	0.42	0.07	0.40	0.75	0.84	0.57	0.19	0.45	0.80	0.90	0.67	0.31

Sep		Oct				Nov			Dec		
12:30	15:30	6:30	9:30	12:30	15:30	9:30	12:30	15:30	9:30	12:30	15:30
1.02	0.51	0.03	0.69	0.86	0.29	0.52	0.69	0.18	0.40	0.60	0.15
0.98	0.50	0.03	0.65	0.81	0.29	0.49	0.65	0.17	0.36	0.56	0.12
0.94	0.49	0.03	0.61	0.78	0.28	0.45	0.61	0.14	0.32	0.51	0.09
0.90	0.48	0.03	0.58	0.73	0.28	0.42	0.56	0.12	0.28	0.45	70.0
0.88	0.46	0.03	0.53	0.67	0.25	0.36	0.51	0.10	0.23	0.39	0.03
0.86	0.43	0.02	0.49	0.64	0.22	0.34	0.45	0.18	0.19	0.36	0.02
0.83	0.42	0.01	0.47	0.60	0.19	0.31	0.41	0.06	0.16	0.30	0.01
0.79	0.40	0.01	0.43	0.56	0.17	0.24	0.36	0.05	0.11	0.24	0.01
0.73	0.38	0.01	0.40	0.50	0.14	0.20	0.30	0.04	0.08	0.20	—
0.69	0.37	—	0.35	0.45	0.13	0.15	0.23	0.02	0.07	0.16	—
0.66	0.37	—	0.32	0.38	0.11	0.12	0.20	0.01	0.03	0.14	—
0.65	0.35	—	0.28	0.35	0.11	0.10	0.15	0.00	0.02	0.09	—
0.62	0.32	—	0.24	0.33	0.10	0.08	0.12	—	—	0.06	—
0.58	0.31	—	0.22	0.31	0.10	0.06	0.10	—	—	—	—
0.54	0.28	—	0.18	0.27	0.10	0.04	0.09	—	—	—	—
0.48	0.26	—	0.13	0.20	0.09	0.01	0.08	—	—	—	—

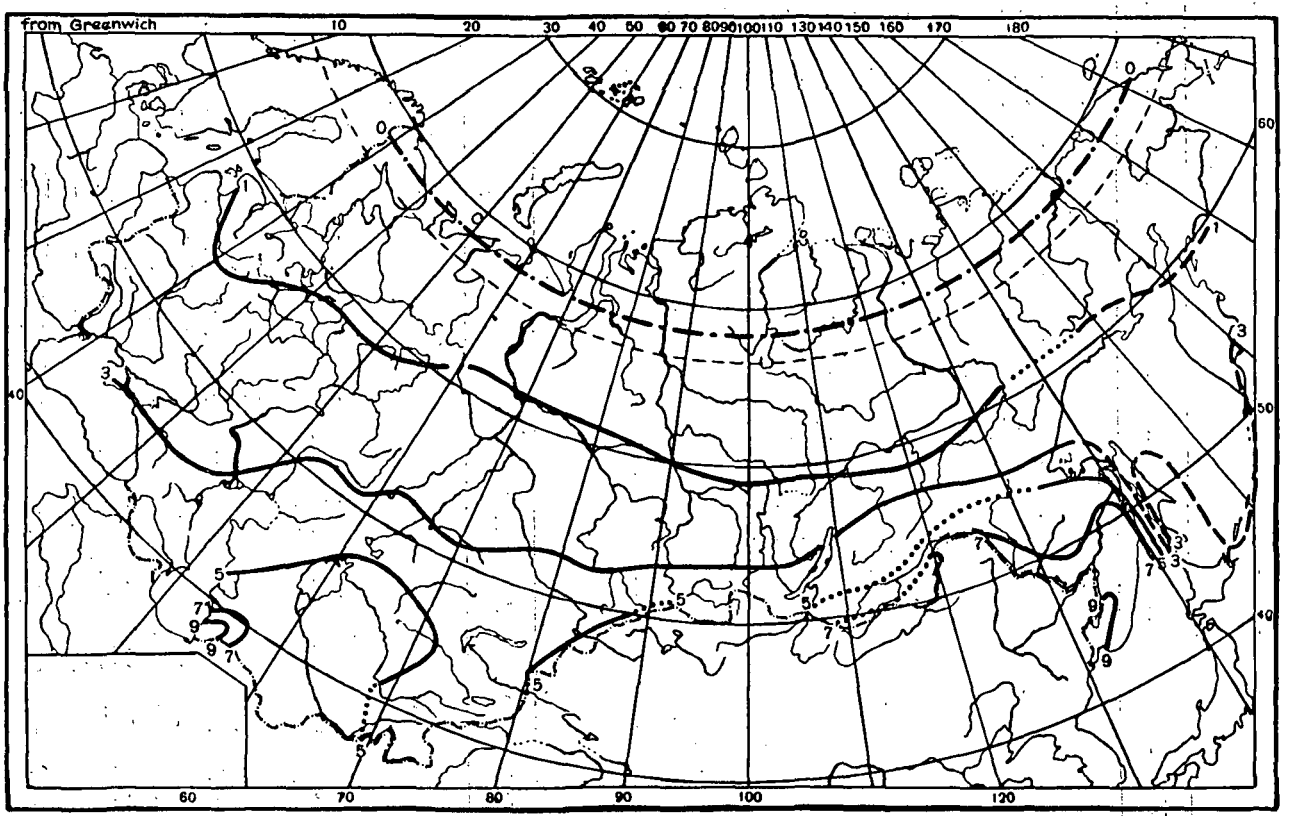

Fig. 5.14. Direct solar radiation on a perpendicular surface (kcal/cm² · mon), December.

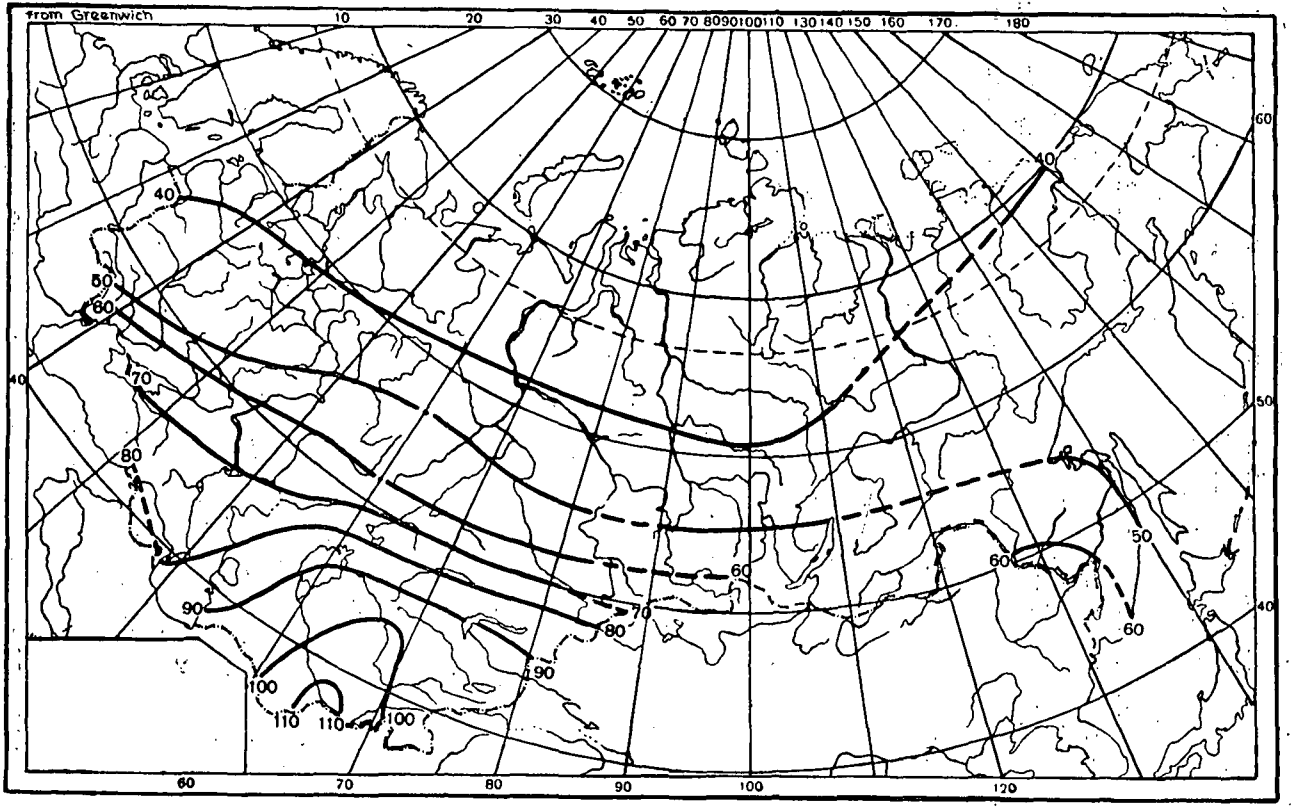

Fig. 5.15. Direct solar radiation on a horizontal surface (kcal/cm²), year.

A chart representing annual amounts of direct solar radiation on a horizontal surface (Fig. 5.15) was compiled in reference [4].

The geographic distribution of direct solar radiation over the earth was analyzed by Bernhardt and Philips [30]. They computed fluxes of direct solar radiation (cal/cm^2·min) for areas of sea of 10 degrees and land between 70° N and 60° S and compiled corresponding charts.

Bernhardt and Philips used the formula they obtained from theoretical parameters as the basis for their computations. Bernhardt made the computation considering turbidity of the atmosphere for a clear sky and Philips took into consideration turbidity and cloudiness. Using the mean monthly values obtained, twelve monthly and one annual charts were compiled for the distribution of direct solar radiation over the earth (separately for the Northern and Southern Hemispheres).

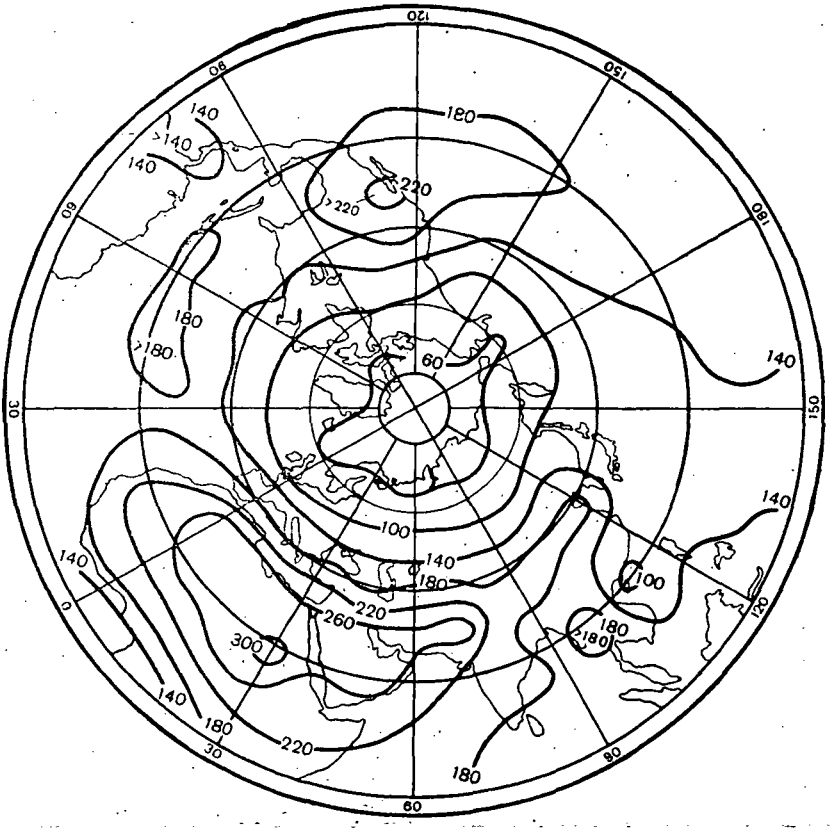

Fig. 5.16a. Direct solar radiation on a horizontal surface considering cloudiness (cal/cm^2·min), year.

Northern Hemisphere.

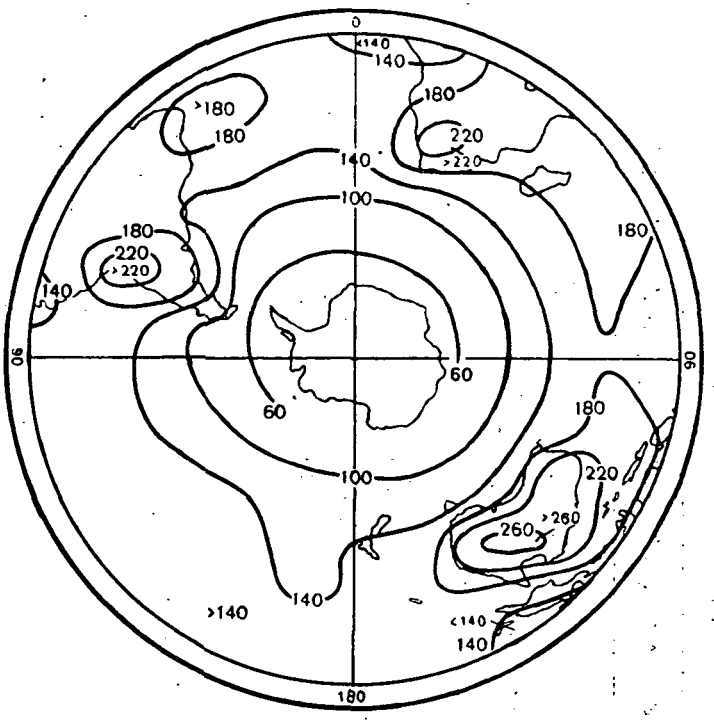

Fig. 5.16b. Direct solar radiation on a horizontal surface considering cloudiness (cal/cm² · min), year.
Southern Hemisphere.

Annual charts of the distribution of direct solar radiation on a horizontal surface considering cloudiness and turbidity of atmosphere have been introduced here as illustrations (Figs. 5.16a and 5.16b).

It is necessary to consider the influence of turbidity on fluxes of direct solar radiation separately. Experimental investigations [9] showed that for the last 25 years the contribution of aerosol components to attenuation of direct solar radiation has increased noticeably. This gradual rise in turbidity has been brought about on account of industrial activity.

Distinct cases of high turbidity of the atmosphere have been registered not only in distinct sections of the earth [37] but on a global scale.

The eruption of volcanoes, especially of the explosive type, is the reason for similar rapid turbidity in a majority of cases. The appearance and the subsequent dynamics of aerosol turbidity in a given section depend on the time of the year and the intensity of the eruption. There is a possibility of dust accumulation in the course of several years in the equatorial stratosphere.

Table 5.24 Attenuation of solar radiation in real atmosphere (cal/cm^2·min) for $m=2$

Station	March			May			July			September			November		
	S_R	ΔS_{H_2O}	ΔS_{aer}	S_R	ΔS_{H_2O}	ΔS_{aer}	S_R	ΔS_{H_2O}	ΔS_{aer}	S_R	ΔS_{H_2O}	ΔS_{aer}	S_R	ΔS_{H_2O}	ΔS_{aer}
Tikhaya Bay	1.33	0.17	0.12	1.29	0.20	0.14	1.26	0.25	0.11	1.32	0.19	0.11			
Dikson Island	1.24	0.18	0.19	1.24	0.20	0.17	1.22	0.26	0.13	1.30	0.21	0.11			
Tiksi Bay	1.22	0.17	0.23	1.24	0.22	0.16	1.21	0.28	0.13	1.30	0.24	0.08			
Markovo	1.27	0.18	0.16	1.20	0.21	0.20	1.16	0.28	0.18	1.29	0.23	0.09			
Klyuchi	1.25	0.18	0.18	1.15	0.22	0.25	1.10	0.29	0.23	1.25	0.26	0.10	1.40	0.19	0.02
Syktyvkar	1.28	0.20	0.14	1.18	0.24	0.20	1.13	0.28	0.21	1.19	0.26	0.18	1.35	0.22	0.04
Moscow	1.14	0.21	0.27	1.02	0.26	0.34	1.01	0.29	0.32	1.10	0.27	0.24	1.32	0.23	0.07
Kaliningrad	1.24	0.23	0.15	1.09	0.26	0.27	1.09	0.29	0.24	1.16	0.28	0.18	1.27	0.25	0.09
Kazan'	1.22	0.20	0.20	1.08	0.25	0.28	1.01	0.29	0.32	1.13	0.26	0.22	1.30	0.21	0.10
Omsk	1.14	0.19	0.28	1.03	0.25	0.34	1.06	0.29	0.27	1.10	0.26	0.26	1.24	0.20	0.16
Semipalatinsk	1.22	0.21	0.18	1.12	0.26	0.23	1.13	0.29	0.21	1.18	0.27	0.17	1.30	0.21	0.10
Irkutsk	1.17	0.20	0.25	1.06	0.23	0.33	1.09	0.29	0.23	1.19	0.25	0.18	1.26	0.20	0.16
Skovorodino	—	—	—	1.22	0.23	0.17	1.15	0.29	0.17	1.28	0.25	0.08	1.27	0.17	0.18
Khabarovsk	1.18	0.18	0.26	1.14	0.25	0.24	1.10	0.31	0.20	1.20	0.27	0.15	1.27	0.18	0.16
Sad-Gorod	1.16	0.20	0.26	1.06	0.26	0.31	1.06	0.33	0.25	1.18	0.28	0.20	1.26	0.21	0.19
Kishinev	1.08	0.23	0.31	0.98	0.27	0.36	1.00	0.30	0.32	1.10	0.28	0.24	1.12	0.25	0.24
Baku	1.12	0.24	0.25	1.00	0.29	0.33	0.94	0.32	0.36	1.00	0.32	0.30	1.17	0.26	0.18
Aral Sea	1.24	0.24	0.14	1.11	0.27	0.24	1.07	0.29	0.26	1.18	0.27	0.17	1.31	0.23	0.08
Tashkent	1.19	0.24	0.18	1.07	0.28	0.27	1.02	0.28	0.31	1.06	0.26	0.30	1.20	0.24	0.18
Ashkhabad	1.14	0.25	0.23	1.02	0.28	0.32	0.93	0.29	0.40	0.96	0.27	0.39	1.16	0.25	0.21

Recent climatological investigations conducted in the USSR [21, 22] confirmed that the contribution of aerosol components in the attenuation of direct solar radiation in the atmosphere of intermediate and lower latitudes is comparable to that due to water vapor. The properties of aerosol attenuation and absorption of direct solar radiation in water vapor over the territory of the USSR at different times of the year are given in Table 5.24. Calculation of attenuation was based on the actinometric and aerological observations at 20 places in the USSR. The computation was conducted for $m=2$.

The above data show that aerosol attenuation is at its maximum in June and July in the major part of USSR territory. In the southern part of the European Territory of the USSR and in Central Asia aerosol attenuation even exceeds the absorption in water vapor (up to 60%), and a similar situation is characteristic of the region of the Steppes along the Volga and Western Siberia. Aerosol attenuation decreases in a North-North-Easterly direction as well as in the major portion of USSR territory during winter.

2.4 Incidence of direct solar radiation on an inclined surface

Solar radiation flux incident on an arbitrarily oriented plane surface may be determined by the relation [14].

$$S_c=S_m \cos i, \tag{5.6}$$

where S_m is flux of solar radiation on a plane perpendicular to the rays for atmospheric mass m ; i—angle of incidence of ray from the sun on a fixed surface. The following relation expresses the course of the angle of incidence thus :

$$\cos i=\cos \alpha \sin h_\odot+\sin \alpha \cos h_\odot \cos \psi_\odot, \tag{5.7}$$

where α is angle of inclination of the surface with respect to horizontal plane ; $h_\odot$—solar altitude ; $\psi=\psi_\odot-\psi_p$, $\psi_\odot$ and ψ_p are solar azimuth and projection of the normal to the surface on a horizontal plane.

The altitude and azimuth of the sun can be determined by the following formula :

$$\sin h_\odot=\sin \varphi \sin \delta_\odot+\cos \varphi \cos \delta_\odot \cos \Omega, \tag{5.8}$$

$$\cos \psi_\odot=\frac{\sin h_\odot \sin \varphi-\sin \delta_\odot}{\cos h_\odot \cos \varphi},$$

$$\sin \psi_\odot=\frac{\cos \delta_\odot \sin \Omega}{\cos h_\odot}, \tag{5.9}$$

where φ is latitude, $\delta_\odot$—inclination of the sun, Ω—hourly angle of the sun at the given time reckoned from the moment of true midday.

While considering equations (5.7)-(5.9), we obtain the following in place of equation (5.6), viz.

$$S_c = S_m [\cos \alpha (\sin \varphi \sin \delta_\odot + \cos \varphi \cos \delta_\odot \cos \Omega) + \sin \alpha \{\cos \psi_p [\tan \varphi (\sin \varphi \sin \delta_\odot + \cos \varphi \cos \delta_\odot \cos \Omega) - \sin \delta_\odot \sec \varphi] + \sin \psi_p \cos \delta_\odot \sin \Omega\}]. \quad (5.10)$$

The last formula determines in a general form the incidence of direct solar radiation on the inclined surface relative to its orientation, specified by angles α and ψ_p for any latitude φ and at different times of the day (Ω) or year ($\delta_\odot$).

For vertical planes oriented toward the east or west the angles of incidence of solar radiation do not depend on the latitude and can be determined throughout by local (solar) times [3] thus :

$$\cos i = \pm \cos \delta_\odot \sin \Omega. \quad (5.11)$$

The angles of incidence of solar radiation on the eastern and western vertical surfaces at the same hours, local time (Ω), appear to be identical over the entire earth.

The solar radiation flux on an inclined surface can usually be evaluated from the given actinometric measurements of the flux of solar radiation on a surface perpendicular to the rays. Similarly a large number of theoretical computations S_c under varying conditions of atmospheric transparency have been obtained. The flux of solar radiation on a surface perpendicular to the rays can be determined from the value of the solar constant and different given values of characteristic atmospheric transparency.

The most detailed theoretical computations were carried out for fluxes of solar radiation on differently oriented surfaces. The results of these computations have been discussed in detail in monograph [14].

The daily course of direct solar radiation for vertical surfaces depends considerably on their orientation. The maximum is observed at solar midday for southern walls. For eastern and western walls the maximum is displaced toward the morning and evening hours respectively. Table 5.25 illustrates the daily course of solar radiation, where the magnitudes S_b/S_r and S_r/S_m are given for differently oriented vertical surfaces in summer and in winter at 60° N.

The daily course of direct solar radiation for differently inclined surfaces of northern and southern orientations at latitudes 42, 50, 60 and 70° is given in Table 5.26. This Table gives hourly fluxes of direct solar

Table 5.25 Daily variation in magnitude of ratio of fluxes of solar radiation on a vertical surface and a surface perpendicular to the rays at 60° N

Real solar time, h		S_r/S_m		S_b/S_m							
				Summer (June 21), $\delta_\odot = 23.5°$					Winter (Dec. 22), $\delta_\odot = 23.5°$		
W	E	Summer	Winter	S	N	W/E	SW/SE	NW/NE	S	W/E	SW/SE
9	15										
10	14						0.02				0.30
11	13						0.23				0.52
12	12	0.80	0.11	0.60		0.00	0.42		0.99	0.00	0.70
13	11	0.79	0.10	0.57		0.24	0.60		0.97	0.24	0.85
14	10	0.74	0.05	0.49		0.46	0.67		0.89	0.46	0.95
15	9	0.70		0.36		0.65	0.71	0.20			
16	8	0.57		0.20		0.79	0.70	0.42			
17	7	0.46		0.01		0.89	0.63	0.62			
18	6	0.34			0.20	0.92	0.51	0.79			
19	5	0.23			0.41	0.89	0.34	0.91			
20	4	0.12			0.60	0.79	0.14	0.98			
21	3				0.76	0.65		1.00			
22	2	0.02									

radiation on different days of the year corresponding to the inclination of the sun equal to +23° [10]. Since the diurnal movement is symmetrical with respect to midday, the Table gives the variation for 12 hours. As is evident from the data in the Table, at a latitude of 50° the fluxes of solar radiation at southern inclinations are close to one another so that the angle of inclination plays an insignificant role.

The diurnal variation of direct solar radiation for northern inclinations becomes increasingly steep with geographic latitude. The computations were carried out for cloudless atmosphere. In [10] we can find the computations for diurnal amounts of heat of direct solar radiation for different inclinations. The annual course of the probable diurnal amounts of solar radiation can be determined primarily by the angle of incidence of the direct rays. The summer minimum, caused by an increase in the angle of incidence of the rays for the highest position of the sun, may be observed in the annual course of diurnal amounts for southern slopes with inclination of 40° at 42° latitude.

Table 5.26 Hourly fluxes of direct solar radiation (cal/cm² . min) . Inclination of sun $\delta_\odot = 23°$

Hourly angle	North				0°	South			
	40°	30°	20°	10°		10°	20°	30°	40°
					$\varphi = 42°$				
0	0.80	1.02	1.18	1.34	1.45	1.52	1.54	1.52	1.42
1	0.70	0.99	1.17	1.31	1.41	1.47	1.49	1.45	1.38
2	0.77	0.94	1.09	1.21	1.29	1.33	1.34	1.30	1.21
3	0.69	0.84	0.96	1.03	1.08	1.09	1.08	1.04	0.96
4	0.63	0.71	0.78	0.82	0.83	0.82	0.78	0.73	0.65
5	0.53	0.56	0.57	0.57	0.55	0.51	0.42	0.37	0.31
6	0.38	0.37	0.35	0.31	0.26	0.22	0.16	0.08	0.02
7	0.20	0.19	0.10	0.04	0.04	0.04	—	—	—
					$\varphi = 50°$				
0	0.60	0.83	1.04	1.22	1.36	1.45	1.51	1.53	1.48
1	0.60	0.82	1.02	1.18	1.32	1.41	1.46	1.47	1.43
2	0.59	0.78	0.95	1.09	1.20	1.28	1.30	1.31	1.26
3	0.57	0.72	0.86	0.96	1.04	1.09	1.10	1.08	1.03
4	0.54	0.64	0.73	0.79	0.82	0.83	0.82	0.79	0.73
5	0.50	0.55	0.57	0.58	0.58	0.56	0.51	0.45	0.39
6	0.41	0.41	0.39	0.36	0.32	0.26	0.21	0.14	0.07
7	0.25	0.26	0.21	0.15	0.10	0.05	—	—	—
					$\varphi = 60°$				
0	0.34	0.58	0.80	1.00	1.18	1.29	1.40	1.46	1.47
1	0.35	0.58	0.80	1.00	1.16	1.29	1.39	1.44	1.44
2	0.38	0.58	0.77	0.91	1.05	1.15	1.25	1.28	1.30
3	0.40	0.56	0.70	0.84	0.96	1.02	1.05	1.07	1.03
4	0.42	0.53	0.62	0.72	0.79	0.81	0.81	0.80	0.77
5	0.43	0.49	0.54	0.58	0.61	0.58	0.56	0.51	0.46
6	0.43	0.44	0.43	0.41	0.43	0.34	0.28	0.22	0.14
7	0.39	0.36	0.32	0.26	0.23	0.13	0.07	0.01	—
8	0.26	0.24	0.20	0.13	0.07	—	—	—	—
9	—	—	—	—	—	—	—	—	—
10	—	—	—	—	—	—	—	—	—
11	—	—	—	—	—	—	—	—	—
12	—	—	—	—	—	—	—	—	—

Table 5.26—*Contd.*

Hourly angle	North					South			
	40°	30°	20°	10°	0°	10°	20°	30°	40°
					$\varphi=70°$				
0	0.06	0.32	0.56	0.78	0.97	1.17	1.26	1.36	1.41
1	0.07	0.32	0.54	0.75	0.95	1.11	1.24	1.33	1.39
2	0.13	0.35	0.55	0.73	0.90	1.01	1.13	1.20	1.23
3	0.22	0.38	0.54	0.69	0.81	0.90	0.98	1.02	1.03
4	0.28	0.41	0.58	0.62	0.70	0.77	0.80	0.81	0.80
5	0.37	0.44	0.50	0.54	0.57	0.58	0.58	0.55	0.51
6	0.44	0.45	0.46	0.45	0.43	0.40	0.35	0.29	0.22
7	0.46	0.46	0.41	0.36	0.30	0.23	0.15	0.07	—
8	0.47	0.41	0.35	0.27	0.18	0.09	—	—	—
9	0.43	0.36	0.28	0.18	0.10	—	—	—	—
10	0.36	0.28	0.23	0.13	0.05	—	—	—	—
11	0.31	0.23	0.19	0.13	0.03	—	—	—	—
12	0.26	0.20	0.13	0.06	0.02	—	—	—	—

The relative values of fluxes and amounts of direct solar radiation, determined with respect to fluxes and amounts for a horizontal surface, are distinctive characteristics of the radiative conditions of inclined surfaces.

For differently oriented vertical surfaces the relative magnitudes of actual X_a and probable X_p diurnal totals of direct solar radiation are given in Table 5.27 [8]. The relative amounts were obtained for the latitude of Minsk ($\varphi=54°$N) for the 16th of each month. The relative magnitudes of diurnal amounts depend on transparency and cloudiness to a lesser extent and can be applied for the entire plotted latitudes.

The relative diurnal amounts of direct solar radiation for different angles of incidence and for different latitudes are similarly given in [10].

The relative magnitudes can be applied for the determination of the actual amounts on the basis of actual sums for a horizontal surface obtained through observations.

Detailed tables for fluxes and amounts of direct solar radiation on differently oriented inclined surfaces can be found in [31, 39, 41, 51].

Table 5.27 Actual and probable diurnal amounts of direct solar radiation [8]

Orientation of slope	Coefficients	Month											
		Jan	Feb	Mar	Apr	May	Jun	Jul	Aug	Sep	Oct	Nov	Dec
South	X_a	4.42	2.60	1.50	0.84	0.50	0.40	0.45	0.69	1.19	2.12	3.70	5.50
	X_p	4.50	2.60	1.50	0.84	0.50	0.40	0.43	0.68	1.20	2.10	3.80	5.40
West	X_a	1.01	0.75	0.69	0.50	0.46	0.43	0.44	0.50	0.61	0.74	0.96	1.20
	X_p	0.92	0.72	0.66	0.58	0.53	0.51	0.53	0.56	0.66	0.74	0.90	1.03
North	X_a	0.00	0.00	0.00	0.01	0.06	0.11	0.09	0.03	0.00	0.00	0.00	0.00
	X_p	0.00	0.00	0.00	0.02	0.09	0.13	0.12	0.04	0.00	0.00	0.00	0.00
East	X_a	0.82	0.62	0.59	0.57	0.54	0.54	0.54	0.56	0.61	0.63	0.70	0.83
	X_p	0.92	0.72	0.66	0.58	0.53	0.51	0.53	0.56	0.66	0.74	0.90	1.03

2.5 Radiative heat flux of solar radiation

Solar radiation absorbed in the atmosphere, according to the computation of M. I. Budyko, compensates approximately 43% of the energy lost in the atmosphere through emission. The results of computations and actinometric balloon probings show that the main contribution to the absorption of solar radiation in the atmosphere and to outgoing radiation comes in the troposphere. The contribution of the stratosphere to outgoing radiation comprises only 3-6%. The minimum of radiative heating on account of absorption of short wavelength radiation in summer in the intermediate latitudes may be observed at an altitude of 14-16 km [17]. The amounts of radiative heating on account of the absorption of solar radiation in the lower troposphere during clear summer days is close to 0.06-0.1 deg/h. In distinct layers the heating may reach 0.2 deg/h. These values were obtained by V. G. Kastrov [12], and similarly in Leningrad State University during balloon investigations [17]. From this it appeared that water vapor and the aerosol component make the greatest, and almost identical, contribution to the absorption of solar radiation in in the lower troposphere. The maximum of radiative heating may be observed at altitudes of 2-5 km (Fig. 5.17). Computations on the absorption of direct solar radiation, carried out by O. A. Avaste [2], confirm the

experimental data. Radiative heating (Fig. 5.17), according to computations, possesses a maximum at altitudes of 2-5 km, its values being close to those obtained through experiment.

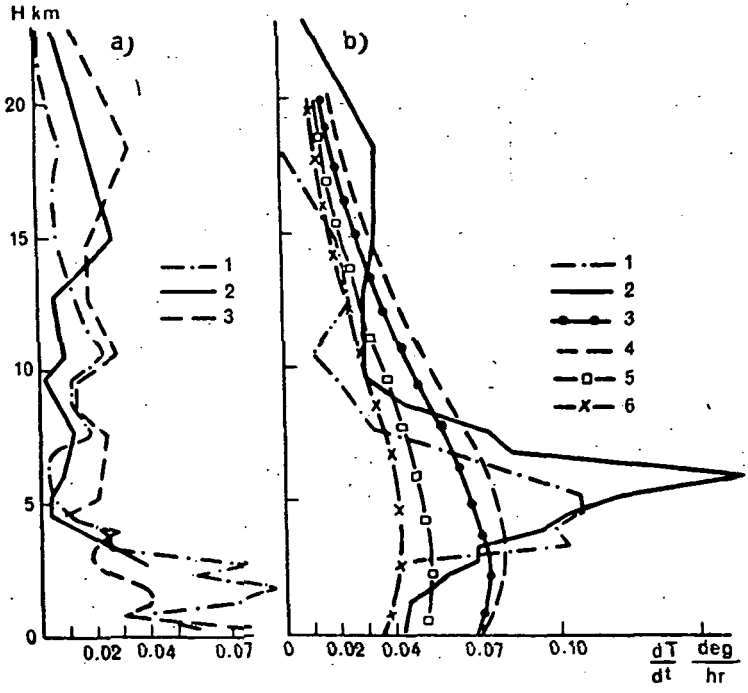

Fig. 5.17. Rate of radiative heating for layer of 50 millibars.

(a) due to absorption in aerosol in summer (1, 2) and in autumn (3); (b) due to absorption in water vapor in October (1), in atmospheric gases in July (2); theoretical values of radiative heating: 3—for $m=1$ and $u'=2.1$ cm; 4—for $m=1$ and $u'=3.0$ cm; 5—for $m=1.5$ and $u'=2.1$ cm; 6—for $m=2$ and $u'=2.1$ cm.

The absorption of direct solar radiation in water vapor and carbon dioxide in a layer of 0-20 km depending on the atmospheric masses is given in Fig. 5.18. The amounts of the solar energy absorbed in layers of 0.5 km thickness for different masses are given in Table 5.28. The computations were carried out with the supposition that the density of water vapor decreases exponentially with the height. If water vapor is localized at some height in the form of a distinct layer, then the absorption of solar radiation can attain a value of 50 mcal/cm^2·min·km. For the case of mean standard model of atmosphere (τ_0 (λ_0)=0.3; $u'=2.1$ cm) for mass $m\sim1$ in the layer 0-20 km, 12% radiation from solar constant is absorbed.

Ohring's [49] computations of the net radiation of the stratosphere (12-55 km) showed that the absorption of ultraviolet radiation in ozone

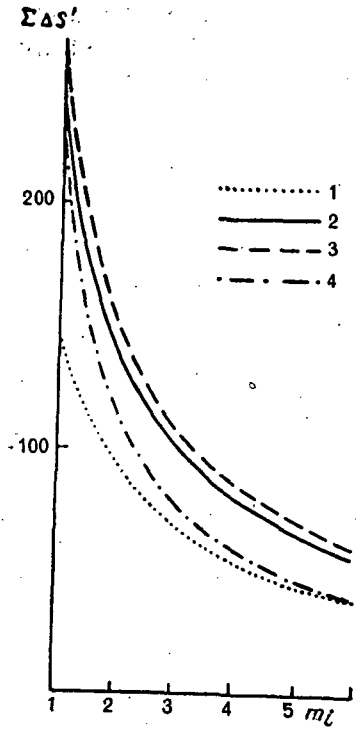

Fig. 5.18. Direct solar radiation in layer 0-20 km depending on atmospheric mass m_i (considering vertical column of unit mass).

1—$\tau_0=0.2$, $u'=0.5$ cm; 2—$\tau_0=0.3$, $u'=2.1$ cm; 3—$\tau_0=0.5$ $u'=3.0$ cm; 4—the relation $f(m_i)c=m_i$ (introduced for comparison).

and infrared solar radiation in water vapor intrinsically compensate the radiative cooling of the stratosphere on account of longwave radiation. Absorption of solar radiation in ozone plays a fundamental role ; it exceeds the absorption in water vapor by approximately four times. The fundamental conclusion of Ohring's researches leads to the finding that the layer of the atmosphere examined does not lie in a state of radiative equilibrium. As a rule radiative cooling may be observed in the lower half of the stratosphere whereas radiative cooling comprising magnitudes of the order of several degrees in a day, may be observed in the upper stratosphere. Results of computations of vertical profiles of radiative variations in temperatures for the belt of 60-70° N are shown in Fig. 5.19. In all cases the maximum of radiative heating is situated in the vicinity of 50 km; consequently the maximum radiant flux of heat is situated at this level. The variation in the temperature above and below 50 km is correspondingly connected with variation in the absorption of ultraviolet radiation in ozone.

Table 5.28 Energy of direct solar radiation, absorbed in atmosphere in layers of 0.5 km, with respect to atmospheric mass of different optical thicknesses and amounts of water vapor (mcal/cm² · min)

$H_k - H_{k-1}$	m										$\overline{K}_{H_2O}$	$\overline{K}_{CO_2}$
	1.000	1.064	1.305	1.500	2.000	2.500	3.000	4.000	5.759	6.000		
	$\tau_0=0.2$; $u'=0.5$ cm											
0-0.5	12.98	21.34	10.44	9.30	7.28	5.98	5.08	3.89	2.72	2.61	4.14	156.2
0.5-1.0	21.28	11.69	9.93	8.87	6.99	5.78	4.93	3.81	2.71	2.61	3.61	148.0
1.0-1.5	11.55	11.01	9.38	8.41	6.66	5.54	4.75	3.70	2.67	2.57	3.14	140.2
1.5-2.0	10.81	10.31	8.82	7.92	6.31	5.27	4.54	3.65	2.59	2.50	2.74	132.6
2.0-2.5	10.06	9.61	8.25	7.43	5.95	4.99	4.31	3.40	2.50	2.41	2.39	125.4
2.5-3.0	9.32	8.91	7.68	6.93	5.58	4.70	4.07	3.23	2.39	2.31	2.08	118.6
3.0-3.5	8.59	8.22	7.11	6.43	5.20	4.40	3.82	3.05	2.28	2.20	1.81	112.0
3.5-4.0	7.88	7.55	6.55	5.94	4.82	4.09	3.57	2.87	2.15	2.08	1.58	105.7
4.0-4.5	7.20	6.90	6.00	5.45	4.46	3.80	3.32	2.68	2.02	1.96	1.38	99.7
4.5-5.0	6.54	6.28	5.48	4.99	4.09	3.50	3.07	2.49	1.89	1.84	1.20	94.0
5.0-5.5	5.93	5.69	4.98	4.54	3.74	3.21	2.83	2.30	1.76	1.71	1.04	88.6
5.5-6.0	5.34	5.14	4.51	4.12	3.41	2.93	2.59	2.12	1.63	1.58	0.91	83.4
6.0-6.5	4.80	4.62	4.06	3.72	3.09	2.67	2.36	1.94	1.50	1.46	0.79	78.5
6.5-7.0	4.30	4.14	3.65	3.35	2.79	2.42	2.14	1.77	1.38	1.34	0.68	73.8
7.0-7.5	3.84	3.70	3.26	3.00	2.51	2.18	1.94	1.61	1.26	1.22	0.60	69.3
7.5-8.0	3.41	3.29	2.91	2.68	2.25	1.96	1.74	1.45	1.14	1.11	0.52	65.0
8.0-8.5	3.03	2.92	2.59	2.38	2.00	1.75	1.56	1.31	1.03	1.01	0.45	61.0
8.5-9.0	2.68	2.58	2.30	2.12	1.78	1.56	1.40	1.17	0.93	0.91	0.39	57.2
9.0-9.5	2.36	2.28	2.03	1.87	1.58	1.39	1.24	1.04	0.83	0.81	0.34	53.5
9.5-10.0	2.08	2.01	1.79	1.65	1.40	1.23	1.10	0.93	0.74	0.73	0.29	50.1
10.0-10.5	1.83	1.77	1.57	1.46	1.23	1.08	0.98	0.82	0.66	0.65	0.26	46.8
10.5-11.0	1.60	1.55	1.38	1.28	1.09	0.96	0.86	0.73	0.59	0.57	0.22	43.7
11.0-11.5	1.41	1.36	1.21	1.12	0.95	0.84	0.76	0.64	0.52	0.51	0.19	40.8
11.5-12.0	1.23	1.19	1.06	0.98	0.84	0.74	0.66	0.56	0.46	0.45	0.17	38.0

Table 5.28—*Contd.*

H_k—H_{k-1}	m										$\bar{K}_{H_2O}$	$\bar{K}_{CO_2}$
	1.000	1.064	1.305	1.500	2.000	2.500	3.000	4.000	5.759	6.000		
12.0-12.5	1.07	1.04	0.93	0.86	0.73	0.64	0.58	0.49	0.40	0.39	0.14	35.4
12.5-13.0	0.94	0.90	0.81	0.75	0.64	0.56	0.51	0.43	0.35	0.34	0.12	32.9
13.0-13.5	0.81	0.79	0.70	0.65	0.56	0.49	0.44	0.38	0.31	0.30	0.11	30.6
13.5-14.0	0.71	0.68	0.61	0.57	0.48	0.43	0.39	0.33	0.27	0.26	0.09	28.4
14.0-14.5	0.62	0.60	0.53	0.49	0.42	0.37	0.34	0.29	0.23	0.23	0.08	26.4
14.5-15.0	0.54	0.52	0.46	0.43	0.37	0.32	0.29	0.25	0.20	0.20	0.07	24.4
15.0-15.5	0.46	0.45	0.40	0.37	0.32	0.28	0.25	0.22	0.18	0.17	0.06	22.6
15.5-16.0	0.40	0.39	0.35	0.32	0.27	0.24	0.22	0.19	0.15	0.15	0.05	20.9
16.0-16.5	0.35	0.34	0.30	0.28	0.24	0.21	0.19	0.16	0.13	0.13	0.05	19.3
16.5-17.0	0.30	0.29	0.26	0.24	0.21	0.18	0.16	0.14	0.11	0.11	0.04	17.8
17.0-17.5	0.26	0.25	0.23	0.21	0.18	0.16	0.14	0.12	0.10	0.10	0.03	16.4
17.5-18.0	0.23	0.22	0.20	0.18	0.15	0.14	0.12	0.10	0.08	0.08	0.03	15.0
18.0-18.5	0.20	0.19	0.17	0.16	0.13	0.12	0.11	0.09	0.07	0.07	0.02	13.8
18.5-19.0	0.17	0.16	0.15	0.14	0.12	0.10	0.09	0.08	0.06	0.06	0.02	12.6
19.0-19.5	0.15	0.14	0.13	0.12	0.10	0.09	0.08	0.07	0.05	0.05	0.02	11.6
19.5-20.0	0.13	0.12	0.11	0.10	0.09	0.08	0.07	0.06	0.05	0.05	0.02	10.6
Σ	148.39	142.14	123.28	111.81	91.01	77.38	67.60	54.47	41.09	39.84	(mcal/cm^2 · min)	
					$\tau_0=0.3$; $u'=2.1$ cm							
0-0.5	17.48	16.57	13.89	12.30	9.33	6.87	5.72	4.23	2.78	2.64	8.49	156.2
0.5-1.0	16.86	16.01	13.48	11.98	9.36	7.69	6.06	4.40	3.02	2.89	7.40	148.0
1.0-1.5	15.14	15.34	12.96	11.55	9.07	7.50	6.41	4.59	3.13	3.00	6.45	140.2
1.5-2.0	15.37	14.62	12.38	11.05	8.72	7.24	6.21	4.86	3.13	3.02	5.62	132.6
2.0-2.5	14.57	13.86	11.77	10.52	8.32	6.93	5.96	4.68	3.42	3.25	4.90	125.4
2.5-3.0	13.75	13.10	11.14	9.98	7.92	6.60	5.69	4.48	3.30	3.19	4.27	118.6

Table 5.28—*Contd.*

3.0-3.5	12.93	12.32	10.51	9.42	7.50	6.27	5.41	4.28	3.16	3.06	3.72	112.0
3.5-4.0	12.11	11.55	9.88	8.87	7.08	5.93	5.13	4.06	3.01	2.91	3.24	105.7
4.0-4.5	11.30	10.79	9.25	8.32	6.66	5.60	4.84	3.85	2.86	2.77	2.82	99.7
4.5-5.0	10.50	10.03	8.62	7.77	6.25	5.26	4.56	3.64	2.71	2.62	2.46	94.0
5.0-5.5	9.71	9.29	8.01	7.23	5.84	4.93	4.28	3.42	2.56	2.48	2.14	88.6
5.5-6.0	8.95	8.56	7.41	6.70	5.43	4.60	4.01	3.21	2.42	2.34	1.86	83.4
6.0-6.5	8.20	7.86	6.82	6.18	5.03	4.28	3.73	3.01	2.27	2.20	1.62	78.5
6.5-7.0	7.49	7.18	6.25	5.68	4.64	3.96	3.46	2.80	2.12	2.06	1.40	73.8
7.0-7.5	6.81	6.54	5.71	5.19	4.26	3.64	3.20	2.60	1.98	1.92	1.22	69.3
7.5-8.0	6.17	5.93	5.19	4.73	3.90	3.34	2.94	2.40	1.84	1.79	1.06	65.0
8.0-8.5	5.57	5.35	4.70	4.29	3.55	3.05	2.70	2.21	1.70	1.65	0.92	61.0
8.5-9.0	5.00	4.81	4.23	3.88	3.22	2.78	2.46	2.02	1.57	1.52	0.80	57.2
9.0-9.5	4.48	4.32	3.80	3.49	2.90	2.52	2.23	1.84	1.44	1.40	0.70	53.5
9.5-10.0	4.00	3.85	3.40	3.13	2.61	2.27	2.02	1.67	1.31	1.27	0.60	50.1
10.0-10.5	3.56	3.43	3.04	2.79	2.34	2.04	1.82	1.51	1.19	1.16	0.52	46.8
10.5-11.0	3.16	3.05	2.70	2.49	2.09	1.82	1.63	1.36	1.08	1.05	0.45	43.7
11.0-11.5	2.80	2.70	2.40	2.21	1.86	1.63	1.46	1.22	0.97	0.94	0.39	40.8
11.5-12.0	2.47	2.38	2.12	1.96	1.65	1.45	1.30	1.09	0.87	0.85	0.34	38.0
12.0-12.5	2.18	2.10	1.87	1.73	1.46	1.28	1.15	0.97	0.78	0.76	0.30	35.4
12.5-13.0	1.91	1.85	1.65	1.52	1.29	1.14	1.02	0.86	0.69	0.68	0.26	32.9
13.0-13.5	1.68	1.62	1.45	1.34	1.14	1.00	0.90	0.76	0.61	0.60	0.22	30.6
13.5-14.0	1.47	1.42	1.27	1.17	1.00	0.88	0.79	0.67	0.54	0.53	0.19	28.4
14.0-14.5	1.29	1.24	1.11	1.03	0.88	0.77	0.70	0.59	0.48	0.47	0.17	26.4
14.5-15.0	1.12	1.09	0.97	0.90	0.77	0.68	0.61	0.52	0.42	0.41	0.14	24.4
					$\tau_0=0.3$; $u'=2.1$ cm							
15.0-15.5	0.98	0.95	0.85	0.79	0.67	0.59	0.54	0.46	0.37	0.36	0.12	22.6
15.5-16.0	0.85	0.83	0.74	0.68	0.59	0.52	0.47	0.40	0.32	0.32	0.11	20.9
16.0-16.5	0.74	0.72	0.64	0.60	0.51	0.45	0.41	0.35	0.28	0.28	0.09	19.3
16.5-17.0	0.65	0.63	0.56	0.52	0.44	0.39	0.36	0.30	0.25	0.24	0.08	17.8
17.0-17.5	0.56	0.54	0.49	0.45	0.39	0.34	0.31	0.26	0.22	0.21	0.07	16.4
17.5-18.0	0.49	0.47	0.42	0.39	0.34	0.30	0.27	0.23	0.19	0.18	0.06	15.0

Table 5.28—*Contd.*

H_k—H_{k-1}	m										K_{H_2O}	K_{CO_2}
	1.000	1.064	1.305	1.500	2.000	2.500	3.000	4.000	5.759	6.000		
18.0-18.5	0.42	0.41	0.37	0.34	0.29	0.26	0.23	0.20	0.16	0.16	0.05	13.8
18.5-19.0	0.37	0.35	0.32	0.29	0.25	0.22	0.20	0.17	0.14	0.14	0.14	12.6
19.0-19.5	0.32	0.31	0.28	0.26	0.22	0.19	0.18	0.15	0.12	0.12	0.04	11.6
19.5-20.0	0.27	0.27	0.24	0.22	0.19	0.17	0.15	0.13	0.11	0.10	0.03	10.6
Σ	234.68	224.24	192.89	173.94	139.94	117.38	101.52	80.45	59.52	57.54		
					$\tau_0=0.5$; $w'=3.0$ cm							
0-0.5	17.89	16.91	14.00	11.69	8.11	6.34	5.13	3.56	2.10	1.96	10.13	156.2
0.5-1.0	17.62	16.69	13.95	12.33	8.98	6.76	5.60	4.08	2.62	2.48	8.83	148.0
1.0-1.5	17.09	16.22	13.63	12.10	9.42	7.48	5.84	4.36	2.95	2.82	7.70	140.2
1.5-2.0	16.41	15.59	13.16	11.72	9.29	7.59	6.47	4.45	3.11	2.99	6.71	132.6
2.0-2.5	15.66	14.89	12.60	11.24	8.86	7.35	6.30	4.92	3.16	3.04	5.85	125.4
2.5-3.0	14.86	14.14	12.00	10.72	8.48	7.05	6.06	4.76	3.37	3.19	5.10	118.6
3.0-3.5	14.04	13.37	11.37	10.18	8.07	6.73	5.80	4.57	3.37	3.25	4.44	112.0
3.5-4.0	13.22	12.60	10.74	9.62	7.65	6.40	5.52	4.36	3.22	3.12	3.87	105.7
4.0-4.5	12.40	11.82	10.10	9.07	7.23	6.06	5.23	4.14	3.07	2.97	3.37	99.7
4.5-5.0	11.58	11.05	9.47	8.51	6.81	5.72	4.95	3.93	2.92	2.82	2.93	94.0
5.0-5.5	10.77	10.29	8.84	7.96	6.40	5.38	4.67	3.71	2.77	2.68	2.55	88.6
5.5-6.0	9.97	9.54	8.22	7.42	5.98	5.04	4.38	3.50	2.62	2.53	2.22	83.4
6.0-6.5	9.20	8.80	7.61	6.88	5.57	4.71	4.10	3.29	2.47	2.39	1.93	78.5
6.5-7.0	8.44	8.09	7.01	6.35	5.16	4.38	3.83	3.08	2.32	2.25	1.68	73.8
7.0-7.5	7.72	7.40	6.44	5.84	4.77	4.06	3.56	2.87	2.18	2.11	1.46	69.3
7.5-8.0	7.03	6.74	5.88	5.35	4.39	3.75	3.29	2.67	2.03	1.97	1.27	65.0
8.0-8.5	6.37	6.12	5.35	4.88	4.02	3.44	3.03	2.47	1.89	1.83	1.10	61.0
8.5-9.0	5.76	5.53	4.85	4.43	3.66	3.15	2.78	2.27	1.75	1.70	0.96	57.2

Table 5.28—*Contd.*

9.0-9.5	5.18	4.98	4.38	4.00	3.32	2.86	2.54	2.08	1.61	1.56	0.83	53.5
9.5-10.0	4.64	4.47	3.93	3.61	3.00	2.60	2.30	1.90	1.48	1.44	0.72	50.1
					$\tau_0=0.5$; $u'=3.0$ cm							
10.0-10.5	4.15	3.99	3.52	3.24	2.70	2.34	2.085	1.73	1.35	1.31	0.62	46.8
10.5-11.0	3.69	3.56	3.15	2.89	2.42	2.11	1.88	1.56	1.23	1.20	0.54	43.7
11.0-11.5	3.28	3.16	2.80	2.58	2.17	1.89	1.69	1.41	1.11	1,08	0.47	40.8
11.5-12.0	2.90	2.80	2.49	2.29	1.93	1.69	1.51	1.26	1.00	0.98	0.41	38.0
12.0-12.5	2.56	2.48	2.20	2.03	1.72	1.50	1.35	1.13	0.90	0.88	0.35	35.4
12.5-13.0	2.26	2.18	1.94	1.79	1.52	1.33	1.20	1.01	0.81	0.79	0.31	32.9
13.0-13.5	1.99	1.92	1.71	1.58	1.34	1.18	1.06	0.89	0.72	0.70	0.26	30.6
13.5-14.0	1.74	1.69	1.50	1.39	1.18	1.04	0.94	0.79	0.64	0.62	0.23	28.4
14.0-14.5	1.53	1.48	1.32	1.22	1.04	0.92	0.82	0.70	0.56	0.55	0.20	26.4
14.5-15.0	1.34	1.29	1.16	1.07	0.91	0.80	0.73	0.62	0.50	0.49	0.17	24.4
15.0-15.5	1.17	0.13	1.01	0.94	0.80	0.71	0.64	0.54	0.44	0.43	0.15	22.6
15.5-16.0	1.02	0.99	0.88	0.82	0.70	0.62	0.56	0.47	0.39	0.38	0.13	20.9
16.0-16.5	0.89	0.86	0.77	0.71	0.61	0.54	0.49	0.42	0.34	0.33	0.11	19.3
16.5-17.0	0.77	0.75	0.67	0.62	0.53	0.47	0.43	0.36	0.30	0.29	0.09	17.8
17.0-17.5	0.67	0.65	0.58	0.54	0.46	0.41	0.37	0.32	0.26	0.25	0.08	16.4
17.5-18.0	0.58	0.57	0.51	0.47	0.40	0.36	0.32	0.28	0.23	0.22	0.07	15.0
18.0-18.5	0.51	0.49	0.44	0.41	0.35	0.31	0.28	0.24	0.20	0.19	0.06	13.8
18.5-19.0	0.44	0.43	0.38	0.35	0.30	0.27	0.24	0.21	0.17	0.17	0.05	12.6
19.0-19.5	0.38	0.37	0.33	0.31	0.26	0.23	0.21	0.18	0.15	0.15	0.05	11.6
19.5-20.0	0.33	0.32	0.29	0.27	0.23	0.20	0.18	0.16	0.13	0.13	0.04	10.6
Σ	258.97	246.33	211.17	182.43	150.65	125.77	108.33	85.23	62.41	60.22		

REMARKS: $\overline{K}_{H_2O}$ and $\overline{K}_{CO_2}$—weighted parameters characterizing the influence of water vapor and carbon dioxide on absorption of solar radiation at the height H_k.

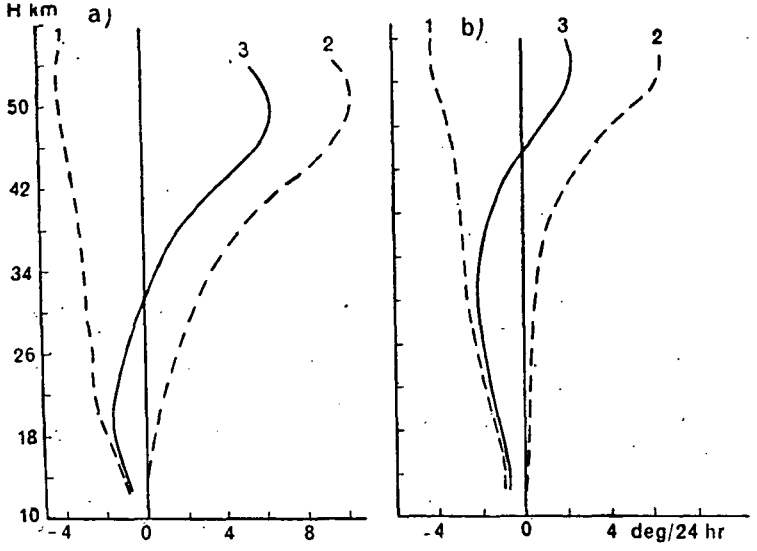

Fig. 5.19. Vertical distribution of radiative temperature variation (deg/24 hrs) in April (a) and October (b). 60-70° N.

1—on account of radiative heat exchange; 2—on account of absorption of solar radiation; 3—total variation in temperature.

As an instance of variations in the diurnal temperature at the altitude of 50 km (5-8°) Johnson showed that the diurnal variation of the absorption of solar radiation in ozone is a fundamental factor of diurnal behavior. These results bear witness to the fact that the thermal condition of the stratosphere is primarily controlled by radiation but in the lower stratosphere the thermal advection, according to computations of Chiu and Greenfield, may dominate over radiation factors.

The thermal condition of the mesosphere can be determined to a large extent by the radiation processes. In the lower mesosphere the fundamental contribution to the shortwave radiant flux of heat is brought about by the absorption of the ultraviolet solar radiation in ozone. The second component which strongly absorbs the far ultraviolet radiation of the sun is molecular oxygen. According to the data of R. Penndorf, the maximum flux of heat due to the absorption of solar radiation in oxygen takes place around an altitude of 100 km; moreover, the radiative variation in temperature in the layer of absorption maxima can reach a value of 5.5 deg/hr. Theoretical investigations of Margetroid and Goody gave a considerably lower value of radiative heating, viz. 10-15 deg/24 h.

The establishment of the existence of a maximum of radiative heating in the vicinity of 80 km is an important result of the theoretical investigations. From these investigations, it is clearly seen that the vertical

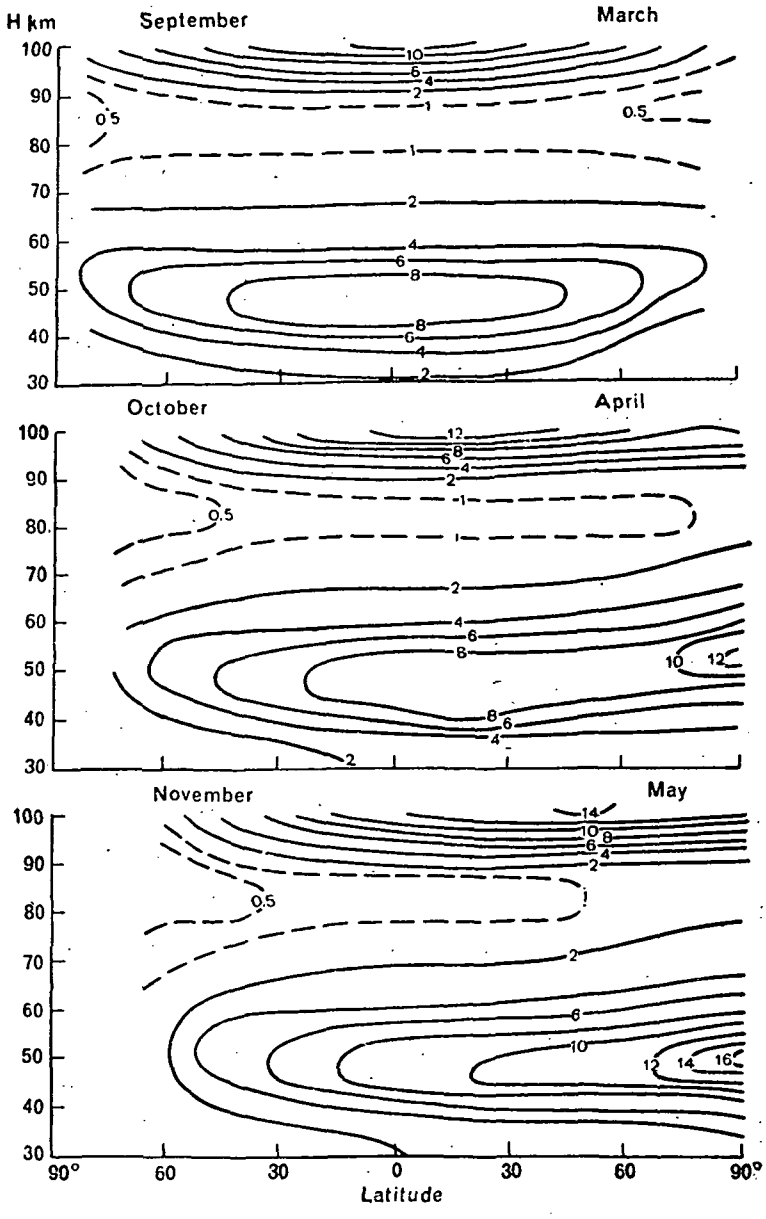

Fig. 5.20 Variation in temperature at different altitudes on account of absorption of solar radiation (deg/24 h).

distribution of shortwave radiative heat flux is similar to the vertical profile of temperature.

The computed meridional cross sections of radiative variations in temperature for different layers are given in Fig. 5.20.

REFERENCES

1. Avaste, O., Kh. Molday and K. S. Shifrin. Spektral'noe raspredelenie pryamoi i rasseyannoi radiatsii (Spectral distribution of direct and scattered radiation). Issledovaniya po fizike atmosfery, vyp. 3, IFA AN E'SSR, 1962.
2. Avaste, O. A. Pritok tepla solnechnoi radiatsii v atmosfere i potok summarnoi radiatsii na poverkhnosti morya (Heat flux of solar radiation in the atmosphere and flux of total radiation on the sea surface). Issledovaniya radiatsionnogo rezhima atmosfery. IFA AN E'SSR, 1967.
3. Averkiev, M. S. Ob odnoi osobennosti osveshcheniya Solntsem vostochnykh i zapadnykh sten zdanii (A peculiarity in the lighting of eastern and western walls of buildings by the sun). Meteorologiya i gidrologiya, No. 5, 1961.
4. Barashkova, E. P. et al. Radiatsionnyi rezhim territorii SSSR (Radiational regime of the Soviet Territory). Gidrometeoizdat, Leningrad, 1961.
5. Belinskii, V. A. and B. A. Semenchenko, Ul'trafioletovaya radiatsiya na razlichnykh vysotakh pri bezoblachnoi ae'rozol'noi atmosfere (Ultraviolet radiation at different heights in cloudless aerosol atmosphere). Trudy GGO, vyp. 184, 1966.
6. Berlyand, T. G. Raspredelenie solnechnoi radiatsii na kontinentakh (Distribution of solar radiation over the continents). Gidrometeoizdat, 1961.
7. Garadzha, M. P. Pryamaya ul'trafioletovaya radiatsiya pri razlichnykh usloviyakh prozrachnosti atmosfery (Direct ultraviolet radiation at different atmospheric transparencies). Geliotekhnika, No. 4. 1966.
8. Gol'berg, M. A. Osobennosti vozmozhnogo i deistvitel'nogo prikhoda pryamoi radiatsii k skloman i stenam v Belorussii (Properties of possible and actual influx of direct radiation on slopes and walls in White Russian SSR). Nauchnye soobshcheniya inta Geologii i geografi AN Lit. SSR, t. XIII, 1962.
9. Davitaya, F. F. O vozmozhnom vliyanii zapyleniya atmosfery na umen'shenie lednikov i poteplenie klimata (Possible effect of atmospheric dust on diminution of glaciers and warming of climate). Izv. AN SSSR, ser. geof., No. 2, 1965.
10. Zakharova, A. F. Radiatsionnyi rezhim severnykh i yuzhnykh sklonov v zavismosti ot geograficheskoi shiroty (Radiational regime of northern and southern slopes with respect to geographical latitudes). Uch. zap. LGU, No. 269, ser. geogr. nauk, vyp. 13, 1959.
11. Kalitin, N. N. O dlinnovolnovoi solnechnoi radiatsii (Longwave solar radiation). AN SSSR, t. 58, No. 7, 1947.
12. Kastrov, V. G. Izmerenie pogloshcheniya solnechnoi radiatsii v svobodnoi atmosfere do 3-5 km (Measurement of solar radiation absorbed in free atmosphere upto 3-5 km). Trudy TsAO, vyp. 8, 1952.
13. Kondrat'ev, K. Ya. Aktinometriya (Actinometry). Gidrometeoizdat, Leningrad, 1965.

14. Kondrat'ev, K. Ya. Luchistaya e'nergiya Solntsa (Radiant energy of the sun). Gidrometeoizdat, Leningrad, 1954.

15. Kondrat'ev, K. Ya., G. N. Gaevskaya and G. A. Nikol'skii. Ae'rostatnye issledovaniya radiatsionnogo balansa sistemy zemnaya poverkhnost'—atmosfera (Balloon investigation on net radiation of the earth's surface—atmosphere system). Kosmicheskie issledovaniya, t. 1, vyp. 3, 1963.

16. Kondrat'ev, K. Ya. and G. A. Nikol'skii. Pryamaya solnechnaya radiatsiya do vysot 30 km i solnechnaya postoyannaya (Direct solar radiation upto the altitude of 30 km and the solar constant). Trudy Vsesoyuznoi konferentsii po nauchnym itogam MGSS, January 1967, Moskva.

17. Kondrat'ev, K. Ya., G. A. Nikol'skii and E. N. Esipova. Ae'rostatnye issledovaniya radiatsionnykh potokov v svobodnoi atmosphere (Balloon investigation of radiative fluxes in a free atmosphere). Izv. AN SSSR, fizika atmosfery i okeana, t. 2, No. 4, 1966.

18. Kondrat'ev, K. Ya., G. A. Nikol'skii and E. N. Esipova. Radiatsionnye potoki i komponenty oslableniya pryamoi solnechnoi radiatsii v troposfere i stratosfere. Trudy Shestogo mezhduvedomstvennogo soveshchaniya po aktinometrii i optike atmosfery (Radiative fluxes and attenuation components of direct solar radiation in the troposphere and stratosphere. Proceedings of the Sixth Interdepartmental Conference on Actinometry and Atmospheric Optics). June 1966, Tartu.

19. Lopukhin, E. A. Spektral'nyi sostav pryamoi solnechnoi radiatsii (Spectral composition of direct solar radiation). Geliotekhnika, No. 1. 1965.

20. Pivovarova, Z. I. Pryamaya solnechnaya radiatsiya na territorii SSSR (Direct solar radiation over the territory of the USSR). Trudy GGO, vyp. 139. 1963.

21. Pivovarova, Z. I. Raspredelenie koe'ffitsienta prozrachnosti atmosfery na territorii SSSR (Distribution of coefficient of atmospheric transparency in the territory of the USSR). Trudy GGO, vyp. 213, 1968.

22. Pivovarova, Z. I. and V. A. Sheffer. Issledovanie rezhima prozrachnosti atmosfery. VII Vsesoyuznoe soveshchanie po aktinometrii i atmosfernoi optike (Study on the regime of atmospheric transparency. The VIIth All-Union Conference on Actinometry and Atmospheric Optics). May, 1968.

23. Pivovarova, Z. I. Kharakteristika radiatsionnogo rezhima pri yasnoi pogode (Characteristics of radiative regime in clear weather). Trudy GGO, vyp. 96, 1959.

24. Rusin, N. P. Meteorologicheskii i radiatsionnyi rezhim Antarktidy (Meteorological and radiative regime of the Antarctic region). Gidrometeoizdat, Leningrad, 1961.

25. Sivkov, S. I. Oslablenie solnechnoi radiatsii v ideal'noi atmosfere (Attenuation of solar radiation in ideal atmosphere). Trudy GGO, vyp. 169, 1965.

26. Sivkov, S. I. Metody rascheta kharakteristik solnechnoi radiatsii (Methods of computing the characteristics of solar radiation). Gidrometeoizdat, Leningrad, 1968.

27. Sitnik, G. F. Novoe opredelenie solnechnoi postoyannoi (Recent determination of the solar constant). Astronomicheskii tsirkulyar, No. 444, 1967.

28. Faraponova, G. P. Nekotorye resul'taty aktinometricheskikh nablyudenii na svobodnykh ae'rostatakh (Some results of actinometric observations from free balloons) Trudy TsAO, vyp. 8, 1952.

29. Aldrich, L. B. and W. H. Hoover. Annals of Astrophysical Observatory, Smithsonian Institute, 7, 1954.

30. Bernhardt, F. and H. Philipps. Die räumliche und zeitliche Verteilung der Einstrahlung, der Ausstrahlung und der Strahlungsbilanz im Meeresniveau. Teil 1. Die Einstrahlung. Abhandl. Meteorol. u. Hydrograph. Dienstes Deutsch. Demok. Rep. Nr 45, 1958.

31. Bögel, A. Die directe Sonnenstrahlung auf westhänge. Zeitschr. für Meteor., Bd 11, H. 3, 1957.

32. Gates, D. M. Radiant energy, its receipt and disposal. Meteorolog. Monographs, v. 6, No. 28, 1965.

33. Drummond, A. J. The extraterrestrial solar spectrum. Proc. IES and ASTM International Symposium on Solar Radiation, Los Angeles, January 1965.

34. Drummond, A. J. et al. New value for the solar constant of radiation. Nature, v. 218, No. 5138, 1968.

35. Dunkelman, L. and R. Scolnik. Solar Spectral Irradiance and Vertical Atmospheric Attenuation in the Visible and Ultraviolet. J. Opt. Soc. Amer., 49, 1959.

36. Elterman, L. Atmospheric Attenuation, 1964, in the Ultraviolet, Visible, and Infrared Regions for Altitudes to 50 km. Environ. Res. Papers No. 46, Air Force Cambridge Res. Lab. 1964.

37. Flowers, E. C. and H. J. Viebrock. Solar radiation: an anomalous decrease of direct solar radiation. Science, v. 148, No. 3669, 1965.

38. Gates, D. M. Spectral Distribution of Solar Radiation at the Earth's Surface. Science, v. 151, No. 3710, 1966.

39. Hand, I. Insolation on cloudless days at the time of solstices and equinoxes. Heating and Ventillating, v. 51, No. 2, 1954.

40. Hardy, J. D. and H. L. Giclas. A search for solar variation. Astronom. J. Chic., 122 (3), Nov. 1955.

41. Hutchinson, F. and M. Cotter. Solar irradiation of east and west inclined surface. Heating, Piping and Air Condit., v. 27, No. 9, 1955.

42. Johnson, F. S. The Solar Constant. J. Meteorology, 11, No. 6, 1954.

43. Johnson, H. L. and B. Iriarte. Lowell Observatory, IV, No. 8, Bull. 96 (1959), pp. 99-104.

44. Johnson, F. S. et al. Rocket Exploration of the Upper Atmosphere. London, Pergamon Press, 1954.

45. Kondratyev, K. Ya. and G. A. Nikolsky. Direct Solar Radiation and Aerosol Structure of the Atmosphere from Balloon Measurements in the Period IQSY. Communications Sveriges Meteor. Hydrol. Institute, Ser. B, No. 28, 1968.

46. Ny-Tsi-Ze et Choong-Shin-Piaw. L'absorption de la lumière par l'ozone. Comptes rend. acad. sc., t. 195, no 4, 1932; t. 196, no 13, 1933.

47. Nicolet, M. Sur la détermination du flux énergetique du raynonnement extraterrestre du Soleil. Archiv f. Met., Geoph. and Biokl., Ser. B, 3, 209, 1951.

48. Nicolet, M. Sur la problème de la constante solarie. Annales d'Astrophys., 14, 249, 1951.

49. Ohring, G. The radiation budget of stratosphere. J. Met. v. 15, No. 5, 1958.

50. Robinson, N. Solar radiation. Elsevier Publ. Comp., Amsterdam, 1966.

51. Sato, T. On the problem of mathematical insolation. Journ. Met. Soc. Japan v. 31, No. 1, 1953.

6. SCATTERED AND REFLECTED RADIATION

PART I. SCATTERED RADIATION OF THE ATMOSPHERE

The amount of radiation scattered in the atmosphere depends to varying extents on a large number of astronomical, physical and geographic factors. Among these may be included the spectral composition of solar radiation, the value of the solar constant, the declination and the hourly angle of the sun, the latitude of the location and altitude above sea level, the amount of scattering and absorbing substances in the atmosphere, cloudiness and the albedo of the underlying surface.

Numerous factors determining the quantity of scattered radiation change continuously in time and space and make computation difficult. To obtain the most probable value of fluxes of scattered radiation at a given time and place, a chain of observations has to be made for the reasons enumerated above.

1. SPECTRAL COMPOSITION OF SCATTERED RADIATION

The intensity of the scattered radiation depends on the wavelength of the incident light and on the number and size of the scattering particles.

In the majority of cases the intensity of scattered radiation increases with decreasing wavelength. As the size of the scattering particle increases, the intensity of scattered radiation also increases and the maximum in the scattered spectrum shifts toward longer wavelengths.

The results of theoretical computations of the spectral compositions of scattered radiation for different scattering media are given in Table 6.1 [22].

Table 6.1 Energy distribution outside the atmosphere in solar spectrum (10^{-3} cal/cm^2 · min) and spectral component of scattered radiation (10^{-6} cal/cm^2 · min) [22]

	$\Delta\lambda$ μ						
	0.28-0.30	0.30-0.32	0.32-0.34	0.34-0.36	0.36-0.38	0.38-0.40	0.42-0.44
Sun	2.6	11.5	21.8	31.3	35.2	36.0	54.3
1 cm^3 of pure dry air	4.4	14.4	21.9	23.5	20.08	16.9	17.2
100 droplets; r=0.1 μ	0.05	0.27	0.44	0.54	0.51	0.45	0.52
25 droplets; r=0.5 μ	0.14	0.78	1.62	1.78	3.52	3.78	6.41
5 droplets; r=1 μ	1.0	4.6	9.2	12.8	14.6	15.1	23.2

	$\Delta\lambda$ μ							
	0.46-0.48	0.50-0.52	0.56-0.58	0.64-0.66	0.70-0.72	0.78-0.80	0.86-0.88	0.98-1.00
Sun	62.6	59.7	54.6	48.4	42.9	35.3	27.1	21.0
1cm^3 of pure dry air	13.7	9.3	4.4	2.8	1.8	0.8	0.5	0.2
100 droplets; r=0.1 μ	0.46	0.36	0.25	0.136	0.09	0.04	60.027	0.015
25 droplets; r=0.5 μ	7.65	7.35	6.67	5.48	4.29	3.04	2.11	1.36
5 droplets; r=1 μ	25.6	20.6	14.4	18.6	20.0	18.0	15.8	12.4

The maximum of scattered radiation in the case of dry, pure air lies in the interval 0.34-0.36 μ and the secondary maximum in the interval 0.42-0.44 μ.

The curves of spectral distribution of scattered radiation from measurements in solar almucanthorat for four angular displacements ψ from the sun, viz. at 20, 50, 90 and 180° [23] are shown in Fig. 6.1. The large number of peaks in the curves of Fig. 6.1 are primarily the result of the influence of Fraunhofer's absorption bands in the solar spectrum outside the atmosphere and in telluric bands, belonging to water and vapor oxygen.

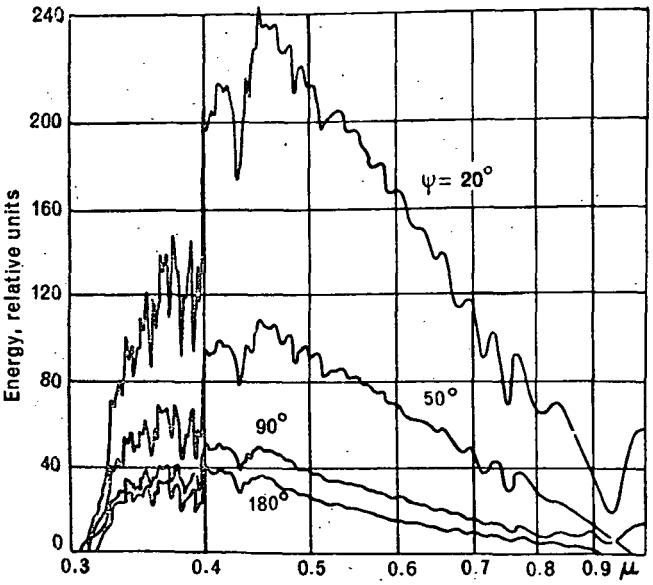

Fig. 6.1. Spectral distribution of scattered radiation at different positions of solar almucanthorat at $h_{\odot}=40°$.
Azimuths of points relative to sun are indicated on curves [23].

Spectral components of scattered radiation change noticeably with respect to the zenith distance of the sun and angular distance of the observed point from the sun from day to day (see Tables 6.2 and 6.3) [11]. At low positions of the sun the spectrum has a maximum which shifts a little toward the blue region of the spectrum as the angular displacement from the sun increases. The most complete angular dependence of the scattered radiation for a clear sky can be seen in Tables 6.4 and 6.5 [19]. The point of minimum intensity in most cases lies on the side directly opposed to the sun at an angular displacement of 85-90° or within the range 70-90°. An increase in intensity with increasing zenith distance of the point of observation may be observed at constant azimuth along with a decrease in I_{λ} with the growth of azimuth for observations on the same almucanthorat.

Table 6.2 Energy distribution in the spectrum of daytime sky on September 2, 1958 [11]

λ nm	ψ°										
	20	40	60	90	120	180	20	40	60	120	180
	$\vartheta_\odot$=85.9-84.3°						$\vartheta_\odot$=80.0-77.8°				
418	9.8	14.3	9.9	9.5	9.3	—	29.0	23.7	22.2	20.1	23.6
422	14.0	20.2	14.0	12.5	13.3	—	33.8	26.3	24.2	21.1	27.0
426	16.5	20.3	14.3	11.7	12.2	—	38.4	28.4	26.7	23.1	28.6
434	18.7	23.5	16.9	13.8	14.9	—	36.5	27.2	25.2	22.1	31.2
438	15.8	21.1	17.3	12.2	13.2	—	36.2	28.0	23.9	21.5	28.3
442	12.7	18.1	13.6	11.0	11.4	—	34.6	23.6	22.1	18.5	24.2
448	17.7	23.6	17.7	14.0	14.7	—	36.5	27.1	23.4	21.0	26.6
474	28.8	—	38.5	20.8	22.4	—	44.5	26.4	26.0	23.6	30.2
492	37.4	41.5	31.2	23.0	23.8	—	43.3	29.7	24.2	21.9	27.8
521	38.3	46.2	32.3	22.4	22.7	—	38.1	25.2	19.8	17.8	22.9
555	33.9	—	26.9	18.3	18.0	—	31.4	20.0	14.7	13.9	17.3
584	30.8	30.7	20.4	13.5	13.0	—	25.6	15.7	10.7	10.2	4.8
662	22.0	8.1	15.3	9.9	6.7	—	21.1	11.7	6.8	7.5	8.4
704	30	—	19.2	11.3	10.3	—	21.5	11.4	5.7	7.8	7.8
	$\vartheta_\odot$=73.2-70.8°						$\vartheta_\odot$=58.1-56.1°				
418	28.8	29.3	20.6	19.9	23.1	26.1	22.1	25.0	18.2	9.1	12.3
422	27.2	28.3	20.1	19.5	22.8	25.7	24.4	24.0	17.6	9.0	10.7
426	29.8	35.7	22.5	20.1	24.0	21.2	24.2	24.0	16.5	8.8	10.2
434	27.9	30.0	31.8	19.0	22.6	25.8	23.4	26.0	17.3	8.6	10.4
438	27.4	34.0	19.8	21.8	21.0	24.2	24.0	24.0	15.7	8.5	9.6
442	25.1	26.0	18.8	16.6	19.5	21.6	22.1	22.0	15.6	8.3	9.5
448	26.5	26.7	19.4	21.8	19.9	21.5	23.4	21.4	14.5	8.5	9.1
474	28.4	35.7	20.6	16.9	20.2	21.6	22.7	26.2	14.2	8.0	8.8
492	37.2	25.2	18.4	15.0	17.8	21.0	20.7	17.5	11.9	7.2	7.3
521	23.4	8.0	14.8	11.9	13.9	14.4	17.4	13.7	9.1	5.4	5.2
555	—	—	—	—	—	—	13.9	10.2	6.4	4.0	3.7
584	—	—	—	—	—	—	11.7	7.2	4.3	3.1	2.5
662	10.8	8.5	5.1	4.2	7.1	5.0	8.6	4.2	2.2	2.0	1.2
704	10.2	7.4	4.4	4.2	4.6	4.7	8.0	2.7	—	1.8	—

REMARKS: $\vartheta_\odot$—angular distance from the sun.

Table 6.3 Energy distribution in the spectrum of daytime sky on January 10, 1959 [11]

λ nm	ψ°					
	60	90	60	90	60	90
	$\vartheta_\odot = 68.3°$		$\vartheta_\odot = 72.3°$		$\vartheta_\odot = 79.6°$	
412	38.1	36.0	48.0	45.0	9.48	48.5
414	28.5	32.8	54.6	49.1	74.6	33.3
417	33.0	26.9	42.8	39.7	41.4	25.5
421	32.3	29.3	34.5	37.7	44.9	25.8
426	31.0	27.0	37.8	31.7	33.0	22.1
429	31.0	27.4	36.1	28.9	30.7	21.0
433	30.8	26.6	34.4	29.5	35.9	20.2
441	29.4	25.0	32.5	25.3	22.4	17.8
445	27.7	22.9	30.8	25.7	25.6	18.8
450	28.9	24.2	30.4	25.9	25.8	16.6
459	29.5	22.9	28.7	24.8	25.3	16.9
468	24.5	19.7	25.2	20.8	20.3	14.2
480	22.4	17.7	22.9	18.8	17.7	13.7
492	19.9	16.5	21.2	17.0	16.1	12.2
504	19.5	14.9	18.7	15.0	13.7	10.5
521	16.6	12.7	17.8	13.2	11.3	9.7
538	14.7	11.0	15.2	11.9	10.1	8.1
560	12.5	9.7	13.2	9.7	6.0	8.0
582	9.6	7.9	11.1	8.3	6.0	6.9
607	8.9	5.6	8.5	6.3	3.3	5.3
631	5.8	3.8	10.2	6.9	2.7	5.8

Fig. 6.2 illustrates the dependence of the spectral composition of scattered radiation on different atmospheric conditions [92]. Let us turn our attention to the brightness minimum caused by absorption bands for the following wavelengths, viz. 360, 390, 430, 590 and 650 nm, and the maximum in the region of wavelengths 370, 420 and 460 nm. The bands essential for the absorption in water vapor (590, 650 and 720 nm) and in oxygen (580, 630 and 690 nm) are absent from the spectrum of a clear sky, but appear in the case of cloudiness or fog.

Table 6.4 Spectral intensity of scattered radiation $I_\lambda \times 10^{-3}$ W/cm² ster at $\vartheta_\odot = 60°$ [19]

$\vartheta°$	$\psi°$									
	10	30	50	70	90	110	130	150	170	180
					$\lambda = 3500$ Å					
75	2.05	1.9	1.7	1.52	1.5	1.3	1.3	1.3	1.5	1.3
60				1.16	1.05	1.0	0.92	0.96	0.72	0.92
45	0.96	1.4	1.2	1.08	0.93	0.85	0.76	0.72		0.7
30	1.05	1.06	1.05		0.72		0.6			
					$\lambda = 4000$ Å					
75	12	9.8	8.7	7.9	7.1	6.8	6.6	6.5	7.1	6.5
60				5.8	5.3	5.0	4.6	4.9	3.9	4.0
45	4.9	7.3	6.0	5.4	4.7	4.2	3.9	3.6		3.2
30	5.2	5.3	5.2		3.9		3.1			2.8
					$\lambda = 5000$ Å					
75	20.5	17	12	11	11	10	10	11	9.5	
60	19	15	9	7.5	6.5	6	5	6	7	6
45	14	10	7.5	6.5	6.5	6	4.5	4.5		
30	8.5	7.5		4.5						
					$\lambda = 6000$ Å					
75	11	8.5	6	7	4	3.5	4	4.5	3.5	4
60	10	5	3	3	2	2	2	4	3	2
45	7.5	4	2.5	2	1.5	1.5	1.5	1.5		2
30	4	3	2		1.5					
					$\lambda = 7000$ Å					
75	9.5	6.5	4	5	3	2.5	3	3	2.5	3
60	11	4	2	1	1	1	1.1	1.5	1.5	1
45	6	3	1	1.5	1.5		1	1		
30	2.5	1	1.5		1					
					$\lambda = 8000$ Å					
75	5.5	3.5	2.2	2.2	1.5	0.95	0.95	1.5	1.5	
60		2	0.95	—	0.75	0.55	0.5	0.7	0.9	0.5
45	3.0	1.5	1	0.8	0.65	—	0.75	0.45	1	1
30	1	0.65	0.7	—	0.45					

Table 6.5 Spectral intensity of scattered radiation $I_\lambda \times 10^{-3}$ W/cm² . ster . μ on November 13, 1967, Karakum Desert $\vartheta_\odot = 65°$ [19]

$\vartheta°$	$\psi°$									
	10	30	50	70	90	110	130	150	170	180
					$\lambda = 3500$ Å					
65	2.0	1.6	1.3	2.4	1.6	1.8	1.3	1.9		
60	3.0	2.5	1.6	1.7	1.3	1.5	1.4	1.6	1.6	1.7
45	0.8	0.8	1.3	0.8	1.0	0.8	0.7	0.8	0.8	0.8
30	0.7	0.7	0.7		0.6		0.6			
					$\lambda = 4000$ Å					
65	17.9	14.4	12.1	21.6	16.6	17.0	11.5	17.5		
60	26	23.1	16.2	16 2	12.7	14.0	18.3	14.7	16.7	16.2
45	8.9	7.8	12.3	8.1	9.8	8.4	7.1	7.2	7.5	7.7
30	6.6	6.7	6.7		6.5		5.9			4.6
					$\lambda = 5000$ Å					
65	52	33	28	21.5	19.5	20	25	25		
60	45.5	36	22	19	12.5	17	19.5	21	11.5	
45		17.5	15.5	13	12.5	10	12.5	12.5	12.5	
30	12.2	11.5	9.8							
					$\lambda = 6000$ Å					
65	27	12	8.0	6.5	5.5	6.0	7.0	6.7		
60	25	15	8.5	9.0	3.0	5.0	5.5	6.5	6.5	
45		4.5	4.5	4.0	3.0	3.5	5.0	5.0	5.0	
30	4.0	3.5	3.0							
					$\lambda = 7000$ Å					
65	25.5	9.5	6.5	5.0	4.3	4.0	5.5	5.5		
60	22	13	7.0	4.5	2.5	4.3	4.2	5.5		
45		3.0	3.0	2.5	3.0	3.2	3.5	3.5		
30	3.0	2.5								
					$\lambda = 8000$ Å					
65	16.5	5.0	2.7	2.4	1.8	1.8	1.5	2.4		
60	10.5	6.6			1.2					
45		1.2			1.2					

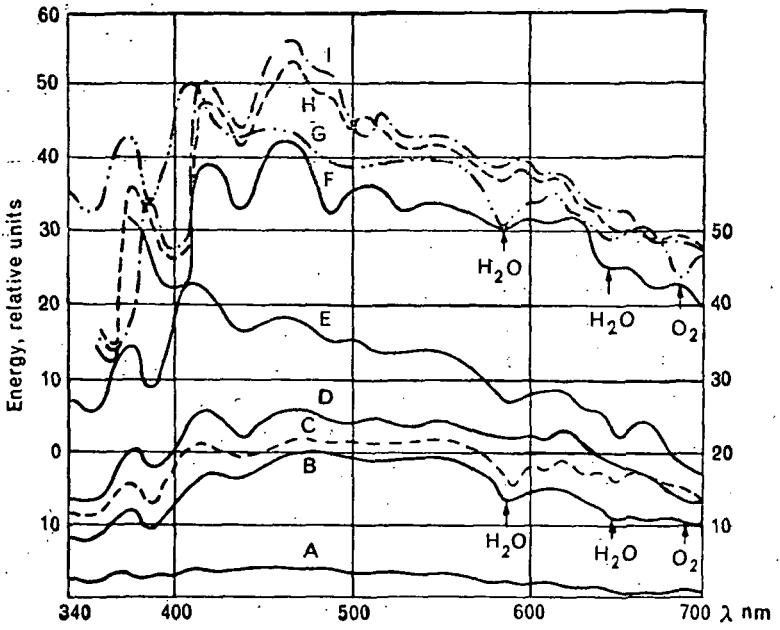

Fig. 6.2. Spectral distribution of scattered radiation for different atmospheric states.

A, C, E—continuous dense cloudiness; B, G—dense cumulus clouds; D—clear sky; F, H, I—fog [92].

The values of fluxes of radiation scattered from the entire hemisphere of the sky [19] when it is clear are given in Table 6.6.

2. ANGULAR DISTRIBUTION OF INTENSITY OF SCATTERED RADIATION

The intensity of scattered radiation resulting from the optical inhomogeneity of the atmosphere varies within wide limits depending on the direction of probe, i.e. it appears to be considerably anisotropic. The properties of the angular distribution of intensity of scattered radiation in cloudless atmosphere can be primarily determined by the form of the scattering function and the optical thickness of the atmosphere in a given direction. Because the scattering functions are prolate, the maximum intensity is always observed in the vicinity of the sun. The maximum intensity of the scattered radiation lies in a horizontal plane at an angular displacement of about 90°. The angular distribution of the intensity of scattered radiation is symmetrical *with respect to the vertical plane in which the sun* is situated (Fig. 6.3). The energy and light intensities in Fig. 6.3 are

Table 6.6 Spectral fluxes of scattered radiation (cal/cm² · min . μ) at the ground on September 24, 1964, Odessa [19]

λ Å	*m*									
	5.6	2.9	2.1	1.7	1.5	1.5	1.7	2.1	3.0	6.0
3286	0.02	0.05	0.07	0.09	0.11	0.11	0.09	0.07	0.04	0.01
3533	0.05	0.10	0.14	0.17	0.20	0.19	0.17	0.14	0.09	0.04
3864	0.11	0.24	0.31	0.38	0.48	0.42	0.34	0.27	0.22	0.13
4111	0.34	0.62	0.78	0.88	0.96	0.88	0.74	0.62	0.44	0.24
4276	0.33	0.60	0.72	0.80	0.90	0.84	0.74	0.60	0.44	0.25
4318	0.33	0.58	0.70	0.78	0.86	0.80	0.68	0.58	0.42	0.24
4359	0.36	0.60	0.73	0.80	0.88	0.84	0.73	0.60	0.44	0.26
4606	0.40	0.64	0.76	0.86	0.90	0.84	0.76	0.64	0.48	0.29
4800	0.42	0.66	0.79	0.88	0.92	0.88	0.78	0.64	0.49	0.30
5019	0.32	0.50	0.58	0.60	0.62	0.60	0.54	0.46	0.36	0.23
5432	0.24	0.36	0.42	0.44	0.46	0.44	0.40	0.28	0.24	0.16
6010	0.17	0.28	0.34	0.35	0.36	0.36	0.32	0.26	0.19	0.11
6258	0.12	0.22	0.28	0.30	0.31	0.28	0.24	0.22	0.16	0.11
6505	0.12	0.22	0.27	0.29	0.29	0.25	0.21	0.18	0.14	0.10
6758	0.16	0.23	0.28	0.29	0.30	0.28	0.23	0.18	0.14	0.10
6918	0.10	0.18	0.22	0.24	0.24	0.21	0.18	0.14	0.12	0.08
7248	0.08	0.13	0.17	0.18	0.19	0.18	0.15	0.12	0.09	0.06
7455	0.10	0.16	0.19	0.20	0.20	0.19	0.16	0.13	0.10	0.07
7620	0.04	0.07	0.09	0.10	0.11	0.12	0.09	0.06	0.05	0.03
7744	0.09	0.14	0.18	0.20	0.20	0.17	0.14	0.11	0.09	0.07
7991	0.07	0.12	0.16	0.17	0.18	0.17	0.14	0.12	0.10	0.06
8157	0.06	0.09	0.10	0.12	0.13	0.12	0.12	0.09	0.07	0.04
8569	0.04	0.10	0.13	0.14	0.14	0.13	0.12	0.10	0.08	0.05
8900	0.04	0.08	0.10	0.10	0.11	0.10	0.10	0.08	0.06	0.04
9147	0.02	0.05	0.06	0.08	0.08	0.08	0.08	0.05	0.04	0.02
9312	0.03	0.04	0.06	0.06	0.06	0.06	0.06	0.06	0.04	0.01
9395	0.01	0.02	0.04	0.04	0.05	0.06	0.05	0.05	0.04	0.02
9643	0.02	0.04	0.08	0.06	0.07	0.08	0.08	0.06	0.06	0.03

given in relative units, the corresponding intensity at the zenith [24] is taken as a unit.

The angular displacement of the region of the maximum intensity from the sun varies with respect to solar altitude and wavelength of the radiation. It decreases with increasing solar altitude, and grows with increasing wavelength [24, 79].

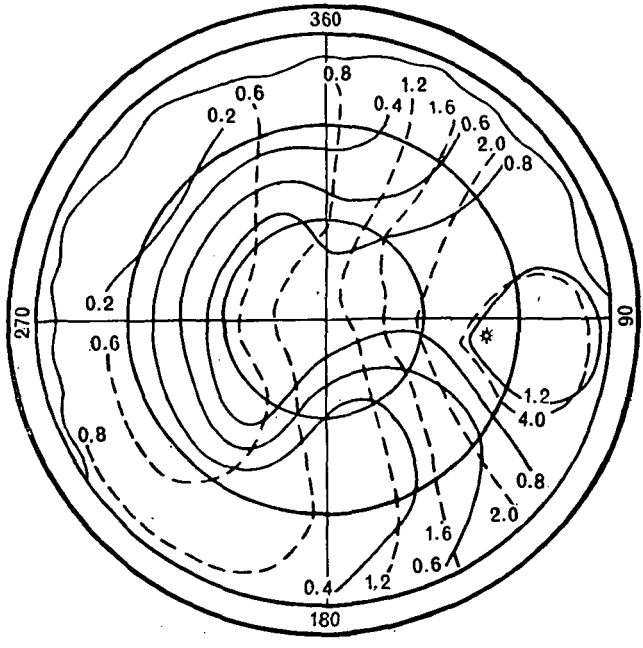

Fig. 6.3. Distribution of relative energy (continuous lines) and light (dotted lines) intensities of scattered radiation over the sky, $h_{\odot}=39°$ [24].

The nature of the angular distribution of energy and light intensities of scattered radiation correspond generally, but a quantitative correspondence is not to be observed (see Fig. 6.3). The quantitative differences may be caused by changes in the spectral composition of scattered radiation with the direction of sighting.

The energy intensity and radiative intensity may differ considerably for many points in the sky (see Table 6.7) [24]. This difference narrows down with increasing altitude. For $h_{\odot} > 60°$ it becomes insignificant.

A close correspondence between the distributions of energy and light intensities of scattered radiation may be observed in the case of continuous cloudiness. An azimuthal dependence of scattered radiation on the intensity is weakly expressed in the case of a continuous stretch of cloudiness and a monotonic decrease in intensity may be observed from the zenith toward the horizon.

Extensive theoretical computations on the field of scattered radiation for a clear atmosphere provide a pattern of the angular distribution of the intensity of scattered radiation similar to that of experimental observations [64].

Table 6.7 Relative magnitudes of energy and light intensities of scattered radiation in clear atmosphere and $h_{\odot}=25°$ [24]

$h°$	$\psi°$	Energy intensity I_D	Light intensity I_F	I_D/I_F
30	10	2.25	1.27	1.77
	40	1.37	1.18	1.16
	70	1.12	1.09	1.03
	100	2.75	1.27	2.16
	130	2.37	1.09	2.18
	160	2.50	1.09	2.29
	190	2.75	1.63	1.69
	220	4.00	2.45	1.64
	250	4.75	4.54	1.05
	280	9.75	13.80	0.71
	310	1.87	3.63	0.52
	340	0.62	1.81	0.34
60	10	0.62	0.90	0.69
	40	0.87	0.90	0.97
	70	1.75	0.90	1.95
	100	2.00	0.90	2.22
	130	2.37	0.90	2.63
	160	2.75	0.90	3.06
	190	3.00	1.09	2.75
	220	3.25	1.63	2.00
	250	3.25	1.81	1.80
	280	3.25	2.18	1.49
	310	1.87	1.81	1.03
	340	1.25	1.45	0.86
90		1.00	1.00	1.00

REMARKS: $h°$, $\psi°$—angular height and azimuth of point.

3. FLUX OF SCATTERED RADIATION FROM DISTINCT ZONES OF THE SKY

3.1 Zonal radiation

Radiation scattered from the annular segments of the sky, encircled by two almucanthorats, is called the zonal radiation. The amount of scattered radiation can be approximately evaluated with the help of data

on zonal radiation in those places where the horizon may be more or less covered. The zonal distribution for clear and cloudy skies for different solar altitudes [22] is given in Table 6.8. The last column of the table shows the relative magnitudes of the zonal radiation for isotropically scattered radiation. The flux of radiation from the entire sky is taken as a unit in all the cases. The variation in magnitude of zonal radiation for a given $h_\odot$ may be brought about by a variation in the following two quantities, viz. area of zone and incident angle of radiation, quantities which are related to zenith separation of the zone in a different manner. As the zenith distances decrease the area of the zone decreases, and the incident angle of radiation on the horizontal surface also decreases. As the zenith angle of the sun decreases the zone of maximum radiation moves to the side of lesser zenith distances of Table 6.9. The zonal distribution of scattered radiation (in relative units) for a cloudless sky at different altitudes of the sun, obtained through observations [44], is given in Fig. 6.4.

Table 6.8 Relative zonal distribution of scattered radiation [22]

Zonal boundaries		Clear		Cloudy	Uniformly bright sky
ϑ_1°	ϑ_2°	$h_\odot = 20°30'$	$h_\odot = 16°30'$	$h_\odot = 7°30'$	
0	10	0.0294	0.0161	0.0390	0.0301
10	20	0.0535	0.0523	0.1307	0.0868
20	30	0.0878	0.0838	0.1943	0.1330
30	40	0.1307	0.1235	0.1591	0.1632
40	50	0.1621	0.1338	0.1375	0.1736
50	60	0.1779	0.1509	0.1467	0.1632
60	70	0.1715	0.1861	0.1173	0.1330
70	80	0.1400	0.1798	0.0509	0.0868
80	82	0.0162	0.0260	0.0086	0.0108
82	84	0.0133	0.0204	0.0067	0.0084
84	86	0.0097	0.0149	0.0050	0.0061
86	88	0.0059	0.0092	0.0031	0.0037
88	90	0.0020	0.0032	0.0011	0.0013
	Entire sky	1.0000	1.0000	1.0000	1.0000

Table 6.9 Fluxes of zonal radiation (10^{-3} cal/cm^2 · min) and the position of maximum in the zones with respect to zenith distance of the sun [22]

$\vartheta_\odot$°	0	30	45	60	75	87
ϑ_{max}	47.5	54.0	60.0	64.5	67.5	69.0
D_z	10.07	9.68	9.44	9.14	7.85	4.03

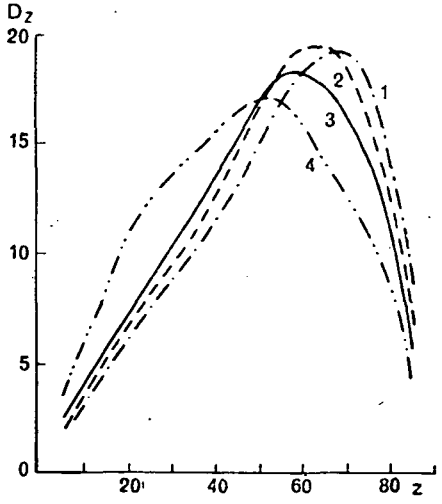

Fig. 6.4. Zonal radiation at different solar altitudes.
1—$h_\odot = 13.5°$; 2—$h_\odot = 26.5°$; 3—$h_\odot = 36°$; 4—$h_\odot = 54.5°$ [44].

The data of fluxes of radiation scattered from separate sections of the sky are useful in evaluating the effect of covering the horizon.

The fluxes of radiation scattered from semi-annular zones of the sky, evaluated from data on measurements of angular distribution of intensity of scattered radiation (intensity was measured along 37 directions), are given in Fig. 6.5. Semi-annular zones are formed by the division of annular zones by a vertical plane that contains the solar vertical. The field of scattered radiation is considerably nonuniform. The fluxes from the semi-annular zone lying on the side of the sun are significantly greater than the fluxes from the semi-annular zones situated away from the sun [63].

The intensity of scattered radiation is distributed all over the sky during continuous stretches of cloudiness (cf. Table 6.10) [44]. The average intensity of scattered radiation for a given zone is evaluated from the formula as follows :

$$\bar{I}_1 = \frac{D_{z,i}}{2\pi \cos z_{av} (\cos z_{i+1} - \cos z_i)} \quad (6.1)$$

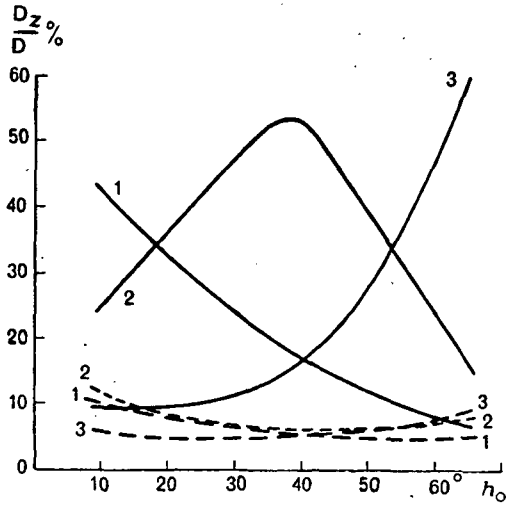

Fig. 6.5. Fluxes of radiation scattered by semi-annular zones.
1—zone 0-28°; 2—zone 28-52°; 3—zone 52-78°; continuous lines—semi-annular rings in the vicinity of the sun; dotted lines—semi-annular rings away from the sun.

Table 6.10 Mean values of zonal radiation D_z and scattered radiation, intensity $\bar{I}$ at the time of a continuous stretch of clouds at a lower level (in relative units) [44]

Zone, deg	0–10	10–20	20–30	30–40	40–50	50–60	60–70	70–80	80–90
D_z	3.5	9.5	14.5	16.5	18.0	16.0	12.5	6.5	3.0
$\bar{I}$	23	22	22	20	21	20	19	15	20

The amount of flux for an isotropically scattered radiation on account of annular zone at an altitude 'h' from the horizon can be expressed by the formula [5] :

$$D_h = \pi I \sin^2 h, \tag{6.2}$$

where I is intensity of scattered radiation (it is identical along all azimuthal directions in the present case). Since the flux from the entire sky equals πI for isotropically scattered radiation it is possible to write $D_h = D \sin^2 h$.

In the case of isotropic approximation the amount of radiation flux due to scattering from an annular ring, bounded by two almucantnorats with angular elevations of h_1 and h_2, can be evaluated from the following formula, viz. :

$$D_h = D\ (\sin^2 h_2 - \sin^2 h_1). \tag{6.3}$$

3.2 Radiation in the vicinity of the sun

The scattered radiation of the zones in the vicinity of the sun (aureole near the sun) depends to a great extent on atmospheric transparency and thus may be considered to be an important characteristic of transparency.

The scattered radiation of the annular zones in the vicinity of the sun, possessing an angular halfwidth of about 2°, comprises approximately 1% of the direct solar radiation under average conditions of atmospheric transparency (Table 6.11). As the area of annular zones in the neighborhood of the sun enlarges according to its distance from the sun, and the ratio D/S changes a little, it is obvious that the intensity of radiation in the vicinity of the sun decreases in accordance with its distance from the sun. To a first approximation this distance can be considered exponential [23].

Table 6.11 Relative magnitudes of radiation in the vicinity of the sun [22]

Zone	Area of zone, deg²	Region of angular distances from the center of solar disc	Halfwidth of the zone	$\frac{D}{S}$ %
I	17.49	27.5′-4°0.25′	1°47′	0.99
II	31.92	1°43.1′-5°25.6′	1 55	0.71
III	44.71	3°3.9′-6°50.6′	1 55	0.70
IV	56.33	4°34.4′-8°15′	1 50	1.12

Clouds, especially of the cirrocumulus and high cumulus types, considerably increase the scattered radiation in the zonal regions near the sun. In this case radiation in the vicinity of the sun comprises up to 15% direct solar radiation.

It is necessary to carry out measurements on direct solar radiation in the presence of clouds around the sun with extreme caution. One must take into consideration the scattered radiation near the sun during measurements on direct solar radiation employing a pyrheliometer or an actinometer.

The relative intensity of radiation near the sun incident on an actinometer can be evaluated from the following formulas [78], viz :

$$\eta = \frac{1}{\pi} \sigma \cos h_{\odot} \Delta\omega e^{\tau m} \tag{6.4}$$

where σ —coefficient of brightness of the sky
m —atmospheric mass
$h_{\odot}$ —solar altitude
τ —optical thickness of atmosphere
$\Delta\omega$—solid angle of the actinometer.

In the case of Yanishevskii's thermoelectric actinometer $\Delta\omega = 2.39 \times 10^{-2}$.

Results of computations using formula 6.4 for the wavelength $\lambda = 0.55$ μ at different solar altitudes and albedo values of the underlying surface A are given in Table 6.12.

Table 6.12 Relative intensity of radiation near the sun under standard conditions [78]

$h_{\odot}^{\circ}$	A										
	0	0.1	0.2	0.3	0.4	0.5	0.6	0.7	0.8	0.9	1.0
0	0.53	0.54	0.55	0.55	0.56	0.57	0.57	0.58	0.59	0.60	0.60
50	0.84	0.85	0.86	0.87	0.88	0.89	0.90	0.91	0.92	0.93	0.94
60	1.07	1.08	1.09	1.10	1.11	1.12	1.13	1.14	1.15	1.16	1.18
70	1.56	1.57	1.58	1.60	1.61	1.62	1.63	1.65	1.66	1.68	1.69
80	3.60	3.62	3.64	3.66	3.66	3.68	3.68	3.70	3.72	3.74	3.80

4. VERTICAL PROFILE OF THE FLUX OF SCATTERED RADIATION

The flux of scattered radiation in a clear sky decreases with the altitude above the ground. As the altitude rises above the sea level there occurs a decrease in the thickness of the atmospheric layer and, subsequently, a decrease in the number of scattering particles.

Observations made over the Kyzyl-Kum Desert show that in the layer between 0.5 and 1.5 km the scattered radiation decreases almost directly in proportion to the pressure. On account of a rapid decrease in the amount of dust the scattered radiation reduces much faster [62].

The variation in the flux of scattered radiation with height is illustrated by data of Table 6.13, obtained through measurements from an airplane over Tashkent. The most noticeable variation in the flux of

scattered radiation may be observed in the layer 1-4 km throughout the year. The mean values of the fluxes of scattered radiation over the seasons of the year are given in this table.

Table 6.13 Fluxes of scattered radiation at different heights (cal/cm² . min) at actual midday [62]

H km	Winter	Spring	Summer	Autumn
0.4	0.148	0.200	0.170	0.178
0.8	0.146	0.199	0.169	0.175
1.3	0.138	0.176	0.162	0.158
2.3	0.125	0.154	0.131	0.138
3.4	0.115	0.129	0.086	0.114
4.4	0.108	0.111	0.058	0.098
5.5	0.101	0.094	0.031	0.081
6.7	0.093	0.080	—	—

The experimental profiles obtained through aerostatic [43] and airplane [35] probings are almost identical (Fig. 6.6). The most noticeable discrepancy exists between theoretical [46] and average experimental profiles in the layer 2-7 cm. A low gradient D may be observed in the layer from 3 to 6 km which is comparatively transparent and stable. Larger gradients D (in absolute magnitude) lie in the layer between 6 and 8 km, as a result of which this layer possesses high turbidity.

The results of theoretical computations show an exponential decrease with height in the flux of scattered radiation with a maximum gradient occurring in the lower layer of 3 km [46, 71, 72].

The greatest variation in the flux of scattered radiation occurs in the layer 0-3 km for low zenith angles of the sun.

There exists an almost linear decrease in the flux of scattered radiation from the height of 4-5 km. The scattered flux becomes practically negligible at 19-20 km.

5. SCATTERED RADIATION ON A HORIZONTAL SURFACE

5.1 Cloudless atmosphere

The flux of scattered radiation grows monotonically (cf. Table 6.14) with increasing solar altitude under stationary conditions of the atmosphere and the underlying surface, whereas the gradient $dD/dh_{\odot}$ decreases.

Similarly the fluxes of scattered radiation for different ranges of the spectrum decrease with rising solar altitude (cf. Table 6.15, where results of theoretical computations for ideal atmosphere [22] have been introduced).

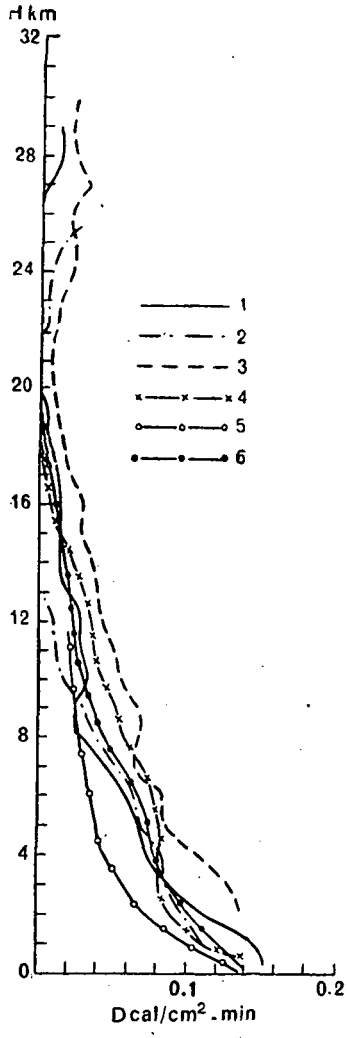

Fig. 6.6. Vertical profiles of scattered radiation from balloon investigations [43].

1—July 1964, $h_\odot$=23-38°, clear; 2—July 1964, $h_\odot$=20-37°, clear; 3—October 1964, $h_\odot$=23°, St. 10/10; 4—October 1964, $h_\odot$=26°, clear; 5—computed profile, $h_\odot$=26.5°, grass [43]; 6—*mean experimental profile over four profiles.*

Table 6.14 Mean values of scattered radiation in a clear sky (cal/cm² · min) [8]

$h^\circ_\odot$	5	10	15	20	25	30	35	40	45	50	55	60	65
D	0.05	0.07	0.10	0.11	0.13	0.14	0.15	0.16	0.17	0.17	0.18	0.19	0.19

Table 6.15 Fluxes of scattered radiation D_r% in different ranges of the spectrum depending on the zenith separation of sun (with respect to fluxes at $\vartheta_\odot = 0^\circ$) [22]

$\vartheta^\circ_\odot$	Dr%			Entire spectrum
	$\lambda < 0.4\ \mu$	$0.4\ \mu \leqslant \lambda \leqslant 0.6\ \mu$	$0.6\ \mu \leqslant \lambda < 0.9\ \mu$	
0	100	100	100	100
15	97.0	99.7	99.8	99.0
30	92.5	97.5	98.9	96.5
45	82.8	94.2	97.9	92.0
60	66.9	88.5	95.7	84.5
75	39.4	75.4	90.8	69.3
87	8.0	34.6	63.3	37.4

The flux of scattered radiation increases at all solar altitudes (Fig. 6.7) with decreasing atmospheric transparency. At higher altitudes of the sun the scattered radiation increases more rapidly with an increase in the turbidity factor [8, 48].

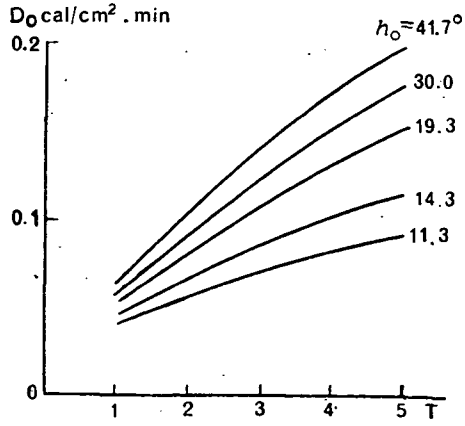

Fig. 6.7. The relation of the flux of scattered radiation to the turbidity factor for clear atmosphere [8].

The nature of the dependence of the scattering radiation flux on the turbidity factor varies according to the relationship between the scattering and the absorption coefficients. The flux of scattered radiation decreases with an increase in the absorption coefficient at constant coefficient of scattering, whereas it increases with an increase in scattering coefficient at constant coefficient of absorption [8].

The scattered radiation increases with the albedo of the underlying surface, especially in the presence of a snow cover. The effect of the albedo of the underlying surface becomes stronger in accordance with the increase in altitude of the sun (Fig. 6.8). Similarly it follows from theoretical computations [59] that the flux of scattered radiation increases linearly with an increase in albedo at all altitudes of the sun. From the data in Table 6.16 [67] it is possible to obtain an idea of the influence of the albedo of snow on the magnitude of scattered radiation.

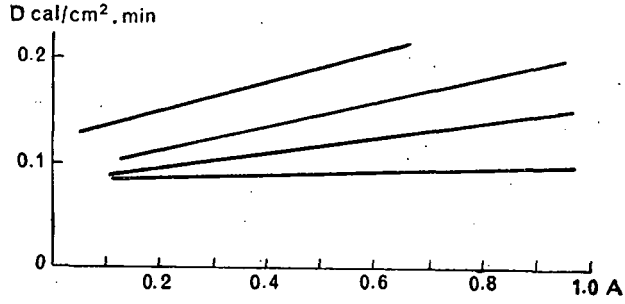

Fig. 6.8. The relation between flux of scattered radiation and albedo of the surface [8].

Table 6.16 Influence of albedo of snow on the magnitude of scattered radiation in clear sky in Central Arctic (cal/cm² . min) [67]

Snow surface	Month	Solar altitude, deg						
		0	5	10	15	20	25	30
				Mean values				
Snow covered	Feb-Apr	0.03	0.06	0.10	0.14	0.16	0.18	0.18
No snow	Jun-Aug	—	0.06	0.08	0.12	0.14	0.14	0.16
				Maximum values				
Snow covered	Mar-Jun	0.05	0.12	0.20	0.28	0.28	0.30	—
No snow	Jul-Aug	0.05	0.06	0.18	0.22	0.23	0.24	—

5.2 Scattered radiation in cloudy atmosphere

The presence of clouds in the atmosphere sharply increases the flux of scattered radiation. The amount of scattered radiation flux in a cloudy sky depends on the quantity and form of the clouds as well as on the altitude of the sun, atmospheric transparency and the albedo of underlying surface. Similarly, the distribution of clouds over the sky and their location relative to the sun influences the flux. The variation in scattered radiation is noticeably reduced when the solar disc is covered by comparison with the presence of direct solar radiation. The scattered radiation increases with rising solar altitude for varying cloudiness ; moreover, this increase becomes more noticeable as the amount of cloudiness increases (Table 6.17) [69]. The scattered radiation increases monotonically with increasing cloudiness in the upper layers. The most intense rise in scattered radiation may be observed with cloud cover of more than 6 on a 10-point scale. Radiation reaches a maximum at cloudiness of 6 tenths in the lower and intermediate layers. Scattered radiation increases for cloudiness rising to 7 tenths with clouds having vertical development at a given solar altitude. However, it decreases with further increase in cloudiness. For continuous cloudiness of Cu and Cb types, scattered radiation is less than that for a cloudless sky.

Table 6.17 Fluxes of scattered radiation (cal/cm² · min) for different solar altitudes and cloudiness $\varphi=60°$ N [69]

Cloudiness, tenths	Altitude of the sun, deg									
	5-10	10-15	15-20	20-25	25-33	30-35	35-40	40-45	45-50	50-55
	Ci, Cs, Cc									
1	0.07	0.08	0.10	0.12	0.13	0.15	0.17	0.18	0.18	0.18
2	0.08	0.09	0.10	0.13	0.13	0.14	0.17	0.17	0.18	0.18
3	0.08	0.10	0.10	0.15	0.17	0.17	0.18	0.18	0.19	0.20
4	0.05	0.12	0.13	0.15	0.16	0.17	0.18	0.18	0.19	0.20
5	0.06	0.12	0.12	0.13	0.15	0.17	0.18	0.18	0.19	0.20
6	0.06	0.12	0.12	0.12	0.15	0.17	0.18	0.18		
7	0.06	0.11	0.12	0.16	0.16	0.19	0.21	0.22	0.23	
8	0.06	0.10	0.10	0.14	0.15	0.19	0.20	0.24	0.24	
9	0.06	0.09	0.12	0.13	0.16	0.16	0.18			0.27
10	0.09	0.13	0.15	0.16	0.16	0.19	0.22	0.24	0.26	0.28
10	0.09	0.14	0.16	0.18	0.20	0.23	0.27	0.30		

Table 6.17—*Contd.*

					As, Ac					
1	0.06	0.08	0.10	0.11	0.14	0.16	0.18	0.20	0.21	
2	0.07	0.11	0.13	0.16	0.17	0.19	0.20	0.22		
3		0.09	0.14	0.20	0.21		0.20			0.20
4	0.05	0.12	0.14	0.16			0.25	0.25		
5		0.12	0.15	0.18	0.19	0.22	0.24	0.25		
6	0.06	0.10	0.16	0.20	0.22	0.26	0.28			
7	0.10	0.10	0.18	0.22	0.24	0.30	0.32	0.32		
8	0.10	0.12	0.18	0.22	0.20	0.25	0.26	0.26	0.34	0.38
9	0.06	0.13	0.16	0.20	0.22	0.25	0.27	0.26	0.36	0.40
10	0.07	0.16	0.23	0.22	0.28	0.32				
10	0.10	0.12	0.18	0.18	0.22					
					Cu, Cb					
1	0.06	0.08	0.11	0.12	0.12	0.16	0.16	0.17	0.18	0.19
2	0.06	0.06	0.17	0.17	0.16	0.18	0.18	0.21	0.21	0.22
3	0.06	0.08	0.14	0.14	0.16	0.23	0.22	0.23	0.23	0.24
4	0.05		0.15	0.20		0.19	0.22	0.24	0.26	0.27
5		0.12			0.17	0.23	0.27	0.29	0.31	
6			0.15	0.22	0.26	0.27	0.28	0.33	0.37	0.42
7	0.05		0.18	0.22	0.26	0.27	0.28	0.35	0.36	0.42
8	0.06	0.16	0.18	0.21	0.30	0.32	0.34	0.35	0.36	0.38
9	0.06	0.18		0.21	0.27	0.31	0.33	0.34	0.35	0.36
10	0.04	0.06	0.10	0.10	0.10	0.07	0.07	0.12	0.12	0.15
					Sc					
1	0.08	0.13								
2		0.10	0.11	0.15	0.19					
3		0.10		0.15	0.19					
4		0.07		0.16						
5		0.08		0.16						
6		0.05	0.12		0.22					
7		0.06	0.12		0.22					
8	0.10	0.10	0.14	0.22						
9		0.11	0.16	0.13	0.21					
10		0.05	0.10	0.13	0.18	0.22	0.24	0.22	0.22	0.24

Investigations on the influence of distinct forms of clouds showed that an increase in cloudiness up to the value $\overline{10}$ leads to an increase in scattered radiation [12] for any cloud formation and any state of the solar disc. Only in the case of the densest Cb does an increase in cloudiness from 8-9 to 10 tenths not result in a growth in scattered radiation. Scat-

tered radiation decreases especially strongly for Sc and Cb upon the disappearance of transillumination in clouds.

The flux of scattered radiation is less in case of any cloud formation completely covering the sun than in the case of moderate brightness of the sun (i.e. translucent sun through clouds imparting a distinct shadow to objects).

There is a practically linear dependence of the scattered radiation flux on solar altitude for different types of cloud [8, 50, 69]. In the Arctic, the main portion of the radiant energy arrives in fractions of scattered radiation because of the peculiar conditions of cloudiness and underlying surface. In comparison with the scattered radiation of a clear sky, the scattered radiation flux doubles for continuous stretches of cloudiness in the upper layer and a snow cover. The highest value of radiation fluxes may be observed for clouds in the intermediate and lower layers [68].

5.3 Daily variations and daily aggregates of scattered radiation

The daily variation of scattered radiation in a clear sky is primarily brought about by the change in altitude of the sun. The maximum of scattered radiation may be observed around midday. The daily variation of D is often asymmetrical with respect to midday because of the decrease in atmospheric transparency in the post midday period. The data in Table 6.14 serve as an illustration of the daily variation of scattered radiation in a clear sky.

The diurnal variation of scattered radiation is very complex and irregular under conditions of variable cloudiness. The variation in the flux of scattered radiation for a continuous stretch of cloudiness can be

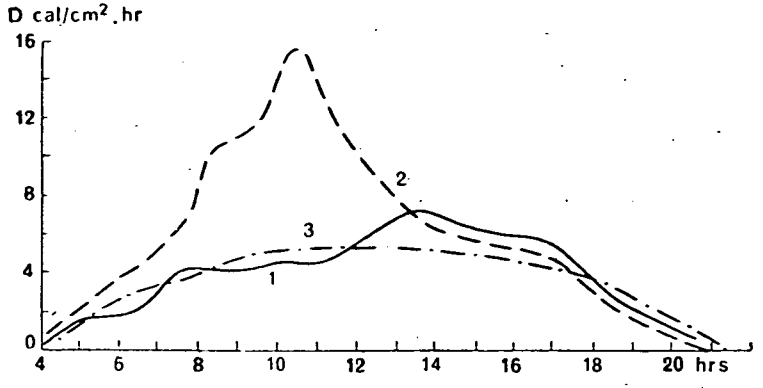

Fig. 6.9. Diurnal variation of scattered radiation.
1—continuous cloudiness; 2—variable cloudiness; 3—clear sky [69].

determined mainly by the variation in the solar altitude, and the daily course attains a maximum around midday (Fig. 6.9) [69].

It is possible to form an idea of the mean daily course of scattered radiation from the hourly amounts (Table 6.18) [69].

Table 6.18 Hourly amounts (cal/cm² . min) of scattered radiation (average over 1950-1960); φ=60° N [69]

Month	Hours																		Maximum
	3-4	4-5	5-6	6-7	7-8	8-9	9-10	10-11	11-12	12-13	13-14	14-15	15-16	16-17	17-18	18-19	19-20	20-21	
Jan							2	3	5	5	3	2							9
Feb					1	3	6	9	10	10	8	6	3	1					12
Mar				2	5	9	11	14	16	15	14	11	9	5	2				16
Apr			2	5	9	12	14	16	18	18	17	15	12	9	5	2			38
May		3	6	9	12	15	17	19	19	19	18	16	14	12	9	5	3	1	41
Jun	2	5	8	10	13	16	18	21	22	21	21	19	16	13	11	7	4	2	43
Jul	1	4	7	10	13	16	18	19	20	20	20	17	15	12	10	7	4	1	41
Aug		1	4	7	10	13	15	17	19	18	17	16	13	10	7	4	1		36
Sept			1	3	6	9	12	14	15	15	13	11	9	5	2				22
Oct					1	4	6	8	9	8	7	6	3	1					16
Nov						1	2	4	5	5	4	2	1						10
Dec							1	2	3	3	2	1							8

The diurnal variation of scattered radiation in winter is expressed more sharply in the northern latitudes where the amount may be distributed over a considerably smaller number of hours. The diurnal amounts show an annual as well as a latitudinal variation (Table 6.19).

Table 6.19 Diurnal amounts of scattered radiation (cal/cm² . min) for recordings averaged over 1950-1960 [69]

Amounts of radiation	Jan	Feb	Mar	Apr	May	Jun	Jul	Aug	Sept	Oct	Nov	Dec
Mean	20	57	113	154	197	229	214	172	115	53	24	12
Minimum	24	70	153	189	245	364	232	181	143	62	32	15
Maximum	18	35	87	129	178	207	200	158	96	44	16	8

The diurnal amounts of scattered radiation differ considerably from the average over many years on particular days. For instance, in Karadag the maximum daily amounts may exceed the minimum by more than 20 times [8].

Latitudinal variation in diurnal amounts of scattered radiation is different at different times of the year. The diurnal amounts of scattered radiation in the South are considerably larger than in the North during winter. The difference between diurnal amounts in the South and in the North is reduced on account of the prolonged day during summer.

5.4 Monthly amounts and annual course of scattered radiation

The monthly amounts of scattered radiation can be determined by the altitude of the sun, by the cloud cover, albedo of the surface and the length of the day. The mean values of monthly amounts of scattered radiation for recordings registered over many years are given in Table 6.20 [8]. Similarly, the midday altitude h_{noon} of the sun, the length of the day on the 15th of the month t and the mean monthly total cloud cover n are given in the Table. As a result of the effect of cloudiness, the month of the maximum amount does not coincide with the month of the maximum altitude of the sun, but is shifted to the neighboring months, viz. May and July. A distinct relation between the monthly amounts and mean monthly degree of cloudiness was not observed. Evidently the quantity of overall cloudiness expressed in tenths does not fully characterize the scattering power of clouds of different forms.

The annual variation in the flux of scattered radiation, corresponding to a specific time, depends mainly on the variation in solar altitude, transparency and cloud cover.

A large amount of scattered radiation in the Arctic region is brought about by a marked cloudiness during summer and by the high reflectivity of the underlying surface which is covered with snow and ice for the greater part of the year.

5.5 Contribution of scattered radiation to total radiation

Scattered radiation comprises an important part of the shortwave balance, especially for varying cloudiness and during winter. On an average the scattered radiation may represent up to 50% of the entire amount. The contribution of scattered radiation depends on the solar altitude, turbidity in the atmosphere and cloudiness. The portion of

Table 6.20 Monthly and annual amounts of scattered radiation [8]

Station, period of observation	Parameter	Jan	Feb	Mar	Apr	May	Jun	Jul	Aug	Sept	Oct	Nov	Dec	Year
Tbilisi 1938-1954	$\Sigma_m D$	2.3	2.9	4.5	5.0	5.4	5.2	5.6	4.8	3.7	2.9	2.2	2.0	46.5
	h_{noon}	27.0	35.4	45.9	50.8	67.0	71.6	70.0	62.6	51.6	40.1	30.0	25.1	
	n	6.3	6.7	6.7	6.3	6.2	5.1	4.5	4.4	5.0	5.5	6.2	6.1	
	t	9.2	10.4	12.1	13.2	14.3	15.0	14.1	13.7	12.4	11.0	9.7	9.0	
Vladivostok 1941-1954	$\Sigma_m D$	2.2	2.7	4.5	5.3	6.2	6.0	6.2	5.4	4.0	3.1	2.2	1.9	49.6
	h_{noon}	25.6	34.0	44.5	55.4	65.6	70.2	68.6	61.2	50.2	38.7	28.6	23.7	
	n	2.9	3.2	4.9	6.4	7.0	8.0	8.7	7.8	5.9	4.6	4.0	3.1	
	t	9.3	10.5	11.8	13.3	14.6	15.3	15.0	13.9	12.6	11.1	9.7	9.0	
Karadag 1938-1951	$\Sigma_m D$	2.2	2.8	4.5	5.5	6.1	5.8	5.5	4.8	3.7	3.4	2.2	1.9	48.4
	h_{noon}	23.8	32.2	42.7	54.6	63.8	68.4	66.8	59.4	48.4	36.9	26.8	21.9	
	n	7.9	7.7	7.4	6.6	5.8	4.7	3.3	3.2	3.9	6.0	7.3	—	
	t	9.0	10.3	11.7	13.3	14.6	15.4	15.1	14.0	12.4	11.4	9.4	8.6	
Irkutsk 1940-1953	$\Sigma_m D$	1.4	2.3	3.8	4.8	5.8	5.4	5.2	4.4	3.5	2.6	1.8	1.3	42.3
	h_{noon}	16.4	24.8	35.3	47.2	56.4	61.0	59.4	52.0	41.0	29.5	19.4	14.5	
	n	7.3	6.3	6.0	6.6	6.8	7.0	7.0	6.7	6.3	7.1	7.4	8.7	
	t	8.1	9.7	11.6	13.7	15.4	16.4	16.0	14.5	12.6	10.6	8.8	7.7	
Vysokaya Dubrava 1941-1952	$\Sigma_m D$	1.3	2.4	4.5	5.6	6.4	6.8	6.7	5.6	3.9	2.5	1.4	0.9	48.0
	h_{noon}	12.0	20.4	30.9	42.8	52.0	56.6	55.0	47.6	36.6	25.1	16.0	10.1	
	n	6.9	6.7	4.0	6.6	7.1	6.9	6.3	6.2	8.1	8.2	8.0	7.5	
	t	7.6	9.5	11.7	14.1	16.3	17.7	17.2	15.2	12.9	10.4	8.2	6.8	
Yakutsk 1938-1949	$\Sigma_m D$	0.7	1.6	3.1	5.2	6.4	6.1	5.8	4.2	2.9	2.0	0.9	0.4	39.3
	h_{noon}	6.7	15.1	25.6	37.5	46.7	51.3	49.7	42.3	31.3	19.8	9.7	4.8	
	n	5.9	5.2	5.4	5.5	6.6	6.9	6.0	6.6	6.6	8.2	7.0	6.7	
	t	6.0	9.0	11.5	14.7	17.5	19.5	18.7	16.0	13.0	10.0	6.0	5.2	

REMARKS: $\Sigma_m D$ is given in kcal/cm . mont; h_{noon}—in degrees, n—in tenths and t—in hours.

scattered radiation decreases as the solar altitude increases. Scattered radiation decreases at constant solar altitude when atmospheric transparency increases (direct solar radiation increases in that case). The ratio D/Q increases with decreasing solar altitude and rising turbidity in the atmosphere and correspondingly S'/Q also decreases (S', D and Q are the fluxes due to direct solar radiation, scattered and total radiation respectively on a horizontal surface). The appearance of cloudiness raises the ratio D/Q which is unity under continuous cloud cover.

The influence of solar altitude and cloudiness appears in the value of the ratio of the monthly amount of radiation to the total radiation (Table 6.21) [69]. During the winter months scattered radiation comprises the main portion of the shortwave radiation received.

Table 6.21 Ratio of monthly amounts of scattered radiation to monthly amounts of total radiation [69]

Jan	Feb	Mar	Apr	May	Jun	Jul	Aug	Sep	Oct	Nov	Dec	Year
0.82	0.71	0.47	0.47	0.44	0.43	0.44	0.52	0.56	0.72	0.78	0.86	0.69

PART II. REFLECTED RADIATION OF THE ATMOSPHERE

6. ANGULAR DISTRIBUTION OF INTENSITY OF REFLECTED RADIATION

The intensity of reflected radiation can be determined by the quantity of radiative energy included in a unit interval of wavelength and in a unit solid angle, passing in a unit time through a unit cross-sectional area situated perpendicular to the direction of reflection.

The ratio of the intensity of radiation reflected from the surface examined to the intensity of radiation reflected from an absolutely white surface under similar conditions of illumination (corresponding to Lambert's law) is known as the luminosity coefficient. The coefficient of luminosity is equal to the albedo for an orthotropic surface (corresponding to Lambert's law), whereas these values differ for all other surfaces.

The angular distribution of intensity of reflected radiation depends on the physical properties and the conditions of the reflecting surface, as well as on the conditions of surface irradiation of the incident radiation. The solar altitude and cloudiness determine the conditions of irradiation.

Thus, the intensity of reflected radiation for a given surface is a function of three angles ; viz. the angle of incidence of the incident radiation, the angle of reflection and the difference between the azimuthal

angles of the directions of incident and reflected radiation. As a rule this function may be represented by means of a vector diagram which is known as the reflection phase function.

In accordance with V. V. Sharonov's classification [70] the reflection indicatrices for natural surfaces in all their variations may be divided into the following four types :

type A—orthotropic phase functions, approximately corresponding to the condition I_R=const (I_R—intensity of reflected radiation) ;

type *B*—phase functions extending in the direction of mirror-reflection of the ray ;

type *C*—phase functions extending in the direction of light sources, characteristic for surfaces which are very roughly cut ; and

type *D*—composite phase functions, characterizing the existence of two maxima ; one in the direction of reflected ray and the other in the direction of source of light.

6.1 Angular distribution of integrated intensity of reflected radiation

For the majority of natural surfaces the characteristic feature of the spatial distribution of the intensity of reflected radiation in a clear atmosphere is the symmetry with respect to the plane containing the solar vertical. The maximum reflected intensity lies on the side of the projection of the sun in the horizontal plane, i. e. in the direction of the reflected ray, whereas the minimum lies on the opposite side (Fig. 6.10). The isolines in Fig. 6.10 are given in relative units, with the intensity of reflection at nadir [26] being accepted as unity. The projection of the sun in the horizontal plane is marked by a circle. The detailed angular distribution of intensity of reflected radiation has been examined for snow covered by an ice crust, and for several vegetative covers (wheat, barley, Sudan grass).

The nature of the spatial distribution of intensity of reflected radiation remains the same during partial cloudiness not obscuring the sun as well as for a clear sky.

Isolines of reflected radiation can be approximately represented by concentric circles with the center at the nadir in case of continuous dense cloudiness, with the intensity of reflected radiation increasing from the lowest point toward the horizon.

For a clear sky a snow covering has a clearly expressed mirror reflection ; a barley surface and Sudan grass have a similar noticeable mirror component (Fig. 6.11 a, b, c) [26].

There is a decrease in the stretching of the reflected phase function with increasing solar altitude.

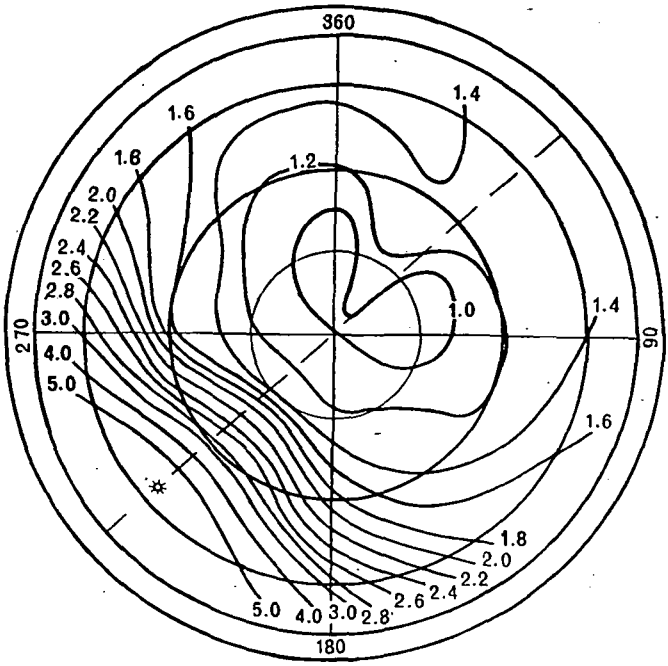

Fig. 6.10. Angular distribution of intensity of radiation from snow covered by an ice crust. No clouds, $h_{\odot}=18.5°$ [26].

It is possible to consider a snow cover among surfaces of type *b* according to Sharanov's classification.

The reflection phase functions from barley and Sudan grass for $h_{\odot}<45°$ are stretched in the direction of the reflected ray and in the direction of the source of light. Reflection phase functions from stubble barley are sharply extended in the direction of incident rays from the sun (Fig. 6.11, c). These vegetative covers relate to type *D* according to Sharanov's classification.

Reflection phase functions for different surfaces obtained from experimental data [83, 93, 98] are given in Tables 6.22-6.24 (the order of position of surfaces has been altered in the tables used).

Reflection coefficients for different nadir angles in the plane of the solar vertical at different solar altitudes are given in these tables.

Laboratory investigations on snow surfaces [101] confirm the presence of reflection at all angles of incidence on the surface. As the angle of incidence increases the reflected component also increases. Snow covered with ice crust shows the highest mirror quality.

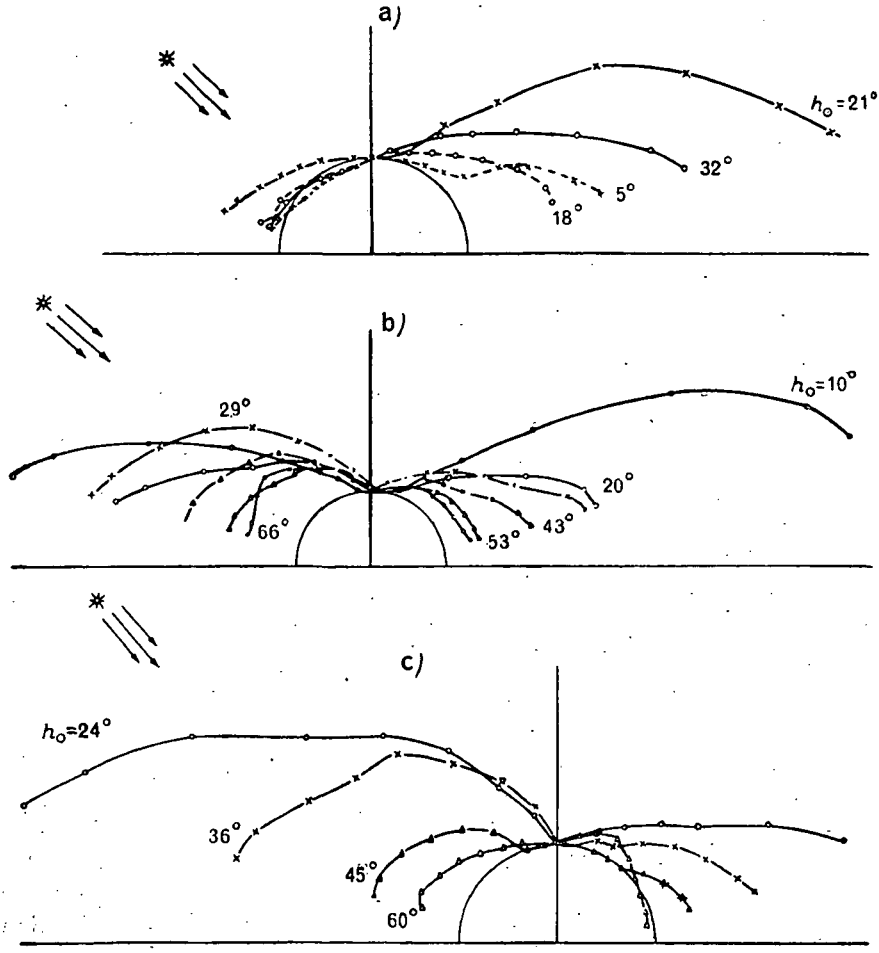

Fig. 6.11. Reflection phase functions in the plane of solar vertical at different solar altitudes.

a—snow : covered by ice crust (1), dry (2); b—green barley; c—stubble of barley [26].

6.2 Spectral characteristics of reflected radiation

The spectral coefficients of brightness for snow cover and meadow are given in Table 6.25 [34]. For a meadow surface the greatest luminosity can be observed at 180°, the least at 0°. As the solar altitude increases the variability of coefficients of brightness weakens along these directions. For a snow cover with frozen crust at all azimuths other than $\psi=0°$, the spectral coefficients of luminosity are almost identical. At $\psi=0°$ the

Table 6.22 Reflection indicatrices at different azimuth angles relative to the sun [93]

Surface description	Zenith angle of the sun, deg	Azimuth of sighting relative to sun, deg	Angle of point of observation, deg							
			0	15	30	45	60	75	80	85
Asphalt, covered by petroleum with a layer of dust	42.0	0	0.061	0.057	0.058	0.060	0.068	0.090	0.104	0.127
		180		0.067	0.080	0.101	0.090	0.086	0.086	0.088
White old concrete	42.2	0	0.266	0.263	0.254	0.254	0.266	0.298	0.320	0.377
		180		0.289	0.313	0.343	0.367	0.350	0.343	0.320
Distorted eroded rubble cover	48.5	0	0.113	0.115	0.119	0.128	0.148	0.194	0.229	
	60.1	90		0.110	0.109	0.116	0.122	0.139	0.147	
	46.0	180		0.126	0.141	0.156	0.166	0.172	0.176	
Tightly packed soil of yellow color	53.2	0	0.243	0.230	0.229	0.239	0.252	0.300	0.330	
	56.5	90		0.243	0.258	0.260	0.276	0.300	0.304	
	51.1	180		0.272	0.313	0.370	0.422	0.432	0.434	
Sand dunes with sharply expressed dry relief	40	0	0.288		0.183		0.337	0.353	—	
	40	90			0.284		0.329	0.306	—	
	40	180			0.246		0.259	0.276	—	
	40	270			0.278		0.410	0.281	—	
Tilled moist podzol	50	0	0.0600	0.0680	0.0646		0.0555			
	50	90		0.0662	0.0953	0.0715	0.0614	0.0761		
	50	270		0.149	(0.180)	0.168	0.168	(0.189)		
Small pine trees situated at equal distances	41.5	0	0.0333	0.0241	0.0214	0.0214	0.0261	0.0379	0.0463	0.0859
		45		0.0222	0.0202	0.0194	0.0210	0.0303	0.0387	0.0549
		90		0.0315	0.0311	0.0317	0.0317	0.0337	0.0387	0.0463
		135		0.0335	0.0382	0.0392	0.0387	0.0438	0.0463	0.0572

Table 6.22—*Contd.*

Surface description	Zenith angle of the sun, deg	Azimuth of sighting relative to sun, deg	Angle of point of observation, deg							
			0	15	30	45	60	75	80	85
Marshy grass, fairly long, greenish-white, a bit dry,	41.5	0	0.088	0.081	0.076	0.077	0.088	0.094	0.096	0.094
surface visible to some extent		180		0.098	0.119	0.146	0.150	0.153	0.153	0.160
Mowed grassy lawn	40.4	0	0.100	0.096	0.098	0.108	0.120	0.149	0.168	—
	39.6	90		0.103	0.110	0.121	0.138	0.159	0.168	—
	39.6	135		0.107	0.125	0.148	0.166	0.178	0.178	—
	39.9	180		0.109	0.109	1.119	0.122	0.125	0.125	—
Leveled green forest (oak and pine)	39.0	0	0.0360	0.0325	0.0291	0.0205	0.0205	0.342	—	—
	37.0	180		0.0410	0.0493	0.0493	0.0820	0.263		
Pine forest	33.5	0	0.0385	0.0385	0.0308	0.0246	0.0246	0.020		
Meadow with dry dense grass in midsummer	45	0	0.0955	0.0897	0.0960	0.0952	0.108	0.129		
	45	90		0.0778	0.0890	0.101	0.111	0.130		
	45	180		0.116	0.131	0.143	0.153	0.170		
	45	270		0.107	0.121	0.134	0.137	0.132		
Dry yellowish sparse grass in the sand toward the	40	0	0.231		0.320		0.342	0.356		
end of summer	40	90			0.163		0.176	0.198		
	40	180			0.295		0.353	0.359		
	40	270			0.262		0.237	0.229		
Calm water of infinite optical depth	41.6	0	0.0222	0.0234	0.0297		0.0567	0.139	0.267	0.461
		45		0.0230	0.0240	0.0272	0.0357	0.107	0.199	0.325
		90		0.0221	0.0222	0.0234	0.0293	0.0711	0.121	0.214
		135		0.0213	0.0212	0.0220	0.0270	0.0665	0.113	0.203
		180		0.0214	0.0212	0.0216	0.0267	0.0718	0.125	0.254

Table 6.23 Reflection indicatrices at different azimuths with respect to the sun [83]

Description of surface	Zenith angle of the sun, deg	Azimuth of sighting relative to sun, deg	Angle of point of sighting, deg							
			0	15	30	45	60	75	80	85
Ocean water, infinitely great optical depth, wind velocity 5 m/sec	77.3	0	0.0230	0.0288	0.0390	0.0550	0.132		0.384	0.358
		45		0.0246	0.0329	0.0417	0.065	0.087	0.104	0.158
		90		0.0242	0.0266	0.0297	0.0373	0.061	0.076	0.093
		135		0.0264	0.0280	0.0309	0.0384	0.072	0.096	0.116
		180		0.0266	0.0288	0.0325	0.449	0.072	0.099	0.125
Calm water in ocean, infinitely great optical depth	77.3	0	0.0152	0.0177	0.0219	0.0408	0.140	—	1.03	1.03
		45		0.0188	0.0200	0.0181	0.0371	0.107	0.190	0.345
		90		0.0139	0.0139	0.0156	0.0388	0.132	0.154	0.243
		135		0.0133	0.0141	0.0160	0.0267	0.0823	0.149	0.345
		180		0.0158	0.0206	0.0425	0.108	0.508	0.823	1.03
Snow with frost on the surface	74.0	0	0.69	0.69	0.73	0.78	0.89	1.20	1.39	1.73
		90		0.64	0.65	0.69	0.72	0.73	0.73	—
Snow with rain cover (rain which does not freeze, forms a layer)	74.0	0	0.73	0.73	0.74	0.79	0.91	1.47	1.81	2.44
		45		0.71	0.71	0.69	0.67	0.62	0.60	0.58
		90		0.73	0.73	0.71	0.72	0.71	0.69	—
		135		0.71	0.74	0.77	0.82	0.89	0.90	—
Snow with layer frozen rain (ice completely covers slightly undulating layer of snow)	74.0	0	0.80	0.80	0.88	1.13	1.900	5.6	8.4	10.90
		45		0.75	0.77	0.72	0.68	0.65	0.61	0.65
		90		0.75	0.75	0.75	0.74	0.72	0.70	0.65
		135		0.76	0.77	0.80	0.81	0.85	0.84	—

Table 6.24 Reflection indicatrices for continuous stretch of cloud cover [98]

Description of surface	Zenith angle of the sun, deg	Azimuth of sighting relative to sun, deg	Angle of point of sighting, deg							
			0	15	30	45	60	75	80	85
Calm water of infinitely great optical depth	51	0	0.0296	0.0314	0.0336	0.0287	0.053	0.197	0.356	0.570
	51	45		0.0302	0.0313	0.0287	0.058	0.229	0.376	0.550
	51	90		0.0306	0.0272	0.0294	0.064	0.229	0.340	0.510
	51	135		0.0279	0.0239	0.0264	0.057	0.182	0.260	0.425
	51	180		0.0273	0.0254	0.0238	0.0421	0.145	0.234	0.459
Snow with frost on the surface	51	0	0.69	0.68	0.66	0.66	0.67	0.67	0.70	—
	51	45		0.66	0.65	0.65	0.66	0.67	0.68	—
	51	90		0.66	0.65	0.66	0.67	0.68	0.69	—
	51	135		0.67	0.65	0.66	0.67	0.69	—	—
	51	180		0.68	0.64	0.65	0.66	0.68	0.69	—
Snow with rain cover	51	0	0.67	0.67	0.67	0.67	0.67	0.67	0.67	0.67
	51	45		0.67	0.66	0.66	0.67	0.67	0.67	0.68
	51	90		0.66	0.77	0.67	0.68	0.68	0.68	—
	51	135		0.65	0.66	0.67	0.68	0.68	0.67	0.69
	51	180		0.67	0.64	0.65	0.67	0.68	0.68	0.69
Snow with frozen crust of rain	51	0	0.74	0.76	0.76	0.76	0.77	0.77	0.77	—
	51	45		0.76	0.76	0.76	0.76	0.77	0.78	—
	51	90		0.74	0.76	0.76	0.76	0.78	0.77	—
	51	135		0.74	0.76	0.77	0.77	0.79	0.78	—
	51	180		0.74	0.74	0.75	0.75	0.76	0.77	—

Table 6.25 Dependence of spectral coefficients of luminosity on azimuth and solar altitude for natural formations [34]

λ μ	In the normal direction	Azimuth 0°					Azimuth 90°				
		$\vartheta=15°$	$\vartheta=30°$	$\vartheta=45°$	$\vartheta=60°$	$\vartheta=75°$	$\vartheta=15°$	$\vartheta=30°$	$\vartheta=45°$	$\vartheta=60°$	$\vartheta=75°$
					Dry valley meadow, $h_\odot=25°$						
400-500	0.028	—	—	—	—	—	0.029	0.030	0.032	0.037	0.047
510-600	0.086	—	—	—	—	—	0.106	0.112	0.125	0.145	0.183
610-650	0.061	—	—	—	—	—	0.080	0.087	0.094	0.103	0.159
730-800	0.573	0.554	0.562	0.548	0.656	0.834	0.797	0.823	0.917	0.933	0.861
810-850	0.673	0.638	0.648	0.645	0.702	0.836	0.888	0.901	0.962	0.969	0.920
					Dry valley meadow, $h_\odot=45°$						
400-500	0.036	0.033	0.033	0.025	0.026	0.032	0.027	0.033	0.034	0.036	0.044
510-600	0.099	0.099	0.102	0.096	0.110	0.134	0.081	0.091	0.104	0.116	0.136
610-650	0.172	0.058	0.064	0.086	0.076	0.093	0.066	0.081	0.072	0.081	0.105
					Snow cover with ice crust, $h_\odot=20°$						
400-500	—	0.432	—	2.675	4.493	7.461	—	—	0.678	0.756	0.830
510-600	0.861	0.457	—	2.350	3.941	6.902	—	—	0.580	0.765	0.770
610-650	—	0.526	—	—	—	—	—	—	—	—	—
730-800	0.702	—	—	—	—	—	0.446	—	0.363	0.457	0.376
810-850	0.611	—	—	—	—	—	0.474	—	0.377	0.464	0.376

Table 6.25—*Contd.*

λ, μ	In the normal direction	Azimuth 180°					Azimuth 270°				
		$\vartheta=15°$	$\vartheta=30°$	$\vartheta=45°$	$\vartheta=60°$	$\vartheta=75°$	$\vartheta=15°$	$\vartheta=30°$	$\vartheta=45°$	$\vartheta=60°$	$\vartheta=75°$
					Dry valley meadow, $h_\odot=25°$						
400-500	0.028	0.026	0.033	0.040	0.052	0.073	—	—	0.051	0.053	0.052
510-600	0.086	0.073	0.092	0.105	0.142	0.199	—	—	0.144	0.159	0.163
610-650	0.061	0.058	0.072	0.083	0.112	0.170	—	—	0.097	0.105	0.120
730-800	0.573	0.544	0.576	0.546	0.780	—	—	—	0.691	0.805	0.823
810-850	0.673	0.636	0.700	0.725	0.929	—	—	—	0.819	0.952	0.966
					Dry valley meadow, $b_\odot=45°$						
400-500	0.036	0.047	0.052	0.052	0.055	0.055	0.037	0.039	0.042	0.044	0.044
510-600	0.099	0.121	0.136	0.141	0.157	0.175	0.113	0.127	0.143	0.144	0.141
610-650	0.172	0.089	0.108	0.128	0.131	0.141	0.076	0.091	0.077	0.098	0.099
					Snow cover with ice crust, $h_\odot=20°$						
400-500	—	—	—	—	0.530	0.599	0.659	—	—	—	—	—
510-600	0.861	—	—	—	0.579	0.728	0.636	—	—	—	—	—
610-650	—	—	—	—	—	—	—	—	—	—	—	—
730-800	0.702	0.626	—	0.688	0.637	0.688	—	—	—	—	—
810-850	0.611	0.706	—	0.662	0.561	0.738	—	—	—	—	—

coefficients of brightness rise sharply at low angles, i.e. mirror reflection may be observed.

The greatest luminosity may be observed at $\psi=0°$ for sand, and at $\psi=180°$ for black clay [91].

The angular distribution of coefficients of luminosity is identical for all ranges of the spectrum in its general features.

The spectral coefficient of luminosity increases with increasing wavelengths for grass surfaces, sand and corrugated slate for continuous cloud cover and for variable cloud [33]. In most cases the form of the reflection phase function does not depend on the wavelength. For partial cloudiness when the underlying surface bears the shadow of clouds, the coefficient of brightness has a very high variability.

6.3 Measurements of reflection characteristics from an airplane

The intensity of reflected radiation, measured from different heights above the surface, depends on the reflection properties of the underlying layer and on the optical properties of the atmospheric layer lying between the ground and the level at which measurements are made (i.e. upon the emission of fog). The angular distribution of intensity of radiation reflected at different levels can be determined from the relation between reflection from the underlying surface and emission through fog.

The integrated coefficients of brightness for specific geographic regions and several forms of cloudiness, obtained by measurements from an airplane [32], vary within considerable limits (Tables 6.26 and 6.27).

Table 6.26 Limits of variation in coefficients of brightness for several geographic zones of the Soviet Union [32]

Zonal characteristics	r %
Forest region	10-38
Forest steppes	11-25
Steppes :	
Don	10-31
Crimea	12-25
Volgograd	10-34
Semidesert	12-25
Water surface	26-38
	1-4

Table 6.27 Limits of variation of brightness coefficient for several types of cloud [32]

Form of cloud	r %
Cu hum.	15-80
Cu med.	2-45
Cu fr.	10-20
Sc op.	20-60
Sc trans.	5-30
Ac trans.	8-15

Airplane measurements of the integrated coefficient of brightness of sandy desert with dunes indicate a wide variation in the angular dependence of the luminosity coefficient, which is caused by the nonuniformity of the underlying surface (sand dunes, solonchak, haloxylon) (Table 6.28) [14].

Measurement of the angular distribution of intensity of reflected radiation with an automatic balloon showed that with a clear atmosphere and albedo of the surface of about 0.20 the total intensity of radiation reflected from the underlying surface and the atmospheric layer rises with an increase in the sighting angle. A sharp increase in the intensity starts at approximately 60° [13].

Airplane measurements of reflection characteristics from a homogeneous sandy surface with sparse vegetation showed that the brightness increases noticeably in the direction of the sun, as observed in the case of dug-up surfaces [31]. The nature of the reflection from uniform sandy surface depends only slightly on the wavelength of the incident radiation. In the direction perpendicular to the solar vertical, reflection from this surface approximates to that due to Lambert's law. Measurements of the reflection phase function from sand dunes in the Kara-Kum desert showed that reflection is anisotropic to a considerable extent [31]. The deviation from Lambert's law increases with an increase in the zenith separation of the sun ; moreover, mirror reflection and back reflection may also be observed.

The brightness coefficient of clouds in the plane of the solar vertical approaches that of Lambert within the angular limits $\pm 30°$. Considerable deviations from Lambert's law may be observed with increase in the angle of sighting, especially for large zenith distances from the sun.

The intensity of reflection does not vary monotonically for continuous cloud cover. Measurements in the plane of the solar vertical show that

Table 6.28 Brightness coefficient (%) above desert [14]

H km	$\theta°$												
	60	50	40	30	20	10	0	−10	−20	−30	−40	−50	−60
1	22.6	21.2	21.1	21.5	22.5	21.5	20.2	17.7	17.0	16.7	16.7	17.8	
4	23.5	21.7	20.9	21.1	22.0	23.0	23.5	22.8	24.0	24.3	25.2	26.7	
6		19.3	18.2	17.0	17.6	17.7	19.1	20.0	21.0	20.7	19.4	20.9	23.3
		26.3	24.5	22.0	22.3	22.2	22.7	23.4	22.4	21.6	21.3	21.6	21.6
7	24.2	21.6	20.1	19.9	21.3	21.0	21.3	18.6	15.8	16.0	18.5	20.7	
8		22.6	20.6	18.4	17.5	16.8	18.3	19.3	18.9	19.2	19.1	19.9	19.6
		16.7	15.7	14.9	14.8	14.5	15.6	16.1	15.6	16.1	16.6	18.7	19.7
9	22.4	20.9	20.4	20.4	21.4	22.0	22.5	22.2	21.9	22.3	24.1	26.2	
1	24.3	21.2	19.5	19.2	20.1	20.9	20.3	20.1	21.5	22.6	25.9	30.1	
		18.2	17.2	15.7	16.1	16.4	18.9	20.7	21.2	22.0	25.7	26.2	27.0
2	22.4	19.8	18.3	17.0	18.5	19.2	17.7	17.1	18.4	19.8	21.6	25.9	
	18.1	17.2	17.8	18.1	19.2	18.7	18.4	18.1	20.9	20.8	23.9	28.9	
3		17.9	15.7	14.7	14.9	15.2	17.4	19.7	20.4	21.5	24.6	26.2	28.3
		18.6	18.9	17.9	17.6	16.1	19.2	20.4	20.6	21.3	24.0	26.2	29.7
4	21.6	18.3	18.3	17.3	17.7	18.4	18.6	17.4	18.6	20.1	21.1	25.3	
	23.0	20.7	19.3	19.3	20.9	21.1	20.8	19.7	20.5	21.5	24.5	29.6	
	21.9	18.9	17.7	17.2	18.0	18.3	19.0	18.6	19.1	20.2	23.4	24.2	

Table 6.28—*Contd.*

H km	θ°												
	60	*50*	*40*	*30*	*20*	*10*	*0*	*−10*	*−20*	*−30*	*−40*	*−50*	*−60*
5	29.0	24.3	21.8	19.6	18.2	17.1	16.4	14.0	13.7	12.8	13.4	10.7	
	27.0	24.4	22.4	21.3	20.7	20.5	18.8	17.2	17.2	16.9	18.6	20.3	
6	12.3	7.7	8.3	12.1	14.2	15.4	15.6	14.9	17.2	18.2	21.5	24.4	
1	30.4	27.8	27.0	24.4	22.1	21.8	19.5	18.0	18.0	18.0	19.5	22.1	
2		26.0	24.4	21.0	21.0	18.3	19.9	20.6	19.9	19.1	19.1	21.0	22.9
3	27.2	24.7	29.3	18.8	18.1	18.8	16.9	15.5	15.5	15.5	16.9	15.1	
4	23.8	20.0	18.1	18.1	18.8	19.6	18.8	17.3	18.8	20.4	23.8	27.0	
5	33.2	27.1	23.6	20.6	19.8	20.6	18.3	18.3	18.3	18.3	20.2	21.4	
6	27.8	23.6	21.8	18.8	19.5	18.8	16.9	15.4	13.9	13.9	15.4	14.3	
7	27.0	25.4	23.8	20.4	20.4	17.1	17.1	15.0	15.0	13.3	13.3	11.7	
8	22.2	20.2	18.1	16.2	17.0	17.8	19.1	17.6	17.6	19.1	22.9	24.2	
9	21.6	21.4	17.6	16.0	14.8	15.8	15.2	13.9	13.9	13.8	15.2	14.4	
10		20.0	20.4	18.8	17.2	15.9	17.2	15.9	15.5	14.7	14.7	15.5	16.7
Average	23.1	21.2	20.2	19.5	19.6	19.7	19.1	17.8	18.0	18.5	20.3	21.8	23.2

the intensity of reflected radiation increases in the direction of the reflected ray. The intensity is distributed equally along all other directions.

Measurement of the intensity of radiation reflected from snow and clouds from a height of 1-4 km showed that in the interval 0.3-1.1 μ snow is brighter than cloudiness of lower and intermediate layers [66], whereas clouds are brighter than snow in the interval 1.4-2.5 μ. A slight lessening of the contrasts at greater altitude has been observed for all spectral intervals, more noticeably so in the shortwave range. Fog plays a fundamental role in the value of intensity of reflected radiation in the interval 1.4-2.5 μ. The values of flux of radiation reflected from snow and fog at the level of 3 km at $\vartheta_\odot = 60°$, $\tau = 0.3$ and a meteorological visual range $D_0 = 10$ km [66] are given in Table 6.29. The flux of radiation reflected from snow in the vicinity of overlapping absorption bands is several times less than flux from fog.

Table 6.29 Fluxes of radiation reflected from snow and fog at a height of 3 km (cal/cm^2 . min) [66]

$\Delta\lambda$, μ	Snow	Fog
1.38-1.50	0.20×10^{-3}	0.34×10^{-3}
1.50-1.53	0.04	0.09
1.70-1.92	0.35	0.39
1.92-2.08	0.04	0.18

Similarly, the theoretical computation of the angular distribution of intensity of reflected radiation for typical underlying surfaces shows an inherent anisotropy in the field of reflected radiation [47]. The intensity of radiation due to fog is essentially anisotropic and increases with height above the surface and with greater albedo of the underlying surface. With increasing zenith separation of the sun at large angles the intensity of radiation of fog B_1 increases over surfaces with low albedo values (water and grass) and decreases over surfaces with large albedo values (snow). A reverse course is observed for the underlying layers. As the height above the ground increases at large angles of sighting the intensity of reflected radiation B_1 decreases for all marked surfaces. The intensity of radiation reflected over snow and grass decreases at all levels with an increase in the zenith angle of the sun. Over water the intensity of reflected radiation decreases with a rise in $\vartheta_\odot$ starting from $\vartheta_\odot < 40°$, whereas for $\vartheta_\odot > 40°$ the intensity increases a little. The angular structure of the field of reflected radiation depends on the relation between

C-5

the magnitudes B_1 and B_2. B_1 increases with $\vartheta_\odot$ at low albedo values, and B_2 rises with increasing albedo, especially at low $\vartheta_\odot$, so that the characteristic angular dependence of intensity of reflection for fog is smooth.

An analysis of the relation between intensity of reflected radiation ($B=B_1+B_2$) and total flux R provides an idea of the conformity of the earth-atmosphere system with Lambert's law (see Table 6.30). The greatest deviation from isotropic reflection ($\eta=0.32$) is obtained for $\theta=85°$ (θ—nadir angle) and $\vartheta_\odot=80°$. As the zenith distance of the sun increases the deviation from Lambertosity decreases with increasing altitude. For low $\vartheta_\odot$ the deviation from isotropy decreases, for large $\vartheta_\odot$ it increases [47].

Table 6.30 $\frac{\vartheta B(\theta)}{R}$ **1/ster [47]**

$\vartheta_\odot$ °	Surface	H km	Nadir angle, deg				
			0	20	40	60	85
	Water	0	0.34	0.34	0.34	0.34	0.34
		1	0.27	0.28	0.29	0.35	0.97
		3	0.27	0.28	0.29	0.36	0.87
		10	0.28	0.28	0.30	0.36	0.77
20	Grass	0	0.40	0.40	0.37	0.27	0.27
		1	0.37	0.37	0.37	0.28	0.42
		3	0.36	0.37	0.35	0.29	0.41
		10	0.35	0.35	0.34	0.29	0.39
	Snow	0	0.34	0.34	0.34	0.34	0.34
		1	0.34	0.34	0.34	0.33	0.34
		3	0.34	0.34	0.34	0.33	0.32
		10	0.34	0.34	0.34	0.33	0.32
	Water	0	0.34	0.34	0.34	0.34	0.34
		1	0.25	0.26	0.29	0.35	1.08
		3	0.24	0.26	0.29	0.37	0.96
		10	0.24	0.26	0.29	0.37	0.89
40	Grass	0	0.40	0.40	0.38	0.27	0.27
		1	0.36	0.36	0.35	0.29	0.48
		3	0.35	0.35	0.34	0.30	0.48
		10	0.33	0.34	0.33	0.30	0.45

Table 6.30—*Contd.*

$\vartheta_\odot$	Surface	H km	Nadir angle, deg				
			0	20	40	60	85
	Snow	0	0.34	0.34	0.34	0.34	0.34
		1	0.34	0.34	0.34	0.34	0.36
		3	0.34	0.34	0.34	0.33	0.35
		10	0.33	0.33	0.34	0.33	0.34
	Water	0	0.33	0.33	0.33	0.33	0.33
		1	0.24	0.25	0.28	0.36	1.08
		3	0.23	0.24	0.28	0.37	1.04
		10	0.23	0.24	0.27	0.38	1.02
60	Grass	0	0.40	0.40	0.37	0.26	0.26
		1	0.34	0.34	0.34	0.30	0.64
		3	0.32	0.32	0.33	0.32	0.65
		10	0.30	0.30	0.30	0.31	0.62
	Snow	0	0.34	0.34	0.34	0.34	0.34
		1	0.33	0.33	0.33	0.34	0.44
		3	0.32	0.32	0.33	0.34	0.45
		10	0.32	0.32	0.33	0.34	0.46
	Water	0	0.34	0.34	0.34	0.34	0.34
		1	0.28	0.28	0.29	0.34	1.00
		3	0.25	0.26	0.27	0.35	1.31
		10	0.24	0.24	0.26	0.36	1.44
80	Grass	0	0.39	0.39	0.37	0.26	0.26
		1	0.27	0.27	0.29	0.32	1.32
		3	0.24	0.24	0.26	0.34	1.55
		10	0.20	0.21	0.24	0.32	1.49
	Snow	0	0.34	0.34	0.34	0.34	0.34
		1	0.29	0.30	0.31	0.34	0.79
		3	0.27	0.28	0.29	0.34	1.00
		10	0.26	0.27	0.28	0.35	1.14

7. VERTICAL PROFILE OF FLUX OF REFLECTED RADIATION

Reflected radiation may be observed only immediately above the ground. A total rising flux, consisting of reflected flux transformed by the

underlying atmospheric layer and the flux of radiation scattered by this very layer, exists at different heights over the earth's surface.

Airplane measurements on the rising flux over Ladogian Lake (aqueous, icy or snow surface depending on the time of the year) and above a field with uniform vegetation show that flux of reflected radiation increases with altitude. The variation of reflected radiation differs with height depending on the type of underlying surface (cf. Table 6.31) [45]. For winters the vertical profile of reflected flux R is more even, for spring it is more uneven. Table 6.31 shows that the values of R depend on the altitude of the sun.

Table 6.31 Fluxes of reflected radiation at different altitudes (cal/cm² . min) [45]

Date	$h_\odot^\circ$	Altitude above the earth's surface, km							
		0	0.2	0.5	1.0	1.5	2.0	2.5	3.0
Jan 25	10.6	0.170	—	0.171	0.179	0.197	0.202	—	0.199
Feb 8	14.0	0.222	—	0.216	0.216	0.224	0.232	—	0.232
Feb 23	20.0	0.221	—	0.222	0.239	0.250	0.258	—	—
Feb 27	22.0	0.248	—	0.262	0.265	0.275	0.274	—	—
Mar 8	18.0	0.293	—	0.301	0.291	0.314	0.325	0.328	0.334
Mar 8	25.0	0.311	—	0.292	0.299	0.304	0.308	0.301	0.310
Apr 20	41.6	0.299	—	0.292	0.294	0.300	0.296	0.308	0.312
Apr 20	27.5	0.262	—	0.274	0.278	0.277	0.300	0.296	0.288
Jun 17	45.0	0.039	—	0.046	0.055	0.077	0.090	—	0.118
Jun 17	52.0	0.033	—	0.044	0.053	0.069	0.076	—	0.108
Jun 18	45.0	0.029	—	0.036	0.045	0.057	0.068	—	0.097
Jun 18	52.0	0.034	—	0.044	0.048	0.054	0.070	—	0.100
Jul 1	45.0	0.041	—	0.062	0.066	0.073	0.092	0.099	—
Jul 1	52.0	—	—	—	0.070	0.093	0.102	—	0.130
Jul 14	43.5	0.049	0.050	0.056	0.060	0.081	0.093	0.101	—
Jul 14	51.0	0.053	0.055	0.057	0.065	0.075	0.089	—	—
Aug 13	40.0	0.044	0.044	0.047	0.059	0.074	—	—	—
Aug 14	37.0	0.043	0.043	0.054	0.067	0.076	0.085	0.095	—
Aug 14	44.0	0.060	0.062	0.063	0.057	0.074	0.081	—	—
Oct 5	25.0	0.077	0.073	0.076	0.088	0.096	0.102	0.105	—
Oct 15	20.0	0.058	—	0.056	0.062	0.074	0.076	—	0.081

Airplane measurements of reflected flux in the region of Tashkent (snow surface, green or dry grass) similarly show that the reflected radiation increases with rising altitude above the earth's surface (Table 6.32) [35].

Table 6.32 Flux of reflected radiation (cal/cm² · min) at different altitudes at true midday [35]

H km	Winter	Spring	Summer	Autumn
0.4	0.214	0.267	0.279	0.212
0.8	0.214	0.271	0.280	0.219
1.3	0.226	0.324	0.275	0.237
2.3	0.238	0.336	0.284	0.262
3.4	0.246	0.344	0.294	0.270
4.4	0.259	0.361	0.279	0.282
5.5	0.263	0.444	0.295	0.293
6.7	0.273	0.394	—	—

The highest vertical gradient for all layers may be observed in summer and the lowest in winter (Table 6.33). The influence of fog is most noticeable at low albedo values [36].

Table 6.33 Gradient of rising radiation flux (cal/cm² · min · km) [35]

Time of year	Thickness of layer, km			
	0-1	1-2	2-3	0-3
Winter	0.004	0.018	0.002	0.008
Spring	0.010	0.012	0.002	0.008
Summer	0.015	0.026	0.023	0.012
Autumn	0.006	0.014	0.005	0.009
Average	0.009	0.018	0.008	0.012

Balloon measurements of the flux of reflected radiation [29, 30, 37] indicate a variation in this flux with respect to the altitudes above the earth's surface and with respect to the nature of the underlying surface.

The profiles of reflected radiation represented in Fig. 6.12 refer to the summer and autumn periods ($A \sim 25\%$); only profile 2 was obtained

in the presence of a snow cover ($A \sim 70\%$) [43]. For a clear sky (curves 3, 11, 13, 15, 16, 19) the flux of reflected radiation steadily rises. The value of R does not exceed 0.27 cal/cm² · min in any case. The value

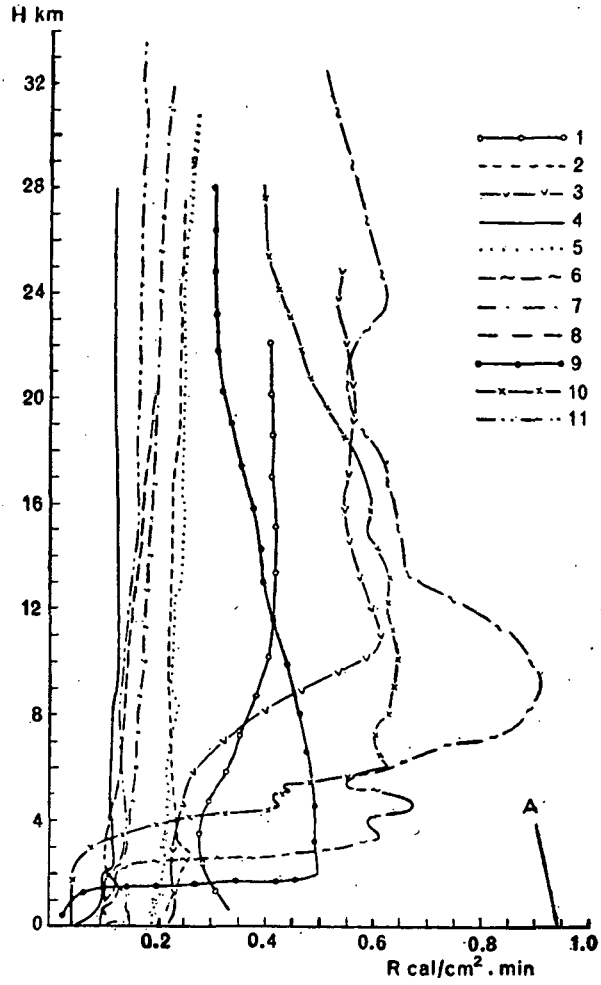

Fig. 6.12. Vertical profiles of reflected shortwave radiation according to balloon investigations [43].

1—Nov. 1961, $h_\odot = 17°$, snow, clear; 2—May 1962, $h_\odot = 55\text{-}58°$, flooded meadow, clear; 3—July 1962, $h_\odot = 59°$, N_s=6-7 tenths; 4—Nov. 1962, $h_\odot = 17°$, steppe, clear; 5—July 1963, $h_\odot = 56\text{-}60°$, fields, clear; 6—Aug. 1963, $h_\odot = 42\text{-}54°$, three layered cloudiness of 6-7 tenths; 7—Aug. 1964, $h_\odot = 20\text{-}38°$, fields, clear; 8—July 1964, $h_\odot = 20\text{-}37°$, fields, clear; 9—Oct. 1964, $h_\odot = 23°$, St 10 tenths; 10—Oct. 1965, $h_\odot = 33\text{-}35°$, three layered cloudiness of 10 tenths; 11—Oct. 1965, $h_\odot = 26°$, steppe, clear; *A*—profile in Antarctica, $h_\odot = 40°$ [77].

of R reaches 0.37 cal/cm^2 · min at 6 km in Central Asia during summers [36]. A still higher value of R=0.93 cal/cm^2 · min was obtained on a clear day in Antarctica at $h_\odot \sim 40°$ at an altitude of about 5 km [77].

The dependence of the values of reflected flux on the altitude of the sun for a clear sky has been traced in Fig. 6.12 (profiles : 11—$h_\odot$=17° ; 19—$h_\odot$=24-27° ; 15 and 16—$h_\odot$=30-35° ; 3—$h_\odot$=57-59° ; 13—$h_\odot$= 56-60°). The dependence of R on $h_\odot$ in the presence of a layer of cloud can be estimated from the profiles 14 and 18 at an altitude of 10 km. The layers of clouds on this day were situated at different altitudes. The flux R rises rapidly to the level of the upper boundary of this cloudy layer.

The theoretical investigations for standard atmosphere confirm the pattern established through experiments [47, 72, 76] ; the value of the flux of reflected radiation rises with the altitude as well as with increasing solar altitude, the rise being more rapid at higher values of the albedo of the reflecting surface.

8. FLUX OF SCATTERED AND REFLECTED RADIATION

The flux of scattered and reflected radiation at an inclined surface depends not only on the angle of inclination of these surfaces but also on their azimuth. The magnitude of flux can be accurately determined, if data about the angular distribution of scattered radiation are available from the following form [22], viz.

$$D_s = \int_0^{2\pi} d\psi \int_{h(\psi)}^{\pi/2} I(h, \psi) \cos i \cos h \, dh, \tag{6.5}$$

where $I(h, \psi)$—intensity of scattered radiation in a direction determined by the spherical coordinates h (angular height) and ψ (azimuth relative to the sun) ; $h(\psi)$ least angular height of a point in the sky at azimuth ψ with respect to the horizontal plane ; i—angle of incidence of radiation at the inclined plane whose cosine can be determined by the following expression :

$$\cos i = \sin \alpha \cos h \cos \psi + \cos \alpha \sin h,$$

where α—angle of inclination of the slope ; $\psi = \psi_\odot - \psi_s$, ψ_s—azimuth of the slope.

The fluxes of radiation scattered on an inclined plane can be computed by numerical integration from the formula (6.5).

For an isotropic scattered radiation (I=const) the flux of radiation scattered on an inclined surface can be determined from the relation [6].

$$D_s = D_h \cos^2 \frac{\alpha}{2}, \qquad (6.6)$$

where D_h—flux of scattered radiation on a horizontal surface.

The relative magnitudes of flux and of total radiation determined with respect to flux and total radiation on a horizontal surface are the distinct features of radiational regime of inclined surfaces.

The difference between the values of flux computed from formulas (5) and (6) are given in Table 6.34 [25]. Orientation of the surface is given by the angle of the slope α and azimuth ψ relative to the azimuth of the sun. In the brackets one finds the deviations of the relative magnitudes of flux in percentages, computed in an isotropic approximation from corresponding values obtained through accurate calculations. In most cases the deviations from "isotropic" values enter because of the limits of error in the measurements of flux of scattered radiation.

For surfaces oriented on the side opposite to the sun ($\psi = 180°$), a decrease in the flux of scattered radiation with an increasing angle of inclination of the slope may be observed ; for surfaces turned toward the sun, a maximum at values of the angle of inclination α_{max} may be observed corresponding to the condition $\alpha_{max} = 90° - h_\odot$.

The angular distribution of intensity of reflected radiation for the majority of natural surfaces is anisotropic. It is necessary to take into consideration this criterion for accurate computations of flux of radiation scattered from an inclined surface.

The relative values of flux of reflected radiation R_s/R_h at differently oriented surfaces can be computed from the given angular distribution of intensity of reflected radiation and from the isotropic approximation [25, 28]. Flux of reflected radiation of an inclined surface in case of isotropic reflection can be determined from the formula

$$R_s = R_h \sin^2 \frac{\alpha}{2}. \qquad (6.7)$$

Evidently for surfaces yielding mirror reflections the formula (6.7) provides a crude evaluation. The flux of radiation on an inclined surface depends considerably on their orientation in the presence of snow covering (Table 6.35). For surfaces turned toward the sun, an isotropic approximation gives much lower values.

In the case of a barley surface the difference between accurate and approximate relative fluxes of reflected radiation is noticeable only for steep inclines (Table 6.36).

The contribution of reflected radiation to the total flux of scattered and reflected radiation on a slope (Table 6.37) for different values of albedo

Table 6.34 Relative fluxes of scattered radiation D_s/D_h for a clear sky [25]

α°	ψ°												$\cos^2\frac{\alpha}{2}$
	0	90	180	270	0	90	180	270	0	90	180	270	
	$h_\odot=15^\circ$				$h_\odot=48^\circ$				$h_\odot=68^\circ$				
15	1.20	0.94	0.79	0.94	1.10	0.94	0.82	0.95	1.05	0.96	0.89	0.98	0.98
	(18.4)	(—4.2)	(—24.0)	(—4.2)	(11.0)	(—4.2)	(—20.0)	(—3.1)	(6.6)	(—2.0)	(—10.1)	(0.0)	
30	1.22	0.86	0.59	0.91	1.14	0.86	0.62	0.86	1.04	0.88	0.68	0.91	0.93
	(23.8)	(—8.1)	(—57.6)	(—2.2)	(18.4)	(—8.1)	(—50.0)	(—8.1)	(10.0)	(—5.7)	(—36.7)	(—2.2)	
60	1.27	0.64	0.41	0.74	1.15	0.62	0.36	0.64	0.89	0.63	0.45	0.68	0.75
	(41.0)	(—17.2)	(—83.0)	(—1.3)	(34.7)	(—21.0)	(—52.0)	(—17.2)	(15.7)	(—19.0)	(—66.6)	(—10.2)	
90	0.94	0.36	0.35	0.43	0.79	0.36	0.22	0.36	0.59	0.35	0.26	0.39	0.50
	(46.8)	(—40.0)	(—43.0)	(—16.3)	(36.7)	(—40.0)	(—128.0)	(—40.0)	(15.3)	(—43.0)	(—92.0)	(—28.2)	

Table 6.35 Relative flux of reflected radiation R_s/R_h % in a clear sky and for $A=0.20$ (barley surface) [25]

α°	$h_\odot=23^\circ$				$h_\odot=44^\circ$				$h_\odot=67^\circ$				$\sin^2\frac{\alpha}{2}$
	N	E	S	W	N	E	S	W	N	E	S	W	
30	6.7	8.4	6.7	6.7	6.1	5.6	6.1	7.6	5.5	4.7	6.7	5.9	6.7
50	21 0	25.2	21.0	21.8	19.3	17.8	19.3	22.8	18.5	15.7	16.2	18.5	17.9
70	39.4	45.4	37.8	38.7	36.0	33.0	35.5	41.6	35.0	30.0	30.0	34.6	32.9
90	58.0	64.7	56.3	55.5	53.3	49.2	52.8	61.5	54.0	46.5	46.0	52.7	50.0

Table 6.36 Relative fluxes of reflected radiation R_s/R_h % in a clear sky in the presence of snow cover [28]

$h_\odot = 30°$, $A = 0.50$

$\alpha°$	$\psi°$				$\sin^2 \frac{\alpha}{2}$ %
	0	90	180	270	
30	13.0 (96)	5.2 (−22)	4.6 (−31)	6.0 (−11)	6.7
50	35.0 (96)	16.8 (−6)	13.8 (−23)	18.5 (3)	17.9
70	60.0 (83)	31.7 (−4)	25.8 (−22)	34.6 (5)	32.9
90	83.0 (66)	48.0 (−4)	40.0 (−20)	53.6 (7)	50.0

Table 6.37 The magnitude of ratio $\frac{R_s}{(D+R)_s}$ % in a clear sky and $h_\odot = 34°$ [28]

$\alpha°$	$A = 0.60$				$A = 0.20$			
	N	S	W	E	N	S	W	E
15	7.3	5.2	6.3	5.9	1.9	1.4	1.6	1.7
30	26.8	15.8	21.8	19.4	8.2	4.9	6.1	6.5
50	54.7	30.0	46.5	37.2	20.2	11.4	15.4	16.4
70	81.4	41.7	63.4	57.0	37.0	19.2	27.7	28.2
90	100.0	51.0	76.5	63.4	43.0	29.2	40.6	43.0

of surface A determines the role of reflected radiation in the radiational regimes of the slopes.

In the presence of snow cover the flux of reflected radiation on a steep incline is higher than the flux of radiation from the sky [28].

The fraction of reflected radiation, with rising values of albedo of the underlying surface from 0.20 to 0.60, in the flux of total radiation is 2-3 times higher than for corresponding surfaces (Table 6.38). In case of inclined planes ($\alpha < 30°$), the contribution of reflected radiation in the flux of total radiation is insignificant. For slopes oriented away from the

sun the reflected radiation plays an important role and in some cases represents the main component in the total flux of radiation on an inclined surface. The fluxes of reflected radiation in a given case can be computed from the approximate formula (6.7). Accurate computation of the flux of reflected radiation for slopes facing the sun must necessarily give considerably higher values.

Table 6.38 The values of ratio $\frac{R_s}{(S+D+R)_s}$% in a clear sky and at different values of albedo of underlying surface [28]

α°	$h_\odot=12°$, $A=0.65$ (⊙ at WSW)				$h_\odot=35°$, $A=0.60$ (⊙ at S)			
	N	S	W	E	N	S	W	E
15	2.4	0.8	0.6	3.7	1.6	0.8	1.1	1.0
30	14.8	2.3	1.7	14.8	13.9	2.6	5.3	3.7
50	29.8	5.0	3.4	32.4	50.8	6.2	19.7	10.2
70	39.0	8.4	5.5	52.5	74.2	11.0	65.6	20.7
90	59.0	12.9	8.0	68.3	99.0	17.4	75.0	39.2

α°	$h_\odot=28°$, $A=0.20$ (⊙ at W)				$h_\odot=34°$, $A=0.20$ (⊙ at E)			
	N	S	W	E	N	S	W	E
15	0.3	0.3	0.2	0.6	0.4	0.3	0.5	0.3
30	1.5	1.5	0.8	6.7	1.8	1.3	5.2	0.9
50	4.8	4.7	1.9	17.5	7.2	3.8	19.2	2.2
70	13.4	12.2	3.5	27.8	30.8	8.8	32.8	4.3
90	37.5	33.4	6.0	43.0	47.0	19.2	41.6	7.4

The evaluation of the flux of radiation scattered on an inclined surface can be achieved with the help of a differently oriented pyranometer, supplied with a special screen which eliminates the flux of reflected radiation. Then the flux of radiation reflected on a given surface with screen and without screen can be determined differently. Daily amounts of reflected radiation on slopes were obtained as a result of detailed measurements over clayey soil with dry grass (Table 6.39) [9]. It is obvious from this Table that it is possible to neglect reflected radiation incident on a plane of 10° inclination. The values of daily amounts of reflected radiation even on an inclined plane with $\alpha=40°$ do not constitute more than 15% of the entire flux of reflected radiation (Table 6.40).

Table 6.39 Daily amounts of reflected radiation (cal/cm² . day) mean value for September. Makhtala [9]

Orientation of slope	α°			
	10	20	30	40
North	1.7	5.6	13.9	25.9
South	1.0	4.2	9.2	18.3
East	2.0	5.1	12.4	23.6
West	1.3	4.7	11.0	23.6
Computation from the formula (13)	1.4	5.3	11.7	20.6

Table 6.40 Relative daily amounts of reflected radiation $\Sigma R_s/\Sigma R_h$ %, mean for September [9]

α°	Orientation of slope			
	North	South	East	West
10	1.0	0.6	1.1	0.8
20	3.2	2.4	2.9	2.7
30	7.9	5.2	7.0	6.2
40	14.7	10.4	13.1	13.4

The flux of radiation reflected and scattered on an inclined plane under continuous cloudiness depends mainly on the angle of inclination of the surface but remains practically independent of the azimuth. In this case, isotropic approximation provides adequate accuracy.

The daily amounts of scattered and reflected radiation for differently oriented surfaces which are not very steep differ only slightly from the corresponding daily amounts for horizontal surfaces (Table 6.41) under a clear sky and albedo around 0.20 [27].

The daily amounts of scattered and reflected radiation can be evaluated from isotropic approximation to a sufficient degree of accuracy using the following equation :

$$\Sigma (D+R)_s = \cos^2 \frac{}{2} \Sigma D_h + \sin^2 \frac{}{2} \Sigma R_h \qquad (6.8)$$

Table 6.41. Relative daily amounts of scattered and reflected radiation $\frac{\Sigma (D+R_s)}{\Sigma D_h}$ under a clear sky, $\varphi = 45°N$ [27]

$\alpha°$	North			South		
	Jun 19	Jul 15	Aug 6	Jun 19	Jul 15	Aug 6
5	1.01	0.98	0.97	1.09	1.04	1.06
10	1.00	0.99	0.95	1.07	1.04	1.08
15	1.00	0.99	0.96	1.07	1.05	1.06
20	1.01	0.99	0.93	1.07	1.05	1.09
30	1.00	0.98	0.93	1.10	1.07	1.17
50	1.03	0.99	0.93	1.18	1.12	1.24
70	1.09	1.01	0.96	1.23	1.12	1.25
90	1.12	1.04	1.00	1.24	1.12	1.23

$\alpha°$	East			West		
	Jun 19	Jul 7	Aug 6	Jun 19	Jul 15	Aug 6
5	1.01	1.01	0.98	1.03	1.00	1.01
10	1.01	0.99	0.97	1.03	1.00	1.02
15	1.03	0.99	1.00	1.03	1.02	1.03
20	1.04	1.01	1.01	1.05	1.03	1.05
30	1.07	1.01	1.04	1.11	1.04	1.08
50	1.14	1.06	1.08	1.20	1.08	1.14
70	1.21	1.08	1.14	1.24	1.12	1.19
90	1.27	1.12	1.16	1.31	1.13	1.21

9. GEOGRAPHIC DISTRIBUTION OF SCATTERED RADIATION

The altitude of the sun, length of day and cloudiness are the chief factors that determine the geographic distribution of scattered radiation.

Slight variability of the geographic distribution of scattered radiation over a given territory is a characteristic feature. The annual amount of scattered radiation across the territory of the USSR varies within the limits 10-15 kcal/cm^2 · yr and possesses a weakly expressed latitudinal course [8]. The minimum annual amounts have been observed in the North-West region of the European Territory of the Soviet Union and

yield a value of 37-39 kcal/cm^2·yr. A second minimum (43-45 kcal/cm^2·yr) has been observed in the desert region of Central Asia. The maximum annual amounts were observed in the Far-East region and in Zakarnat'e, viz. 51-53 kcal/cm^2·yr.

Twelve monthly charts of the distribution of scattered radiation over the territory of the Soviet Union are given in monograph [8]. The charts for December (Fig. 6.13) and June (Fig. 6.14) have been included here as an illustration. A latitudinal distribution of scattered radiation is characteristic for the winter period. Monthly amounts increase in a North to South direction from 0 to 25 kcal/cm^2·mon and in February from 0.8 to 3.5 kcal/cm^2·mon. On account of the increase in the length of the day during spring the latitudinal course of scattered radiation is destroyed by the high albedo values in the Northern latitudes and by the considerable variation in mean monthly cloudiness in distinct regions. A weakly expressed latitudinal variation of scattered radiation is present in March and its value increases from North to South from 2 to 4.5 cm^2·mon. In April the latitudinal course varies within the limits 5-6 kcal/cm^2·mon. A redistribution of monthly amounts of scattered radiation has been observed for May. In the North these amounts increase to 10-11 kcal/cm^2·mon. on account of the long day, whereas in the South the amounts decrease to 6-5 kcal/cm^2·mon.

The monthly amounts of scattered radiation decrease in June from North to South from 12.5 to 4.5 kcal/cm^2·mon.

The maximum of scattered radiation in the North is the result of the greater length of the day. The maximum amount of scattered radiation has been observed in Central Asia (5 kcal/cm^2·mon), where it differs slightly from the amount of radiation under a clear sky.

There is an insignificant variation in scattered radiation over the territory of the Soviet Union during the autumn months, and a feature of the distribution of the monthly amounts of radiation is the transition from the summer to the winter season.

On account of the properties of cloudiness and underlying surfaces in the Arctic region the fundamental part of the radiative energy incident on the earth's surface contributes to scattered radiation. Such a large occurrence of scattered radiation is not observed in the Antarctic region, insofar as clouds of the lower stratum corresponding to rising scattered radiation in this region are observed less frequently than in the Arctic. Scattered radiation forms the main portion of the net radiation in the element received in the Arctic regions, whereas direct solar radiation is the main portion in the Antarctic region.

The properties of the scattered radiation received under varying conditions of the sky in the Arctic as well as in the Antarctic regions are most distinctly manifested in the relation between scattered radiation D

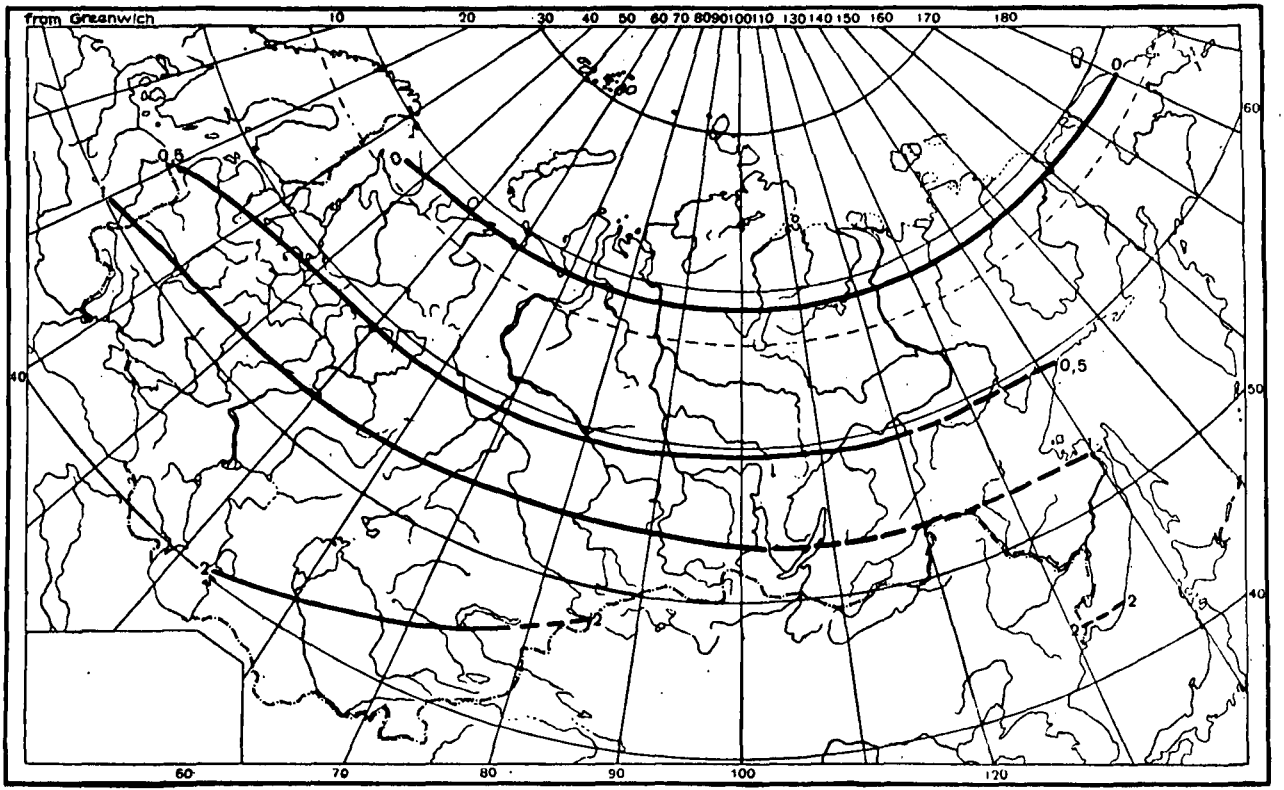

Fig. 6.13. Geographic distribution of scattered radiation in December [8].

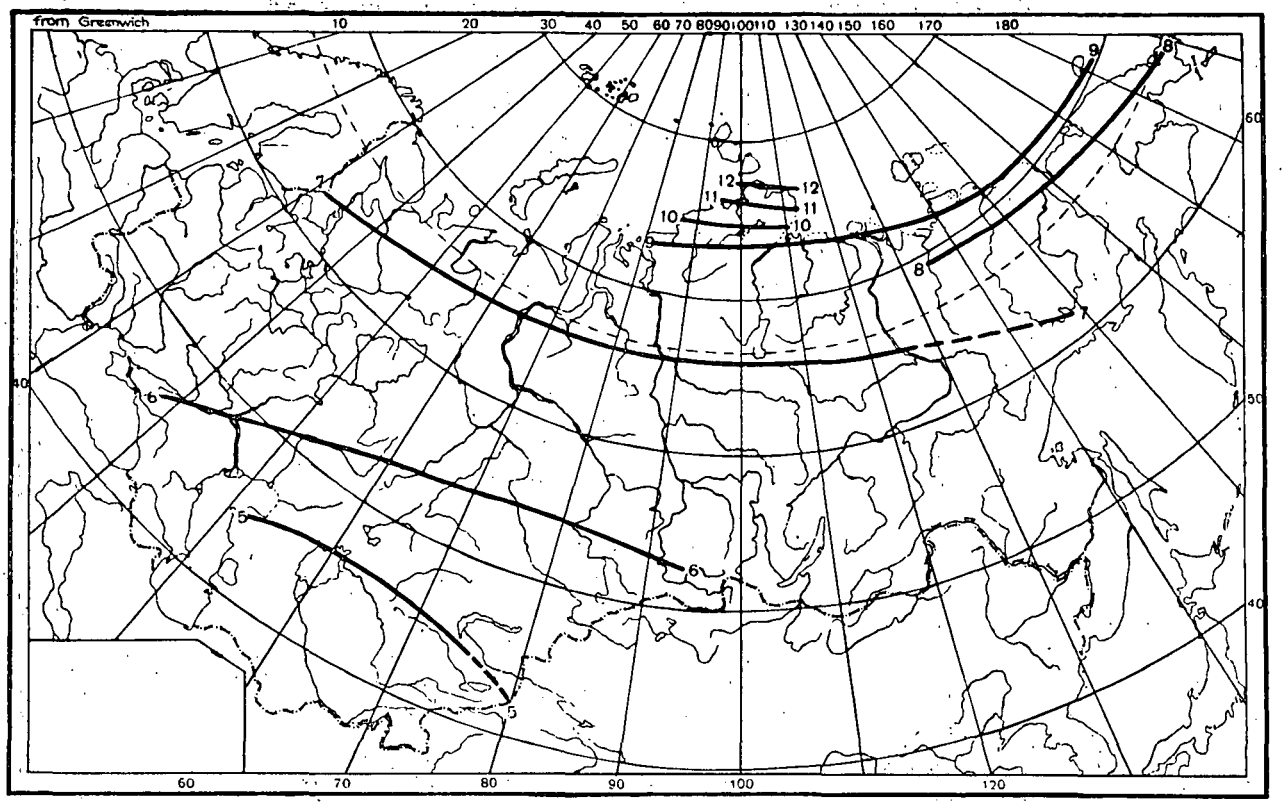

Fig. 6.14. Geographic distribution of scattered radiation in June [8].

and total radiation Q [68]. For altitudes of the sun above 25°, a clear sky and the presence of snow cover, scattered radiation comprises 20-25% of the total radiation received, whereas in the absence of snow it is 15-20%.

For altitude of the sun below 15° the contribution of scattered radiation even under a clear sky becomes 40-60% of the total radiation.

An analogous picture has been observed in the Antarctic region (Table 6.42) for large solar altitudes (above 15°), the ratio D/Q at all stations comprising 10-20% [49].

Table 6.42 Ratio of scattered radiation to total radiation for a clear sky (a) and for average conditions of cloudiness (b) [49]

Station	Method of calculation	Altitude of the sun, deg								
		5	10	15	20	25	30	35	40	45
Oasis	*a*	0.46	0.24	0.20	0.18	0.17	0.13	0.12	0.11	0.10
	b	1.00	0.67	0.61	0.52	0.50	0.46	0.43	0.44	0.42
Mirnyy	*a*	0.45	0.30	0.25	0.22	0.19	0.15	0.13	0.13	0.12
	b	0.86	0.67	0.58	0.55	0.52	0.48	0.44	0.43	0.42
Pioneer	*a*	0.33	0.19	0.18	0.17	0.16	0.15	0.14	0.14	
	b	0.44	0.35	0.37	0.33	0.28	0.30	0.35	0.40	
Vostok-1	*a*	0.55	0.32	0.26	0.22	0.18	0.15	0.14		
	b	0.78	0.55	0.43	0.40	0.36	0.34	0.32		
Komsomol'skaya	*a*	0.42	0.28	0.24	0.20	0.17	0.15	0.14		
	b	0.67	0.39	0.33	0.29	0.25	0.22	0.20		
Vostok	*a*	0.55	0.30	0.25	0.19	0.16	0.14	0.13		

The contribution of scattered radiation to the total radiation in the presence of clouds rises sharply and comprises 30-50% Q at a high altitude of the sun in the Antarctic region; in the Arctic it represents 30-40% for clouds in the lower stratum and 60-90 % for clouds in the intermediate and lower strata.

The mean annual amounts of scattered radiation in the Arctic region change only a little from 41.6 kcal/cm^2 · yr in Pacific Bay to 47.9 kcal/cm^2 · yr at Kotel'nyy Island.

An interesting comparison of fluxes of radiation in the Antarctic and Arctic regions is given in Table 6.43.

Table 6.43 Annual amounts of scattered radiation in Antarctic regions for average cloudiness [49]

Station	D kcal/cm^2 . yr	Q kcal/cm^2 . yr	$\frac{D}{Q}$
	Antarctic region		
Mirnyy	46.7	94.5	0.49
Pioneer	35.5	108.9	0.33
Komsomol'skaya	36.5	131.2	0.28
Vostok	22.3	120.1	0.19
	Arctic region		
Cape Schmidt	44.0	72.4	0.61
Tiksi Bay	42.6	70.3	0.61
Dickson Island	46.9	65.3	0.72
Uedineniya Island	44.4	58.6	0.76

It is obvious from the Table that the yearly amounts of scattered radiation in the Arctic region between the latitudes 68-80° and along the coast of the Antarctic region (Mirnyy station) are almost identical. However, if we consider the yearly values of total radiation in the Arctic region to be significantly lower than the values in the Antarctic region, then the contribution of scattered radiation in the portion of the net radiation received in the Antarctic region is considerably lower even on the coast as compared to the Arctic region.

With the help of the accumulated data of observations it is possible to construct a schematic chart of distribution of the ratio of scattered total radiation for the Northern Hemisphere [10]. These charts are used for the evaluation of the amount of scattered radiation in the total radiation from the sun incident on the earth's surface. The region of predominance of scattered over direct radiation covers a large portion of the earth. In view of the predominance of cloudy weather at equatorial and at high latitudes the scattered radiation is more than the direct radiation in the course of an entire year, and at moderate latitudes this happens mostly during the autumn months.

At high latitudes of the Northern Hemisphere scattered radiation during spring and summer months comprises 50-60% of the value of total radiation, during autumn and winter months its contribution increases to 80-100%.

Minimum values of scattered radiation were observed in regions of low cloud cover in the tropical and subtropical latitudes. The contribu-

tion of scattered radiation over the period of an entire year does not exceed 20-30% of total radiation.

Table 6.44 represents the distribution of scattered radiation with respect to latitude obtained from observations in clear weather at 150 actinometric stations in the USSR over the period 1952-1958.

The first schematic charts of the geographic distribution of scattered radiation over the earth were published in 1958 by F. Bernghardt and H. Phylipps [82]. They computed the mean monthly intensity of scattered radiation (mcal/cm^2 · min) for the quadrant of 10° for sea and land between 70° N and 60° S.

10. OUTGOING SHORTWAVE EMISSION OF THE EARTH-ATMOSPHERE SYSTEM (RESULTS OF THEORETICAL COMPUTATIONS)

The atmosphere transforms solar emission mainly as a result of the process of multiple scattering and intrinsic absorption. The main portion of direct solar radiation, scattered and reflected emission comes from the visible and near infrared region of the spectrum.

In order to compute the outgoing shortwave emission it is necessary to know the scattering function, coefficients of scattering and absorption, survival probability of the vertical quantum distribution of the above-mentioned optical properties in the atmosphere and the reflection properties of the underlying surface, as well as to take into consideration the curvature of the atmosphere, polarization and refraction of radiation.

For the evaluation of shortwave radiation in the ultraviolet region of the spectrum the following should be taken into consideration : scattering on aerosol and molecules of air, as well as absorption in air (Hartley's band λ=0.22-0.32 μ, Huggin's band λ=0.30-0.345 μ); whereras in the visible region of the spectrum scattering by molecules of air and aerosol should be considered but not inherent absorption ; in the near infrared region of the spectrum one should take into consideration single scattering aerosol and absorption in water vapor and carbon dioxide.

The effect of actual cloudiness in the emission of radiation has not yet been adequately considered.

10.1 Parallel-plane model of Rayleigh's atmosphere

Voluminous theoretical computations of the outgoing emission for a parallel-plane model of the atmosphere have been accomplished for conditions of orthotropic reflection of the earth's surface for the following values of albedo, viz. 0 ; 0.25 ; 0.80 [65, 86, 89]. The results are given in the form of separate Tables for the following values of optical thickness τ and corresponding wave lengths λ, thus :

Table 6.44 Scattered radiation in clear sky (cal/cm^2 · min) from data of

Latitude	Jan			Feb			Mar				Apr	
	9 30	12 30	15 30	9 30	12 30	15 30	6 30	9 30	12 30	15 30	6 30	9 30
38°C	0.10	0.13	0.08	0.12	0.15	0.11	0.04	0.14	0.16	0.13	0.10	0.18
40	0.10	0.13	0.08	0.13	0.15	0.11	0.04	0.14	0.17	0.13	0.10	0.18
42	0.10	0.13	0.08	0.13	0.15	0.10	0.05	0.15	0.17	0.13	0.10	0.18
44	0.10	0.13	0.07	0.12	0.15	0.10	0.05	0.15	0.17	0.13	0.10	0.18
46	0.10	0.13	0.07	0.15	0.16	0.11	0.05	0.16	0.18	0.14	0.11	0.19
48	0.09	0.13	0.07	0.15	0.16	0.11	0.06	0.17	0.19	0.14	0.11	0.19
50	0.09	0.13	0.06	0.14	0.17	0.11	0.06	0.17	0.19	0.14	0.10	0.18
52	0.08	0.12	0.05	0.13	0.17	0.10	0.05	0.16	0.20	0.14	0.10	0.18
54	0.07	0.11	0.05	0.11	0.16	0.09	0.05	0.15	0.18	0.13	0.09	0.17
56	0.06	0.10	0.05	0.10	0.14	0.08	0.05	0.15	0.17	0.13	0.09	0.16
58	0.06	0.09	0.04	0.10	0.13	0.07	0.04	0.14	0.16	0.12	0.09	0.16
60	0.05	0.07	0.03	0.09	0.12	0.06	0.04	0.13	0.15	0.11	0.09	0.16
62	0.03	0.07	0.02	0.08	0.11	0.05	0.04	0.13	0.14	0.10	0.09	0.16
64	—	0.06	—	0.08	0.11	0.05	0.04	0.13	0.14	0.10	0.10	0.17
66	—	0.06	—	0.07	0.10	0.05	0.04	0.12	0.14	0.10	0.10	0.17
68	—	—	—	0.06	0.09	0.04	—	0.11	0.14	0.10	0.10	0.17

Latitude	Jul					Aug					Sept	
	6 30	9 30	12 30	15 30	18 30	6 30	9 30	12 30	15 30	18 30	6 30	9 30
38°C	0.12	0.19	0.20	0.17	0.06	0.10	0.18	0.19	0.16	0.04	0.07	0.16
40	0.12	0.18	0.20	0.17	0.06	0.10	0.17	0.18	0.16	0.04	0.07	0.16
42	0.12	0.18	0.20	0.17	0.07	0.10	0.17	0.18	0.16	0.04	0.07	0.16
44	0.12	0.18	0.19	0.16	0.07	0.10	0.17	0.18	0.16	0.04	0.06	0.15
46	0.12	0.18	0.19	0.16	0.07	0.10	0.17	0.19	0.15	0.04	0.06	0.15
48	0.12	0.18	0.19	0.16	0.08	0.10	0.17	0.19	0.15	0.05	0.07	0.15
50	0.12	0.18	0.19	0.16	0.08	0.09	0.17	0.18	0.15	0.05	0.07	0.14
52	0.12	0.17	0.19	0.16	0.08	0.09	0.16	0.17	0.15	0.05	0.07	0.13
54	0.12	0.17	0.18	0.16	0.08	0.09	0.15	0.17	0.14	0.05	0.06	0.12
56	0.11	0.17	0.18	0.15	0.08	0.09	0.15	0.17	0.13	0.05	0.06	0.12
58	0.11	0.16	0.18	0.15	0.08	0.08	0.14	0.16	0.13	0.05	0.06	0.12
60	0.11	0.15	0.15	0.13	0.08	0.08	0.14	0.15	0.13	0.05	0.05	0.11
62	0.11	0.14	0.13	0.12	0.08	0.08	0.13	0.13	0.12	0.06	0.05	0.10
64	0.11	0.14	0.13	0.12	0.08	0.08	0.12	0.13	0.11	0.06	0.05	0.09
66	0.11	0.14	0.13	0.12	0.09	0.08	0.11	0.13	0.11	0.06	0.05	0.09
68	0.11	0.13	0.13	0.12	0.09	0.08	0.10	0.12	0.10	0.05	0.05	0.09

a network of actinometric stations (mean values for several years)

Apr			May					Jun				
12 30	15 30	18 30	6 30	9 30	12 30	15 30	18 30	6 30	9 30	12 30	15 30	18 30
0.20	0.16	—	0.11	0.18	0.19	0.16	0.05	0.11	0.17	0.18	0.16	0.07
0.20	0.16	—	0.11	0.18	0.19	0.16	0.05	0.11	0.17	0.18	0.16	0.07
0.20	0.16	—	0.11	0.17	0.19	0.16	0.05	0.11	0.17	0.18	0.15	0.07
0.20	0.16	—	0.11	0.17	0.19	0.16	0.05	0.11	0.17	0.17	0.15	0.07
0.20	0.16	—	0.11	0.19	0.19	0.16	0.06	0.12	0.18	0.18	0.16	0.07
0.20	0.15	0.04	0.11	0.19	0.20	0.16	0.06	0.12	0.19	0.19	0.16	0.07
0.19	0.15	0.04	0.12	0.18	0.19	0.15	0.06	0.12	0.19	0.19	0.16	0.08
0.19	0.14	0.04	0.12	0.18	0.18	0.15	0.07	0.12	0.18	0.18	0.16	0.09
0.17	0.14	0.04	0.12	0.18	0.18	0.15	0.07	0.12	0.18	0.18	0.16	0.09
0.17	0.14	0.04	0.12	0.18	0.17	0.15	0.08	0.12	0.17	0.18	0.16	0.10
0.17	0.13	0.04	0.12	0.16	0.16	0.14	0.08	0.12	0.16	0.17	0.15	0.10
0.17	0.13	0.05	0.11	0.15	0.16	0.14	0.08	0.11	0.15	0.16	0.15	0.09
0.17	0.13	0.05	0.10	0.15	0.16	0.14	0.08	0.11	0.15	0.15	0.14	0.09
0.18	0.14	0.05	0.10	0.14	0.16	0.14	0.09	0.11	0.15	0.15	0.14	0.09
0.18	0.15	0.05	0.10	0.14	0.16	0.14	0.09	0.11	0.14	0.15	0.14	0.09
0.18	0.16	0.06	0.10	0.14	0.16	0.14	0.09	0.11	0.17	0.15	0.17	0.09

Sept		Oct				Nov			Dec		
12 30	15 30	6 30	9 30	12 30	15 30	9 30	12 30	5 30	9 30	12 30	15 30
0.17	0.14	0.05	0.13	0.14	0.11	0.11	0.12	0.08	0.10	0.11	0.06
0.17	0.14	0.05	0.13	0.14	0.11	0.11	0.12	0.07	0.10	0.11	0.06
0.17	0.13	0.05	0.13	0.14	0.11	0.11	0.12	0.07	0.10	0.11	0.06
0.17	0.12	0.04	0.12	0.14	0.09	0.10	0.12	0.07	0.09	0.11	0.04
0.17	0.12	0.04	0.12	0.14	0.09	0.10	0.12	0.06	0.09	0.11	0.04
0.16	0.12	0.04	0.12	0.13	0.09	0.09	0.12	0.05	0.09	0.11	0.04
0.15	0.12	0.04	0.11	0.12	0.09	0.08	0.11	0.05	0.08	0.10	0.04
0.15	0.12	0.04	0.11	0.11	0.08	0.08	0.10	0.04	0.07	0.10	0.02
0.15	0.12	0.04	0.10	0.11	0.08	0.07	0.10	0.04	0.06	0.09	—
0.14	0.12	—	0.10	0.11	0.07	0.06	0.09	0.03	0.05	0.08	—
0.14	0.11	—	0.08	0.11	0.07	0.06	0.07	0.02	0.05	0.06	—
0.13	0.10	—	0.07	0.08	0.05	0.05	0.06	0.02	0.03	0.06	—
0.12	0.09	—	0.07	0.07	0.05	0.04	0.06	—	0.03	0.04	—
0.11	0.07	—	0.05	0.05	0.05	0.04	0.05	—	—	—	—
0.11	0.07	—	0.05	0.05	0.04	0.03	0.04	—	—	—	—
0.10	0.07	—	0.05	0.06	0.03	0.02	0.04	—	—	—	—

τ	1.00	0.50	0.25	0.15	0.10	0.05	0.02
$\lambda\,\mu$	0.3120	0.3715	0.4365	0.4950	0.5460	0.6440	0.8090

The Tables show the values of outgoing emission at the level of the upper boundary of the atmosphere, as well as the values of Stokes' parameters, degree of polarization and the angles between the plane of polarization and the vertical plane for a given azimuth.

Results of computations on the angular distribution of intensity of outgoing emission [88] for different optical thicknesses along the solar vertical indicate a considerable increase in intensity along the directions close to the horizon (Fig. 6.15). This can be caused by a rise in the amount of single-scattering as a result of the increase in the optical thickness of the atmosphere at horizontal level.

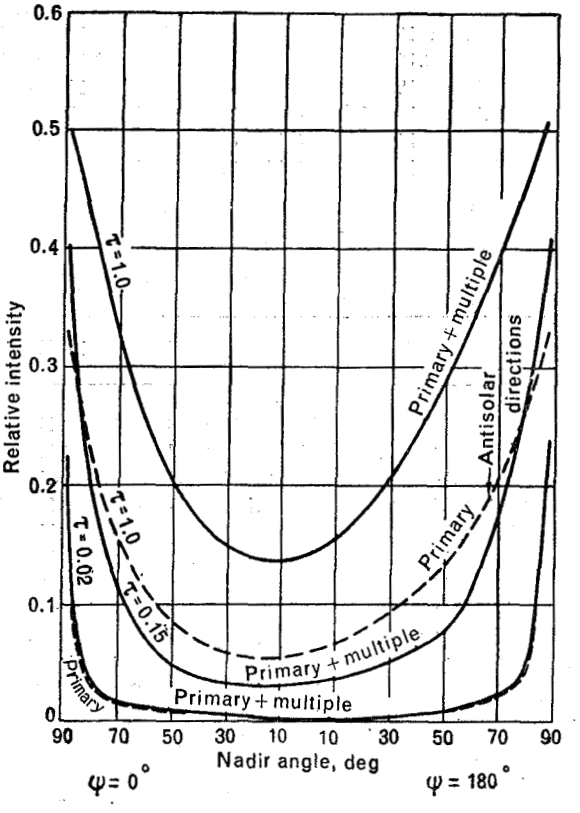

Fig. 6.15. Angular distribution of intensity of outgoing emission (in relative units) in the plane containing the solar vertical for different optical thicknesses (cos $\vartheta_\odot$=0.40; A=0) [88].

The effect of the albedo of the underlying surface on the angular distribution of intensity of outgoing emission is illustrated by the data in Fig. 6.16, where the results of computations for $\tau=0.15$; $\cos\vartheta_{\odot}=0.80$ and $A=0$; 0.25 ; 0.80 are shown. A decrease in intensity occurs at the level of the horizon in the case of a higher albedo value ($A=0.80$). Reflection from the earth's surface carries the main contribution to the outgoing emission for low optical thickness.

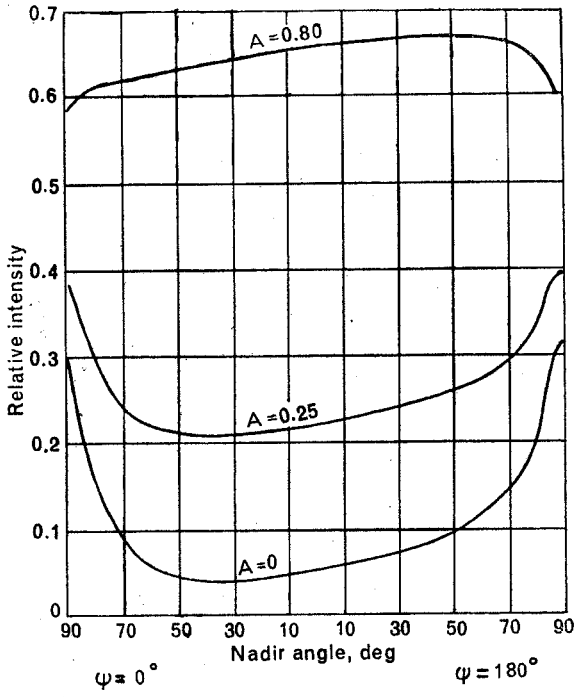

Fig. 6.16. Angular distribution of intensity of outgoing emission (in relative units) in the plane containing solar vertical for different albedo values of earth's surface ($\tau=0.15$; $\cos\vartheta_{\odot}=0.80$) [88].

The azimuthal dependence of the outgoing emission can be determined mainly by the scattering function. The fundamental principles of angular distribution of the outgoing emission along the solar vertical are typical for any other azimuth relative to the solar vertical (Fig. 6.17).

The maximum emission does not occur in the antisolar direction as in the case of single scattering but is shifted considerably toward the horizon. In the immediate vicinity of the horizon (toward the antisolar direction)

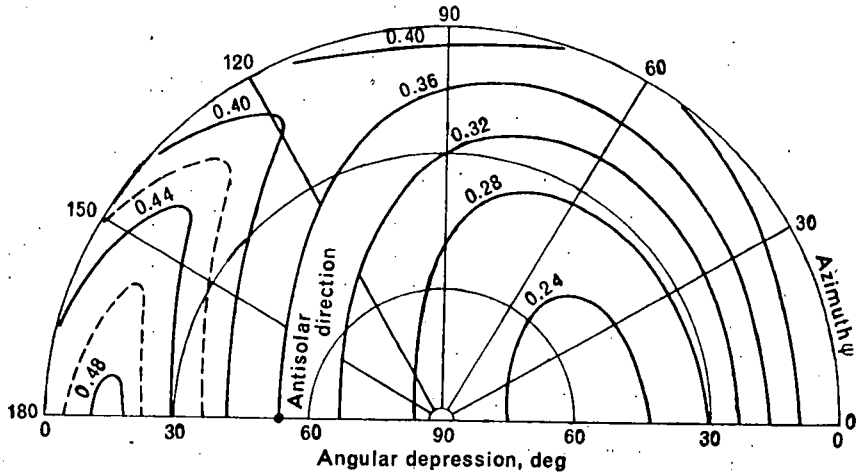

Fig. 6.17. Isophots of angular distribution of intensity of angular emission (in relative units) for altitude of sun=53° (τ=1.0; cos $\vartheta_\odot$=0.80; A=0) [88].

a drop in the outgoing emission may be observed. An increase at the level of the horizon takes place for other azimuthal angles. A maximum brightness may be observed near the horizon for low optical thicknesses. Consideration of Lambert's reflection does not give rise to azimuthal variation in the brightness field in the atmosphere which is horizontally uniform, although it affects the magnitude of the intensity of outgoing emission.

The dependence of the intensity of outgoing emission on the zenith angle of the sun has been studied for an orthotropic underlying surface (A=0.25) in the direction of the lowest point (nadir) for the wavelength interval of 0.312-0.803 μ [95]. The intensity of radiation at nadir decreases monotonically for increasing zenith angles of the sun.

The influence of a real nonorthotropic underlying surface (silica sand and red clay) on the field of shortwave outgoing emission has been investigated [90]. The intensity of scattered radiation can be computed using Chandrashekar's method [65] for two wavelengths λ=0.492 μ and λ =0.643 μ. In the case under examination the main contribution to the intensity of outgoing emission comes from radiation directly passing through the atmosphere, reflected by the surface and again passing directly through the atmosphere. The effect of reflection from red clay for λ= 0.643 μ is especially noticeable. Quartz sand reflects both wavelengths strongly. Reflected radiation in the red and near infrared regions of the spectrum for large albedo values (desert sand) [91] predominates in the outgoing reflection. Diffuse back reflection in the atmosphere occurs in the short wavelength region of the spectrum at large nadir angles ($\theta > 60°$).

Consideration of higher order scattering is important for the computations of polarization [80]. The computations for outgoing radiation give the same values for the degree of polarization and the same pattern for planes of polarization as for scattered outgoing emission [88]. The maximum contribution to atmospheric brightness is the result of multiple scattering in the vicinity of the horizon at azimuth ψ=90°. The degree of polarization decreases as the amount of multiple scattering increases, with the exception of the region of sky in the vicinity of the sun. For the scattering angle γ=90° the degree of polarization is 100% for single scattering, whereas for multiple scattering it decreases to 70%.

The computations of outgoing emission in the ultraviolet region were obtained for the interval $\Delta\ \lambda$=0.20-0.32 μ, for different positions of the sun and directions of sighting [17, 96, 97, 105]. The intensity of outgoing radiation is a minimum around λ=0.24 μ in agreement with the computations. Only single scattering (small optical thickness τ=0.18) was considered in the upper layer for the two-layered model of the atmo-

sphere. Multiple scattering was taken into consideration [105] in the lower layer where $\tau \sim 1.0$. The computations were carried out for Rayleigh scattering function using the relation:

$$\varkappa(\gamma) = \frac{3}{4}(1+\cos^2\gamma) \text{ and } \lambda = 0.229\ \mu,\ A = 0$$

The qualitative characteristics of the angular distribution of outgoing radiation in the presence of ozone and in its absence coincide. The error on account of neglect of multiple scattering (in the absence of ozone) becomes 8-15% for zenith angles of the sun $\theta_\odot < 50°$ and angles of sighting $\theta < 50°$. As the absorption in ozone increases these errors rapidly decrease. For the parallel planes model of the atmosphere, whose density changes with the height exponentially, data on the vertical distribution of ozone obtained from rocket measurements [17, 18, 99] to 70 km and extrapolated to 100 km were utilized.

In the figures for ozone bands corresponding to $\lambda > 0.3\ \mu$ aerosol scattering was considered. The atmosphere was divided into several layers, within whose limits the scattering function was considered invariable. Computations of vertical and angular distribution of intensity of multiple scattered radiation were accomplished for the following wavelengths : 0.25 ; 0.28 ; 0.32 μ [16]. In the region of strong absorption the intensity increases with increasing angle θ, especially at large $\theta_\odot$. The intensity does not depend on θ in the fringes for bands of weak absorption when $\theta_\odot$ is small. This contradicts the results showing a neutral course for intensity of outgoing radiation [97]. This contradiction shows that the single-scattering approximation is extremely crude for fringes of the band where multiple scattering is known to exist.

The spectral distribution of outgoing shortwave radiation can be determined by the spectral composition of the incident solar radiation and the optical properties of the atmosphere and the underlying surface.

The greatest variation in the spectral structure of the outgoing radiation field may be observed for $A = 0$, especially at high solar altitudes. In this case the flux of radiation is approximately proportional to λ^{-4}. For non zero values of surface albedo ($A = 0.25$) the spectral dependence of outgoing radiation is noticeably weaker.

Table 6.45 shows the result of computations of the spectral albedo of the earth-atmosphere system, i.e. Rayleigh's atmosphere for any albedo value of the underlying surface. For selected albedo values of the surface the spectral distribution of the outgoing radiation can be determined by the spectral course in the selected albedo value.

In the case of unselected albedo values for the earth's surface the albedo of the above system decreases with increasing wavelength. This

Table 6.45 Spectral albedo of the earth-atmosphere system—Rayleigh's atmosphere [88]

A	$\cos\theta_\odot$	λ Å					
		3150	4000	5000	6000	7000	8000
0	0.02	0.754	0.638	0.565	0.503	0.430	0.325
0	0.10	0.705	0.552	0.396	0.247	0.154	0.094
0	0.40	0.550	0.304	0.152	0.079	0.044	0.024
0	0.80	0.400	0.181	0.085	0.039	0.022	0.013
0	1.00	0.345	0.148	0.068	0.033	0.017	0.009
0.25	0.02	0.791	0.712	0.665	0.625	0.574	0.494
0.25	0.10	0.752	0.643	0.536	0.427	0.362	0.319
0.25	0.40	0.623	0.445	0.345	0.298	0.276	0.285
0.25	0.80	0.492	0.347	0.293	0.271	0.260	0.257
0.25	1.00	0.450	0.322	0.280	0.264	0.256	0.255
0.80	0.02	0.922	0.910	0.904	0.896	0.885	0.865
0.80	0.10	0.918	0.892	0.866	0.842	0.826	0.815
0.80	0.40	0.860	0.830	0.812	0.805	0.803	0.800
0.80	0.80	0.811	0.798	0.798	0.798	0.798	0.799
0.80	1.00	0.794	0.792	0.794	0.796	0.798	0.799

change is especially noticeable for $A=0$ and high solar altitudes. Reflection from the earth's surface increases the albedo value for all wavelengths especially in the region of minimum attenuation of radiation. For $A=0.80$ and high solar altitudes scattering in the atmosphere lowers the albedo value of the system slightly in comparison with the ground albedo. The spectral distribution for outgoing radiation (W/m^2 for 0.1 μ) for $A=0$ and different solar altitudes is given in Fig. 6.18. The distribution of energy in the spectrum of solar radiation outside the atmosphere is provided by Nicolet's data (cf. Chapter 5).

The magnitudes of integrated flux of outgoing radiation for the region 0.32-0.80 μ depend to a large extent on the albedo value of the earth's surface, especially for high solar altitudes. For a variation in A from 0 to 0.80 the flux of the outgoing radiation for $\theta_\odot=0°$ increases from 51.8 to 609.6 W/cm^2. A corresponding variation in the albedo of the system in the first case consists of 0.067-0.792 and in the second 0.519-

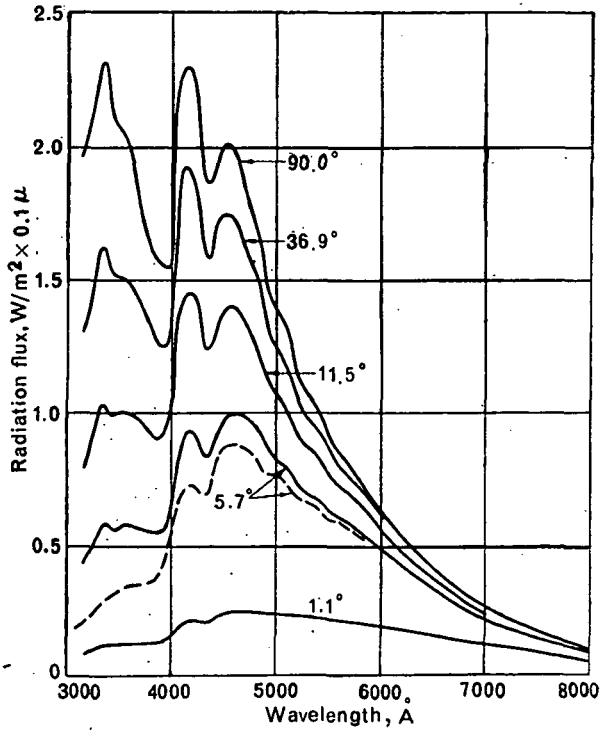

Fig. 6.18. Energy distribution in the spectrum of outgoing radiation (W/m^2, 0.1 μ) at $A=0$ and at different solar altitudes ($\cos \vartheta_\odot = 1.0; 0.40; 0.20; 0.10; 0.02; 0.0$).

Dotted curve is the spectral distribution of outgoing scattered radiation [88].

0.890. Hence the albedo of the system depends on solar altitude, increases with a decrease in the latter for $A=0$ and changes comparatively little at $A=0.80$. Approximate computations of the integrated (for the entire solar spectrum) albedo of the earth, as a planet, gave the value 7.6% [88] for $A=0$. If the absorption effect of solar radiation is taken into consideration, this value decreases to 6.9%.

10.2 Parallel plane model of a real atmosphere

In a real atmosphere it is necessary to take into consideration scattering and absorption of solar radiation in aerosol. In most investigations the absorption in aerosol and horizontal inhomogeneity of atmosphere are neglected.

In the two-parameter scheme of Shifrin and Minin [73] the mean standard model of the atmosphere was used, where the concentration of aerosol decreases exponentially [102]. A closed optical scheme of natural clear atmosphere (not considering its curvature) was constructed so that it was possible to determine any characteristic of the atmosphere from a few known characteristics. Such a scheme requires the application of the following empirical data: 1—aerosol structure of clear atmosphere [102], 2—spectral transparency of atmospheric aerosol [107] and 3—form of scattering function in atmosphere [94].

The horizontal visual range at the level of the earth's surface D_0 and spectral optical thickness of the atmosphere $\tau(\lambda)$ are the initial parameters to be determined experimentally.

The intensity of outgoing radiation can be computed for weighted average of the scattering function ($\lambda=0.55\,\mu$) for different values of optical thickness of the atmosphere, albedo of surface, zenith angles of the sun and angles of sighting [73, 75]. From the given data it is possible to determine the intensity of outgoing radiation for any value of albedo between 0 and 1 within an error of 3%. Errors in computing the intensity of outgoing radiation according to Sobolev's method used in [73] do not exceed 15% even for highly stretched scattering function and for large optical thickness ($\tau=0.80$) [3].

As the angle of sighting θ increases, so does the intensity of outgoing radiation. Intensity increases almost linearly with an increase in the albedo of the underlying surface, but the ratio $I_{\theta=85°}/I_{\theta=0°}$ decreases

Table 6.46 Ratio of intensity of outgoing radiation at the horizon ($\theta=85°$) to the intensity at the lowest point ($\theta=0°$) [75]

	$\psi°$								
$\theta_\odot°$	0	90	180	0	90	180	0	90	180
	$D_0=50$ km, $\tau=0.2$			$D_0=20$ km, $\tau=0.3$			$D_0=4$ km, $\tau=0.5$		
				$A=0$					
20	4.36	3.75	3.93	3.98	3.36	3.40	3.79	3.11	3.08
40	7.43	4.66	5.53	6.47	3.92	4.35	7.38	3.43	3.68
60	14.14	5.45	7.67	12.42	4.40	5.75	18.67	3.67	4.28
80	32.62	6.26	10.16	43.18	6.53	10.42	81.35	4.61	5.81
				$A=1.0$					
20	4.15	3.96	7.01	2.96	2.81	2.81	1.69	1.62	1.62
40	5.02	4.21	4.46	3.62	2.97	3.08	2.14	1.69	1.72
60	7.63	4.52	5.33	5.98	3.33	3.60	4.45	1.84	1.95
80	20.24	5.29	7.51	23.52	4.63	6.64	25.90	2.43	2.79

(Table 6.46). As the zenith angle of the sun $\theta_{\odot}$ increases the intensity of outgoing radiation decreases at the nadir.

Computations for brightness of the outgoing radiation for a two-layered plane atmosphere which is horizontally homogeneous were obtained for the case of pure scattering [7, 64], corresponding to the transition conditions in the visible region of the spectrum. In the upper layer ($\tau'=\frac{1}{4}\tau$) Rayleigh's scattering function can be accepted, whereas in the lower layer the functions accepted are stretched according to [94]. Reflection from the earth's surface is considered to be of the Lambert type. Computations are carried out for different values of optical thickness τ, zenith angles of the sun $\theta_{\odot}$, azimuth ψ, angle of sighting θ and albedo of the earth's surface A.

Isophot charts at the level of the upper boundary of the atmosphere [64] are considered for an analysis of angular distribution of intensity of outgoing radiation. Isophots are situated in the vicinity of parallels for large and small zenith angles of t e sun. Small azimuth variations in the intensity of outgoing radiation are distinctly shown.

With an increase in turbidity in the atmosphere and angle of sighting the intensity increases for $A=0$. The intensity of outgoing radiation decreases as the extent of the scattering function increases. The dependence of the form of the function is relatively weaker, so that anisotropy in scattering could be roughly considered in the first approximation. and the scattering could be assumed to be isotropic if the angle of observation is not extremely wide.

The difference between intensities of outgoing radiation corresponding to different scattering functions decreases as the albedo of the underlying surface increases. Consideration of the albedo of the underlying surface decreases the effect of anisotropy in scattering.

The following conclusions are derived on the basis of the computations carried out [7]:

1. The dependence of intensity of outgoing radiation upon θ, ψ and τ for noticeable reflection from the earth's surface ($A \geqslant 0.2$) is considerably counterbalanced ;
2. Reflection strengthens the dependence of outgoing radiation from zenith distance of the sun $\theta_{\odot}$;
3. The contribution to albedo is insignificant for strong scattering ($\tau=0.6$, $\theta \geqslant 75°$; $\psi=0°$) and minimum flux of direct solar radiation ($\theta_{\odot} > 75°$) ;
4. It is possible to consider intensity of outgoing radiation independently of $\theta_{\odot}$, θ and τ to a rough approximation for $\theta_{\odot} \geqslant 75°$ and $A \geqslant 0.2$;
5. For high positions of the sun reflection from the earth's surface may increase the intensity of outgoing radiation 5-15 times.

Brightness of the atmosphere for $A=0$ has a minimum either in the direction of the lowest point, or in the solar vertical and in vertical directions close to it, i.e. close to $\theta=0°$. The horizon on the side of the sun is brighter than the horizon on the opposite side almost by 20-30% for small $\theta_\odot$ and by 50-100% for large $\theta_\odot$ ($\theta_\odot \geqq 75°$). The brightness of the solar horizon rapidly increases with increasing atmospheric turbidity and the zenith distance of sun whereas the brightness on the side away from the sun changes slowly. Along other vertical directions the angular distribution of the intensity of outgoing radiation becomes more symmetrical and in the direction perpendicular to the solar vertical the distribution of brightness is completely symmetrical. The brightness does not change near the horizon for small angles $\theta_\odot$ and for large $\theta_\odot$ decreases twice as much as compared with the brightness in the direction of the solar vertical.

The solar horizon may appear brighter in Rayleigh's atmosphere than on the opposite horizon. Molecular atmosphere turns out to be brighter than turbid atmosphere especially for small θ and large $\theta_\odot$. Turbid atmosphere is brighter than Rayleigh's only in the vicinity of the solar horizon.

In a cloudy sky the outgoing radiation does not depend so much on the position of the sun as in the case of a clear atmosphere [20].

For large albedo values A and small zenith angles of the sun $\theta_\odot$ the difference between intensities of outgoing radiation in a Rayleigh and a non-Rayleigh atmosphere is small [7]. The course of intensity of outgoing radiation with respect to $\theta_\odot$ is considerably different for different angles of sighting [38]. Intensity of radiation in the direction $\theta=15°$ decreases slightly with increasing $\theta_\odot$; the opposite behavior has been observed in the direction $\theta=75°$.

The results given above confirm the calculations for the parallel-plane model of real atmosphere [84, 85] where single scattering in aerosol is computed accurately, and multiple scattering in molecules has been considered on the basis of tables [89].

The data on brightness of the real atmosphere considered as a plane when single scattering occurs in the medium and aerosol particles are distributed according to Young's formula, is given in the form of tables [81]. The single scattering approximation is justified for small optical thickness. For large values of τ multiple scattering in Rayleigh's atmosphere can be evaluated from data in [89].

The computations on intensity of the outgoing radiation in the presence of sharply defined aerosol layers were carried out for the case of noctilucent clouds localized between 75 and 80 km [17].

The results of computations on integrated intensity of outgoing shortwave radiation, including the visible and near infrared region of the spectrum, show that the general patterns of the angular distribution of outgoing radiation named above hold true for integral shortwave radiation

as well [74]. While computing integrated intensity [74] it is assumed that the earth's surface reflects according to Lambert's law. Similarly computations have been accomplished for the case of non-Lambertian reflection in red atmosphere [4].

In the near infrared region of the spectrum computations on outgoing radiation have been carried out for strong absorption bands in water vapor and outside this band ($\lambda=1.68\ \mu$). Integrated intensity in the intervals $\Delta\lambda=0.4\text{-}0.7\ \mu$ and $\Delta\lambda=0.7\text{-}1.0\ \mu$ have been computed. It was shown that in the visible region of the spectrum, scattered radiation provides a noticeable contribution to the intensity of outgoing radiation. The angular distribution of intensity of outgoing radiation in the visible region for nonorthotropic reflective surfaces is illustrated in Fig. 6.19.

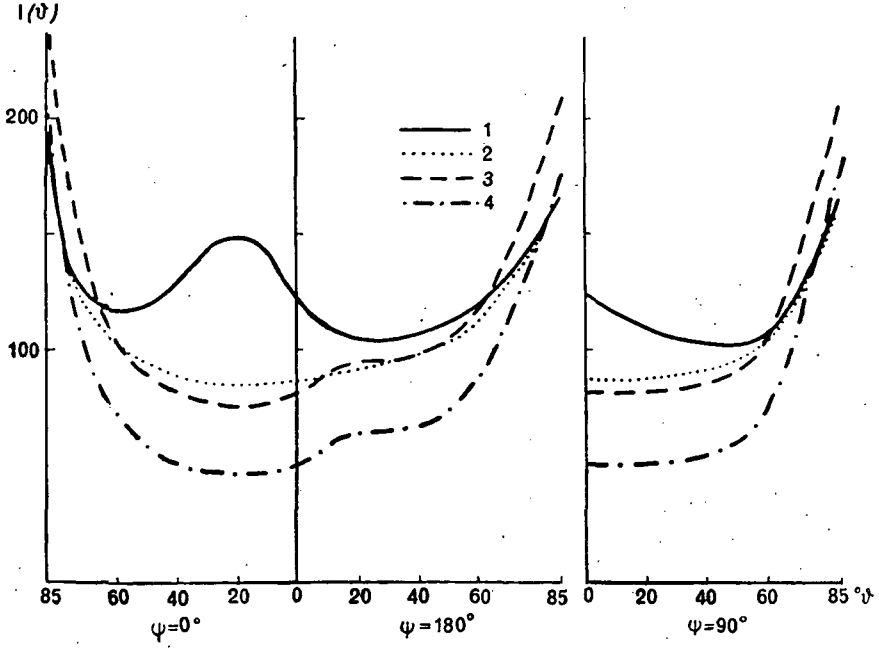

Fig. 6.19. Dependence of intensity of outgoing radiation above sea in visible region of the spectrum ($\lambda=0.55\ \mu$, $\tau=0.3$) on the angle of sighting θ for $\psi=0$; 90 and 180°.

1—nonorthotropic reflective surface [71]; 2—$A=0$ according to [71]; 3—$A=0.058$ according to [75]; 4—$A=0$ according to [75].

The results of computations are available for the case of reflection of solar radiation in a nondispersive layer of infinite thickness with strong anisotropic scattering [87] ; this condition results in the presence of a dense layer of clouds. It was shown that the albedo of an infinite layer increases with a rising zenith angle of the sun ; moreover, a thick layer of clouds

reflects nonorthotropically. Brightness of the horizon in the presence of the sun exceeds the brightness in the opposite direction. There exists an explicit dependence on the azimuth and a bright region has been observed, viz. the solar track, which is confirmed by airplane and sputnik measurements [21, 87].

Variation in the spectral composition of the outgoing shortwave radiation is caused mainly by the following three factors :

1. scattering in fluctuating densities ;
2. scattering on aerosol ; and
3. selective absorption in water vapor in the near infrared region of the spectrum.

Similarly it is necessary to consider absorption in ozone and carbon dioxide. In a real atmosphere as well as in Rayleigh's, a slight decrease in the intensity of the outgoing radiation may be observed with increasing wavelength (for $A=0$). This dependence on λ becomes extremely weak for $A>0$; whereas an increase in intensity may occur for a large albedo ($A=0.80$) with increase in λ. These variation could be explained by the combination of two factors as follows :

1. intensity of radiation scattered by the atmosphere into the cosmos always decreases with increase in λ; and
2. intensity of radiation reflected from the earth's surface and attenuated by the atmosphere in any case increases with rising values of λ for nonselective albedo.

For real underlying surfaces with clearly marked spectral dependence of the albedo there exists a more complex relation between intensity of the outgoing radiation and λ. Consideration of spectral variation of albedo has a decisive significance in the determination of energy distribution in the spectrum of the outgoing radiation [38].

The effect of the horizontal heterogeneity of the atmosphere on the outgoing radiation has not been studied in detail. An estimate of the effect of horizontal heterogeneity showed that the flux of outgoing radiation computed while considering the heterogeneity of the radiation field may differ sharply from the corresponding flux computed with the assumption of isotropy [38]. For instance, in the region $0\leqslant\theta\leqslant 60°$ (for $A=0$) and in the region $60\leqslant\theta\leqslant 75°$ (for $A=0.80$) the isotropic flux can be twice as much as the flux computed while assuming arisotropy.

10.3 Spherical model of the atmosphere

Consideration of the sphericity of the atmosphere is one of the difficult tasks of radiation transfer. The transfer equation of polarized

radiation in spherical atmosphere is considerably more complex than the corresponding equation for a two-dimensional atmosphere [100].

The following conclusions were arrived at from results of computing outgoing radiation in a spherical atmosphere [106], obtained for a model of pure scattering in Rayleigh atmosphere for reflection from the earth's surface according to Lambert's law.

1. For $A=0$ an increase in the brightness near the edge of the light side of the planetary disc is observed.
2. The maximum of reflected intensity shifts from the boundary of the disc toward the point below the sun when the albedo of the surface increases.
3. The gradient of relative intensity is greatest in the direction of the large circle of the planet, including incident and reflected rays which intersect at the center of the planet.
4. The effect of multiple scattering on the intensity of the outgoing radiation is more clearly marked for small phase angles ρ_0 (the phase angle of the planet is the angle at the center of the planet between the direction of the sun and the direction of sighting) and for low magnitudes of A. For $\rho_0=16.26°$ and $\tau=1.0$ an increase in intensity near the boundary of the disc on the illuminated portion of the planet can be observed; for $\tau=0.25$ a minimum in intensity can be observed in the vicinity of the nadir. This effect disappears with the rise in ρ_0 and A.
5. For $\rho_0=0$ intensity distribution in the vertical direction is symmetrical. For large values of A intensity falls toward the horizon, for small values of A the reverse is true.
6. If $\rho_0=0$ and A is small, then in the plane of the solar vertical an increase in intensity from the line dividing the illuminated and the unilluminated part of the planetary disc (terminator) is observed. For a high value of A the position of the maximum depends on ρ_0 and lies in the vicinity of the point below the sun.
7. For high values of A an increase in brightness with rising τ may be observed. This effect decreases with increasing A, indicating the predominance of reflected radiation.
8. The gradient of brightness in the vicinity of the terminator rises with increasing A. Higher order scattering has little influence of the value of this gradient, with the exception of the case of large angles ρ_0 and small values of A.

An approximate computation of sphericity for the earth's atmosphere has been accomplished in [103, 104]. The problems of transfer theory of nonpolarized emission in a spherical atmosphere have been examined in detail in [41, 42, 51-54, 60, 61]. An analytical expression for the mean

intensity of multiple scattering of light has been obtained for a constant coefficient of absorption [61]. A model of the spherical atmosphere was studied, in which the attenuation coefficient decreases exponentially with height [41]. The following quantities were evaluated with the help of results obtained :

1. brightness of the planet in the vicinity of the terminator for an atmosphere of infinite optical thickness, for spherical scattering characteristics and phase angle $\rho_0=90°$ (Table 6.47) ; and
2. brightness of zenith for terrestrial observations of different zenith distances of the sun (Table 6.48).

Table 6.48 shows the values of I_1, which is the intensity caused by scattering of the first order for spherical phase function and I_n—the intensity due to higher order scattering. The computations were carried out for a spherical function of scattering $\varkappa(\gamma)=1$, for different values of zenith distances of the sun $\theta_\odot$, for optical thickness of atmosphere τ and albedo of ground A. It follows from this Table that the relative role of higher order scattering changes only a little with the variation of zenith distance of the sun. However, this conclusion is based on the application of an approximate theory.

The values of complete brightness of the zenith in spherical atmosphere for the Rayleigh scattering function are given in Table 6.49.

The mean intensity of multiple scattering of light in a spherical atmosphere, whose density is a constant or changes exponentially, has been computed for the point below the sun and for terminator for at $\varkappa(\gamma)=1$, $\omega_0=1$ and $\tau=0.1$-0.3 [51-53]. For $\tau=0.2$-0.3 the radiational

Table 6.47 Luminosity of the planet in the vicinity of terminator in units of $10^{-3}\ \frac{1}{\pi}\ S_{0,\lambda}$ ($\pi S_{0,\lambda}$ is the solar constant) [41]

$\theta_\odot$	I_1	I	I'	$\theta_\odot$	I_1	I	I'
80°	38.5	148	145	90°	6.85	21.7	0
82	32.2	120	113	91	4.42	13.6	0
84	25.8	92.6	82.9	92	2.52	7.71	0
86	19.2	65.8	54.6	93	1.24	3.76	0
87	15.9	52.7	40.7	94	0.505	1.52	0
88	12.7	41.6	26.8	96	0.0425	0.127	0
89	9.05	31.0	13.3	98	0.0133	0.0396	0

Table 6.48 Values of I_1 and ΔI_n in units of $10^{-3}\frac{1}{\pi}S_{0,\lambda}$ ($S_{0,\lambda}$ is solar constant) [41]

$\theta_\odot$	I_1	I_n, $\tau=0.1$		I_1	I_n, $\tau=0.3$	
		$A=0.2$	$A=0.8$		$A=0.2$	$A=0.8$
80°	18.2	3.3	7.4	30.2	12.8	22.6
82	17.2	2.9	6.0	26.2	11.0	18.4
84	15.8	2.4	4.8	21.6	8.9	14.4
86	13.7	2.0	3.4	16.2	6.6	10.3
87	12.3	1.7	2.8	13.3	5.4	8.4
88	10.6	1.4	2.2	10.4	4.3	6.5
89	8.6	1.1	1.7	7.72	3.19	4.85
90	6.35	0.8	1.18	5.38	2.20	3.35
91	4.12	0.52	0.78	3.40	1.39	2.12
92	2.34	0.29	0.44	1.92	0.78	1.17
93	1.14	0.14	0.21	0.931	0.379	0.705
94	0.458	0.057	0.087	0.375	0.152	0.232
96	0.0382	0.0048	0.0072	0.0312	0.0128	0.0195
98	0.0119	0.0016	0.0022	0.00975	0.00398	0.00600

Table 6.49 Vertical luminosity in spherical atmosphere on earth for Rayleigh's scattering in units of $10^{-3}\frac{1}{\pi}S_{0,\lambda}$ ($S_{0,\lambda}$ is solar constant) [41]

$\theta_\odot$	$\tau=0.1$		$\tau=0.3$	
	$A=0.2$	$A=0.8$	$A=0.2$	$A=0.8$
80°	17.3	21.4	36.2	45.8
82	16.0	19.2	31.0	38.6
84	14.4	16.7	25.3	30.6
86	12.2	13.7	18.9	22.4
87	11.0	12.1	15.6	18.4
88	9.33	10.2	12.1	14.3
89	7.54	8.14	9.0	10.6
90	5.56	5.95	6.26	7.39
91	3.62	3.87	3.94	4.67
92	2.04	2.19	2.20	2.61
93	1.00	1.07	1.08	1.41
94	0.402	0.432	0.435	0.515
96	0.0338	0.0362	0.0364	0.0432
98	0.0107	0.0113	0.0114	0.0134

regime along the terminator can be completely determined by multiple scattering. Similarly the brightness during twilight has been computed while considering molecular sphericity [55] and aerosol atmosphere [56, 57]. The first order scattering for different angles of sunset at the horizon $\varepsilon_\odot$ and the height of spaceship at H=400 km were also evaluated. Table 6.50 gives the values of the brightness aureole of the earth's spherical atmosphere in case of pure Rayleigh sacttering ($\varkappa(\gamma)=\frac{3}{4}(1+\cos^2\gamma)$, $\psi=0°$) and angles of sunset $\varepsilon_\odot$=2-4°.

The brightness of the twilight halo of a spherical atmosphere considering aerosol and multiple scattering was computed by the Monte-Carlo method [39, 40]. It was shown that for computation of brightness of the night horizon it is possible to take into consideration only first order scattering if the observer is situated sufficiently far from the line of the terminator.

Computation of the intensity of outgoing radiation in the near infrared region for a spherical earth at the level of 300 km was carried out by considering single scattering and absorption in water vapor and carbon dioxide [1, 2]. The following fundamental conclusions were drawn.

1. For A=0 an increase in intensity of radiation at the horizon outside the absorption bands is sharper than within these bands.
2. Intensity distribution for A=0 can be determined from zenith distance of the sun, scattering function $\varkappa(\gamma)$ and the increase in optical thickness in the direction of the horizon.
3. For $A\geq 0.1$ the intensity distribution of the outgoing radiation can be determined by the reflection of the radiation. For sufficiently high A the atmospheric brightness in the direction of the horizon falls.
4. In the presence of a reflecting surface, the intensity of radiation at the nadir decreases with increase in τ (λ), since attenuation of solar radiation in the atmosphere before and after reflection rises. For variation in τ (λ) from 0.2 to 0.5 above clouds the intensity of radiation changes only a little at the nadir since the contribution of scattered radiation is small in the layer above the clouds.
5. The effect of atmosphere on the albedo of the earth-atmosphere system outside the absorption bands is insignificant. The value of the albedo of this system sharply decreases in the absorption bands of the atmosphere. In the near infrared region of the spectrum the atmosphere reflects back less than 2% of the incident solar radiation.

Table 6.50 Spectral brightness of twilight halo of molecular atmosphere (earth's) in units of $\frac{1}{\pi} S_{o,\lambda}$ ($S_{o,\lambda}$ is solar constant) [55]

θ	λ μ				
	0.40	0.45	0.50	0.55	0.60
			$\varepsilon_\odot = 2°, \psi = 0°$		
70°12 35″	0.184×10^{-11}	0.217×10^{-7}	0.349×10^{-5}	0.634×10^{-4}	0.348×10^{-3}
70 22 35	0.119×10^{-5}	0.541×10^{-4}	0.390×10^{-3}	0.110×10^{-2}	0.191×10^{-2}
70 32 35	0.221×10^{-3}	0.905×10^{-3}	0.169×10^{-2}	0.215×10^{-2}	0.224×10^{-2}
70 42 35	0.801×10^{-3}	0.154×10^{-1}	0.205×10^{-1}	0.227×10^{-1}	0.227×10^{-1}
70 52 35	0.179×10^{-1}	0.209×10^{-1}	0.207×10^{-1}	0.191×10^{-1}	0.166×10^{-1}
71 2 35	0.194×10^{-1}	0.178×10^{-1}	0.152×10^{-1}	0.123×10^{-1}	0.970×10^{-2}
71 12 35	0.149×10^{-1}	0.119×10^{-1}	0.905×10^{-2}	0.668×10^{-2}	0.484×10^{-2}
72 12 35	0.216×10^{-3}	0.116×10^{-3}	0.650×10^{-4}	0.382×10^{-4}	0.233×10^{-4}
73 12 35	0.266×10^{-5}	0.591×10^{-6}	0.314×10^{-6}	0.177×10^{-6}	0.108×10^{-6}
74 12 35	0.925×10^{-8}	0.453×10^{-8}	0.237×10^{-8}	0.132×10^{-8}	0.769×10^{-9}
			$\varepsilon_\odot = 4°, \psi = 0°$		
70°12′35″	0.231×10^{-12}	0.376×10^{-8}	0.802×10^{-6}	0.186×10^{-4}	0.128×10^{-3}
70 22 35	0.364×10^{-6}	0.231×10^{-4}	0.221×10^{-3}	0.819×10^{-3}	0.173×10^{-2}
70 32 35	0.165×10^{-3}	0.926×10^{-3}	0.227×10^{-2}	0.365×10^{-2}	0.468×10^{-2}
70 42 35	0.209×10^{-2}	0.398×10^{-2}	0.530×10^{-2}	0.590×10^{-2}	0.506×10^{-2}
70 52 35	0.524×10^{-2}	0.615×10^{-2}	0.620×10^{-2}	0.582×10^{-2}	0.523×10^{-2}
71 2 35	0.627×10^{-2}	0.585×10^{-2}	0.515×10^{-2}	0.442×10^{-2}	0.375×10^{-2}
71 12 35	0.521×10^{-2}	0.435×10^{-2}	0.357×10^{-2}	0.292×10^{-2}	0.240×10^{-2}
72 12 35	0.214×10^{-3}	0.148×10^{-3}	0.105×10^{-3}	0.753×10^{-3}	0.542×10^{-4}
73 12 35	0.361×10^{-5}	0.215×10^{-5}	0.132×10^{-5}	0.841×10^{-6}	0.554×10^{-6}
74 12 35	0.477×10^{-7}	0.267×10^{-7}	0.159×10^{-7}	0.990×10^{-8}	0.638×10^{-8}

Table 6.50—*Contd.*

θ	λ μ				
	0.65	0.70	0.75	0.80	1
			$\varepsilon_\odot = 2°, \psi = 0°$		
70°12′35″	0.968×10^{-3}	0.178×10^{-2}	0.253×10^{-2}	0.305×10^{-2}	0.305×10^{-2}
70 22 35	0.248×10^{-2}	0.275×10^{-2}	0.274×10^{-2}	0.256×10^{-2}	0.154×10^{-2}
70 32 35	0.209×10^{-2}	0.184×10^{-2}	0.158×10^{-2}	0.133×10^{-2}	0.903×10^{-2}
70 42 35	0.214×10^{-1}	0.194×10^{-1}	0.170×10^{-1}	0.149×10^{-1}	0.791×10^{-1}
70 52 35	0.139×10^{-1}	0.115×10^{-1}	0.930×10^{-2}	0.762×10^{-2}	0.330×10^{-2}
71 2 35	0.747×10^{-2}	0.569×10^{-2}	0.435×10^{-2}	0.333×10^{-2}	0.129×10^{-2}
71 12 35	0.350×10^{-2}	0.252×10^{-2}	0.185×10^{-2}	0.137×10^{-2}	0.487×10^{-3}
72 12 35	0.146×10^{-4}	0.946×10^{-5}	0.629×10^{-5}	0.431×10^{-5}	0.122×10^{-5}
73 12 35	0.633×10^{-7}	0.400×10^{-7}	0.260×10^{-7}	0.174×10^{-7}	0.460×10^{-8}
74 12 35	0.468×10^{-9}	0.294×10^{-9}	0.190×10^{-9}	0.128×10^{-9}	0.337×10^{-10}
			$\varepsilon_\odot = 4°, \psi = 0°$		
70°12′35″	0.428×10^{-2}	0.920×10^{-3}	0.149×10^{-2}	0.200×10^{-2}	0.252×10^{-2}
70 22 35	0.271×10^{-2}	0.349×10^{-2}	0.395×10^{-2}	0.410×10^{-2}	0.313×10^{-2}
70 32 35	0.522×10^{-2}	0.532×10^{-2}	0.514×10^{-2}	0.475×10^{-2}	0.289×10^{-2}
70 42 35	0.566×10^{-2}	0.520×10^{-2}	0.465×10^{-2}	0.408×10^{-2}	0.222×10^{-2}
70 52 35	0.460×10^{-2}	0.401×10^{-2}	0.344×10^{-2}	0.293×10^{-2}	0.150×10^{-2}
71 2 35	0.317×10^{-2}	0.268×10^{-2}	0.225×10^{-2}	0.188×10^{-2}	0.934×10^{-3}
71 12 35	0.198×10^{-2}	0.164×10^{-2}	0.135×10^{-2}	0.112×10^{-2}	0.540×10^{-3}
72 12 35	0.393×10^{-4}	0.290×10^{-4}	0.215×10^{-4}	0.163×10^{-4}	0.622×10^{-5}
73 12 35	0.375×10^{-6}	0.261×10^{-6}	0.187×10^{-6}	0.136×10^{-6}	0.474×10^{-7}
74 12 35	0.427×10^{-8}	0.292×10^{-8}	0.207×10^{-8}	0.151×10^{-8}	0.512×10^{-9}

REFERENCES

1. Avaste, O. A. Metod rascheta intensivnostei i potokov ukhodyashchego izlucheniya pri sfericheskoi Zemle v blizkoi infrakrasnoi oblasti spektra (Method of calculating the intensities and fluxes of outgoing radiation for a spherical earth in the near infrared region of the spectrum). Trudy GGO, vyp. 166, 1964.
2. Avaste, O. A. Resul'taty raschetov intensivnostei i potokov ukhadyashchego izlucheniya pri sfericheskoi Zemle v blizkoi infrakrasnoi oblasti spektra (Results of computations on intensity and fluxes of outgoing radiation for spherical earth in the near infrared region of the spectrum). Trudy GGO, vyp. 166, 1964.
3. Avaste, O. A. and V. S. Atroshenko. O tochnosti metoda V. V. Soboleva (On the accuracy of V. V. Sobolev's method). Izv AN SSSR, ser. geogr., No. 3, 1960.
4. Avaste, O. A., Yu. A. R. Mullamaa and K. S. Shifrin. Pole ukhodyashchei korotkovolnovoi radiatsii v vidimoi i blizkoi infrakrasnoi oblastyakh spektra pri neortotropnoi podstilayushchei poverkhnosti (The field of outgoing shortwave radiation in visible and near infrared regions of the spectrum for nonorthotropic underlying surfaces). Issledovaniya po fizike atmosfery IFA AN E'SSR, No. 6, 1964.
5. Averkiev, M. S. Geograficheskoe izobrazhenie zakrytosti gorizonta (Geographic representation of horizon's shielding). Meteorologiya i gidrologiya, No. 5, 1960.
6. Aizenshtat, B. A. and M. E. Zuev. Nekotorye cherty teplovogo balansa pechanoi pustyni (Some features of thermal balance of sandy deserts). Trudy Tash. GO, 5, 1952.
7. Artoshenko, V. S. et al. Trudy IFA AN SSSR, No. 3, 1962.
8. Barashkova, E. P., V. L. Gaevskii, L. N. D'yachenko, Z. I. Pivovarova and K. M. Lugina. Radiatsionnyi rezhim territorii SSSR (Radiative regime of the territory of the USSR). Gidrometeoizdat, Leningrad, 1961.
9. Belyaeva, I. P. Potoki otrazhennoi i rasseyannoi radiatsii na sklony (Fluxes of radiation reflected and scattered on slopes). Trudy GGO vyp. 107, 1961.
10. Berlyand, T. G. Teplovoi balans Severnogo polushariya. Sb. "A. I. Voeikov i sovremennye problemy klimatologii" (Thermal balance of the Northern Hemisphere. Coll. "A. I. Voeikov and the contemporary problems of climatology". Gidrometeoizdat, 1956.
11. Boiko, P. N. Nekotorye dannye o raspredelenii e'nergii v spektre dnevnogo neba (Some information about the distribution of energy in the spectrum of daytime sky). Trudy VNMS, t. VI, 1963.
12. Gal'perin, B. M. and L. P. Seryakova. Rasseyannaya i summarnaya solnechnaya radiatsiya pri razlichnykh usloviyakh (Scattered and total solar radiation under different conditions). Trudy GGO, vyp. 152, 1964.
13. German, A. I. Izmerenie uglovogo raspredeleniya intensivnosti radiatsii s avtostratostatov (Measurement of angular distribution of intensity of radiation from automatic stratospheric balloons). Trudy TsAO, vyp. 70, 1966.
14. German, A. I., et al. Uglovoe raspredelenie otrazhennoi radiatsii po dannym poletov na samolete IL-18 (Angular distribution of reflected radiation from the data collected during flights of airplane IL-18). Trudy TsAO, vyp. 70, 1966.
15. Germogenova, T. A. O vliyanii polyarizatsii na raspredelenie intensivnosti rasseyannogo izlucheniya (The effect of polarization on the intensity distribution of scattered radiation). Izv. AN SSSR, ser. geofiz No. 6, 1962.

16. Germogenova, T. A. O kharaktere resheniya uravneniya perenosa dlya ploskogo sloya (On the nature of the solution of the transition equation for a plane layer). Zhurnal vychisl. tekhniki, t. 1, No. 6, 1961.

17. Germogenova, T. A. and M. S. Malkevich. Pole otrazhennoi radiatsii Zemli v polose pogloshcheniya ozona 0.20-0.34. I. Spektral'noe raspredelenie (The field of reflected radiation of the earth in the absorption band of ozone 0.20-0.34. I. Spectral distribution). Izv. AN SSSR, fizika atmosfery i okeana, t. 1, No. 9, 1965.

18. Germogenova, T. A. and L. D. Krasnokutskaya. Uglovoe i vertikal'noe raspredelenie otrazhennoi radiatsii Zemli v polose pogloshcheniya ozona 0.20-0.34 μ (Angular and vertical distribution of reflected radiation of the earth in the absorption band of ozone 0.20-0.34 μ). Izv. AN SSSR, fizika atmosfery i okeana, t. 2. No. 11, 1966.

19. Grishechkin, V. S. and V. V. Mikhailov. Spektral'naya yarkost' bezoblachnogo neba (Spectral luminosity of cloudless sky). Problemy fiziki atmosfery, vyp. 7. Izd. LGU, 1967.

20. Gromova, N. V. and E. M. Feigel'son. Udkhodyashchaya radiatsiya v oblachnoi atmosfere (Outgoing radiation in cloudy atmosphere). Izv. AN SSSR, fizika atm. i okeana, t. 1. No. 9, 1965.

21. Kozlov, V. P. and E. O. Fedorova. K voprosu o prostranstvennom raspredelenii yarkosti oblakov nizhnego yarusa (On the problem of spatial distribution of luminosity in clouds of lower stratum). Izv. AN SSSR, ser. geofiz, No. 7, 1962.

22. Kondrat'ev, K. Ya. Luchistaya e'nergiya Solntsa (Radiant energy of the sun). Gidrometeoizdat, Leningrad, 1954.

23. Kondrat'ev, K. Ya. Aktinometriya (Actinometry). Gidrometeoizdat, Leningrad, 1965.

24. Kondrat'ev, K. Ya., L. A. Kudryavtseva and M. P. Manolova. Raspredelenie e'nergeticheskoi i svetovoi intensivnosti rasseyannoi radiatsii atmosfery po nebesnomu svodu (Distribution of energy and light intensities of atmospheric scattered radiation over the sky). Vestnik LGU, No. 5, 1965.

25. Kondrat'ev, K. Ya and M. P. Manolova. Radiatsionnyi balans sklonov (Net radiation of slopes). Vestnik LGU, No. 10, 1958.

26. Kondrat'ev, K. Ya. and M. P. Manolova. Uglovoe raspredelenie intensivnosti radiatsii, otrazhennoi estestvennymi podstilayushchimi poverkhnostyami (Angular distribution of intensity of radiation reflected by natural underlying surfaces). Vestnik LGU, No. 10, 1957.

27. Kondrat'ev, K. Ya. and M. P. Manolova. Dnevnoi khog i dnevnye summy rasseyannoi i summarnoi radiatsii na razlichno orientirovannykh sklonakh (Daily course and daily amounts of scattered and total radiation on differently oriented slopes). Vestnik LGU, No. 4, 1958.

28. Kondrat'ev, K. Ya. and M. P. Manolova. Prikhod korotkovolonovoi radiatsii na razlichno orientirovannye poverkhnosti pri nalichii snezhnogo pokrova (Influx of shortwave radiation on differently oriented surfaces in the presence of snow cover). Nauchnye soobshcheniya in-ta geologii i geografii. AN Lit.SSSR, t. XIII, 1962.

29. Kondrat'ev, K. Ya., G. N. Gaevskaya and G. A. Nikol'skii. Ae'rostatnye issledovaniya radiatsinonnogo balansa sistemy zemnaya poverskhnost'-atmosfera (Balloon investigation of net balance of the earth's surface-atmosphere system). Kosmicheskie issledovaniya, t. 1, vyp. 3, 1963.

30. Kondrat'ev, K. Ya., G. A. Nikol'skii and E. N. Esipova. Ae'rostatnye issledovaniya radiatsionnogo potoka v svobodnoi atmosfere (Balloon investigation of radiation flux in free atmosphere). Izv. AN SSSR, fizika atmosfery i okeana, t. II, No. 4, 1966.

31. Korzov, V. I. and L. B. Krasil'shchikov. Samoletnye izmereniya indikatris yarkosti podstilayushchei poverskhnosti (Airplane measurement of luminosity coefficients of underlying surface). Trudy GGO, vyp. 203, 1967.

32. Kostyanoi, G. N. and L. A. Pakhomova. Izmereniya koe'ffitsienta yarkosti podstilayushchei poverkhnosti i oblakov s samoleta (Measurement of coefficient of brightness of underlying surfaces and clouds from an airplane). Trudy TsAO, vyp. 66, 1965.

33. Krasil'shchikov, L. B. and N. P. Pyatovskaya. Spektral'nye indikatrisy otrazheniya nekotorykh poverkhnostei pri estestvennom osveshchenii v oblachnyi den' (Spectral reflection coefficients for several surfaces in natural lighting on a cloudy day). Trudy GGO, vyp. 86, 1957.

34. Krinov, E. L. Spektral'naya otrazhatel'naya sposobnost' prirodnykh obrazovanii (Spectral reflective capability of natural formations). Moskva-Leningrad, 1947.

35. Lopukhin, E. A. Vertikal'nye profili sostavlyayushchikh radiatsionogo balansa v Uzbekistane (Vertical profiles of components of radiation balance in Uzbekistan). SANIGMI, vyp. 11 (26), 1963.

36. Lopukhin, E. A. K voprosu ob izmenenii korotkovolnovoi radiatsii s vysotoi Solntsa i s vysotoi mesta nablyudeniya (On the problem of the variation of shortwave radiation with solar altitude and with the height of the place of observation). Trudy SANIGMI, vyp. 16 (31), 1963.

37. L'vova, E. M. Izmereniya summarnoi radiatsii Solntsa i al'bedo Zemli do vyso t 10-20 km (Variation of the total radiation of the sun and of albedo of the earth upto the height of 10-20 km). Trudy TsAO, vyp. 16, 1956.

38. Malkevich, M. S. Uglovoe i spektral'noe raspredelenie radiatsii, otrazhennoi Zemlei v mirovoe prostranstvo. Iskusstvennye sputniki Zemli (Angular and spectral distribution of radiation reflected by the earth in space. Artificial satellites of the earth). vyp. 14, 1962.

39. Marchuk, G. I. Rasul'taty resheniya nekotorykh zadach atmosfernoi optiki metod om Monte-Karlo (Results of the solution of some problems on atmospheric optics by the Monte-Carlo method). Izv. AN SSSR, fizika atmosfery i okeana, 3, No. 4, 1967.

40. Marchuk. G. I. and G. A. Mikhailov. O reshenii zadach atmosfernoi optiki metodom Monte-Karlo (The solution of problems on atmospheric optics by Monte-Carlo method). Izv. AN SSSR, fizika atmosfery i okeana, 3, No. 3, 1967.

41. Minin, I. N. and V. V. Sobolev. Rasseyanie sveta v sfericheskoi atmosfere (Scattering of light in spherical atmosphere). Kosmicheskie issledovaniya, 2, vyp. 4., 1964.

42. Minin, I. N. and V. V. Sobolev. K teorii rasseyaniya sveta v planetnykh atmosferakh (On the theory of scattering of light in planetary atmosphere). Astronomicheskii zhurnal, 40, No. 3, 1963.

43. Nikol'skii, G. A. Komponenty radiatsionnogo balansa v atmosfere do vysot 30 km (Components of net radiation in the atmosphere up to the height of 30 km). Problemy fiziki atmosfery, coll. No. 8, 1969.

44. Pyldmaa, V. O. O raspredelenii rasseyannoi radiatsii po nebosvodu (On the dis-

tribution of scattered radiation over the sky). Issledovaniya po fizike atmosfery. In-t fiziki i astronomii AN E'SSR, No. 4, 1963.

45. Pyatovskaya, N. P. Potoki korotkovolonvoi radiatsii v svobodnoi atmosfere (Fluxes of shortwave radiation in free atmosphere). Trudy GGO, vyp. 109, 1961.

46. Pyatovskaya, N. P. E'ksperimental'naya proverka rascheta potokov korotkovolnovoi radiatsii v real'noi atmosfere (Experimental verification of the calculation of shortwave radiative flux in the atmosphere). Trudy GGO, vyp. 183, 1966.

47. Pyatovskaya, N. P. Uglovaya struktura polya otrazhennoi radiatsii (Angular structure of the field of reflected radiation). Trudy GGO, vyp. 183, 1966.

48. Ross, Yu. and O. A. Avaste. Rasseyannaya radiatsiya v Tartu (Scattered radiation in Tartu). Issledovaniya po fizike atmosfery. IFA, AN E'SSR, No. 1, 1959.

49. Rusin, N. P. Meteorologicheskii rezhim Antarktidy (Meteorological regime of Antarctic region). Gidrometeoizdat, Leningrad, 1961.

50. Sivkov, S. I. K metodike vychisleniya vozmozhnykh summ radiatsii (On the method of computing possible amounts of radiation). Trudy GGO, vyp. 160, 1964.

51. Smoktii O. I. Mnogokratnoe rasseyanie sveta v odnorodnoi sfericheski-simmetrichnoi planetnoi atmosfere (Multiple scattering of light in homogeneous and spherically symmetrical planetary atmosphere). Izv. AN SSSR, fizika atmosfery i okeana, 3, No. 3, 1967.

52. Smoktii, O. I. Ob opredelenii yarkosti neodnorodnoi sfericheski-simmetrichnoi planetnoi atmosfery (On the determination of luminosity of non homogeneous spherically symmetrical planetary atmosphere). Izv. AN SSSR, fizika atmosfery i okeana, 3. No. 4. 1967.

53. Smoktii, O. I. Mnogokratnoe rasseyanie sveta v neodnorodnoi sfericheski-simmetrichnoi planetnoi atmosfere (Multiple scattering of light in nonhomogenous spherically symmetrical planetary atmosphere). Izv. AN SSSR, fizika atmosfery i okeana, 3, No. 5, 1967.

54. Smoktii, O. I. Mnogokratnoe rasseyanie sveta v sfericheskoi planetnoi atmosfere (Multiple scattering of light in spherical planetary atmosphere). Izv. komissii po fizike planet Astrosoveta AN SSSR, vyp. 6, 1969.

55. Smoktii, O. I. Mnogokratnoe rasseyanie sveta v molekylyarnoi sfericheskoi atmosfere (Multiple scattering of light in molecular spherical atmosphere). Vestnik LGU, ser. fiziki, vyp. 6, 1969.

56. Smoktii, O. I. Rasseyanie sveta v ae'rozol'noi sfericheskoi atmosfere (Scattering of light in spherical aerosol atmosphere). Izv. AN SSSR, fizika i okeana, 5, No. 15, 1969.

57. Smoktii, O. I. O priblizhennom opredelinii yarkosti sumerechnogo oreola real'noi zemnoi atmosfery v oblasti 0.40-1.06 mkm (On the approximate determination of the luminosity of twilight aerosol of terrestrial atmosphere in the region 0.40-1.06 μ). Izv. AN SSSR, fizika atmosfery i okeana, 5. No. 8, 1969.

58. Sobolev, V. V. Priblizhennoe reshenie zadachi o rasseyanii sveta v srede s proizvol'noi indikatrisoi rasseyaniya (An approximate solution of the problem of scattering of light in a medium with arbitrary scattering functions). Astronom, zh., 20, No. 5-6, 1943.

59. Sobolev, V. V. O rasseyanii sveta v atmosferakh Zemli i planet (On the scattering of light in the atmosphere of the earth and planets). Uch. zap. ser. LGU, ser. matematich. vyp. 18, 1949.

60. Sobolev, V. V. and I. N. Minin. Rasseyanie sveta v sfericheskoi atmosfere (Scattering of light in spherical atmosphere). I. Iskusstvennye Sputniki Zemli, vyp. 14, 1962.

61. Sobolev, V. V. and I. N. Minin. Rasseyanie sveta v sfericheskoi atmosfere (Scattering of light in spherical atmosphere). 2. Kosmicheskie issledovaniya, 1, vyp. 2, 1963.

62. Faraponova, G. P. and V. G. Kastrov. Aktinometricheskie nablyudeniya v nizhnei troposfere nad Kyzyl-Kumami (Actinometric observations in lower troposphere above Kyzyl-Kum mountains). Trudy TsAO vyp, 13, 1954.

63. Fedorova, M. P. Potoki rasseyannoi radiatsii ot otdel'nykh uchastkov neba na naklonnye poverkhmosti (Flux of scattered radiation from distinct segments of the sky on an inclined surface). Problemy fiziki atmosfery, 3, 1965.

64. Feigel'son, E. M., et al. Raschet yarkosti sveta v atmosfere pri anizotropnom rasseyanii (Computation of luminosity of light in atmosphere for anistropic scattering). Trudy IFA AN SSSR, No. 1, 1958.

65. Chandrasekhar, S. Perenos luchistoi e'nergii (Transfer of radiant energy). IL, 1953.

66. Chapurskii, L. I. E'ksperimental'nye issledovaniya spektral'nykh yarkostnykh kharakteristik oblakov, atmosfery i podstilayushchei poverkhnosti v intervale dlin voln 0.3-2.5 mkm (Experimental investigation on spectral luminosity characteristics of clouds, atmosphere and underlying surfaces in the interval of wavelength 0.3-2.5 μ). Trudy GGO, vyp. 196, 1966.

67. Chernigovskii, N. T. Nekotorye kharakteristiki radiatsionnogo klimata Tsentral'noi Arktiki. Radiatsionnyi i teplovoi balans Artiki (Some characteristics of radiational climate in Central Arctic region. Net radiation and thermal balance of the Arctic region). Trudy AANII, t. 229, 1961.

68. Chernigovskii, N. T. and M. S. Marshunova. Klimat Sovetskoi Arktiki (Climate of Soviet Arctic region). Gidrometeoizdat, Leningrad, 1965.

69. Chizhevskaya, M. P. Rasseyannaya radiatsiya po nablyudeniyam v voeikove (Scattered radiation from the observation in Voekov). Trudy GGO, vyp. 129, 1962.

70. Sharonov, V. V. Sovremennoe sostoyanie optiki prirodnogo landshafta (Contemporary state of optics of natural landscapes). Trudy VNMS, t. V, 1963.

71. Shifrin, K. S. and O. A. Avaste. Potoki korotkovolnovoi radiatsii v bezoblachnoi atmosfere (Flux of shortwave radiation in cloudless atmosphere). Issledovaniya po fizike atmosfery, IFA AN E'SSR, No 2, 1960.

72. Shifrin, K. S. et al. Teoriya spektral'nykh potokov korotkovolnovoi radiatsii v real'noi atmosfere (Theory of spectral flux of shortwave radiation in real atmosphere). Trudy VNMS, t. 6, 1963.

73. Shifrin, K. S. and I. N. Minin. K teorii negorizontal'noi vidimosti (On the theory of nonhorizontal visibility). Trudy GGO, vyp. 68, 1957.

74. Shifrin, K. S., V. Ya. Kolomiitsev and I. P. Pyatovskaya. Opredelenie potoka ukhodyashchei korotkovolnovoi radiatsii s pomoshch'yu iskusstvennogo sputnika Zemli (Determination of the flux of outgoing shortwave radiation with the help of artificial earth satellite). Trudy GGO, vyp. 166, 1964.

75. Shifrin, K. S. and N. P. Pyatovskaya. Tablitsy naklonnoi dal'nosti vidimosti i yarkosti dnevnogo neba (Tables of visual range on a slope and luminosity of daily sky). Gidrometeoizdat, Leningrad, 1959.

76. Shifrin, K. S. and N. P. Pyatovskaya. Pole korotkovolnovoi radiatsii nad tipichnymi podstilayushchimi poverkhnostyami (Field of shortwave radiation above typical underlying surfaces). Trudy GGO, vyp. 166, 1964.

77. Shlyakhov, V. I. Nekotorye osobennosti radiatsionnykh protsessov v nizhnei troposfere Antarktidy (Some peculiarities of radiative processes in lower troposphere in the Antarctic region). Trudy TsAO, vyp. 32, 1959.

78. Shubova, G. L. Intensivnost' okolosolnechnoi radiatsii v standartnykh usloviyakh (Intensity of radiation in the vicinity of the sun under standard conditions). Trudy GGO, vyp. 170, 1965.

79. Yaroslavtsev, I. N. Raspredelenie yarkosti po nebu (Distribution of brightness in the sky). Izv. AN SSSR, ser. geofi z. No. 1, 1953.

80. de Bary, E. and K. Bullrich. Effects of higher-order scattering in molecular atmosphere. J. Opt. Soc. Am., v. 54, No. 12, 1964.

81. de Bary, E., B. Brann and K. Bullrich. Tables related to light scattering in turbid atmosphere, v. I-III, AFCRL 65-71 (I-III) Special reports, No. 33, U. S. Air Force Office of Aerospace Research, 1965.

82. Bernghardt, F. and H. Phylipps. Die räumliche und zeitliche Verteilung der Einstrahlung, der Ausstrahlung und der Strahlungsbilanz im Meeresniveau. Abhandl. Meteorol. Hydrol. Dienst DDR, H. 45, 1958.

83. Boileau, A. R. and J. I. Gordon. Atmospheric properties and reflectances of ocean water and other surfaces for a low Sun. Appl. Opt., 5, No. 5, 1966.

84. Bullrich, K. Scattered radiation in the atmosphere and the natural aerosol. Adv. in Geophys., vol. 10, 1964.

85. Bullrich, K. et al. Research on atmospheric optical radiation transmission. Met. Geoph. Inst., Johannes Guttenberg Univ., Mainz, Germany Sci. Rep. No. 3, 1965, Contract AF 68 (052)—595.

86. Chandrasekhar, S. and D. D. Elbert. The illumination and polarization of the sunlight sky on the Rayleigh scattering. Trans. Am. Phil. Soc., New Series, vol. 44, 6, 1954.

87. Chu, C. M. et al. Numerical solution for multiple anisotropic scattering. IGES Electromagnetic Scattering, 567-582, Pergamon Press, N. Y., 1963.

88. Coulson, K. L. Characteristics of the radiation emerging from the top of Rayleigh atmosphere. 1: Intensity and polarization; 2: Total upward flux and albedo. Planet. Space Sci., v. 1, No. 4, 1959.

89. Coulson, K. L., J. Dave and Z. Sekera. Tables related to radiation emerging from a planetary atmosphere with Rayleigh scattering. Univ. of California Press, Berkeley, Berkeley—Los Angeles, 1960.

90. Coulson K. L., E. L. Gray and G. M. B. Bouricius. Effect of surface reflection on planetary albedo. Icarus, vol. 5, No. 2, 1966.

91. Coulson K. L. Effects of relation properties of natural surface in aerial reconnaissance. Appl. Opt., v. 5, No. 6, 1966.

92. Das, S. R. and V. D. P. Sastri. Spectral distribution and color of tropical daylight. JOSA, v. 55, No. 3, 1965.

93. Duntley, S. G. et al. Visibility. Appl. Optics, 3. No. 5, 1964.

94. Foitzik, L. and H. Zchaeck. Messungen der spektralen Zerstreuungs-funktion bodennaher dust bei guter Sicht, Dunst und Nebel. Zs. f. Meteorol., v. 7, No. 1, 1953.

95. Fraser, R. S. Apparent contrasts of objects on the earth's surface as seen from above the earth's atmosphere. JOSA, v. 54, No. 3, 1964.

96. Friedman, R. M., R. D. Rawcliffe and C. E. Meloy. Radiance of the upper atmosphere in the middle ultraviolet. J. G. Soc., v. 68, No. 21, 1963.

97. Green, A. E. S. Attenuation by ozone and earth's albedo in the middle ultraviolet. Appl. Opt., v. 3. No. 2, 1964.

98. Gordon, J. I. and P. V. Church. Overcast sky luminance and directional luminous reflectances of objects and backgrounds under overcast skies. Appl. Opt., 5, No. 6, 1966.

99. Jonson, E. S. and L. D. Pursell. Direct measurement of the vertical distribution of atmospheric ozone to 70 km altitude. J. Geoph. Res., v. 57, No. 2, 1952.

100. Lenoble, J. and Z. Sekera. Equation of radiative transfer in a planetary spherical atmosphere. Proc. Nat. Acad. Sci. USA, 47, No. 3, 1961.

101. Middleton, W. E. and A. G. Mungall. The luminous directional reflectance of snow. JOSA, 42, No. 8, 1952.

102. Penndorf, R. The vertical distribution of Mie particles in the troposphere. J. Met., v. 11, No. 3, 1954.

103. Robley, R. La diffusion multiple dans l'atmosphère déduite des observations crepusculaires. Ann. Geophys., 8, n° 1, 1952.

104. Sato, T. The intensity of scattered light for each wavelength in Rayleigh atmosphere composed of spherical shells. J. Met. Soc. Japan, 40. No. 3, 1962.

105. Sekera, Z. and J. V. Dave. Determination of ozone from the measurement of diffusely reflected ultraviolet solar radiation. Planet. Space Sci., vol. 5, No. 2, 1961.

106. Sekera, Z. and W. Viezee. Distribution of the intensity and polarization of the diffusely reflected light over a planetary disk. R-389-RR, a report prepared for U. S. Air Force project RAND Contract No. AF 49 (638)-700, Nov. 1961.

107. Schmolinsky, F. Die Wellenlängenabhängigkeit der Sichtweit und der Koeffizienten der Dustextinktion. Meteorol. Z., v. 61, No. 6, 1944.

108. Viezee, W. and P. A. Davis. Evidence of the dependence of reflected solar radiation on viewing geometry in TIROS IV radiation data sample. J. Appl. Met., vol. 4, No. 5, 1965.

7. TOTAL RADIATION

Problems relating to the study of direct and scattered radiation have been examined in Chapters 5 and 6. Direct and scattered radiation taken together represent the total shortwave radiation. The present chapter is devoted to the description of the patterns of variations in the total radiation with respect to the sun, atmospheric transparency, degree of cloudiness, period of sunshine and height of elevation above the earth's surface.

1. SPECTRAL COMPOSITION OF TOTAL RADIATION

The spectrum of solar radiation registered at the earth's surface is very complex. The processes of scattering on air molecules, water droplets and other particles suspended in the atmosphere, the process of absorption of radiation reflected from the earth's surface, etc. are the fundamental processes which determine the transformation of solar radiation in the atmosphere in the ultraviolet and visible regions of the spectrum.

The spectral composition of radiation recorded is extremely sensitive to variations in solar altitude and the optical state of the atmosphere and also depends on the nature of the underlying surface and the orientation of

the receptive surface of the apparatus.

Extensive experimental investigations on the spectral composition of total radiation have been carried out by many researchers [25, 37, 38, 64, 70, 79].

Measurements carried out by a group of researchers [25] showed that the energy maximum in the spectrum (480 nm) at the earth's surface is shifted relative to the spectrum outside the atmosphere by approximately 20 nm (Fig. 7.1). The extremes observed refer to the absorption bands of separate components of the atmosphere. The absorption bands of oxygen (510, 630, 760 nm) and water vapor (720, 820, 930 nm) are the most intense among these and a wide band, probably of extra-atmospheric origin, is situated in the vicinity of 430 nm. A decrease in the curvature of spectral distribution in the shortwave region of the spectrum is determined by the effect of the absorption bands of ozone (Hartley's band) ; intense Fraunhofer's lines are found in this droplet (365, 360, 405 nm).

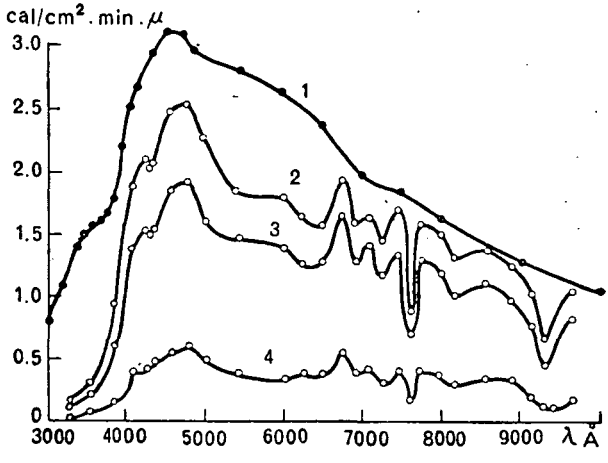

Fig. 7.1. Energy distribution in the spectrum of solar radiation.

1) values outside the atmosphere; values at the earth's surface in case of clear sky; Odessa, September 24, 1962 [26]; 2) $m=1.45$; 3) $m=2.1$; 4) $m=5.6$.

The magnitudes of spectral fluxes of total radiation for a clear sky are given in Table 7.1.

Table 7.2. is of interest because of the practical application of the results on the measurement of radiation in different spectral ranges. The data provide the ratio of spectral fluxes of total radiation for different masses of atmosphere to spectral flux, corresponding to the mass of atmosphere at zenith.

Table 7.1 Spectral fluxes of total radiation (cal/cm² · min . μ) at the level of the earth's surface. Odessa, September 24, 1964

λ, Å	*m*									
	Before noon					Afternoon				
	5.6	2.9	2.1	1.7	1.5	1.5	1.7	2.1	3.0	6.0
3286	0.03	0.06	0.10	0.13	0.14	0.13	0.12	0.08	0.05	0.02
3533	0.06	0.12	0.20	0.26	0.27	0.25	0.24	0.16	0.11	0.05
3864	0.12	0.31	0.60	0.86	0.94	0.82	0.72	0.52	0.30	0.10
4111	0.38	0.88	1.36	1.73	1.88	1.77	1.70	1.28	0.80	0.30
4276	0.40	0.94	1.52	1.93	2.09	2.02	1.84	1.32	0.86	0.32
4318	0.38	0.88	1.48	1.89	2.02	1.93	1.80	1.30	0.84	0.31
4359	0.44	0.92	1.52	1.93	2.05	2.04	2.00	1.40	0.88	0.33
4606	0.54	1.16	1.84	2.26	2.46	2.48	2.28	1.76	1.10	0.36
4800	0.58	1.24	1.90	2.33	2.53	2.55	2.40	1.84	1.20	0.40
5019	0.48	1.04	1.60	2.11	2.26	2.12	1.90	1.44	0.92	0.30
5432	0.44	0.96	1.44	1.71	1.85	1.77	1.84	1.32	0.76	0.24
6010	0.36	0.94	1.38	1.64	1.78	1.80	1.76	1.24	0.70	0.20
6258	0.34	0.80	1.24	1.56	1.61	1.65	1.60	1.20	0.72	0.19
6505	0.38	0.92	1.26	1.60	1.57	1.59	1.64	1.16	0.72	0.21
6758	0.52	1.04	1.64	1.93	1.92	1.88	1.92	1.44	0.84	0.21
6918	0.36	0.80	1.26	1.55	1.57	1.56	1.52	1.12	0.60	0.12
7083	0.40	0.92	1.40	1.64	1.62	1.59	1.56	1.16	0.68	0.20
7248	0.30	0.74	1.16	1.42	1.44	1.42	1.32	1.00	0.60	0.17
7455	0.40	0.90	1.32	1.56	1.68	1.74	1.56	1.12	0.64	0.20
7620	0.16	0.40	0.68	0.84	0.87	0.88	0.80	0.60	0.32	0.08
7744	0.40	0.80	1.28	1.60	1.57	1.49	1.48	1.10	0.68	0.20
7991	0.36	0.80	1.16	1.42	1.50	1.45	1.36	1.04	0.64	0.18
8157	0.28	0.66	1.00	1.24	1.30	1.20	1.08	0.80	0.48	0.15
8569	0.34	0.72	1.08	1.28	1.37	1.33	1.20	0.96	0.56	0.16
8900	0.32	0.64	0.96	1.18	1.23	1.20	1.16	0.80	0.50	0.14
9147	0.20	0.50	0.76	0.96	1.02	0.97	0.90	0.68	0.40	0.08
9312	0.12	0.26	0.44	0.54	0.65	0.64	0.60	0.40	0.20	0.04
9395	0.08	0.29	0.46	0.66	0.72	0.72	0.70	0.42	0.22	0.04
9643	0.17	0.50	0.84	1.06	1.10	0.96	0.84	0.60	0.38	0.06

Table 7.2 Ratio of spectral flux of total radiation for different atmospheric masses to spectral flux corresponding to atmospheric mass at zenith. Clear sky. Odessa, September 24, 1962

λ, Å	*m*						
	2.9	2.1	1.7	1.5	1.7	2.1	3.0
3237	20	42	66	100	68	46	27
3485	23	45	70	100	75	52	32
3817	22	34	69	100	66	52	27
4065	23	46	65	100	78	58	35
4562	24	46	70	100	76	59	34
5376	22	50	72	100	84	56	29
6691	28	52	82	100	86	59	32
7334	28	54	79	100	82	56	29
8512	28	54	79	100	80	61	34

Condit and Grum [64] carried out detailed measurements on energy distribution in total radiation for different solar altitudes and conditions of cloudiness. They investigated radiation fluxes on a surface inclined at an angle of 15° relative to the vertical and azimuth (relative to the sun) angles of 0, 30, 45 and 180°, and similarly on a vertical surface as well as a surface perpendicular to the direction of the solar rays.

The effect of a variation in solar altitude on the spectral composition of total radiation in the case of a clear sky is shown in Fig. 7.2. These measurements showed that the appearance of light smoke causes a "reddening" of total radiation. With the appearance of cloudiness the transformation of the spectrum becomes insignificant, whereas it vanishes in continuous dense cloudiness. The variation in the spectral composition of total radiation depending on different atmospheric conditions is shown in Fig. 7.3. Obviously, with the appearance of fog the "blue" component of the spectrum is noticeably diminished ; with the appearance of cloudiness it grows and only slightly exceeds the value for a clear sky in the presence of continuous dense cloudiness.

The spectral composition of total radiation changes with the angle of inclination of the receiving surface. The total radiation is more "blue" for measurements on a perpendicular plane and more "red" for measurements on a normal plane as compared with incident radiation on a plane at an angle of 15°.

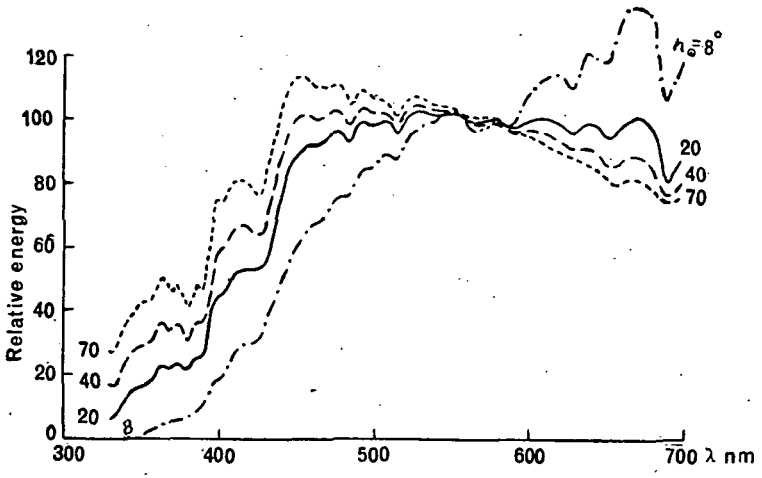

Fig. 7.2. Energy distribution in the region 15-0° of the spectrum of total radiation for solar altitudes of 8, 20, 40, 70° in the case of clear sky [64].

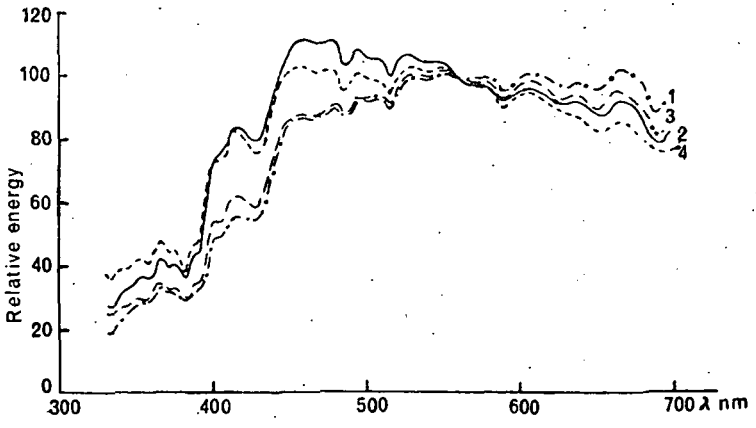

Fig. 7.3. Energy distribution in the region 15-0° of the spectrum of total radiation for solar altitudes of 40° [64].

1—fog, 2—clear sky, 3—thin clouds, 4—continuous dense cloudiness.

An increase in the azimuth causes the "blueness" of the radiation in the sky. This effect is noticeable at low altitudes of the sun, whereas for solar altitudes close to the maximum it becomes weaker. One of the basic results of experimental investigations on the spectral composition of total radiation is the conclusion that the spectral distribution of total radiation in the region of the spectrum 0.35-0.80 μ for cloudless and partially cloudy sky remains approximately constant in the course of a day. It is

not difficult to understand the reasons for the absence of a relation between spectral composition of total radiation and solar altitudes. A gradual depletion of solar radiation in the blue and violet rays occurs with the diminution of solar altitude, as a result of which a "reddening" of solar radiation may be observed. However the relative proportion of scattered light, richer in the blue and violet rays, in the total radiation rises as the solar altitude decreases. This increase in the proportion of shortwave scattered radiation practically compensates for the attenuation of radiation in the blue and violet regions of the solar spectrum. Thus the spectral composition of total radiation does not undergo any substantial variation with changing solar altitude.

2. TOTAL RADIATION INCIDENT ON A HORIZONTAL SURFACE

2.1 Dependence of total radiation on solar altitude

The flux of total radiation in a cloudless sky depends on the latitude of the place, inclination and altitude of the sun, optical properties of the atmosphere and underlying surface.

Measurements obtained at different geographic places show that the magnitude of the flux of total radiation rises with the increase in solar altitude. Tables 7.3, 7.4 and 7.5 clearly illustrate this dependence for the Arctic, Antarctic and temperate latitudes [14, 15, 50]. It is possible to visualize from the data in these tables that in spite of a significant difference in the geographical location of these places there is almost no change in the observed intensities of total radiation at identical solar altitudes in a cloudless sky.

Table 7.3 Intensity of total radiation in cloudless sky (cal/cm² . min) [14]

Station	Solar altitude, deg						
	5	10	15	20	25	30	40
Dreifuyushchie	—	0.20	0.33	0.47	0.61	0.74	—
Cape Chelyuskhin	0.06	0.18	0.31	0.43	0.56	0.68	—
Helsinki	0.08	0.18	0.30	0.42	0.55	0.66	0.86
Pavlovsk	0.09	0.18	0.29	0.41	0.55	0.69	0.96
Karadag	—	0.18	0.32	0.45	0.56	0.69	0.93
Blue Hill	—	—	0.31	0.44	0.55	0.69	0.93

Table 7.4 Total solar radiation in cloudless sky (cal/cm² . min) [15]

Region	Month	Altitude of the sun, deg												
		5	10	15	20	25	30	35	40	45	50	55	60	65
Central Asia	Apr	0.09	0.19	0.30	0.43	0.55	0.68	0.80	0.92	1.02	1.12	1.22	1.36	—
	May	0.05	0.17	0.29	0.42	0.55	0.67	0.79	0.91	1.02	1.11	1.20	1.36	1.43
	Jun	—	0.16	0.28	0.38	0.51	0.63	0.75	0.86	0.97	1.07	1.16	1.31	1.38
	Jul	—	0.16	0.28	0.39	0.51	0.63	0.75	0.86	0.97	1.07	1.16	1.30	1.35
	Aug	0.06	0.18	0.29	0.40	0.52	0.63	0.75	0.86	0.96	1.07	1.18	1.31	—
	Sept	0.05	0.17	0.29	0.42	0.54	0.66	0.79	0.90	1.01	1.11	1.20	1.34	—
Far East Region of the USSR	Apr	0.08	0.20	0.31	0.44	0.58	0.71	0.84	0.96	1.07	1.17	1.26	1.31	—
	May	—	0.18	0.30	0.43	0.55	0.68	0.80	0.91	1.01	1.11	1.21	1.29	1.34
	Jun	—	0.17	0.30	0.43	0.55	0.67	0.78	0.89	1.00	1.11	1.20	1.27	1.32
	Jul	—	0.17	0.30	0.42	0.54	0.67	0.79	0.88	0.98	1.08	1.17	1.23	1.28
	Aug	0.09	0.19	0.30	0.42	0.54	0.66	0.77	0.89	1.00	1.10	1.17	1.22	—
	Sept	0.09	0.18	0.30	0.44	0.58	0.70	0.82	0.93	0.91	—	—	—	—
	Oct	0.19	0.20	0.35	0.48	0.60	0.72	0.86	0.98	—	—	—	—	—
Cape Chelyuskin	Jul-Aug	—	0.18	0.31	0.43	0.56	0.68	—	—	—	—	—	—	—

Table 7.5 Mean values of intensity of total radiation in a clear sky in the Antarctic region at different altitudes of the sun (cal/cm² · min) [50]

Station	Years	Altitude of the sun, deg								
		5	10	15	20	25	30	35	40	45
Oasis	1956-1957	0.11	0.25	0.40	0.55	0.70	0.85	1.00	1.14	1.24
Mirnyy	1956-1957	0.11	0.23	0.38	0.54	0.68	0.83	0.98	1.11	1.20
Modkheim	1958	0.11	0.24	0.39	0.55	0.69	0.84	0.99	1.12	—
Pionerskaya	1956-1958	0.12	0.26	0.40	0.53	0.69	0.83	0.97	1.09	1.14 (43°)
Vostok-1	1957	0.11	0.25	0.42	0.55	0.72	0.86	1.00	1.13 (39°)	—
Komsomol'skaya	1958	0.12	0.28	0.45	0.64	0.81	0.98	1.13	—	—
Vostok	1958	0.10	0.26	0.43	0.61	0.79	0.96	1.10	—	—
Sovetskaya	1958	0.12	0.29	0.45	0.62	0.78	0.95	1.09	—	—
South Pole		0.12	0.27	0.40	0.58	0.70 (23.5°)	—	—	—	—

REMARKS: The altitude of the sun for which intensity is given is indicated in parentheses.

The dependence of the flux of total radiation on the altitude of the sun can be analytically represented by the following formula :

$$Q = \frac{S_0 \cos \vartheta_\odot}{1 + f \sec \vartheta_\odot}, \tag{7.1}$$

where S_0 is solar constant ; $f = \varepsilon\tau_0$ — a parameter whose magnitude depends on the properties of the atmosphere and the underlying surface (ε — fraction of light scattered back, τ_0 — optical thickness of atmosphere in the direction of the vertical) ; $\vartheta_\odot$ — zenith distance of the sun.

This formula was obtained independently by L. C. Makhotkin [43], M. E. Berlyand [7], K. Ya. Kondrate'v and G. P. Volkova [26].

The values of the coefficient f theoretically obtained by Berlyand for different months and latitudes are given in Table 7.6. Mean values of the parameter f [4] over many years were obtained on the basis of observations in a clear sky at many places situated at different latitudes.

Tables 7.6 and 7.7 show that the parameter f possesses an annual variation, which to a significant extent may be caused by the variation in the amount of water vapor in the atmosphere, variation in albedo of the underlying surface and other factors. The parameter f reaches a maximum value in June-July. The computed and measured values of parameter f are in close enough agreement among themselves.

It is possible to make completely reliable computations of the daily variation of total radiation with the help of the formula (7.1). In spite of its simplicity the formula enables us to establish a satisfactory correspondence between the computed and measured values of Q.

To a first approximation there is a direct proportionality between the flux of total radiation and the altitude of the sun $h_\odot$ on account of the linear dependence of one upon the other.

In a more simplified form the dependence $Q\,(h_\odot)$ can be represented by the following equation :

$$Q = 0.0252 h_\odot \tag{7.2}$$

as suggested by N. I. Chel'tsov [59]. The formula (7.2) cannot be sufficiently generalized and is applicable for computations to a first approximation. The coefficient of proportionality in the formula (7.2) changes not only for different places of observation but also at a specific place, since besides the dependency $Q\,(h_\odot)$ there exist other dependencies, in particular the dependency on atmospheric transparency.

In the case of cloudiness the relation between the flux of total radiation and the altitude of the sun becomes considerably more complex. In the presence of continuous cloudiness in the lower stratum the flux of total

Table 7.6 Values of parameter f with respect to latitude of place and time of year [7]

Latitude, deg	Jan	Feb	Mar	Apr	May	Jun	Jul	Aug	Sept	Oct	Nov	Dec
30	0.030	0.060	0.080	0.140	0.170	0.190	0.190	0.165	0.120	0.090	0.070	0.070
40	0.030	0.045	0.085	0.120	0.165	0.185	0.190	0.170	0.130	0.100	0.075	0.070
50	0.055	0.065	0.085	0.110	0.150	0.175	0.180	0.175	0.140	0.100	0.085	0.070
60	0.045	0.070	0.090	0.110	0.140	0.160	0.165	0.165	0.155	0.090	0.055	0.035

Table 7.7 Average values of parameter f over many years [4]

Station	Jan	Feb	Mar	Apr	May	Jun	Jul	Aug	Sept	Oct	Nov	Dec
Tbilisi	0.09	0.11	0.11	0.17	0.23	0.25	0.25	0.23	0.19	0.13	0.10	0.11
Odessa	0.07	0 11	0.09	0.15	0.19	0.23	0.23	0.21	0.16	0.14	0.06	0.07
Kiev Vysokaya	0.06	0.08	0.09	0.16	0.21	0.26	0.23	0.22	0.17	0.11	0.07	0.06
Dubrava	0.05	0.11	0.08	0.19	0.18	0.21	0.24	0.18	0.14	0.15	0.10	0.08
Voeikovo	0.05	0.05	0.11	0.14	0.20	0.22	0.22	0.21	0.11	0.12	0.10	0.04

radiation varies approximately proportionally to the altitude of the sun; in the case of cloudiness of intermediate and upper strata this linear dependency is eliminated.

2.2 The effect of cloudiness on the incidence of radiation

The cloudiness of different strata and forms exerts a varying influence on the flux of total radiation which may increase or decrease. In the case of clear solar disc ($\odot^2$) the appearance of cloudiness leads to an increase in Q since scattered radiation increases significantly. As a result of a marked decrease in direct solar radiation on the projection of clouds on solar disc ($\odot$, $\odot^\circ$, C)* the magnitude of total radiation varies considerably.

It is possible to evaluate the effect of 10 tenths cloudiness on the magnitude of Q from Table 7.8. Also Table 7.9 shows the results of observations on total radiation under conditions of moderate sunshine for 10 tenths cloudiness in the upper stratum. These results were obtained by B. M. Gal'perin [15] for different geographic regions. The Table shows that in regions with large repetitions of atmospheric fronts in summer periods the clouds of the upper stratum, which differ in density, considerably decrease the total radiation.

If the mean values of Q in moderate sunshine are only slightly lower than for a sun free from clouds, especially for Cu, then they decrease sharply on transition to weak sunshine.

Table 7.8 Dependence of intensity of total radiation (cal/cm² . min) on forms of clouds in 10 tenths cloudiness [4]

Form of cloud	Altitude of sun, deg					
	0-10	10-20	20-30	30-40	40-50	50-60
St	0.06	0.10	0.17	0.24	0.40	—
Sc	0.06	0.11	0.19	0.23	0.31	0.40
Ac	0.06	0.14	0.30	0.35	0.45	0.66
Clear	0.08	0.30	0.56	0.80	1.06	1.23

* $\odot^2$—solar disc completely uncovered ; $\odot$—moderate sunshine
$\odot^\circ$—weak sunshine; C—sun completely covered by clouds.

Table 7.9 Mean values of total radiation in cloudiness ⊙ of 10/0 Ci, Ci and Cs (cal/cm² . min) [15]

Region	Altitude of sun, deg								
	10	15	20	25	30	35	40	45	50
Central Asia	0.18	0.30	0.41	0.52	0.64	0.74	0.86	0.97	1.04
Southern region of USSR	0.17	0.28	0.40	0.51	0.63	0.74	0.86	0.98	1.06
Far East region of USSR	0.14	0.24	0.36	0.47	0.59	0.70	0.81	0.93	1.04
North West region of European Territory of USSR	0.15	0.25	0.35	0.46	0.56	0.66	0.77	0.86	0.94

Airplane measurements of total radiation in the Arctic region [55] show that the presence of cloudiness over ice increases total radiation on an average by 5%, over water surface—on an average by 13%.

A smaller collection of clouds at a high altitude, i.e. the presence of cloudiness in upper and intermediate strata, and strong secondary reflection of shortwave radiation in clouds in the Antarctic region entail an increase in the flux of total radiation, comparable with the arctic region. The data of measurements of Q given in the article by N. P. Rusin [50] provide a fairly complete picture of the variation in total radiation with respect to the solar altitude and cloudiness in the Eastern Antarctic region. The magnitude of the intensity of total radiation can differ widely on account of the secondary reflection of shortwave radiation from the lower boundary of cloudiness as well as with respect to the density of clouds in different regions of the Antarctic region for the same form of clouds.

Averaging of the results of observations on total radiation in moderate latitudes [13] for different forms and quantities of clouds and also depending on the state of the solar disc, shown in Table 7.10, indicates that the total radiation attenuates most markedly in cloudiness of the lower stratum, which completely absorbs direct solar radiation. Clouds of the upper stratum exert less influence. A variation in the state of the solar disc causes a significant variation in the flux of scattered radiation, so that total radiation undergoes a lot of variation in 10 tenths cloudiness of the upper stratum. The fluctuation in radiation is considerably less in $\odot^{\circ}$ than in $\odot^{2}$ and $\odot$. The data in Table 7.10 show that total radiation, when the solar disc is uncovered and there is considerable cloudiness of Cu or Ac (Sc) types, exceeds radiation in clear sky by almost 20%.

Table 7.10 Mean values of total solar radiation (cal/cm² . min) depending on the quantity and type of cloud, altitude of the sun and state of solar disc [13]

Clouds		State of solar disc	Altitude of sun, deg										
tenths	form		5	10	15	20	25	30	35	40	45	50	55
0/0	—	⊙²	0.07	0.18	0.31	0.43	0.55	0.66	0.79	0.90	1.01	1.11	1.20
2-3	Ci, Ci & Cs	⊙²	0.07	0.17	0.30	0.42	0.55	0.68	0.80	0.90	1.00	1.10	1.18
		⊙	0.05	0.14	0.27	0.40	0.52	0.65	0.77	0.88	0.98	1.06	
	Ac & Sc	⊙²	0.06	0.17	0.29	0.40	0.53	0.65	0.76	0.88	1.00	1.11	1.23
		⊙	0.06	0.16	0.28	0.39	0.51	0.63	0.74	0.86	0.97		
	Cu	⊙²		0.16	0.29	0.42	0.55	0.67	0.80	0.93	1.03	1.14	1.24
		(⊙)		0.16	0.29	0.42	0.54	0.66	0.79	0.92	1.02	1.11	1.20
4-5	Ci & Ci, Cs	⊙²		0.17	0.29	0.42	0.55	0.67	0.78	0.89	1.00	1.10	1.20
		⊙	0.06	0.16	0.28	0.40	0.52	0.64	0.76	0.87	0.98	1.08	1.18
	Ac & Sc	⊙²	0.07	0.18	0.32	0.44	0.56	0.69	0.82	0.95	1.08	1.18	
		(⊙)	0.07	0.18	0.30	0.42	0.54	0.66	0.78	0.90	1.02	1.13	1.24
	Cu	⊙²		0.19	0.31	0.44	0.56	0.69	0.82	0.96	1.09	1.21	1.30
		⊙		0.18	0.30	0.43	0.55	0.69	0.82	0.94	1.06	1.16	1.26
	Cu, Ac & Sc	(⊙°)			0.13	0.17	0.21	0.24	0.28	0.31	0.35	0.39	0.43
6-7	Ci & Ci, Cs	⊙²		0.17	0.29	0.43	0.55	0.68	0.80	0.91	1.02	1.12	1.21
		⊙	0.06	0.15	0.26	0.37	0.48	0.60	0.71	0.83	0.94	1.05	1.17
	Ac & Sc	⊙²	0.07	0.20	0.32	0.45	0.58	0.70	0.82	0.95	1.08	1.20	1.32
		⊙		0.20	0.32	0.43	0.55	0.67	0.79	0.90	1.02	1.14	1.26
		(⊙°)		0.12	0.17	0.23	0.28	0.33	0.38	0.43	0.48		

Table 7.10—*Contd.*

Clouds		State of solar disc	Altitude of sun, deg										
tenths	form		5	10	15	20	25	30	35	40	45	50	55
	Cu & Cu, Cb	⊙²		0.19	0.31	0.44	0.58	0.73	0.87	1.01	1.14	1.25	1.34
		(⊙)		0.17	0.30	0.43	0.56	0.70	0.83	0.96	1.10	1.21	1.30
		(⊙°)		0.12	0.16	0.20	0.24	0.28	0.32	0.36	0.40	0.44	0.48
8-9	Ci & Ci, Cs	⊙²		0.18	0.30	0.42	0.54	0.66	0.78	0.90	1.02	1.14	1.26
		⊙	0.07	0.16	0.26	0.39	0.51	0.63	0.74	0.85	0.94	1.04	1.13
		(⊙°)			0.13	0.18	0.25	0.31	0.38	0.45	0.52		
	Ac & Sc	(⊙²)		0.20	0.35	0.50	0.65	0.80	0.94	1.10	1.25	1.36	1.44
		⊙	0.07	0.17	0.27	0.39	0.41	0.64	0.76	0.89	1.02	1.14	1.27
		(⊙°)		0.10	0.16	0.21	0.27	0.33	0.39	0.45	0.50	0.56	0.62
	Cu & Cu, Cb	(⊙²)								1.05	1.20	1.32	1.42
	Cu	⊙					0.66	0.78	0.90	1.03	1.17	1.29	1.42
	Cb, Cu & Sc	(⊙)°				0.20	0.24	0.29	0.33	0.38	0.42	0.47	0.51
$\frac{10}{10}$	Ci & Ci, Cs	⊙	0.06	0.15	0.25	0.35	0.46	0.56	0.66	0.77	0.86	0.94	0.98
10	Cs & Cs, Ci	(⊙)	0.06	0.14	0.24	0.34	0.45	0.55	0.66	0.74	0.79	0.84	0.88
		(⊙°)	0.04	0.09	0.16	0.22	0.28	0.34	0.41	0.47			
$\frac{10}{10}$	Ac & Sc	(⊙)	0.06	0.16	0.27	0.38	0.48	0.59	0.69	0.80	0.93	1.04	
$\frac{10}{10}$	Cb, Cu & Sc	⊙°		0.10	0.15	0.21	0.27	0.32	0.38	0.43	0.48	0.53	0.58
10	Ac & Ac, Cu	(⊙°)				0.19	0.28	0.37	0.45	0.53	0.60	0.67	
	Sc & Sc, Cu	(⊙°)				0.19	0.24	0.29	0.35	0.42	0.49	0.55	

REMARKS: Indication of sunshine in parentheses denotes approximate values for certain solar altitudes in the Table.

The accumulation of experimental data leads to the necessity of analytically defining the relation between total radiation and cloudiness. The formula, suggested by Ångström relates 24-hr amounts of total radiation in cloudiness and without clouds with respect to duration of sunshine in the following manner, viz ;

$$\Sigma Q_g = \Sigma Q \left[1 + (1-\eta) \frac{s}{s_0} \right], \tag{7.3}$$

where ΣQ_g, ΣQ are the diurnal amounts of total radiation in cloudy and clear sky respectively ; s, s_0—actual and probable periods of sunshine in hours; and $\eta = 0.235$. Ångström's formula was later defined more accurately for different geographic positions [62, 72, 77].

On the basis of observed data S. I. Savinov [52, 53] suggested the following formula :

$$Q = S\,(1-\alpha)\,(1-c\bar{n}), \tag{7.4}$$

where S—direct solar radiation in clear sky, $\bar{n} = 1 - \bar{S}$, $\bar{S}$—ratio of true observed amount of direct solar radiation to the possible amount in a clear sky, c=constant, $\alpha = \frac{D}{S}$, where D—scattered radiation in clear sky.

Savinov-Ångström's formula given below is applied most often in climatological computations for the determination of the amount of total radiation :

$$\Sigma Q_g = \Sigma Q\ [1-(1-k_g)n_g], \tag{7.5}$$

where ΣQ_g and ΣQ are the actual and probable amounts of total radiation; $k_g = Q_1/Q$ is an empirical coefficient defining the transmission of short-wave radiation in clouds, and n_g is mean degree of cloudiness in fractions of unity.

The computations carried out by T. G. Berlyand [9] provided information about the variation in coefficient k_g with respect to the latitude of the locale which brought about a change in a number of factors, especially the physical properties, form and density of cloudiness, solar altitude and albedo value. Table 7.11 shows only the general picture of the variation in coefficient k_g with latitude which, however, varies not only with latitude but with the time of year, and similarly with longitude and altitude above sea level and with respect to the form of clouds.

Table 7.11 Variation in coefficient K_g with latitude [9]

φ	75	70	65	60	55	50	45	40
k_g	0.55	0.50	0.45	0.40	0.38	0.36	0.34	0.33
φ	35	30	25	20	15	10	5	0
k_g	0.32	0.32	0.32	0.33	0.33	0.34	0.34	0.35

The values of coefficient k_g for nine places in the Soviet Union (Table 7.12), arising from the data on observation for total radiation, were computed by E. P. Barashkova [3] using the improved formula of Savinov-Ångström (7.5).

Observations made in the mountain region showed that the coefficient k_g rises with elevation. This is clearly manifested in the winter months, since the presence of snow increases the reflection of shortwave radiation (Table 7.13).

On the basis of observations made in the Alps, J. Dirmhirn [65] suggested the application of the following formula for the determination of values of coefficient k_g with respect to altitude H of the point of observation above sea level :

$$k_H=0.01\ (21+0.03H). \tag{7.6}$$

For conditions in the Caucasus and Tyan' Shan', Borzenkov [11] modified the relation suggested by Dirmhirn and computed coefficient k_H according to the following relation :

$$k_H=0.01\ (k_0+0.05H), \tag{7.7}$$

where k_0 is value of k_g at ground level, which rises with increasing latitude and attains a maximum value beyond the Arctic circle.

It was established by Marshunova [42] from data on computations at Arctic stations that besides latitudinal variation there exists a change in coefficient k_g with longitude. The values of coefficient for conditions in the Arctic region are shown in Table 7.14.

From the observations of diurnal amounts of total radiation measured in Pavlovsk and Sverdlovsk and similarly from the information on cloudiness and atmospheric phenomena from April to October, Gal'perin [16] obtained reasonably complete data on the relation between k_g and mean daily cloudiness for different forms and types of cloud.

The average value $k_g=0.22$, indicated by B. M. Gal'perin for the case of continuous cloudy cover of the lower stratum, corresponds to the value $\alpha=0.23$ obtained by Ångström. According to the observations of Dirmhirn [65] $\alpha=0.22$-0.23 and according to S. Tams [80] $\alpha=0.18$-0.22.

Table 7.12 Mean coefficients k_g in formula of S. I. Savinov [3]

Station	φ	Jan	Feb	Mar	Apr	May	Jun	Jul	Aug	Sept	Oct	Nov	Dec	Year
Tbilisi	41°43′	0.58	0.56	0.60	0.63	0.54	0.51	0.53	0.54	0.52	0.52	0.49	0.58	0.55
Vladivostok	43 07	0.75	0.77	0.63	0.48	0.44	0.42	0.41	0.41	0.46	0.40	0.50	0.70	0.53
Karadag	44 54	0.54	0.60	0.56	0.62	0.64	0.62	0.52	0.51	0.52	0.55	0.53	0.49	0.56
Saratov	51 34	0.70	0.69	0.62	0.59	0.57	0.55	0.65	0.45	0.55	0.50	0.51	0.61	0.58
Irkutsk	52 16	0.64	0.60	0.68	0.70	0.58	0.53	0.51	0.53	0.59	0.69	0.71	0.70	0.62
Kuibyshev	53 15	0.66	0.62	0.60	0.60	0.58	0.42	0.45	0.35	0.39	0.56	0.44	0.60	0.52
Sverdlovsk	56 44	0.76	0.74	0.69	0.59	0.53	0.57	0.52	0.47	0.45	0.44	0.52	0.66	0.58
Voeikovo	59 57	0.42	0.59	0.68	0.52	0.54	0.58	0.56	0.50	0.47	0.31	0.29	0.34	0.48
Yakutsk	62 01	0.77	0.82	0.83	0.74	0.52	0.48	0.43	0.38	0.45	0.44	0.73	0.74	0.61

Table 7.13 Values of coefficient k_H at different elevations in mountains [11]

Station	Altitude, m	Jan	Feb	Mar	Apr	May	Jun	Jul	Aug	Sept	Oct	Nov	Dec	Mean annual values
Makhachkala	34	0.20	0.12	0.31	0.42	0.45	0.41	0.35	0.32	0.12	0.25	0.13	0.15	0.27
Telavi	562	0.27	0.22	0.26	0.35	0.44	0.30	0.32	0.35	0.24	0.21	0.24	0.24	0.29
Tsalka	1469	0.36	0.42	0.21	0.35	0.35	0.30	0.48	0.34	0.30	0.23	0.36	0.33	0.34
Leninakan	1556	0.34	0.32	0.38	0.33	0.57	0.56	0.24	0.41	0.38	0.24	0.28	0.14	0.35
Martuni	2000	0.50	0.54	0.43	0.33	0.39	0.46	0.42	0.38	0.39	0.47	0.44	0.44	0.43
Kazbegi	3650	0.28	0.34	0.47	0.46	0.50	0.53	0.43	0.33	0.46	0.39	0.48	0.35	0.42
Tyan-'Shan'	3600	0.58	0.61	0.70	0.65	0.64	0.44	0.36	0.35	0.29	0.46	0.60	0.64	0.53

Table 7.14 Values of coefficient k_g for computation of total radiation in Arctic region [42]

Station	Mar	Apr	May	Jun	Jul	Aug	Sept	Oct	Nov
Dreifuvushchie	0.85	0.75	0.75	0.70	0.50	0.50	0.70	0.70	—
Tikhaya Bay	0.80	0.65	0.60	0.55	0.40	0.35	0.40	0.50	—
Uedineniya Islands	0.85	0.75	0.70	0.60	0.50	0.40	0.40	0.50	—
Dickson Islands	0.85	0.75	0.70	0.55	0.50	0.45	0.45	0.50	—
Cape Chelyuskin	0.85	0.75	0.75	0.65	0.50	0.45	0.45	0.50	—
Tiksi Bay	0.85	0.80	0.75	0.60	0.50	0.50	0.45	0.45	0.50
Cape Schmidt	0.80	0.75	0.70	0.60	0.50	0.50	0.45	0.45	0.50

Dirmhirn's data virtually coincide with Tams' data for 5 tenths Ac clouds. The value of coefficient k_g he obtained equals 0.85. With an increase in points of cloudiness the coefficient k_g diminishes more significantly than for clouds situated at a lower level.

In Albrecht's formula [61] for computation of radiation, in analogy to the formula [7.5], the coefficient k_g can be evaluated from the relation :

$$k_g = f\left(\frac{n_g}{n_l}\right) \varphi\,(h_m),$$

where $\left(\frac{n_g}{n_l}\right)$ is ratio of total cloudiness to lower, $\varphi\,(h_m)$—mean maximum altitude of the sun for a given month. For the determination of function f and φ Albrecht suggested the following expression :

$$f\left(\frac{n_g}{n_l}\right) = \left(0.615 + 0.157\,\frac{n_g}{n_l}\right)$$

(for $\frac{n_g}{n_l} > 4$ the function maintains a constant value 1.243) and :

$$\varphi\,(h_m) = 0.50 + 0.14 \text{th}\left(\frac{h_m - 34.5^\circ}{17^\circ}\right)$$

The value of functions f and φ are given in Tables 7.15 and 7.16.

All the formulas given above take into consideration the relation between total radiation and mean cloudiness and, as is obvious from the measurement data, the quantity Q undergoes different variation with respect to the stratum of cloudiness. This relation may be expressed in the following form :

$$Q_g = Q\,[1 - (c_l\, n_l + c_l\, n_l + c_u\, n_u)], \tag{7.8}$$

where n_l, n_l, n_u are the amounts of clouds of lower, intermediate and upper layers in fractions of unity ; c_l, c_l, c_u —coefficients of radiation attenuated in clouds of the corresponding layers which may be obtained from the relation :

$$C = \frac{Q - Q_l}{Q_l} \tag{7.9}$$

Here Q_l is the total radiation in continuous cloudiness of the corresponding stratum. Computations provide the following mean values of the coefficients, viz :

Table 7.15 Values of function $f\left(\frac{n_a}{n_1}\right)$ [61]

$\frac{n_a}{n_1}$	0	1	2	3	4	5	6	7	8	9
1	0.772	0.788	0.803	0.819	0.835	0.850	0.866	0.882	0.898	0.913
2	0.929	0.945	0.960	0.976	0.992	1.007	1.023	1.039	1.055	1.070
3	1.086	1.102	1.117	1.133	1.149	1.164	1.180	1.196	1.212	1.227
4	1.242	1.243	1.243	1.243	1.243	1.243	1.243	1.243	1.243	1.243

Table 7.16 Values of function φ (h_m) [61]

h m	φ (h_m)	h m	φ (h)	h m	φ (h)	h m	φ (h)
0	0.365	25	0.428	50	0.601	75	0.638
5	0.368	30	0.464	55	0.617	80	0.639
10	0.375	35	0.504	60	0.627	90	0.640
15	0.386	40	0.543	65	0.632		
20	0.403	45	0.577	70	0.636		

$c_l=0.8$, $c_l=0.5$; $c_u=0.2$ for $h_\odot > 20°$; $c_u=0.4$ for $h_\odot < 20°$.
According to data of Haurwitz [69] using an 11-year period of observations, $c_l \simeq 0.8$; $c_l \simeq 0.5$-0.6.

P. P. Kuz'min [39, 40] and V. S. Samoilenko [54] who used a relation of the following type :

$$Q_g=Q[1-c_l n_l-C_{lu}(n_g-n_l)], \tag{7.10}$$

(where c_{lu}—coefficient for intermediate and upper cloudiness) obtained the following values of the coefficients :

$c_l=0.67$, $c_{lu}=0.14$ (P. P. Kyz'min);
$c_l=0.76$, $c_{lu}=0.37$ (V. S. Samoilenko).

Berlyand and Novosel'tsev [8] theoretically evaluated the magnitude of the coefficients C_l. For clouds of lower stratum with thickness equal to 800 m, $c_l \approx 0.8$ during summertime in the European Territory of the Soviet Union ; moreover, it varies from 0.70 to 0.82 for a variation in solar altitude from 10 to 60°. The value of c_l also increases with an increase in solar altitude ; on an average it equals approximately 0.5. For cloudiness of upper stratum :

$c_u=0.4$ for $h_\odot=10°$; $c_u=0.3$ for $h_\odot=30°$; and $c_u=0.2$ for $h_\odot=50°$.

The computed values of coefficients are in close agreement with the empirical values given above.

An analysis of the results of observations shows that the dependency on the degree of cloudiness is not linear. In view of this Berlyand [9] suggested the use of a quadratic relation for the computation of the amount of total radiation follows :

$$\Sigma Q_g=\Sigma Q[1-(a+bn_g)n_g], \tag{7.11}$$

where a and b are constants, $b=0.38$, a varies with altitude as shown in Table 7.17.

Table 7.17 Dependence of coefficient a on altitude [9]

$\varphi°$	0	5	10	15	20	25	30	35	40
a	0.38	0.40	0.40	0.39	0.37	0.35	0.36	0.38	0.38
$\varphi°$	45	50	55	60	65	70	75	80	85
a	0.38	0.40	0.41	0.36	0.25	0.18	0.16	0.15	0.14

The application of formula (7.11) guarantees high accuracy in computation.

2.3 The dependence of total radiation on the duration of sunshine

V. N. Ukraintsev [56] studied the relation between total radiation and duration of sunshine with the object of simplifying the evaluation of amount of total radiation and suggested the following formula :

$$\Sigma Q = ms + n, \tag{7.12}$$

where ΣQ is the mean diurnal amount of total radiation on a horizontal surface, s is the duration of sunshine in hours; m, n are empirical coefficients, averaged over altitudes. The mean monthly values of these coefficients are shown in Tables 7.18 and 7.19. The coefficients m and n change in the course of a year and with respect to latitudes. The accuracy of this formula was verified by Berlyand at many places, and thus it was established that the deviations of computed amounts from measured values do not exceed by 5-10% in summer and during winter the difference is somewhat larger.

In analyzing the recordings of actinometric observations for different locations in the USSR, Barashkov [3] showed that the Ukrain-

Table 7.18 Mean monthly values of coefficient m for different latitudes [56]

Latitude	Jan	Feb	Mar	Apr	May	Jun	Jul	Aug	Sept	Oct	Nov	Dec
35° N	28.0	32.0	35.5	39.0	40.0	41.6	42.7	39.3	35.5	30.8	28.6	26.1
40	22.5	27.0	33.5	38.0	37.5	39.5	39.0	36.0	33.4	26.3	23.2	19.4
45	17.5	22.0	30.6	36.5	35.5	36.8	35.0	32.2	30.6	22.7	18.2	14.6
50	13.0	17.0	26.5	33.0	33.3	34.3	31.7	28.1	26.8	20.3	15.2	11.4
55	9.6	14.2	21.9	30.0	31.2	31.8	29.9	26.6	23.8	18.1	12.0	7.6
60	7.0	11.5	17.3	25.2	29.0	29.3	28.6	26.0	21.0	15.7	9.2	4.1
65	—	9.5	13.8	17.7	24.5	25.7	27.0	24.3	17.9	11.6	6.7	—
70	—	—	12.3	12.5	16.0	21.0	23.3	20.6	13.5	7.4	—	—

Table 7.19 Mean monthly values of coefficients n at different latitudes [56]

Latitude	Jan	Feb	Mar	Apr	May	Jun	Jul	Aug	Sept	Oct	Nov	Dec
35° N	130	160	200	250	280	300	290	270	230	200	140	120
40	100	130	160	200	220	230	220	200	170	150	100	90
45	70	100	130	160	180	190	180	170	140	110	80	65
50	50	80	110	150	160	170	160	150	130	100	55	40
55	30	60	100	140	145	160	145	130	120	80	35	25
60	15	42	95	125	135	150	130	110	90	50	20	12
65	—	30	85	190	230	200	160	90	70	40	—	—
70	—	—	85	270	400	300	250	170	100	40	—	—

tsev formula must be correct for computation of the amount of total radiation. The coefficients m and n, for instance, at many locations depend linearly on the solar altitude at midday, determined on the 15th of the month under examination.

S. I. Sivkov [49] suggested a formula which relates the monthly amounts of total radiation to the duration of sunshine in a month S_m and to the solar altitude $h_{\odot noon}$ at midday on the 15th of the month, thus :

$$\Sigma Q = 0.0049\ (s_m)^{1.31} + 10.5\ (\sin h_{\odot noon})^{2.1} \qquad (7.13)$$

This formula enables us to determine monthly amounts Q in the interval of latitude 35-65° within an error of $\pm 10\%$.

The nomogram (Fig. 7.4), constructed according to formula (7.13), can be applied to quickly determine the approximate value of the monthly amounts of total radiation.

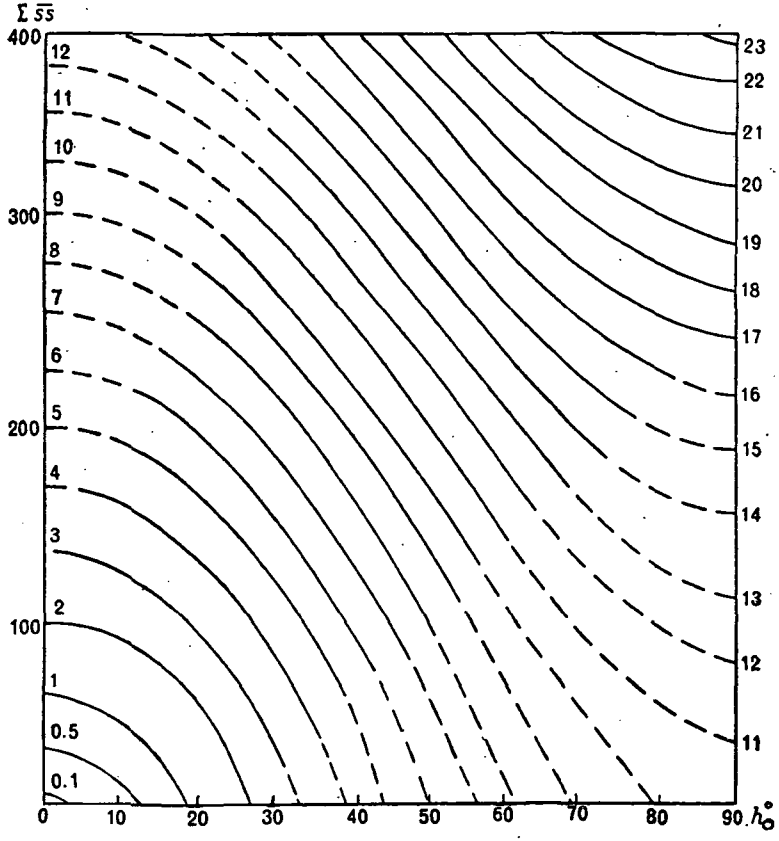

Fig. 7.4. Nomogram for approximate determination of monthly amounts of total radiation [51].

$h_{\odot}^{\circ}$—solar altitude at midday.

2.4 The effect of atmospheric turbidity on total incoming radiation

The variation in the flux of total radiation may be caused not only by a change in solar altitude and cloudiness but also by a change in the optical properties of the atmosphere and underlying surface.

With an increase in transparency the flux of direct solar radiation, appearing as a component part of total radiation, increases, whereas the flux of scattered radiation decreases. However, a decrease in the flux of direct radiation is not fully compensated for an increase in the flux of direct radiation resulting in an increase in the flux of total radiation with increased transparency at all latitudes, with the exception of winter months at high altitudes ($\varphi \sim 70°$). In summer the total radiation increases by 18-22% and in winter by 21-26% for a change in coefficients of transparency from 0.70 to 0.85.

It is possible to see from data in Table 7.20, obtained by Pyatnenkov [45] in the Arctic region, that total radiation changes at constant albedo for a variation in the transparency coefficient from $P_1=0.780$ to $P_1=0.830$ by 0.01 cal/cm^2 · min at $h_\odot=5°$, and for $h_\odot=25°$ by 0.06 cal/cm^2 · min.

Table 7.20 The dependence of total radiation on solar altitude and atmospheric transparency for $A=0.70$-0.90 [45]

P_1	Solar altitude, deg				
	5	10	15	20	25
0.830	0.10	0.25	0.40	0.56	0.71
0.780	0.09	0.21	0.37	0.51	0.65

Insofar as transparency changes with respect to specific local conditions, on account of these variations the latitudinal course of total radiation is altered to a considerable extent. Table 7.21 shows that the difference in coefficients of transparency for places situated almost at the same latitude causes a variation in the flux of total radiation.

Gal'perin [13] showed that a noticeable variation in Q with respect to time, caused by the variation in atmospheric transparency, takes place during the change of seasons. Thus, for instance, in July Q was 97% of average magnitude and in April and October it is 106 and 103% respectively. Variation in atmospheric transparency cause the mean values of total

Table 7.21 Variation in total radiation with respect to variation in atmospheric transparency [1]

Latitudinal zone	Month	Location	Coefficient of transparency P_2	Monthly amount for central zone
55-57°	July	Moscow ($\varphi=55°45'$)	0.760	20910
		Sverdlovsk ($\varphi=56°50'$)	0.792	21710
41-43°	May	Vladivostok ($\varphi=43°07'$)	0.738	20970
		Tashkent ($\varphi=41°20'$)	0.794	22330

radiation to be less in the middle of summer than in early summer when the solar disc is fully uncovered or there is moderate sunshine or cloudiness of 2-3 and 4-5 tenths.

In the case of a clear sky the difference in the flux of total radiation on account of variation in transparency may be about 12%, for 6 tenths cloudiness it is approximately 38%, and under continuous cloud it can become 68%.

Averkiev [1] examined the question of variation of total radiation in the case of a clear sky depending on the variation in atmospheric transparency in different months for latitudes of 40, 50, 60 and 70°.

The greatest absolute variations in total radiation with respect to the turbidity factor occur at high solar altitudes. For instance, at $h_\odot = 41.7°$ ($m=1.5$) a variation in the turbidity factor between 2 and 4 leads to a change in the intensity of total radiation from 1.03 to 0.88 cal/cm² · min., for $h_\odot = 11.3°$ ($m=5$) the change is from 0.20 to 0.22 cal/cm² · min.

Using actinometric recordings at the networks, Sivkov [49] and Pivovarov [48] obtained the relation between intensity of total radiation and solar altitude at different atmospheric transparencies.

2.5 Variation in total radiation with albedo value of underlying surface

In order to obtain the most accurate values of total radiation it is necessary to take into account the effect of the albedo of the underlying surface on the incident total radiation. In view of this, Averkiev [1] suggested the following formula for computation of total radiation :

$$Q_A = Q\left(\frac{0.96}{1+A\gamma_r}\right), \tag{7.14}$$

where Q_A—total radiation considering albedo of underlying surface A,

Q —total radiation computed by Averkiev for different months,
γ_r —fraction of reflected radiation, returning to the earth,
$\gamma_r = 0.2 + 0.5\, n_g$ (n_g = cloudiness in fractions of unity).

It is especially important to consider the effect of albedo in the presence of snow cover. This is illustrated in the data of Pyatnenkov [47] (Table 7.22).

Table 7.22 Dependence of total radiation upon $h_\odot$ and albedo of underlying surface [45]

P_1		Altitude of the sun, deg							
		5	10	15	20	25	30	35	40
830	Q_1	0.10	0.25	0.40	0.56	0.71	—	—	—
	Q_2	0.08	0.21	0.34	0.49	0.63	—	—	—
	Q_1/Q_2	1.25	1.19	1.18	1.14	1.13	—	—	—
780	Q_1	0.09	0.21	0.37	0.51	0.65	0.76	0.93	1.06
	Q_2	0.07	0.18	0.32	0.45	0.58	0.71	0.83	0.96
	Q_1/Q_2	1.28	1.17	1.16	1.13	1.12	1.11	1.11	1.10

REMARKS: Q_1 at A=0.70-0.90; Q_2 at A=0.08-0.20.

This dependence is more distinctly observed in probable monthly amounts of total radiation. Thus, for instance, P_1=0.780 at constant coefficient of transparency, but at different albedo values it was shown that:

A=0.70-0.90 $\qquad \sum_{VI} Q = 26.3$ kcal/cm^2 · mon.

A=0.08-0.90 $\qquad \sum_{VI} Q = 22.9$ kcal/cm^2 · mon.

i. e. on account of an increase in albedo the probable amount Q rose by 15%.

Fig. 7.5 shows the variation of intensity of total radiation with respect to altitude of sun $h_\odot$, atmospheric transparency P and albedo A.

It is necessary to take into consideration the magnitude of the area whose albedo influences the incident total radiation while evaluating albedo values. The albedo value of the surface entering into the formula (7.14) represents a mean value of albedo for a particular region, surrounding the point of observation with a radius given by:

$$r = 2h_g \tan \varphi,$$

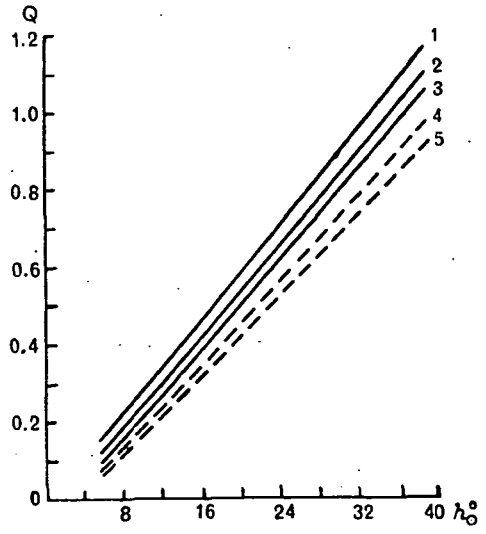

Fig. 7.5. Dependence of total radiation $h_\odot$, P_1, and A, in clear sky [47].
At A=0.70-0.90; (1) P_1=0.860, (2) P_1=0.800, (3) P_1=0.740;
At A=0.08-0.20; (4) P_1=0.800, (5) P_1=0.740.

where h_g —height of cloudiness, φ—angle between the normal and the direction of the segment of cloudy layer from which reflected radiation is admitted.

If $h_g = 4$ km, then $r \approx 35$ km, and when $h_g \cong 2$ km, $r \approx 15$-20 km.

These values are extremely important for stations located on islands where albedo possesses two values in the vicinity of the dividing line between land and sea. Computations for the case of a cloudy sky enabled Pyatnenkov to determine the distance r_m, for which the influence of the albedo of any underlying surface (in particular, sea) will be maximum. For $r_m = 500$ m (i.e. instrument is situated at a distance of 500 m from the sea) the magnitude of the influence of sea albedo on incident radiation is 8-10%, at $r_m = 50$ m, it is 35-40% whereas the influence of sea albedo disappears at r_m = 2-3 km.

3. VARIATION OF TOTAL RADIATION WITH ALTITUDE

3.1 Vertical distribution of total radiation in clear sky

Observations on net radiation and its constituents, primarily total and reflected shortwave radiation, were similarly carried out from airplanes and free balloons [5, 6, 12, 17, 18, 20, 22-24, 27-29, 36, 41, 46, 51, 57, 58, 60, 67, 68, 75, 76].

The aim of these investigations consists in studying the attenuation factors of shortwave radiation in the atmosphere and obtaining information about the magnitude of the radiation flux of heat due to shortwave radiation at different levels in the atmosphere.

Scientists in the USSR employed standard actinometric instruments for measurements of radiation flux. They devised special methods of measuring and handling of data, of studying the characteristics of the instruments under varying conditions of the surrounding medium. Many difficulties and errors arises in the application of standard actinometric apparatus for measurements in free atmosphere. For their construction the following had to be taken into consideration : receiving surface of the instrument is not horizontal, optical inhomogeneity of the underlying surface, the dependence of the apparatus on temperature and pressure of air, the effect of the reflection of radiation from the frame of the airplane or balloon, variation of zonal and spectral distribution of the radiation flux, difference in the temperature regime of the radiation receptor and galvanometers, and similarly obtained results of variation with respect to time.

The most elaborate method of airplane measurements with the help of pyranometers was developed by Kastrov [20, 21, 58]. In order to include the variation in flux of total radiation caused by a change in solar altitude, the measured shortwave flux is derived at a given time according to the following empirical formula :

$$F^{\downarrow}_{\odot} = \frac{F^{\downarrow}_{sw}}{S^{*}_{0} \sin h_{\odot}} = a - b\sqrt{m}, \qquad (7.15)$$

where $m = \operatorname{cosec} h_{\odot}$ is the atmospheric mass in the direction of the sun, $F^{\downarrow}_{sw}$ — downward flux of shortwave radiation, S^{*}_{0} —solar constant for a given day, $h_{\odot}$ — altitude of the sun, a and b are empirical constants. It is necessary to have data on measurements at one level for different values of m in order to determine a and b. The number of atmospheric masses for an arbitrary height H above the surface can be determined from the following relation :

$$m_{H} = m_{0} \frac{p_{H}}{p_{g}},$$

where m_0, p_0 are the number of atmospheric masses and pressure of air at the surface, p_H is the pressure of air at the level H.

The suggested method of deduction can be employed only in the case of a clear sky. The appearance of large optical inhomogeneity in the atmosphere introduces significant errors in the data derived.

Airplane measurements at moderate and high altitudes show that flux of total radiation in the troposphere rises according to the elevation by 0.05 kcal/cm² · min for 1 km; moreover, this gradient decreases slightly with altitude.

Pyatovskaya [46] carried out numerous measurements on the flux of shortwave radiation in the lower stratum of the troposphere over various homogeneous surfaces at all seasons of the year in the case of a clear sky and in cloudiness of not more than 2 tenths. Measurements showed that the total radiation almost always increases with altitude, a decrease being observed only when the sun is covered by invisible cirrus clouds. The gradient of total radiation for layers of 0-1, 1-2, 2-3 km and for distinct seasons of the year according to data from flights is given in Table 7.23. From the Table it is obvious that the gradient of total radiation decreases with altitude, viz. in the layer between 0-1 km it constitutes on an average 0.076 cal/cm² · min · km, in the layer between 2-3 km it is 0.034 cal/cm² · min · km. ΔQ is considerably higher in spring and summer than in autumn and winter.

Table 7.23 The gradient of downward flux of radiation according to seasons (cal/cm² · min · km) [46]

Season	Thickness of layer, km			
	0-1	1-2	2-3	0-3
Winter	0.045	0.046	0.021	0.037
Spring	0.115	0.050	0.015	0.060
Summer	0.120	0.078	0.070	0.089
Autumn	0.052	0.036	0.028	0.039
Mean	0.076	0.052	0.034	0.056

Early actinometric measurements with airplanes and balloons enabled scientists to obtain an idea of the variation in radiative fluxes only in the lower part of atmosphere, up to 5-8 km. Wider possibilities opened up with balloon probing. The elevation of the actinometric apparatus [27-29] in unmanned balloons to a height of 25-30 km enabled scientists to obtain complex information about profiles of radiation fluxes and meteorological elements, and similarly to explain the relation between them and estimate the influence of cloudiness on radiative fluxes.

The vertical profiles of total radiation for clear days (Fig. 7.6) can be divided into three series; viz. the upper curves relative to flights

conducted under high sun ($h_{\odot}$=52-60°) ; i.e. when the variation in the altitude of the sun is 4-5° in the course of the flight. The two lower curves, being the vertical profiles of Q, were obtained at an earlier hour than the first, when $h_{\odot}$ changed by 10° in the course of the flight. The value of the flux of total radiation is slightly less in this case, and the variation in the entire flight constitutes at most about 0.5 cal/cm² · min. The third series of curves refers to a low position of the sun around 19.5° and 17°. In these flights the altitude of the sun varied by approximately 1° during the time the apparatus was airborne. The greatest variation in total radiation, in the lower stratum of probing, was caused by high turbidity in the lower layers of the atmosphere and attenuation of solar radiation in fog.

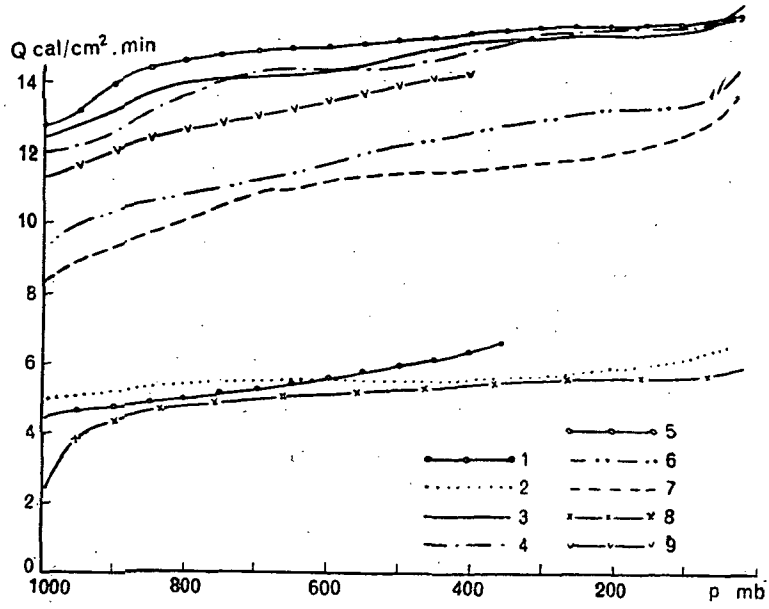

Fig. 7.6. Vertical profiles of total radiation in case of clear sky [28]
(1) June 7, 1961; (2) Nov 14, 1961; (3) May 25, 1962; (4) May 30, 1962; (5) June 12, 1962; (6) July 7, 1962; (7) July 12, 1962; (8) Nov 22, 1962; (9) July 19, 1963.

The total radiation increases with the range of elevation of the apparatus. However, the gradient varies considerably with height. If it constitutes about 0.25 cal/cm² · min for the first series of curves in the lower layer at 500 millibars, then it diminishes to half its value for the 500-15 mb layer. The variation in gradient Q is connected not only with the height of the apparatus, but also with the variation in solar altitude during the time of the flight. The value of the flux of total radiation

decreases along with a diminution in $h_\odot$ in the course of the entire flight. Q varies approximately by 0.36 cal/cm² · min on the variation of $h_\odot$ by 5° and for $\Delta h_\odot = 10°$ it varies by 0.52 cal/cm² · min.

According to the data of Pyatovskaya [46], the relation between Q and $h_\odot$ at different levels is not linear, and the change of total radiation at different levels for low solar altitudes ($h_\odot < 20°$) is considerably less than at large angles. Attenuation of total radiation in the 0-3 km layer constitutes on an average 0.18 cal/cm² · min.

Information about total radiation up to a height of about 30 km obtained by a group of researchers [27-29] remains unsupplemented and it is not possible to carry out a comparison with data for other geographical locations but it should be observed that the value of the flux of total radiation in 1.28 cal/cm² · min obtained by L'vova [41] at a height of 14.9 km for $h_\odot = 48°$, corresponds to the data from one of the flights described in [28] in which the value of the flux of total radiation constitutes 1.26 cal/cm² · min at a height of about 15 km for the same solar altitude.

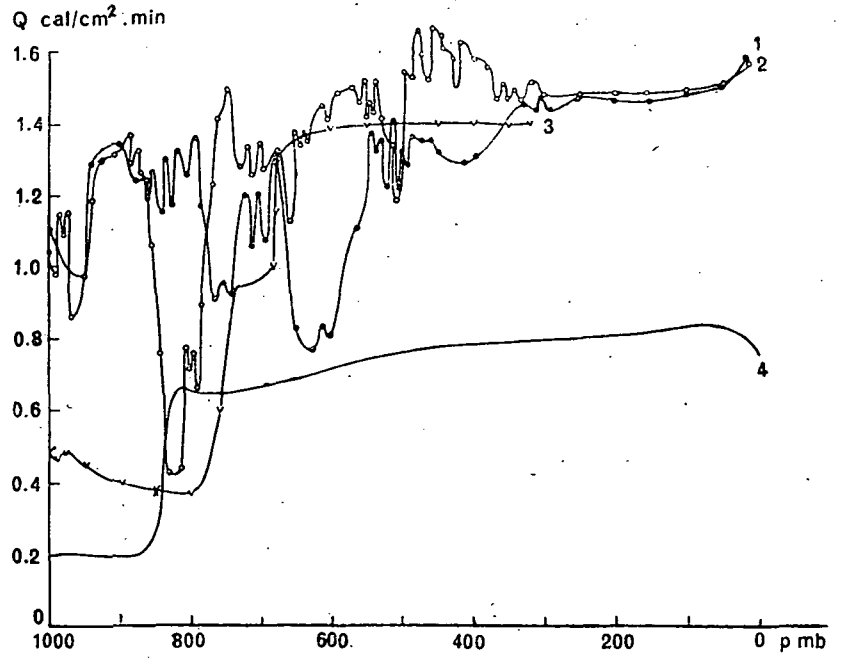

Fig. 7.7. Vertical profiles of total radiation in the presence of cloudiness.
(1) June 22, 1962; (2) July 4, 1962; (3) July 6, 1963; (4) Oct 23, 1964.

3.2 Influence of cloudiness on total radiation in a free atmosphere

In the case of variable cloudiness (Fig. 7.7., curves 1 and 2) it is difficult to talk of any pattern of variation in the flux of radiation with the height. The situation may be simplified if continuous dense cloudiness is observed (curves 3, 4) as happened in the case of the 12th flight (curve 3) carried out on July 6, 1963 when Ci, As and St were observed in an aggregate of 10 tenths cloud in the layer between 1.9 km and 3.1 km, or in the 17th flight (Oct 23, 1964) when continuous stratocumulus cloud was observed in the layer between 1 km and 1.9 km. If in the case of variable cloudiness the total radiation experiences most of the intermittent variations then in the presence of continuous cloudiness Q varies sharply by a factor of one or two depending on the number of cloudy layers. Sharp differences in the values of the flux of total radiation between the 12th and 17th flights were similarly caused by the difference in solar altitudes. In the 12th flight $h_{\odot}=55.2\text{-}60.5°$, and in the 17th flight $h_{\odot}=26\text{-}24°$.

4. RADIATIVE HEATING IN THE TROPOSPHERE AND STRATOSPHERE

4.1 Absorption of shortwave radiation in a free atmosphere

It is possible to estimate the magnitude of absorbed radiation and radiative heating from a knowledge of net radiation and its constituents in the troposphere and stratosphere.

On measuring the upward flux $F_{sw}^{\uparrow}$ and downward flux $F_{sw}^{\downarrow}$ of shortwave radiation at different levels in free atmosphere, it is possible to evaluate the balance of shortwave radiation thus :

$$B_{sw}(z)=F_{sw}^{\downarrow}(z)-F_{sw}^{\uparrow}(z). \tag{7.16}$$

The absorption of radiation in the layer z_1-z_2 will be equal to the difference measured at levels z_1 and z_2 given as follows :

$$q=B_{sw}(z_2)-B_{sw}(z_1). \tag{7.17}$$

The radiative variation of temperature (radiative heating), brought about by absorption in radiation can be determined from the relation :

$$\frac{dT}{dt}=\frac{1}{c_p\rho}\frac{q}{\Delta z}, \tag{7.18}$$

where c_p—specific heat at constant pressure, ρ—density of air.

Going over from altitude to the corresponding values of pressure, and considering $\Delta p = \rho\, g\, dz$ and expressed in cal/cm² · min it is possible to estimate the radiative variation of atmospheric temperature in degrees per hour from the formula :

$$\frac{dT}{dt} = -\frac{0.981 \times 60 \times q}{0.24\ (p_2 - p_1)} = 245\ \frac{q}{\Delta p}. \qquad (7.19)$$

Here p_1 and p_2 are pressures in millibars at altitudes z_1 and z_2 respectively.

These formulas hold good only in the case of horizontal optical homogeneity of the atmosphere and the underlying surface. In reality this condition may not always be observed.

V. G. Kastrov [20] carried out an evaluation of heating in the absence of horizontal optical homogeneity of the underlying surface and atmosphere. If the underlying surface under examination has a high albedo value ($A = 0.82$) and the surrounding surface has rather low albedo values ($A = 0.27$) then the influence of the horizontal optical inhomogeneity of the underlying surface should be considered while working with data at heights above 1 km. If the ratio of albedo values is reversed, then the effect of horizontal optical inhomogeneity is insignificant.

The airplane measurements showed [18] that the effect of optical inhomogeneity is slightly reduced if the measurements are carried out over an underlying surface which has been divided into sufficiently small segments, i.e. 5-10 km.

Actinometric airplane measurements showed that the value of the shortwave radiation absorbed in the lower troposphere varies considerably

Table 7.24 Absorption of solar radiation q according to seasons (cal/cm² · min) [46]

Season	Thickness of layer, km			
	0-1.0	1.0-2.0	2.0-3.0	0-3.0
Winter	0.041	0.028	0.019	0.088
Spring	0.105	0.040	0.014	0.159
Summer	0.105	0.072	0.044	0.221
Autumn	0.028	0.022	0.019	0.069
Mean	0.070	0.041	0.024	0.135

from layer to layer. It is obvious from the data in Table 7.24, obtained by N. P. Pyatovskaya [46], that the radiation absorbed changes noticeably in the course of a year and decreases with height. For a layer of 0-3 km on an average over a year the value of q is 0.135 cal/cm² · min whereas according to the data of N. I. Goisa [17] it is a little less than 0.125 cal/cm² · min.

The fundamental properties of vertical profiles of absorbed shortwave radiation can be determined from measurements of flux absorption from descending radiation in water vapor, aerosol, and clouds, from the variation in the flux of shortwave radiation reflecting the inhomogeneity of the underlying surface and from the atmosphere itself.

According to the data from balloon probing up to an altitude of 30 km [30], in the case of a clear sky and in the absence of strong horizontal heterogeneity the magnitude of absorbed shortwave radiation increases with increasing thickness of the layer of probing. The gradient of absorbed shortwave radiation decreases as the layer of probing increases ; it attains a maximum value in the lower layer of 200 millibars (Table 7.25).

Table 7.25 Absorbed shortwave radiation in layers $p_{1000}-p_z$ [30]

p mb	Flight number						
	1	2	3	4	9	10	11
1000-950	—0.009	0.085	0.051	0.103	0.089	0.060	0.235
1000-900	—0.003	0.116	0.093	0.152	0.128	0.100	0.259
1000-850	0.025	0.142	0.128	0.207	0.158	0.129	0.277
1000-800	0.054	0.166	0.140	0.239	0.170	0.156	0.289
1000-750	0.067	0.180	0.143	0.269	0.183	0.189	0.294
1000-700	0.073	0.185	0.149	0.283	0.201	0.225	0.303
1000-650	0.081	0.185	0.160	0.287	0.213	0.229	0.310
1000-600	0.088	0.177	0.179	0.288	0.235	0.246	0.314
1000-550	0.098	0.159	0.201	0.290	0.261	0.247	0.320
1000-500	0.109	0.141	0.228	0.300	0.277	0.254	0.328
1000-450	0.116	0.125	0.249	0.315	0.289	0.257	0.333
1000-400	0.120	0.115	0.266	0.326	0.302	0.260	0.338
1000-350	0.126	0.102	0.278	0.349	0.321	0.269	0.345
1000-300	—	0.083	0.288	0.377	0.337	0.277	0.350
1000-250	—	0.077	0.293	0.382	0.354	0.284	0.355
1000-200	—	0.076	0.291	0.385	0.362	0.299	0.355
1000-150	—	0.077	0.285	0.378	0.362	0.315	0.365
1000-100	—	0.102	0.278	0.369	0.362	0.329	0.354
1000-50	—	0.136	0.303	0.340	0.379	0.356	0.363
1000-15	—	0.148	0.350	0.286	0.413	0.395	0.376

The vertical profile of absorbed radiation, computed for 50 millibar layers, is considerably more complex. The highest values of absorbed radiation have been recorded in a lower layer of 50 mb. Sometimes they can be replaced by the minimum values in the neighboring 50 mb layer (Fig. 7.8). To some extent this is explained by the fact that detailed vertical profiles of heat flux and the quantity q refer to layers in which the absorbing mass decreases with altitude ; moreover, in the given case the influence of horizontal optical heterogeneity is considerable.

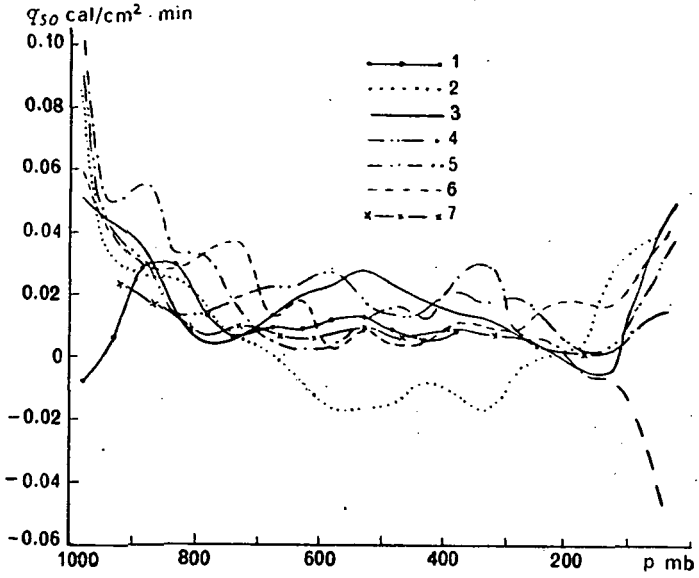

Fig. 7.8. Vertical profiles of absorbed radiation [31].
1—For conditions of cloudiness see Fig. 7.6.

In spite of considerable differences between distinct profiles it is obvious that the layer 1000-800 mb most strongly absorbs shortwave radiation.

A noticeable inhomogeneity of the underlying surface and considerably distorted vertical profile of shortwave balance can lead to the appearance of negative values of q_{50}. This has no physical significance and once again confirms the necessity of formulating a more refined method of measurement and computation (at the time of ascent the balloon may rise to a considerable height above the starting point, and this denotes the fact that the optical properties of the underlying surface and atmosphere may vary considerably).

Computations on absorption of shortwave radiation in water vapor according to Möller's [73] and Kastrov's [19] formulas, accomplished

by many researchers, showed that basically the observed values considerably exceed the computed values. An increase of measured absorption over absorption on account of water vapor can be caused by the presence of dust in the atmosphere, as shown by Kastrov [20, 22, 58] and other researchers [17, 46, 57]. These investigations showed that the role of dust in overall absorption on an average is the same as that of water vapor. Absorption in dust present in the atmosphere can be greater than the absorption of shortwave radiation on account of water vapor.

Sometimes the values of excessive absorption undergo rather wide variations, for instance, around Minsk in 1951-1953, very large coefficients of absorption in the lower layer (15% in 1 km) were recorded, but in 1955 excessive absorption was not detected [23, 51]. Excessive absorption was not noticed in measurements carried out by Fritz [67] and Berezina [6].

According to the data of Pyatovskya [46] absorption on account of water vapor ΔH_2O decreases with altitude ; it is at a maximum in summer

Tables 7.26 Increase in observed values of absorption of shortwave radiation over values of absorption on account of water vapor in layers with thickness $p_{1000}-p_z$ and 50 mb [31]

Δp mb	Flight number				Δp mb	Flight number			
	3	4	9	10		3	4	9	10
	$\left(\frac{q}{\Delta H_2O}\right)_{p_{1000}-p_z}$					$\left(\frac{q}{\Delta H_2O}\right)_{50}$			
1000-950	3.5	5.4	5.6	4.6	1000-950	3.5	5.4	5.6	4.6
1000-900	3.8	4.3	4.0	3.9	950-900	4.2	3.0	2.5	3.2
1000-850	3.6	4.2	3.3	3.4	900-850	3.1	3.9	1.8	2.4
1000-800	2.8	3.7	2.8	3.1	850-800	0.9	2.1	0.9	2.2
1000-750	2.3	3.4	2.7	3.0	800-750	0.2	2.0	1.7	2.5
1000-700	2.0	3.0	2.7	2.9	750-700	0.5	0.8	2.5	2.6
1000-650	1.8	2.6	2.6	2.6	700-650	0.9	0.2	1.8	0.3
1000-600	1.8	2.3	2.7	2.5	650-600	1.7	0.08	3.8	2.1
1000-550	1.9	2.1	2.8	2.4	600-550	2.2	0.2	3.9	0.2
1000-500	2.0	2.0	2.7	2.3	550-500	3.3	1.0	1.8	1.0
1000-450	2.0	2.0	2.6	2.2	500-450	3.0	1.7	1.2	0.4
1000-400	2.1	2.0	2.5	2.1	450-400	5.7	1.6	2.2	0.6
1000-350	3.2	2.1	2.6	2.1	400-350	10.0	5.2	6.3	2.2
1000-300	2.3	2.2	2.7	2.1	350-300	12.5	9.6	8.0	2.0
1000-250	2.3	2.2	2.8	2.1	300-250	0.0	3.1	24.3	1.9
1000-200	2.3	2.2	2.9	2.2	250-200	—2.8	—3.8	6.2	6.2
1000-150	2.2	2.2	2.8	2.2	200-150	—6.7	—10.0	0.0	3.2
1000-100	2.1	2.1	2.8	2.3	150-100	—3.9	—22.5	0.0	14.0
1000-50	2.3	1.9	2.8	2.4	100-50	2.3	—12.1	4.2	5.4
1000-15	2.4	1.5	2.8	2.4	50-15	5.0	—3.4	2.6	2.6

and at a minimum in winter. Taking the average over a year for the layer 0-3 km ΔH_2O comprises 0.042 cal/cm^2 · min.

The computations obtained in [30] showed a noticeable increase in measurement of absorbed radiation over the calculated values. Measured absorption in shortwave radiation is greater than ΔH_2O by 1.8-5.6 times. The most excessive absorption occurs in the lower layers of the atmosphere, from 50-200 mb in extent (Table 7.26). Further increase in the thickness of the layer changes the ratio $q/\Delta H_2O$ very little.

In the case of layers at 50 mb, the increase in observed values of absorbed shortwave radiation over radiation absorbed in water changes noticeably from layer to layer and even changes sign. On the one hand this is connected with a horizontal optical inhomogeneity of the atmosphere and the properties of the vertical distribution of moisture, and on the other hand with the defects in the methods of determining radiation.

The values of $q/\Delta H_2O$, obtained by Pyatovskaya [46] for the lower troposphere, decrease with altitude and change unnoticeably with season. Averaged over a year this ratio equals 3.2.

4.2 Radiative heating of the troposphere and stratosphere

Absorption of shortwave radiation by the atmosphere leads to the heating of the troposphere and stratosphere. The rate of radiative heating can be evaluated from the relation (7.20). According to data from airplane measurements the values of radiative variations in temperature caused by absorption of shortwave radiation vary within wide limits from 0.01 to 0.3 deg/hr. Kastrov [22] obtained the following values for different layers of atmosphere from the observed data :

$$z_{av} < 1 \text{ km} \quad \frac{dT}{dt} = 0.08 \pm 0.01 \text{ deg/hr}$$

$$1 \text{ km} \leqslant z_{av} \leqslant 3 \text{ km} \quad \frac{dT}{dt} = 0.09 \pm 0.01 \text{ deg/hr}$$

$$3 \text{ km} \leqslant z_{av} \leqslant 5 \text{ km} \quad \frac{dT}{dt} = 0.06 \pm 0.01 \text{ deg/hr}$$

The rate of radiative heating changes not only with altitude but also in the course of a year. Pyatovskaya's computations showed that radiative heating comprises 0.10 deg/hr when averaged over a year for the layer 0-3 km; and N. I. Goisa [17] gave values close to this number. Shlyakhov [60] obtained values of radiative heating of air of same order (0.1 deg/hr) through airplane measurements in the Antarctic region. V. I. Belov [5]

obtained a rate of radiative heating of 0.6 deg/24 hrs for coastal regions of the Antarctic region and Antarctic slopes for a layer of 0.2-2 km, and for a layer 3.2-4.0 km a value of 0.4 deg/24 hrs; for sea covered by ice in a layer 0.2-2 km $\frac{dT}{dt}$=0.5 deg/24 hrs, whereas in a layer 2-4 km $\frac{dT}{dt}$ = 0.25 deg/24 hrs.

The values of radiative heating obtained by a group of researchers [24] for a layer of atmosphere of 0.5-5 km in the region of the spectrum 0.3-2.5 μ, varied within the limits 0.09-0.23 deg/hr and worked out at 0.13 deg/hr when averaged over all flights. These data are in close agreement with the data of Roach [75]. Radiative heating equals 0.16 deg/hr in the region of the spectrum 0.6-0.25 μ.

The values of radiative heating, according to data obtained in high altitude actinometric probings (Table 7.27), decrease in proportion to an increase in the layer of probings. Only in the case of a very dusty lower layer of probing does an increase in heating occur, and it becomes practi-

Table 7.27 Radiative temperature variations (deg/hr) on account of absorption of shortwave radiation in layers $p_{1000}-p_z$ [30]

p mb	Flight number						
	1	2	3	4	9	10	11
1000-950	—0.033	0.298	0.201	0.436	0.404	0.294	0.323
1000-900	—0.006	0.237	0.203	0.343	0.301	0.245	0.529
1000-850	0.037	0.204	0.194	0.321	0.250	0.211	0.399
1000-800	0.061	0.185	0.162	0.282	0.204	0.191	0.321
1000-750	0.062	0.163	0.134	0.255	0.176	0.185	0.267
1000-700	0.056	0.142	0.117	0.225	0.162	0.184	0.232
1000-650	0.054	0.122	0.108	0.196	0.147	0.160	0.205
1000-600	0.052	0.103	0.106	0.173	0.142	0.151	0.183
1000-550	0.051	0.083	0.106	0.155	0.141	0.134	0.167
1000-500	0.052	0.066	0.109	0.144	0.135	0.124	0.154
1000-450	0.050	0.054	0.108	0.138	0.128	0.114	0.143
1000-400	0.048	0.045	0.106	0.131	0.122	0.106	0.134
1000-350	0.046	0.037	0.103	0.130	0.120	0.101	0.126
1000-300	—	0.028	0.099	0.130	0.117	0.097	0.119
1000-250	—	0.024	0.094	0.123	0.115	0.093	0.113
1000-200	—	0.023	0.088	0.117	0.110	0.092	0.106
1000-150	—	0.022	0.081	0.108	0.104	0.091	0.100
1000-100	—	0.027	0.075	0.100	0.098	0.090	0.094
1000-50	—	0.034	0.077	0.087	0.097	0.092	0.092
1000-15	—	0.037	0.086	0.071	0.103	0.098	0.091

cally stationary at higher altitudes, $\frac{dt}{dt}$ varies very markedly in the lower troposphere from flight to flight.

The vertical profiles of radiative temperature variation computed for layers of 50 mb (Fig. 7.9) vary widely during transition from one layer to another. The reasons for this variation were discussed above.

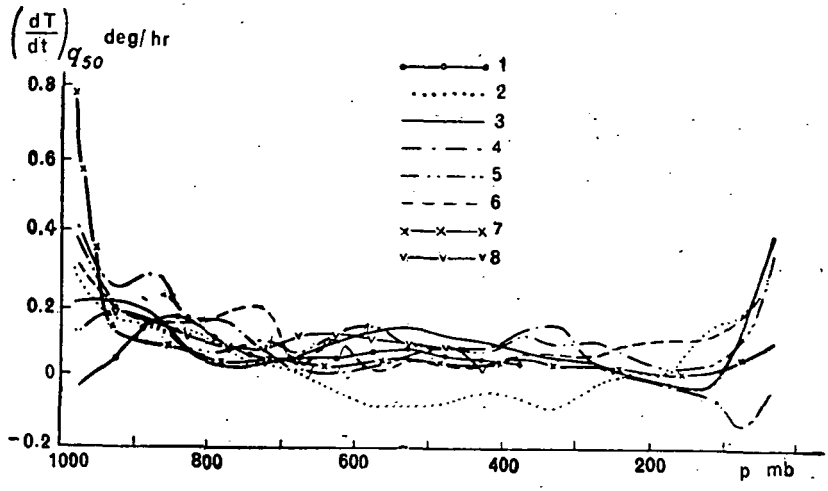

Fig. 7.9. Vertical profiles of radiative temperature variation [30]. **For conditions of cloudiness see Fig. 7.6.**

The results of theoretical computations of the radiative heating of the troposphere from absorption of solar radiation conducted by London [71] give a value of 0.004-0.025 deg/hr for clear sky and 0.004-0.033 deg/hr for a cloudy sky. Moreover a maximum of radiative heating is approximately situated in the zone from 2 to 4 km. Above 5 km the values of radiative heating show a decrease. These maxima cannot be detected from experimental data as shown above.

The radiative temperature variation caused by absorption of radiation in water vapor is considerably less than the observed values. This can be visualized from the data in Table 7.28. The ratio $(dT/dt)\, q_{50}/\left(\frac{dT}{dt}\right)_{H_2O_{50}}$ changes within wider limits than the ratio $(dT/dt)q/(dT/dt)_{H_2O}$ and even changes sign. This occurs due to the fact that in the higher layer of atmosphere the absorption of radiation from water vapor is very small, but from measurement of data it becomes noticeable. The radiative heating of water vapor comprises in all a thousandth part of a degree in an hour.

Table 7.28 Increase in the observed radiative heating over radiative heating due to absorption of shortwave radiation in water vapor in the layers $p_{1000}-p_z$ and 50 mb thickness [31]

Δp mb	Flight number				Δp mb	Flight number			
	3	4	9	10		3	4	9	10
	$\left(\frac{dT}{dt}\right)_q / \left(\frac{dT}{dt}\right)_{H_2O}$					$\left(\frac{dT}{dt}\right)_{q_{50}} / \left(\frac{dT}{dt}\right)_{H_2O_{50}}$			
1000-950	3.3	4.4	4.7	3.8	1000-950	3.3	4.4	4.7	3.8
1000-900	3.6	3.5	3.4	3.2	950-900	3.8	2.3	2.1	2.6
1000-850	2.8	3.6	2.7	2.8	900-850	2.8	2.9	1.5	2.0
1000-800	2.4	3.2	3.2	2.5	850-800	0.8	1.8	0.8	1.9
1000-750	2.2	2.7	2.9	2.4	800-750	0.2	1.6	1.6	2.2
1000-700	1.8	2.4	2.7	2.4	750-700	0.5	0.7	2.4	2.4
1000-650	1.8	2.3	2.5	2.4	700-650	0.9	0.2	1.7	0.3
1000-600	1.9	2.3	2.5	2.9	650-600	1.7	0.07	3.6	2.1
1000-550	2.0	2.1	2.3	2.3	600-550	2.3	0.2	3.8	0.2
1000-500	2.1	2.0	2.0	2.2	550-500	3.1	0.9	1.7	1.0
1000-450	2.8	2.1	2.1	2.2	500-450	3.8	1.7	1.3	0.5
1000-400	2.9	2.2	2.4	2.1	450-400	6.6	1.7	2.2	0.6
1000-350	3.0	2.4	2.6	2.1	400-350	7.2	5.0	7.5	2.2
1000-300	3.0	2.6	2.7	2.0	350-300	11.2	10.4	13.8	2.4
1000-250	2.9	2.5	2.7	2.1	300-250	14.0	3.7	28.6	3.1
1000-200	2.7	2.5	2.5	2.1	250-200	—4.8	4.6	12.0	9.2
1000-150	2.4	2.3	2.4	2.0	200-150	—7.6	—26.5	0.0	8.9
1000-100	2.1	2.1	2.2	2.1	150-100	—5.3	—72.3	0.0	8.7
1000-50	1.8	1.6	2.1	1.8	100-50	8.5	—16.3	13.6	9.8
1000-15	0.7	0.3	0.7	0.8	50-15	3.7	—2.5	2.4	3.0

In computations carried out by Kastrov [20] for data averaged over a year it was shown that $\left(\frac{dT}{dt}\right)_q / \left(\frac{dT}{dt}\right)_{H_2O} = 2.1$, whereas in some cases this ratio attains a value of 6.

N. P. Pyatovskaya [46] obtained a value of this ratio equal to 4.7 when averaged over a year for the layer of less than 1 km, whereas for the layer 0-3 km it is 3.2. Moreover, the ratio $\left(\frac{dT}{dt}\right)_q / \left(\frac{dT}{dt}\right)_{H_2O}$ decreases with altitude from layer to layer in the course of all seasons of the year. This bears witness to the fact that aerosol contributes substantially to the radiative heating.

4.3 Effect of cloudiness on radiative heat inflow

The vertical distribution of radiative fluxes is most markedly distorted by cloudiness.

It is possible to directly determine the amount of transmission, absorption and reflection of solar radiation in clouds through actinometric measurements made from airplanes. Unfortunately, lack of sufficient quantities of experimental data prevents scientists from solving this problem completely.

Sufficiently complete measurements on transmission and absorption of shortwave radiation in stratiformis clouds were carried out by Neuburger [74] in 1948 and by Chel'tsov [59] in 1952. Measuring the upward and downward fluxes of shortwave radiation, Neuburger discovered that for St type of clouds of thickness around 450 m the value of absorbed radiation changes from 5 to 9%.

The measurements of Chel'tsov, conducted for different forms of stratiformis clouds during spring and autumn, showed that the magnitude of transmission of solar radiation is closely connected with the albedo value of clouds and depends on the thickness and form of clouds. For Ac with thickness of 200 m it amounts to 43%, for Sc of the same thickness it is 59%. When the thickness of the layer Sc increases to 500 m the magnitude of transmission diminishes to 24%. The mean values of absorption according to the data from 26 flights carried out by Chel'tsov in Arkhangelsk, is 3.5% and according to data from 16 flights over Moscow it is 7.2%.

This difference in values is caused by an increase in the thickness of the clouds over Moscow. The mean rate of radiative heating, corresponding to the values of absorption obtained, amounts to 0.23 deg/hr for Arkhangelsk, and 0.31 deg/hr for Moscow.

Airplane measurements of total radiation, carried out by Timerev [55] in the Arctic region enabled scientists to evaluate the attenuation of total radiation in clouds from the relation :

$$P_g = \frac{Q_1 - Q_2}{Q_1} \times 100,$$

where P_g is the total attenuation of radiation as a percentage, and Q_1 and Q_2 are the total radiations at the upper and lower boundaries of cloudiness in cal/cm^2 · min respectively.

The magnitude of attenuation of total radiation decreases with the solar altitude and comprises 13% on an average for Ci, Cs; St, Sc—59%; As-Ns and Ac—60% ; As—38% and Ac—37%.

According to Koptev's [36] measurements carried out in the Arctic region, layers of cloud of 10 tenths (Sc and St) of thickness between 200-500 m absorbs 2-8% radiation, and for any increase in liquid phase in clouds

under conditions existing when precipitation occurs, and for clouds of thickness 300-800 m the absorption of radiation rises to 27%.

A magnitude of absorption of radiation around 20% was obtained as a result of three airplane flights carried out by Fritz and MacDonald [68] over complex systems of frontal cloudiness with the upper boundary at the level of 7-8 km.

In one of the flights, carried out by Gaevskii [12] in the summer of 1952, it was shown that Cu cong clouds with lower boundary at a height of 1.3 km and upper boundary at 2.7 km absorb up to 21% of shortwave radiation.

Robinson [76] derived values of approximately the same order. Through airplane measurements he obtained a mean value of absorbed radiation equal to 22%.

Computations carried out in [63] showed that above the peaks of clouds absorption of shortwave radiation is greater than at the same altitude in a clear sky, which in all probability is connected with the increase in moisture in the first case. The absorption decreases below the lower boundary of clouds. Within the clouds it is a little greater than at the same level in a clear sky.

While carrying out an evaluation of the rate of radiative heating for a cloudy sky in the Antarctic region Belov [5] observed that the value of radiative heating above the clouds remains approximately of the same order as in the absence of clouds whereas at the same time below clouds the radiative heating decreases by 1.5-2 times as compared with a clear sky.

The wide variations in the radiation flux during transmission through clouds introduces significant variations in radiative heating, which may change from 0.086 to 0.339 deg/hr at the upper boundary of cloudiness. Moreover, accurate values of absorbed radiation and radiative heating can be obtained only through simultaneous measurements on the upper and lower boundaries of clouds.

The available information on the absorption of shortwave radiation and radiative heating in the case of a cloudy sky indicates a considerable variation in their values.

To a great extent absorption of shortwave radiation and radiative heating depend on the thickness, form, water content and height of clouds, for which accurate values are not always known.

5. INCIDENCE OF TOTAL RADIATION ON AN INCLINED SURFACE

Fluxes of total radiation on an inclined surface can be determined by the same factors as fluxes on horizontal surfaces as well as by the angle

of inclination and azimuth of the surface with respect to the azimuth of the sun. The fluxes of total radiation on inclined surfaces similarly depend on the albedo of the underlying surface and other surrounding objects. The evaluation of fluxes of the total radiation on inclined surfaces is a very complex problem.

In order to determine fluxes of total radiation on differently inclined surfaces it is necessary to use the data for a horizontal surface and the relative values of fluxes for inclined surfaces. The relative values for inclined surfaces can be determined as a ratio of flux of total radiation on a given inclined surface Q_{in} to the flux of total radiation on horizontal surface Q in identical conditions. If the relative magnitudes are to be denoted by k_{in} ($k_{in}=Q_{in}/Q$), then the flux Q_{in} can be determined by the simple relation :

$$Q_{in}=k_{in}\,Q. \tag{7.20}$$

The relative values of the fluxes depend mainly on the solar altitude and orientation of the surface and to a lesser extent on the albedo of the underlying surface and atmospheric transparency. Thus the measurements obtained at one place can be used for any other place, if the albedo

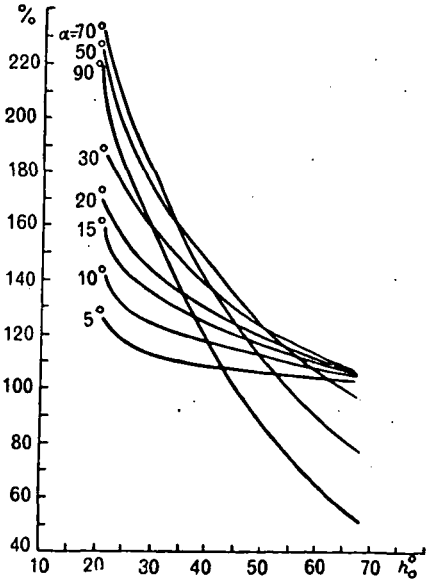

Fig. 7.10. Dependence of magnitude of relative flux of total radiation $\frac{(S+D+r)_{in}\,\%}{S+D}$ on the altitude of sun for slopes with azimuth 180° relative to azimuth of sun in cloudless sky [32].

of the underlying surface does not change too much. In the presence of a snow cover the relative values of fluxes differ noticeably from the values obtained for summer conditions [33]. The relative values of fluxes of total radiation for differently oriented surfaces in clear atmosphere are graphically represented in Figs. 7.10-7.12 [32]. The curves are constructed from measurements at latitude $\varphi = 45°$ N at varying solar altitudes for summer periods. The angles of inclination of the surfaces relative to

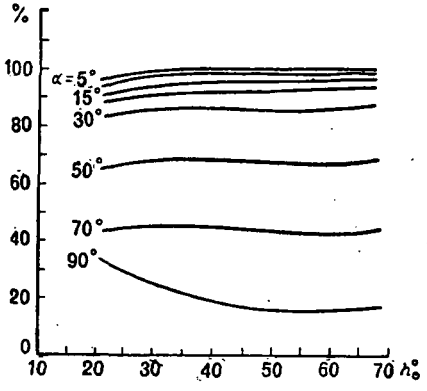

Fig. 7.11. Dependence of values of relative flux of total radiation $\frac{(S+D+r)_{in}\%}{S+D}$ on the solar altitude for slopes with azimuth 90° and 270° [32].

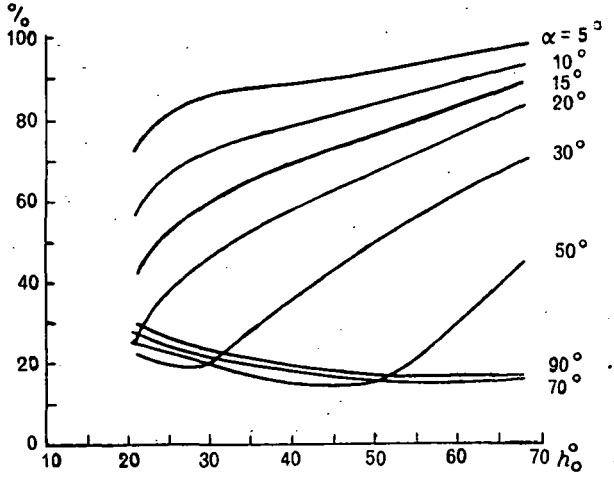

Fig. 7.12. Dependence of values of relative flux of total radiation $\frac{(S+D+r)_{in}\%}{S+D}$ on solar altitude for slopes with azimuth 180° relative to azimuth of sun under cloudless sky [32].

the horizontal plane are marked on the curves. In all the cases, with the exception of slopes inclined toward the South, the incidence of total radiation on the slope is less than on the horizontal surface.

In the presence of a snow cover, when the albedo of the surface is 60-70%, the relative values of the flux of total radiation increase, especially in case of steep slopes [33].

It is obvious from data of Table 7.29 [44] that at $h_\odot > 30°$ southern and eastern (western) slopes, situated at $\varphi = 60°$N, receive more total radiation than horizontal surfaces at solar altitudes $h_\odot < 30°$, only eastern and western slopes receive more total radiation than the horizontal surface.

7.29 Relative values of flux of total radiation Q_{in}/Q on differently oriented surface in a cloudless sky [44]

$h_\odot$°	α°	Slope			$h_\odot$°	α°	Slope		
		southern	eastern and western	northern			southern	eastern and western	northern
50	10	1.13	1.03	0.87	30	10	1.05	1.23	0.94
	20	1.20	1.03	0.73		20	1.05	1.47	0.85
	30	1.26	1.04	0.57		30	1.05	1.62	0.77
	40	1.27	1.04	0.39		40	1.04	1.76	0.67
	60	1.22	0.80	0.18		60	0.90	1.85	0.40
	90	0.97	0.50	0.19		90	0.62	1.71	0.27
40	10	1.08	1.15	0.89	20	10	0.98	1.28	1.01
	20	1.13	1.26	0.76		20	0.95	1.63	0.99
	30	1.16	1.34	0.63		30	0.90	1.92	0.97
	40	1.17	1.41	0.48		40	0.85	2.07	0.91
	60	1.07	1.39	0.23		60	0.67	2.30	0.75
	90	0.79	1.15	0.21		90	0.45	2.21	0.48

Approximate computations on the flux of total radiation on an inclined surface under a clear sky can be made from individual constituents. Thus the flux of direct solar radiation can be computed exactly from the following formula :

$$S_{in} = S\,(\cos\alpha \sin h_\odot + \sin\alpha \cos h_\odot \cos \psi_{in}) \qquad (7.21)$$

where S is flux of direct solar radiation on a perpendicular surface, α—angle of inclination of the surface, ψ_{in}—azimuth of surface with respect to the azimuth of the sun.

The flux of scattered radiation on an inclined surface can be approximately evaluated for the case of isotropically scattered radiation by the following formula :

$$D_{\text{in}}=D\cos^2\frac{\alpha}{2}\ . \tag{7.22}$$

The flux of reflected radiation on an inclined surface for isotropic reflection can be computed from an analogous formula as follows :

$$R_{\text{in}}=R\sin^2\frac{\alpha}{2}\ , \tag{7.23}$$

where R is flux of reflected radiation on horizontal surface.

In reality, the scattered and reflected radiations are essentially nonisotropic. At high solar altitudes, when the fraction of scattered radiation is large, it is necessary to take into account the nonisotropy of scattered radiation. At high solar altitudes the flux of total radiation on slopes can be evaluated by assuming scattered radiation to be isotropic.

The daily course of the flux of total radiation depends mainly on the orientation of inclined surfaces caused primarily by a variation in the angle of incidence of the solar rays. The daily course of total radiation differs considerably for surfaces of different orientation [35]. The maximum for total radiation on southern slopes has been observed at midday. For western and eastern slopes the maximum shifts with respect to midday and the amount of displacement depend on the angle of inclination of the slope. According to observation at 45° N the following relation for shifting of maximum for time Δt to the angle of inclination of the surface α was obtained :

α deg	5	10	15	20	30	50	70	90
Δt hr · min	0:30	1:00	1:15	1:30	2:00	3:00	3:00	4:00

For a vertical surface, oriented toward the north, three maxima of the incident total radiation have been observed ; weakly expressed midday maximum, morning and evening. The last two are caused by the appearance of direct solar radiation and are distinctly expressed.

The daily amounts of total radiation for differently oriented inclined surfaces depend mainly on the orientation of these surfaces, as is evident from the data of Table 7.30 [35]. The values $\Sigma Q_{\text{in}}/\Sigma Q$ for northern slopes are less than unity and decrease with the increasing angle of inclination of the slope α. Southern slopes of a curvature up to 30° receive total

radiation which is almost the same as that for a horizontal surface ($\Sigma Q_{in}/\Sigma Q$ is close to unity). The incidence of total radiation on steep southern slopes decreases considerably as compared with the incidence on a horizontal surface. The eastern and western slopes always receive lesser amounts of total radiation than a horizontal surface.

Table 7.30 Relative daily amounts of total radiation $\Sigma Q_{in}/\Sigma Q$ according to observations in clear sky ($\varphi = 45°$ N, Karadag, 1956) [35]

$\alpha°$	South			East (West)			North		
	Jun 19	Jul 15	Aug 6	Jun 19	Jul 15	Aug 6	Jun 19	Jul 15	Aug 6
5	1.02	1.02	1.05	1.00	1.00	1.01	0.98	0.98	0.97
10	1.03	1.03	1.05	0.99	0.98	1.00	0.95	0.95	0.92
15	1.03	1.04	1.06	0.97	0.96	0.97	0.92	0.91	0.86
20	1.02	1.02	1.07	0.95	0.94	0.94	0.88	0.86	0.82
30	0.98	1.02	1.06	0.90	0.90	0.88	0.79	0.78	0.71
50	0.85	0.91	0.98	0.78	0.78	0.79	0.57	0.55	0.44
70	0.65	0.72	0.80	0.66	0.66	0.67	0.31	0.30	0.24
90	0.42	0.47	0.55	0.52	0.54	0.55	0.24	0.24	0.22

For dense cloudiness (cf. Table 7.32) the difference between $\Sigma Q_{in}/\Sigma Q$ for different days is not great. With increasing angles of inclination of the surface the relative amounts decrease [34]. The data shown in Tables 7.31 and 7.32 are more accurate as compared with data in [34].

Approximate computation of daily amounts of total radiation for differently oriented surfaces can be made from the following formula:

$$\sum Q_{in} = \sum S_{in} + \cos^2 \frac{\alpha}{2} \sum D + \sin^2 \frac{\alpha}{2} \sum R, \qquad (7.24)$$

as suggested by Aisenshtat [2].

The mean monthly and daily amounts of radiation on an inclined surface, computed from a formula analogous to (7.24), are given in Table 7.33 [78]. The amounts are evaluated for surfaces oriented southward at latitude $\varphi = 35°$ N.

The daily amounts of total radiation on an inclined surface oriented southward and computed for clear atmosphere and for $\varphi = 30°$ N are given in [66]. Orientations with respect to all directions of light have been examined for vertical surfaces. In addition, computations for surfaces perpendicular to direct solar radiation have also been made.

Table 7.31 The daily amounts (cal/cm² . day) and relative values of daily amounts of total radiation in a cloudless sky and in the presence of snow cover $\varphi = 60°$ N [34]

Orientation of slope	$\alpha°$	Dec 11, $A=0.97$		Mar 22, $A=0.75$		Mar 26, $A=0.70$		Apr 4, $A=0.80$	
		ΣQ_{in}	$\frac{\Sigma Q_{in}}{\Sigma Q}$	ΣQ_{in}	$\frac{\Sigma Q_{in}}{\Sigma Q}$	ΣQ_{in}	$\frac{\Sigma Q_{in}}{\Sigma Q}$	ΣQ_{in}	$\frac{\Sigma Q_{in}}{\Sigma Q}$
N	15			212	0.67	260	0.67	313	0.92
	30			41	0.13	100	0.26	149	0.44
	45	78.7	0.72	67	0.21	102	0.27	126	0.37
	60	59	0.55	100	0.32	116	0.30	131	0.41
	75	22	0.20						
	90			132	0.42	133	0.35	169	0.50
E	15			369	1.17	382	0.99	404	1.19
	30			288	0.91	348	0.90	350	1.03
	45	44	0.40	408	1.29	380	0.99	476	1.40
	60	62	0.57	401	1.26	415	1.08	374	1.09
	75	63	0.58						
	90			358	1.13	329	0.94	357	1.05
S	15			489	1.54	490	1.27	538	1.58
	30							556	1.63
	45	201	1.86	612	1.93	611	1.59	543	1.59
	60	218	2.02	715	2.96	704	1.83	726	2.14
	75	257	2.37						
	90							550	1.62
W	60	127	1.17	361	1.14	358	0.93	481	1.41
	90			424	1.34	429	1.12	545	1.60

Table 7.32 Daily amounts (cal/cm² . min) and relative values of daily amounts of total radiation in continuous cloudiness and snow cover [34]

Orientation of slope	$a°$	Nov 28, 10/10 St, $A=0.80$		Dec 12, 10/10 St, $A=0.80$		Dec 18, 10/10 St, $A=0.90$		Mar 15, 10/10 St, $A=0.75$	
		ΣQ_{in}	$\frac{\Sigma Q_{in}}{\Sigma Q}$	ΣQ_{in}	$\frac{\Sigma Q_{in}}{\Sigma Q}$	ΣQ_{in}	$\frac{\Sigma Q_{in}}{\Sigma Q}$	ΣQ_{in}	$\frac{\Sigma Q_{in}}{\Sigma Q}$
N	45	16	0.84	17	0.85	16	0.84	67	0.84
	60	12	0.64	13	0.65	12	0.63	52	0.65
	75	13	0.66	13	0.65	12	0.63	66	0.83
E	45	21	1.10	22	1.10	20	1.10	83	1.04
	60	17	0.88	17	0.85	16	0.84	70	0.88
	75	16	0.84	17	0.85	15	0.80	68	0.85
S	45	19	1.00	20	1.00	19	1.00	80	1.00
	60	19	1.00	19	0.95	18	0.90	79	0.99
	75	15	0.80	16	0.80	15	0.80	64	0.80
W	60	16	0.84	16	0.80	15	0.80	65	0.81

Table 7.33 Daily amounts of total radiation (cal/cm² · day) on an inclined surface oriented southward at $\varphi = 35°$ N [78]

$\alpha°$	Jan	Feb	Mar	Apr	May	Jun	Jul
45	376	287	376	388	385	346	367
35	359	284	379	404	411	370	391
25	337	280	375	417	428	391	414
15	303	267	366	418	441	404	428
0	240	234	341	409	447	414	436

$\alpha°$	Aug	Sept	Oct	Nov	Dec	ΣQ_{in}	$\frac{\Sigma Q_{in}}{\Sigma Q}$
45	397	331	315	316	338	4221	1.057
35	408	341	315	308	322	4292	1.074
25	433	345	308	295	299	4322	1.082
15	441	343	299	273	271	4254	1.065
0	438	329	267	227	212	3993	1.000

Errors in the computation of daily amounts of radiation on account of application of isotropic approximation for scattered and reflected radiation are considerably less than for computation of the fluxes of total radiation on an inclined surface.

6. GEOGRAPHIC DISTRIBUTION OF TOTAL RADIATION

The widespread network of actinometric and meteorological stations and the refinement of the method of computation of values of total radiation made possible the construction of distribution charts of solar radiation over the earth. The geographic distribution of average yearly and monthly values of total radiation are shown in 13 charts found in "An Atlas of the Heat Balance of the Earth" edited by Budyko. Computations made at 2,100 places on land and 250 points in the oceans as well as observations at 300 actinometric stations were used in the construction of these charts. The use of this voluminous material covers quite well all the climatic zones of the continents with the exception of high altitude regions.

The computation of monthly values of total radiation can be made according to the formula suggested by Berlyand [9] as follows:

$$Q_g = Q\,[1 - (a + bn)\,n].$$

The values of coefficients a and b are given in Table 7.22. The monthly values were obtained with an accuracy of 8-10% and the annual values 3-4%.

Table 7.34 Total solar radiation in a cloudless sky (kcal/cm². month)

φ°	Jan	Feb	Mar	Apr	May	Jun	Jul	Aug	Sept	Oct	Nov	Dec
90 N	0	0	0.1	10.0	21.9	26.0	23.8	12.9	2.4	0	0	0
85	0	0	0.7	10.2	21.8	25.8	23.4	13.1	3.0	0	0	0
80	0	0	2.4	10.8	21.4	25.2	23.0	13.4	4.3	0.5	0	0
75	0	0.5	4.0	11.7	21.0	24.5	22.2	13.8	5.8	1.3	0	0
70	0	1.6	6.0	13.1	20.5	23.6	21.2	14.6	7.5	2.7	0.5	0
65	0.7	2.8	8.0	14.5	20.1	22.8	21.0	15.6	9.5	4.3	1.4	0.2
60	1.8	4.3	9.9	16.0	20.8	22.9	21.4	16.7	11.3	6.1	2.6	1.1
55	3.1	6.2	11.7	17.3	21.4	23.4	21.9	17.9	12.9	7.8	4.0	2.3
50	4.8	8.2	13.3	18.5	22.2	23.7	22.6	19.1	14.4	9.7	5.8	3.9
45	6.7	10.3	14.8	19.5	22.6	23.9	23.2	20.1	15.8	11.5	7.8	5.9
40	8.8	12.2	16.4	20.3	23.0	24.0	23.4	20.9	17.0	13.2	9.7	7.7
35	10.7	14.0	17.6	21.0	23.0	24.0	23.6	21.6	18.1	14.7	11.4	9.7
30	12.5	15.5	18.6	21.4	23.0	23.8	23.4	21.8	19.1	16.1	13.1	11.5
25	14.1	16.8	19.5	21.6	23.0	23.4	23.1	21.8	19.8	17.4	14.6	13.1
20	15.5	17.9	20.2	21.6	22.5	22.8	22.6	21.6	20.4	18.5	16.1	14.7
15	16.9	19.0	20.8	21.4	21.9	22.0	21.9	21.2	20.9	19.3	17.4	16.1
10	18.1	19.8	21.1	21.2	21.2	21.0	21.1	20.6	21.2	20.1	18.5	17.5
5	19.3	20.4	21.4	21.0	20.2	19.9	20.0	20.0	21.3	20.6	19.5	18.8

Table 7.34—*Contd.*

φ°	Jan	Feb	Mar	Apr	May	Jun	Jul	Aug	Sept	Oct	Nov	Dec
0	20.2	20.9	21.5	20.4	19.3	18.8	19.1	19.3	21.2	21.2	20.4	19.2
5S	20.1	21.4	21.4	19.9	18.3	17.6	17.9	18.3	20.8	21.4	21.8	21.0
10	22.0	21.8	21.1	19.2	17.7	16.3	16.3	17.3	20.4	21.4	21.8	22.0
15	22.6	22.0	20.6	18.3	16.0	14.9	15.4	16.1	19.7	21.3	22.4	22.9
20	23.2	22.0	20.0	17.2	14.7	13.4	13.8	14.9	18.9	21.0	22.6	23.6
25	23.6	22.0	19.4	16.0	13.0	12.0	12.6	13.6	18.0	20.6	23.0	24.1
30	23.9	21.8	18.6	14.9	11.9	10.6	11.1	12.1	17.0	20.1	23.0	24.6
35	24.0	21.3	17.6	13.6	10.4	9.0	9.6	10.6	15.9	19.5	23.0	25.0
40	24.0	20.6	16.4	12.2	8.7	7.3	8.1	9.0	14.3	18.7	22.8	25.2
45	24.0	19.9	15.2	10.7	7.1	5.5	6.3	7.3	13.4	17.7	22.4	25.2
50	23.6	18.9	13.8	9.2	5.4	3.8	4.6	5.5	12.0	16.6	21.8	25.0
55	23.2	17.8	12.3	7.5	3.8	2.3	3.0	3.8	10.3	15.4	21.2	24.6
60	22.6	16.6	10.8	5.6	2.4	1.0	1.6	2.3	8.5	14.1	21.0	24.4
65	22.4	15.3	9.1	3.9	1.1	0.1	0.4	1.0	6.7	12.6	20.8	24.5
70	22.6	14.2	7.3	2.2	0.1	0	0	0	5.0	11.4	21.0	24.9
75	23.2	13.4	5.7	0.9	0	0	0	0	3.5	10.4	21.2	25.4
80	24.0	12.8	4.3	0	0	0	0	0	2.1	9.7	21.9	26.0
85	24.6	12.4	2.9	0	0	0	0	0	0.9	9.2	22.4	26.6
90	24.9	12.3	1.7	0	0	0	0	0	0	9.0	22.6	27.0

The values of Q under conditions of clear sky are given in Table 7.34.

At large and moderate latitudes the zonal nature of the distribution of the annual values of total radiation is observed, whereas in the tropical latitudes the zonal character is destroyed (Fig. 7.13).

The highest values of total radiation can be observed in the high pressure belts of both the hemispheres. The maximum value of Q has been recorded in the North-East of Africa and the central region of Arabia, viz. regions of extremely low cloudiness. The regions of high cloudiness and monsoon climate are characterized by a diminution in the quantity of total radiation. The annual amounts of total radiation change on an average from 60 to 200 kcal/cm^2 · yr over the entire earth.

The distribution of total radiation during the winter months is characterized by a rapid decrease in solar radiation from the equator toward the poles (Fig. 7.14). With increasing latitudes the total radiation changes less in the Southern Hemisphere than in the Northern. The zero isoline passes north of the Northern Arctic Circle, further south its total radiation increases, reaching a value of 22 kcal/cm^2 · mon. The zonal character of isolines of Q is destroyed at low latitudes, and the region of maxima and minima of total radiation coincide with the region of raised and lowered cloudiness. In July a reverse picture has been observed (Fig. 7.15). In the Northern Hemisphere the total radiation changes almost unnoticeably, and in the Southern Hemisphere a rapid decrease in Q with increasing latitudes may be observed.

In March and September the isolines of total radiation qualitatively suggest a distribution shown in the annual chart. In these cases the highest values of total radiation have been similarly observed in regions of tropical deserts. For the remaining months the distribution of total radiation possesses a character intermediate between those indicated above.

The Arctic and Antarctic regions receive a large quantity of heat in the summer months. Here the effect of low solar altitudes is compensated by the considerable length of the day. The monthly amounts Q, obtained in the Arctic region during summer, are close to the values Q for tropical deserts. It is clear from the data in [42] that the annual amounts of total radiation decrease according to the rise in latitude. The values of total radiation are higher in the Eastern Arctic region than in the Western. In the annual course a minimum Q may be observed during the winter months, a maximum in May-June. The longest uninterrupted incidence of solar radiation for the entire earth is enjoyed by the Antarctic Plateau [50] during summer. The monthly amounts of total radiation change from 20 kcal/cm^2 · mon on the coast to 30 kcal/cm^2 · mon on the mainland, which exceeds the values of Q obtained in tropical deserts. The Eastern Antarctic region, lying in the relatively inaccessible polar region, appears

C-6

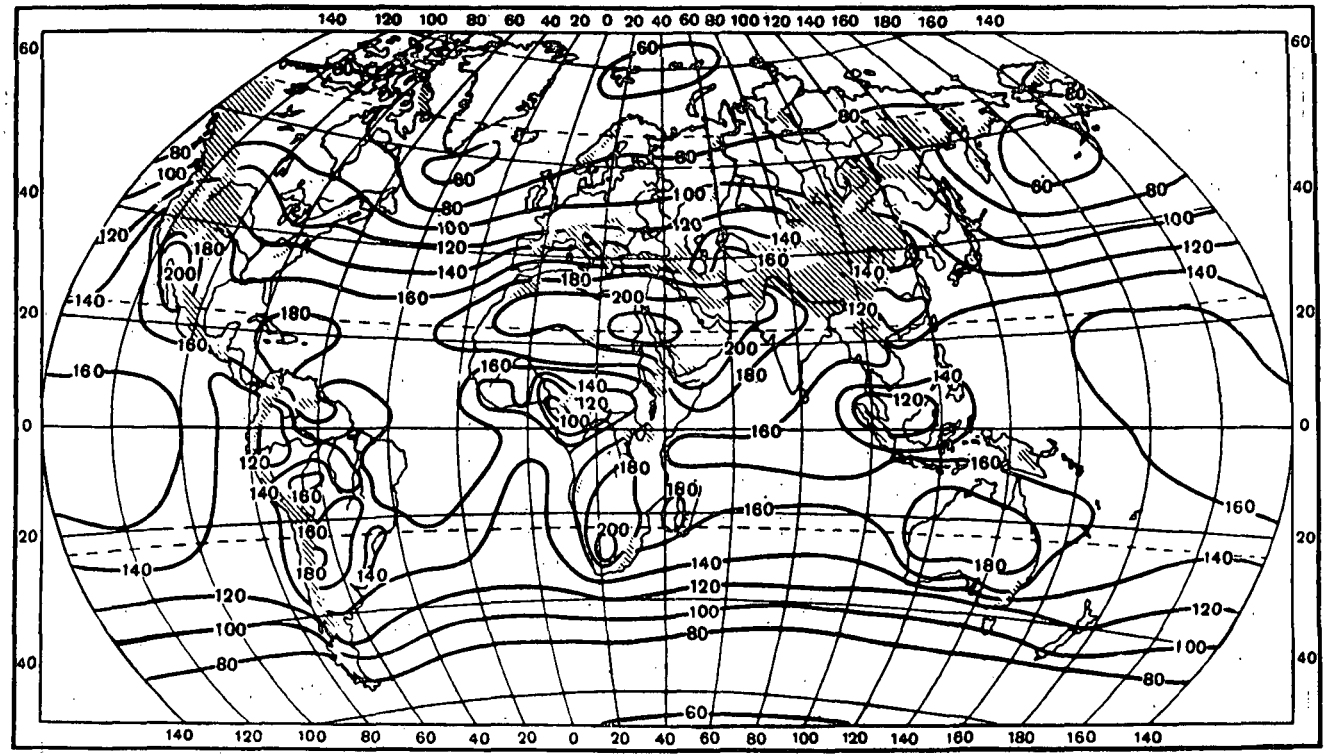

Fig. 7.13. Geographic distribution of mean annual amounts of total radiation.

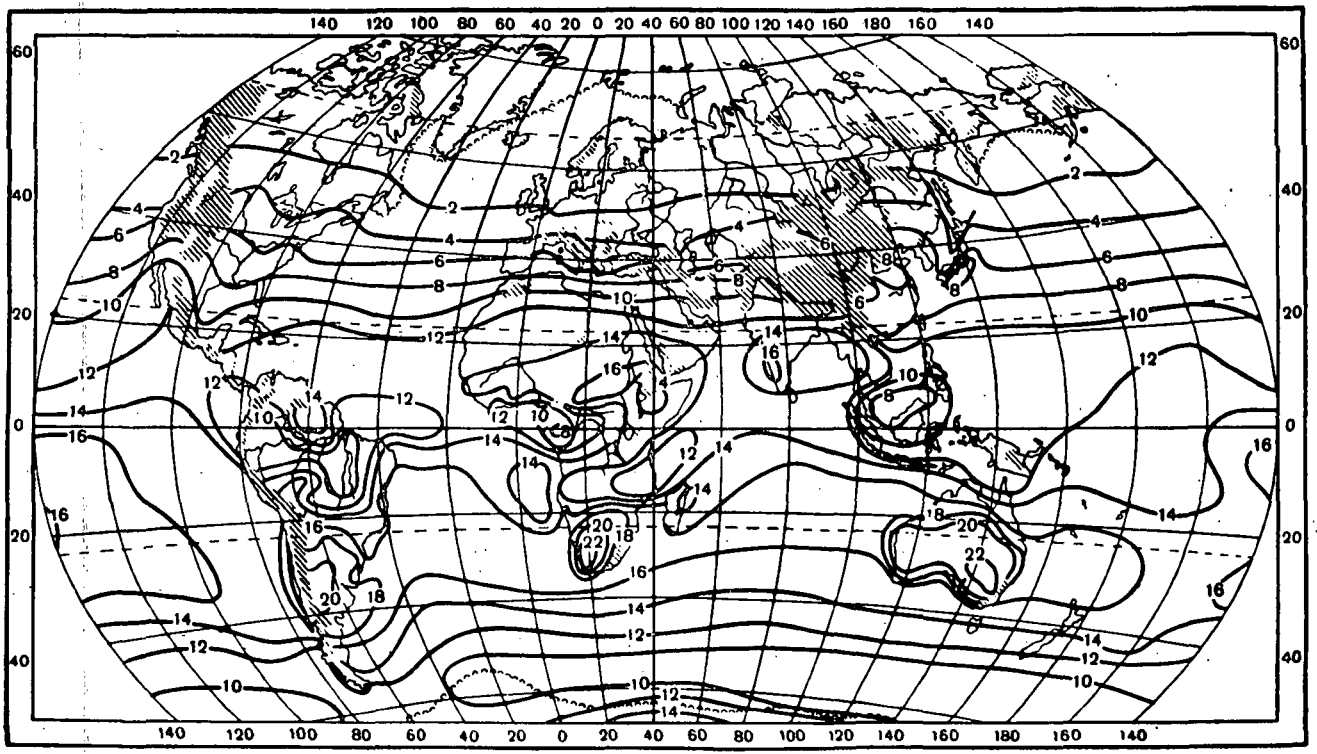

Fig. 7.14. Geographic distribution of mean monthly amounts of total radiation, January.

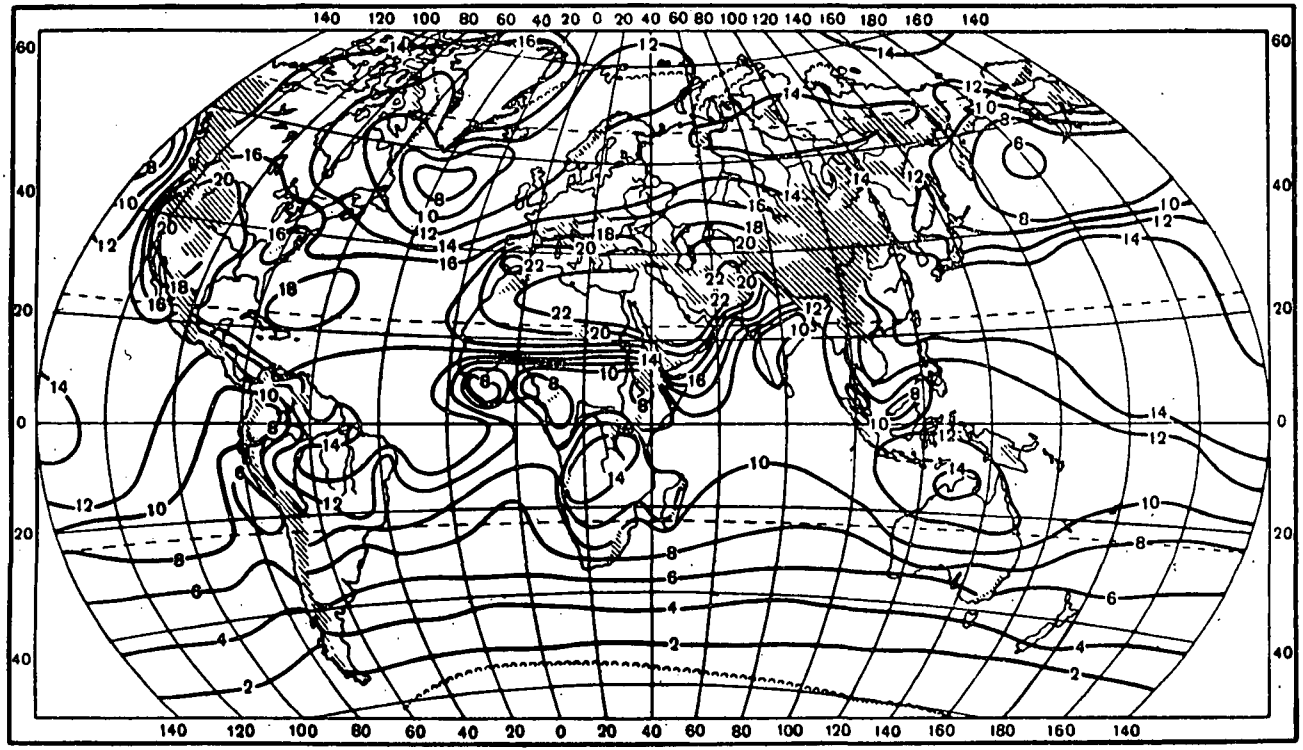

Fig. 7.15. Geographic distribution of mean monthly amounts of total radiation, July.

not only as an absolute pole of coldness but also as an absolute pole of heat of solar radiation. Even though the monthly amounts of total radiation in the course of a year are close to zero in the Antarctic region from one to five or six months, the annual amount Q in Antarctic territory is more than 100 kcal/cm^2 · yr, which turns out to be 20-30% more than the annual amounts for the Arctic region.

It should be recalled that all the given values of monthly and annual amounts represent mean values which may vary considerably from year to year and from month to month. Using uninterrupted observations on solar radiation in the course of sufficiently long intervals of time it is possible to evaluate the variation of the incident solar radiation. From the data on observations at stations situated in different climatic regions of the earth, Berlyand [10] obtained values characterizing the variation of solar radiation. The ratio of the maximum value of incident total radiation to the minimum values was considered an example of this characteristic. The least variability of diurnal amounts of total radiation has been observed in desert regions. The maximum amounts at the equator exceed the minimum by 5-6 times. The greatest variability is found to occur in the regions of monsoon climate.

An analysis of the variability of monthly amounts of total radiation showed that the variation of Q increases from winter to summer. The greatest variation of monthly Q was observed in moderate latitudes, the lowest in tropical latitudes.

As the investigations of Pivovarova [47] have shown, the variability of total radiation is less than that of direct, as a consequence of the leveling of the variations on account of scattered radiation. An examination of variations over many years of the incident shortwave radiation depends on the relation between direct and scattered radiation, and often total radiation changes less than its constituents. According to Pivovarova's [47] data, the extreme deviations in the annual amounts of and total radiation worked out at $\pm$ 6%; for monthly amounts Q is $\pm$ (6-10%) in summer and 15-16% during winter.

Consideration of variations in the perpetual path of the incoming shortwave radiation is necessary for the solution of many applied problems relating to the evaluation of perennial radiation regimes.

REFERENCES

1. Averkiev, M. S. *Summarnaya radiatsiya i ee komponenty pri bezoblachom nebe i zavisimost' ot prozrachnosti atmosfery dlya shirot 40-70°* (Total radiation and its components in clear sky and dependence on atmospheric transparency for latitudes 40-70°). Vestn. MGU No. 4, 1958.

2. Aizenshtat, B. A. Metod opredeleniya radiatsionnogo balansa sklonov (A method of determining net radiation of slopes). Meteorologiya i gidrologiya, No. 2, 1952.

3. Barashkova, E. P. Nekotorye zakonomernosti v rezhime summarnoi radiatsii (Some patterns in the regime of total radiation). Trudy, vyp. 80, 1959.

4. Barashkova, E. P. et al. Radiatsionnyi rezhim territori SSSR (Radiational regime of the territory of the USSR). Gidrometeoizdat, 1961.

5. Belov, V. F. Pogloshchenie solnechnoi radiatsii v svobodnoi atmosfere nad morem Deivisa i Antarkticheskim sklonom (Absorption of solar radiation in atmosphere above Davis Sea and Antarctic slope). Trudy TsAO, vyp. 45, 1962.

6. Berezina, L. S. Izmerenie pogloshcheniya solnechnoi radiatsii v raione Odessy (Measurement of absorption of solar radiation in the region of Odessa). Trudy YkrNIGMI, vyp. 8, 1957.

7. Berlyand, M. E. *Predskazanie i regulirovanie teplovogo rezhima prizemnogo sloya* atmosfery (Prediction and regulation of thermal regime of atmosphere in the vicinity of the earth's surface). Gidrometeiozdat, Leningrad, 1956.

8. Berlyand, M. E. and E. P. Novosel'tsev. K teorii zavisimosti summarnoi radiatsii ot oblachnosti (The theory of the dependence of total radiation on cloudiness). Nauchn. soobshch. In-ta geologii i geografii AN Lit.SSR, t. XIII, 1962.

9. Berlyand, T. G. Raspredelenie solnechnoi radiatsii na kontinentakh (Distribution of solar radiation over the continents). Gidrometeoizdat, Leningrad, 1961.

10. Berlyand, T. G. Izmenchivost' solnechnoi radiatsii, postuayushchei k poverkhnosti zemli (Variability of solar radiation incident on the earth's surface). Trudy, GGO, vyp. 179, 1965.

11. Borzenkova, I. I. K metodike rascheta summarnoi radiatsii dlya uslovii gornogo plato (On the method of calculating total radiation for the conditions of a mountain plateau). Trudy GGO, vyp. 179, 1965.

12. Gaevskii, V. L. Izmerenie radiatsionnykh potokov v oblakakh (Measurement of radiative fluxes in clouds). Trudy GGO, vyp. 46, 1955.

13. Gal'perin, B. M. and L. P. Seryakova. Rasseyannaya i summarnaya solnechnaya radiatsiya pri razhlichnykh usloviyakh (Scattered and total solar radiation under different conditions). Trudy GGO, vyp. 152, 1964.

14. Gal'perin, B. M. O summarnoi radiatsii v Arktike (On the total radiation in the Arctic region). Trudy, AANII, t. 229, 1961.

15. Gal'perin, B. M. and L. P. Seryakova. Osnovnye zakonomernosti korotkovolnovoi radiatsii i dnevnogo radiatsionnogo balansa pri razlichnoi oblachnosti (Fundamental patterns of shortwave radiation and daily radiative balance for different cloudiness). Trudy LGMI, vyp. 22, 1964.

16. Gal'perin, B. M. Sutochnyi prikhod summarnoi solnechnoi radiatsii pri razlichnykh oblakakh (Diurnal influx of total solar radiation for different clouds). Trudy GGO, vyp. 125, 1962.

17. Goisa, N. I. Pogloshchenie solnechnoi radiatsii v svobodnoi atmosfere v raione Kieva (Absorption of solar radiation in free atmosphere in the region of Kiev). Trudy YkrNIGMI, vyp. 3, 1955.

18. Goisa, N. I. Metodika aktinometricheskikh izmerenii s samoleta IL-14 (Method of actinometric measurements from the airplane IL-14). Trudy YkrNIGMI, vyp. 55, 1966.

19. Kastrov, V. G. O nagrevanii atmosfery blagodarya pogloscheniyu solenchnoi radiatsii vodyanym parom (On the heating of atmosphere on account of absorption of solar radiation in water vapor). Trudy TsAO, vyp. 6, 1952.

20. Kastrov, V. G. Izmerenie pogloshcheniya solnechnoi radiatsii v svobodnoi atmosfere do 3-5 km (Measurement of solar radiation absorbed in free atmosphere up to 3-5 km). Trudy TsAO, vyp. 8, 1952.

21. Kastrov, V. G. Opredelenie zavisimosti chuvstvitel'nosti pirauometrov Yanishevskogo ot davleniya (The determination of the dependence of sensitivity of Yanishevskii's pyranometer on pressure). Trudy TsAO, vyp. 13, 1954.

22. Kastrov, V. G. Pogloshchenie solnechnoi radiatsii v nizhnei troposfere (Absorption of solar radiation in lower troposphere). Trudy TsAO, vyp. 32, 1952.

23. Kastrov, V. G. O resul'tatakh izucheniya oslableniya solnechnoi radiatsii v svobodnoi atmosfere i sutochnom khode temperatury (On the results of the study of attenuation of solar radiation in free atmosphere and diurnal course of temperature). Trudy VNMS, t. VI, 1963.

24. Katulin, V. A. et al. Samoletnyi pribor dlya izmereniya radiatsionnogo zondirovaniya atmosfery (Airplane instruments for measuring radiative probing of atmosphere). Trudy GGO, vyp. 166, 1964.

25. Kondrat'ev, K. Ya. et al. Issledovanie spektral'nogo sostava korotkovolnovoi solnechnoi radiatsii (Study of the spectral composition of shortwave solar radiation). Izd. AN SSSR, fizika atmosfery i okeana, vyp. 9, 1965.

26. Kondrat'ev, K. Ya. and G. P. Volkova. Sutochnyi khod i vozmozhnye summy summarnoi radiatsii (Diurnal course and probable amounts of solar radiation). Meteorologiya i gidrologiya, No. 7, 1958.

27. Kondrat'ev, K. Ya., G. N. Gaevskaya and G. A. Nikol'skii. Vertikal'nyi profil' radiatsionnogo balansa i ego sostavlyayushchikh v svobodnoi atmosfere v dnevnoe vremya (Vertical profile of radiative balance and its components in free atmosphere during day time). ISZ, vyp. 14, 1962.

28. Kondrat'ev, K. Ya., G. N. Gaevskaya and G. A. Nikol'skii. Ae'rostatnye issledovaniya radiatsionnogo balansa sistemy zemnaya poverkhnost'—atmosfera (Aerostatic investigation of radiative balance of the earth's surface—atmosphere system). Kosmicheskie issledovaniya, t. 1, vyp. 3, 1963.

29. Kondrat'ev, K. Ya., G. A. Nikol'skii and N. M. Evdokimova. Vertikal'nye profili radiatsionnogo balansa i ego sostavlyayushchikh po dannym izmerenii 1963-1964 gg. (Vertical profiles of radiative balance and its components from the data of measurements in 1963-1964). Problemy fiziki atmosfery, vyp. 4, LGU, 1966.

30. Kondrat'ev, K. Ya. and G. N. Gaevskaya. Radiatsionnye izmeneniya temperatury v svobodnoi atmosfere (Radiative temperature changes in free atmosphere). Problemy fiziki atmosfery, vyp. 3, LGU, 1965.

31. Kondrat'ev, K. Ya. and G. N. Gaevskaya. Osnovnye faktory, opredelayushchie radiatsionnoe nagrevanie atmosfery za schet pogloshcheniya korotkovolnovoi radiatsii (Fundamental factors which determine the radiative heating of atmosphere on account of absorption of shortwave radiation). Problemy fiziki atmosfery, vyp. 4, LGU, 1966.

32. Kondrat'ev, K. Ya. and M. P. Manolova. Radiatsionnyi balans sklonov (Radiative balance of slopes). Vestn. LGU, No. 10, vyp. 2, 1958.

33. Kondrat'ev, K. Ya. and M. P. Manolova. Prikhod korotkovolnovoi radiatsii na razlichno orientirovannye naklonnye poverkhnosti pri nalichii snezhnogo pokrova (Influx of shortwave radiation on differently oriented inclined surfaces in the presence of snow cover). Nauchn, soobshch. In-ta geologii i geografii AN Lit.SSR, t. XIII, 1962.

34. Kondrat'ev, K. Ya. Aktinometriya (Actinometry). Gidrometeoizdat, Leningrad, 1965.

35. Kondrat'ev, K. Ya. and M. P. Manolova. Dnevnoi khod i dnevnye summy rasseyannoi i summarnoi radiatsii na razlichno orientirovannykh sklonakh (Daily course and daily amounts of scattered and total radiation on differently oriented slopes). Vestn. LGU, No. 4, 1958.

36. Koptev, A. P. Aktinometricheskie issledovaniya s samoleta v Arktike (Actinometric investigation in the Arctic region from an airplane). Nauchn. soobshch. In-ta geologii i geografii AN Lit.SSSR, t. XIII, 1962.

37. Krinov, E. L. and V. V. Sharonov. Spektrofotometricheskie issledovaniya summarnoi i rasseyannoi dnevnoi osveshchennosti (Spectrophotographic investigation of total and scattered daytime illumination). Zh. geofiziki, 6, vyp. 2-3, 1936.

38. Krinov, E. L. Spektral'naya dnevnaya osveshchennost' gorizontal'noi poverkhnosti v predelakh infrakrasnoi oblasti spektra (Daily spectral illumination of horizontal surface within the limits of infrared region of the spectrum). Issl. po fotometrii i sensitometrii, coll. TsNIGAIK, No. 1, 1939.

39. Kuz'min, P. P. Metod opredeleniya maksimal'noi intensivnosti snegotayaniya (A method for determining the maximum intensity of melting of snow). Trudy GGI, vyp. 24 (78), 1950.

40. Kuz'min, P. P. Issledovanie parametrov formul snegotayaniya (Investigation on the parameters of the formula for melting of snow). Trudy, GGI, vyp. 32, (86), 1951.

41. L'vova, E. M. Izmerenie summarnoi radiatsii solntsa i al'bedo zemli do vysoty 10-20 km (Measurement of total radiation of the sun and albedo of earth up to the height of 10-20 km). Trudy TsAO, vyp. 16, 1956.

42. Marshunova, M. S. Osnovnye zakonomernosti radiatsionnogo balansa podstilayushchei poverkhnosti i atmosfery v Arktike (Fundamental patterns of net radiation of the underlying surface and the atmosphere in the Arctic region). Trudy AANII, t. 229, 1961.

43. Makhotkin, L. G. Itogi rabot po izucheniyu variatsii pryamoi solnechnoi radiatsii (Conclusion of the work on variation of direct solar radiation). Trudy GGO, vyp. 80, 1959.

44. Mukhenberg, V. V. Nekotorye osobennosti prikhoda solnechnoi radiatsii na naklonnye poverkhnosti (Some peculiarities of the influx of solar radiation on an inclined surface). Trudy GGO, vyp. 179, 1965.

45. Pyatnenkov, B. A. Vliyanie al'bedo na prikhod summarnoi radiatsii v Arktike (The effect of albedo on the influx of total radiation in the Arctic region). Trudy AANII, t. 217, 1959.

46. Pyatovsakaya, N. P. Potoki korotkovolnovoi radiatsii v svobodnoi atmosfere (Flux of shortwave radiation in free atmosphere). Trudy GGO, vyp. 109, 1961.

47. Pivovarova, Z. I. Kolebaniya solnechnoi radiatsii po nazemnym izmereniyam (Fluctuation of solar radiation according to terrestrial measurements). Trudy GGO, vyp. 193, 1967.

48. Rukovodstvo po kontrolyu aktinometricheskikh nablyudenii (A manual on the standardization of actinometric observations). Gidrometeoizdat, Leningrad, 1962.

49. Rukovodstvo gidrometeorologicheskim stantsiyam po registratsii radiatsii (A guidebook on the hydro-meteorological stations for recording radiation). Gidrometeoizdat, 1961.

50. Rusin, N. P. Meteorologicheskii i radiatsionnyi rezhim Antarktidy (Meteorological and radiational regimes of the Antarctic region). Gidrometeoizdat, Leningrad, 1961.

51. Savikovskii, A. I. Nablyudeniya nad solnechnoi radiatsii v svobodnoi atmosfere (Observation on solar radiation in free atmosphere). Trudy, TsAO, vyp. 23, 1957.

52. Savinov, S. I. Sootnoshenie mezhdy oblachnost'yu, prodolzhitel'nostyu solnechnogo siyaniya i summami pryamoi i rasseyannoi radiatsii (Relation between cloudiness, duration of daylight and the amount of direct and scattered radiation). Meteorol. vestn., No. 1, 1931.

53. Savinov, S. I. O formulakh, vyrazhayushchikh pryamuyu i rasseyannuyu radiatsiyu v zavisimosti ot stepeni oblachnosti (On the formulas expressing direct and scattered radiation with respect to the degree of cloudiness). Meteorol. vestn. Nos. 5-6, 1933.

54. Samoilenko, V. S. Formirovanie temperaturnogo rezhima morei (Formulation of the temperature regime of the seas). Gidrometeoizdat, Leningrad, 1959.

55. Timerev, A. A. Summarnaya radiatsiya i al'bedo po nablyudeniyam s samoleta v Arktike v 1963 g (Total radiation and albedo according to observations from an airplane in the Arctic region in 1963). Trudy AANII, t. 273, 1965.

56. Ukraintsev, V. N. Priblizhennoe vychislenie summ pryamoi i rasseyannoi radiatsii (Approximate computation of amounts of direct and scattered radiation). Meteorologiya i gidrologiya, No. 6, 1939.

57. Faraponova, G. P. Nekotorye resul'taty aktonometricheskikh nablyudenii na svobodnykh ae'rostatkh (Some results of actinometric observations from free balloons). Trudy TsAO, vyp. 8, 1952.

58. Faraponova, G. P. and V. G. Kastrov. Aktinometricheskie nablyudeniya v nizhnei troposfere nad Kyzyl-Kumami/(aprel'-mai) 1951 g [Actinometric observations in lower troposphere above Kyzyl-Kum (April-May) 1951]. Trudy TsAO, vyp. 13, 1954.

59. Chel'tsov, N. I. Issledovanie otrazheniya, propuskaniya i pogloshcheniya solnechnoi radiatsii oblakami nekotorykh form (Investigation on reflection, transmission and absorption of solar radiation in clouds of several forms). Trudy TsAO, vyp. 8, 1952.

60. Shlyakhov, V. I. Nekotorye osobennosti radiatsionnykh protsessov v Antarktide (Some peculiarities of radiation processes in the Antarctic region). Trudy TsAO, vyp. 32, 1959.

61. Albrecht, F. Methods of computing global radiation. Geofisica pura e applicata, vol. 32, III, 1955.

62. Black, J. N. The distribution of solar radiation over the earth's surface. Archiv für Meteor., Geoph. und Biokl., ser. B, Bd, 6, 1956.

63. Clapp, P., F. Winninghoff and G. Fisher. Vertical distribution of atmospheric heating and cooling at Washington, D. C. June-July 1961. Technical Memorandum No. 21, 1962.

64. Condit, H. R. and F. Grum. Spectral energy distribution of day-light. JOSA, vol. 54, No. 7, 1964.

65. Dirmhirn, J. Untersuchungen über die Himmelstrahlung in die Ostalpen. Archiv für Met., Geoph. und Biokl., Ser. B, Bd 2, H. 4, 1951.

66. Elhers, M. K., and A. M. Khalil. *Total radiation on vertical and inclined surfaces* during cloudless days in the UAR. Pure and Applied Geophysics, vol. 60, 1965/1.

67. Fritz, S. The albedo of the ground and atmosphere. Bull. Amer. Met. Soc., vol. 29, No. 6, 1948.

68. Fritz, S. and T. H. MacDonald. Measurements of absorption of solar radiation by clouds. Bull. Amer, Met. Soc., vol. 32, No. 6, 1951.

69. Haurwitz, B. Insolation in relation to cloudiness and cloud density. J. Met., vol. 5, No. 2, 1945.

70. Hendorson, S. T. and D. Hodgkiss. The spectral energy distribution of daylight. Brit. J. Appl. Phys., vol. 14, No. 125, 1963.

71. London, J. The distribution of radiational temperature change in the Northern Hemisphere during March. J. Met., vol. 9, No. 2. 1952.

72. Lunelund, H. Über die Helligkeit in Finnland. Soc. Scient. Fennica Coment. Ph. Math., vol. 8, No. 17, 1935.

73. Mügge, R. and F. Möller. Zur Berechnung von Strahlungsströmen und Temperaturänderungen in Atmosphären von belibiegen Aufbau. Zeitschr. für Geopchys. Bd. 8, H. 1-2, 1932.

74. Neiburger, M. Reflection, absorption and transmission of insolation by stratus clouds. J. Meteor., vol. 6, No. 2, 1959.

75. Roach, W. T. Some aircraft observations of fluxes of solar radiation in the atmosphere. Quart. J. Roy. Met. Soc., vol. 87, No. 373, 1961.

76. Robinson, C. D. Some observations from aircraft of surface albedo and absorption of cloud. Arch. Meteor., Geophys. und. Biokl., Bd 9, No 1, 1958.

77. Sapsford, C. M. An estimation of solar energy radiation for Australia. Austral. J. Sci., vol. 20, No. 4, 1957.

78. Sekihara, K. The amount of solar radiation falling on a tilted surface in Tokyo. Papers in Meteor. and Geophys., vol. XVI, No. 1, 1965.

79. Teylor, A. H. and G. P. Kerr. The distribution of energy in the visible spectrum of daylight. JOSA, vol. 31, No. 1, 1941.

80. Thams, C. Sonnen und Himmelstrahlung in Locarni-Monti. Geofisica pura et vol. XIV, B. 3-4, 1949.

8. THERMAL RADIATION OF THE ATMOSPHERE

The thermal radiation of the atmosphere and the earth's surface is concentrated in the infrared region of the spectrum, viz., 4-120 μ. The wavelength at which thermal radiation of the earth's surface and the atmosphere begins to predominate during the day and the energy contribution of reflected and scattered solar radiation becomes negligible depends on the solar altitude, the direction in which radiation is propagated, the height of observation and other factors. However, it can be assumed in almost every case that thermal radiation of terrestrial origin predominates in the region of wavelengths $\lambda > 4$ μ, and for $\lambda < 2$ μ the reflected and solar radiations predominate [13, 23, 46, 57]. Both the sources of radiation are comparable in the spectral interval 2-4 μ, with a minimum of radiation in the neighborhood of 3 μ. This is observed in the daily spectra of the atmosphere and different terrestrial objects and brought about by the presence of two components of radiation, one of which decreases with increasing λ and the other increases [46, 54].

1. SPECTRAL COMPOSITION OF THERMAL RADIATION OF THE ATMOSPHERE

The intrinsic thermal radiation of the atmosphere may be primarily characterized by the distinctive fact that gases comprising the basis of atmosphere, viz. nitrogen, oxygen and argon do not participate in radiation, whereas active gases (from the point of view of the generation of infrared radiation) are present in the atmosphere in insignificant and often variable quantities.

Table 8.1.

Active component	Isotope formula	Molecular weight	Type of molecules	Volume content, %
Water vapor	H_2O	18.0	Asymmetrical gyrostat	0-7
Carbon dioxide	CO_2	44.0	Linear asymmetrical	0.01-0.1 (mean 0.03)
Methane	CH_4	16.0	Spherical gyrostat	0.02
Ozone	O_3	48.0	Asymmetrical gyrostat	0-0.01
Nitrous oxide	N_2O	44.0	Linear asymmetrical	0.005

The second fact presents considerable difficulty since the variability of the amount of gas and the absence of a practicable method of measuring it in such insignificant concentrations (besides measuring humidity) prove to be a hindrance in the exact interpretation of observations made on the radiation spectrum and lessens the accuracy of computations.

The role of the components enumerated above in the study of infrared radiation is different. The most important contribution belongs to water vapor.

The water molecule H_2O (the isotopic variations of molecules whose spectral properties are not manifested in emission spectra because of their low concentrations, will not be examined either now or later) pertains to the "asymmetrical gyrostat" type and may be characterized by the small moments of inertia, differing considerably from one other [10, 56]. The vibrational and rotational spectra of its radiation appear to be very complex and in the presence of comparatively large quantities of water vapor in the atmosphere modify the entire infrared spectrum of the atmosphere in the interval 4-120 μ (more than 99% of outgoing radiation and back radiation of the atmosphere is concentrated in this interval). Laboratory measurements and theoretical quantum mechanical computations show

that in the spectral range from 4.5 to 10 μ vibrational and rotational transitions play a fundamental role, in particular, the principal band ν_2—6.25 μ (1595 cm^{-1}), and from 10 μ onward only rotational transitions, i.e. mainly the band with the center at 50 μ. The distant edges of this band appear as an important factor in the radiation properties of the atmospheric transparency window of 8-12 μ and the spectral range beyond 17 μ.

The molecule of carbon dioxide [10, 56] is linear and symmetrical and does not possess a distinct rotational spectrum. The principal bands, ν_3—4.3 μ (2380 cm^{-1}) and ν_2—14.7 μ (673 cm^{-1}), play a basic role in the infrared region. The effect of the band ν_3, appearing in the interval of wavelengths 13-17 μ, becomes more significant since it occurs in the segment of the spectrum having an intensity close to the maximum (at the absolute temperature of the earth's surface). In the limits 12-18.5 μ carbon dioxide has several more low intensity bands of upper state, caused by vibrations perpendicular to the direction of propagation. They attain a maximum partly in the principal band ν_2.

Ozone may be characterized by the principal bands ν_1—9.1 μ (1110 cm^{-1}, weak intensity), ν_2—14.1 μ (710 cm^{-1}) and ν_3—9.6 μ (1043 cm^{-1}) [56]. However the last band alone considerably affects the radiation since it is more intense and appears in the region of the transparency window of the atmosphere where both the upper layer (for upward radiation) and the lower layer (in case of back-radiation) do not screen off the radiation of ozone.

The role of methane and nitrous oxide is inconsequential and appears exclusively in the transparency window where the following bands are situated, viz. methane ν_4—7.66 μ (1306 cm^{-2}) the practically overlapping the longwave edge of the band of water vapor ν_2, and the band of nitrous oxide, with centers at 7.78 μ (1285 cm^{-1}), 8.56 μ (1167 cm^{-1}) and 17 μ (589 cm^{-1}) [56].

From Kirchhoff's law we see that the emission and absorption spectra are identical. However, they manifest themselves in different ways. In the first place it is necessary to notice that intrinsically the absorption functions, and, consequently, the absorption spectra, depend only a little on the temperature of the gases, which plays a principal role in the intensity of emission spectra. Thus anisotropy in the atmospheric emission may be determined exclusively from the anisotropy in the distribution of gases, and the anisotropy in radiation can be similarly determined by the thermal structure. This is most clearly demonstrated in the comparison of the spectra of upward radiation at the radii with the back-radiation spectra at the zenith (Figs. 8.1-8.3) : the maxima and minima have here changed places. This can be explained by the fact that the entire contribution to downward radiation comes from the atmosphere, and the atmosphere not

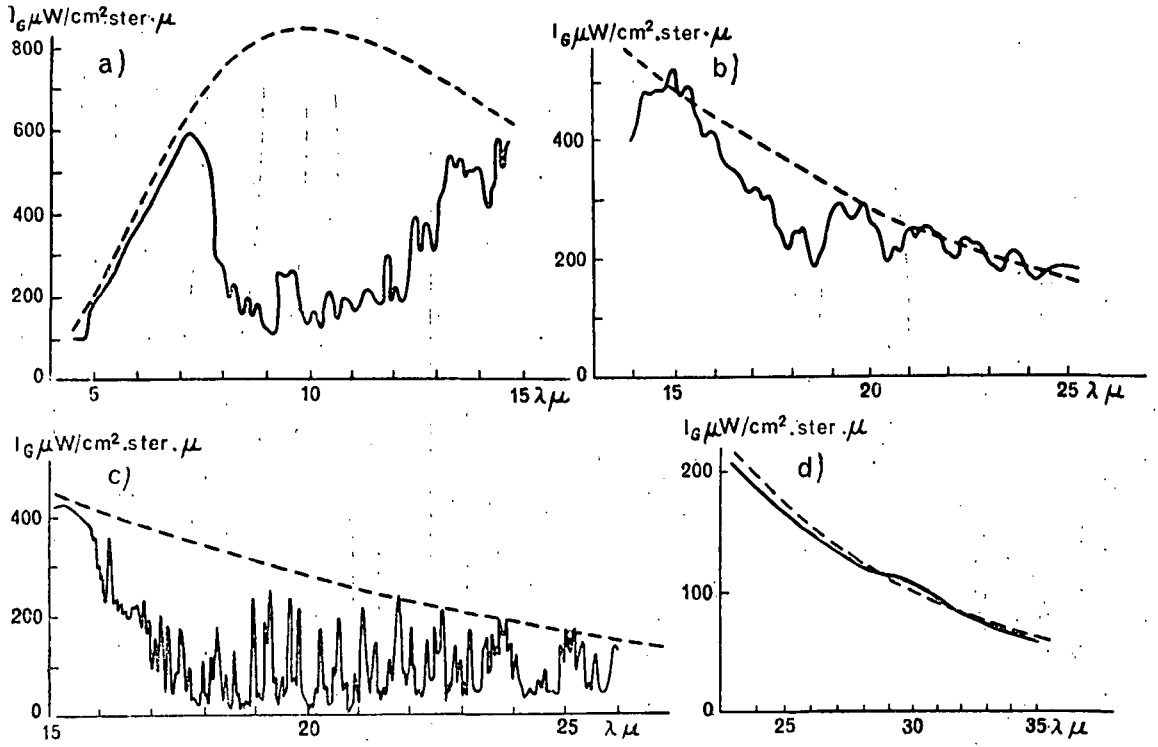

Fig. 8.1. Spectral distribution of intensity of atmospheric back-radiation at the level of the earth's surface (1) and intensity of radiation of a perfectly black body (2).

(a) July 22, 1965, 1 hr. 15 min., Kaunas. temperature of surface layer 15° C, resolution 0.1 μ [1]; (b) October 16, 1963, 21 hrs., Rostov-on-Don, temperature of surface layer 3° C, resolution 0.15 μ [25]; (c) February 17, 1961, 18 hrs. 19 min. Jungfrau, temperature of surface layer –5.5° C [48]; (d) December 20, 1964, 22 hrs. Leningrad, temperature of surface layer 3° C, resolution 0.8 μ [24].

only emits upward radiation but also screens off radiation of the comparatively warm earth's surface. In case of back-radiation the maxima in strong absorption bands (6.3 μ, 15 μ) are caused by the fact that here the radiation is generated by the surface and, consequently, warmer layers of the atmosphere, and at the same time the very cold layer contributes to back-radiation in the transparency window. In the case of upward radiation in bands of strong absorption the main contribution belongs to the upper cold layers which completely screen off the more intense radiation of lower layers and the earth's surface.

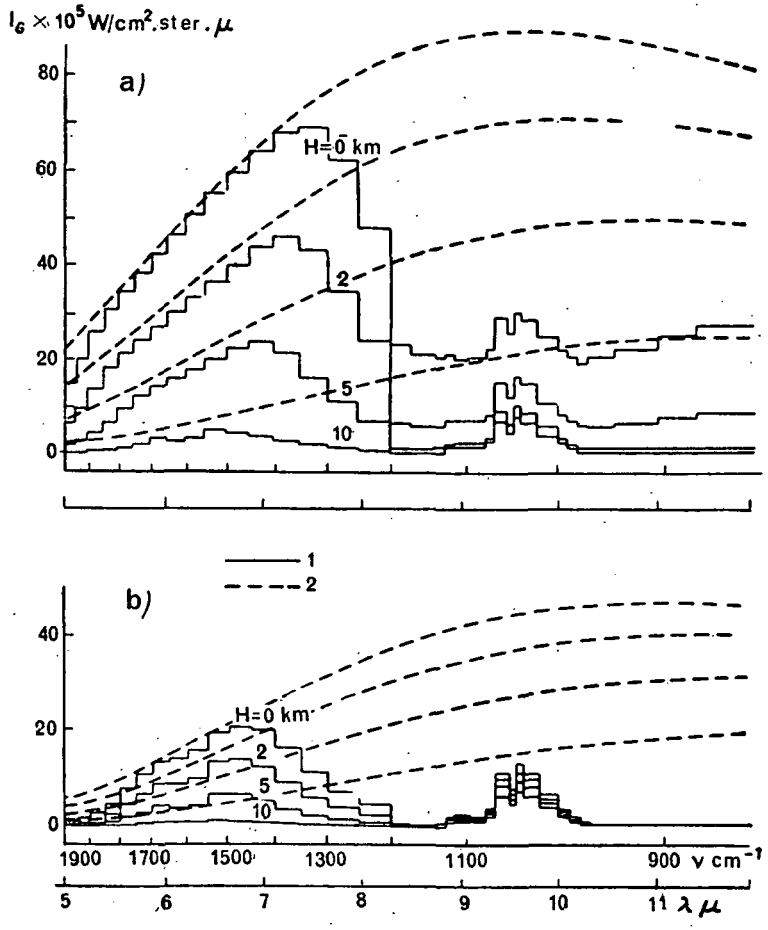

Fig. 8.2. Spectral distribution of intensity of atmospheric downward radiation at different altitudes (1) and intensity of radiation of perfectly black body (2).

(a) summer in moderate latitudes, high relative humidity, zenith [42];

(b) winter in moderate latitudes, low relative humidity, zenith [42].

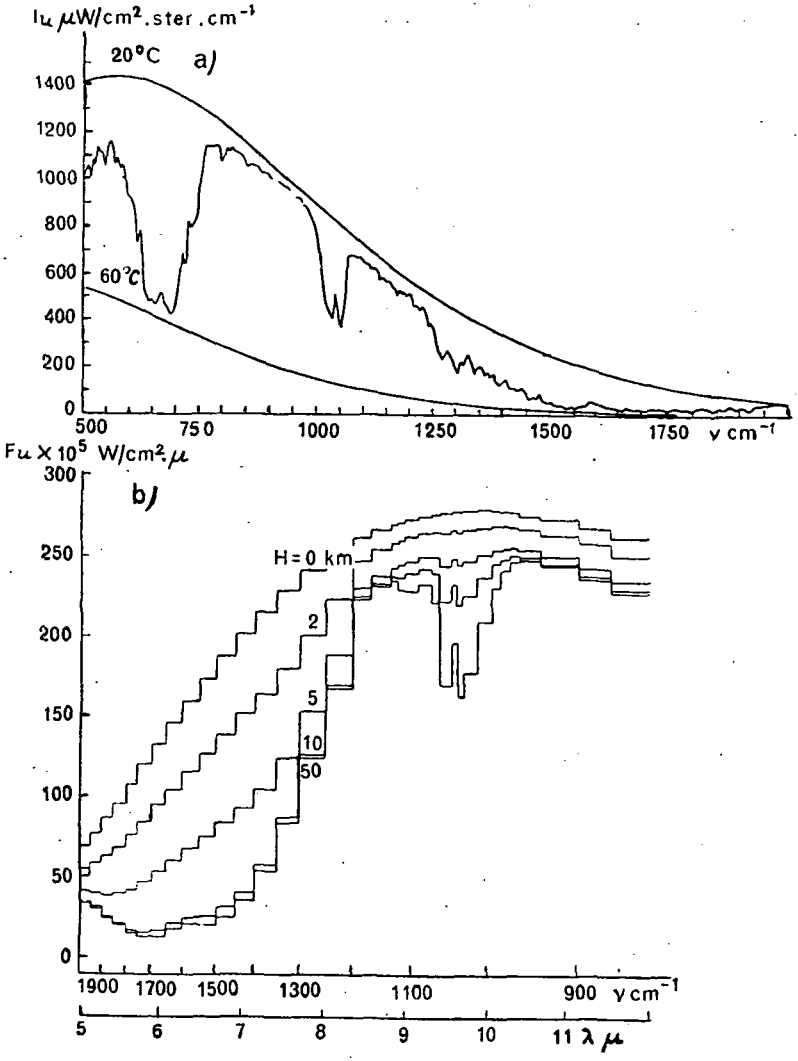

Fig. 8.3. Spectral distribution of upward atmospheric radiation.
(a) intensity of radiation of May 8, 1966, Texas, height 33.5 km, surface temperature 20° C [50];
(b) radiation flux; summer in moderate latitudes with high relative humidity, nadir [42].

Emission spectra can be computed and measured with much less accuracy in spectral resolution than absorption spectra at the present. This may arise because of the unsatisfactory values of the emission functions

of the thermal structure and distribution of radiative computations and in experiments with the low values of energy of radiation registered.

Typical spectra of atmospheric back radiation at the earth's surface under clear sky [1, 24, 25] are shown in Fig. 8.1. The characteristic properties are radiation maxima situated in the spectral ranges 6-8, 9-10, 13-17 μ and minima in the transparency windows 8-12 μ, 18.8 μ and 20.5 μ. Thus the principal band ν_2 of water vapor with center at 6.25 μ provides an overwhelming contribution from 5 to 8 μ. The shifting of the absolute maximum toward 7.5 μ shows that the atmospheric radiation can be determined by the overlapping of the contour of band ν_2 of the curve of energy distribution in the radiation spectrum of a perfectly black body; for temperatures of 280-300° K the latter exhibits a sharp decrease toward short wavelengths.

An increase in radiation from 10 to 15 μ can be explained by the influence of the farther edge of a rotational band of water vapor with center at 50 μ and overlapping radiation of the fundamental band ν_2 of carbon dioxide ($\lambda=13$ μ).

A number of weaker radiation bands are found in the transparency window 8-12 μ. In the shift from 8 to 9 μ, caused by continuous radiation of the band 6.3 μ of water vapor, the following bands are easily seen : 8.4 μ (H_2O), 8.59 μ (N_2O) and 8.82 μ (H_2O). The intense double peaked radiation band of ozone extends from 9.1 to 9.8 μ. Beyond 10 μ the following bands are characteristic members : 10.6 μ (CO_2), 10.8 μ (CO_2), 11.1 μ (H_2O), 11.4 μ (H_2O—overlapping of bands with centers at 11.34 and 11.5 μ), 11.87 μ (H_2O), 12.1 μ (H_2O+CO_2), 12.45 (H_2O—overlapping of bands 12.41 and 12.53 μ), 12.7 μ (CO_2) and 13.1 μ (CO_2+H_2O). The following windows are the most transparent, viz. 8.35, 8.7, 9.08, 10.29, 11.14, 11.7, 11.96 and 12.19 μ.

In the interval 13-17 μ the fundamental band ν_2 of carbon dioxide plays a principal role, and the following bands play a secondary role, viz. 14.4, 14.7, 15.0, 15.4, 16.2, 16.7 μ (all of CO_2) and 17 μ (N_2O).

In the interval 17-25 μ the radiation may be determined exclusively by the continuous radiation of the shortwave edge of the H_2O band with center at 50 μ and by its overlapping of weak rotational bands of water vapor.

Analogous members have also been examined in the spectrum, registered with high spectral resolution in mountainous areas, i.e. under conditions of low temperatures and lesser quantities of water precipitation [48], and similarly in the spectra of upward radiation (Fig. 8.3). A redistribution of energy in the case has been explained above.

The transformation of the spectral distribution of radiation with respect to height may be determined primarily by the stratification of the atmosphere [42]; however, one can observe many general patterns. The

radiation in strong absorption bands (5-7 μ) is an approximation to the radiation of a black body at a temperature equal to the temperature at the corresponding level in the atmosphere. Moreover the lower the location of the level under examination the higher the moisture content of the atmosphere (Fig. 8.2). Downward radiation falls sharply with altitude in transparency windows, whereas upward radiation does not change measurably (Fig. 8.3). The correction on account of emission of back-radiation in ozone depends broadly on the height. The screening action of ozone on upward radiation is substantial only for heights comparable to or exceeding the altitude of maximum concentration of ozone.

Cloudiness changes the character of energy distribution considerably in downward radiation spectra, the latter approximating the radiation of a black body and decreasing the number of components. This takes place because the radiation of upper cold layers of the atmosphere in the transparency windows is displaced by the radiation of the lower boundary of cloudiness[1] at a temperature close to that of the surface. As the lower boundary of cloudiness descends, the leveling of the spectra becomes stronger. On the other hand, there is an increasing smoothness in spectra of the outgoing radiation with a rise in altitude of the upper boundary of cloudiness. In some cases [23] the ozone minimum even disappears, although the main body of ozone is situated above the clouds.

2. ANGULAR DISTRIBUTION OF THERMAL RADIATION OF THE EARTH'S SURFACE AND THE ATMOSPHERE

The object of the present section is to characterize the fundamental pattern of the energy distribution of thermal radiation of the earth's surface and atmosphere in space.

2.1 Downward atmospheric radiation

Computations and measurements show [11, 16, 26, 42 and 47] that the intensity of downward radiation increases in a clear atmosphere with an increase of the zenith angle ϑ (Fig. 8.4)[2]. A sharp increase in the intensity of radiation occurs only at the horizon. An insignificant variation

[1] This is justified by the assumption of complete nontransparency of the boundary of cloudy cover.

[2] The zenith angle ϑ, which specifies the direction of radiation, is measured from the local vertical. In case of downward radiation of the atmosphere the vertical to be considered is directed below, and in case of upward radiation above, thus $0 \leqslant \vartheta^\circ \leqslant 90$.

in radiation energy may be observed for low zenith angles. At small altitudes, atmospheric downward radiation in the vicinity of the horizon can be close to the radiation of a perfectly black body at the temperature of the surrounding air or even equal to a perfectly black body radiation. For instance, measurements [47] carried out at points situated at different heights above sea-level show that in the region of the spectrum 2-40 μ, at any rate, up to a height of 4.3 km, thermal radiation in the horizontal direction equals that of perfectly black radiation at the temperature of air at the point of observation.

As absorption increases in a spectral interval the angular dependence of downward radiation of the atmosphere $I_G(\vartheta)$ becomes weaker. In the spectral regions of extremely intense absorption, atmospheric radiation becomes equal to perfectly black body emission in all directions. Thus

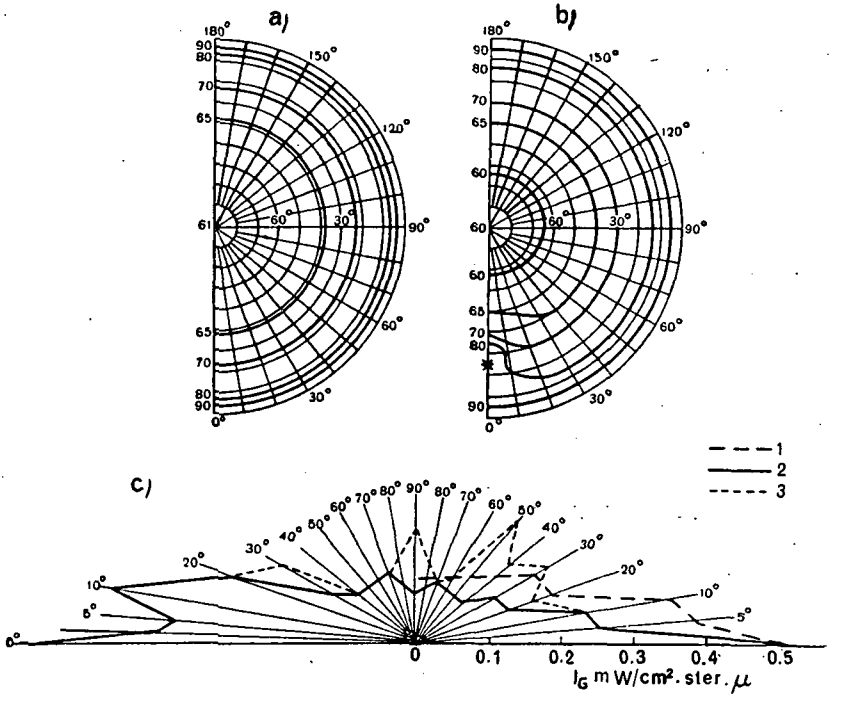

Fig. 8.4. Angular distribution of intensity

(a, b) Isophot of intensity of back-radiation in clear atmosphere (W/m² · ster) in the Colorado, 4.3 km above sea level); (c) the dependence of the intensity of back-radiation cloudiness (Feb. 20, 1966) from measurements on ground [11]; 1—in solar vertical; 2—in of back-radiation of clear atmosphere on the zenith angle in the spectral interval in [42]; (e) the dependence of intensity of back-radiation in a clear atmosphere of with low relative humidity,

the radiation of the sky is black even at the zenith [42, 46] and does not depend on ϑ (Fig. 8.4 d), on the earth's surface in the central regions of the absorption bands 6.3 μ of H_3O and 15 μ of CO_2. The angular dependence I_G (ϑ) is weaker in moist warm atmosphere than in the case of dry and cold atmosphere [42].

The dependence of radiation on the zenith angle in the presence of thick cloud is likewise insignificant [11, 16 and 33]. Thus, integral radiation is practically isotropic, irrespective of the height of the clouds [16]. As Table 8.2 shows, even for the values $w_H \cong 2.66$ g/cm² the intensity of radiation for $\vartheta = 85°$ differs from the intensity at the zenith by not more than 10% (w_H—amount of water vapor in a column of atmosphere between clouds and the ground). For comparison it may be pointed out that

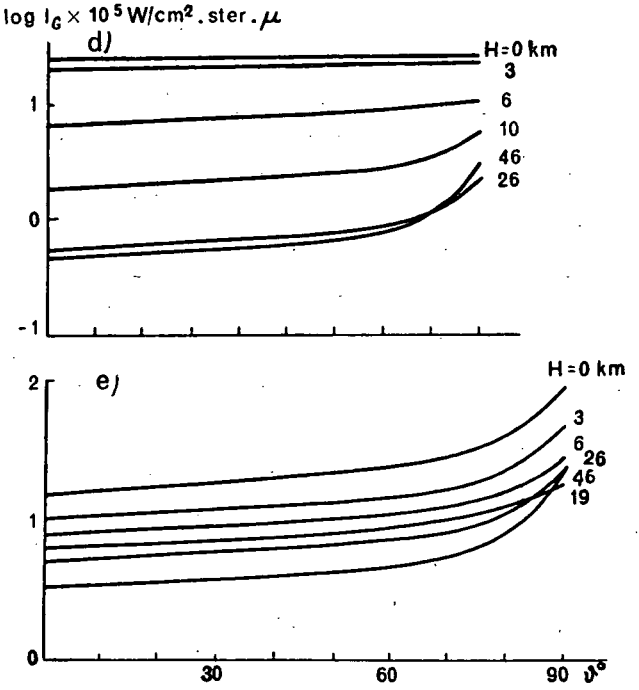

of back-radiation of the atmosphere.

region 2-40 μ at (a) nighttime and (b) daytime from measurements [47] (Pike's Peak, of the atmosphere on angular height θ ($\theta = 90° - \vartheta$) in the window 8-12 μ in partial the perpendicular direction; 3—the same after 10 minutes; (d) dependence of intensity 6.90-7.14 μ during winter at moderate latitudes with high relative humidity, computations zenith angle in the spectral interval 9.68-9.85 μ during summer in moderate latitudes computation in [42].

the mean value of $I_G(\vartheta)/I_G(0) \cong 130\%$ according to measurements [16] for a clear sky at $\vartheta = 85°$ (it is approximately identical for wide intervals of values of atmospheric moisture contents varying from 0.4-3.0 g/km²).

Table 8.2 Mean values of relative intensity of integral back-radiation of atmosphere $I_G(\vartheta)/I_G(0)$ at the surface of the earth [16]

w_H g/cm²	θ°									
	0	10	20	30	40	50	60	70	80	85
0.34	100	100	100	100.1	100.2	100.5	100.8	101.0	102.0	102.5
1.12	100	100	100	100.4	100.6	101.0	101.2	102.0	103.0	104.5
2.66	100	100	100	101.1	101.2	101.7	103.0	104.0	108.0	110.5

In most spectral ranges the angular distribution of back-radiation is more sharply defined (Fig. 8.4d) as the height above the ground increases. However, in the absorption bands of ozone the altitudinal behavior of the dependency of $I_g(\vartheta)$ may vary in a different manner as a result of the peculiar vertical distribution of the O_3 concentration in the atmosphere (cf. Section 3 of Chapter 1). Thus in the absorption band 9.6 μ of O_3 up to a height 15-20 km the change in intensity of back-radiation with the change in zenith angle attenuates according to the distance from the earth's surface (Fig. 8.4e). For instance, a gradual increase in the dependence $I_G(\vartheta)$ begins at the altitude of maximum concentration in ozone.

The variation in intensity of atmospheric back-radiation for a change in the azimuthal angle is negligibly small for dense cloudiness and similarly for a clear sky, if the spectral frequencies under examination possess a sufficiently strong absorption [46]. The field of integral atmospheric back radiation may serve as an example of weak azimuthal anisotropy (Fig. 8.4a and b)[1]. An increase in the intensity of integral radiation at the solar azimuth during daytime can be brought about not by thermal radiation of the atmosphere, but by solar radiation scattered in the near infrared region of the spectrum. This radiation contributes noticeably to the radiation of the atmosphere in the spectral interval 2-40 μ on account of strong "forward" scattering in the sections of the sky in the vicinity of the sun.

In the spectral regions of weak absorption the azimuthal asymmetry

[1] Atmospheric back-radiation in the spectral range 2-40 μ may be considered integral.

of the field of atmospheric back-radiation is somewhat higher. However, the azimuthal variations in intensity of radiation become noticeable only in the zone of the sky adjoining the horizon ($\vartheta > 70°$) [11, 46].

The monotonic nature of the dependence of the downward radiation on the zenith angle (Fig. 8.4c), examined above, is naturally eliminated under conditions of partial cloudiness. Besides, partial cloudiness significantly increases azimuthal anisotropy of the radiation field. The effect of an overcast sky or of distinct background cloud with a clear sky on the angular dependence of downward radiation becomes weaker as the absorption in the given spectral interval and its separation from the near infrared region of the spectrum increases. The last case occurs because in this region of the spectrum large relative variations in Planck's function, and consequently, larger relative variations in atmospheric radiation, correspond to insignificant variations in temperature (see [23]).

2.2 Upward emission

The atmosphere and the underlying surface are the sources of upward radiation. As a rule the intensity of upward radiation I_u (ϑ) decreases with an increase in the angle [42] in a clear sky (infrared darkening toward the horizon may be observed). In the angular interval from $\vartheta = 0$ to $\vartheta = \vartheta_b$ a slow variation in intensity of radiation takes place, and when $\vartheta > \vartheta_b$ the magnitude of I_u (ϑ) falls sharply (ϑ_B—zenith angle at which the earth's boundary is visible from the point of observation).

With the increase of height infrared darkening at the horizon strengthens (Fig. 8.5a). It is obvious from the diagram that at ground level and vicinity the outgoing radiation is practically independent of ϑ (in computations of [42] whose results are given in Fig. 8.5a[1], the earth's surface and atmosphere are accepted as horizontally homogeneous, so that the earth's surface may be considered as smooth and radiating like a perfectly black body). However, under natural conditions the angular distribution of outgoing radiation can be characterized through many maxima and minima [23, 52, 67], which result because the conditions indicated above are not satisfied, but which are usually accepted in theoretical computations of the intensity of upward emission (Fig. 8.5b, c)[2]. For instance, the maxima of radiation for scanning the surface in the mountains (Fig. 8.5b)

[1] The values of I_u are computed only for ϑ equal to 0, 70, 80 and 90°, so that the curves for, $v > v_b$ given here are tentative.

[2] Negative values of angular height θ ($|\theta| = 90° - \vartheta$) correspond to sighting of lower hemisphere (earth's surface), whereas positive values correspond to sighting of the upper hemisphere.

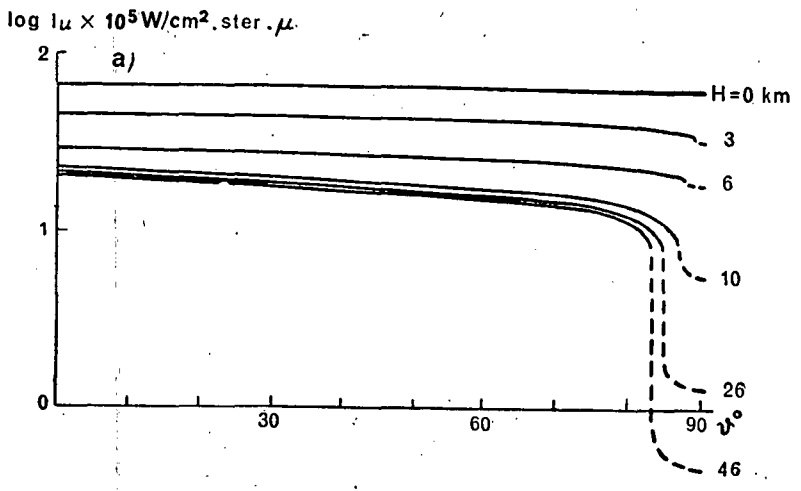

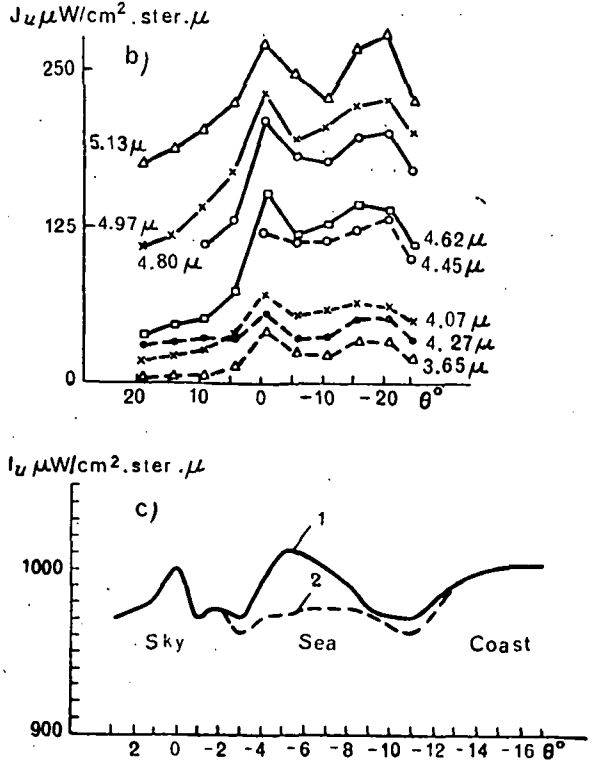

Fig. 8.5. Angular distribution of intensity of outgoing emission. (a) spectral interval 6.90-7.14 μ, clear summer atmosphere of moderate latitudes with low relative humidity, computation from [42]; (b) different spectral intervals, in the afternoon, near the earth's surface, September 20, 1956. Pike's Peak, Colorado (height above sea level 3.6 km), clear sky, measurement in [52]; (c) wavelength 10 μ, in the vicinity of ocean surface east of Coco Beach (Florida), June 24, 1957, 21 hrs, partial cloudiness, measurements [52]. 1—stormy water surface; 2—calm water surface.

is related to the parts of the mountainous zones illuminated by the sun, which are warmer than the regions in shadow.

As in the case of downward radiation of atmosphere, the angular distribution of upward radiation depends on the magnitude of absorption in the spectral interval and its position in the spectrum, stratification of the atmosphere, conditions of cloudiness and height of the underlying surface. Recently the effect of these factors in I_u (ϑ) has been analyzed mainly for the level of the upper boundary of radiative atmosphere or height outside the radiative atmosphere, i.e. for outgoing radiation.

Thanks to investigations from artificial satellites the angular distribution of outgoing radiation has been elaborately studied, employing high angular resolution (see [23]). Later we will separately examine the angular dependence of outgoing radiation and show the effect of the indicated factors on $I_u(\vartheta)$.

2.3 Outgoing radiation

Evidently, the intensity of outgoing radiation falls toward the boundary of the atmosphere, i.e. in sighting the earth-atmosphere system an infrared darkening may be observed (Fig. 8.6). This darkening may either exhibit a continuous character (the function $I(\vartheta)$ decreasing at all times with increase in zenith angle), or may finally occur at distinct angular intervals (for instance an infrared glow occurs toward the boundary of the terrestrial disc, and only at very large zenith angles may the intensity of radiation decrease). The variations in the intensity of radiation are not large in the case of a clear sky and dense cloud while sighting a large portion of the planetary disc. As the distance of the spectral interval is increased from the near infrared region of the spectrum, there is a corresponding slowing down in the variation of intensity of radiation with rising ϑ and a decrease in the overall infrared darkening (or glowing) toward the boundary of the earth taken as a flat disc (compare spectral ranges 6 and 7, 8 and 9 in Fig. 8.6 in pairs, absorption in each pair of segments being almost identical). Furthermore, as the height of the upper boundary of cloud increases, the spectrum ranges become more transparent, and the angular dependence $I_u(\vartheta)$ in the limits of sighting of a large portion of the terrestrial disc becomes naturally weaker as the atmosphere above the underlying surface becomes drier.

The effect of atmospheric stratification on the angular distribution of the outgoing radiation manifests itself in the following manner. An infrared darkening toward the boundary of the earth may be observed in most spectral ranges being examined (Fig. 8.6). However, when the stratosphere provides the chief contribution to outgoing radiation at increasing ϑ then an infrared glow may occur since the mass of gas radiating

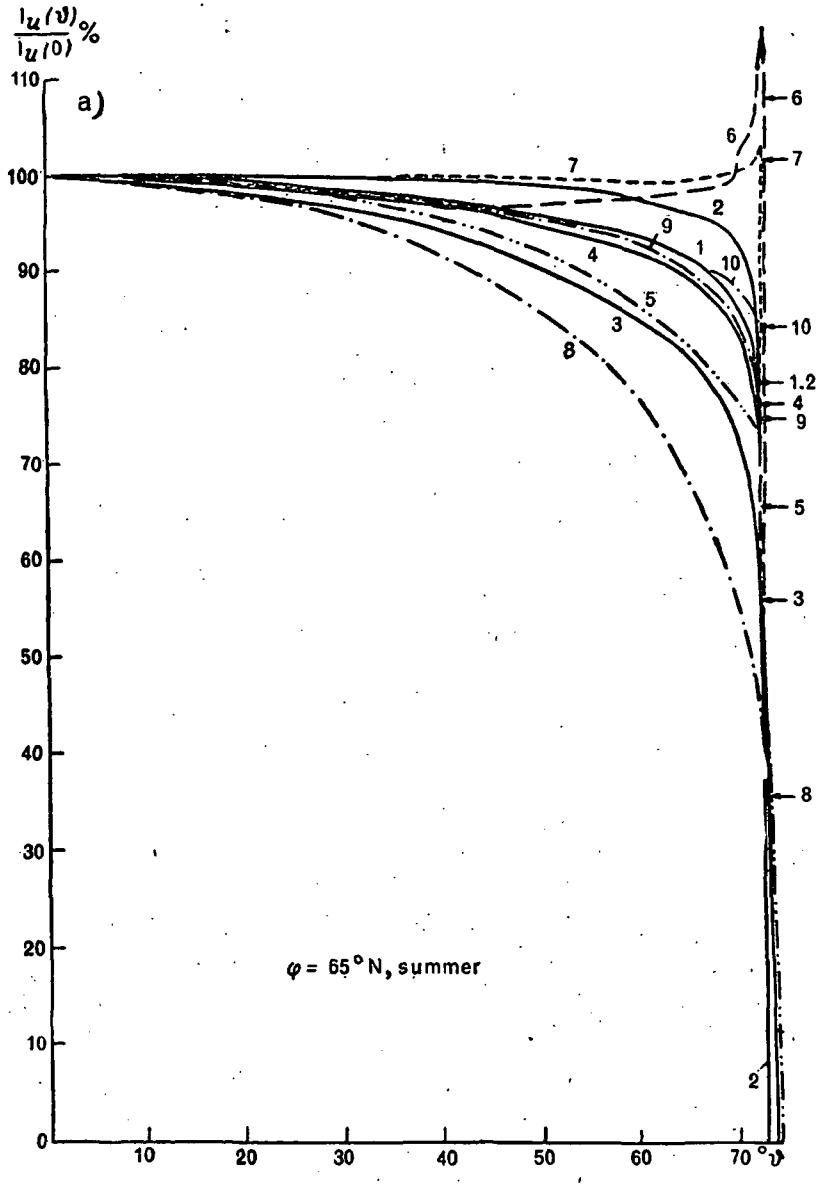

Fig. 8.6. Relative angular distribution of intensity of outgoing radiation for the

(a) general course of angular dependency $I_u(\vartheta)/I_u(0)$; 1—integral radiation, 2—segment in atmospheric window 10.55-11.01 μ, 3—absorption tion band 9.6 μ O_3 (9.01-10.29 μ), 6—band of very strong absorption H_2O (6.49-6.58 μ), (5.00-5.05 μ), 9—band of weak absorption of H_2O (17.86-18.52 μ), 10—region of H_2O (40-120 μ). Horizontal arrows in

at a comparatively high temperature increases with increasing zenith angle (temperature rises with height in the stratosphere), and this appears as the determining factor in the large contribution of the stratosphere to the outgoing radiation. Thus the intensity of outgoing radiation begins to grow as the boundary of the planetary disc is approached for moist and

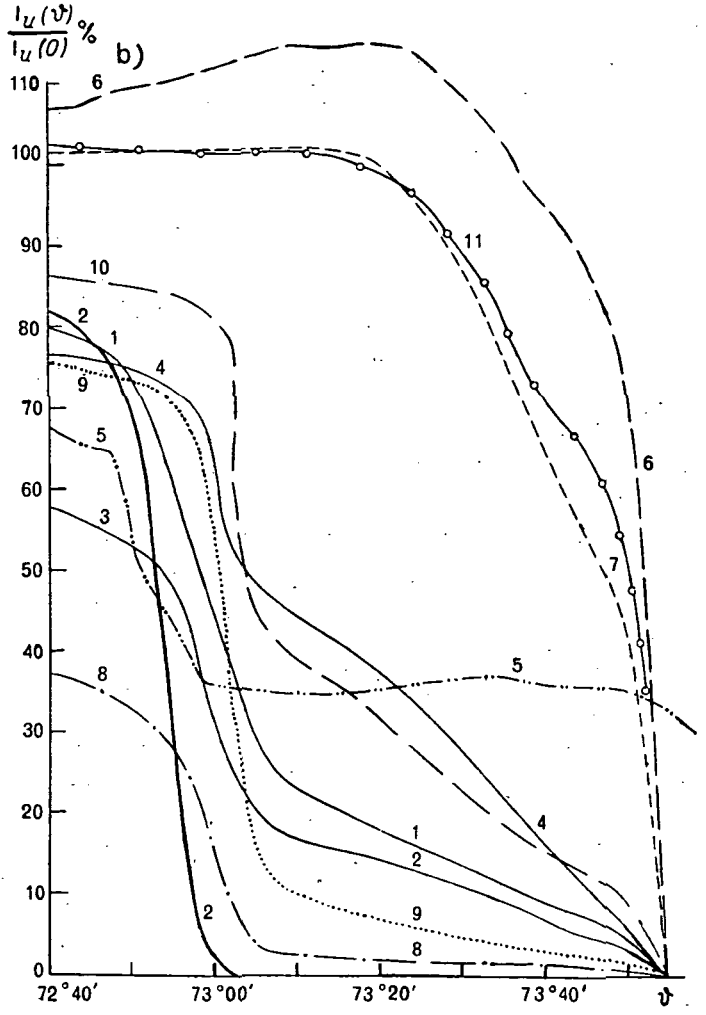

altitude 300 km ($\vartheta_b = 72° 45'$) according to computations in [29, 30], 65° N, summer.
(b) angular distribution at wide zenith angles $\vartheta > \vartheta_b$.
band 6.3 μ of H_2O (4.88-8.70 μ), 4—absorption band 15 μ of CO_2 (12-18 μ), 5—absorp-
7—band of very strong absorption H_2O (41.7-45.5 μ), 8—band of weak absorption H_2O
rotational absorption band of H_2O (18-40μ), 11—region of rotational absorption band of
Fig. 8.6 a show the magnitude of $\frac{I_\omega(\vartheta)}{I_u(O)}$ at $\vartheta = \vartheta_{cr}$.

warm stratosphere (65° N, summer) in spectral frequencies of strong absorption, viz. 6, 7 and 11. An analogous phenomenon (only to a lesser extent) has been observed for the stratification under examination (65° N, summer) and in regions of not so strong absorption 4 and 5 and even in the window 8.70-12.00 μ in the case of an underlying surface at low temperature (high cloudiness with upper boundary at 9 km). Similarly it may be brought about by the substantial contribution of the stratosphere to the outgoing radiation for large ϑ in the spectral intervals points out for the combination of an underlying surface at low temperature and a warm and moist stratosphere.

Computations and results of the artificial satellite measurements show that in the central part of the 15 μ absorption band of CO_2 an infrared glow may be observed for any atmospheric stratification, since in this region of intense absorption the radiation always originates in the stratosphere as a result of the presence of a significant amount of carbon dioxide (see [23]).

There is a sharp fall in the intensity of outgoing radiation in the narrow angular interval in the region of sighting of an atmosphere (large zenith angles: $\vartheta > \vartheta_b$). In those regions of atmospheric window 8-12 μ in which water vapor alone absorbs, an infrared darkening toward the boundary of the atmosphere may be accomplished most sharply, abruptly and rapidly (Fig. 8.6b). It may be noticed that for low zenith angles it is natural that the variation in the intensity of radiation with rising ϑ is weak as compared to these spectral intervals.

The general character of the variation of I_u with respect to variation of ϑ for $\vartheta > \vartheta_b$ is sufficiently stable in the spectral frequencies excluding the interval of very strong absorption situated in the near infrared region of the spectrum. Here the angular dependence of outgoing radiation undergoes noticeable stratificational variation. In the center of the band 15 μ of CO_2 one must observe the maximum resemblance in the angular distribution of outgoing radiation obtained for different atmospheric stratifications.

In partial cloudiness the dependence of the intensity of outgoing radiation on the zenith angle cannot be represented by such smooth curves as shown above. In this case the sharp maxima and minima in the course of I_u (ϑ) make it possible to disguise infrared darkening toward the edge of the atmosphere. Theoretical investigations show that this is possible in transparency regions of the spectrum, situated in the atmospheric window 8-12 μ in the near infrared region (spectral intervals of weak absorption and the near infrared region of the spectrum are most sensitive to variation under conditions of cloudiness). In the distant infrared region of the spectrum there is very little likelihood of screening infrared darkening toward the boundary of the atmosphere by the inhomogeneity of angular distribution of outgoing radiation caused by partial cloudiness of different

strata or inhomogeneity in atmospheric stratification even in wide spectral intervals (18-40, 40-120 μ). Only the central part of the absorption bands of carbon dioxide gas 15 μ can compare in this respect with the distant infrared region of the spectrum for wavelengths $\lambda<18$ μ.

Azimuthal anisotropy of the field of outgoing radiation within the observational limits of the terrestrial disc in a clear sky and in dense cloudiness is not large. However, for $\vartheta>\vartheta_b$ it becomes important. In the presence of partial cloudiness the azimuthal dependence of the intensity of outgoing radiation is extremely significant even for the sighting of central parts of planetary disc. Naturally, the azimuthal anisotropy is greatest in spectral ranges which are sensitive to the appearance of clouds and inhomogeneity in atmospheric stratification.

Measurements by rockets and artificial satellites ascertain many of the patterns [23, 36] examined above. However judging by the experimental data, the altitude of the radiative atmosphere is evidently considerably higher than that accepted in theoretical computations (40-60 km). Besides, intensive infrared radiation of the atmosphere in a horizontal direction (spectral region 2.5-8.0 μ) was discovered during Soviet cosmic experiments [40] at altitudes of 250-300, 420-450 and around 500 km. The maximum intensity of this radiation is either comparable to or exceeds the intensity of outgoing radiation at nadir. Meanwhile it is difficult to interpret the radiation registered as the thermal radiation of the horizontal layers of rarefied atmosphere. Evidently the mechanism of radiation is different.

2.4 Effective radiation

The intensity of the effective radiation I_{eff} ($I_{eff}=I_u-I_G$) decreases with a rise in the zenith angle [16, 42]. The greatest drop in radiation has been observed for directions close to the horizontal. For $\vartheta=90°$, the magnitude of I_{eff} is zero at all altitudes within an optically active and horizontally uniform atmosphere since $I_u=I_G$.

The overall character of angular dependence I_{eff} (ϑ) is preserved for variations in atmospheric stratification and rather weakly depends on the spectral interval and altitude [42].

In the presence of partial cloudiness the smooth curve of the function I_{eff} (ϑ), found in a clear sky and in dense cloudiness, must be distorted by so many maxima and minima. Azimuthal anisotropy of the field of effective radiation, which is weak in cloudless atmosphere and in the case of dense cloud [16], naturally rises in partial cloudiness.

3. VERTICAL PROFILE OF RADIATION

Several results of the determination of vertical distribution of upward,

downward and effective fluxes of atmospheric thermal radiation as well as vertical profiles of thermal radiative fluxes have been derived in this section. Fluxes and influxes of integral thermal radiation, and their magnitudes in different spectral intervals, have been examined.

It is already known [22], that in cloudless atmosphere for normal stratification of temperature the upward and downward fluxes of integral thermal radiation as a rule decrease with altitude. The effective flux of radiation, on the other hand, rises with altitude in a free atmosphere. However, within the limit of the entire troposphere this rise is more or less linear. The rise in effective radiation slows down in the vicinity of the stratosphere. The presence of cloud, especially of the dense type, is reflected in the profiles of radiation by the distortion in the monotonic variation of flux.

Several examples of vertical distribution of atmospheric thermal radiation are shown in Fig. 8.7 (from the articles [43, 59]). The vertical profiles of radiation introduced here have been obtained for moderate latitudes.

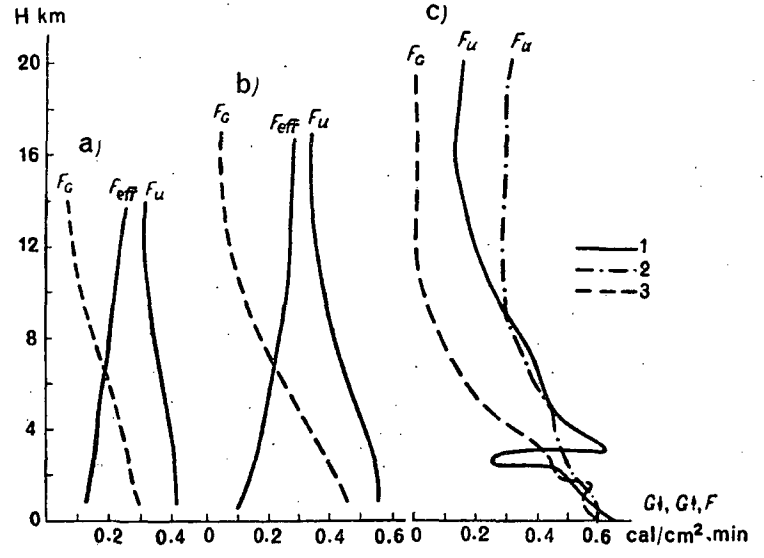

Fig. 8.7. Vertical profiles of downward F_G, upward F_u and effective fluxes of thermal radiation.

(a) USA, winter, averaged values [59]; (b) USA, summer, averaged values [59]; (c) USSR, single layered cloudiness of lower stratum, day [43]; 1—July, 2, 3—October.

A complete investigation on the vertical and meridional variability of integral flux of atmospheric thermal radiation has been carried out by G. N. Kostyan and N. A. Zaitseva. Thus a large amount of data on the vertical and geographical distributions of the field of atmospheric thermal radiation has been accumulated through measurement of radiation by

actinometric radioprobings at different geographic locations. According to data in [31], both downward and upward fluxes of thermal radiation decrease with height at a rate of 250×10^{-5} to 400×10^{-5} cal/cm^2 · min, from 160×10^{-5} to 240×10^{-5} cal/cm^2 · min in 100 m in the troposphere and from 30×10^{-5} to 40×10^{-5} cal/cm · min in 100 m in the stratosphere (downward flux). The gradient for upward flux in the stratosphere is close to zero. In [19, 43], as well as in some investigations by foreign scientists [49, 61] a slight increase in upward fluxes of thermal radiation with height has been recorded in the stratosphere. Evidently this is brought about by peculiarities of the vertical distribution of temperature in the stratosphere, viz. isothermy and inversion of temperature.

An analysis of the variability of effective radiation in free atmosphere has been carried out in [34, 61, 65] on the basis of actinometric probing of the atmosphere. According to data from these investigations the most characteristic problem of vertical profiles of effective radiation consists in its rise with height approximately to a level of 10-13 km, followed by a subsequent decrease in the region of the tropopause and further rise in the stratosphere.

The correlation between effective radiation and cloudiness has been examined in [34, 43]. It has been observed that the anomaly in the distribution of effective radiation is related to the influence of cloudiness. The decrease in the effective radiation on account of the effect of cloud at several altitudes constitutes 0.19 cal/cm^2 · min. As a rule a slight increase in effective radiation with altitude takes place in the layer 1.5-3.0 km in the presence of clouds, and a sharp decrease occurs in the layer 7-10 km. During winter, when the amount of moisture in the atmosphere is not large, cloudiness can increase the effective radiation at high altitudes (as compared to a cloudless condition), thereby redistributing the net radiation in the atmosphere. In the layer of clouds near the earth's surface the effective radiation decreases if there is no increase in the temperature of the underlying surface and isothermy below clouds is not destroyed. The variation in upward fluxes of thermal radiation during winter in the transition from "clear" to "cloudy" and vice versa can become 10-12% in one direction within two to four hours. In cloudy conditions during wintertime one can observe not only a decrease in the upward flux as compared to cloudless conditions, but also an increase in it [34]. In the opinion of the author of this article the values of atmospheric back-radiation on the earth's surface in dense cloudiness may be approximately 20-40% higher than the corresponding flux in clear sky for normal stratification of temperature.

The mean winter profiles of effective radiation for the North Atlantic, computed with the help of the radiation nomograms of V. Elsasser, are given in the Table 8.3. The low magnitudes and anomalous vertical

course of radiation in the lower troposphere are evidently caused by cloudiness in the lower troposphere.

Table 8.3 Mean values of effective atmospheric radiation F_{ett} cal/cm² . min in winter, 1956-57, in the North Atlantic [55]

Place of measurement	p mb					
	1000	850	700	500	300	200
1	0.062	0.069	0.163	0.173	0.181	0.224
2	0.063	0.042	0.169	0.194	0.209	0.274
3	0.066	0.027	0.168	0.187	0.224	0.280
4	0.054	0.038	0.170	0.220	0.253	0.283
5	0.056	0.039	0.127	0.189	0.206	0.262
6	0.066	0.060	0.141	0.206	0.226	0.266
7	0.057	0.039	0.179	0.218	0.239	0.297
8	0.075	0.046	0.180	0.236	0.265	0.321

The vertical profiles of thermal radiation for five models of cloudless atmosphere from results of theoretical computations by the author of this article are given in Table 8.3. The models of atmosphere examined may be briefly characterized in the following manner:

I. standard atmosphere (model ARDC-1959),
II. dry summer in moderate latitudes,
III. damp summer in moderate latitudes,
IV. dry winter in moderate latitudes, and
V. damp winter in moderate latitudes.

A comparison of these results with corresponding vertical profiles of radiation in Fig. 8.7 shows that the theoretical magnitudes of the integral flux of effective radiation for "damp" atmospheric models III and V agree satisfactorily with mean leveled experimental profiles of flux at corresponding times of the year. However, the rate of decrease with altitude of downward thermal radiation obtained, on the basis of theoretical values, is noticeably higher than that obtained from experimental data, and consequently in the upper troposphere and stratosphere the theoretical values of back-radiation are lower than experimental values. It should also be

observed that vertical profiles of thermal radiation under real, specific synoptic (weather) situations may differ significantly from mean theoretical values.

Table 8.4 The values of integrated fluxes is of downward F_G and effective F_{eff} atmospheric thermal radiation for models of atmospheric I-V (region of the spectrum 2000-225 cm^{-1})

p mb	H km	Model				
		I	II	III	IV	V
		F_G cal/cm^2 · min				
1013	0	0.384	0.378	0.456	0.183	0.220
898	1	0.326	0.324	0.382	0.160	0.195
795	2	0.274	0.272	0.322	0.138	0.169
617	4	0.195	0.193	0.233	0.102	0.131
472	6	0.130	0.128	0.162	0.072	0.097
265	10	0.042	0.044	0.068	0.035	0.050
76	18	0.024	0.024	0.034	0.021	0.028
12	30	0.013	0.011	0.019	0.008	0.014
0.9	50	0.003	0.003	0.007	0.003	0.005
		F_{eff} cal/cm^2 · min				
1013	0	0.142	0.186	0.108	0.152	0.115
898	1	0.180	0.222	0.153	0.169	0.133
795	2	0.204	0.248	0.185	0.183	0.146
617	4	0.240	0.286	0.224	0.205	0.169
472	6	0.270	0.316	0.252	0.222	0.188
265	10	0.315	0.357	0.294	0.242	0.211
76	18	0.320	0.364	0.311	0.250	0.227
12	30	0.326	0.375	0.325	0.261	0.239
0.9	50	0.345	0.386	0.343	0.270	0.254

Vertical profiles of integral flux of atmospheric thermal radiation have been examined above. However, the character of the vertical distribution of the spectral flux of radiation can in many cases differ noticeably from the distribution of integral radiation. As an illustration we introduce the vertical profiles of spectral fluxes of downward and effective radiations for different spectral frequencies obtained on the basis of results computed by the present author (Tables 8.5 and 8.6). The rate at which atmospheric

downward radiation decreases with altitude depends strictly on wavelength λ (or on the wave number ν). The spectral dependence of vertical profiles of effective radiation (Table 8.6) is clearly expressed. If there is an absence of inversion in the vertical course of effective radiation in the frequency intervals 400-375 cm^{-1}, and 940-900 cm^{-1}, then in the central regions of the absorption band of water vapor, ozone and carbon dioxide inversion may be observed either in the middle of the troposphere (wave number about 1500 cm^{-1}) or in upper troposphere (wave number about 650 cm^{-1}), and in the center of absorption band of ozone (about 1040 cm^{-1}). The range of altitudes within whose limits the effective radiation decreases with height is extremely large, viz. from 5 to 30 km.

A great deal of research work has been devoted to the investigation of the field of radiative fluxes of heat in the atmosphere (see for instance [12, 20, 22, 31, 49, 51, 55 and 58-62]). Radiative cooling of air [20] is usually observed in free atmosphere in the absence of cloudiness. The characteristic distribution of radiative cooling with altitude in clear atmosphere is shown in Fig. 8.8. It is obvious that the temperature stratification in the vicinity of the earth's surface has a considerable influence on the vertical profile of radiative temperature variation up to a height of the order of 700-600 mb. The minimum of absolute values of radiative cooling is situated above the tropopause.

Table 8.5 The values of spectral fluxes of incoming thermal radiation for standard model of atmosphere in different spectral intervals (10^{-5} W/cm^2 . μ)

H km	$\Delta\nu$ cm^{-1}				
	1550-1500	1040-1033	940-900	675-650	400-375
0	149.9	101.3	59.80	178.4	54.22
1	122.3	77.31	32.77	162.8	50.75
2	97.12	61.52	16.90	146.7	46.61
3	79.73	51.50	8.340	134.2	42.24
5	51.80	39.99	1.754	110.8	30.20
7	30.29	33.68	0.2965	89.37	16.57
10	7.055	28.72	0.00894	61.68	3.152
18	3.678	25.96	0.00152	46.73	1.500
30	4.224	21.28	0.00051	26.69	1.089
40	4.374	13.61	0.00015	16.07	0.7298
50	1.976	2.333	0.00002	6.206	0.2777

Table 8.6 Values of spectral fluxes of effective radiation for standard atmospheric model in different spectral intervals (10^{-5} W/cm · μ^2)

H km	$\Delta\nu$ cm^{-1}				
	1550-1500	1040-1033	940-900	675-650	400-375
0	2.579	153.4	192.2	1.469	0.4300
1	11.64	174.2	217.5	6.820	1.858
2	14.39	184.4	230.5	9.516	3.320
3	17.32	188.9	236.2	12.34	5.699
5	13.09	190.4	239.8	11.56	13.05
7	11.76	187.6	239.8	11.19	23.01
10	16.54	179.7	239.5	10.93	33.22
18	16.41	145.1	239.7	12.77	34.21
30	16.29	116.2	239.0	37.94	34.66
40	18.91	129.6	239.0	58.14	35.31
50	24.15	145.9	238.4	72.88	35.96

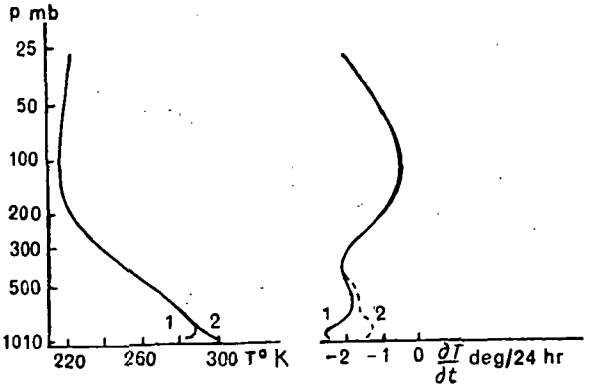

Fig. 8.8. Vertical profiles of temperature and corresponding radiative temperature variations in cloudless weather in the ease of temperature inversion at the surface of the earth (1) and without inversion (2) the influence of ozone on $\partial T/\partial t$ is not taken into consideration [51].

According to data in [61], radiative cooling in the troposphere caused by thermal radiation amounts on an average to 1-2 deg/24 hrs upto a level of 200 mb. At heights 3, 6 and 10 km stable maxima of the radiative cooling have been observed in a clear sky, and radiative heating has been observed below the tropopause. Radiative temperature variation in the stratosphere on an average exceeds the values in the troposphere by five

times, and the values may be far more variable. The vertical profiles of radiative cooling for different climatic and synoptic conditions are given in [68]. The maximum values $|\partial T/\partial t|$ are around -3 deg/24 hrs. In the case of clear weather the maximum of radiative cooling may be situated at heights between 8 and 10 km. The Arctic, where this maximum is situated at about a height of 1.5 km, appears to be an exception. The minimum magnitudes $|\partial T/\partial t|$ have been observed at the height of the tropopause and similarly at the earth's surface.

The author of this article has computed the variation in radiative temperature for clear weather in the case of the atmospheric models I-V mentioned above. The results of computations of $|\partial T/\partial t|$ for the spectral frequencies 2000-225 cm^{-1} show that radiative cooling has been observed at all heights in the atmosphere (of the order of 2-3 deg/24 hrs.) in the vicinity of the earth's surface and in the upper stratosphere (Table 8.7) for the atmospheric models examined in cloudless weather. The minimum values of $|\partial T/\partial t|$ have been recorded in the range of altitudes 10-20 km, and this minimum is lower during winter than in summer. The high values of radiative cooling at the earth's surface occur in this case because rapid changes in temperature at the earth's surface are not considered (it is assumed that the temperature of air at the earth's surface is equal to the effective radiative temperature of the earth). However, consideration of the rapid jumps in the temperature of the "earth's surface-air" as well as of the detailed behavior of temperature and moisture in the surface layer can give very serious deviations of vertical distribution of the radiant influx of heat from the average "model" behavior. For instance, it is

Table 8.7 Radiative variation of temperature $\partial T/\partial t$ deg/24 hrs for standard atmospheric model in different regions of the spectrum

H km	$\Delta\nu$ cm^{-1}				
	2000-1200	1170-940	800-550	525-225	2000-225
0	—0.47	—0.44	—0.69	—0.40	—2.60
1	—0.22	—0.25	—0.38	—0.22	—1.46
2	—0.18	—0.13	—0.45	—0.42	—1.45
4	—0.060	—0.020	—0.30	—0.56	—1.08
6	—0.070	0.014	—0.25	—0.89	—1.26
10	—0.040	0.044	—0.020	—0.69	—0.71
18	—0.003	0.18	—0.39	—0.053	—0.28
30	—0.030	0.11	—2.09	—0.79	—2.80

shown in [71, 72] that a consideration of rapid jumps in temperature of the order of 3-5° K even changes the sign of the radiant influx of heat and the influence of this jump on the magnitude of $\partial T/\partial t$ can be distinctly traced up to a height of 5 km. In this manner extremely accurate and detailed information about the values of meteorological parameters in the atmosphere is required for a reliable determination of the radiant influx of heat.

The influence of cloudiness on values of the radiant influx of heat has been investigated by L. M. Gradus and E. M. Feigel'son [12]. They computed the integral flux of thermal radiation at different altitudes of cloudy layers for thickness of underlying and overlying cloudy layers. It was shown that radiative cooling decreases considerably in the layer below the clouds as compared to clear atmosphere, dipping almost to zero in cloudiness of the lower and intermediate strata. Radiative cooling has been observed above the clouds as well. Thus, in case of multilayered cloudiness, and similarly for inversion layers and layers of fog and aerosol in the atmosphere, extremely complex vertical profiles of the radiant influx of heat with inversion have been observed showing sharp changes in magnitude and sign. This has been confirmed by the results in [31, 49, 55, 62]. In [31] the following conclusion has been arrived at, viz. that in general the troposphere and stratosphere are heterogeneous with respect to radiative properties and can have layers with high values of the rate of radiative cooling, averaging 0.04-0.05 and 0.02-0.06 deg/hr respectively. In the region of the troposphere one may observe layers with radiative heating up to 0.03 deg/hr, although the mean rate of variation in the radiative temperature of the tropopause is around zero.

It is interesting to note that the effect of cloudiness on the magnitudes of the radiative influx of heat in most cases appears even at high altitudes in the atmosphere. Thus, for instance, the data on variability of magnitudes $\partial T/\partial t$ in the absorption band of ozone 9.6 μ at altitudes from 10 to 33 km with respect to variation in cloud conditions are given in [58]. According to results in this reference the magnitudes of radiative heating decrease three to five times with the upper boundary at a height of 9 km in the stratosphere as a result of transition from a clear sky to cloudiness.

Comprehensive theoretical computations for the determination of vertical, seasonal and geographic variations of the radiative influx of heat under conditions of average cloudiness were accomplished by London and Davison. (The fundamental results of their computations are given in [20].) According to the data of these researchers, as a rule the maximum of cooling is situated in the middle of the troposphere, directly above the zone of maximum frequency of recurrence of the upper boundary of cloudiness.

The values of radiative cooling in the middle region of the troposphere and above the tropopause obtained in [55] (see Table 8.8) are

extremely high. It should be noticed that radiative heating has been observed almost in all cases in the lower layers (1000-850 mb).

Table 8.8 Mean values of radiant influx of heat $\partial T/\partial t$ deg/24 hrs in winter 1956-57 from data of eight stations in North Atlantic Territory [55]

Station	p mb				
	1000-850	850-700	700-500	500-300	300-200
1	—0.27	—3.68	—0.29	—0.24	—2.50
2	0.82	—5.00	—0.73	—0.45	—3.83
3	1.42	—5.56	—0.56	—1.10	—3.32
4	0.55	—5.21	—1.47	—0.96	—1.17
5	0.69	—3.46	—1.83	—0.50	—3.32
6	0.69	—3.31	—1.92	—0.59	—2.36
7	0.62	—5.54	—1.15	—0.62	—3.42
8	1.00	—5.29	—1.66	—0.85	—3.31

An investigation on vertical distribution of the radiant influx of heat in the stratosphere is of special interest. In view of the low values of density of air at these altitudes even a small influx of heat introduces a noticeable amount of variation in radiative temperature. On the other hand, the determination of the concentration of absorbing substances in the stratosphere is associated with large relative errors and as a result of this noticeable errors in the radiant influx of heat may arise. Hence the values of $\partial T/\partial t$, obtained for the stratosphere in concrete synoptic situations and in a "model" atmosphere, may differ widely and any degree of accuracy demands a special study.

The majority of researchers (see, for instance [51, 55, 61, 65]), as already explained above, observe that there is far more radiative cooling in the stratosphere than in the troposphere, and that the magnitudes of $|\partial T/\partial t|$ rise with altitude. It should be noticed that a review of the vertical and geographic distribution of variations in radiative temperature in the stratosphere has been undertaken in the monograph by Kondrat'ev [20].

Thermal radiation is of interest in the separate evaluation of the rule of each of the fundamental absorbing components of the atmosphere in the establishment of variations in radiative temperature. Fig. 8.9 shows vertical profiles, averaged over a year, of $\partial T/\partial t$ for absorption bands of water vapor, and similarly for bands of carbon dioxide 15 μ and ozone 9.6 μ [60]. From these results it follows that the absorption band of O_3 introduces radiative heating in the atmosphere at altitudes of 15-30 km, carbon

dioxide causes a cooling of the atmosphere which is especially marked at altitudes above 15-20 km; radiative cooling, caused by water vapor, attains a maximum in the upper troposphere and upper stratosphere. Analogous conclusions have been drawn in the works of T. Sasamori, D. London, S. D. Walshaw and the present author (see Table 8.7).

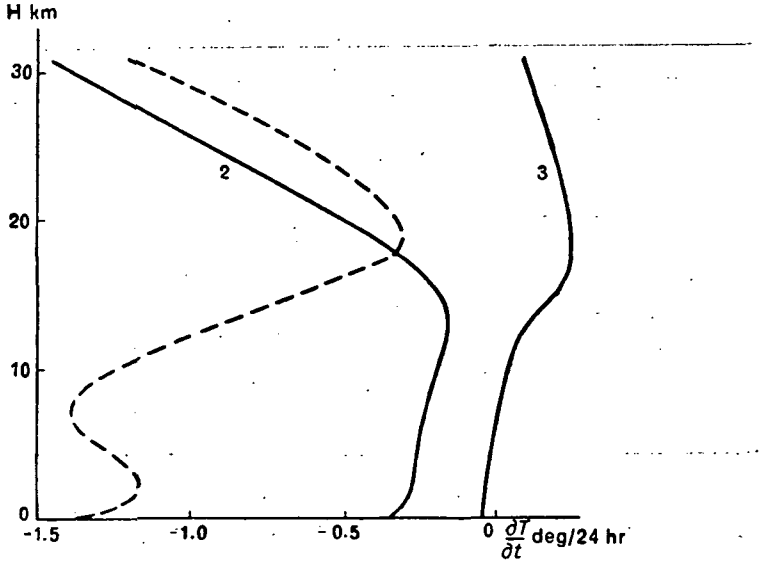

Fig. 8.9. Vertical profiles (averaged over the entire earth) of variations in radiative temperature caused by water vapor (1), carbon dioxide (2) and ozone (3) [60].

Similarly computations on spectral distribution of vertical profiles $\partial T/\partial t$ for the atmospheric models I-V, mentioned above, have been carried out by the present author. As an illustration the results on computation of $\partial T/\partial t$ for several narrow spectral ranges at different altitudes in the atmosphere are given in Table 8.9. The data in this table show that one cannot draw any conclusions regarding integral radiation for negative values of $\partial T/\partial t$; and that all the spectral values of $\partial T/\partial t$ are negative; in fact the values of $\partial T/\partial t$ are positive or close to zero at several heights in most spectral intervals. The resulting negative values of radiative variations of temperature can be obtained as a result of very large values of radiative cooling in several spectral ranges (for instance, in the distant infrared region).

The results of computations on the vertical distribution of the radiant influx of heat in narrow spectral intervals have been derived in the works of Kondrat'ev, Styro and Zhvalev (for a concrete synoptic situation in

Table 8.9 The values of radiative temperature variations $\partial T/\partial t$ deg/24 hr in case of standard atmospheric model for different spectral intervals

H km	$\Delta\nu$ cm^{-1}				
	1550-1500	1040-1033	833-800	675-650	400-375
0	—0.0262	—0.0129	—0.0975	—0.0453	—0.0289
2	—0.0051	—0.0037	—0.0427	—0.0233	—0.0322
4	0.0059	—0.0004	—0.0194	0.0023	—0.0643
6	0.0020	0.0012	—0.0058	0.0014	—0.1081
8	—0.0057	0.0025	0.0004	0.0001	—0.1104
10	—0.0062	0.0046	0.0015	0.0055	—0.0597
14	0.0001	0.0106	0.0002	—0.0050	—0.0078
18	—0.0006	0.0188	—0.0002	—0.0851	—0.0057
22	0.0008	0.0285	—0.0006	—0.1534	—0.0073
26	0.0012	0.0279	—0.0020	—0.2786	—0.0154
30	—0.0097	0.0020	—0.0049	—0.5931	—0.0419

Rostov-on-Don). The results of this investigation showed that radiative cooling occurs at all heights in all spectral intervals examined.

It may be mentioned that the data on vertical distribution of radiative temperature variation are only approximate in most cases. Since the values of $\partial T/\partial t$ are dependent on the detailed structure of vertical profiles of temperature and thermal radiation in the atmosphere, as well as on the absorbing substance, extremely accurate and detailed information about the values of meteorological parameters in the atmosphere is required in order to determine these quantities reliably, especially at the earth's surface and, obviously, on the surface of clouds as well. It is known that the results of computations on the radiant influx of heat by different methods differ considerably. The relative errors in the radiative influx of heat at low absolute values are especially large, since the approximate method of computation guarantees only a limited degree of accuracy.

4. GEOGRAPHIC DISTRIBUTION OF LONGWAVE BALANCE IN THE ATMOSPHERE AND ITS COMPONENTS

The data on geographic distribution of atmospheric thermal radiation, available in literature, refer chiefly to longwave balance in the atmosphere and to its components, i.e. to the effective radiation of the underlying surface and outgoing radiation.

4.1 Outgoing radiation

The magnitude of the outgoing radiation has been computed by Vinnikov (8, 9) from the formula which was obtained by solving the transition equation of longwave radiation in the atmosphere. The following suggestions were made with respect to these results. Temperature of the air was considered to be linearly dependent on height and the variation of mass of water vapor in the troposphere to be related to height through an exponential function.

The magnitudes of outgoing radiation F_∞ were computed at 260 places uniformly distributed on the earth, and the time and space variation of the outgoing radiation was determined.

Charts of monthly and annual amounts of outgoing radiation were obtained as a result of these investigations. As an illustration, Figs. 8.10a and 8.10b give distribution charts of monthly amounts of outgoing radiation on the earth for the months of January and July.

An analysis of the charts of monthly and annual amounts of outgoing radiation shows that the field of outgoing radiation is fairly homogeneous and the values of outgoing radiation changes within limits of comparatively small range for monthly and annual amounts. A rise in the values of F_∞ from the poles to the tropical region may be observed in all charts. Such a state of affairs can be explained primarily by an increase in the mean temperature of the troposphere and secondly by the decreasing cloudiness in the high-pressure belts.

The monthly amounts F_∞ in January change from 10 kcal/cm^2 · mon at high latitudes to 16 kcal/cm^2 · mon in the tropics, and in July from 12 kcal/cm^2 · mon to 18 kcal/cm^2 · mon respectively.

The annual amounts vary from values less than 140 kcal/cm^2 · yr in the region of polar latitudes to values exceeding 200 kcal/cm^2 · yr in the regions of North Africa and Arabia.

The maximum values of outgoing radiation have been observed above deserts for low latitudes, where the high temperature of air at low moisture content and insignificant cloudiness may be found.

In places with noticeable cloudiness and sufficiently high moisture in the air (equatorial region) the values of outgoing radiation decrease considerably but a continuous band of lowered values of F_∞ is not observable. The variation in the values of F_∞ depends on the moisture content of the atmosphere and presence of cloudiness.

The zonal distribution of outgoing radiation is noticeably distorted under the influence of cold and warm sea currents.

The warm current of the Gulf Stream and the cold Peruvian current, which exert a considerable influence on the nature of isolines in the course of a year, may serve as distinct examples.

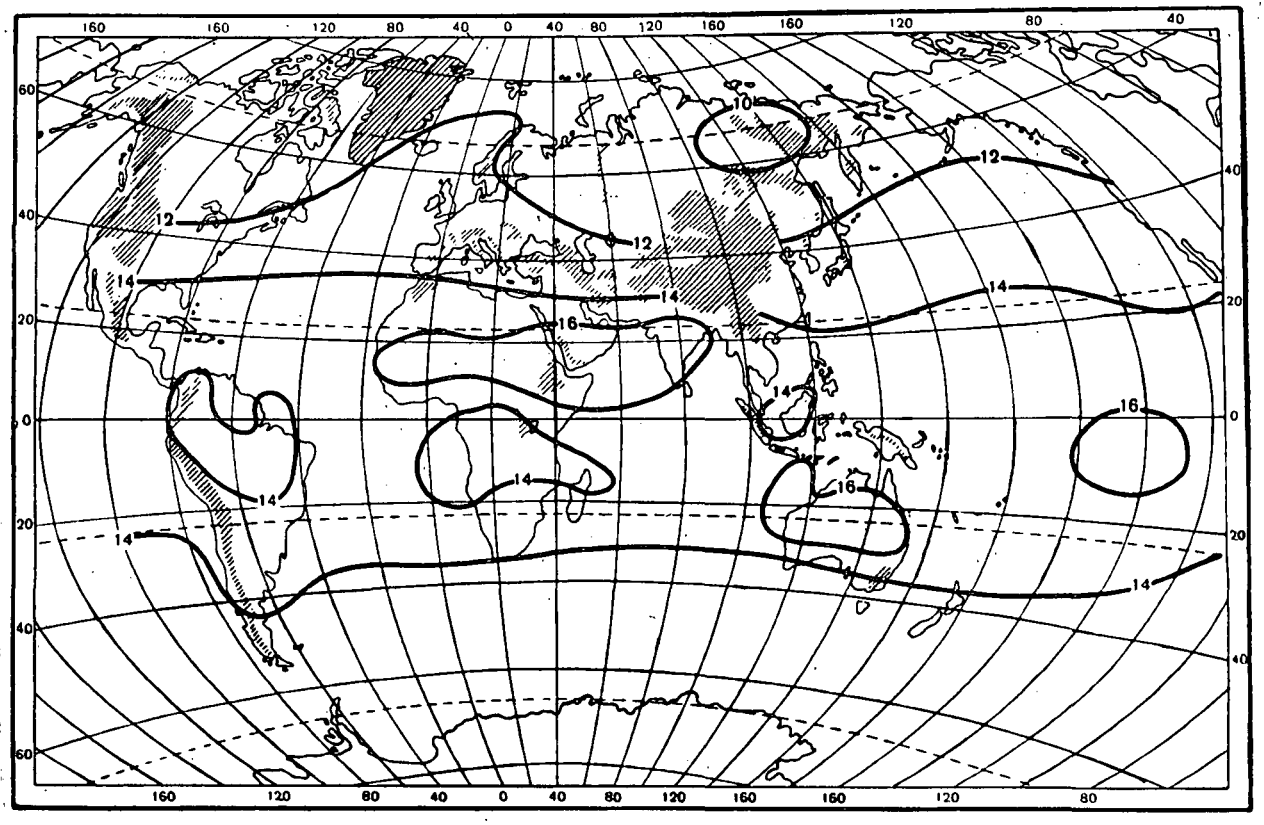

Fig. 8.10a. Geographic distribution of monthly amounts of outgoing radiation (kcal/cm²) [8, 9], January.

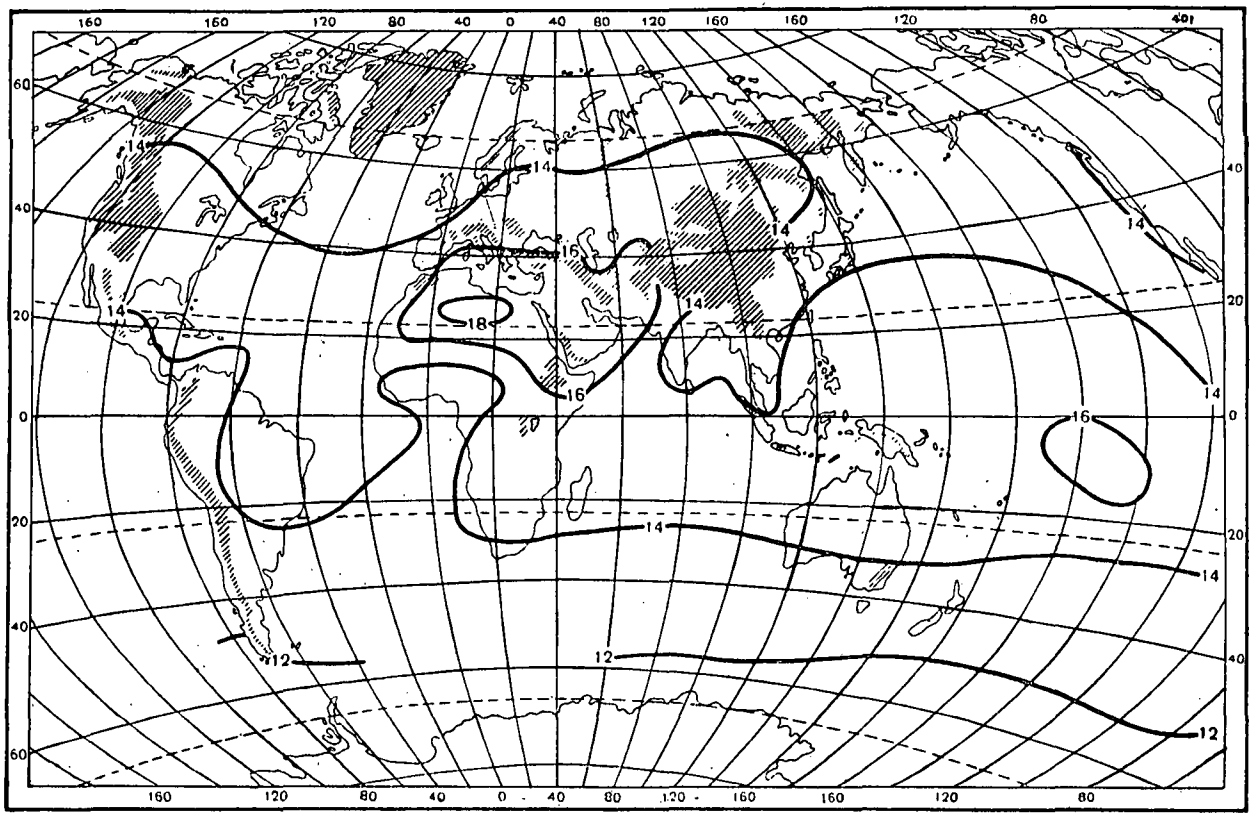

Fig. 8.10b. Geographic distribution of monthly amounts of outgoing radiation (kcal/cm²) [8, 9], July.

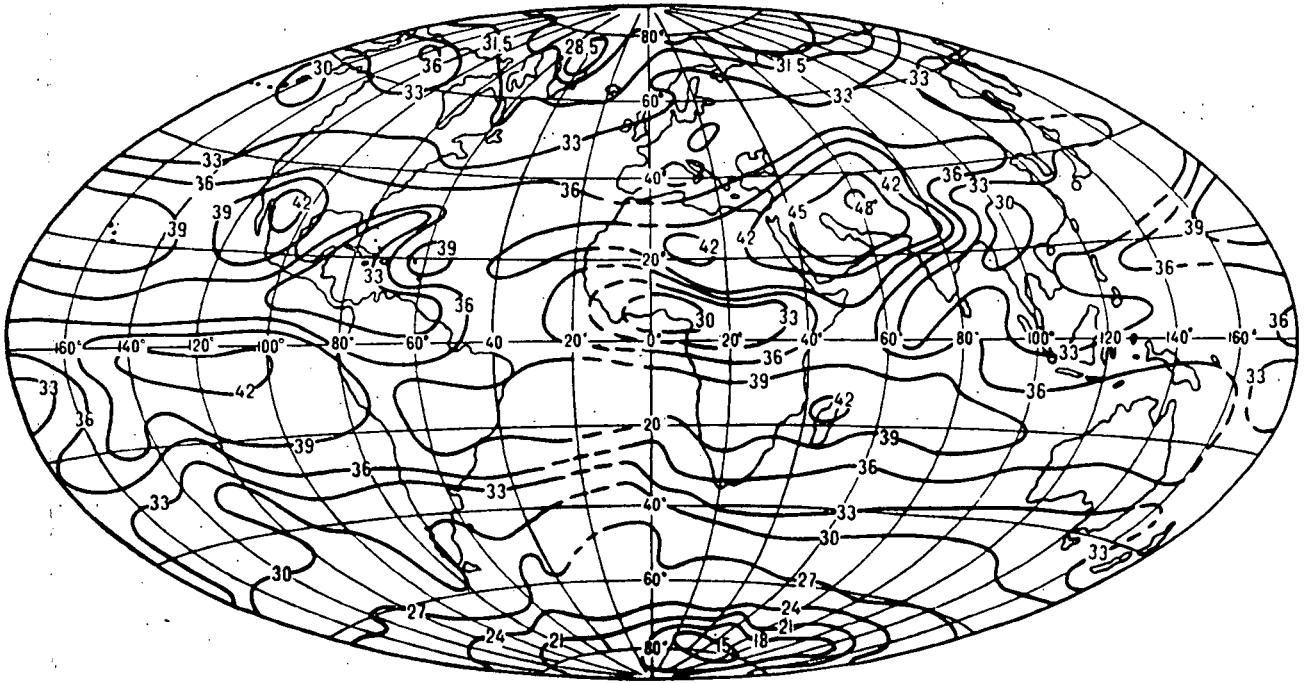

Fig. 8.11 Outgoing radiation (10^{-2} cal/cm^2 . min) June 1-15, 1966, after measurements from satellite "Nimbus II" [64].

The shifting of the thermal equator toward the North from the geographic equator and the large oceanity of the Southern Hemisphere also affect the distribution of the field of outgoing radiation. All this leads to the fact that on an average thermal radiation of the Southern Hemisphere is lower than that of the Northern.

Extremely widespread and most reliable experimental investigations on the outgoing radiation of the earth-atmosphere system were carried out by Raschke and Pasternak [64] and similarly examined in the works of Raschke, Miller and Bandeen [63]. Employing the data of measurements from "Nimbus-II" which (as distinct from the satellite "Tairos") was at first set in a polar orbit, the authors were able to construct charts of distribution of outgoing longwave radiation over the earth, averaged for the period from 1 to June 15, 1966 (Fig. 8.11). The results of measurements of outgoing longwave radiation for data from the satellite "Nimbus-II" in June, 1966, have been discussed in [63].

4.2 Effective radiation of the underlying surface

The effective radiation of the underlying surface F_0 was computed by Efimova and Strokina [17, 18] from theoretical formulas while taking into consideration its dependence on the temperature of the underlying surface, temperature stratification of the atmosphere and its moisture content and cloudiness (a linear relation between the effective radiation and cloudiness is accepted).

The geographic distribution of effective radiation of the underlying surface over the earth is represented here in the form of charts for the two months, viz. January (Fig. 8.12a), July (Fig. 8.12b), being taken from [17, 18].

The maximum values of effective radiation averaged over a year, of the order of 80-90 kcal/cm^2 · yr, have been recorded in regions with high temperature of the underlying layer and low values of moisture and cloudiness. This is found to take place in the deserts and in arid regions in tropical latitudes. Considerably lower values of effective radiation (of the order of 30-40 kcal/cm^2 · yr) have been observed in the region of trade-winds and above the oceans. This happens on account of increased moisture in the air and some increase in cloudiness.

In the presence of polar latitudes (Arctic and Antarctic), where in the course of a year one finds low temperatures of the underlying surface, inversion in winter and considerable cloudiness in summer, the maximum of effective radiation has been recorded (less than 20 kcal/cm^2 · yr).

The presence of cold and warm oceanic currents exerts a considerable influence on the course of isolines of effective radiations. The cold currents may slightly decrease the value of effective radiation, whereas warm currents may somewhat increase it.

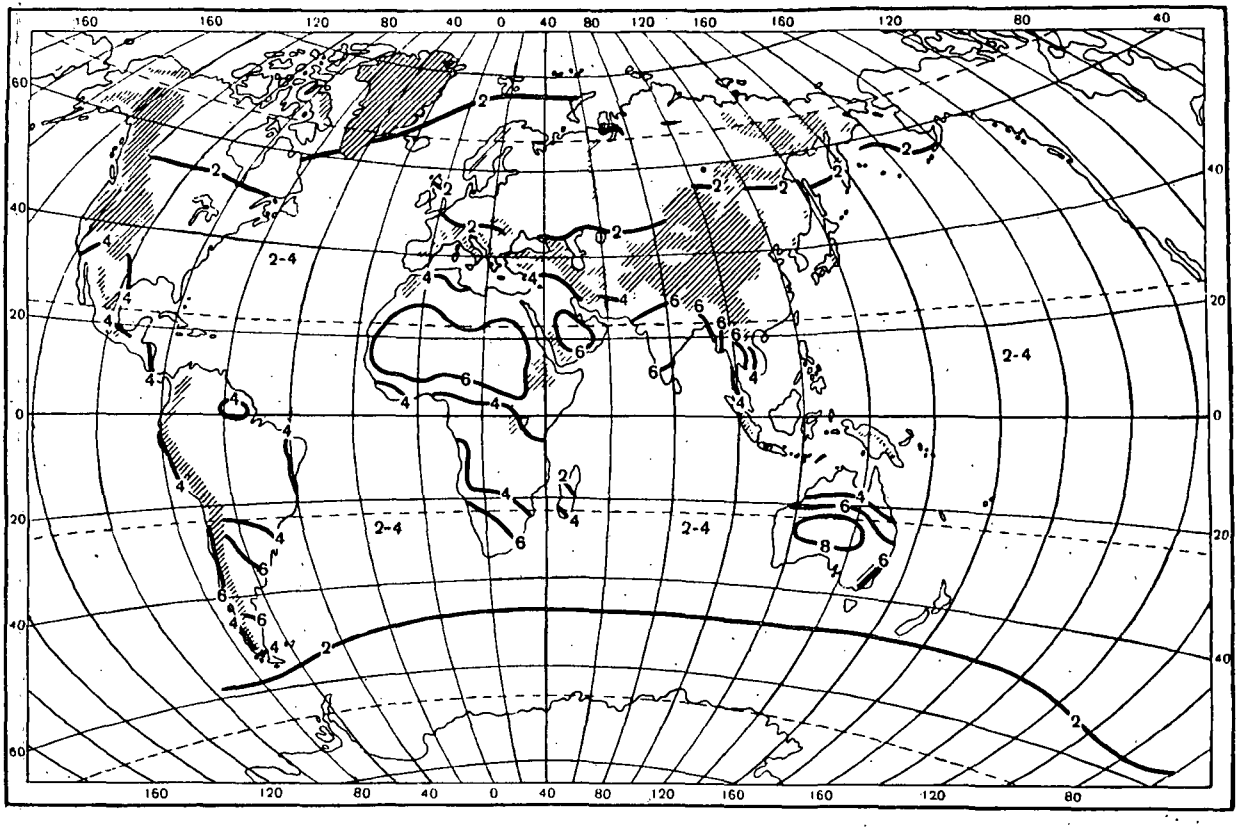

Fig. 8.12a. Effective radiation of surface (kcal/cm²) [17, 18], January. Monthly amounts.

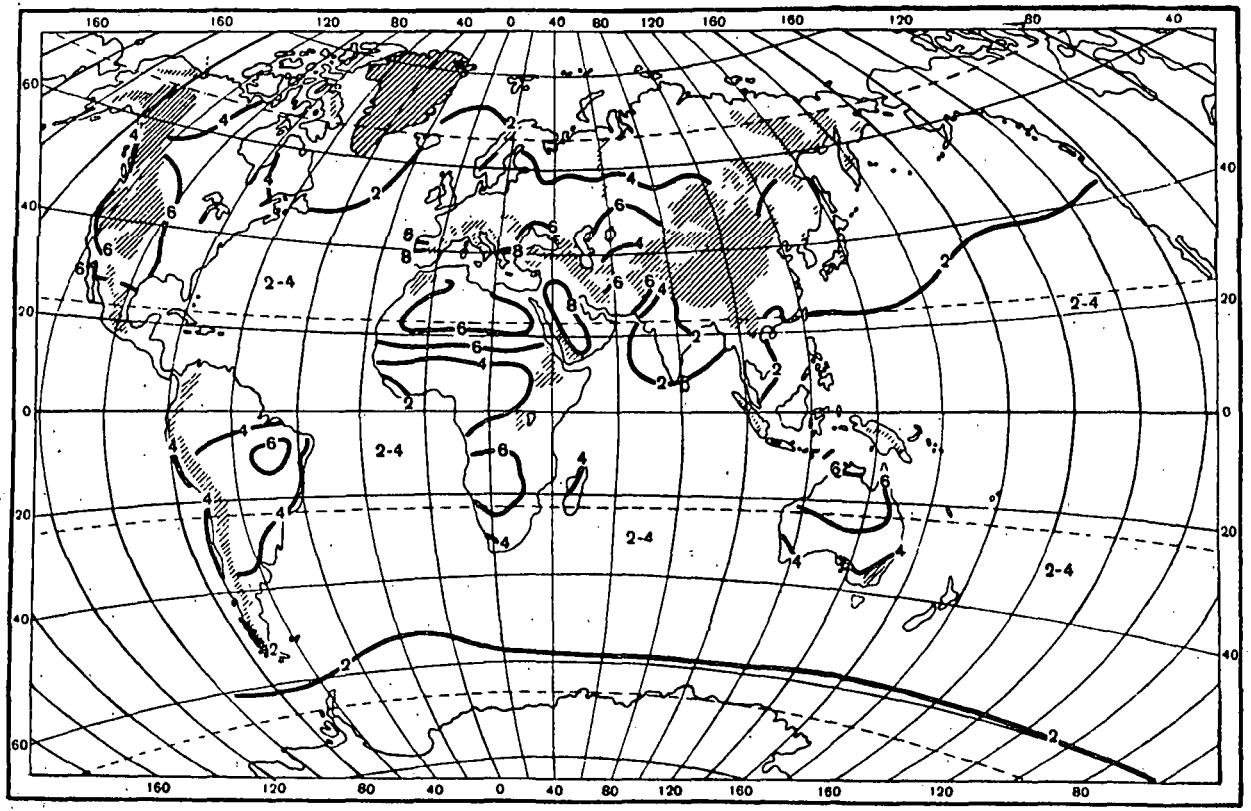

Fig. 8.12b. Effective radiation of surface (kcal/cm²) [17, 18]. July. Monthly amounts.

The character of isolines of effective radiation of the underlying surface in the average monthly and yearly charts exhibits analogous fundamental features. However, the properties of the season being studied may in this case exert a specific influence.

The distribution charts of effective radiation are simpler in the Northern Hemisphere during wintertime than in summer. In January the isolines have an almost latitudinal direction whereas in July this is somewhat distorted.

The highest value of effective radiation in the Northern Hemisphere has been observed in the desert region of Africa and Asia. In the Southern Hemisphere the maximum occurs in January (summer) above the desert region of Central Australia and comprises values exceeding 8 kcal/cm² · mon.

In the Southern Hemisphere the value of effective radiation of the underlying surface in July (winter) increases as one proceeds from the pole (2.0 kcal/cm² · mon) to the tropics. The maximum values (above 6 kcal/cm² · mon) have been recorded in the regions of the Australian and South Africa deserts. In the tropics and less arid subtropical regions the value of effective radiation decreases considerably and constitutes values of the order of 3.5-5.0 kcal/cm² · mon, and in the zone of moderate latitudes it is 2.5-3.0 kcal/cm² · mon.

L. N. D'yachenko [14] derived distribution charts of annual and monthly amounts of effective radiation of the surface over the Soviet Union territory, being constructed on the basis of measured data. An analysis and comparison with analogous charts were carried out simultaneously, the latter being constructed according to data computed by Efimova.

While constructing and analyzing these charts the values of effective radiation were examined, taking into consideration the following, viz. distribution of air temperature over the territory of the USSR, the amount of precipitation, the number of days with precipitation and the amounts of solar radiation. In addition, they employed charts of average cloudiness given in the works of T. G. Berlyand [4].

A comparison between measured and computed values of effective radiation for the territory of the USSR provides a sufficiently close agreement.

An analysis of measurements shows that the entire territory of the Soviet Union is characterized by a monotonic decrease in the effective radiation with increase in latitude. The lowest annual amounts have been recorded in the North and consist of the value of 20 kcal/cm² · yr. The field of effective radiation in the Northern region of the USSR is diffuse and possesses low gradients.

The maximum values of annual sums F_0 have been recorded in Central Asia (in Kara Kum desert and in the region of Mt. Karabil), attaining values of the order of 700 kcal/cm² · yr.

In the monthly distribution charts of F_0 [14] the isolines pass through 1 kcal/cm² · mon. An analysis of the charts shows that the value of effective radiation changes during winter (December, January and February) from 1 kcal/cm² · mon in the North to 4 kcal/cm² · mon in the South.

In Central Asia in the region of the Kara Kum desert the values F_0 exceed 3 kcal/cm² · mon in December and January and 4 kcal/cm² · mon in February. Similarly monthly amounts F_0 are found to occur in the Far East region of the USSR.

In Northern and Central Parts of the territory of the USSR the field of effective radiation is extremely diffused. The monthly amounts F_0 vary around 1 kcal/cm² · mon.

An increase in effective radiation has been observed in the entire territory of the USSR with increasing heat influx during springtime. It varies in values below 2 kcal/cm² · mon in the North to values above 5 kcal/cm² · mon in the Southern region of Central Asia.

During summers (June, July, August) the monthly amounts of effective radiation attain the annual maximum. They exceed the values 8 kcal/cm² · mon in some instances in the Southern region of Central Asia. The highest temperatures in the Soviet Union and insignificant cloudiness have been recorded in this region.

In September, October and November the values of effective radiation gradually decrease to 1 kcal/cm² · mon in the North and to 4 kcal/cm² · mon in the South.

4.3 The longwave balance of the atmosphere

The longwave balance of the atmosphere (radiant heat influx in the entire thickness of atmosphere due to longwave radiation) may be determined as the difference between two radiative fluxes : viz. effective radiation at the earth's surface and the outgoing radiation.

In an overwhelming majority of cases the longwave balance of the atmosphere is negative since the atmosphere, in effect, loses heat on account of longwave radiation.

In order to emphasize the importance and necessity of studying longwave components of radiative heat influx in the atmosphere, we will carry out qualitative evaluation of heat balance and its distinct components [7, 20].

According to modern representation, albedo of the earth as a planet equals 0.35. Thus shortwave radiation absorbed by the earth equals 168 kcal/cm² · yr.

Shortwave solar radiation amounting to 130 kcal/cm² · yr falls at the earth's surface. If the average weighted value of albedo of the earth's surface equals 0.14, then it absorbs solar energy q_e is equal to 112 kcal/cm² · yr,

and reflects 18 kcal/cm² · yr. Consequently that part of heat which is absorbed by the earth's atmosphere equals 56 kcal/cm² · yr and comprises almost one-third of the quantity of radiation absorbed by the earth's surface.

There is a decrease in the thermal loss of the earth's surface on account of longwave radiation. The effective radiation F_0 at the level of the earth's surface constitutes 40 kcal/cm² · yr on an average. Finally the earth's surface receives about 72 kcal/cm² · yr in the form of energy of the net radiation which is dispersed partially in vaporization (59 kcal/cm² · yr) and in a turbulent heat exchange in atmosphere (13 kcal/cm² · yr).

The overall quantity of longwave radiation of the earth F_∞, or the outgoing radiation at the level of the upper boundary of the atmosphere, averaged over a year for the whole earth, is equal to the quantity of absorbed solar radiation q_s i.e. 168 kcal/cm² · yr. Thus the difference of heat in the atmosphere and radiation ($B_{LW}=F_0-P_\infty$) comprises 128 kcal/cm² · yr. This difference is compensated in the absorbing atmosphere by solar radiation (56 kcal/cm² · yr) and by heat influx caused by the condensation process in water vapor (59 kcal/cm² · yr) and in turbulent heat transfer (13 kcal/cm² · yr).

The numerical characteristics of distinct components of the thermal balance of the earth given above clearly emphasize the importance and significance attached to the magnitude of the radiative influx of heat on account of longwave radiation in the overall heat balance of the earth-atmosphere system.

The geographic distribution of the longwave balance of atmosphere over the earth is examined below.

L. H. D'yachenko and K. Ya. Kondrat'ev [15] constructed world maps of monthly and annual amounts of longwave balance of atmosphere on the basis of computed data.

As indicated above, the magnitude of the longwave balance of atmosphere B_{LW} is negative. Absolute values of B_{LW} are employed for the construction of charts for convenience. The charts were constructed from the data of 260 places uniformly distributed on the earth. This number includes 165 stations situated on land and 95 in the oceans.

The regions of polar latitudes (above 80° N and 70° S) and mountainous regions were not surveyed because of insufficient volume of necessary data. It may be noticed that the mountainous regions are shaded in the charts. The overall area investigated comprises 460.1×10^6 km² and the entire area of the earth is 510×16^6 km².

The isolines pass through 20 kcal/cm² in the charts on distribution of annual amounts of longwave balance of the atmosphere. In the monthly charts they pass through 2 kcal/cm². In [15] the charts of distribution of annual amounts of longwave balance of atmosphere and 12 other monthly charts are shown. Here we show only two charts, viz. for

July and January.

One can easily see while examining the charts constructed that the field of atmospheric longwave balance is sufficiently homogeneous and the range of variation of the monthly and even the annual amounts is not large. A gradual increase in the magnitudes of B_{LW} takes place from the poles toward the equator in all charts.

An analysis of annual amounts of the longwave balance of the atmosphere shows that these amounts change from magnitudes of less than 100 kcal/cm^2 · yr) in polar latitudes to 160 kcal/cm^2 · yr in the equatorial region. The isolines mostly differ in latitudinal direction. Discontinuities in isolines reflecting horizontal inhomogeneity of the temperature take place on the boundary between land and sea.

A certain amount of nonzonality in the course of isolines has been recorded over cold and warm oceanic currents. A decrease in the longwave balance of atmosphere B_{LW} is related to cold currents. This occurs, for instance, above cold Peruvian currents or above branches of currents of Western winds on the North-West coast of Australia. The increase in the amount of longwave balance of atmosphere corresponds to warm currents. This increase was recorded above the warm Gulf Stream current, above a branch of the North Pacific ocean current and above warm currents of the Indian Ocean.

These data show that there exists a possibility of discovering sea currents from the artificial satellites, since the field of outgoing radiation and the field of radiant heat influx in the atmosphere are sensitive to the presence of these currents.

The large oceans of the Southern Hemisphere and the position of the thermal equator toward the North from the geographic equator lead to the fact that on an average the heat influx in the atmosphere is greater in the Southern Hemisphere than in the Northern.

It should be observed that maximum values of longwave balance equal 140-160 kcal/cm^2 · yr occur above the ocean in the region of warm equatorial currents where a cloudy sky is frequently found.

The absolute maximum of longwave heat influx in the atmosphere was recorded above the Pacific Ocean. It is 163 kcal/cm^2 · yr. A comparison of the distribution charts of the annual amounts of longwave balance of atmosphere B_{LW} over the earth, with analogous charts for outgoing radiation F_∞ and for effective radiation of underlying surface F_0 shows that outgoing radiation considerably affects the magnitude of the longwave balance of the atmosphere over the oceans. The longwave balance above the continents may be determined by the effective radiation of the earth's surface.

In view of this it should be observed that the minimum values B_{LW} are found to occur above deserts where the maximum value of the effective

radiation of the surface F_0 was recorded as caused by high temperature, low moisture content in the atmosphere and low cloudiness.

Thus, for instance, in the Northern Hemisphere a noticeable decrease of annual amounts B_{LW} was recorded in the desert region of Northern Africa and Arabia, where B_{LW} is less than 120 kcal/cm² · yr. In the Southern Hemisphere a considerable diminution of the longwave balance of atmosphere was recorded above the Great Sandy Desert of Australia and the South African deserts. The absolute minimum was recorded in the region of the Kalahari Desert in South Africa where the B_{LW} is less than 100 kcal/cm² · yr.

Table 8.10 Mean latitudinal values of B_{LW} kcal/cm² · yr

Latitude	Area of land, %	Area of sea, %	Total area of the zone, $\times 10^2$ cm²	B_{LW} av			ΣB_{LW} of the zone
				Above land	Above sea	Mean for the zone	
90-80°N	10	90	3.9	111			
80-70	29	71	11.6				
70-60	72	28	18.9	115	118	116	21.9×10^{18}
60-50	57	43	25.6	114	121	117	30.0
50-40	52	48	31.5	112	120	116	36.6
40-30	43	57	36.4	110	129	121	44.1
30-20	38	62	40.2	119	139	131	52.7
20-10	26	74	42.8	126	150	144	61.7
10-0	23	77	44.1	132	150	146	64.5
0-10°S	24	76	44.1	131	151	146	64.5
10-20	22	78	42.8	131	147	144	61.7
20-30	23	77	40.2	113	135	130	52.3
30-40	12	88	36.4	111	127	125	45.6
40-50	3	97	31.5	114	125	124	39.1
50-60	1	99	25.6	118	120	120	30.8
60-70	10	90	18.9				
70-80	78	22	11.6				
80-90			3.9				
80°N 70°S	29	71	460.1	119.0	136.0	131.5	

The mean values of the longwave balance of atmosphere for the earth equals 131.5 kcal/cm² · yr (Table 8.10). The average value of the longwave balance for land is 119.0 kcal/cm² · yr, and for sea 136.0 kcal/cm² · yr. These values were computed while considering the fact that land covers 20% and sea 71% of the entire area of the earth.

Similarly L. W. D'yachenko and K. Ya. Kondrat'ev [15] obtained the annual amounts of longwave balance of atmosphere for different latitudinal zones of the earth (cf. Table 8.10). They are found while considering the "weight" of sea and land for each latitudinal zone.

An analysis of Table 8.10 shows that the radiant current of heat for the entire thickness of atmosphere increases from the poles toward the equator.

It should be noticed that the mean value of the balance for the Southern Hemisphere is slightly higher than for the Northern Hemisphere. This is explained by the large oceanity of the Southern Hemisphere.

We will now examine the monthly distribution charts of the longwave balance of atmosphere. In the monthly charts (Fig. 8.13a and 8.13b) one may observe a picture which is analogous to some extent to the distribution picture of annual amounts of B_{LW}. A clear minimum can be distinguished during winter in the Northern Hemisphere in the region of Siberian anticyclone when the warm Gulf Stream current increases the value of the heat influx in the atmosphere as in the North Atlantic.

The position of the maximum B_{LW} changes slightly from season to season. During summer it is situated in the vicinity of the tropics, whereas during winter it may shift in the direction of the equator.

An examination of the charts constructed enables us to establish that the highest absolute values of monthly amounts of longwave balance of atmosphere have been recorded above the ocean in the vicinity of the equator. In July the maximum influx of heat in the atmosphere shifts a little towards the North from the equator. It is more than 12 kcal/cm² · mon (in the Pacific Ocean it is more than 13 kcal/cm² · mon). In January a reverse picture has been observed. The maxima shift toward the South from the equator. They exceed the values 12 kcal/cm² : mon (in the Pacific Ocean it is 13 kcal/cm² · mon).

A further analysis of the monthly charts shows that the maxima of the values of heat influx in the atmosphere in a given case is similarly related to the maximum values of outgoing radiation (F_∞ 16=kcal/cm² · mon) which have been recorded above the oceans.

Similarly an analysis of the year-to-year variation of the monthly amounts of longwave balance of atmosphere has been carried out [15] for different climatic zones of the earth. Fig. 8.14 illustrates the variation of longwave balance of atmosphere in the course of a year in different landscapes and climatic zones.

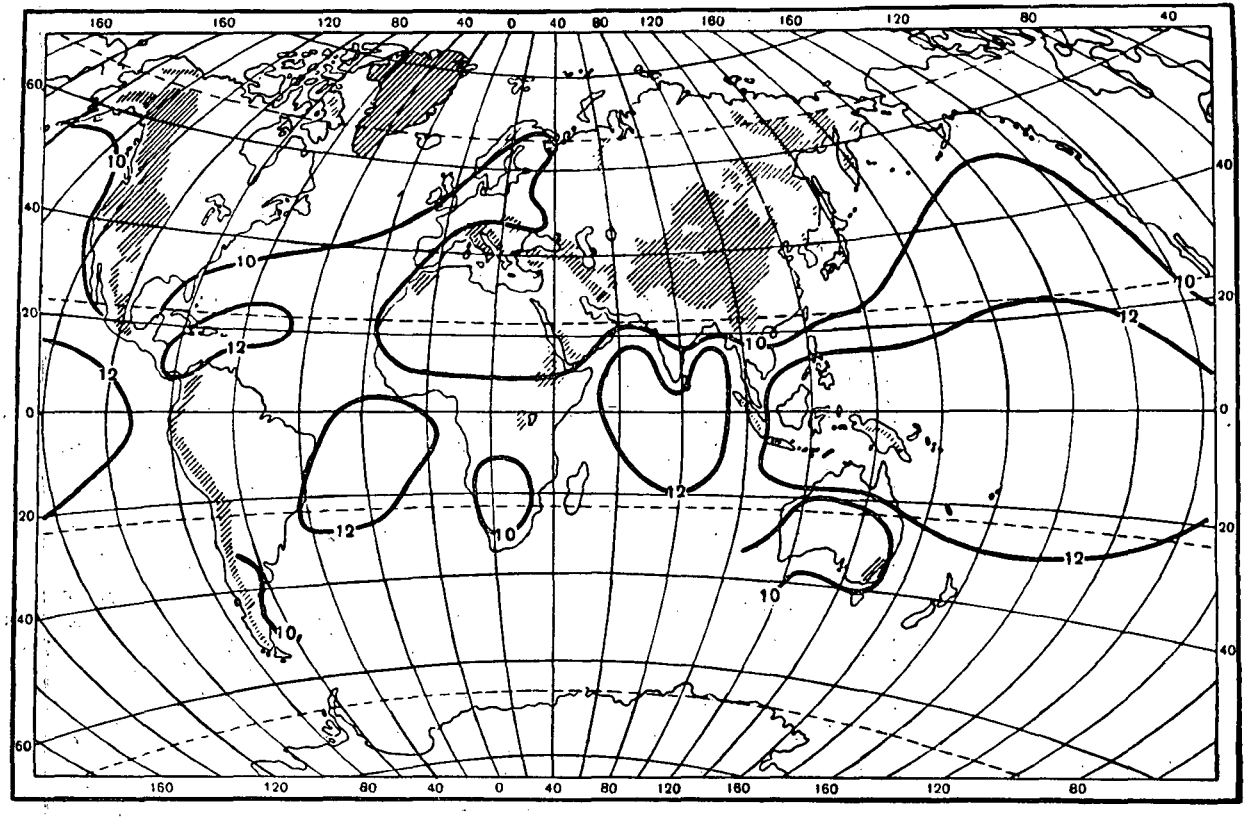

Fig. 8.13a. Geographic distribution of monthly amounts of longwave balance of atmosphere (kcal/cm²) ([15]. January.

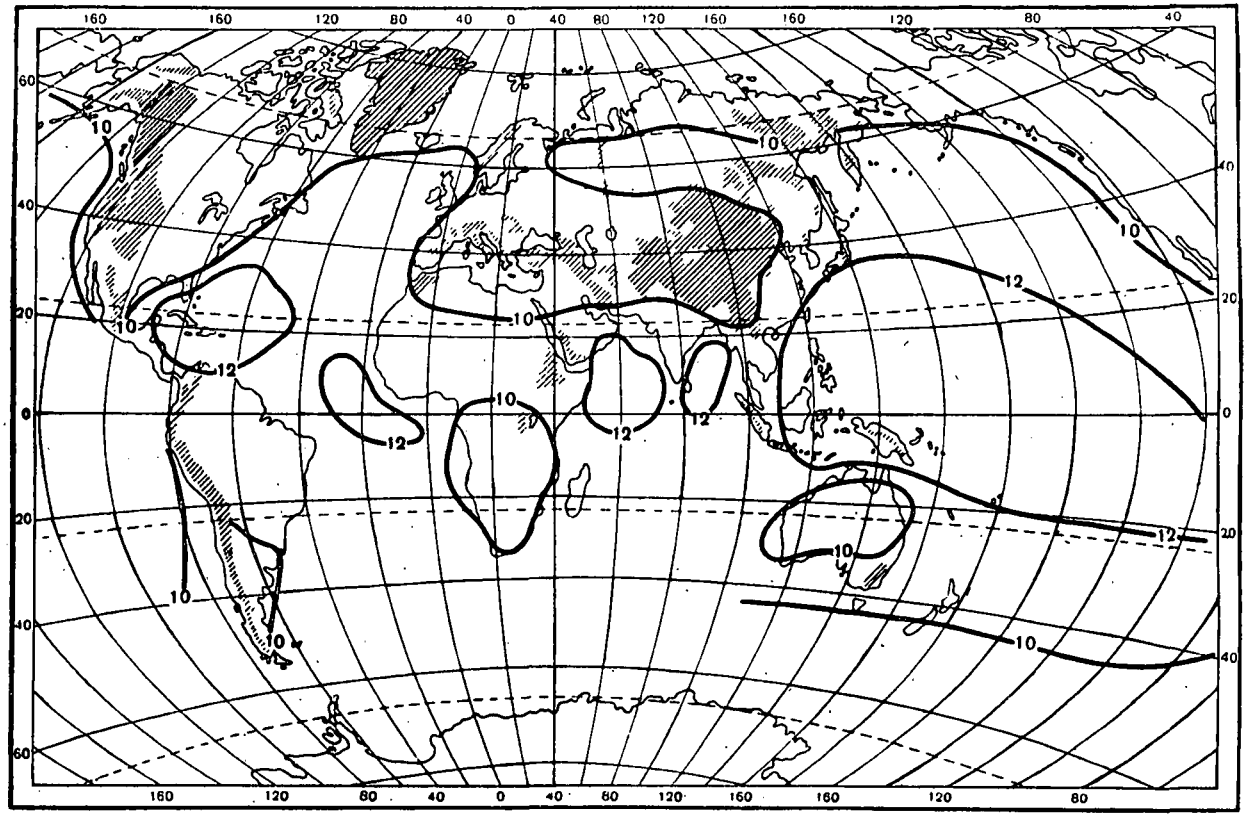

Fig. 8.13b. Geographic distribution of monthly amounts of longwave balance of atmosphere (kcal/cm²) [15] July.

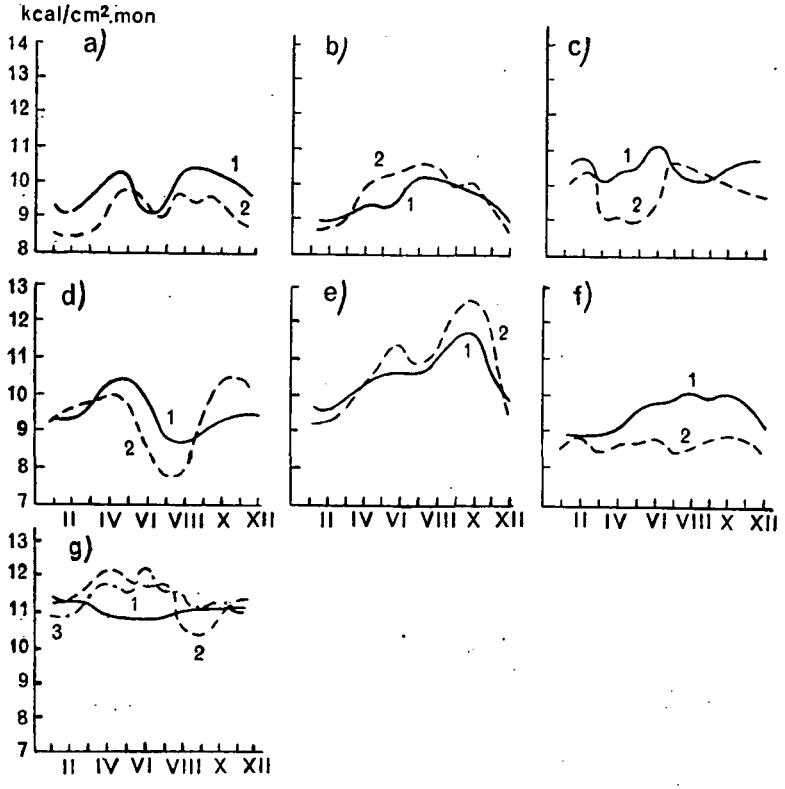

Fig. 8.14. Annual variation of longwave balance of the atmosphere in different landscapes and climatic zones [15]

a) Tundras : 1—Amderma; 2—Cape Barrow; b) summer zone of moderate latitudes: 1—Sverdlovsk; 2—Fort Nelson; c) zone of forest steppes and steppes of moderate latitudes: 1—Rostov-on-Don; 2—El Paso; d) 1—land area of subtropical latitudes (Tashkent); 2—Mediterranean climate (Rome); e) zone of equatorial monsoon; 1—Fort Lami; 2—Calcutta; f) zone of tropical deserts: 1—Wadi Halfa; 2—Alice Springs; g) zone of equatorial climate of tropical deserts; 1—Sao Gabriel; 2—Batavia, 3—Singapore.

5. FLUXES OF ATMOSPHERIC THERMAL RADIATION ON DIFFERENTLY ORIENTED PLANES

5.1 Fluxes at the ground level

In clear sky and in dense cloudiness the fluxes of atmospheric heat radiation on differently oriented inclined surfaces situated on the ground depend on the angle of inclination of the surface and remain practically independent of its azimuth. The latter is connected with the fact that

azimuthal variations in intensity of radiation under the conditions indicated are so small that it is not possible to consider them (see section 2, Chapter 8).

The flux of effective radiation of inclined surfaces may be determined by the relation analogous to (6.5).

In the case of isotropic effective radiation ($I_{eff}(\vartheta, \psi)=\text{const}$) for an inclined surface the following relation holds

$$F_s=F_h \cos^2 \frac{\alpha}{2}, \tag{8.1}$$

where F_h is effective radiation of horizontal surface.

The effective radiation of slopes which are not very steep can be determined from the approximate formula :

$$F_s \simeq F_a \cos \alpha. \tag{8.2}$$

The measurements of effective radiation of inclined surfaces with the help of Yanishevskii's pyrgeometer fastened on a theodolitic installation showed that the approximate formula (8.2) provides sufficient accuracy for surfaces with an angle of inclination $\alpha<30°$ [28]).

The dependence of the relative effective radiation of inclined surfaces (with respect to effective radiation of horizontal surface) on the angle of inclination of the surface for cloudless atmosphere [27] is shown in Fig. 8.15 for integral radiation. The results of measurements accomplished during nighttime are indicated by points. The dependence of $F_s//F_h$ on α according to data of computations is denoted by continuous lines. Calculations were conducted according to a formula, analogous to (6.5), using numerical integration over the given angular distribution of effective radiation. Computations were made for the following values of w_∞, viz. 1.0, 1.8 and 4.0 g/cm^2 (w_∞—total content of water vapor in a vertical column of atmosphere of unit cross section). In the figure the pointed lines denote curves for isotropic approximation ($F_s=F_h \cos^2 \frac{\alpha}{2}$) and for cosine law ($F_s=F_h \cos \alpha$).

The discrepancies between measurements and calculated values lie within the limits of errors in measurement. The behavior of the curves depends broadly on the total content of water vapor in the atmosphere. Thus in practice the effective radiation of inclined surfaces under a clear sky can be computed from the effective radiation of a horizontal surface, which increases the relative values of F_s/F_h corresponding to intermediate curves in Fig. 8.15. If the value of w_∞ is known then the computations will be more accurate.

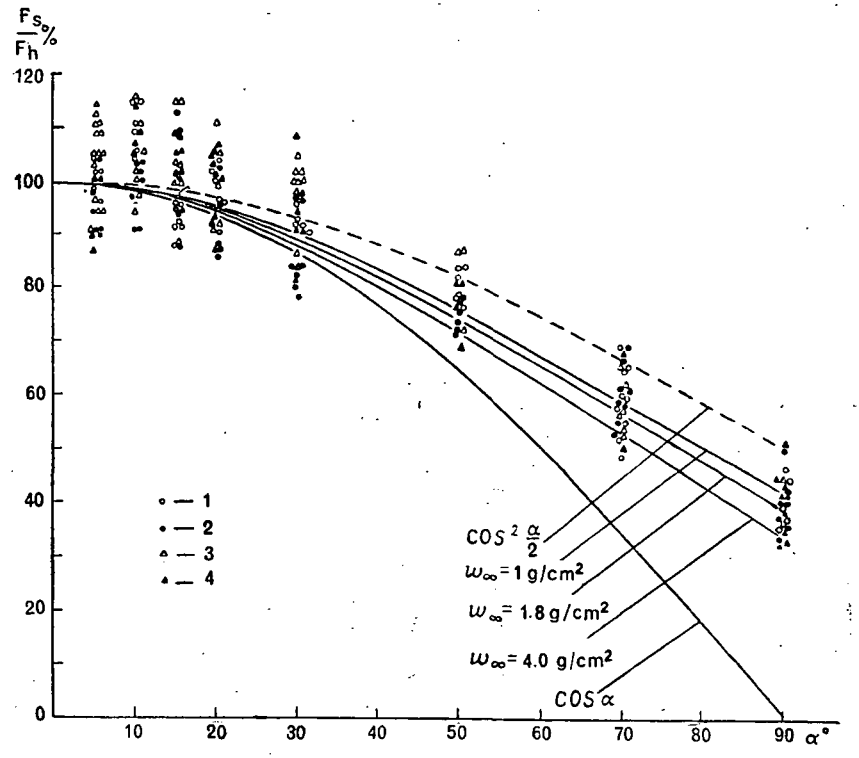

Fig. 8.15. Dependence of the magnitudes of relative effective radiation of slopes on angles of inclination of the slope under clear sky.

1—northern slopes; 2—southern; 3—eastern; 4—western.

The computations carried out above relate to the case when the inclined and horizontal surfaces, situated side by side, possess identical temperature and are perfectly black, i.e. between these surfaces there is no heat transfer or multiple reflection.

If the temperature of the inclined and horizontal surfaces are T_s and T_h respectively, then the supplementary flux of effective radiation on the horizontal surface F_t, brought about by radiative heat transfer between the surfaces can be evaluated from the following formula [21]; viz.

$$F_s = \delta\sigma\left(T_s^4 - T_h^4\right)\sin^2\frac{\alpha}{2}, \tag{8.3}$$

where δ is relative radiative capability of the slope and horizontal surfaces and σ is Stefan-Boltzmann's constant. The radiative heat transfer between slope and horizontal surface must be considerable during daytime when there exists a noticeable temperature difference between them.

5.2 Flux of outgoing longwave radiation

The fluxes of outgoing longwave radiation on planes situated at a known height in the atmosphere depend on the orientation of these planes as well as on the angular structure of the field of outgoing longwave radiation which is essentially nonisotropic in most cases.

The fluxes of outgoing longwave radiation have been computed for two stratifications of the atmosphere, with respect to latitudes 0 and 65° N, and calculations have been made for summer and winter periods [23] for 65° N. Besides, computations were carried out for a clear atmosphere and under conditions of dense cloudiness with upper boundary at a height of 3 to 9 km. The corresponding data on angular distribution of integrated intensity of outgoing longwave radiation [29, 30] were utilized in the calculations.

The fluxes of outgoing radiation were obtained for surfaces inclined with respect to the earth's normal from 0 to 180° at intervals of 10°. The azimuthal orientation has not been considered in this case, because the angular structure of the field of outgoing longwave radiation for stratification of horizontally homogeneous atmosphere examined lacks azimuthal dependence. The results of computations of flux of outgoing longwave radiation for intervals of wavelengths 4.88-120 μ are shown in Tables 8.11-8.13, where F_α is the flux of radiation on a surface inclined at an angle α (the angle between normal to surface and earth's normal) and F_0 is the flux of radiation on a horizontal surface ($\alpha = 0$) turned toward the earth. The relative values are of interest because they show most distinctly by how much the radiation regime of differently oriented surfaces differs from the radiation regime of the horizontal surface. Moreover, the relative values are more convenient for a comparison of computations for a real field and for an isotropic field of outgoing current.

An analysis of the data obtained shows that there exists a monotonic decrease in the flux of outgoing radiation as the angle of inclination of the surface increases in most cases examined for cloudless atmosphere and for dense cloudiness. A practically linear and very sharp decrease in flux was recorded for an increasing angle of inclination of the surface for values of α from 40 to 90°. The value of the flux of outgoing longwave radiation changes as the surface turns from 0 to 160° for all the stratifications of cloudless atmosphere within the limits of 1.5×10^{-2} W/cm^2 to 0.001×10^{-2} W/cm^2. For surfaces turned at an angle $\alpha = 170°$ the flux of outgoing radiation is practically nil. Here, besides the decrease in the visible portion of the earth's surface with increasing angle of inclination of the irradiated surface, a drop in the intensity of outgoing longwave radiation with increasing nadir angles is also significant. As a result, the flux of outgoing radiation rapidly decreases with an increase

in the angle of inclination of the receiving surface.

The value of the outgoing radiation current decreases in dense cloudiness as the upper boundary of the layer of clouds rises. Moreover, a decrease in the flux of outgoing radiation with increasing angle of inclination of the surface occurs noticeably slower under dense cloud than in a clear atmosphere. The value of the flux of outgoing radiation under dense cloud for inclinations of receiving surface from 0 to 160° varies from 2.3×10^{-2} W/cm² to 0.001×10^{-2} W/cm² when the upper boundary of the layer of clouds H_t lies at a height of 3 km and from 1.7×10^{-2} W/cm² to 0.0005×10^{-2} W/cm² when $H_t = 9$ km.

Table 8.11 Fluxes of outgoing longwave radiation (10^{-2} W/cm²) on surfaces of different orientations at the height of 300 km ($4.88 < \lambda < 120$ μ) equator, summer

α°	Clear atmosphere		Dense cloudiness				Isotropic emission F_α/F_0 %
			H_t=3 km		H_t=9 km		
	F_α	F_α/F_0 %	F_α	F_α/F_0 %	F_α	F_α/F_0 %	
0	2.42	100.0	2.26	100.0	1.62	100.0	100.0
10	2.39	98.8	2.23	98.7	1.59	98.1	98.5
20	2.28	94.2	2.13	94.2	1.52	93.8	94.0
30	2.12	87.6	1.98	87.6	1.42	87.6	87.8
40	1.93	79.8	1.80	79.6	1.29	79.6	80.2
50	1.72	71.1	1.61	71.2	1.16	71.6	72.0
60	1.49	61.6	1.40	61.9	1.01	62.3	63.0
70	1.26	52.1	1.19	52.6	0.856	52.8	53.8
80	1.03	42.6	0.974	43.1	0.707	43.6	44.7
90	0.801	33.1	0.758	33.5	0.554	34.2	35.2
100	0.613	25.3	0.581	25.7	0.426	26.3	28.1
110	0.432	17.8	0.411	18.2	0.304	18.8	21.0
120	0.282	11.6	0.270	11.9	0.201	12.4	14.3
130	0.163	6.73	0.157	6.94	0.118	7.28	8.8
140	0.0707	2.92	0.0686	3.04	0.0526	3.25	4.3
150	0.0209	0.863	0.0205	0.91	0.0162	1.00	1.7
160	0.00063	0.03	0.00068	0.03	0.00058	1.04	0.3

Table 8.12 Fluxes of outgoing longwave radiation (10^{-2} W/cm^2) on surfaces of different orientations at the height of 300 km ($4.88 < \lambda < 120\ \mu$), 65°N, summer

$\alpha°$	Clear atmosphere		Dense cloudiness				Isotropic emission F_α/F_0 %
			H_t=3 km		H_t=9 km		
	F_α	F_α/F_0 %	F_α	F_α/F_0 %	F_α	F_α/F_0 %	
0	2.26	100.0	2.07	100.0	1.45	100.0	100.0
10	2.22	98.2	2.04	98.6	1.43	98.6	98.5
20	2.12	93.8	1.95	94.2	1.36	93.8	94.0
30	1.98	87.6	1.81	87.4	1.27	87.6	87.8
40	1.80	79.6	1.65	79.7	1.16	80.0	80.2
50	1.61	71.2	1.48	71.5	1.04	71.7	72.0
60	1.40	61.9	1.29	62.3	0.912	62.9	63.0
70	1.19	52.6	1.10	53.1	0.777	53.6	53.8
80	0.977	43.2	0.903	43.6	0.644	44.4	44.7
90	0.762	33.7	0.706	34.1	0.507	35.0	35.2
100	0.585	25.9	0.544	26.3	0.392	27.0	28.1
110	0.414	18.3	0.387	18.7	0.281	19.4	21.0
120	0.273	12.1	0.255	12.3	0.187	12.9	14.3
130	0.159	7.03	0.149	7.19	0.111	7.65	8.8
140	0.0703	3.11	0.0667	3.22	0.0504	3.48	4.3
150	0.0213	0.942	0.0204	1.00	0.0159	1.10	1.7
160	0.00075	0.03	0.00074	1.04	0.00063	1.04	0.3

The above computations enable us to make some general evaluation of the latitudinal and seasonal variability of the values of the flux of outgoing longwave radiation. It should be observed that at the equator the flux of outgoing radiation for any orientation of the surface exceeds the corresponding values at 65°N for a clear sky or for identical conditions of cloudiness.

For cloudless conditions the variations at latitude 65° appear considerably more than latitudinal variations during summer conditions. From the data obtained it is seen that during summer the clouds exert a greater influence on the flux of outgoing radiation than during winter.

Table 8.13 Flux of outgoing longwave radiation (10^{-2} W/cm^2) on surfaces of varying orientations at height of 300 km ($4.88 < \lambda < 120\ \mu$), 65° N, winter

$\alpha°$	Clear atmosphere		Dense cloudiness				Isotropic emission F_α/F_0 %
			H_t=3 km		H_t=9 km		
	F_α	F_α/F_0 %	F_0	F_α/F_0 %	F_α	F_α/F_0 %	
0	1.68	100.0	1.63	100.0	1.16	100.0	100.0
10	1.66	98.8	1.60	98.2	1.15	99.1	98.5
20	1.58	94.2	1.53	93.9	1.09	94.0	94.0
30	1.47	87.5	1.42	87.1	1.02	87.9	87.8
40	1.34	79.8	1.30	79.8	0.931	80.2	80.2
50	1.20	71.4	1.16	71.2	0.836	72.1	72.0
60	1.05	62.5	1.01	62.0	0.730	62.9	63.0
70	0.888	52.8	0.859	52.7	0.621	53.5	53.8
80	0.732	43.6	0.709	43.5	0.514	44.3	44.7
90	0.572	34.0	0.554	34.0	0.404	34.8	35.2
100	0.440	26.2	0.426	26.1	0.312	26.9	28.1
110	0.312	18.6	0.303	18.6	0.223	19.2	21.0
120	0.206	12.3	0.200	12.3	0.148	12.8	14.3
130	0.120	7.14	0.117	7.17	0.0871	7.51	8.8
140	0.0338	1.98	0.0519	3.18	0.0394	3.40	4.3
150	0.0162	1.0	0.0158	1.0	0.0122	1.05	1.7
160	0.00055	0.03	0.00054	0.03	0.00045	0.4	0.3

From data appearing in Tables 8.11-8.13 it is possible to observe that the nature of the dependence of relative values of the flux of radiation on the angle of inclination in clear atmosphere appears to be the same as for conditions of dense cloud and, moreover, it is identical for all cases examined. Thus the dependence of the relative values of the flux of outgoing longwave radiation on the angle of inclination of the surface is practically universal and obviously differs a little from the same dependence computed for isotropic outgoing radiation. Noticeable differences between real and isotropic relative fluxes have been observed only in those cases when the angle of inclination of the surface is above 90°. Thus for $\alpha<90°$ in case of approximate computations of relative values of fluxes of

outgoing longwave radiation in differently oriented surfaces in the atmosphere one can use the isotropic approximation. However, further investigation for the case of partial, horizontally inhomogeneously distributed, cloudiness is necessary.

Evidently in this case the dependence of relative values of fluxes on the angle of inclination of the surface will be considerably more variable than under conditions of cloudless sky or dense cloud. In partial cloudiness the relative fluxes may be more than unity ($F_\alpha/F_0>1$, if the surface is oriented on the side of the uncovered part of the earth's surface, and the clouds are situated directly below the satellite).

Using the available data on the angular distribution of intensity of outgoing longwave radiation for a clear atmosphere and for dense clouds, it is possible to artificially simulate a field of outgoing radiation for the case of partial cloudiness, taking half of the radiation field from computations for cloudless atmosphere and the other half from computations for dense cloud. In real conditions this case can be introduced. For a given distribution of cloudiness the effect of the azimuthal orientation of the receiving surface should be more substantial.

The computation of fluxes of outgoing radiation on differently oriented surfaces from an artifically simulated field of outgoing longwave radiation in partial cloudiness gives only an approximate qualitative evaluation. In real conditions the presence of partial cloudiness must effect the stratification of the atmosphere in adjacent regions in the same way as the presence of large openings would influence the stratification of the atmosphere in the layer above the clouds.

Some of the results of the calculations of the above-mentioned models (cf. [23]) are shown in Table 8.14. The computations were made for two latitudes (0 and 65° N) when half of the visible portion of the earth's surface is covered by a layer of clouds with upper boundaries at altitudes of 3 to 9 km. The surface is oriented on the side of cloudy covering ($\psi=0°$) and on the opposite side the uncovered portion of the earth's surface ($\psi=180°$). It is natural to expect that the receiving surface turned toward the cloud cover receives less longwave radiation as compared to the surface turned toward the uncovered earth. It is obvious from the data obtained that the azimuthal orientation of the receiving surface for clouds at an altitude of 3 km considerably affects the influx of longwave radiation. The difference between the values of flux of outgoing inclinations and opposite azimuths in this case becomes 3-5%. For clouds at a height of 9 km the influence of azimuthal orientation appears to be more important. The differences between the values of F_α for surfaces with identical and opposite azimuths in this case become 20%. Here it is necessary to notice that the above-mentioned differences have been observed for surfaces with angles of inclinations from 40 to 90°.

Table 8.14 The flux of outgoing longwave radiation (10^{-2} W/cm^2) at a height of 300 km in partial cloudiness, 65° N, winter

α°	3 km				9 km				F_α/F_0 % (isotropic)
	ψ=0°		ψ=180°		ψ=0°		ψ=180°		
	F_α	F_α/F_0 %	F_α	F_α/F_0 %	F_α	F_α/F_0 %	F_α	F_α/F_0 %	
0	1.66	100.0	1.66	100.0	1.46	100.0	1.46	100.0	100.0
10	1.63	98.2	1.64	98.8	1.41	96.6	1.47	100.7	98.5
20	1.55	93.4	1.56	94.0	1.32	90.4	1.43	97.9	94.0
30	1.44	86.7	1.46	88.0	1.20	82.2	1.36	93.2	87.8
40	1.31	78.9	1.33	80.1	1.06	72.6	1.27	87.0	80.2
50	1.17	70.5	1.20	72.3	0.931	63.8	1.15	78.8	72.0
60	1.02	61.4	1.04	62.7	0.791	54.2	1.02	69.9	63.0
70	0.863	52.0	0.886	53.4	0.654	44.8	0.880	60.3	53.8
80	0.710	42.8	0.732	44.1	0.528	36.2	0.731	50.1	44.7
90	0.554	33.4	0.572	34.4	0.404	27.7	0.572	39.2	35.2
100	0.426	25.7	0.439	26.4	0.312	21.4	0.439	30.1	28.1
110	0.306	18.2	0.312	18.8	0.223	15.3	0.312	21.4	21.0
120	0.200	12.0	0.206	12.4	0.148	10.1	0.206	14.1	14.3
130	0.117	7.0	0.120	7.2	0.0869	6.0	0.120	8.2	8.8
140	0.0519	3.1	0.0533	3.2	0.0393	2.7	0.0533	3.6	4.3
150	0.0158	0.952	0.0162	0.976	0.0122	0.836	0.0162	1.1	1.7
160	0.0005	0.0001	0.0005	0.0301	0.0004	0.0274	0.0005	0.0342	0.3

The relative values of fluxes of outgoing longwave radiation on different surfaces for identical conditions of cloudiness at different latitudes are very close to each other.

The results of these computations similarly show that for surfaces with angles of inclination up to 25° the fluxes of outgoing radiation do not vary by more than 10% as compared with the flux on horizontal surface. Starting with the angle of inclination $\alpha=30°$ the relative flux of outgoing radiation decreases with a rising angle of inclination practically linearly. The vertically oriented surfaces receive about 34% of the radiation flux incident on the horizontal surface.

On the basis of computations made on fluxes of outgoing longwave radiation it is possible to approximately evaluate the angle of the cone (with apex at the receiving surface), which includes the specific portion of

radiation flux from the earth and atmosphere, incident on the given surface. The magnitude of the angle which includes 90% of the flux incident on the surface of different orientation is almost 60°. Only for a surface with an angle of inclination from 70 to 90° the angle of the cone (or the so-called effective zone) is about 70°. The magnitude of the effective zone which comprises 50% of the flux of outgoing longwave radiation is almost 30° for the surface with an angle of inclination between 70° and 45-50° for surfaces with an angle of inclination from 70° to 90°. For surfaces having $\alpha > 90°$ similar evaluation was not carried out since such surfaces already "do not see" the central portion of the underlying surface being situated directly below the satellite.

The fundamental results of theoretical computations shown in this paragraph are the definite dependence of the values of the flux of outgoing longwave radiation on the angle of inclination of the receiving surface, situated in the atmosphere at a height of 300 km. The calculations conducted showed that the dependence of values of the flux of outgoing radiation on the angle of inclination of the surface possesses a qualitatively identical character for cloudless atmosphere as well as for dense cloudiness under conditions of horizontally homogeneous atmosphere. Evidently for partial and nonuniformly distributed cloudiness the dependence of the flux of outgoing radiation on the orientation of the receiving surface will be considerably more complex because the influx of radiation will depend not only on the angle of inclination but also on the azimuth of the surface. Similarly the data obtained provided an opportunity to use isotropic approximation for the determination of relative values of the flux of outgoing radiation in a horizontally homogeneous atmosphere (at least up to an angle of inclination of 90°).

6. CHARACTERISTICS OF MESOSTRUCTURE OF THERMAL RADIATION FIELD OF THE EARTH AS A PLANET

In solving many of the problems of atmospheric optics as well as various allied problems it is necessary to take into consideration the properties of time, space and the space-time structure of the field of outgoing radiation of the earth as a planet.

The numerous and variegated factors which exert an influence on the radiational regime of the atmosphere in most cases enable us to indicate the arbitrary nature of the field of the earth's radiation. This approach is justified by the fact that the volume of results of direct measurements on radiation has become so large recently that their complete analysis for concrete experiments is not feasible in practice. Only statistical models of analysis and development enable us to represent experimental data in compact form.

The arbitrary character of outgoing radiation implies that the full characteristics of the earth's radiations may be obtained from the law of distribution of probable error in the energy levels with respect to some average value. However, the limitations on this information only indicate the approximate determination of the law which is equivalent to passing over to an incomplete description of the structure of the radiation field.

6.1 Statistical method of describing radiation field

While using the methods of incomplete statistical analysis one is forced to neglect some portion of the basic information. Thus the applicability of any method depends on the importance of this lost information for the solution of any concrete problem. The following methods are used :

a) *The distribution function of radiation with respect to levels.* If $P_J(\mathcal{J})$ is probability density of distribution of radiation with respect to levels then the magnitude $P_J(\mathcal{J})d\mathcal{J}$ determines the probability for radiation energy found in the intervals from $\mathcal{J}$ to $\mathcal{J}+d\mathcal{J}$.

It must be borne in mind that a specific distribution $P_J(\mathcal{J})$ corresponds to specific conditions of measurements (characteristics of equipment, time of day, season, geographic coordinates, etc.). Moreover, this method does not take into consideration the space-time structure of the radiation field.

b) *Autocorrelation functions of radiation.* By autocorrelation function we mean a measure of mutual connection between the results of observations on radiation divided into intervals of time. Often autocorrelation functions over space coordinates as well as n-dimensional autocorrelation functions are used.

Let us suppose that the variability of a field in time t has been studied. Then, if the field $\mathcal{J}$ is statistically stationary in time, the autocorrelation function has the following form, viz.

$$\mu(\Delta t)=\lim_{T\to\infty}\frac{1}{2T}\int_{-T}^{T}\mathcal{J}(t)\,\mathcal{J}(t+\Delta t)\,dt. \tag{8.4}$$

The function $\mu(\Delta t)$ is a continuous even function, having the greatest value, equal to the average value of the square of the function $\mathcal{J}(t)$ at $\Delta t=0$. If $\mathcal{J}(t)$ does not contain implicit periodical components the autocorrelation function asymptotically approaches the square of the mean value of $\mathcal{J}(t)$.

c) *The spectrum of Viner-Khinchin (Wiener-Kirchoff) emission.* The Wien-Kirchoff spectrum (for the smooth density spectrum) when $\mathcal{J}(t)$ has stationary value, is the Fourier Cosine-Transform of the autocorrelation function, viz.

$$W(\omega)=\frac{2}{\pi}\int_0^\infty \mu(\Delta t)\cos\omega\Delta t\, d(\Delta t). \tag{8.5}$$

The information contained in the autocorrelation function and the Wien-Kirchoff spectrum is identical and in this respect there is no difference between the methods indicated. The relative usefulness of any of these methods is determined only by the convenience of its further application or by the experimental difficulties in recording corresponding characteristics.

Although the autocorrelation function and the Wien-Kirchoff spectrum are adiabatic methods only for the description of standard, ergodic and Gaussian fields, it is possible to obtain many results, especially for linear systems, with their help. There exist radio-technical instruments for the direct determination of the correlation function of electrical signals with respect to time.

d) *Characteristic function of radiation.* The time-dependent function can be determined from the expression:

$$b(\Delta t)=\lim_{T\to\infty}\frac{1}{2T}\int_{-T}^{T}[\mathcal{J}(t)-\mathcal{J}(t+\Delta t)]^2\, dt \tag{8.6}$$

and is yet another characteristic of the mean correlation between the values of radiation at different moments of time. It is easily seen that the function $\mu(\Delta t)$ and $b(\Delta t)$ are related by the following viz.

$$b(\Delta t)=2<\mathcal{J}^2(t)>_t-2\mu(\Delta t), \tag{8.7}$$

which is justified for a stationary field (value $<\mathcal{J}^2(t)>_t$ is the mean value of the square of intrinsic function).

The space structure function can be determined in an analogous manner.

e) *Entropy of probability distribution of radiation.* The most general measure of the indeterminancy of the arbitrary function $\mathcal{J}$ is the entropy of distribution $P_{\mathcal{J}}(\mathcal{J})$, determined by the following expression.

$$H_e(P_{\mathcal{J}})=\int P_{\mathcal{J}}(\mathcal{J})\log P_{\mathcal{J}}(\mathcal{J})\, d\mathcal{J}, \tag{8.8}$$

where integration is carried over the entire region of variation of values of $\mathcal{J}$.

The entropy H_e becomes zero only in the case where the value J can be completely determined. In all the remaining cases entropy is positive at a given scattering maximum for normal probability distribution.

A detailed account of the indicated methods can be found in special literature on mathematical statistics and similarly in [53, 66], directly relating to the problem of description of emission structure.

6.2 Peculiarities of statistical description of the radiation field

From the point of view of the observer using a typical optical equipment the radiation field represents a source of information on at least two spatial measurements. In simpler cases this information can be given as a function of right-angled coordinates on a plane surface. However, generally the original surface of recording is curved. This situation complicates the procedure of statistical description of the structure of radiation. For instance, in the case of optical instruments scanning the field of the earth's outgoing radiation from the sky, the representation of the original information in the spherical coordinate system connected with the instrument is important since it bears a specific characteristic in mathematical language.

In most cases of practical interest it is impossible to unconditionally assume ergodicity, stability and isotropy of the radiation field. If the direction in which measurements are carried out differs insignificantly from the vertical, the radiation can be considered, under some supplementary conditions, to be stable, ergodic and isotropic up to the zenith angles, at which the earth still appears to be two-dimensional. However, as the ray of light approaches the horizon, the nonsphericity of the earth and the effects mentioned here cast their influence, viz. a distortion of the form in foreshortening, rising influence of atmospheric radiation and absorption, refraction, shadow effect, etc., which change the average radiation and its variation considerably. It is obvious that any characteristic of the field obtained by averaging over all the zenith angles contains a large amount of information. Consideration of anisotropy and nonstability is a difficult task which, however, considerably raises the quality of the solution of the problem under investigation.

The important property of radiation field includes the fact that the probability function of radiation intensity is not Gaussian. In particular the radiation intensity cannot have negative values. Moreover, it is evident that many real situations can be described by distributions with several maxima (for instance, radiation in partial cloudiness). Similar functions cannot be approximated by curves of normal distribution. Thus

we see that these spatial and statistical characteristics, such as the Wien-Kirchoff spectrum and autocorrelation function, contain extremely limited and in most cases insufficient information about the state of the field under investigation. Thus, for instance, in the problems of detecting false alarms, probability is of great interest, being determined by the probability curves of the distribution of background variations. It is known that autocorrelation function does not satisfactorily describe the form of these curves if the distribution curve is not Gaussian. In these cases a knowledge of the distribution functions of probability density is essential.

6.3 Methods of determination and some results of computations of structural characteristics of the field of outgoing radiation

Two methods of determining the statistical characteristics of the radiation field are possible which supplement and control each other. The first of these includes a statistical development and analysis of direct experimental data on radiation. In this the physical principles determining the mechanism of the passage of radiation through terrestrial atmosphere do not play a significant role. Perhaps detailed statistical information can be obtained in this manner. However the working out of the experimental material demands a significant expenditure of labor, and does not always enable us to consider the effect of the properties of the instrument being used on the results of observation.

On the other hand, the statistical properties of the radiation field can also be studied theoretically. In the presence of characteristics of the spatial structure of the meteorological parameters of the atmosphere, which affect its optical properties, the equation of radiative transfer can be used not only for the computation of average values but also for the determination of the characteristics of the radiation field.

(a) *The structural characteristics of the radiation field from direct measurements.* The volume of specific information on the statistical structure of the emission field found in literature as of now is not large. Below we will examine the results of statistical analysis of the field of outgoing radiation from the data of meteorological satellites "Tairos-II' and "Tairos-III", given in [5, 6]. The results of measurement on radiation accomplished with the help of narrow-angle (angular vision 5°) five-channeled radiometers are contained in atlases of charts [69, 70]. The data from the satellite "Tairos-II" were interpolated in charts in networks at intervals of 40 miles, and data of "Tairos-III", in networks at intervals of 1.25° and 2.5° arcs of the meridian at the equator. The dimensions of the portion of the spectrum registered in each of the channels are given in Table 8.15.

Table 8.15

Channel	Spectral range	
1	6-6.5 μ	(absorption band of water vapor)
2	8-12 μ	(transparency window of atmosphere)
3	0.2-6 μ	(spectral range of reflected solar radiation)
4	8-30 μ	(integrated thermal radiation)
5	0.55-0.75 μ	(range of spectral sensitivity of television camera)

Because of the errors in measurements of radiation the data of channels 3 and 5 of the artificial satellite "Tairos-II" are not reliable, and the data of these channels of "Tairos-III" are also not accurate, but they are suffi-

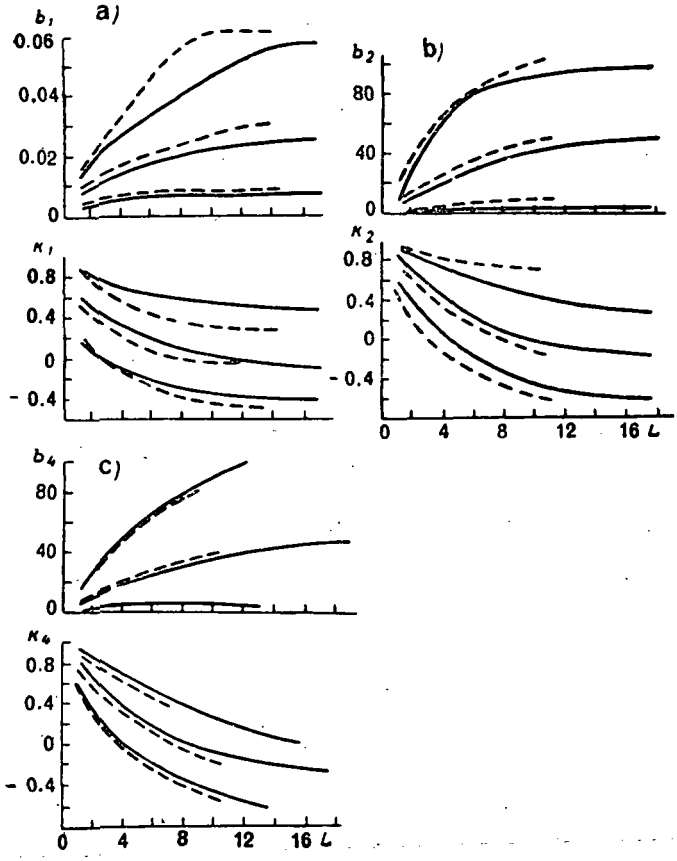

Fig. 8.16. Structural functions b and autocorrelation coefficient of the emission field.
a—channel 1, *b*—channel 2, *c*—channel 4.

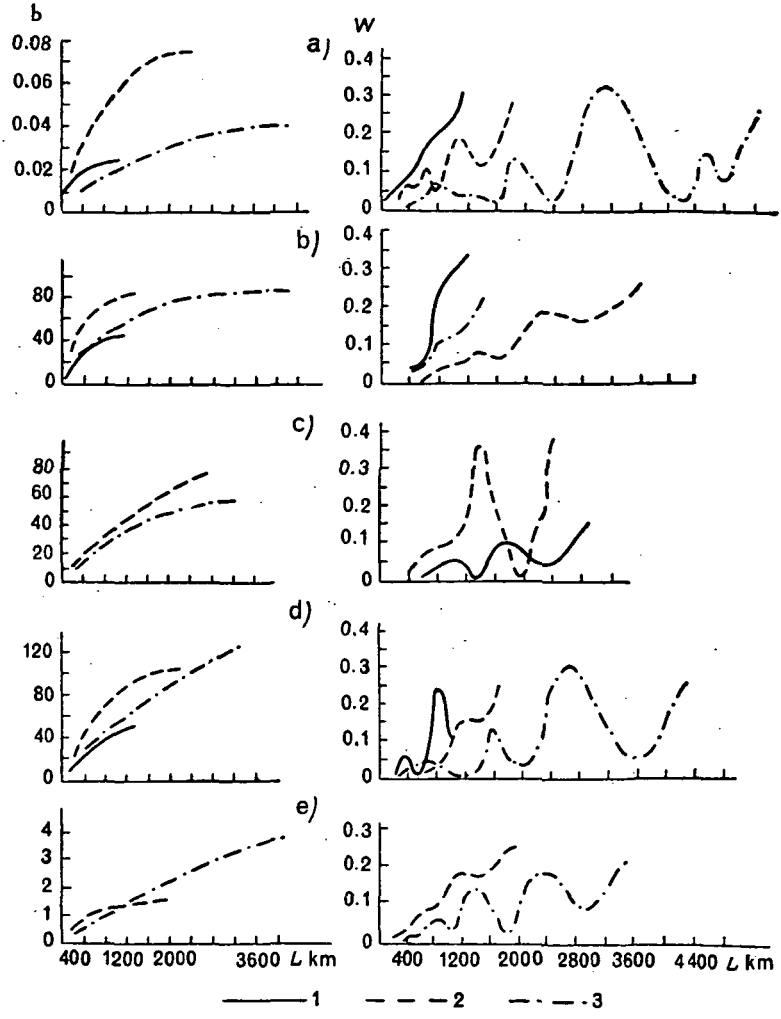

Fig. 8.17. Structural function *b* and spectral density *W* of the radiation field using networks at intervals of 40 miles (1), 1.25° (2) and 2.5° (3).
a—channel 1, *b*—channel 2, *c*—channel 3, *d*—channel 4, *e*—channel 5.

ciently good for the purpose of differentiating cloud systems. Measurements on the satellite "Tairos-II" were made during winter, and data on "Tairos-III" relate of summertime. The results of computations are given in Figs. 8.16 and 8.17.

For the verification of isotropy of the analyzed fields of radiation analogous computations were carried out with a choice of original values at assemblies situated perpendicular to the primary direction. The

results of computation are shown in the graphs by dotted lines. Evidently the field of integrated radiation can be considered to be isotropic with a fair degree of accuracy; to some extent this is justified for radiation in the absorption bands of water vapor.

The fundamental properties of the statistical characteristics obtained have been discussed in the references cited, viz. [5, 6].

We will now introduce more examples of the statistical approach to the analysis of the outgoing radiative field. The result of observations from "Tairos-II" for the construction of intermediate latitudinal profiles of outgoing thermal radiation have been used in [45]. The data were incorporated into two groups, referring to observations above continents and water areas. Computations of mean square values of variation in radiation were carried out. It appeared that in general this value changes with latitude for radiation above land to a greater extent than above sea. The numerical values of mean square deviation [45] are in agreement with the results of [5, 6].

Reference [37] gives the results of statistical development of measurements on the spectral distribution of outgoing radiation of the earth-atmospheric system, obtained by artifical satellite of the series "Cosmos". The results are shown in the form of one-dimensional laws of intensity distribution of outgoing radiation in energy units for segments of the spectrum of width from 1 to 2 microns in the range 7-26 μ.

From the results of statistical analysis of the spectrograms obtained from the satellite "Cosmos-45" the two-dimensional law of intensity distribution of terrestrial radiation [35] was obtained for several spectral intervals of width 1 μ in the range of the spectrum 7-15 μ. Numerical characteristics of these distributions are given (mutual correlation moments and coefficient of mutual correlation).

Several characteristics of combinations of spectral intervals were selected for working out. As expected there appears a great measure of correlation between intensity in emission bands of the same atmospheric gas with values of the absorption coefficient close to each other. A minimum coupling was found in spectral intervals corresponding to absorption bands of different gases.

Naturally, the data introduced characterize the spatial structure of the emission field only in the most general features. The limitations on the application of original information prevent a more detailed analysis. In particular, the very form of the experimental material did not permit a solution of these problems, such as the determination of the characteristics of very small-scale inhomogeneity of emission, the analysis of variations of different origin, the study of time and angular structure of the emission field. The analysis of the last problem is complicated in that to date it has not been possible to obtain sufficiently detailed experimental data on

the properties of thermal radiation of the region close to the planetary horizon. Improved apparatus and methods of observations will enable the widespread application of statistical modes of analysis.

(b) *Application of the transfer equation for the investigation of the structure of the emission field.* The difficulties in statistical analysis of experimental data on emission have increased the interest in the second method of evaluating the structural characteristics of emission field. Theoretical computations on the intensity of outgoing thermal radiation for different models of atmosphere enable scientists to accomplish a qualitative evaluation of the sensitivity of radiation in different segments of the spectrum to the characteristics of the atmospheric state (i.e. distribution of temperature, pressure and optically active components). On these computations are based the evaluation of dispersion and autocorrelation functions of variations of integral emission brought about by cloudiness [2]. The values determined in this manner are close to experimental values [5].

Generally the dependence of statistical properties of radiation in any spectral range on the atmospheric state can be determined on the basis of analyzing the equation of radiative transfer in the medium with arbitrarily distributed optical characteristics. The process of radiative transfer may be examined from the mathematical point of view as a process of formation of an arbitrary signal in a system with arbitrary transmission characteristics. The investigation of these formations has been worked out in detail in the statistical theory of bonds (see, for instance, [41]), whose results can be utilized indirectly in atmosphere optics as well.

The works [3, 38, 39] have been devoted to the investigation of several statistical properties of the solution of the transfer equation. In [3] the effect of variation of optical density of the atmosphere on the transmission function has been determined on the assumption that the variation distribution is normal. The results obtained were used for the working out of the criterion for accepting model emission computations. In [38, 39] a relation has been obtained which establishes the dependence between characteristics of spatial structure of temperature, moisture and cloudiness fields and the corresponding characteristics of the intensity field of longwave emission ($\nu < 3000$ cm^{-1}). The analysis was performed for linear approximation with respect to variations of original meteorological parameters. Examples of several structural characteristics of intensity of ascending radiation are given, computed for the regions of strong and weak absorption in water vapor from data in [44].

One must, thus, expect that a statistical analysis of the transition equation which permits the application of wide material of meteorological observations will be extremely promising.

REFERENCES

1. Ashcheulov, S. V., K. Ya. Kondrat'ev and D. B. Styro. Analiz spektrov protivoizlucheniya atmosfery (An analysis of the spectra of atmospheric downward radiation). Problemy fiziki atmosfery, vyp. 5, LGU, 1967.
2. Baryshev, V. A. *Mezostruktura polya integral'nogo izlucheniya Zemli kak planety* (Mesostructure of the field of integral emission of earth considered as a planet). Izv. AN SSSR, fizika atmosfery i okeana, t. 1, No. 8, 1965.
3. Baryshev, V. A. O vliyanii sluchainykh neodnorodnostei atmosfery na intensivnost' ukhodyashchego teplovogo izlucheniya Zemli (The effect of arbitrary inhomogeneity of atmosphere on the intensity of outgoing thermal radiation of the earth). Problemy fiziki atmosfery, vyp. 3. LGU, 1965.
4. Berlyand, T. G. Raspredelenie solnechnoi radiatsii na kontinentakh (Distribution of solar radiation over the continents). Gidrometeoizdat, Leningrad, 1961.
5. Borisenkov, E. P., Yu. P. Doronin and K. Ya. Kondrat'ev. Strukturnye kharakteristiki polya izlucheniya Zemli kak planety (Structural characteristics of radiation field of earth as a planet). Kosmicheskie issledovaniya, t. I, vyp. 1, 1963.
6. Borisenkov, E. P., Yu. P. Doronin and K. Ya. Kondrat'ev. Strukturnye kharakteristiki polei ukhodyashchei radiatsii po dannym ISZ "Tairos-III" (Structural characteristics of field of outgoing radiation from the data of ISZ (Artificial Earth Satellite) "Tairos-III"). Kosmicheskie issledovaniya, t. III, vyp. 3, 1965.
7. Budyko, M. I. Teplovoi balans zemnoi poverkhnosti (Thermal balance at the earth's surface). Gidrometeoizdat, Leningrad, 1956.
8. Vinnikov, K. Ya. Ukhodyashchee izluchenie sistemy Zemlya-atmosfera (Outgoing radiation of the earth-atmosphere system). Trudy GGO, vyp. 168, 1965.
9. Vinnikov, K. Ya. Novyi raschet teplovogo balansa sistemy Zemlya-atmosfera (Recent computation of thermal balance of the earth-atmosphere system). Meteorologiya i gidrologiya, No. 8, 1965.
10. Gertzberg, G. Kolebatel'nye i vrashchatel'nye spektry mnogoatomnykh molekul (Vibrational and rotational spectra of polyatomic molecules). IL, 1949.
11. Gorodetskii, A. K. and G. P. Filippov. Nazemnye izmereniya izlucheniya atmosfery i podstilayushchei poverkhnosti v oblasti spektra 8-12 mkm (Terrestrial measurements of atmospheric and underlying surface radiation in the spectral interval 8-12 μ). Izv. AN SSSR, fizika atmosfery i okeana, t. IV, No. 2, 1968.
12. Gradus, L. M. and E. M. Feigel'son. Vliyanie oblachnosti na radiatsionnyi pritok tepla v atmosfere (The effect of cloudiness on radiative flux of heat in the atmosphere). Izv. AN SSSR, fizika atmosfery i okeana, t. 1, No. 7, 1965.
13. Jameson, J. E. et al. Fizika i tekhnika infrakrasnogo izlucheniya (The physics and technology of infrared radiation. Translated from the English). Izd-vo "Sovestskoe radio", 1965.
14. D'yachenko, L. N. Raspredelenie e'ffektivnogo izlucheniya po territorii SSSR (Distribution of effective radiation over the territory of the USSR). Trudy GGO, vyp. 152, 1964.
15. D'yachenko, L. N. and K. Ya. Kondrat'ev. Raspredlenie dlinnovolnogo balansa atmosfery po zemnomu sharu (Distribution of longwave atmospheric balance over the earth). Trudy GGO, vyp. 170, 1965.

16. Elovskikh, M. P. and K. Ya. Kondrat'ev. Uglovoe raspredelenie intensivnosti teplovogo izlucheniya atmosfery (Angular distribution of intensity of atmospheric thermal radiation). Izv. AN SSSR, ser. geofiz., No. 5, 1957.

17. Efimova, N. A. K metodike rascheta mesyachnykh velichin e'ffektivnogo izlucheniya (On the method for computing monthly values of effective radiation). Meteorologiya i gidrologiya, No. 10, 1961.

18. Efimova, N. A. and L. A. Strokina. Raspredelenie e'ffektivnogo izlucheniya na poverkhnosti zemnogo shara (Distribution of the effective radiation on the earth's surface). Trudy GGO, vyp. 139, 1963.

19. Zaitseva, N. A. and G. N. Kostyanoi. Meridional'noe izmenenie polya dlinnovolnovoi radiatsii v atmosfere nad Tikhim okeanom (po dannym korablei pogody) [Meridional variation over Pacific Sea of the field of longwave atmospheric radiation (from the data of weather ships)]. Izv. AN SSSR, fizika atmosfery i okeana, t. II. No. 12, 1966.

20. Kondrat'ev, K. Ya. Aktinometriya (Actinometry). Gidrometeoizdat, Leningrad, 1965.

21. Kondrat'ev, K. Ya. Luchistaya e'nergiya Solntsa (Radiant energy of the sun). Gidrometeoizdat, Leningrad, 1954.

22. Kondrat'ev, K. Ya. Luchistyi teploobmen v atmosfere (Radiative heat exchange in atmosphere). Gidrometeoizdat, Leningrad, 1956.

23. Kondrat'ev, K. Ya. et al. Pole izlucheniya Zemli kak planety (Radiant field of the earth as a planet). Gidrometeoizdat, Leningrad, 1967.

24. Kondrat'ev, K. Ya., S. V. Ashcheulov and D. B. Styro. Spektr sobstvennogo izlucheniya atmosfery v diapazone dlin voln ot 25 do 35 mkm (Spectrum of inherent radiation of atmosphere in the spectral range from 25 to 35 μ). Problemy fiziki atmosfery, coll. 4, LGU, 1966.

25. Kondrat'ev, K. Ya., S. V. Ashcheulov and D. B. Styro. Sravnenie izmerennykh i rasschitannykh spektrov sobstvennogo izlucheniya atmosfery (A comparison of the measured and computed spectra of inherent atmospheric radiation). Vestnik LGU, ser. fiziki i khimii, No. 22, 1965.

26. Kondrat'ev, K. Ya. and M. P. Elovskikh. Raspredelenie intensivnosti e'ffectivnogo izlucheniya i protivoizlucheniya po nebosvodu (Intensity distribution of effective radiation and downward radiation over the sky). Izv. AN SSSR, ser. geofiz., No. 5, 1955.

27. Kondrat'ev, K. Ya. and M. P. Manolova. Radiatsionnyi balans sklonov (Radiation balance of slopes). Vestnik LGU, ser. fiziki i khimii, No. 10, 1958.

28. Kondrat'ev, K. Ya. and E'. L. Podol'skaya. E'ffektivnoe izluchenie sklonov (Effective radiation of slopes). Izv. AN SSSR, ser. geofiz., No. 4, 1953.

29. Kondrat'ev, K. Ya. and K. E. Yakushevskaya. Uglovoe raspredelenie ukhodyashchego teplovogo izlucheniya v razlichnykh oblastyakh spektra (Angular distribution of outgoing thermal radiation in different regions of spectra). ISZ (Artificial Earth Satellite), vyp. 14, 1962.

30. Kondrat'ev, K. Ya. and K. E. Yakushevskaya. Uglovoe raspredelenie teplovoi radiatsii sistemy Zemlya-atmosfera v raslichnykh oblastyakh spektra (Angular distribution of thermal radiation of the earth-atmosphere system in different spectral ranges). Trudy GGO, vyp. 166, 1964.

31. Kostyanoi, G. N. Predvaritel'nye resul'taty aktinometricheskogo zondirovaniya atmosfery v 1961 g. v antitsiklonicheskikh usloviyakh (Preliminary results of acti-

nometric probing of atmosphere in 1961 under anticyclonic conditions). Trudy TsAO, vyp. 49, 1963.

32. Kostyanoi, G. N. Ob izmenenii polya dlinnovolnovoi radiatsii v svobodnoi atmosfere v zimnii period (On the variation of the field of longwave radiation in free atmosphere during w nter time). Izv. AN SSSR, fizika atmosfery i okeana, t. I, No. 8, 1965.

33. Kuznechik, O. P., V. V. Dolinin and I. A. Kobak. E'nergeticheskaya yarkost' neba v oblasti 4.5-5.2 mkm (Energy brightness of the sky in the range 4.5-5.2 μ). DAN BSSR, t. XI, No. 11, 1967.

34. Kurilova, Yu. V. O vozmozhnostyakh meteorologicheskoi interpretatsii dlinnovolnovoi radiatsii (The possibility of a meteorological interpretation of longwave radiation). Trudy MMTs, vyp. 8, 1965, 76-86.

35. Lebedinskii, A. N. et al. Korrelyatsionnye zavisimosti spektralnoi intensivnosti infrakrasnogo izlucheniya Zemli v kosmos (Correlational dependence of spectral intensity of earth's infrared radiation in cosmos). Geomagnetizm i ae'ronomiya, t. VIII, No. 1, 1968.

36. Lebedinskii, A. I., T. G. Polyakova and V. I. Tulupov. Uglovoe i spektral'noe raspredelenie infrakrasnogo izlucheniya Zemli v kosmos vblizi gorizonta po nablyudeniyam so sputnikov (Angular and spectral distribution of infrared radiation of the earth in cosmos in the vicinity of the horizon from observations made by an artificial satellite). Geomagnetizm i ae'ronomiya, t. VIII, vyp. 2, 1968.

37. Lebedinskii, A. I. et al. Statisticheskie kharakteristiki izlucheniya Zemli v kosmos v diapazone dlin voln 7-26 mkm (Statistical characteristics of the radiation of the earth in cosmos in the spectral range 7-26 μ). Geomagnetizm i ae'ronomiya, t. VII, No. 3, 1967.

38. Malkevich, M. S. O svyazi mezhdu kharakteristikami vertikal'noi struktury polya dlinnovolnovoi radiatsii i polei temperatury i vlazhnosti (On the relation between the characteristics of vertical structure of the field of longwave radiation and the temperature and moisture distribution). Izv. AN SSSR, fizika atmosfery i okeana, t. 1, No. 10, 1965.

39. Malkevich, M. S. O prostranstvennoi strukture polya dlinnovolnovoi izlucheniya Zemli (On the spatial structure of the field of longwave radiation of the earth). Izv. AN SSSR, fizika atmosfery i okeana, t. 11, No. 4, 1966.

40. Markov, M. N., Ya. I Merson and M. P. Shamilev. Sloi verkhnei atmosfery, izluchayushchie v infrakrasnoi oblasti spektra. Sb. "Issledovaniya kosmicheskogo prostranstva" (The layers of upper atmosphere radiating in the infrared spectral range. Coll. "Study of cosmic space"). Izd-vo "Nauka", 1965.

41. Middleton, D. Vvedenie v statisticheskuyu teoriyu svyazi (Introduction to the statistical theory of bonds). Izd-vo "Sovetskoe radio", 1961.

42. Niilisk, Kh. Yu. and R. O. Noorma. O spektral'nom raspredelenii intensivnosti i potokov teplovogo izlucheniya v svobodnoi atmosfere. Sb. "Issledovaniya radiatsionnogo rezhima atmosfery" (On the spectral distribution of intensity and fluxes of thermal radiation in free atmosphere. Coll. Study of radiational regime of atmosphere). Tartu, 1967.

43. Nikol'skii, G. A. and E. N. Esipova. Izmereniya radiatsionnogo balansa v svobodnoi atmosfere s pomoshch'yu balansomerov s polie'tilenovoi zashchitoi (Measurements on net radiation in free atmosphere with the help of balancemeter provided with a polythene shield). Problemy fiziki atmosfery, coll. 4, Izd. LGU, 1966.

44. Popov, S. M. Nekotorye statisticheskie kharateristiki vertikal'noi struktury polei temperatury i vlazhnosti (Some statistical characteristics of vertical structure of the temperature and moisture distributions). Izv. AN SSSR, fizika atmosfery i okeana, t. 1, No. 1, 1965.

45. Astling, E. G. and L. H. Horn. Some geographical variations of terrestrial radiation measured by TIROS II. J. Atm. Sci., v. 21, No. 1, 1964.

46. Bell, E. E. et al. Spectral radiance of sky and terrain at wave lengths between 1 and 20 microns. II. : Sky measurements. J. Opt. Soc. Am., v. 50, No. 12, 1960.

47. Bennet, H. E., J. M. Bennet and M. R. Nagel. Distribution of infrared radiance over a clear sky. J. Opt. Soc. Am., v. 50, No. 2, 1960.

48. Bolle, H. J. The influence of atmospheric absorption and emission on infrared detection range. Infrared Physics, v. 5, No. 3, 1965.

49. Businger, J. A. and P. M. Kuhn. On the observation of total and net atmospheric radiation. J. Meteorol., v. 17, No. 4, 1960.

50. Chaney, L. W., L. T. Lon and M. T. Surh. A Fourier transform spectrometer for the measurement of atmospheric thermal radiation. Technical Report 05863-12-T, May 1967, The University of Michigan.

51. Davis, D. A. The application of infrared flux models to atmospheric data. J. Appl. Meteor., v. 4, No. 2, 1965.

52. Eisner, L. et al. Spectral radiance of sky and terrain at wave length between 1 and 20 microns. III : Terrain measurements. J. Opt. Soc. Am., v. 52, No. 2, 1962.

53. Eldering, H. G. Method for the complete description of infrared sky backgrounds. J. Opt. Soc. Am., v. 51, No. 12, 1961.

54. Ginsburg, N., W. R. Fredrikcson and R. Paulson. Measurements with spectral radiometer. J. Opt. Soc. Am., v. 50, No. 12, 1960.

55. Godbole, R. V. A preliminary investigation of radiative heat exchange between the ocean and the atmosphere. J. Appl. Met., v. 2, No. 5, 1963.

56. Goody, R. M. Atmospheric radiation. I : Theoretical basis. Oxford, 1964 (Translation into Russian. Izd-vo "Mir", 1967).

57. Hovis, W. A. Jr. and M. Tobin. Spectral measurements from 1.6 to 5.4 μ of natural surfaces and clouds. Appl. Opt., v. 6, No. 8, 1967.

58. Kennedy, S. J. Energy generation through radiative processes in the lower stratosphere. Massachusetts Institute of Technology, Department of Meteorology, Planetary Circulations Project, Report No. 11, 1964.

59. Kuhn, P. M., V. E. Suomi and G. L. Darkow. Soundings of terrestrial radiation flux over Wisconsin. Month. Weath. Rev., v. 87, No. 4, 1959.

60. Manabe, S. and F. Möller. On the radiative equilibrium and heat balance of the atmosphere. Month. Weath, Rev., v. 87, No. 12, 1961.

61. Mani, A., C. R. Sreedharan and V. Srinivasan. Measurements of infrared radiative fluxes over India. J. Geoph. Res., v. 70, No. 18, 1965.

62. Möller, F. The pattern of radiative heating and cooling in the troposphere and lower stratosphere. Proc. Roy. Soc., Ser. A, v. 236, No. 1205, 1956.

63. Raschke, E., F. Möller and W. Bandeen. The radiation balance of the earth-atmosphere system over both polar regions obtained from radiation measurements of the

Nimbus II meteorological satellite. Goddard Space Flight Center. Greenbelt, Maryland, X-622-67-460, September 1967.

64. Raschke, E. and M. Pasternak. The global radiation balance of the earth-atmosphere system obtained from radiation data of the meteorological Satellite Nimbus II. Goddard Space Flight Center, Greenbelt, Maryland, X-622-67-383, Aug. 1967.

65. Riehl, H. Radiation measurements over the Carribean sea during the autumn of 1960. J. Geophys. Res., v. 67, No. 10, 1962.

66. Robinson, D. Z. Methods of background description and their utility. Proc. IRE, v. 47, No. 9, 1959.

67. Saunders, P. M. Radiance of sea and sky in the infrared 800-1200 cm^{-1}. J. Opt. Soc. Am., v. 58, No. 5, 1968.

68. Staley, D. O., and P. M. Kuhn. Measurements of radiative cooling through two intense baroclinic zones in the middle troposphere. J. Meteorol, v. 18, No. 2, 1961.

69. Tiros II Radiation Data Catalogue. Goddard Space Flight Center, 1961.

70. Tiros III Radiation Data Catalogue. Goddard Space Flight Center, 1962.

71. Zdunkowski, W. G. and F. G. Jonson. Infrared flux divergence calculations with newly constructed radiation tables. J. Appl. Meteor., v. 4, No. 3, 1965.

72. Zdunkowski, W., D. Henderson and V. J. Hales. The effect of atmospheric haze on infrared radiative cooling rates. J. Atm. Sci., v. 23, No. 3, 1966.

9. NET RADIATION

1. NET RADIATION AND ITS MEASUREMENT

1.1 Constituents of net radiation

By net radiation we mean the resulting or residual radiation flux after exchange of radiation at the boundary or within the atmospheric layer, or in the boundary and atmospheric layer considered together. The radiant energy absorbed at the boundary or in the layer can be assigned the plus sign (influx) and the emitted energy the minus sign (scattering). During daytime all the components of net radiation participate in a radiative exchange, particularly the following : shortwave, i.e. direct solar radiation on horizontal surface S_h, scattered (D) and reflected (R) radiations; longwaves—atmospheric radiation E_a and radiation of underlying surface E_u. The net radiation for the underlying surface can be determined according to the formula :

$$B = S_h + D - R + kE_a - E_u, \tag{9.1}$$

where k is absorbing capacity of the underlying surface. It is possible to transform equation (9.1) in the following manner :

$$B = Q(1 - A) - F_0, \tag{9.2}$$

where $Q = S_h + D$ is the total radiation, $A = \frac{R}{Q}$ is albedo of the under-

lying surface and $F_0 = E_u - kE_a$ is the effective radiation of the underlying surface.

Only longwave components participate in the radiative exchange of the underlying surface during nighttime so that the following equation holds :

$$B_{LW} = -F_0 = kE_a - E_u. \tag{9.3}$$

The net radiation of the underlying layer can be measured with the help of a radiometer situated horizontally at a distance of 1.0-1.5 m from the surface. The measurements taken with the radiometer during ascent give information about net radiation of the layer of atmosphere lying below together with the underlying surface. On the upper boundary of the atmosphere we obtain data on the net radiation of the earth's surface-atmosphere system as follows :

$$B_s = S'_0 (1 - A_s) - F_\infty = Q (1 - A) + q - F_\infty, \tag{9.4}$$

where S'_0 is the solar constant on the particular day at a horizontal surface, A_s is the albedo of the earth's surface-atmosphere system, F_∞ is the outgoing thermal radiation and q is the shortwave radiation absorbed in the entire thickness of the earth's atmosphere.

The net radiation of the atmosphere can be obtained as the difference of simultaneously measured values of net radiation on the upper and lower boundaries of the atmosphere, thus :

$$B_a = B_s - B = q - (F_\infty - F_0). \tag{9.5}$$

Evidently during nighttime $B_a < 0$, since $F_\infty > F_0$ always. As a rule during daytime, $B_a > 0$ [15]. Climatological computations always show that the average diurnal value $B_a < 0$. This means that the nighttime cooling exceeds daytime heating and that absorption of solar radiation in aerosol is usually not taken into consideration in computing the incoming part of B_a, and absorption of solar radiation is neglected. For moderate latitudes during summer B_a can attain a value of 0.2 cal/cm^2 · min at midday, and B_s attains a value of 1 cal/cm^2 · min (for a layer of atmosphere of 27 km).

1.2 Measurement of net radiation

The measurement of net radiation of the underlying surface and all the more so of the net radiation of the atmosphere or the earth's surface-atmosphere system is an extremely laborious and taxing task as compared

with the measurement of the shortwave constituents. The instruments widely used for a network of observations on net radiation are the following : Yanishevskii's open radiometer in the USSR, Shulze's radiometer with polythene shielding in Europe, Kew's radiometer in England, Gier and Dunkel's open radiometer with blowers and Funk's radiometer with polythene shielding in Australia. In addition, the Ångström compensation pyrgeometer is also used for measurements during nighttime. Shulze's and Ångström's apparatus allow measurement of upward and downward fluxes separately, whereas the remaining three instruments measure net radiation directly. All the above-mentioned instruments are of the thermoelectric type with black receiving surfaces. The essential differences in their structure can be mainly accounted for by the different methods of shielding from the wind. Shulze's and Funk's instruments use hemispherical polythene shields, and the other instruments have open receiving surfaces. The constructional details of these instruments can be found in [8, 27]. Fig. 9.1 shows the above-mentioned radiometers being compared in Aspendale (Australia).

The application of polythene filters completely eliminates the effect of the wind, but then the graduation of the instrument and working out of the results becomes complicated. In practice the use of radiometers

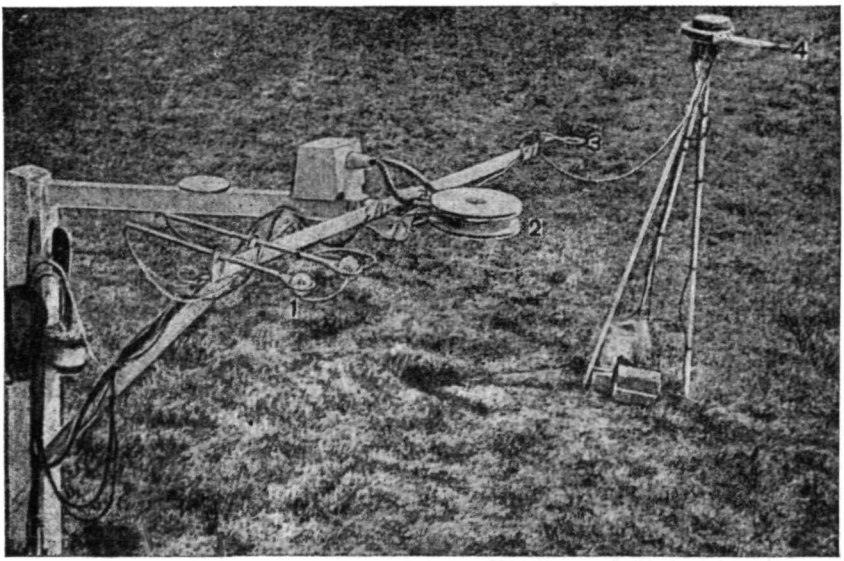

Fig. 9.1. Radiometers of different types being compared to Aspendale.

1—Funk's radiometer; 2—Shulze's radiometer;

3—Yanishevkii's radiometer; 4—Kew's radiometer.

showed that it is necessary to apply only hemispherical shields or at least a shield approximating that in form.

The application of a polythene shield is completely justified for a continuous recording of net radiation of the underlying surface or for measuring the gradient of net radiation. The use of a polythene shield in a radiometer is imperative for measurements made in free atmosphere. For accurate measurements of values of net radiation in free atmosphere it is useful to employ paired radiometers [23], which divide the balance into upward and downward fluxes and with the help of a given albedo pyranometer distinguish all the constituents of net radiation. After the introduction of angular, spectral, thermal and barometric and several other modifications in the components it is possible to obtain net radiation within an error of about 5%. Recently separate measurements on net radiation have been made, using a standard radiometer with an accuracy not exceeding 10%.

2. NET RADIATION OF AN UNDERLYING SURFACE

2.1 Variation of net radiation with time

Of the majority of factors exerting a noticeable influence on the components of net radiation, the following fundamental factors may be distinguished, viz. the altitude of the sun, cloudiness, atmospheric stratification and the nature of the underlying surface. The influence of these factors determines the character of variations with time as well as the geographic distribution of the net radiation of the underlying surface.

The net radiation of the underlying surface can be positive as well as negative depending on the time of day and the season. Negative values of net radiation have usually been observed during nighttime. Similarly the mean monthly values of net radiation of the underlying surface may become negative during winter (for latitudes above 40° N and 40° S).

The diurnal course of the values of net radiation of the underlying surface and its constituents in clear weather for Central Asia are shown in Fig. 9.2 [3].

The effect of solar altitude on the magnitude of net radiation can be traced from the data given in Table 9.1 [6].

The influence of cloudiness on the diurnal variation of net radiation in different seasons is shown in Table 9.2 [21].

The cloudiness in summer and autumn leads to a noticeable decrease in the values of net radiation.

The variation in the degree of cloudiness affects the values of net radiation to a considerable extent (at $h_{\odot} = 40°$ and constant albedo) as shown here :

Degrees of cloudiness, tenths	3	4	5	6	7	8
Net radiation cal/cm² · min	0.46	0.45	0.43	0.42	0.40	0.38

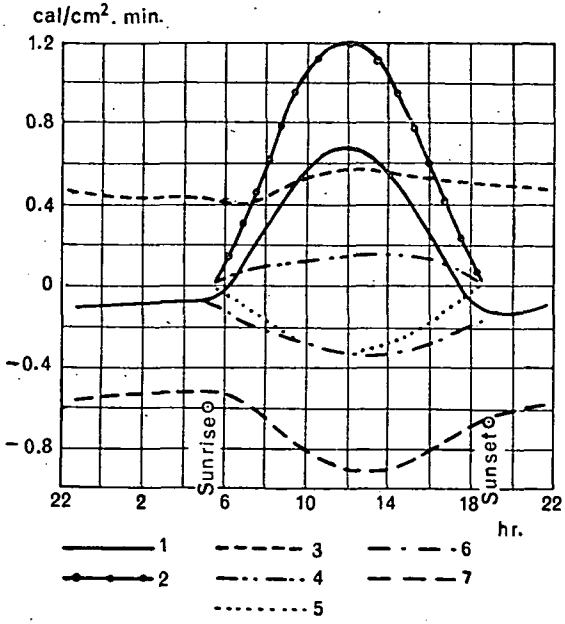

Fig. 9.2. Diurnal course of mean values of net radiation of underlying surface and its constituents in clear weather for Central Asia.

1—net radiation; 2—direct solar radiation; 3—atmospheric back radiation; 4—scattered radiation; 5—reflected shortwave radiation; 6—effective radiation; 7—emission of underlying surface.

Table 9.1 Mean dependence of net radiation of underlying surface upon solar altitude (cal/cm² · min) [6]

Condition of underlying surface	Albedo %	Altitude of the sun, deg							
		0	5	10	15	20	25	30	35
Without snow	15-25	—0.07	—0.04	0.03	0.12	0.21	0.32	0.41	0.48
Snow cover	50-80	—0.05	—0.04	—0.01	0.05	0.10	0.17	0.23	0.29

In the annual variation of the daily amounts of net radiation and of its constituents for moderate latitudes (Hamburg) [33], shown in Fig. 9.3, the definite influence of seasonal variations of solar altitudes on the values of net radiation and of its constituents is apparent.

Table 9.2 Diurnal variation of net radiation in clear and cloudy weather according to seasons (cal/cm² · min)

Time of day, hr	Clear				Cloudy			
	Summer	Autumn	Winter	Spring	Summer	Autumn	Winter	Spring
0	—0.063	—0.092	—0.088	—0.076	—0.018	—0.018	—0.034	—0.029
4	—0.022	—0.070	—0.102	—0.068	—0.013	—0.013	—0.016	—0.024
8	0.392	0.045	0.077	0.123	0.098	0.053	—0.007	0.054
12	0.632	0.390	0.028	0.355	0.247	0.085	0.019	0.107
16	0.312	0.120	—0.064	0.154	0.175	—0.006	—0.008	0.068
20	—0.042	—0.080	—0.082	—0.048	—0.04	—0.012	—0.007	0.004
0	—0.070	—0.079	—0.070	—0.060	—0.019	—0.003	—0.005	—0.019

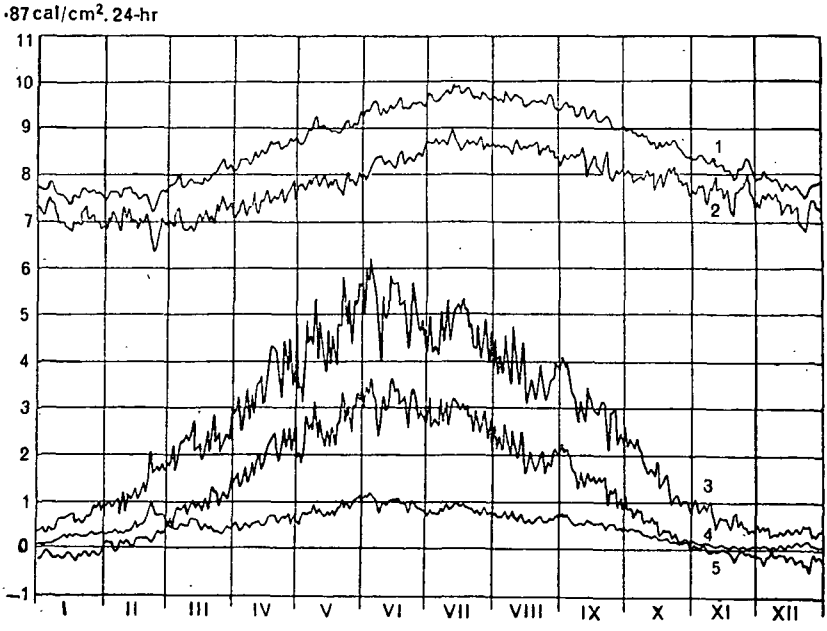

Fig. 9.3. Annual variation of daily amounts (average for 10 years) of net radiation of underlying surface and its constituents in Hamburg.

1—upward flux of the longwave radiation; 2—atmospheric back radiation; 3—resultant radiation; 4—reflected radiation; 5—net radiation.

2.2 Geographic distribution of net radiation of an underlying surface

The occurrence of polar days and nights in the Arctic and Antarctic regions is the basic condition of the radiation regime in these regions of the earth. An analysis of the data on the net radiation was carried out separately for the light and dark periods. For nighttime the mean values of the balance were found by way of averaging over separate data obtained under specific conditions of cloudiness. For the daytime the averaging of values of net radiation was carried out in the same manner as for its constituents at specified solar altitudes.

Because of the scarcity of observations on net radiation in the Arctic and Antarctic regions it is impossible to obtain information about time and space variations only from the material on observations. Thus, theoretical computations of the net radiation and its constituents received fairly wide acceptance. The methods and results of computations are detailed in a monograph [26].

According to the data of Chernigovskii and Marshunova (Table 9.3) the net radiation has simple annual variations in all Arctic regions with a maximum in summer and a minimum in winter. Positive net radiation has been observed from May to August and in the case of the sea being free of ice, even in September. The balance attains a maximum in July and comprises a value of 7-8 kcal/cm^2 · mon at the polar stations and in some polar seas, whereas in the region of ice drifts it reaches a value of 3-4 kcal/cm^2 · mon.

The geographic distribution of net radiation was studied by Chernigovskii and Marshunova [26] in the Arctic region for 12 months. As an example we give here (Fig. 9.4) the annual distribution chart of net radiation in the Arctic region.

In the annual chart of net radiation the zero isoline in the Western part of the Arctic region passes through 80° N and in the Eastern part drops toward the south to 73° N. The net radiation in the Central Arctic region is negative. The net radiation of the island surfaces, continental coasts and Arctic seas averaged over a year is positive. The maximum values have been observed in the region of the Barents sea (25-30 kcal/cm^2 · yr).

The radiation regime of the Antarctic region [25] is extremely characteristic. The annual net radiation is everywhere negative (with the exception of surfaces free from snow and ice). Thus, for instance, the annual amount of net radiation B at Komsomol'sk station constitutes −12.2 kcal/cm^2 · yr, and in Mirnyy (in different years) it varies from −3.5 to −9.1 kcal/cm^2 · yr. In those places where the surface is free from snow and ice, the annual net radiation attains higher values (above 75 kcal/cm^2 · yr

Table 9.3 Annual variation of net radiation in the Arctic region (kcal/cm² . mon) [26]

Place of observation	Jan	Feb	Mar	Apr	May	Jun	Jul	Aug	Sept	Oct	Nov	Dec	Year
Pole	—2.0	—1.9	—1.9	—0.7	1.6	3.2	3.6	1.5	—0.8	—1.3	—1.9	—2.1	—2.7
85° N, 0° E	—2.0	—1.9	—1.9	—0.5	1.7	3.2	3.8	1.5	—0.6	—1.3	—1.9	—2.0	—1.9
85° N, 80° E	—2.2	—2.0	—2.0	—0.6	1.7	3.3	3.7	1.6	—0.6	—1.3	—1.8	—2.2	—2.4
85° N, 160° E	—2.2	—2.0	—1.9	—0.8	1.5	3.3	3.8	1.8	—0.6	—1.4	—2.0	—2.3	—2.8
80° N, 135° E	—2.3	—2.3	—2.2	—0.6	1.6	3.1	3.8	1.8	—0.2	—1.2	—2.0	—2.7	—3.2
80° N, 160° E	—2.4	—2.2	—2.2	—0.6	1.6	3.4	3.6	1.9	—0.6	—1.3	—2.1	—2.5	—3.4
80° N, 185° E	—2.4	—2.2	—2.1	—0.4	1.5	3.4	3.8	1.9	—0.6	—1.3	—2.0	—2.2	—2.6
80° N, 210° E	—2.2	—2.0	—2.0	—0.2	1.5	3.2	3.9	1.7	—0.7	—1.3	—2.0	—2.2	—2.3
75° N, 160° E	—2.4	—2.2	—1.9	—0.5	1.5	3.1	3.9	1.8	—0.1	—0.9	—2.2	—2.5	—2.4
75° N, 180° E	—2.2	—2.2	—1.9	—0.5	1.5	3.1	3.7	1.8	—0.3	—0.9	—2.2	—2.5	—2.6
Kara Sea													
South West part	—2.2	—2.0	—1.6	—0.2	1.5	5.6	6.8	5.2	1.5	—2.3	—2.1	—2.3	7.9
North East part	—2.5	2.2	—1.8	—0.3	1.5	4.8	5.4	3.4	—0.2	—2.4	—2.2	—2.4	1.1
Laptev Sea													
Western part	—2.5	—2.2	—1.7	—0.4	1.7	5.0	6.0	3.6	0.9	—2.4	—2.5	—2.5	3.0
Eastern part	—2.5	—2.1	—1.7	—0.3	1.6	4.8	5.9	4.5	1.5	—2.3	—2.5	—2.5	4.4
East Siberian Sea													
Western part	—2.2	—1.9	—1.8	—0.4	1.6	4.2	5.4	3.8	1.4	—1.6	—2.3	—2.2	4.0
Eastern part	—2.2	—1.9	—1.7	—0.4	1.6	3.7	5.0	3.1	1.3	—1.6	—2.3	—2.2	2.4
Chukchi Sea	—2.4	—1.8	—1.4	—0.2	2.5	7.6	7.9	5.0	2.0	—2.0	—2.2	—2.4	12.6
Uedineniya Island	—2.3	—2.2	—2.0	—0.4	1.8	5.6	8.5	4.3	—0.2	—1.5	—2.1	—2.5	7.0
Cape Chelyuskin	—2.5	—2.2	—2.2	—0.5	1.0	3.6	8.3	3.9	—0.5	—2.0	—2.2	—2.6	2.1
Dickson Island	—2.0	—1.7	—1.7	—0.4	1.6	5.6	8.4	4.2	0.2	—2.0	—2.2	—2.2	7.8
Kotel'nyy Island	—2.4	—2.2	—1.8	—0.2	2.4	7.9	7.2	4.5	—0.2	—1.8	—2.2	—2.6	8.6
Tiksi Bay & Mostakh Island	—2.4	—2.1	—1.4	—0.1	2.0	8.1	8.9	4.4	0.5	—1.7	—2.3	—2.5	11.4
Cape Schmidt	—2.4	—1.8	—1.4	—0.2	2.0	7.4	8.7	4.9	1.1	—1.4	—2.1	—2.3	12.5
Cape Ualen	—2.5	—1.9	—1.5	—0.5	1.9	10.0	9.1	4.5	1.4	—0.8	—1.7	—2.0	16.0

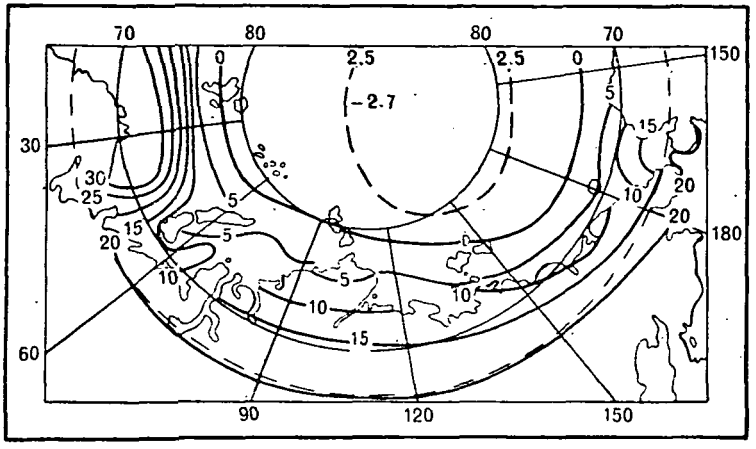

Fig. 9.4. Distribution of annual amounts of net radiation in the Arctic region (kcal/cm² · yr).

at Oasis). Thus, the monthly amounts of net radiation for a large part of the Antarctic region are positive only in the course of three to four months in a year.

The mean monthly amounts of net radiation obtained as the product of mean diurnal amounts B and the average number of days in a month (30.4) are given in Table 9.4.

A general idea of the distribution of monthly amounts of balance over the territory of the USSR is given in Table 9.5 [6], from which it follows that the monthly amounts of net radiation increase with the latitude in the course of a whole year. The properties of atmospheric circulation and the nature of the underlying surface (albedo of surface) affect the distribution of the balance to a considerable extent.

The chart of geographic distribution of the annual amounts of net radiation in the territory of the USSR is shown in Fig. 9.5 [24]. Obviously, the annual net radiation is everywhere positive and varies from 20 kcal/cm² · yr in the North to 60 kcal/cm² · yr in the South.

The geographic distribution of net radiation is primarily zonal. However, a weak tendency of growth in net radiation has been observed in the Western regions. A reverse phenomenon takes place in the Eastern regions of the territory surveyed.

It is usual to regard the period between November and February as the winter season in the case of the USSR, since it is in this period that the net radiation is negative in the major portion of the territory. In these months, especially in December and January, the distribution of net radia-

Table 9.4 Mean monthly amounts of net radiation (kcal/cm²)

Station	Jan	Feb	Mar	Apr	May	Jun	Jul	Aug	Sept	Oct	Nov	Dec	Year
Mirnyy	+ 2.0	+1.2	—1.4	—1.5	—1.7	—2.3	—1.9	—1.8	—1.5	—0.3	+1.5	+ 2.7	—5.0
Pioneer	+ 1.5	—0.4	—1.1	—1.5	—1.5	—1.6	—1.6	—1.6	—1.5	—0.5	+0.7	+ 1.7	—7.4
Vostok 1	+ 0.5	—0.4	—1.1	—1.3	—1.3	—1.4	—1.4	—1.3	—1.3	—0.7	+0.3	+ 1.0	—8.4
Komsomol'sk	+ 0.6	—0.1	—0.8	—0.8	—0.9	—0.9	—0.9	—0.9	—0.8	—0.3	+0.4	+ 1.0	—4.4
Vostok	+ 0.6	—0.1	—1.0	—1.1	—0.6	—0.8	—1.0	—1.2	—0.9	—0.3	+0.4	+ 0.8	—5.2
Soviet	—	—	—1.1	—0.8	—0.9	—1.1	—0.9	—1.2	—1.1	0.0	—	—	—
Oasis	+10.5	+6.8	+2.7	—1.4	—1.8	—2.0	—1.8	—1.1	+1.3	+4.8	+7.8	+11.8	+37.6
Port Martin	+ 5.3	+2.1	+0.5	—2.6	—2.9	—2.9	—3.0	—2.2	—3.2	—1.1	+0.3	+ 4.4	—5.3
Modheim	+ 0.3	—0.5	—0.8	—1.3	—1.5	—1.4	—1.4	—1.4	—1.1	—0.5	—0.1	+ 0.7	—9.0
Little America	+ 1.3	+0.1	—0.7	—1.0	—1.5	—3.9	—1.4	—1.2	—0.8	—0.8	+1.2	+ 1.9	(—6.8)
Scott	+13.3	+5.5	+0.1	—1.9	—2.7	(—2.0)	—2.9	—2.5	—2.1	0.4	3.5	9.5	+18.2

Table 9.5 Mean amounts of net radiation with respect to latitude (kcal/cm²) [6]

Latitude, deg	Jan	Feb	Mar	Apr	May	Jun	Jul	Aug	Sept	Oct	Nov	Dec	Year
38 N	1.5	2.7	3.8	6.1	8.4	8.8	8.5	7.8	5.4	3.5	1.7	0.8	59.0
40	0.8	2.0	3.6	5.8	8.3	8.8	8.5	7.6	5.3	3.0	1.3	0.5	55.5
42	0.4	1.3	3.4	5.6	8.2	8.8	8.5	7.5	5.2	2.6	0.8	0.1	52.4
44	0.0	0.8	3.0	5.5	8.1	8.8	8.5	7.3	5.0	2.3	0.5	—0.2	49.6
46	—0.2	0.5	2.7	5.4	8.0	8.8	8.5	7.1	4.7	2.0	0.3	—0.4	47.4
48	—0.4	0.2	2.3	5.3	7.9	8.8	8.5	6.9	4.5	1.8	0.0	—0.5	45.3
50	—0.5	0.0	2.0	5.2	7.8	8.8	8.4	6.7	4.2	1.5	—0.2	—0.7	43.2
52	—0.5	—0.2	1.6	5.1	7.6	8.7	8.3	6.4	3.8	1.1	—0.4	—0.7	40.8
54	—0.6	—0.3	1.2	4.7	7.5	8.5	8.2	6.1	3.4	0.8	—0.5	—0.8	38.2
56	—0.6	—0.4	0.7	4.3	7.4	8.4	8.0	5.8	3.0	0.5	—0.6	—0.8	35.7
58	—0.7	—0.5	0.2	3.7	7.2	8.3	7.9	5.6	2.7	0.3	—0.6	—0.8	33.3
60	—0.8	—0.6	—0.2	3.2	6.9	8.3	7.8	5.4	2.4	0.1	—0.7	—0.8	31.0
62	—0.8	—0.6	—0.4	2.2	6.5	8.2	7.8	5.3	2.1	—0.1	—0.7	—0.9	28.6
64	—0.7	—0.6	—0.4	1.3	6.0	8.2	7.7	5.1	1.9	—0.2	—0.8	—1.0	26.5
66	—0.7	—0.6	—0.4	0.6	5.5	8.2	7.7	4.9	1.6	—0.4	—0.9	—1.0	24.5
68	—0.7	—0.6	—0.4	0.1	5.0	8.3	7.6	4.5	1.3	—0.7	—0.7	—1.0	22.7

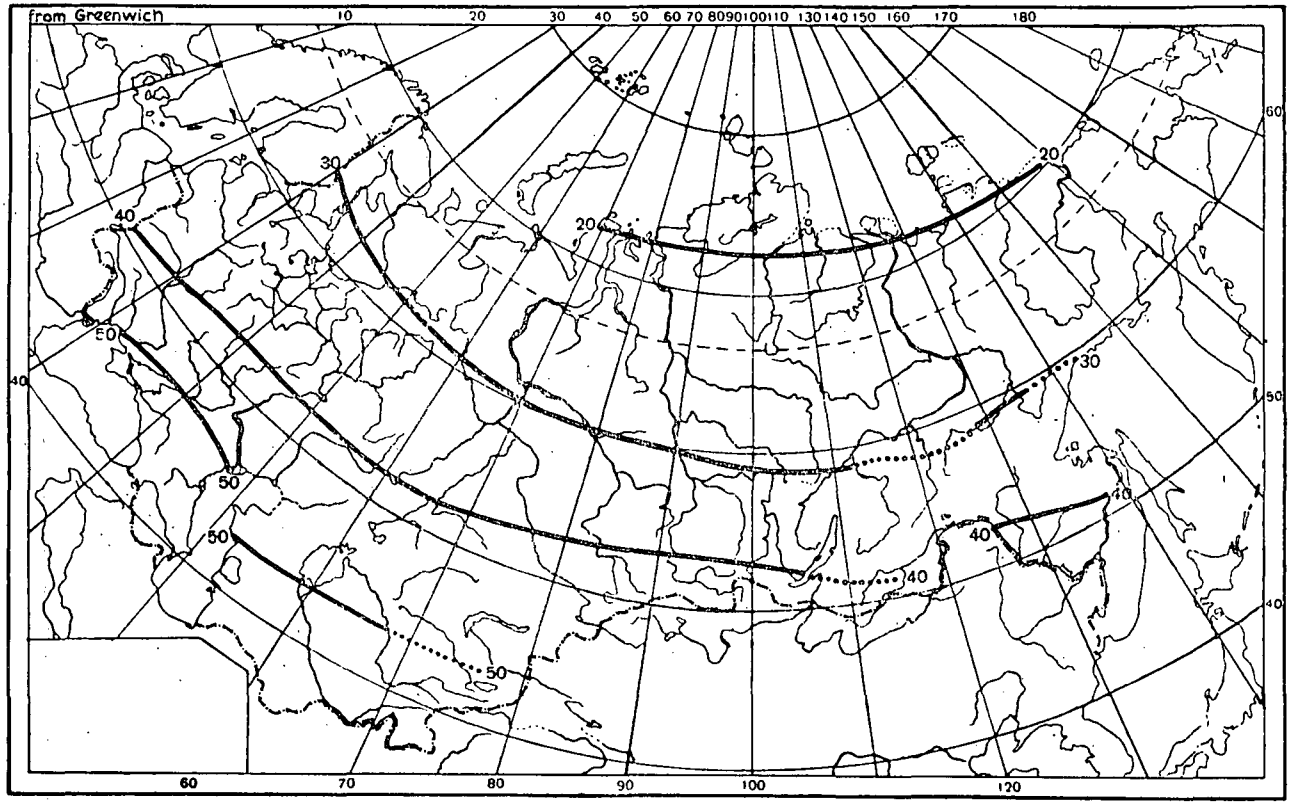

Fig. 9.5. Distribution of annual amounts of net radiation in the territory of the USSR (kcal/cm² · yr.)

tion differs from the latitudinal distribution. The negative values of monthly amounts of the balance diminish in the North-Western region of the European Territory of the USSR under the influence of western transfer and the intense cloudiness connected with it, and in Eastern Siberia under the influence of a steady anticyclone and inversions connected with it.

The summer season (June, July) is characterized by small variations of net radiation over the territory. In August the net radiation diminishes universally and especially noticeably in the North.

Table 9.6 shows the results of computations on average latitudinal distribution of annual amounts of net radiation of land, oceans and the entire surface of the earth. These results were obtained by Budyko, Efimova, Zubenok and Strokina [9].

Table 9.6 Mean latitudinal distribution of annual amounts of net radiation (kcal/cm² · yr) of land, oceans and the entire surface of the earth [9]

Latitude in degrees	Ocean	Land	Mean
70-60 N	23	20	21
60-50	29	30	30
50-40	51	45	48
40-30	83	60	73
30-20	113	69	96
20-10	119	71	106
10-0	115	72	105
0-10 S	115	72	105
10-20	113	73	104
20-30	101	70	94
30-40	82	62	80
40-50	57	41	56
50-60	28	31	28
Entire earth	82	49	72

The construction of charts [11], characterizing the geographic distribution of mean amounts of net radiation for the earth's surface (Fig. 9.6), was carried out on the basis of a large amount of data computed by Efimova. An analysis of this chart shows that the variation in net radiation in transition from land to sea occurs spasmodically, expressed in the discontinuities of isolines in the vicinity of coastal areas. This is brought about by the sharp variation in the albedo of the underlying surface in view of the significantly lower values of albedo of the ocean surfaces than for land. The net radiation of the latter as a rule exceeds the net radiation of land.

From Fig. 9.6 it is seen that the net radiation is positive for the entire

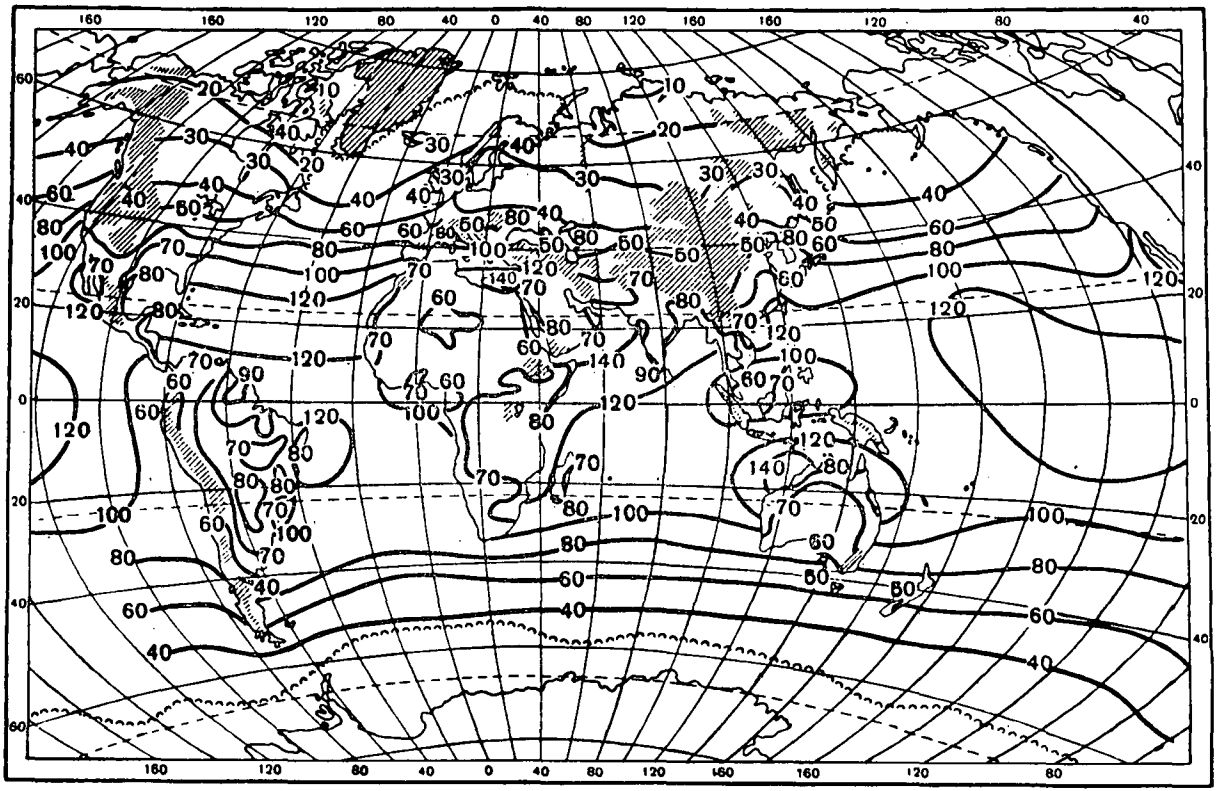

Fig. 9.6. Distribution of average annual amounts of net radiation for the earth's surface (kcal/cm² · yr).

surface of the earth and varies from values close to zero in Central Africa and 10 kcal/cm² · yr in the vicinity of the boundary of perpetual ice to 80-95 kcal/cm² · yr in tropical latitudes. Nevertheless, annual amounts of net radiation can be negative, obviously, in the regions with constant or continuous ice or snow cover, i.e. in some Arctic and Antarctic regions.

The distribution of net radiation in the cold and moderate zones of the earth can be considered approximately zonal, since during summer and winter the underlying surface is comparatively homogeneous in large territories. In land regions the magnitude of net radiation is very much lowered. This situation can be explained by the large albedo values in deserts and considerable dispersion of heat as a result of the high temperature of the desert surface. Inconsequential magnitudes of net radiation are found in monsoon regions brought about by the increased cloudiness during the warm season of the year.

The maximum values of net radiation of the surface above the oceans have been observed in the regions of the Indian Ocean, East of the Arabian Peninsula and off North-Western Australia. The maximum on land occurs for grasslands with low cloudiness but with sufficient moisture, and for the evergreen tropical forests.

An analysis of the monthly charts for January (Fig. 9.7 a) and July (Fig. 9.7 b) leads to the following conclusions :

In January the net radiation is negative in the North from 45-47° N and positive in the remaining surface of the earth with the exception of regions in the vicinity of the South Pole.

Positive net radiation rises toward the equator, attaining a value of 8-12 kcal/cm² · mon. It changes comparatively little in the oceans south of the equator, where it has a value of 8-12 kcal/cm² · mon in the oceans and 6-8 kcal/cm² · mon on land.

In July the lowest values have been recorded in the polar basin, being of the order of 4 kcal/cm² · mon. An extremely homogeneous radiation field with values of the order of 8 kcal/cm² · mon has been observed in the moderate latitudes of the Northern Hemisphere.

Such a diverse distribution of net radiation determines the formulation of continental air masses above these regions. The summer values of the balance in tropical and equatorial latitudes vary within large limits according to territory. The lowest values, viz. 4.5-5.0 kcal/cm² · mon, correspond to the regions of greatest cloudiness during the equatorial monsoons. The maximum values of 8-10 kcal/cm² · mon have been observed in regions with a favorable combination of moisture and cloudiness.

2.3 Net radiation of slopes

The determination of the net radiation of differently oriented inclined

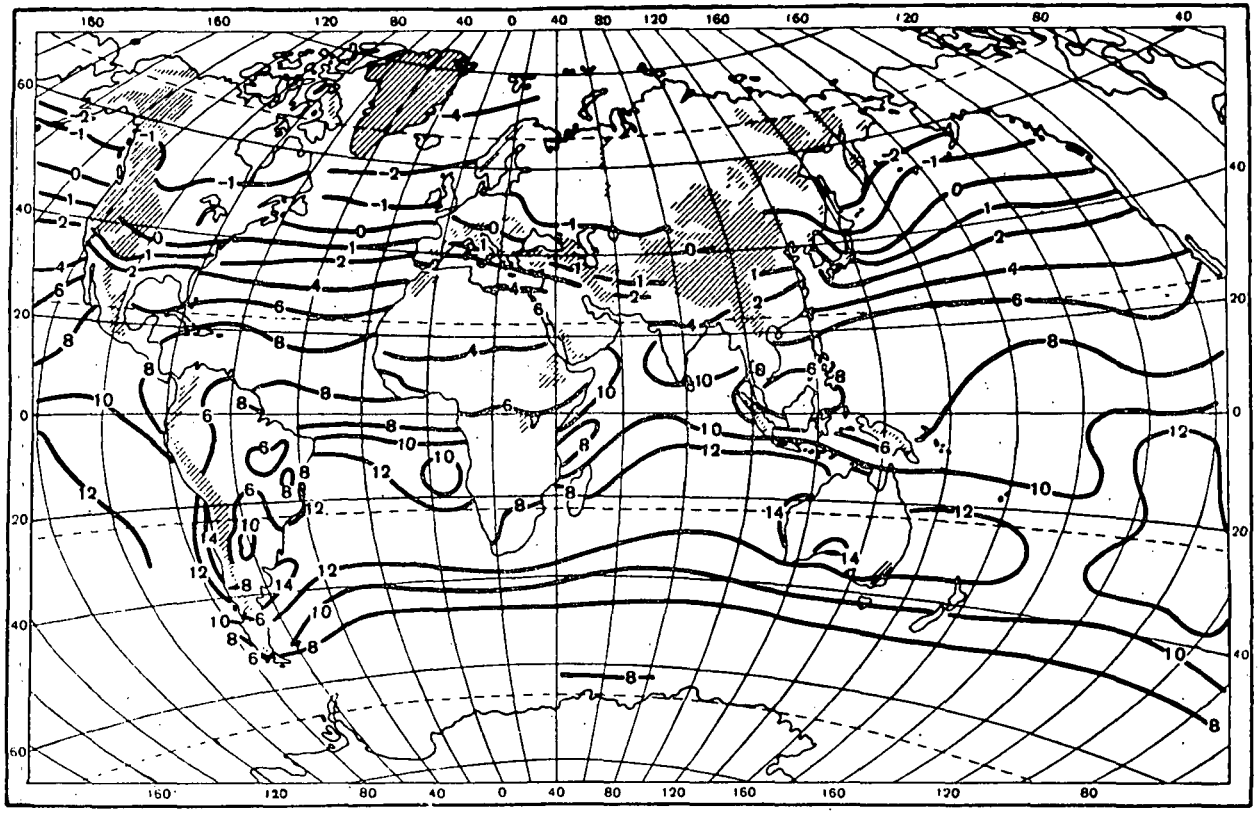

Fig. 9.7a. Monthly amounts of net radiation on the surface of earth (kcal/cm² . mon). January.

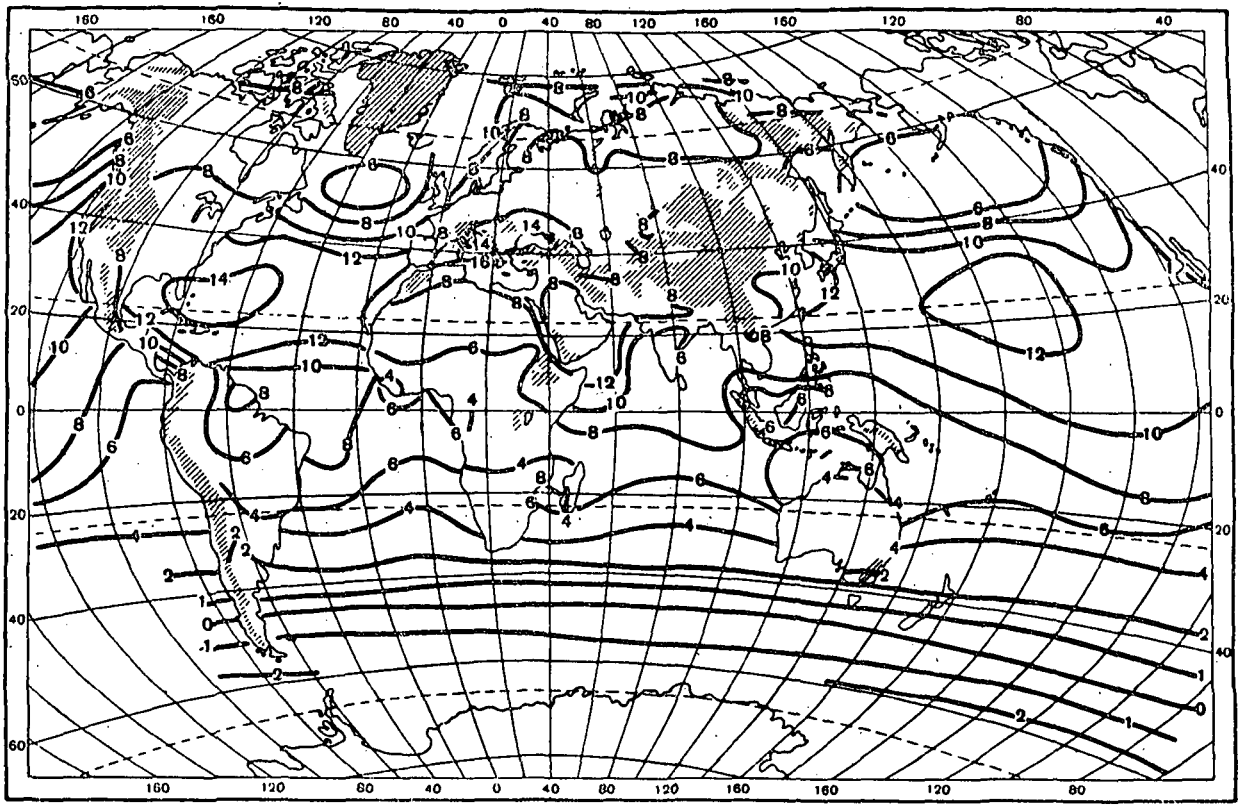

Fig. 9.7b. Monthly amounts of net radiation on the surface of earth (kcal/cm² · mon) · July.

surfaces is required for the solution of different problems in the fields of construction, heliotechnology and meteorology in mountainous regions.

The net radiation of an inclined surface or natural mountain slope can be described by the following relation :

$$B_{in} = (S_s + D_s + R_s)\ (1 - A_s) - F_s - U_s, \tag{9.6}$$

where S_s, D_s, R_s are the fluxes of direct, scattered and reflected radiations respectively on the inclined surface, A_s—the albedo of the inclined surface, F_s—the effective radiation of the slope and U_s—the exchange of longwave radiation between the surface of the slope and the reflecting horizontal surface.

The exchange of longwave radiation between the slope and horizontal surface can be determined from the following expression [1]:

$$U_s = \left(\delta_s \sigma T_s^4 - \delta_h \sigma T_h^4 \right) \sin^2 \frac{\alpha}{2}, \tag{9.7}$$

where δ_s and δ_h are the emissive capabilities of the inclined and the adjoining horizontal surfaces respectively, T_s and T_h—the temperature of the inclined and horizontal surfaces respectively, σ—the emission constant, and α—the angle of inclination of the slope.

If the slope and the horizontal surface possess equal emissive capabilities, then the expression (9.7) can be rewritten in the following manner :

$$U_s = \delta \sigma \left(T_s^4 - T_h^4 \right) \sin^2 \frac{\alpha}{2}. \tag{9.8}$$

The determination of the distinct constituents of the net radiation of slopes has been examined in Chapters 5-8. In this section the net radiation of slopes as a whole will be examined.

There are limited data in literature on the study of the radiation regime of mountain slopes in distinct geographic regions [2, 4, 22] or of differently oriented plane surfaces under ideal conditions [16].

Equation (9.6) describes the case of an isolated slope (or plane inclined surface) with an evenly horizontal surface placed before it and the horizon completely covered. One comes across such conditions extremely rarely in nature. In natural conditions one must take into consideration the covering up of the horizon by mountains or structures and determine the fluxes of reflected radiation from the surroundings on the surface under examination. It is expecially important to consider this while computing melting of snow in the mountains. This problem remains unsolved to date. For each concrete problem one is forced to carry out special actinometric measurements on the components of the net radiation.

The difference between the net radiation of a horizontal surface and inclined surfaces is clearly characterized by the relative magnitudes of the net radiation. Relative values of the net radiation can be determined as the ratio of the net radiation of an inclined surface to the value of the net radiation of the horizontal surface.

Fig. 9.8 a, b shows the dependence of relative values of the net radiation upon the angle of inclination and azimuth of the surface at different solar altitudes and clear atmosphere, constructed from the data on measurements [16]. The orientation of surfaces according to countries in daylight is denoted by letters on corresponding curves. From the figures it is seen that the influence of the azimuthal orientation on the values of the net radiation diminishes with increase in solar altitude. For surfaces turned toward the sun, the maximum of relative values of the radiation (B_{in}/B_h) were recorded at the angle of inclination of the surface $\alpha \approx 90° - h_\odot$, which is most clearly expressed at low solar altitudes. For low and intermediate solar altitudes the net radiation of inclined surfaces turned toward the sun is considerably greater than the net radiation for a horizontal surface.

A maximum of B_{in}/B_h has been recorded for surfaces oriented on the side away from the sun; moreover, for certain values of the angle of inclination of the surface the net radiation is negative at low solar altitudes.

The curves of slopes turned away from the sun exhibit a positive net radiation on account of the rise in the flux of negative radiation and decrease of the effective radiation. A monotonic decrease in values of B_{in}/B_h has been observed for slopes with azimuth 90° and 270° with respect to the sun as the angle of inclination of the surface increases.

Fig. 9.9 shows the dependence of relative values of the net radiation on the angle of inclination and azimuth of a surface under dense cirrus cloud.

From a comparison between Figs. 9.8a and 9.9 it is seen that under dense cirrus cloud the azimuthal dependence of B is less than in a cloudless sky.

The zone of negative net radiation in this case is missing in view of the increase in flux of the scattered radiation and decrease in effective radiation brought about by the influence of cloudiness.

3. NET RADIATION OF THE ATMOSPHERE AND THE EARTH-ATMOSPHERE SYSTEM

3.1 Incoming and diffuse components of net radiation of the atmosphere and the earth-atmosphere system

The incoming part of the net radiation of the atmosphere B_a consists

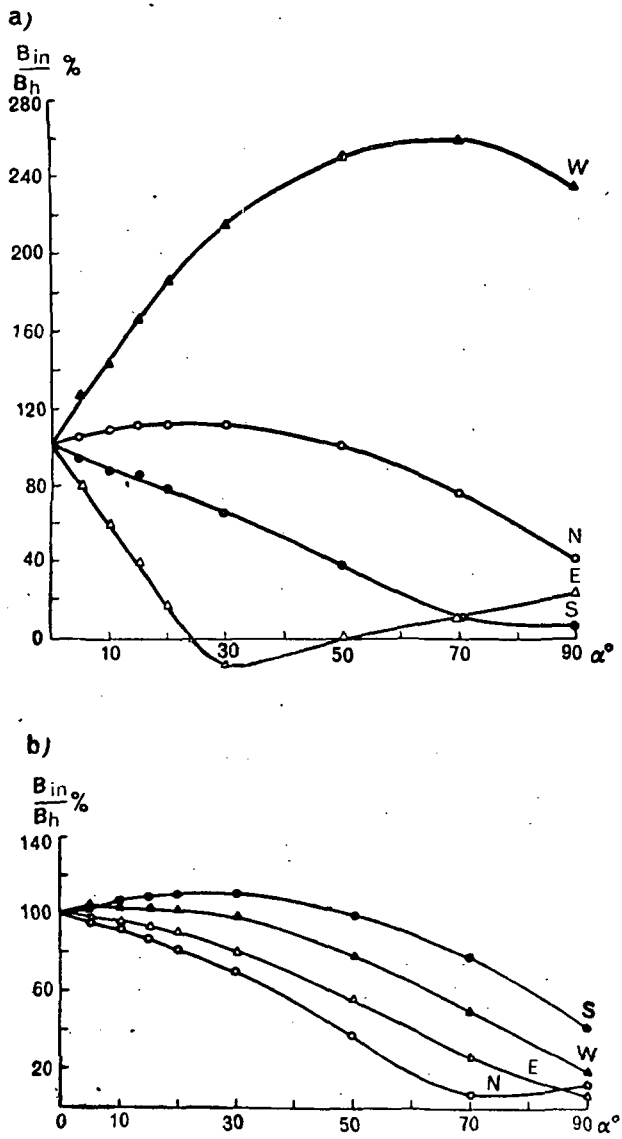

Fig. 9.8. The dependence of relative values of the radiation of slope (B_{in}/B_h) upon the angle of inclination α and azimuth of the surface.

a—Karadag, 16 hrs. 53 min, June 20, 1956; $h_\odot = 27°$, $\psi_\odot = 268°$, clear, wind 1 m/sec, SE;
b—Karadag, 12 hrs. 32 min, June 20, 1956; $h_\odot = 66°$, $\psi_\odot = 199°$, clear, wind 1 m/sec, SE.

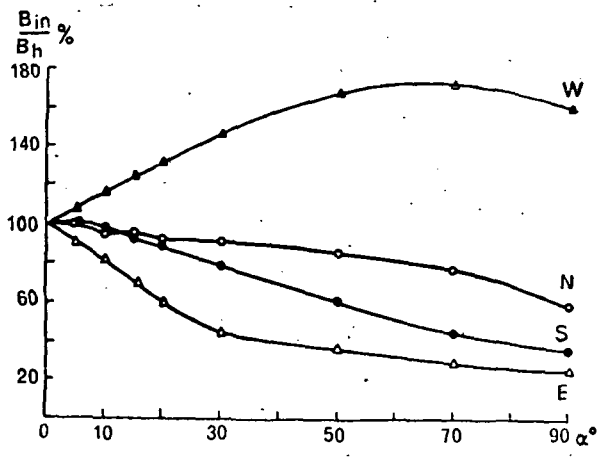

Fig. 9.9. Dependence of relative values of the net radiation of the slope (B_{in}/B_h) on the angle of inclination α and azimuth of the surface.
Karadag, June 16, 1956, 16 hrs. 49 min; $h_\odot = 28°$, $\psi_\odot = 269°$, cloudiness of 10 tenths Ci wind 1 m/sec, SE.

of direct solar radiation absorbed in the atmosphere and scattered radiation q, as well as thermal radiation of the underlying surface U_a absorbed in the atmosphere. The diffuse component can be determined by the loss of heat on account of atmospheric thermal radiation in the direction of the earth's surface and in space. The first component of diffuse part of atmospheric net radiation is the atmospheric radiation E_a and the second is the atmospheric emission in space E_∞.

Thus the equation of atmospheric net radiation will have the following form :

$$B_a = U_a + q - E_a - E_\infty . \tag{9.9}$$

If it is assumed that P_a is the transmission capability of the atmosphere for thermal radiation, then thermal radiation of the underlying surface absorbed in the atmosphere can be represented in the form $U_a = (1 - P_a) F_f$, where F_f is the upward flux of thermal radiation at the level of the underlying surface.

Thus the magnitude $F_b - E_a = F_0$ is the effective radiation of the underlying surface and $P_a F_a + E_\infty = F_\infty$ is the outward radiation of the underlying surface and atmosphere in space. After transformation the equation of atmospheric net radiation can be written in the form :

$$B_a = F_0 - F_\infty + q. \tag{9.10}$$

Direct solar and scattered radiation absorbed in the underlying surface and atmosphere constitute the incoming constituent of the net radia-

tion of the earth's surface-atmosphere system B_s, whereas the outgoing radiation is the dispersed part. Thus the equation of net radiation of the earth-atmosphere system has the following form :

$$B_s = S'_0 (1 - A_e) - F_\infty, \tag{9.11}$$

where S'_0 is the influx of solar radiation beyond the boundary of the atmosphere and A_e is the albedo of the earth as a planet.

The local values of net radiation of the earth's surface-atmosphere system and its constituents can be obtained from the experimental data on aerostatic probings in an atmospheric layer of 27 km thickness given in Table 9.7 [15].

Table 9.7 Net radiation of the earth's surface-atmosphere system (cal/cm² · min)

Date	B_{sw}	q	q%	B_s	B_a	A_s%	A_e%	Cloudiness
May 25, 1962	1.38	0.35	19.3	0.98	0.18	15.3	17.9	Clear
May 30	1.23	0.29	16.1	0.74	0.087	22.0	18.8	„
Jun 5	—	—	—	0.85	0.15	—	—	„
Jun 12	1.04	—	—	0.75	0.006	33.9	16.3	„
Jun 22	1.02	0.11	—	0.63	—0.019	34.1	18.3	St, Cu
Jul 4	—	—	—	0.68	0.15	—	18.5	St, Cu
Jul 7	1.15	0.41	22.2	0.58	0.20	20.0	23.2	Clear
Jul 12	1.08	0.39	21.6	0.70	0.11	20.9	20.9	„
Nov 22	0.45	0.37	64.4	0.12	0.084	20.1	22.0	„

REMARKS: B_s and B_{SW} are the complete and shortwave radiative balance of the system: A_s and A_e are albedo of system and earth's surface.

Table 9.8 Global net radiation (cal/cm² · min) according to measurements of "Nimbus-II", 1966

Period	A_c %	q	F_∞	B_s
May 16-31	30.1	0.341	0.339	+0.002
Jun 1-15	30.6	0.337	0.342	—0.005
Jun 16-30	30.1	0.338	0.345	—0.007
Jul 1-15	29.1	0.343	0.346	—0.003
Jul 16-28	29.5	0.342	0.345	—0.003

REMARKS: Data have been obtained considering the value of solar constant as 1.95 cal/cm² · min [Chapter 5 of the present collection of articles 34, 45].

The global values of net radiation of the earth's surface-atmosphere system and its constituents, from data of "Nimbus-II", are given in Table 9.8 [32].

It is obvious from the Table that mean global net radiation varies around zero value which indicates small deviations of the earth's surface-atmosphere system from the radiation equilibrium. Global values of albedo, viz. $A_e \approx 30\%$, are considerably lower than those obtained earlier (34-42%).

3.2 Geographic distribution of net radiation of the atmosphere and of the earth-atmosphere system

Insofar as the average annual temperatures of the earth as a whole vary only a little with time, the absorbed radiation of the earth-atmosphere system for the whole earth must be on an average equal to the outward radiation. This condition of net radiation of the earth-atmosphere system being equal to zero serves as a reliable criterion of the correctness of the method suggested and the results obtained. Adding the magnitudes of absorbed radiation for the entire earth, it is found to equal 161 kcal/cm^2 · yr. The outgoing radiations thus came out to be 162 kcal/cm^2 · yr. There is a satisfactory agreement.

In the "Atlas of Thermal Balance of the Earth" under the editorship of M. I. Budyko [5] a global chart of net radiation of the earth-atmosphere system has been offered (Fig. 9.10).

Table 9.9 gives average latitudinal values of absorbed radiation of the earth-atmosphere system $S'_0\ (1-A_e)$, outward radiation F_∞ and net radiation of the earth-atmosphere system B_s for June and December.

Table 9.9 Mean latitudinal course of monthly values of net radiation of the earth's surface-atmosphere system and its components (kcal/cm^2)

Latitude, deg	$S'_0\ (1\text{-}A_c)$	F_∞	B_s	$S'_0\ (1\text{-}A_c)$	F_∞	B_s
		June			December	
70 N	15.4	12.9	2.5	0.0	11.4	—11.4
60	17.2	13.4	3.8	0.7	11.7	—11.0
50	18.3	13.6	4.7	2.6	12.3	— 9.7
40	19.0	14.1	4.9	5.7	13.1	— 7.4
30	19.1	14.6	4.5	9.6	14.3	— 4.7
20	18.5	14.2	4.3	12.8	14.8	— 2.0
10	17.2	13.3	3.9	15.5	14.1	1.4
0	15.5	12.7	2.8	16.9	13.1	3.8

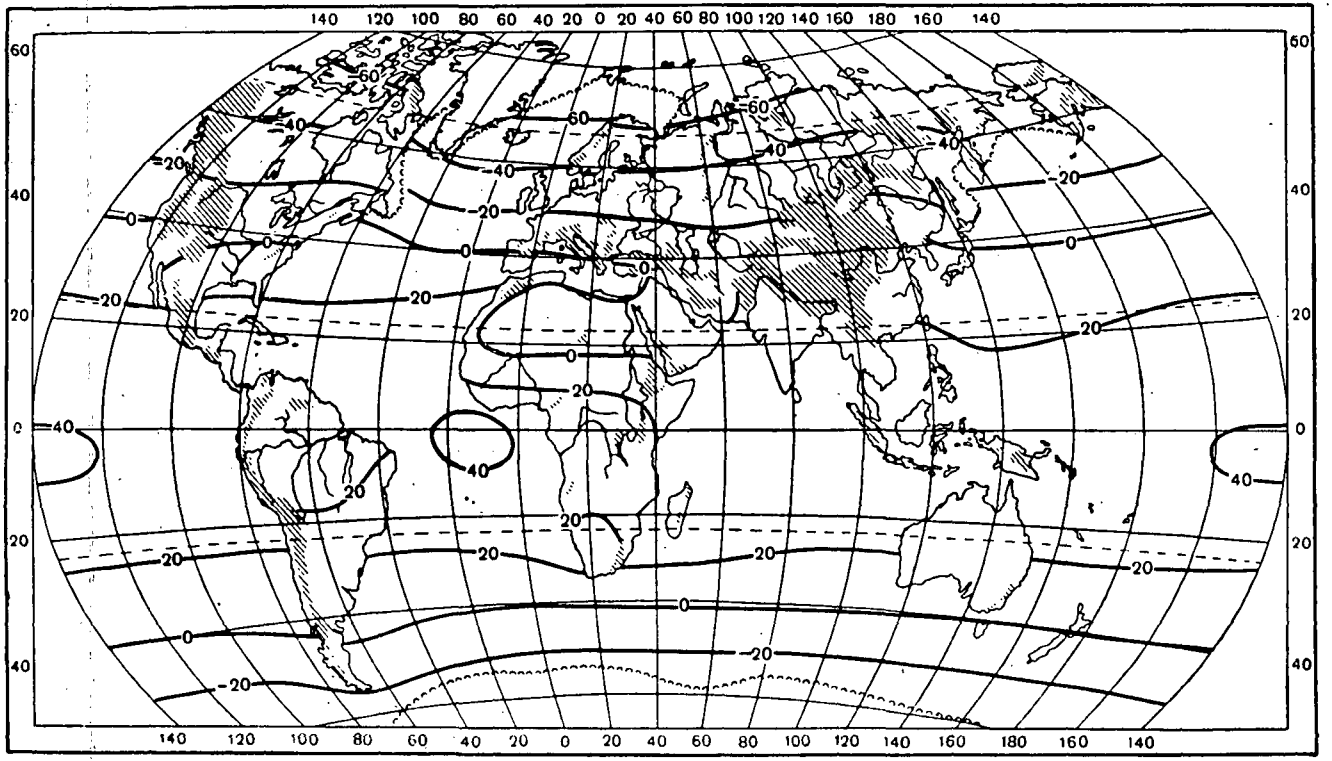

Fig. 9.10. Annual amounts of net radiation of the earth-atmosphere system (kcal/cm² · yr).

While computing the values of net radiation of the underlying surface from values of the net radiation of the earth-atmosphere system, T. G.

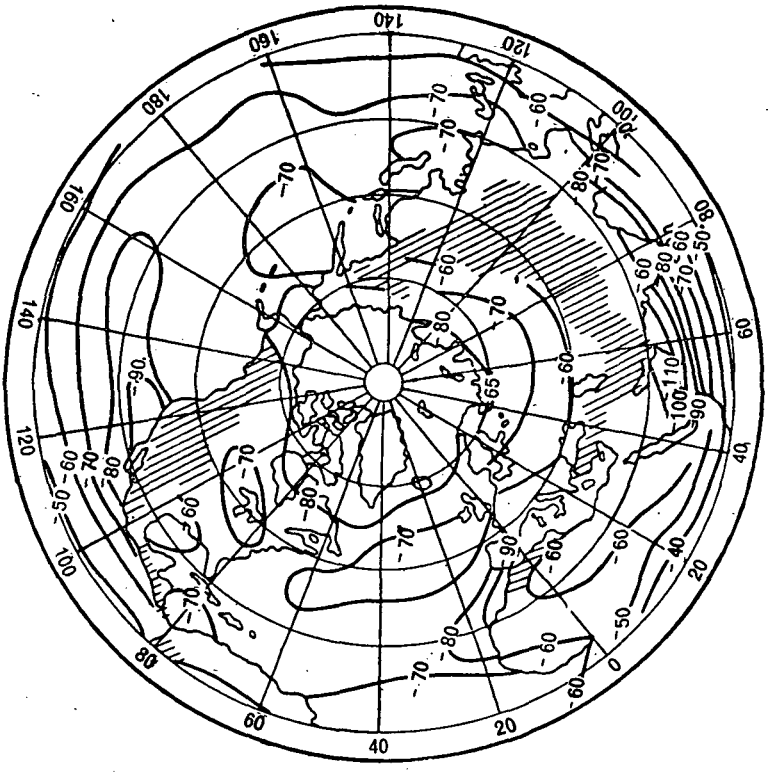

Fig. 9.11. Annual amounts of atmospheric net radiation for the Northern Hemisphere (kcal/cm² · yr).

Berlyand [7] obtained the amount of net radiation of the atmosphere and constructed monthly and annual charts for the Northern Hemisphere.

Here we introduce the annual (Fig. 9.11) and two monthly charts characterizing the warm (Fig. 9.12a) and cold (Fig. 9.12b) periods of the year. An analysis of these charts indicates a comparatively small spatial variation of the net radiation. This is especially seen in summer when the latitudinal variation in absorbed solar radiation and outward radiation is around 4-6 kcal/cm² · mon. A more significant variation of net radiation has been observed in December (from −10 kcal/cm² · mon at high latitudes to −4 kcal/cm² · mon at low latitudes). Similarly the annual net radiation shows a noticeable geographic variability.

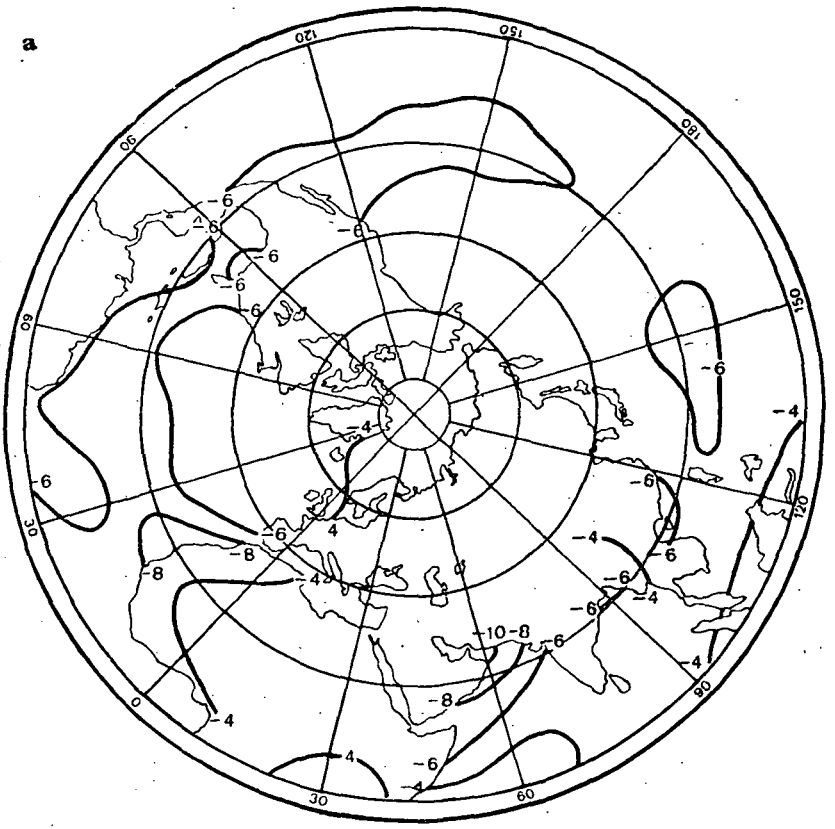

Fig. 9.12a. Monthly amounts of atmospheric net radiation for the Northern Hemisphere (kcal/cm² · mon). June.

Computations of the average latitudinal distribution of atmospheric net radiation were accomplished by Berlyand and Vinnikov (Table 9.10).

Table 9.10 Average latitudinal distributions of atmospheric net radiation (kcal/cm² · yr)

Latitude, deg,	B_a	Latitude, deg,	B_a
70-60 N	70	0-10 S	74
60-50	60	10-20	76
50-40	60	20-30	74
40-30	69	30-40	71
30-20	82	40-50	64
20-10	83	50-60	57
10-0	76	Entire earth	72

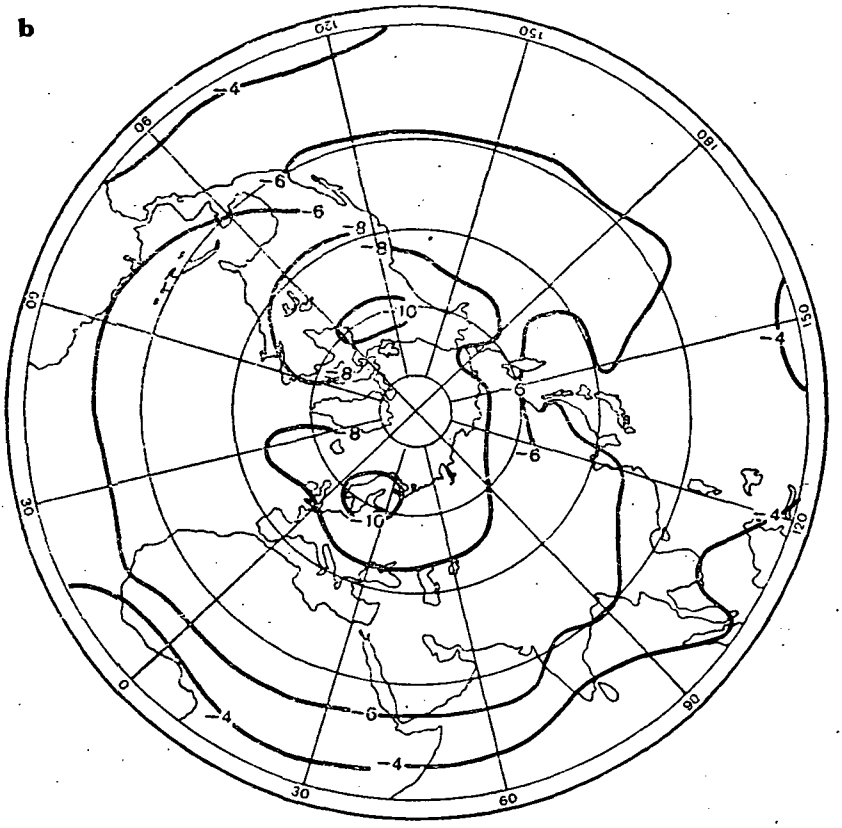

Fig. 9.12b. Monthly amounts of atmospheric net radiation for the Northern Hemisphere (kcal/cm² · mon). December.

Many foreign scientists, besides Soviet scientists, have dealt with the question of the geographic distribution of atmospheric net radiation and the earth-atmosphere system.

Table 9.11, constructed by Möller [30], shows a comparison of the results of computations of average annual values of atmospheric net radiation and its constituents for different latitudinal zones obtained by various scientists.

In [28] Möller and many others scientists have given charts of the geographic distribution of mean annual values of atmospheric net radiation over Europe and parts of the Atlantic Ocean for January, March, May and September of 1955.

Table 9.11 Comparison of results of computations of atmospheric net radiation (cal/cm² · 24 hr) and its constituents

	30-50° N	40-60° N	60-90° N
	Bauer and Phillips (1934)		
q	90	82	81
$F_\infty - F_0$	217	233	227
B_a	127	151	146
	Hutton (1954)		
q	121	99	59
$F_\infty - F_0$	359	333	287
B_a	238	234	228
	London (1957)		
q	96	83	65
$F_\infty - F_0$	305	280	230
B_a	209	197	165
	Möller (1959)		
q	92	79	55
$F_\infty - F_0$	300	291	262
B_a	208	212	207

3.3 Vertical profiles of net radiation

Here the profiles of total B and longwave B_{LW} balances will be examined. The term "net radiation" will imply total radiation balance B.

The values of net radiation at different levels in the troposphere and stratosphere can change within wide limits from negative values of the order of -0.4 cal/cm² · min (at nighttime) to positive values of 1.2-1.4 cal/cm² · min (daytime for large $h_\odot$). Moreover, these extreme values are most often recorded in clear weather at latitudes between 10 and 30°.

At intermediate latitudes in daytime ($h_\odot > 15°$) the net radiation is positive at all heights. The maximum values 1-1.2 cal/cm² · min can be obtained during summer at noon time above water surfaces or any other underlying surface with low albedo. The value of net radiation is unconditionally affected by the state of the air mass situated above and below the radiometer. The pure air mass under other similar conditions results in higher values of net radiation. Variation in the solar altitude and in the quantity of cloud above or below the radiometer acts most distinctly on the values of net radiation.

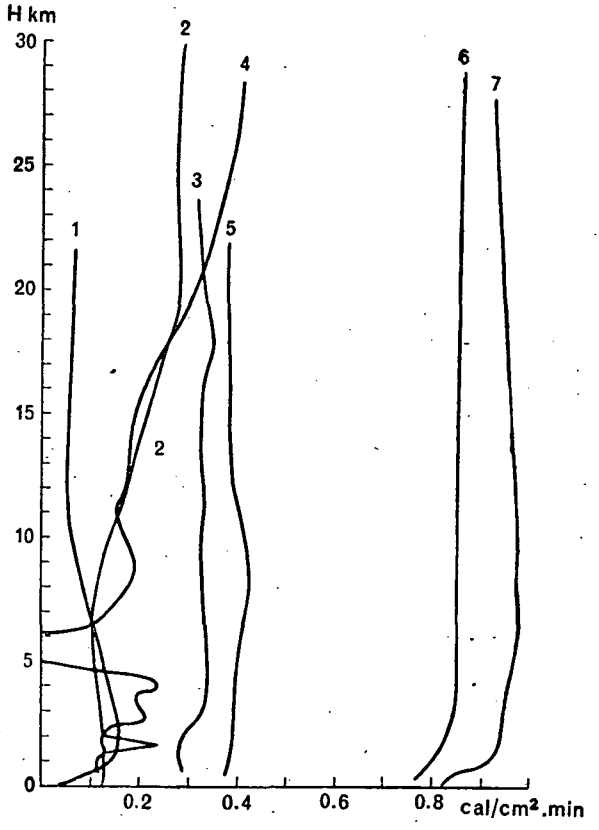

Fig. 9.13. Vertical profiles of net radiation.

1—Nov 14, 1961, $h_\odot = 19°$, clear; 2—Oct. 23, 1964, $h_\odot = 26.5°$, 10 point St.; 3—July 22, 1964, $h_\odot = 26.5°$, clear; 4—Oct. 1, 1965, $h_\odot = 35°$, 10 point, multilayered; 5—Oct. 21, 1965, $h_\odot = 26.5°$, clear; 6—June 5, 1962, $h_\odot = 56°$, clear; 7—May 25, 1962, $h_\odot = 57°$, clear.

The fundamental patterns of the vertical course of net radiation can be studied from the data of actinometric probings carried out by LGU. Fig. 9.13 shows several vertical profiles of net radiation from daily measurements in balloons, rising to a height of 30-33 km. The method of measurement and more detailed results are given in [23]. Each profile refers to a particular solar altitude. The values of net radiation with respect to altitudes were obtained with an accuracy of 10%.

Profile 1 (above 11 km) characterizes the course of net radiation in the stratosphere above a snow surface ($h_\odot = 19°$). The values of balance in this case are low, the highest value being $B = 0.06$ cal/cm² · min. The value of net radiation in the stratosphere is practically constant. The

tropospheric part of the profile was obtained above an underlying surface with lower albedo.

Profiles 3, 6 and 7 refer to summer periods ($h_\odot = 26.5°$ and 56°). Profile 7 shows maximum possible values of net radiation for the latitude $\varphi > 50°$. All the above-mentioned four profiles have been obtained in cloudless weather and under conditions of comparatively clear air masses. The small variation in magnitudes of B from a height of 6 km (profiles 3, 6 and 7) and from a height of 11 km for the case described by profile 1, indicate that the state observed at these heights is close to the state of radiant equilibrium. If there is no distortion in the horizontal homogeneity of the underlying surface during ascent, then a radiant equilibrium may be observed from a height of 3-5 km.

Profiles 2, 4 and 5 characterize the action of aerosol components on the values of the net radiation. In the case of profile 4, it is known that on this day the amount of the aerosol component in the lower stratosphere considerably exceeded the mean value. On the other hand, from the profile of reflected radiation (Fig. 6.17, profile 18), as well as from the profile of reflected balance 4, it is obvious that the variation in fluxes in the stratosphere generally comprises 0.25 cal/cm^2 · min, i.e. the variation in the upward shortwave flux causes a change in net radiation. Thus the rise in net radiation is connected with the presence of aerosol which "eats up" the high values of the albedo of clouds (the aerosol layer may be thought of as some semitransparent gray body with albedo from 20 to 40% depending on the aerosol concentration and thickness of the layer). This conclusion is confirmed by profile 2, which has segments with perceptible growth (7-18 km). In this case one may notice a layer (2-6 km) with anomalous turbidity above the layer of clouds.

From the instance quoted it is obvious that the state of radiant equilibrium is easily distorted above an underlying surface with large albedo. The increased aerosol concentration above these surfaces is the reason for the nonequilibrium of the components of net radiation.

Profile 5 shows the action of the aerosol component (raising of concentration) on the net radiation in a cloudless situation. The stratospheric aerosol, situated in this case between the heights of 9 and 16 km, increases the albedo of the troposphere underlying surface system, and consequently lowers the value of net radiation (drop above 9 km). Evidently aerosol exerts an influence on effective radiation of the earth's surface also.

It thus follows that the aerosol component prevents the establishment of radiant equilibrium; moreover, there is a shift in the equilibrium in the presence of cloudiness toward radiative heating (rise of net radiation at a height of 15-25 km, profile 4). A shift of radiant equilibrium toward radiative cooling has been observed in the presence of cloudiness and in the case where the aerosol layer is situated between the instrument and

the earth's surface (net radiation possesses a tendency to decrease, profile 5).

Thus, in the majority of cases radiant equilibrium is brought about in the stratosphere under conditions of nonturbid air masses and in the absence of cloud formations in the low-lying layers.

In the upper troposphere conditions close to radiant equilibrium

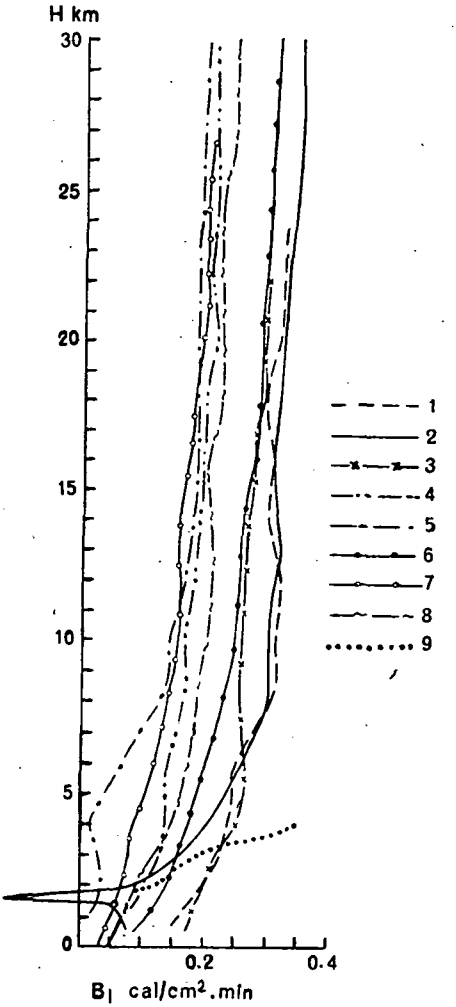

Fig. 9.14. Vertical profiles of longwave net radiation.
1—July 22, 1964, $h_{\odot}=26.5°$; 2—October 23, 1964, $h_{\odot}=26.5°$; 3—October 21, 1965, $h_{\odot}=26.5°$; 4—summer, night, clear (TsAO); 5—summer, night, cloudy (TsAO); 6—summer, night, USA; 7—equatorial regions (TsAO); 8—tropical regions (TsAO); 9—experimental profile, summer, Central Asia.

appear mostly at low solar altitudes (<25°). To some extent the last position is justified for lower stratosphere as well.

Let us now turn our attention to the vertical distribution of the longwave balance. During daytime a longwave balance can be obtained if total and reflected radiations are measured along with net radiation so that the following holds :

$$B_{LW} = \frac{\alpha_{1L} + \alpha_{2L}}{2}\left(n_{pt} - \frac{Q}{\alpha_{1s}} + \frac{R}{\alpha_{2s}} \right), \tag{9.12}$$

where α_{1L}, α_{2L}, α_{1s} and α_{2s} are the longwave and shortwave transition multiples for the first and second sides of the radiometer (α_1 and α_2 may not differ by more than 2%), n_{pt}—indicator of the radiometer adjusted for temperature and pressure (for measurements in free atmosphere); Q and R are the total and reflected radiations, measured by the pyranometer (taking into consideration the angular and spectral connections for pyranometer as well as for radiometer).

During actinometric probing carried out at LGU the researchers employed a coupled radiometer besides the radiometer with a polythene shielding, which enabled them to obtain longwave fluxes and balance with an accuracy of 5% in the troposphere and not less than 10% in the stratosphere. The profiles of longwave balance are shown in Fig. 9.14. The curves 1, 2 and 3 characterize B_{LW} for daily conditions in summer (1) and in autumn (2, 3) and profile (2) was obtained in cloudy weather (St 10/10). The curves 1 and 3 characterize the latitudinal course of B_{LW} for typical conditions (close to average) in clear weather during summer and autumn.

The curves 4-9 have been introduced for comparison, so that the first five profiles (4-8) characterize mean values of B_{LW} obtained with the help of actinometric radioprobing during nighttime, and profile 9 describes the course of B_{LW} in the layer between 2-4 km from the results of daily airplane probings in Central Asia [20].

Profiles 4-5 show average values of the longwave balance for cloudless (4) and cloudy (5) weather during the summer period from the data of eight stations for actinometric radioprobing above the territory of the USSR and from data recorded on the vessel "Voeikov" in the tropics [18].

Average values of longwave balance for near equatorial (0-5°) and tropical (15-20° in winter and 25° in summer) latitudes are shown in profiles 7 and 8 [19].

Profile 6 characterizes mean values of longwave balance during summer at nighttime above the territory of the USA [29].

Values of B_{LW} approaching wintertime by night and day in dense cloudiness are not large; i.e. from -0.03 to -0.08 cal/cm^2 · min; and B_{LW} attains the value of -0.13, -0.17 cal/cm^2 · min in the surface layer during daytime in clear weather.

As can be seen from Fig. 9.14, a longwave balance can be found mainly in the troposphere from heights of 7-10 km, whereas B_{LW} above this layer rises slowly (from absolute values in all cases). The maximum value (-0.36 cal/cm^2 · min) was obtained at a height of 28 km (profile 2) in dense cloudiness at a height of 1-2 km and anomalous turbidity in the layer above the clouds. The minimum (absolute) values of B_{LW} were obtained in the middle of the cloudy layer (profiles 2, 4) where the longwave balance becomes zero. The rise of B_{LW} in the layer 2-7 km (profile 2) occurred as a result of the unusually high temperature, moisture content and aerosol concentration at these heights on October 23, 1964, as compared with the conditions on Nov. 21, 1965 (profile 3), when the air was at a temperature of 18° below, and the moisture content seven times less at a height of 5 km than on October 23, 1964. Surface values of B_{LW} are not large and vary within the limits of -0.05 to -0.08 cal/cm^2 · min at night and may reach -0.15 cal/cm^2 · min during the day.

The difference between daytime (profiles 1, 2, 3 and 9) and nighttime (profiles 4-8) values of B_{LW} appears in the troposphere as well as in the stratosphere. The autumnal daytime profile (2) is closest to the average nightly profiles; in the stratosphere it is practically coincident with mean summer profiles (6) constructed from the data of Suomi (USA). The maximum difference between the summer profiles 1 and 6 exists in the troposphere (15-20%) and decreases in the stratosphere to 10%. Slightly higher differences between the daytime and nighttime summer profiles may be noticed on comparison of average summer profile (1) with the data of nighttime actinometric radioprobing of TsAO. In this case the difference becomes 30%.

A comparison of the data of daytime and nighttime probings shows that the formation of profiles occurs in the daytime at low heights. This is clearly demonstrated by profile 9, which was obtained at a high solar altitude. Significant variations in profiles can be brought about by the raised aerosol concentration where the course of profiles 2 and 9 at altitudes of 2-4 km assists in the process.

The effect of cloudiness on the values of B_{LW} can be estimated from profile 5. At almost all altitudes the absolute values of B_{LW} in this case are lower than in other profiles. The altitudes of 11.5-17 km are an exception since the minimum values of B_{LW} (on the absolute scale) were obtained in equatorial latitudes (profile 7).

The highest average values of B_{LW} (on the absolute scale) from the data of TsAO were recorded in tropical regions (profile 8).

Thus the daily summer values of longwave balance in the troposphere can be higher than average nighttime values (profile 6) by 15-20% ; in the stratosphere the difference decreases to 10%. The mean values of B_{LW} in autumn (profile 3) differ from mean summer values in the dark period of the day (6) only in the troposphere. The mean values of B_{LW}

from the data of nighttime actinometric radioprobing in the USSR and USA for the same season, differ by 15-25% in the lower troposphere and up to 30% in the stratosphere.

The vertical distribution of the values of longwave balance during daytime depends mainly on the altitude of the upper boundary of cloud cover and on the quantity of solar radiation absorbed in any atmospheric layer, i.e. ultimately on the stratification of active components of the atmosphere.

3.4 Radiant influx of heat

We will now examine the resultant influx of heat in the atmosphere up to an altitude of 55 km, received on account of (shortwave and longwave) constituents of net radiation.

There has been insufficient theoretical and experimental work to establish radiative variation from the data on vertical distributions of total balance. This is explained by the fact that the experimental investigation of net radiation in daytime presents many difficulties of a methodological nature which can be overcome only through complications of measuring apparatus (as was done in the aerostatic complex of LGU [23]) or by constructing instruments which measure the radiant influx of heat indirectly. Definite progress has been achieved in this direction [10].

In theoretical works in the majority of cases radiative cooling of the atmosphere on account of longwave radiation (Chapter 8, sec. 3) has been considered, as also to a lesser extent radiative heating due to absorption of shortwave radiation (Chapter 8, sec. 3), and not so comprehensively the variations in radiative temperatures for complete net radiation. The most interesting results are found in [13]. From Ohring's investigations [31] it follows that in the entire layer of the stratosphere radiant equilibrium is absent at all altitudes, with the exception of a narrow transition zone in the region 35-45° N. South of this range the net radiation of the stratosphere is positive, and to the North it is negative. Consequently conditions may appear for interlatitudinal advection heat.

The computations of Ohring and Pressman convincingly prove that the thermal regime of the stratosphere primarily controls radiation. However, the insufficient reliability of the original data for computations, and likewise differences in the methods of computation, lead to the results of the computations of different authors varying considerably even with respect to the fundamental properties of the profile of variations in radiative temperature. The values of variations in the radiative temperature in the atmospheric layer studied experimentally were obtained as the difference between values of net radiation in the upper and lower boundaries of this layer,

and with respect to the difference in pressures at the boundaries of the layers, as follows :

$$\frac{dT}{dt} = \frac{1}{c_p \rho} \frac{\partial B}{\partial z} = -245 \frac{\Delta B}{\Delta p} \text{ deg/hr}, \tag{9.13}$$

where $\Delta B = B(z_2) - B(z_1)$ is the increase in net radiation expressed in cal/cm^2·min; Δp is the difference in pressures in millibars at these levels; z_2 and z_1 are the heights of upper and lower boundaries of the layer being examined. The accuracy attained in this manner is not high (small differences in large values) since the daily vertical profiles B depend on many parameters[1] whose influence on the indicators of the instrument must be determined and eliminated. But the introduction of one solar altitude and consideration of inhomogeneity of the underlying layer for data of the total net radiation obtained in the upper troposphere and stratosphere has not been achieved to date with high accuracy.

Besides, the transition to formula (9.13) from the derived formula with respect to final differences is justified only for small Δp, but in practice while working with aerostatic data on daily probing the application of steps for heights below 0.5 km is insignificant on account of inaccuracy in the profile itself.

The experimental data on the variation in radiative temperature have been obtained only up to a height of 28 km. More detailed observations can be found in [14, 17]. Fig. 9.15 shows several profiles of variations in radiative temperature developed with the consideration of observations

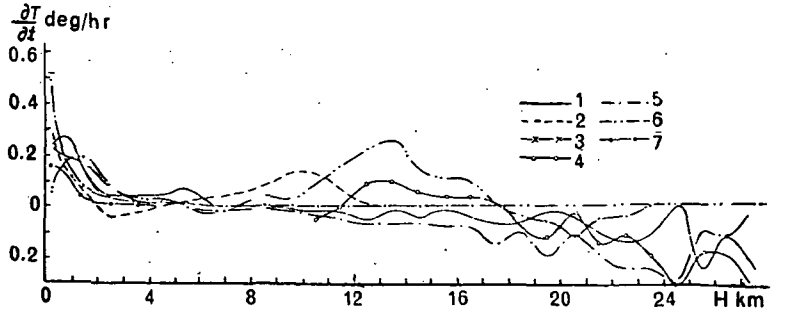

Fig. 9.15. Variations in radiative temperature in troposphere and lower stratosphere from the data on complete net radiation. 1962.

1—May 25; 2—July 12; 3—June 3; 4—July 4; 5—May 30; 6—July 7; 7—November 22.

[1] Variation in $h_\odot$, influence of temperature and pressure on the instrument, when it is not horizontal and inhomogeneity of underlying surface.

made above on the possible sources of error (profiles for which variations in solar altitudes are insignificant and comparatively homogeneous underlying surface, for instance, absence of cloudiness). From the course of profiles it is obvious that radiative heating predominates in the lower 2 km layer during May through November and sometimes the values of heating becomes 0.4 deg/hr. The radiative variation is comparatively small in the layer 2-10 km and fluctuates about zero value.

The results obtained by Kastrov [12] at heights of 3-5 km show that during summer the values of radiative heating and cooling are close to each other and become 0.06-0.08 deg/hr. Thus the radiative effect of variation with respect to temperature approaches zero during daytime.

The results of probing in May (profiles 1, 5) show that cooling starts from a height of 9-10 km.

Localized maxima of radiative heating were recorded in the three probings in the month of July (2, 4 and 6) in the layer 9-14 km. The course of profiles (3, 4) shows that during summer the transition to radiative cooling takes place at altitudes of 17-18 km, whose values become −0.3 deg/hr at a height of 24-27 km. The second group of profiles shows that the case of radiant equilibrium is possible. The course of net radiation profiles in the stratosphere for other days, shown in Fig. 9.13 (1-5), confirms the observed regularity in distribution of variations in radiative temperature.

REFERENCES

1. Aizenshtat, B. A. Metod opredeleniya radiatsionnogo balansa sklonov (Method of determining net radiation of slopes). Meteorologiya i gidrologiya, No. 2, 1952.
2. Aizenshtat, B. A. Teplovoi balans i mikroklimat vlazhnykh gornykh dolin (Thermal balance and microclimate of moist mountain valleys). Trudy SANIGMI, vyp. 35 (50), 1967.
3. Aizenshtat, B. A. and M. V. Zuev. Nekotorye cherty teplovogo balansa pechanoi pustyni (Some features of thermal balance of sandy deserts). Trudy GGO, vyp. 6 (7), 1952.
4. Aizenshtat, B. A. and M. V. Zuev. Radiatsionnyi rezhim, teplovoi balans i mikroklimat gornoi doliny (Radiational regime, thermal balance and microclimate of mountain valley). Trudy SANIGMI, vyp. 6 (21), 1961.
5. Atlas teplovogo balansa zemnogo shara (Atlas of thermal balance of the earth—Under the editorship of M. I. Budyko). Mezhvedomstvennyi Geofizicheskii komitet i GGO, Moskva, 1968.
6. Barashkova, E. P. et al. Radiatsionnyi rezhim territorii SSSR (Radiational regime of the territory of USSR). Gidrometeoizdat, Leningrad, 1961.
7. Berlyand, T. G. Teplovoi balans atmosfery severnogo polushariya. A. I. Voeikov i sovremennye problemy klimatologii (Thermal balance of atmosphere in the Northern Hemisphere. A. I. Voeikov and contemporary problems of climatology). Gidrometeoizdat, Leningrad, 1956.

8. deBrishambo, Sh. P. Solnechnoe izluchenie i radiatsionnyi obmen v atmosfere (Solar radiation and radiative exchange in atmosphere). Izd-vo. "Mir", 1966.

9. Budyko, M. I. et al. Teplovoi balans poverkhnosti Zemli (Thermal balance of the earth's surface). Izv. AN SSSR, ser. geogr. No. 1, 1964.

10. Eliseev, A. A. Priemnik dlya izmereniya radiatsionnykh izmenenii temperatury (A receiver for the measurement of radiative temperature variations). Trudy GGO, vyp. 205, 1967.

11. Efimova, N. A. Radiatsionnyi balans poverkhnosti sushi zemnogo shara (Net radiation of land surface on the earth). Tr. Vsesoyuznogo nauchnogo meteor. soveshcheniya, t. IV, 1962.

12. Kastrov, V. G. Izmerenie poglosheniya solnechnoi radiatsii v svobodnoi atmosfere do 3-5 km (Measurement of absorption of solar radiation in free atmosphere up to 3-5 km). Trudy TsAO, vyp. 8, 1952.

13. Kondrat'ev, K. Ya. Aktinometriya (Actinometry). Gidrometeoizdat, Leningrad, 1965.

14. Kondrat'ev, K. Ya. and G. N. Gaevskaya. Radiatsionnye izmeneniya temperatury v svobodnoi atmosfere (Radiative temperature variations in free atmosphere). Problemy fiziki atmosfery, coll. No. 3, LGU, 1965.

15. Kondrat'ev, K. Ya., G. N. Gaevskaya and G. A. Nikol'skii. O radiatsionnom balanse atmosfery (Net radiation of atmosphere). Problemy fiziki atmosfery, No. 3, LGU, 1965.

16. Kondrat'ev, K. Ya. and M. P. Manolova. Radiatsionnyi balans sklonov (Net radiation of slopes). Vestnik, LGU, No. 10, 1958.

17. Kondrat'ev, K. Ya., G. A. Nikol'skii and E. N. Esipova. Ae'rostatnye issledovanniya radiatsionnykh potokov v svobodnoi atmosfere (Aerostatic investigation on radiative fluxes in free atmosphere). Izv. AN SSSR, fizika atmosfery i okeana, t. II, No. 4, 1966.

18. Kostyanoi, G. N., N. A. Zaitseva and V. I. Shlyakhov. Organizatsiya seti aktinometricheskogo zondirovaniya v SSSR i nekotorye predvaritel'nye resul'taty issledovaniya polya radiatsii s pomoshch'yu ARZ (Organization of the network of actinometric probing in the USSR and some preliminary results of the investigation on the radiation field with ARZ (Aleksandrov Radio Plant). Trudy soveshchaniya po ae'rologicheskomu zondirovaniyu. Tbilisi, 1967.

19. Koshel'kov, Yu. P., V. P. Koval'kov and A. Ya. Petinova. Srednee raspredelenie potokov dlinnovolnovoi radiatsii v atmosfere nizkikh shirot Tikhogo okeana (Mean distribution of fluxes of longwave radiation in atmosphere of lower latitudes of the Pacific Ocean). Geofiz. byull., No. 18, 1968.

20. Lopukhin, E. A. Issledovaniya raspredeleniya sostavlyayushchikh radiatsionnogo balansa nad Srednei Aziei (Investigation on the distribution of components of net radiation over Central Asia). Trudy SANIGMI, vyp. 16 (31), 1963.

21. Mukhenberg, V. V. Radiatsionnyi i teplovoi balans raiona Leningrada (Radiative and thermal balance of the region of Leningrad). Meteorologiya i gidrologiya, No. 4, 1953.

22. Mukhenberg, V. V. Radiatsionnyi balans sklonov (Net radiation of slopes). Metorologiya i gidrologiya, No. 7, 1963.

23. Nikol'skii, G. A. and E. N. Esipova. Izmereniya radiatsinnogo balansa v svobodnoi atmosfere s pomoshch'yu balansomerov s polie'tilenovoi zashchitoi (Measurement

of net radiation in free atmosphere with the help of radiometer provided with a polythene shield). Problemy fiziki atmosfery, No. 4, LGU, 1966.

24. Pivovarova, Z. I. and T. G. Pleshkova. O radiatsionnom rezhime SSSR po materialam nablyudenii seti stantsii (On the radiational regime of USSR from the information of observations at the network of stations). Trudy VNMS, t. IV, 1962.

25. Rusin, N. P. Meteorologicheskii i radiatsionnyi rezhim Antarktidy (Meteorological and radiational regime of the Antarctic region). Gidrometeoizdat, Leningrad, 1961.

26. Chernigovskii, N. T. and M. S. Marshunova. Klimat Severnoi Arktiki (radiatsionnyi rezhim) [Climate of Soviet Arctic region (radiational regime)]. Gidrometeoizdat, 1965.

27. Yanishevskii, Yu. D. Aktinometricheskie pribory i metody nablyudenii (Actinometric instruments and method of observations). Gidrometeoizdat, Leningrad, 1957.

28. Kasten, F. et al. On the heat balance of the troposphere. Final Reports on Contract AF 61 (052)—18, Mainz, 1959.

29. Kuhn, P. M., V. E. Suomi and G. L. Darkow. Soundings of terrestrial radiation flux over Wisconsin. Mon. Wea. Rev., v. 87, No. 4, 1959.

30. Möller, F. Der Strahlungshaushalt der Troposphäre. Meteor. Rund., Bd 13, H. 3, 1960.

31. Ohring, G. The radiation budget of the stratosphere. Journ. Meteorol., v. 15, No. 5, 1958.

32. Raschke, E. and W. R. Bandeen. The radiation balance of the earth-atmosphere system obtained from measurements of the Nimbus II meteorological satellite. 48th Meeting AMS, Jan-Feb 1968. San Francisco.

33. Schulze, R. Das Strahlungsklima der Erde. Strahlentherapie, 130, 1965.

NASA
TT F-678

Radiation Characteristics of the Atmosphere and the Earth's Surface

Kondrat'ev

Amerind